12-31-2005

The implementation of nanoimprint lithography for the fabrication of patterned magnetic media

Daniel David Marks
Rowan University

The Implementation of Nanoimprint Lithography for the Fabrication of Patterned Magnetic Media

by

Daniel David Marks

A Thesis Submitted to the

Graduate Faculty in Partial Fulfillment of the

Requirements for the Degree of

MASTER OF SCIENCE

Department: Electrical and Computer Engineering
Major: Engineering (Electrical Engineering)

Approved:

_____
In Charge of Major Work

_____
For the Major Department

_____
For the College

Members of the Committee:

_____

_____

Rowan University
Glassboro, NJ
2005

ACKNOWLEDGEMENTS 4
ABSTRACT 5
1 INTRODUCTION 6
2 MAGNETIC HARD DISK DRIVE RECORDING TECHNOLOGY 17
2.1 Fundamentals of the Read sensor 17
2.1.1 MR Effect 18
2.1.2 MR Read sensor 21
2.1.3 GMR Read sensor 26
2.2 Fundamentals of the Write Head 31
2.2.1 Karlqvist Head Model 33
2.2.2 Write Process 35
2.3 Magnetic Recording Media 39
2.3.1 Thin-Film Disk Structure 40
2.3.2 The Magnetostatic Field 42
2.3.3 Macroscopic and Microscopic Properties 45
2.4 Limitations of Present-Day Magnetic Recording Technology 53
2.5 Next-Generation Magnetic Recording Technologies 61
2.5.1 AFC Media 61
2.5.2 Perpendicular Recording 64
2.5.3 Patterned Magnetic Media 67
2.6 Conclusion 70
3 SURVEY OF TECHNOLOGIES CAPABLE OF FABRICATING PATTERNED MAGNETIC MEDIA 72
3.1 Interference Lithography 74
3.1.1 Principle of Interference Lithography 75
3.1.2 Anti-Reflective Coating 77
3.1.3 Interference Lithography Systems 79
3.1.4 An Assessment of Interference Lithography 83
3.2 Self-Assembly Patterning 84
3.2.1 Physical and Molecular Self-Assembly 85
3.2.2 Self-Assembled Monolayers 86
3.2.3 Self-Assembly of Nanocrystals 89
3.2.4 Self-Assembly through Heterogeneous Nucleation 91
3.2.5 Self-Assembly of Block Copolymers 93
3.2.6 An Assessment of Self-Assembly Patterning 96
3.3 Nanoimprint Lithography 97
3.3.1 Imprinter Fabrication 98
3.3.2 Anti-Adhesive Agent 106
3.3.3 Imprinting 110
3.3.4 Post Processing 114
3.3.5 An Assessment of Nanoimprint Lithography 118
3.4 Conclusion 119
4 IMPLEMENTATION AND RESULTS 120
4.1 Equipment and Materials 121
4.1.1 Imprinting Press: Construction 123
4.1.2 SEM: Imaging and Writing a Pattern 127
4.2 Material Processing 131

4.3 Imprinter Fabrication 134
4.3.1 SiO_2 Imprinter Fabrication 135
4.3.2 HSQ Imprinter Fabrication 143
4.4 F_{13}-TCS Anti-Adhesive Application 152
4.4.1 Initial Process 153
4.4.2 Results of Implementing the Anti-Adhesive Coating 154
4.5 Imprinting 157
4.5.1 Initial Imprinting Process 157
4.5.2 Most Effective Imprinting Process 160
4.5.3 Results of Imprinting 164
4.6 Post Processing 171
4.6.1 Fabrication of Patterned Magnetic Media Using a Single Layer 171
4.6.2 Fabrication of Patterned Magnetic Media Using the Type 4 Bilayer 174
4.7 Magnetic Measurements 176
4.8 Conclusion 176
5 CONCLUSION 179
6 FUTURE RECOMMENDATIONS 183
APPENDIX A: IMAGES 184
A.1 Imprinters 186
A.1.1 SiO_2 Imprinters 186
A.1.2 HSQ Imprinters 200
A.2 Imprinted Samples 223
A.2.1 Single Layer Resist 223
A.2.2 Type 1 Bilayer Coating 244
A.2.3 Type 2 Bilayer Coating 253
A.2.4 Type 3 Bilayer Coating 256
A.2.4 Type 4 Bilayer Coating 258
A.3 Samples: Etched and Patterned Permalloy Dots 266
A.3.1 Single Layer 266
A.3.2 Type 4 Bilayer 283
REFERENCES 290

ACKNOWLEDGEMENTS

I would like to express my gratitude to my family and friends for their continued support throughout not only graduate school, but also my entire education. I would especially like to thank my Mom, Dad, brothers, and dog for always being there for me. The generosity, love, and guidance that my parents have bestowed upon me through all aspects of life has been unparalleled. I only hope that one day I can repay them for everything they have done for me. My Brother Scott's innate ability to provide comic relief has always made things easier. He is my best friend, and has made me a proud older brother. I would also like to thank my advisor, Dr. Robert Krchnavek, for his support and guidance. His advice and kindness made the daunting task of writing a thesis easier. Furthermore, I would like to thank my committee members, Dr. Linda Head and Dr. Sam Lofland along with Dr. Jeff Hettinger for his continual help with laboratory equipment. I would also like to thank Dr. Sam Lofland for taking measurements of the magnetic media. Finally, I would like to thank my fellow graduate students for their direct help with work and also for their companionship. I would especially like to thank Nate Clarke, Rob Groove, and Amy Vanderslice.

ABSTRACT

Advances in technology are having profound effects throughout society. This is no truer than in the way information is being stored. The primary form of information storage for at least the past to millennium has been paper. Today, an ever increasing amount of information is being stored electronically. An increased demand for high-performance, low-cost information storage has been a major catalyst in increasing the popularity of hard drives. In 2002, two exabytes of original information was stored on hard drives. This is ten times the amount of all printed material in the world if it were converted to electronic files. To keep up with this demand, the capacity of hard drives has increased by at least 60% annually since 1991. The capacity has mainly increased by scaling down the relevant dimensions much in the same way that has been done with microprocessors. Scaling cannot indefinitely be used to increase the capacity of hard drives that employ longitudinal magnetic recording. Before long, the superparamagnetic effect will limit the achievable information capacity of hard drives using conventional recording. Therefore, new technologies will be needed. Perpendicular recording, one of several new technologies, will make its entrance into the market later this year in a hard drive designed by Toshiba for Apple's iPod music player. It is said that the hard drive will have an areal bit density of 133 Gbits/in^2. This is an increase of 75% over what is currently available today. However, the hard drive will still employ a continuous magnetic medium. Even greater densities can be achieved if the magnetic medium is physically patterned into isolated bits. This technology, known as patterned magnetic media, has the potential of achieving areal bit densities greater than 1 Tbit/in^2. The challenge is finding a way to fabricate it. A high-throughput, low-cost pattern generation technology is needed. Research completed with nanoimprint lithography demonstrates that it can be used to fabricate patterned magnetic media. Several patterns of magnetic media were fabricated with densely packed sub-20-nm features that would produce an areal bit density of at least 258 Gbits/in^2.

1 INTRODUCTION

Present day society is in an era where there is a continually increasing demand for high-performance, low-cost, nonvolatile information storage systems. This is a result of several factors that include a greater demand for desktop computers and workstations, the growth of storage-hungry graphics and multimedia applications, and the use of removable drives in noncomputer consumer applications. It is also a result of a continually increasing collection of storable information available to millions of people. In 2002, the University of California conducted a study and found that approximately 2 exabytes of original information ranging from email messages to MP3 files were stored on hard drives [1]. If all the printed material in the world were stored on hard drives, it would still be ten times less than 2 exabytes of information.

The primary form of information storage today is the hard disk drive (HDD). The hard drive industry has been trying to keep on pace with the electronics and information boom. Hard drives have seen their capacity increase by at least 60% per year since 1991. Despite this growth, a physical barrier will eventually be approached that will limit the amount of information that can be stored in a given area with conventional magnetic recording technology. In order to sustain the increasing capacity of information storage in hard drives, new magnetic recording technologies need to be developed. One type of technology that shows great potential is patterned magnetic media which can be created cost effectively by nanoimprint lithography (NIL).

Information storage has progressed over time becoming more efficient and less expensive today. Prior to the invention of the printing press in 1444, all information was handwritten onto paper. Not remarkably, it was uncommon for people to own any types of written material because of the cost. It required three years worth of rent on a decent-sized estate to purchase the readings of the Bible stored on paper. The invention of printing revolutionized the method with which information was recorded by making it faster to produce written materials. Therefore, prices of books decreased, and the spread of information increased rapidly. Now with electronics, storing information has become even easier and cheaper. The price of information storage today is somewhere between $0.0005 and $0.001 per megabyte. At this price, the entire Bible, if assumed to require only a few megabytes, can be stored on a hard drive for a fraction of a cent.

Despite the differences between past and present information storage, there have always been the same goals in mind as the technology progresses. Since its inception, information storage has undergone major advancements aimed towards cost reduction and increased information capacity per unit area. Improving those features together creates a high-quality information storage device. There is also one other feature that should be mentioned when discussing information storage. That is whether or not the device is nonvolatile; the stored information does not degrade rapidly over time. Both paper and hard drives can store information for years without degradation. Contrastingly, random access memory in a computer is volatile, and all the information stored in it is lost when the power is switched off.

The idea of using paper to store written information was discovered by the Egyptians in 3000 B.C., but it was not until 105 A.D. in China that the modern method of creating paper was discovered by T'sai Lun. For the past 5000 years up until a few decades ago, paper has been the primary medium of information storage. Today, printed documents still hold the vast majority of reliable information published in books, newspapers, and journals. If stored as digital data, all printed material in the world would require 0.2 exabytes of storage. This is under the assumption that 1 typewritten page requires 2 kilobytes. However, the University of California's study found that when discussing all the information in the world that is being stored, printed documents only comprised 0.01% of the total original information stored in 2002 [1]. In the study conducted, all the original information in the world being stored in 2002 was considered no matter how meaningful or meaningless it was to the public population. While printed documents still contain most of the reliable information, they only constitute a small portion of all the information being stored today.

There are three other main methods of nonvolatile information storage methods being used today besides paper. These are film, magnetic media, and optical storage. Together these methods accounted for the other 99.99% of information storage in 2002. Some of the devices that fall into these categories of information storage methods are magnetic tape drives, magnetic hard disk drives, magnetic floppy disk drives, phase-change optic disk drives, holographic optical storage, magneto-optic disk drives, and magnetic random access memory. Another type of nonvolatile storage device that does not fall into the above categories is semiconductor flash memory.

Despite all these methods, magnetic media has been the most dominant form of information storage over the past several years. Furthermore, hard disk drives have been the magnetic media device experiencing the most growth. In 2002, 92% of new information was stored on magnetic media. Forty percent of this amount was stored in hard drives. Videotapes stored the second highest percentage of information under magnetic media with 27%. Hard drives have also experienced a 114% increase in information storage from 1999 to 2002. This was the highest increase out of not only magnetic media devices, but also all other forms of media. Hard drives have become the choice for information storage over the past several years.

Why have hard drives become the most favorable type of information storage device over the past few years? It is because the industry has been able to sustain several trends over a long period of time through key technological advancements. They have been able to decrease prices per unit of storage while increasing storage capacity. The industry measures storage capacity in terms of areal bit density in which a bit is a region of average magnetization in one of two possible directions representing either a logic one or zero. Areal bit density is the amount of data represented by bits that can be stored in a given area on a hard disk platter and is expressed in bits per square inch. In more technical terms, it is the product of linear bit and track density. Linear bit density is the number of bits along an inch of one track and is expressed in bits per inch. Track density is the number of tracks per inch along a radius of the disk expressed in tracks per inch. Figure 1.1 shows that areal bit density has been increasing since the first hard drive was distributed in 1956 [2]. It has increased 35 million times from its original value in 1956.

Price trends of storage systems are dependent on some factors more than others. Unit costs of dynamic random access memory (DRAM) caches and buffers, electronics such as controllers, cooling systems, and cabling have had a small effect on declining prices [2]. However, major decreases in price can be attributed to areal bit density increases of 60 to 100% per year for the past 10 to 15 years. Figure 1.2 compares the price of storage on disk drives, paper, and semiconductor memory. Over the past 25 years the price of hard disk drive storage has dropped from $100/MB to under $0.001/MB. Furthermore, price declines from year to year have experienced a change. Somewhere around the mid to late 1990's the price trend became steeper and declines averaged 37 to 50%. This was in response to the 60 to 100% per year

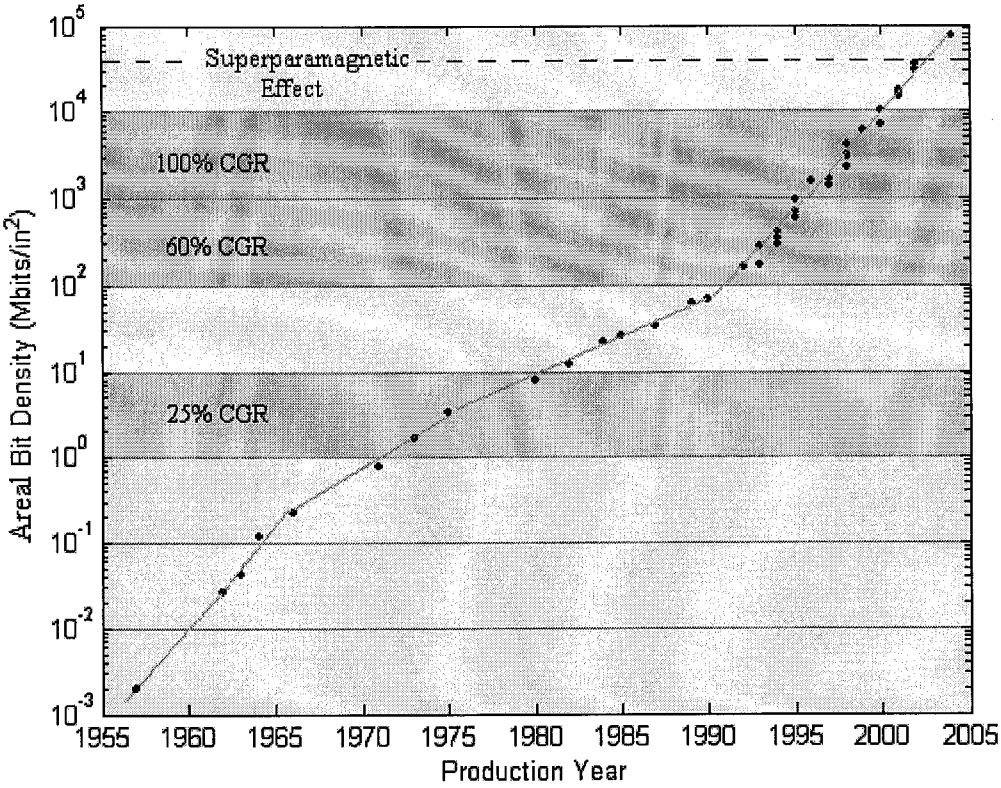

Figure 1.1 Hard disk drive areal bit density in Mbits/in^2 trend over the past half a century. CGR is compound growth rate.

compound growth rate (CGR) of areal bit density that can be seen in Figure 1.1. It can be seen that approximately at this time, the cost of disk drive storage has become cheaper than film and paper costs. This has been responsible for the growth and popularity of using hard disk drives for information storage.

The growth that the hard disk drive industry has seen has been as dramatic and paralleled only by the semiconductor industry. With this comparison, it might seem obvious to use solid state semiconductor memory devices for mass information storage. Semiconductor memory already has the advantage of much quicker access times than hard drives. Table 1.1 shows the amount of time it takes to read or write information into cells of three different types of semiconductor memory: DRAM, static random access memory (SRAM), and flash memory [3]. Compared to these times, the average seek time of a present-day hard drive is between 4 and 8 ms. The seek time is the time needed to move from an arbitrary track to the target track without being ready to read [4]. From this information, it appears that semiconductor memory has an apparent advantage over hard drives.

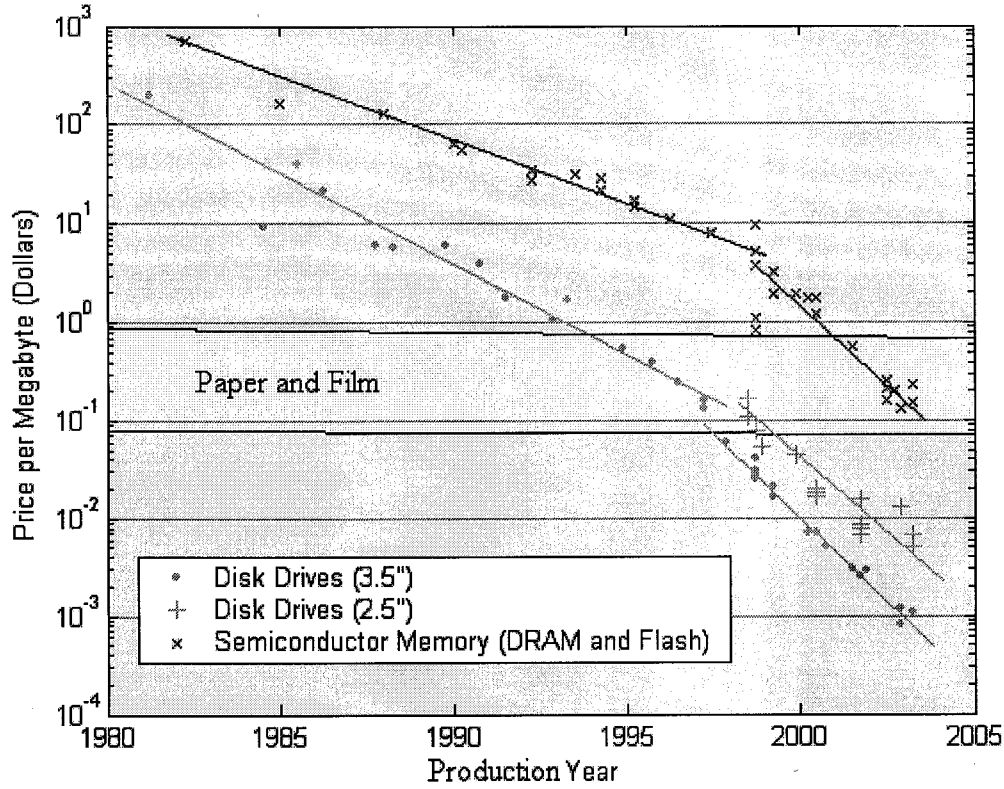

Figure 1.2 Cost of storage for hard disk drives, paper and film, and semiconductor memory over the past quarter century.

If access time was the only factor to consider, semiconductor memory would be the main form of mass information storage. However, because hard drives have a cheaper cost per megabyte basis as seen in Figure 1.2, they are the main form of mass information storage. From 1980 to 1990, the bit density of hard drives shadowed the bit density of semiconductor memory, but from 1990 to 2000, the density of disk drives increased at a faster pace than that of semiconductor memory as seen in Figure 1.3 [5]. Due to this, the price of hard drive storage has remained much cheaper than semiconductor memory. With these trends, it is highly unlikely that semiconductor cost per megabyte will catch up with that of hard drives any time in the foreseeable future.

There have been key advancements in technology that have allowed hard drives to make remarkable strides in price reduction and capacity increases over the years cementing their place as the primary form of mass information storage. The advancements in technology have been aimed towards increasing linear bit and track density. Increasing linear bit density over time has depended on the scaling down of the head to disk space known as the flying height, the gap size

Table 1.1 Operation times of various types of semiconductor memory devices.

Operation	*DRAM (Volatile)*	*SRAM (Volatile)*	*Flash (Nonvolatile)*
Write time	50 ns	8 ns	1 μs
Read time	50 ns	8 ns	60 ns

of the head, and the thickness of the magnetic media [5]. Increasing track density over time has depended on the reduction in track misregistration, innovations in servo systems, higher sensitivity in heads, and advances in track width control [6]. By increasing both of these parameters, areal bit density due to their dependency is increased.

Greater linear bit and track densities stemmed from developments in the areas of magnetic media and head design. While there have been a wealth of developments in these areas, there are a few major ones to point out. These are the ones that resulted in significant trend changes. Two major developments in magnetic media have been the introduction of thin films and recently antiferromagnetically coupled (AFC) media [7]. Recording heads experienced a major change in 1979 when IBM introduced thin-film heads. They were able to be fabricated with the same photolithographic techniques used by the semiconductor industry. Head design was then changed again in 1991 when IBM introduced magnetoresistive (MR) heads which were able to provide five to ten times higher sensitivity compared to that of thin-film heads. This created an abrupt trend change as can be seen in Figure 1.1. The introduction of MR heads resulted in a 60% annual growth rate of areal bit density. Then in 1997, IBM introduced giant magnetoresistive (GMR) heads based on a similar concept to MR heads, but having more sensitivity. This further increased the annual growth rate from 60 to 100%.

The astounding technological advancements in the hard drive industry can be observed by a comparison of the first hard drive with present-day models. The random access method of accounting and control (RAMAC) produced by IBM was the first hard drive to be used beginning in 1957. It consisted of fifty 24-inch diameter disks that together could store a total of 5 MB for a rental cost of $130 per month [5]. In the first quarter of 2005 Hitachi, which purchased IBM's hard drive division, came out with a hard drive capable of storing 500 GB on five 3.5-inch disks for an end cost of $500. Further information on this hard drive can be found at Hitachi's website [4].

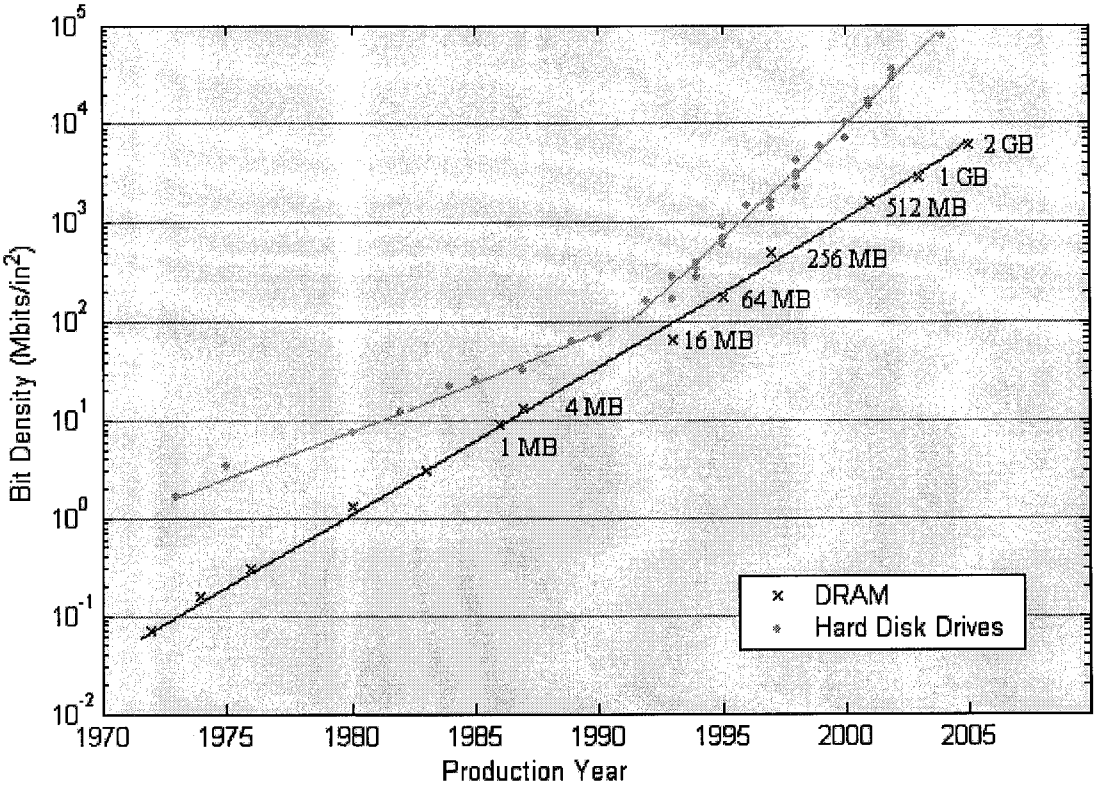

Figure 1.3 Comparison of bit density in Mb/in^2 between hard disk drives and Semiconductor DRAM.

The area of an individual bit in a hard drive along with its inverse, areal bit density, has reached staggering proportions today. The RAMAC hard drive had an areal bit density of 0.002 Mbits/in^2 which translates into a bit area of 0.323 mm^2. Hitachi's new hard drive has an areal bit density of 76 Gbits/in^2 which translates into a bit area of 0.0085 μm^2. Furthermore, Seagate has shown in the lab that they can achieve a data storage areal density of 101 Gbits/in^2 using their technology [8]. An areal density of 101 Gbits/in^2 means that the bit length is 41 nm and the track width is 160 nm translating into an area of only 0.00656 μm^2. A greater significance than the area is that with those dimensions the track width to bit length ratio is only 4:1. Table 1.2 shows the progressions of bit dimensions over the years along with the corresponding areal bit densities.

The only other device that has dimensions comparable to the bit size of a present day hard drive is a microprocessor. Intel's Pentium 4 Prescott processor can be used for a comparison. The bulk of Intel's microprocessors are still made using the 0.13-μm process; however, in the fourth quarter of 2003 Intel began shipping products built using a 90-nm process technology. They were made using strained silicon on a 300-mm wafer. The 90-nm process can

Table 1.2 Progression of hard drive bit dimensions.

Year	*Track Width (μm)*	*Bit Length (μm)*	*Areal Bit Density (Mbits/in^2)*
1957	1270	254	0.002
1962	508	48.8	0.026
1966	255	11.5	0.220
1971	132	6.29	0.776
1973	84.9	4.50	1.69
1980	50.3	1.67	7.68
1984	18.3	1.58	22.3
1987	11.8	1.67	32.8
1989	11.4	0.924	61.6
1992	9.47	0.431	158
1995	3.51	0.199	923
2000	0.915	0.071	10000
2005	0.202	0.042	76000

produce a MOSFET gate width of 50 nm. In comparison, the bit length in a hard drive that is available to consumers today is approximately 40 nm. While the minimum feature size is comparable, the Pentium processor is 112 mm^2 and a typical 3.5-inch diameter hard drive platter is 6207 mm^2. More information on Intel's 90-nm process can be found at their website [9].

In order to keep increasing areal bit density, the bit size needs to be scaled down. This is what has been going on since the first hard drive was developed. However, eventually a physical limit of the minimum bit size will be reached. It was originally predicted that the minimum achievable bit size would be approximately 200 x 50 nm. Original predictions have shown that areal bit densities will be limited to a maximum of 40 to 70 Gbits/in^2 with conventional magnetic recording [10]. The limit is caused by the superparamagnetic effect which is the spontaneous magnetization reversal caused by thermal energy fluctuations. It occurs when the magnetic grains that make up a bit become too small to be thermally stable. Therefore a logic value of one could flip to zero or vice versa without any writing operation taking place. This would lead to instability of the stored data and eventual data loss. Further explanation of the superparamagnetic effect will be discussed in the next chapter.

IBM found a way to push back the superparamagnetic effect for the time being with a breakthrough known as AFC media. It will allow bit dimensions to be scaled further and still work with the conventional longitudinal magnetic recording. Longitudinal recording is the

method used in all hard drives today where the medium magnetization is parallel to the disk plane. AFC media is made up of three layers. There is an ultra-thin layer of ruthenium sandwiched between two magnetic layers. The ruthenium layer forces the adjacent layers to orient themselves in opposite directions making the entire multilayer structure appear much thinner than it actually is [7]. Therefore smaller bits can be written on AFC media, and because of the media's overall thickness, they will not loose their magnetization from the superparamagnetic effect. AFC media is expected to allow areal bit density to surpass 100 Gbits/in^2.

The revolutionary technology that IBM developed will allow longitudinal magnetic recording used hard disk drives to temporarily avoid the superparamagnetic effect. Areal bit densities could reach the 100 to 200 Gbits/in^2 range. Eventually there will be no hiding from the superparamagnetic effect using longitudinal recording. Therefore a new technology is needed to extend the yearly increase of areal bit density. Several storage methods are being researched including some nonmagnetic methods such as holographic and atomic storage devices. Of the magnetic methods one is perpendicular recording. As mentioned earlier, all hard drives today use longitudinal recording. Perpendicular recording is when the medium magnetization is normal to the disk plane. For reasons that will later be discussed, perpendicular recording could increase areal bit density by a factor of 4. The only downside to using perpendicular recording is that it would cause a delay in development.

The type of technology that the remainder of this paper will focus on is patterned magnetic media. As of today, all hard disk drives have continuous magnetic surfaces. Each bit is not physically separated from neighboring bits. However, if bits were isolated from each other by non-magnetic material, it is possible that areal bit density could be increased by a factor of 10. It would be illogical to expect that success could simply be achieved by isolating bits. Other areas of scaling would be very difficult at these densities. Head sensitivities, track densities, and head-to-medium spacing far superior to those of today would be needed. The head-to-medium spacing would have to be on the order of 2 nm which is about the size of the lubricant molecule. These challenges are significant, but are not impossible especially if what has been done in the last half a century is taken into consideration. Despite the significance of these challenges, this paper will focus primarily upon experiments to test the feasibility of creating patterned magnetic media through a low-cost, high-throughput method.

An investigation into creating patterned magnetic media through NIL has been conducted. NIL is a relatively new technology capable of producing sub-50 nm features. Patterns are transferred from an embossing mask to a substrate by mechanically compressing a polymer resist layer. There are other techniques that can be used to create patterned magnetic media; however, none of them show the promise of possessing the high-throughput and low-cost that NIL does. There are several processing steps that are used to create patterned magnetic media. These include imprinter fabrication, imprinting or pattern transfer, post processing cleaning steps, application of a magnetic layer, and a procedure to liftoff the polymer.

The primary objective of this thesis is to provide an investigation of how patterned magnetic media can be created by NIL in an eventual effort to further increase the areal bit density of hard disk drives. A discussion of how the superparamagnetic effect will limit the growth of areal bit density using longitudinal magnetic recording on continuous magnetic media surfaces in present-day hard disk drives will illustrate the eventual need for patterned magnetic media. The next chapter will present an overview present-day head and disk components of a hard drive, and how the superparamagnetic effect is seen when components are continually scaled down. The chapter will conclude with an in-depth look at what is being done now to push back the superparamagnetic effect and what new technologies are being developed for the future, perpendicular recording and patterned magnetic media. A detailed survey of methods that can be used to create patterned magnetic media will be given in chapter 3. Results will be shown along with problems encountered in creating nanoscale features by NIL in chapter 4. Chapter 4 will also discuss measurements conducted on nanoscale magnetic particles created through NIL. Finally, chapter 5 will provide closing remarks and what further work needs to be done to create patterned magnetic media through NIL.

The main goal is to sustain the growth of areal bit density in hard drives despite the impending superparamagnetic effect. From the first hard drive that was introduced until today, areal bit density has been constantly increasing. Why is it necessary or where does the demand come from for greater capacity hard disk drives? Society is in the information age today, and massive amounts of information, whether important or needless, is being created at an alarming rate. In 2002, five exabytes of new information was created and 92% of that was stored on magnetic media [1]. Furthermore, greater density hard drives are in demand because of an increased demand of desktop computers, workstations, and laptops. The growth of storage-

hungry graphics and multimedia applications, along with the use of small drives in non-computer consumer applications has created a demand for hard drive storage. The popularity of hard drives along with a need for increased storage capacity provides a justifiable reason to create new technologies to keep increasing capacity.

2 MAGNETIC HARD DISK DRIVE RECORDING TECHNOLOGY

The fundamental premise of magnetic recording is to bring the magnetically active recording head in close proximity with the magnetic recording medium. The inductively generated stray fields in the write gap of the head are used to record a transition in the medium. When a magnetic recording medium with written magnetic transitions passes underneath the GMR read sensor, the magnetic field produced by each transition is sensed. In order to complete this process, a magnetic hard disk drive has four main components. These components are: the data detection electronics and write circuit; the mechanical servo and control system; the interface to the microprocessor; and the magnetic read/write head and magnetic disks that together form the head-disk assembly.

This chapter will cover the theory behind the head-disk assembly in an effort to provide a conclusive look at where magnetic recording technology is now and where it is going. Specific attention is being paid towards the head-disk assembly because an understanding of it will paint a clear picture of how patterned magnetic media can further increase areal bit density. Therefore, the first three sections will draw on the present-day methods used for the read sensor, write head, and magnetic media to allow for the high density magnetic recording that is achieved today. These methods include the reduction of the size of the write head through modeling, GMR read sensors, thin film disks, and longitudinal recording. As the bit size continues to be scaled down, problems arise as mentioned earlier. This will be discussed as well as the theory on the new technologies that could solve these problems such as AFC media, perpendicular recording, and specifically patterned magnetic media.

2.1 Fundamentals of the Read sensor

There are three requirements that need to be met when considering a read sensor. It should efficiently convert medium magnetization changes into sufficiently high current or voltage signals. This needs to be done with minimal noise being produced. It also needs to detect signals at high areal bit densities without a sizeable degradation to the signal. Finally and most importantly, the process, materials, and fabrication need to be cost effective. There have

been numerous research endeavors looking into the feasibility of using semiconductor devices such as "Hall Effect" transducers and arrays of transistors for read sensors; however, MR read sensors were the first to meet all three requirements.

MR read sensors were the first to employ the magnetoresistance effect; however, they are now out-dated and are no longer used in hard drives. There are two other types of read sensors that employ a stronger variation of the effect. The first type that is currently used in all commercial hard drives today is the GMR read sensor. It exploits the quantum property of spin direction to sense transitions in magnetic media. The second type is the tunneling magnetoresistive (TMR) read sensor which is still being researched. It exploits the property of quantum tunneling to sense transitions. The GMR read sensor is described in section 2.1.3, and the TMR read sensor will not be covered in this thesis.

2.1.1 MR Effect

Magnetoresistance is a property that causes certain metals to experience a change of resistivity in the presence of a magnetic field. On an atomic level it can be attributed to spin-orbit coupling [11]. The magnetoresistance of a ferromagnetic material is characterized by two components of resistivity. One is resistivity parallel to the magnetization, $\rho_{\parallel}$, and the other is perpendicular to the magnetization, $\rho_{\perp}$. An expression describing magnetoresistance in terms of resistivity can be derived from Ohm's law and trigonometric properties. Consider an electrical field, *E*, present in an MR material as seen in figure 2.1(a). Using Ohm's law, the electrical field parallel and perpendicular to the magnetization of the material can be given by

$$\begin{aligned} E_{\parallel} &= j_{\parallel}\rho_{\parallel} \\ E_{\perp} &= j_{\perp}\rho_{\perp} \end{aligned} \tag{2.1}$$

where $j_{\parallel}$ is the current density parallel to the magnetization and $j_{\perp}$ is the current density perpendicular to the magnetization

The final equation describing magnetoresistance is going to be in terms of resistivity; therefore, expressions for current density are needed. Expressions for parallel and perpendicular

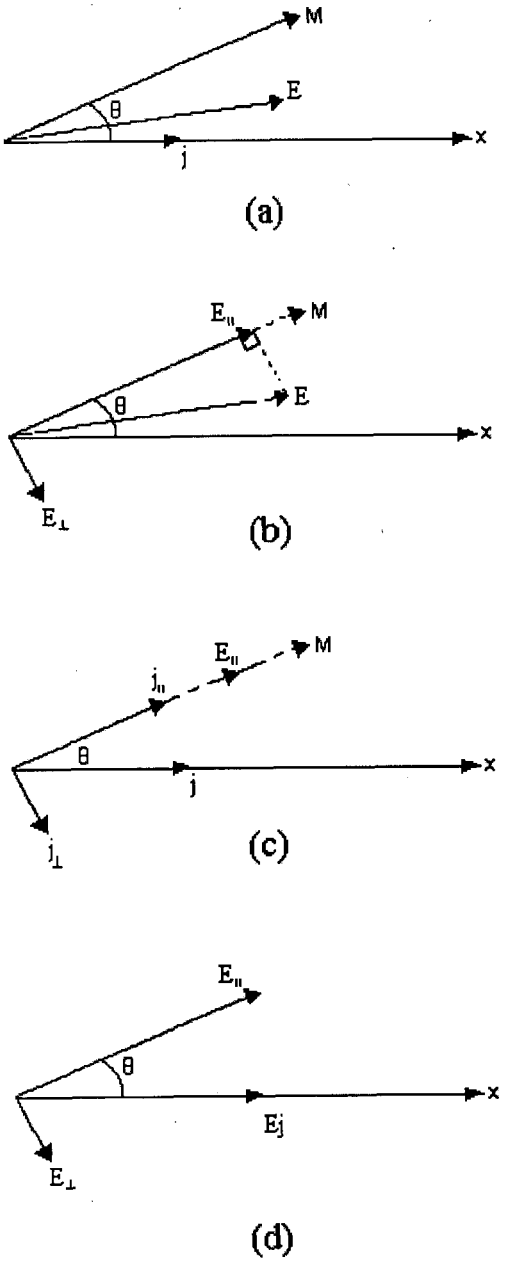

Figure 2.1 (a) The applied electric field to a material with a certain magnetization with an angle, θ, to the horizontal which produces a current density. **(b)** Electric field resolved into a component parallel to the magnetization and perpendicular to it. **(c)** Resolving the current density into a parallel and perpendicular component. **(d)** Using vector geometry to solve for the electric field, E_j, parallel to the current density, j.

current density can be obtained by using right-angle triangle trigonometric properties. Using the cosine of the triangle as seen in figure 2.1(c), the parallel current density can be found. The perpendicular current density can be found using the sine of the triangle as seen in figure 2.1(c). The resulting expressions are

$$\cos(\theta) = \frac{j_{\|}}{j} \Rightarrow j_{\|} = j\cos(\theta)$$
$$\sin(\theta) = \frac{j_{\perp}}{j} \Rightarrow j_{\perp} = j\sin(\theta) \tag{2.2}$$

where j is the current density. These equations can then can be substituted into equation 2.1 of Ohm's law for the parallel and perpendicular electrical fields. Next, the electrical field, $\vec{E}$, parallel to the current density, $\vec{j}$, can be found using vector geometry as seen in figure 2.1(d). Then the modified expressions of Ohm's law for the parallel and perpendicular fields just found can be substituted into the electrical field parallel to the current density. The resulting equations are

$$E_j = E_{\|}\cos(\theta) + E_{\perp}\sin(\theta)$$
$$E_j = \rho_{\|} j\cos^2(\theta) + \rho_{\perp} j\sin^2(\theta) \tag{2.3}$$

The equations of 2.3 yield the magnetic field in the direction of the current density, E_j, and the second one can be solved to give the resistivity along the current direction. Current density is divided out of the right side yielding an equation in terms of resistivity, and then a trigonometric identity is used to group the parallel and perpendicular resistivity. The resulting equation is

$$\frac{E_j}{j} = \rho_{\|}\cos^2(\theta) + \rho_{\perp}\sin^2(\theta)$$
$$\rho_j = (\rho_{\|} - \rho_{\perp})\cos^2(\theta) + \rho_{\perp} \tag{2.4}$$

where $\Delta\rho_m = \rho_{\|} - \rho_{\perp}$ and $\rho_o = \rho_{\perp}$ resulting in the final equation of

$$\rho = \rho_o + \Delta\rho_m \cos^2(\theta). \tag{2.5}$$

The value of $\Delta\rho_m / \rho_o$ is known as the magnetoresistive ratio. It can be seen from the ratio that magnetoresistance is characterized by the parallel and perpendicular components of

resistivity as was mentioned earlier. The ratio provides the percentage change in resistivity that a material exhibits when it is subjected to an external magnetic field. The alloy of nickel and iron mixed together in an 81/19 composition known as Permalloy has been the material of choice for MR read sensors. The electrical and magnetic properties of Permalloy are dependent on film thickness and the deposition method. When these two parameters are properly adjusted, thin film elements of Permalloy exhibit magnetoresistivity between 2 and 3% of the intrinsic resistivity of the material [5].

2.1.2 MR Read sensor

Major growth in areal bit density beginning around 1991 can be attributed to the implementation of MR read sensors in hard drives. They had significant advantages over inductive read sensors that were being used at the time. The signal from the MR read sensor is independent of the velocity of the spinning disk because it measures the flux from the magnetic media unlike the inductive head that measures the change in flux with time. Therefore, the disk does not have to be spun at a certain velocity to experience a large signal using a MR read sensor. Furthermore, unlike an inductive head, it has a low inductance. This means that it can operate efficiently at high frequencies. Finally, an MR read sensor exhibits a higher signal per unit track width in comparison to an inductive head. Therefore, smaller track widths became possible resulting in higher areal bit densities.

A schematic of an MR read sensor flying over a basic magnetic media surface can be seen in figure 2.2. The horizontal beam is the head material which will be referred to as the MR element, and the vertical beams are conductor leads. There is neither a biasing element nor shield in this schematic. An MR read sensor is typically created by depositing an MR material such as Permalloy onto a substrate in the presences of a magnetic field. The field creates a desired direction of magnetization with an easy axis of magnetization in the direction of the field [5]. In figure 2.2, the easy axis is aligned parallel to the current running through the center.

The MR read sensor is a magnetic flux sensing device that responds to the vertical field above the magnetic media averaged over the height of the MR element. The magnetization, *M*, seen in figure 2.2 is normally parallel with the current direction. This is until it encounters an

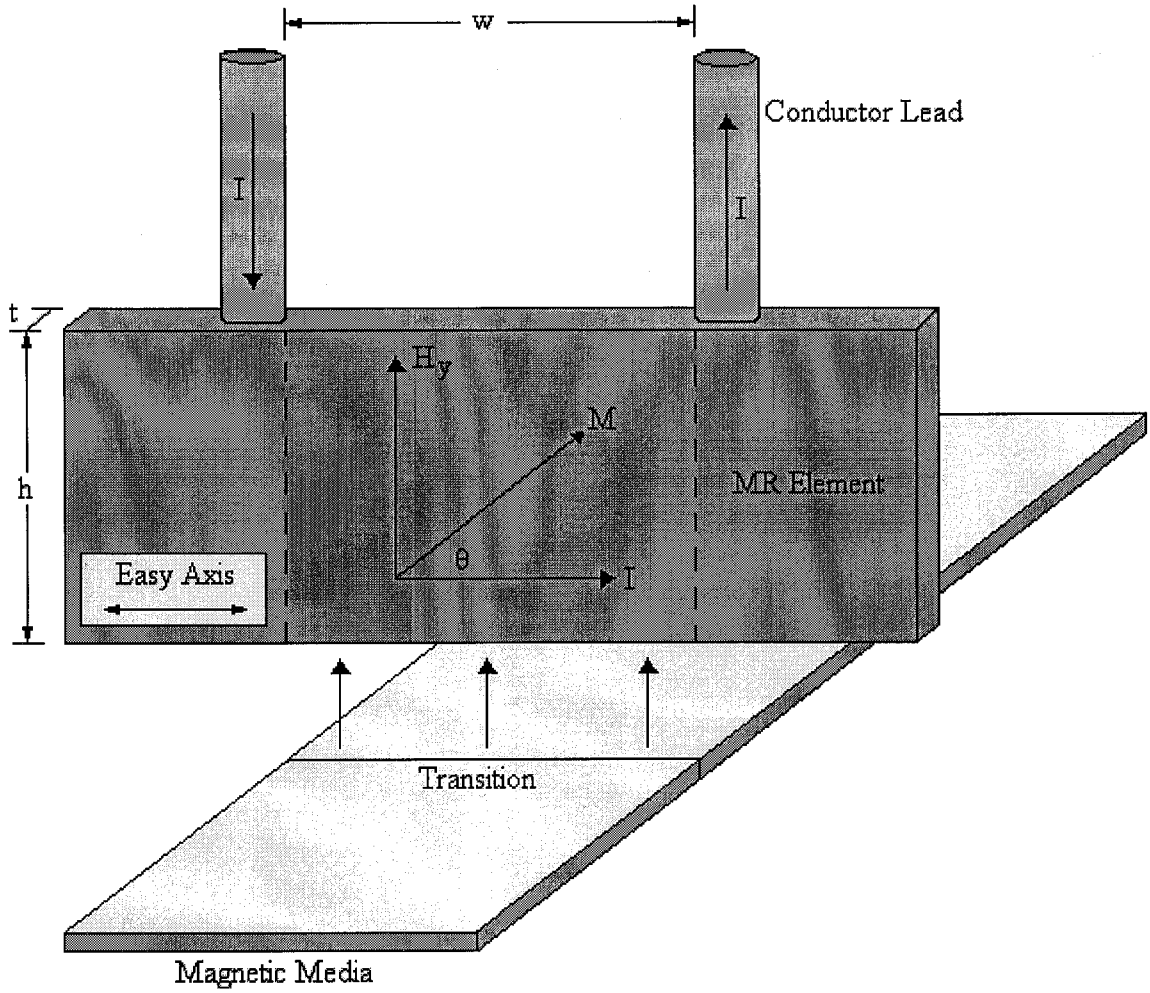

Figure 2.2 Basic unshielded and unbiased MR read sensor passing over top a transition in the magnetic media. The rectangular block is the MR element composed of and the two vertical columns attached to it are the leads carrying the current.

external magnetic field, H_y, from the media. This causes M to rotate to some angle θ with respect to the easy axis. When the current is flowing constantly through the MR element and the rotation of M occurs due to an external magnetic field, the resistivity of the strip changes in accordance to equation 2.5. The change in resistivity is only a function of the angle between the magnetization and current [5]. The resistivity of the MR element is at a maximum, $\rho_o+\Delta\rho_m$, when the magnetization is parallel to the current. The resistivity is at a minimum, ρ_o, when the magnetization is perpendicular to the current. A constant current and a changing resistivity result in a changing readback voltage that the circuitry is able to register.

The transfer curve for an MR read sensor can be obtained by adjusting equation 2.5. It has been proven that by minimizing the magnetic energy, the angle of magnetization as a function of the external magnetic field, H_y, can be found [2] by

$$\sin(\theta) = \frac{H_y}{H_o} \tag{2.6}$$

where $H_o = H_k + H_d$. H_k is the anisotropy field related to the easy axis and H_d is the demagnetizing field that is a function of the shape and saturation magnetization of the MR element. The demagnetizing field can be approximated by tM_s/h where M_s is the saturation magnetization, t is the thickness, and h is the height of the MR element seen in figure 2.2. If considering an ideal case, $H_o = H_k$ because the height of the MR element is assumed to be infinitely greater than the thickness. Using these assumptions, equation 2.5 becomes

$$\rho = \rho_o + \Delta\rho_m \left[1 - \left(\frac{H_y}{H_k} \right)^2 \right] \tag{2.7}$$

which can be used to plot the transfer curve of the MR element.

The transfer curve for an ideal MR element is seen in figure 2.3(a). It is a plot of resistivity of the MR element versus the external magnetic field caused by the magnetic media resulting in a parabola. The values used to create the curve were those of Permalloy. They are $\Delta\rho_m = 2.5\%$, $\rho_o = 20\ \mu\Omega\cdot cm$, $H_k = 400\ A/m$. It can be seen that the resistivity starts at 20 μΩ·cm and increases to 20.5 μΩ·cm which is a 2.5% change in resistivity. Furthermore, the parabola has limiting values of $\pm H_k$. There are two main features to extrapolate from this graph. One is that the graph is clearly an ideal case, and the second is that the MR element is not sensitive to the external magnetic field at $H_y = 0$.

The transfer curve shown in figure 2.3(a) is an ideal case because the MR element height is assumed to be much greater than the thickness. In a non-ideal case, a practical MR element height such as 1 to 3 μm would be used. In this case the parabola shown in figure 2.3(a) would expand at the base to become more bell shaped as seen in an illustration in figure 2.3(b). The

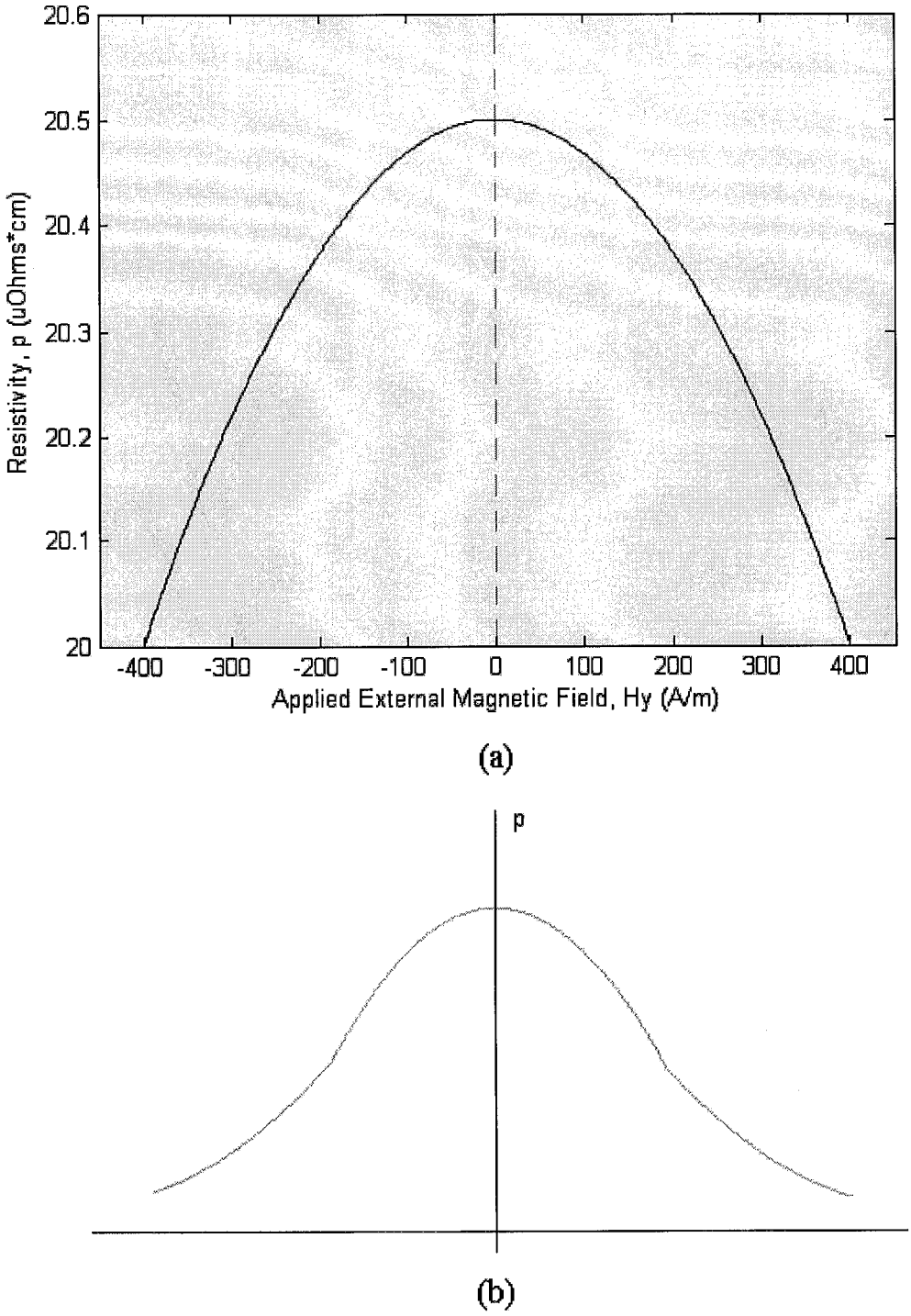

Figure 2.3 (a) Graphed transfer curve of an ideal MR element. Values of Permalloy were used to obtain the graph. **(b)** Illustration of a transfer curve of a non-ideal element where the height of the element is not considered infinitely greater than its thickness.

expanding of the transfer curve at the base is due to the presence of a non-uniform demagnetization field and easy axis dispersion that was not seen when the thickness of the MR element as seen in figure 2.2 was infinitely large [10]. The demagnetization field is generated at the boundary of the MR element and opposes the external magnetic field, H_y. Therefore, at the boundaries of the MR element, the summation of demagnetization field and the external magnetic field is approximately zero resulting in a small rotation of the magnetization, M. However, the demagnetization is very small at the center of the MR element, so the external magnetic field has the most effect of rotating the magnetization here.

At the top of the transfer curve, the MR element is not sensitive to the external magnetic field. This also occurs at the bottom of the non-ideal curve where it expands to form a bell-shape. This is because the slope is very close to zero at these points. For the most efficient operation of the MR read sensor, it is desirable for small changes in the external magnetization field to produce large changes in resistivity. This occurs when the slope is at a maximum. By taking the derivative of equation 2.5 with respect to the magnetization angle, the following equation is obtained

$$\frac{\partial \rho}{\partial \theta} = -\Delta \rho_m \sin(2\theta). \tag{2.8}$$

It is seen that the slope is a maximum when the angle between magnetization and current, θ, is 45° or approximately half of H_k. This occurs at the linear points in the graph. Therefore, a bias field perpendicular to the easy axis and sense current is needed, so that the MR read sensor can operate at a maximum linear slope. This is known as transverse biasing [10].

The MR read sensor pictured in figure 2.2 as mentioned earlier is not shielded. For high density recording in disk drives, shields are required on both sides of the MR read sensor. Shields are generally 1 to 3 μm thick and create a gap within which the MR read sensor, biasing configuration, and conductors are located. The purpose of the shield is not only to protect the MR read sensor from undesired external fields but also provide a better resolution of compacted fields from closely spaced magnetic transitions. Shields are often made from materials that have a high permeability within the applicable frequency range such as Permalloy, ferrites, Sendust, or amorphous substances [5].

The theory behind MR read sensors is not complicated. A constant current is sent through an MR element that is parallel to the easy axis. Normally the magnetization is parallel to the current and easy axis. When an external magnetic field is sensed from the transitions in the magnetic media, the magnetization rotates to some angle with respect to the easy axis. Because of the principle of magnetoresistance, this causes the resistivity in MR materials such as Permalloy to change. If the MR element is biased properly, the change in resistivity is linear. A changing resistivity and constant current produces a readback voltage. Despite a simple concept, the design and mass production took a great deal of engineering work that required micromagnetic modeling. MR read sensors are responsible for an abrupt increase in areal bit density. Their greater ability of sensing smaller magnetic fields and producing greater readback signals from them than inductive heads, allowed for smaller bit sizes. However, the MR read sensor technology was eventually replaced. Today, all consumer hard disk drives employ GMR read sensors.

2.1.3 GMR Read sensor

Most hard drives today employ GMR read sensors because of their ability to provide a larger detected signal of a smaller field on magnetic media. The GMR effect was first detected in FeCr multilayers [12]. It is a multilayer of non-magnetic materials sandwiched in between two magnetic materials. Without the presence of a magnetic field, the two magnetic layers are antiferromagnetically coupled. In its simplest definition antiferromagnetically coupled means the magnetization of the layers is antiparallel or facing in opposing directions. When a strong enough magnetic field is applied, the magnetizations of the two magnetic layers align parallel to each other in the same direction creating a significant drop in resistivity. A drop in resistivity as high as a factor of 2 has been recorded [10]. This is sometimes referred to as the ferromagnetic or saturated state.

The reason that the ferromagnetic state experiences a much lower resistivity than that of the antiferromagnetic state lies in the realm of quantum mechanics. According to quantum mechanics, all electrons possess an intrinsic angular momentum or spin. This angular momentum corresponds to two possible states that an electron can be in, spin up or spin down. In some instances it is possible for an electron to be in both states at the same time [13]. GMR

capitalizes on this intrinsic spin nature of electrons. Even though it was not mentioned MR materials also capitalized off of this spin to some degree. Electrical resistivity is dependent upon the scattering of electrons within a material. Depending on its magnetic direction, a single-domain magnetic material will scatter electrons with an up or down spin differently. When the magnetic layers in GMR read sensors are antiferromagnetically coupled, the resistance is high because spin up electrons that are not scattered in one layer can be scattered in the other. When the layers are aligned in the same direction, all of the spin up electrons are able to pass through both layers with minimal scattering yielding a much lower resistivity. The spin down electrons are not able to pass through the magnetic materials in either state.

Read sensor applications of GMR utilize planar geometry which is favorable because magnetostatic interactions constrain the magnetization to lie in the plane. The GMR effect can either be seen as current-in-the-plane (CIP) or current-perpendicular-to-the-plane (CPP). With CIP, the current flows parallel to the layers of material in the GMR read sensor. With CPP, the current flows perpendicular to these layers of material. The effect is stronger with CPP, but it has not been used in any commercial products yet because of a low resistance across the thin-films [14].

The GMR ratio is derived from quantum mechanic expressions where the resistance is dependent upon the orientation of the electron spin [11]. The resulting equation for the GMR ratio is

$$GMR = \frac{R_{ap} - R_p}{R_p} \tag{2.9}$$

where R_p is the resistance when the magnetizations of the two layers are aligned parallel to each other in the same direction, the ferromagnetic state, and R_{ap} is the resistance when the magnetizations of the layers are not aligned parallel, the antiferromagnetic state. Like the MR ratio, the GMR ratio is the ratio of the maximum resistance change over the minimum resistance. The first GMR ratios of multilayers that were observed were far greater than MR ratios. In the first type of GMR multilayer, Fe/Cr, a ratio of 85% at 4.2 K was observed. A ratio of 220% was seen in a $Co_{95}Fe_5$/Cu multilayer at 4.2 K and 110% at room temperature [10].

Despite the large ratios seen in the lab, the field sensitivity of GMR multilayers turned out to be lower than the MR ratio of $Ni_{81}Fe_{19}$, Permalloy. The magnetic saturation field needed to overcome the antiferromagnetic coupling in the magnetic layers was too great to employ in hard drives. For example, in a FeCr multilayer, 1.6×10^{6} A/m is required to overcome the antiferromagnetic coupling [10]. It turns out that GMR multilayers were too difficult to implement in a read sensor for magnetic recording. Therefore, a device known as a GMR spin valve was developed. A spin valve is a sample consisting of a GMR trilayer. One layer is magnetically soft meaning it is sensitive to small magnetic fields. It is known as the free layer. Then there is a layer that is magnetically hard meaning that it is not sensitive to moderately sized fields. This layer is referred to as the pinned layer. It is pinned by a layer of antiferromagnetic material. Therefore when a magnetic field is applied, the free layer of the structure aligns with the pinned layer. This creates the change in resistance, but because one layer is pinned this operation requires less of a magnetic field.

The first spin valve design consisted of NiFe/Cu/NiFe/FeMn. Since then, there have been several variations in the materials used for spin valves resulting in greater MR ratios. The NiFe/Cu/NiFe/FeMn spin valve was able to produce a GMR ratio of 4%. Table 2.1 shows the various spin valves that have been produced and their respective GMR ratios. A graphic illustration of the second and third spin valve can be seen in figure 2.4. There are two extra types of materials used in these spin valves. There is tantalum (Ta) which is a seed layer used to support desirable film texture and morphology and there is cobalt (Co) which is used to enhance interfacial spin-dependent scattering [10]. It can be seen in figure 2.4(a) that the FeMn layer pins the magnetization of the top NiFe layer. This occurs through a principle known as exchange anisotropy [5]. The spin valve shown in figure 2.4(a) is referred to as a top spin valve because the top layer is pinned by the antiferromagnetic layer. The spin valve shown in figure 2.4(b) is a bottom spin valve naturally because the bottom layer is pinned. The resulting differences in the GMR ratios between the two types can be seen in Table 2.1. The hallmark of spin valves has been that the ferromagnetic or antiferromagnetic interactions between the NiFe layers are much weaker than in the GMR multilayer. The bottom NiFe magnetization can switch under a field as small as 480 A/m.

Table 2.1 Progression of material composition and orientation of the pinned layer of spin valves and the resulting GMR ratio.

Spin Valves (Material Composition)	*Orientation (Pinned Layer)*	*GMR Ratio (%)*
NiFe/Cu/NiFe/FeMn	Top	4
Si/Ta/NiFe/Co/Cu/Co/NiFe/FeMn	Top	9
Si/Ta/FeMn/NiFe/Co/Cu/Co/NiFe	Bottom	12
Si/NiO/Co/Cu/Co	Bottom	19
Si/NiO/Co/Cu/Co/Cu/Co/NiO	Symmetrical	25

A comparison of MR ratios versus magnetization orientation between a GMR spin valve read sensor and an MR read sensor made of Permalloy can be seen in figure 2.5. The graph was obtained using the ratio for a GMR spin valve given by

$$\frac{\Delta R}{R_o} = \frac{\Delta R_m}{R_o}\left[\frac{1-\cos(\theta_2 - \theta_1)}{2}\right] \tag{2.10}$$

where θ_1 and θ_2 are the orientation angles of the magnetizations of the pinned and free ferromagnetic layers respectively [10]. The equation characterizing the MR effect, equation 2.5, was also used to create the graph. From the graph, it can clearly be seen how much greater the GMR effect in a spin valve is than the MR effect. However, it takes a magnetization rotation of 180° to reach the maximum change in resistance in a spin valve compared to 90° in an MR read sensor.

Finally, an illustration of the hysteresis loop of a spin valve can be seen in figure 2.6. The two loops in the graph are the two ferromagnetic layers, the free layer and the pinned layer. It can be seen that the pinned layer is far from zero which is appropriate. Since its magnetization is pinned by the antiferromagnetic layer, it takes a much greater applied field to switch the magnetization than that of the free layer. The free layer in an ideal case should switch magnetization at zero, but because in the real case it is coupled to the pinned layer there is a slight offset [15]. The flat regions of the graph are where the layers are not aligned in the same direction and the greatest resistance is experienced. The sloped region of the graph is where the free layer switches magnetization and the resistance decreases.

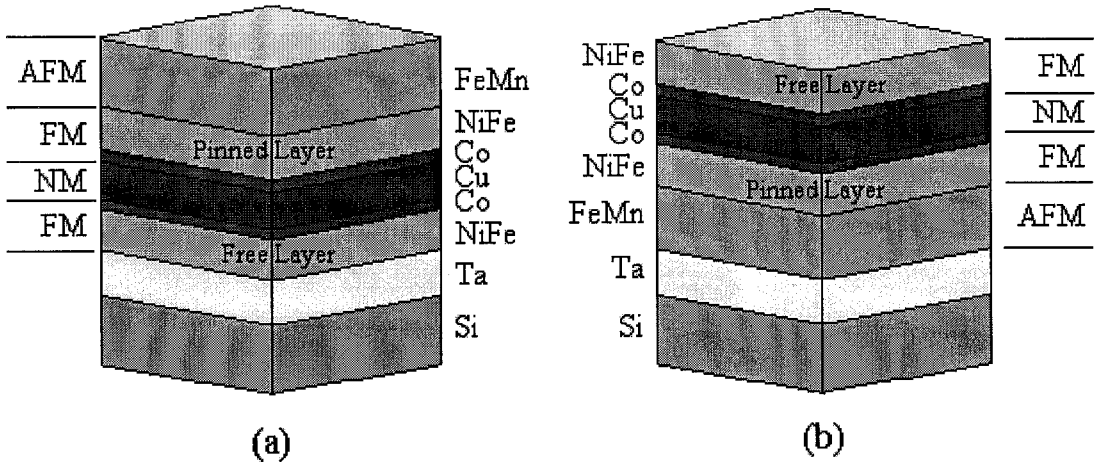

Figure 2.4 AFM is antiferromagnetic, FM is ferromagnetic, and NM stands for non-magnetic. **(a)** Schematic of layers of material in a top spin valve. **(b)** Schematic of layers of material in a bottom spin valve.

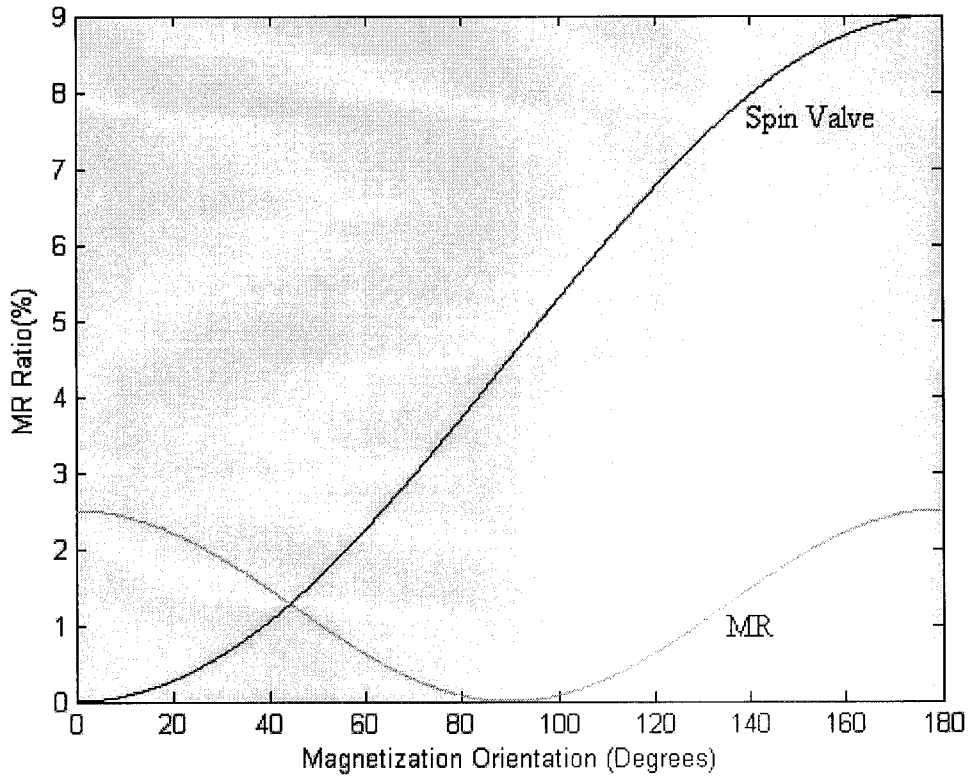

Figure 2.5 The MR ratios of a GMR spin valve read sensor and a MR read sensor versus their magnetization orientations in degrees.

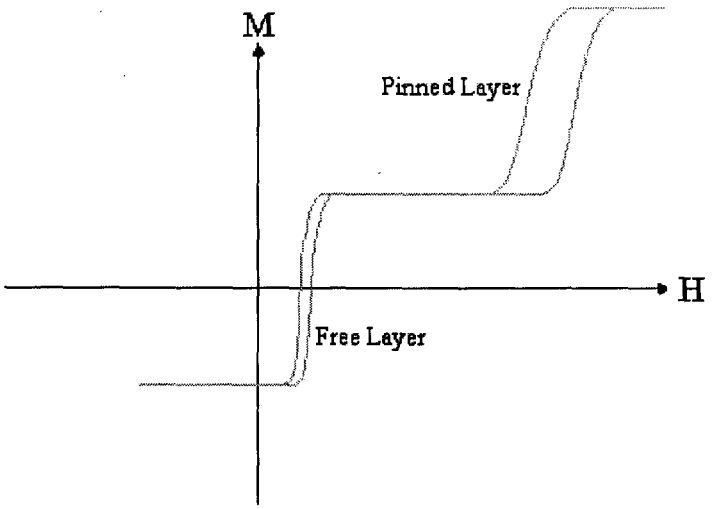

Figure 2.6 An illustration of the hysteresis loop of a GMR spin valve read sensor.

2.2 Fundamentals of the Write Head

Before the introduction of MR read sensors, inductive read/write technology was used. A single thin-film inductive head was used to perform both the write and read processes in a hard drive. This method became obsolete with the arrival of MR and then later GMR read sensor technology. Today, dual-element thin-film inductive-write and GMR read sensors have become the prevailing technology form in hard disk drives. Having separate elements for read and write functions allows for each to be optimized separately. Mainly, there are stricter requirements for read sensors than there are for write heads to fulfill when attempting to achieve higher areal bit densities. The main requirement for a thin-film inductive write head is that it needs to deliver a large write field with a sharp field gradient at a specified magnetic spacing.

To achieve greater areal bit densities in hard drives, the dimensions of the write head need to be scaled down. This is because the bit area is defined during the writing process and therefore depends on the dimensions of the write head. A cross sectional view of a thin-film inductive write head is shown in figure 2.7. The width of the two magnetic poles along the direction perpendicular to the cross sectional view, in the plane perpendicular to the paper, is approximately the trackwidth written to the magnetic media. A current is passed through the coils creating a magnetic field that emanates from the write gap. The direction of the field is dependent on the current. New patterning technologies are being used to develop smaller write

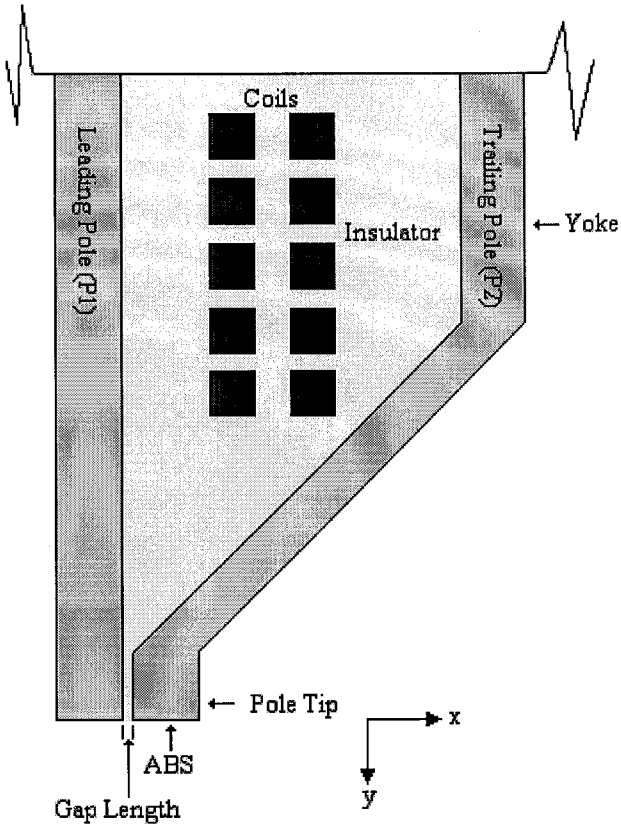

Figure 2.7 Cross sectional view of a thin-film inductive write head. ABS stands for air bearing surface.

heads to achieve smaller and more controlled track widths [16]. To attain higher linear densities, a smaller write gap length is needed. The dimensions of the pole tip width and the write gap length in an effort to create greater track and linear densities are rivaling the dimensions used in the semiconductor industry.

Very few times are there no consequences in scaling down the dimensions of a magnetic or electronic device. The write head is no exception. To create higher linear densities, it was said that a smaller gap length is needed. However, a reduction in the size of the write gap translates into a weaker write field strength. To offset a decrease in the write field strength, different pole materials are used with a greater magnetic moment. Using materials with greater magnetic moments for the write poles is also favorable because they are needed for achieving adequate write performance on high coercivity magnetic media. There has been a trend to increase the coercivity of the media in order to increase the linear density without reducing the stability of the recorded data.

In order to understand how thin-film inductive write heads are designed and used today, the magnetic field produced from the head and the write process need to be discussed. The magnetic field produced from an inductive write head is tremendously complex because of the head geometry. Head fields can be solved numerically by finite element modeling, boundary element modeling, or micromagnetic modeling [11,17]. Analytical methods such as conformal mapping, Green's functions, or transmission line modeling can also be used to model head fields [10]. The simplest and most useful model which will be discussed here is the Karlqvist head model. After the Karlqvist head model is discussed, the write process will be reviewed with attention paid towards the Williams-Comstock model.

2.2.1 Karlqvist Head Model

The Karlqvist model is an analytical model than can be used to approximate the field emanating from the write gap of a thin-film inductive write head. The Karlqvist head field corresponds to infinitely wide and symmetric write poles. Since the width of the poles is normal to the *x-y* plane in figure 2.7, the problem becomes a two-dimensional one in the *x-y* plane. The assumptions made by the Karlqvist model about the surface potential are not very accurate either near the write gap corners or the air bearing surface. The Karlqvist model makes two other assumptions. First the permeability of the magnetic core is infinite. Second, the magnetic potential varies linearly across the gap yielding a constant magnetic potential at the gap surface equal to the deep-gap field [18].

The x and y components of the Karlqvist head field can be derived from a simplified form of the Green's function expressing surface potential and the head deep-gap field [18]. The resulting fields are:

$$H_x(x,y) = \frac{H_g g}{\pi} \frac{y}{x^2 + y^2}$$
$$H_y(x,y) = -\frac{H_g g}{\pi} \frac{x}{x^2 + y^2} \tag{2.11}$$

where x is the position along the track, y is the spacing between the magnetic media and the air-bearing surface of the write head, g is the write gap length, and H_g is the head deep-gap field. These equations represent the x and y components of a magnetic field produced by a line current located at the write-head gap edge. These field components can be evaluated for all x and y, but are only valid for the region above the write head surface as seen in figure 2.7.

The head fields H_x and H_y components of the field are plotted in figure 2.8 as a function of position along the track and with a constant spacing between the magnetic media and the air bearing surface of the write head. The plots are independent of both the head deep-gap field and write-gap length. In both (a) and (b) of figure 2.8, three values of spacing between the magnetic media and the air-bearing surface were used to show the resulting field. As the spacing between the magnetic media and the air-bearing surface of the write head increases, the field amplitudes decrease and the pulses widen. This is a major concern because the amplitude and shape of the head field are important in the writing process. Further inspection of the H_y field component in figure 2.8 (b) shows that the field in the y direction at the gap center is zero. The H_y field component peaks at the points where the H_x field component is at 50% of its maximal value. This is intriguing, but the H_x field component of the Karlqvist head field is the most important because it is most relevant to present-day longitudinal magnetic recording. The H_x field component is parallel to the magnetic media which is the same direction that the media is magnetized in longitudinal magnetic recording.

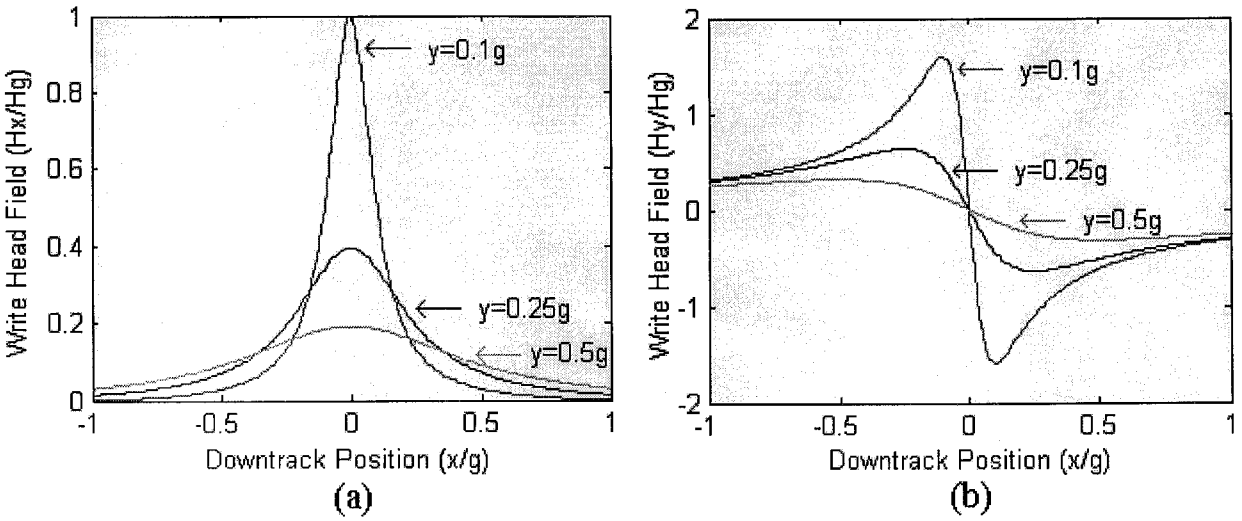

Figure 2.8 (a) The x-component of the Karlqvist head field versus the downtrack position. **(b)** The y-component of the Karlqvist head field versus the downtrack position.

2.2.2 Write Process

The write field produced by the head needs to be greater than the coercivity of the media in order to magnetize it in the direction of the field. The coercivity is the magnetic field needed to switch the magnetization direction. Applying a field equal to the coercivity of the media will only reverse half of its magnetization. This is because the hysteresis loop of the magnetic media is not perfectly square. A field 2 to 3 times greater than the coercivity of the media is applied to reverse the magnetization. By switching the direction of the field from the write head by means of the current, magnetization transitions are written to the magnetic media. A schematic of the write process can be seen in figure 2.9. Each transition when being read corresponds to a voltage pulse with a finite amplitude and finite half-amplitude pulse width (PW_{50}). These two parameters limit how close voltage pulses can be spaced and still detected by the read sensor. Transitions are related to bits by the coding scheme used. The present-day coding scheme used by magnetic recording is known as non-return-to-zero modified (NRZI) coding. The presence of a transition represents a logic one and the absence of a transition represents a logic zero. Therefore, the linear density is limited by how close transitions can be written.

In order to analyze the write process analytically, the Williams-Comstock model can be used. It is a simple model that provides a viable means to study the longitudinal recording process. It also provides a simple analytical formula for the transition length. The model makes two assumptions. Investigations have shown that the transitions have zigzag boundaries because it is a state requiring less magnetostatic energy than a straight line boundary [19]. Also, thin-film magnetic media is composed of miniature grains that tend to form magnetic clusters due to exchange interactions. This leads to the zigzag transition boundaries. It is analogous to randomly placing a bunch of different sized marbles in a boxed area and then trying to draw a line as straight as possible through the center of the boxed area around the marbles. A zigzag appearing line will be created. The first assumption is that the Williams-Comstock model ignores the zigzag transition boundaries. The shape of the transition is described by a function similar to that of the arctangent.

The second assumption provides that a sharp magnetization transition yields a large magnetization gradient. Therefore, for the writing process, a square hysteresis loop for the magnetic media and a large write head field gradient are desirable. Furthermore, the

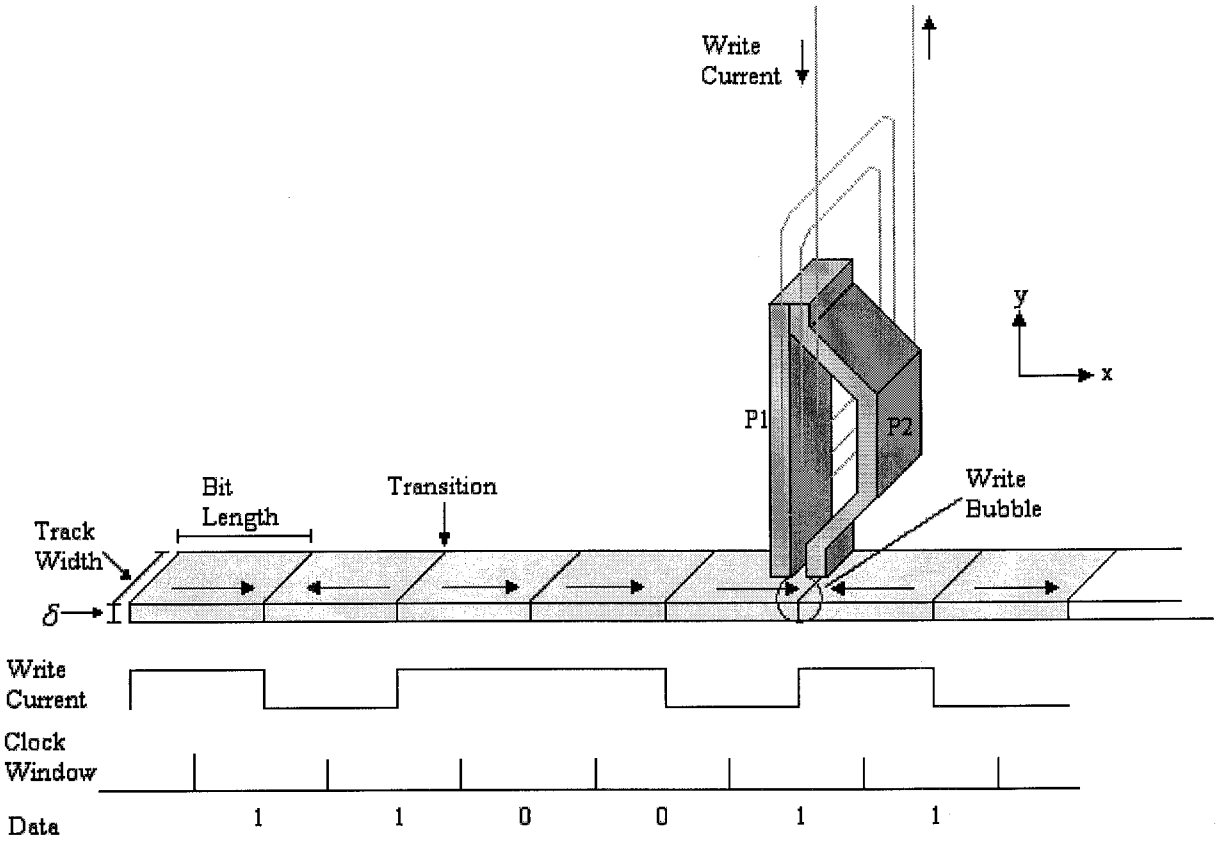

Figure 2.9 Basic schematic of inductive write process with a thin-film inductive write head.

demagnetizing field should be made as small as possible because it opposes the head field and broadens the magnetic transition in the write process. As long as the write bubble penetrates the magnetic media, a transition will be written. However, further considerations need to be made to find the final shape of the transition and its center which should be at the trailing edge of the write bubble [10].

The Williams-Comstock model can be used to derive the transition parameter of a transition written by a Karlqvist head field. The transition parameter is used by the industry as a measure to define the narrowest possible transition to increase linear density [5]. The transition parameter is defined by

$$a = \sqrt{\frac{M_r \delta}{\pi H_c} \frac{y}{Q}} \tag{2.12}$$

when the coercive squareness of the thin-film magnetic media is close to one. The coercive squareness is related to the slope of the magnetic field of the hysteresis loop. It is a measure of how square a hysteresis loop is. To attain a high linear density, the transition parameter is constantly reduced. Naturally to reduce the transition parameter, the variables in the denominator of the equation need to be increased and those in the numerator need to be decreased. The coercive field of the magnetic media, H_c, is increased but within the limits that it can still be written to by an inductive write head. The remanence thickness product, $M_r\delta$, where M_r is the remnant magnetization and δ is the thickness of the magnetic media is reduced. However, it still needs to be large enough to maintain a readback signal. Finally, the magnetic spacing between the magnetic media and the air-bearing surface of the write head, d, is decreased where $y = d + \delta/2$. This spacing has to remain large enough though so that there is no excessive wear or the head does not crash.

As mentioned previously, it is easier to switch the magnetization of the media when its hysteresis loop is more square. This is a quality determined by the type of material being used. Therefore, the materials that are being used for the magnetic media along with the write head need to be chosen carefully. For a given write-head material, there is a maximal coercive field of the media for which it is able to overwrite. Furthermore, the magnetic spacing and write gap length limit the maximum coercivity that it can overwrite. Permalloy used to be the chosen material for the poles of the write head. A graph showing the maximum medium coercivity that is overwritable by Permalloy is shown in figure 2.10(a). The equation used to produce the graph is calculated from the Karlqvist equations. It is defined by

$$H_{c,\max} = 0.268 M_s \tan^{-1}\left(\frac{g/2}{d+\delta}\right) \tag{2.13}$$

under the assumption that the coercive squareness of the media is 0.85 [10]. Coercive squareness is a measure of how square the hysteresis loop of a material is. The M_s value for Permalloy is 102 kA/m.

As the coercivity of the magnetic media is increased to reduce the transition parameter, elements of the write head need to be adjusted. Materials with greater magnetic moments capable of overwriting greater coercivities are being implemented. One of these materials is

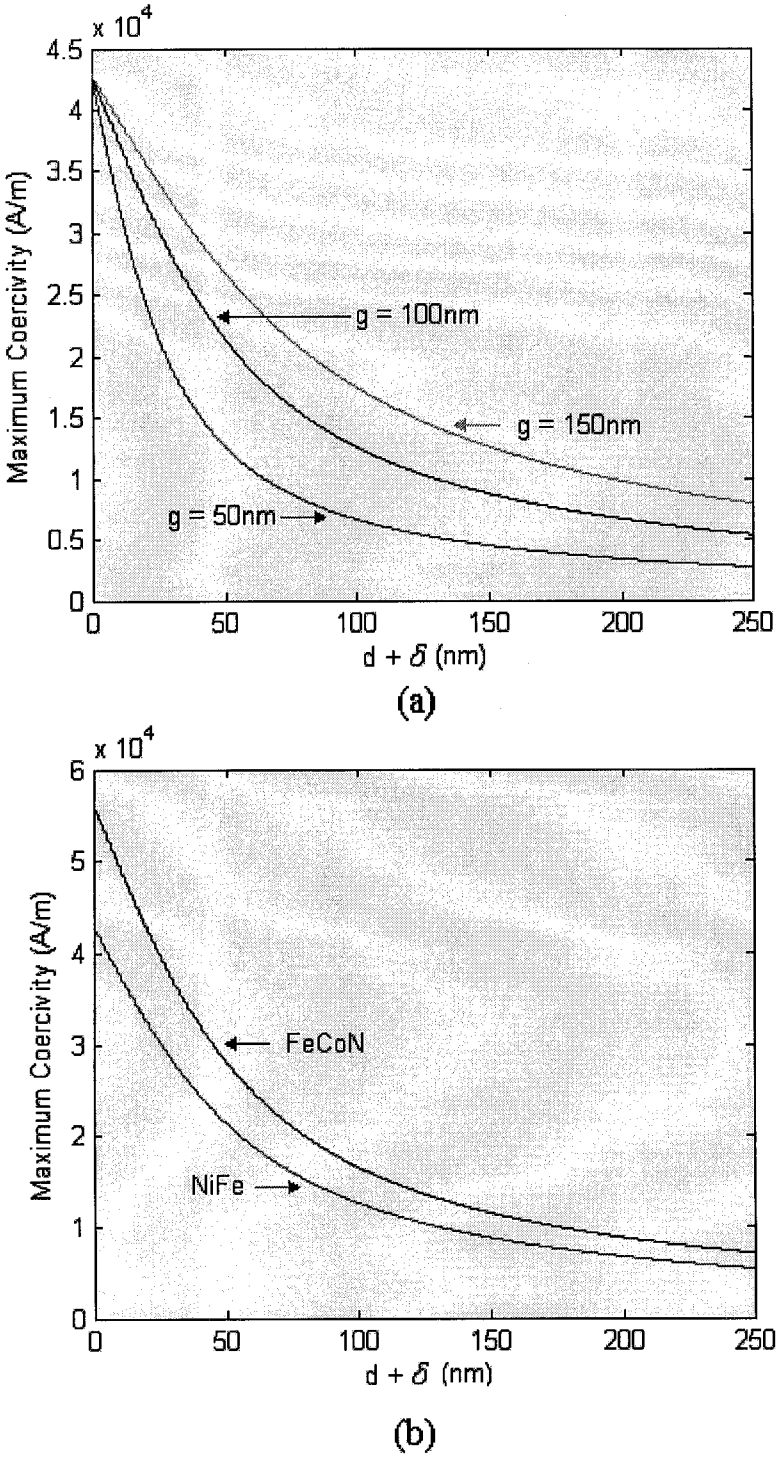

Figure 2.10 (a) Maximum medium coercivity overwritable by NiFe write heads versus magnetic spacing and medium thickness for various write gap lengths. **(b)** A comparison of maximum medium coercivity overwritable by NiFe and FeCoN write heads versus magnetic spacing and medium thickness for a write gap length of 100 nm.

FeCoN. It is being used on the bottom of the top pole of the writer and has a M_s value of 134 kA/m [20]. The graph showing the maximum overwritable coercivity of FeCoN is seen in figure 2.10(b). As stated earlier, a large head field gradient is an important concern to the writing process. The maximal head-field gradient is in part a function of the magnetic spacing and write gap length. Reducing the magnetic spacing is the most effective way of raising the head-field gradient. However, this does not mean that the write-gap length has not been modified. Write-gap lengths of 90 nm and below are being implemented today.

2.3 Magnetic Recording Media

Typically, in order to achieve greater areal bit densities, all relevant media and head parameters are scaled to smaller sizes. Eventually, the current technology is not capable of allowing smaller sizes or there is a different technology that can do it better. This was the case with read sensor technology as the inductive read sensor was phased out to adopt the MR read sensor and then eventually the GMR spin-valve read sensor. Magnetic media has experienced similar changes in its respective technology. Particulate media was used exclusively as a recording surface for the first 25 years of the hard drive industry. It was created by dissolving ferromagnetic particles in a solvent and spin coating the substrate with the material. Eventually, greater areal bit densities could not be achieved by simply scaling the parameters to smaller sizes with this technology. The coating was too thick and not a pure enough ferromagnetic material.

Since particulate media could no longer increase areal bit densities, thin-film technology was adopted. Thin-film media consists of complex multilayer structures that are sputter coated onto a substrate. This allows for completely pure ferromagnetic materials to be used and much thinner layers resulting in greater areal bit densities. Recently, the size of a bit using thin-film media has become so small that it is bordering being thermally unstable. In order to increase thermal stability without compromising recording performance, antiferromagnetically coupled (AFC) media technology is now being implemented. It has the same overall structure and design as thin-film media; however, it uses two magnetic layers separated by a non-magnetic spacer to record transitions. The scheme is very similar to the GMR effect used in present-day read sensors.

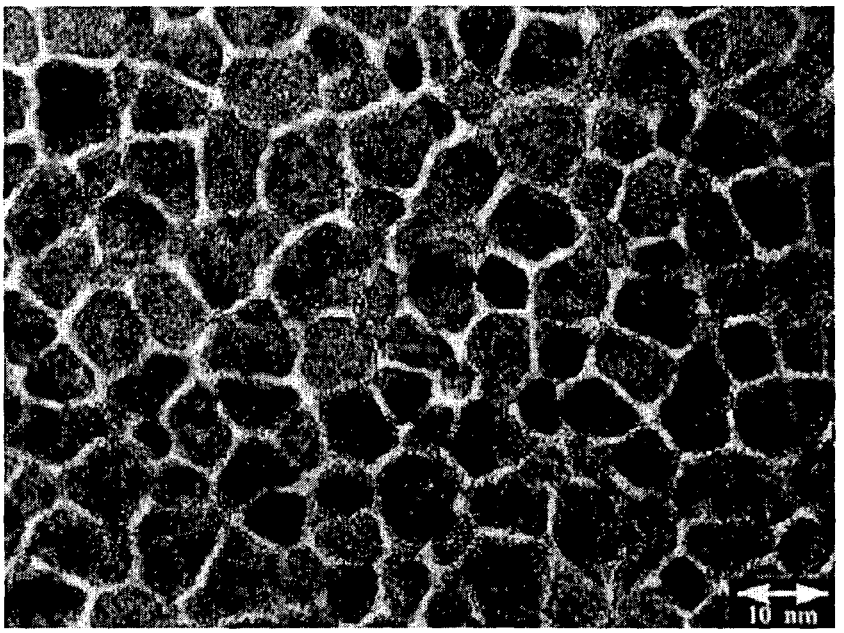

Figure 2.11 A top down view of the magnetic grains that make up the magnetic media layer in a hard disk drive.

Today, hard-disk drives utilize longitudinal magnetic recording on a rigid disk of continuous magnetic thin-film media composed of nanometer-sized magnetic grains. As mentioned previously, longitudinal magnetic recording technology is based on the magnetization of the media positioned parallel to the disk plane. A top-down view of the magnetic layer of a hard drive platter can be seen in figure 2.11. The darker shaded areas are the individual magnetic grains. A collection of these grains create an average magnetization that essentially represents a bit. This region is referred to as a bit even though it is the transition between such a region and another with opposing magnetization that creates a logic one. The actual boundaries of a bit are not physical but more so magnetic. In order to sustain an adequate signal-to-noise ration (SNR), the number of grains in each bit need to be maintained above a certain value. Therefore, the grain size must decrease as the bit size decreases. If the grain size is not reduced with the bit size, the transition region will be too large resulting in greater noise levels.

2.3.1 Thin-Film Disk Structure

A thin-film disk is a complex multilayer structure where each layer serves its own purpose and is continually optimized to provide higher areal bit densities. A cross-sectional

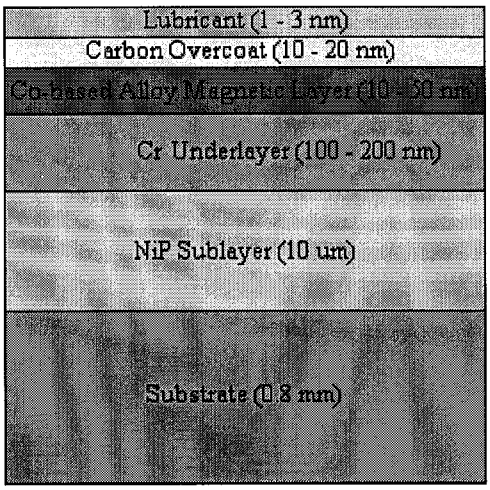

Figure 2.12 Cross sectional view of the individual layers of a thin-film disk used in a hard drive. The figure is not drawn to scale.

view of a thin-film disk can be seen in figure 2.12. The substrate, which is 0.8-mm thick, is usually aluminum, ceramic, or glass. The substrate needs to be a hard surface for structural support and have the capability of being polished to high tolerances. However, substrates can no longer be polished smooth enough for the required areal bit densities so a nickel-phosphorous (NiP) sublayer is used. The NiP sublayer is 10-μm thick and is capable of being polished to a 1 nm RMS finish. Usually the sublayer is textured with circumferential grooves that measure a 3 to 5 nm roughness. The purpose of doing this is to minimize head stiction to the disk surface and to induce a circumferential magnetic anisotropy to produce uniform magnetic readback signals.

The next layer seen is a 100 to 200-nm thick underlayer of usually chromium (Cr). The purpose of the underlayer is to control the magnetic properties and the microstructures of the magnetic layer [5]. A Cr underlayer is primarily used because of its epitaxial relations to the Co-based alloys used in the magnetic layer. These epitaxial relations are used to align the easy axes of magnetization of the magnetic layer in the plane of the disk. Furthermore, the amount of noise in the magnetic layer can be reduced by varying the magnetic grain structure via the Cr underlayer. The underlayer is a very useful tool in forming the magnetic layer. The magnetic layer varies in thickness from 20 to 50 nm and is formed from ferromagnetic materials. Cobalt-based alloys are primarily used because of their large magnetocyrstalline anisotropy resulting in high coercivities. Cobalt by itself is highly ferromagnetic; however, it has too low of a coercivity. By forming alloys with platinum (Pt), Ta, chromium (Cr), and nickel (Ni) coercivities in the range of 80 kA/m to 240 kA/m can be achieved. Chromium is an important

extra element in the magnetic layer because of its ability to reduce corrosion and also to cause the precipitation of other crystalline phases at grain boundaries aiding in noise reduction.

The last two layers are mainly protective coatings. The layer that covers the magnetic layer is an amorphous carbon overcoat that ranges in thickness from 10 to 20 nm. The purpose of the overcoat is to protect the magnetic layer from the recording head when it makes contact with the surface and also to provide a support structure for the lubricant. The purpose of the lubricant is to reduce the friction between the overcoat and the recording head. The lubricant is a perfluoropolyether organic polymer with a thickness of 1 to 3 nm. It exhibits several key properties that enable it to be a high-quality lubricant. It has a chemical inertness, a low vapor pressure to prevent loss by evaporation, a low contact angle which promotes a uniform coating of the carbon overcoat, and a chemical affinity for the overcoat preventing spin-off.

2.3.2 The Magnetostatic Field

The magnetization of each bit in the magnetic layer of the media produces its own magnetic field. This magnetostatic field produced from the magnetization is known as the demagnetizing field. In a uniformly magnetized material, the demagnetization field is related to the magnetization by

$$\vec{H}_d(\vec{r}) = -\ddot{N}(\vec{r}) \cdot \vec{M} \tag{2.14}$$

where $\vec{M}$ is the magnetization, $\ddot{N}(\vec{r})$ is the demagnetizing tensor which is a function of position independent of the magnetization, and $\vec{H}(\vec{r})$ is the demagnetization field [10]. $\vec{H}(\vec{r})$ can be modeled by a distribution of volume charges inside the magnetic media and surface charges above the media. It is given by

$$\vec{H}(\vec{r}) = -\frac{1}{4\pi}\iiint\left(\nabla \cdot \vec{M}(\vec{r}')\right)\frac{\vec{r}-\vec{r}'}{\left|\vec{r}-\vec{r}'\right|^3}d^3r' + \frac{1}{4\pi}\iint\left(\vec{n}' \cdot \vec{M}(\vec{r}')\right)\frac{\vec{r}-\vec{r}'}{\left|\vec{r}-\vec{r}'\right|^3}d^2r' \tag{2.15}$$

which is the Biot-Savart law subjected to superposition. It solves for the magnetic field anywhere in space from the source of the field. The integral term on the left hand side of the equation is the magnetization inside an object, and the term on the right is the magnetization on the surface of the object. The term $\nabla \cdot \bar{M}(\vec{r}')$ is the volume charge density and $\vec{n}' \cdot \bar{M}(\vec{r}')$ is the surface charge density, both of which are derived from Gauss's law. The point at which the field is being measured is $\vec{r}$ and the source point or where the field is created is $\vec{r}'$. When dealing with bar magnetic or uniformly magnetized rectangular prisms like this case with bits in magnetic media, the $\nabla \cdot \bar{M}(\vec{r}')$ term goes to zero [11].

When the first integral drops out due to the $\nabla \cdot \bar{M}(\vec{r}')$ term going to zero, the second integral term of the equation can be used to show the x and y field components produced by a transition. The ideal case would be to have a step transition where the transition has no length and the direction of magnetization changes completely after crossing an infinitely small barrier. However, this is not the case in reality. The transition has some defined length making it impossible for the direction of magnetization to change after crossing an infinitely small barrier. The former case is favorable because the longer a transition, the more noise it produces. A real transition in magnetic media is usually closely approximated by an arctangent function. Figure 2.13(a) shows the magnetization changes corresponding to step and arctangent transitions. The second part of the figure shows how the types of transitions would appear in the magnetic media. It can be seen that with a real transition, it requires a finite distance before the direction of magnetization can fully change.

Equation 2.15 can be derived into a pair of equations describing a finite transition and a pair of equations defining an arctangent transition. The only difference between the two pairs of equations is that the pair describing the step transition has a transition parameter of zero. The plot of the x field component produced by the arctangent transition can be seen in figure 2.14. It can be seen that the x component is opposite of the write field as it should be since it is the demagnetizing field produced from the magnetization of a bit in the media.

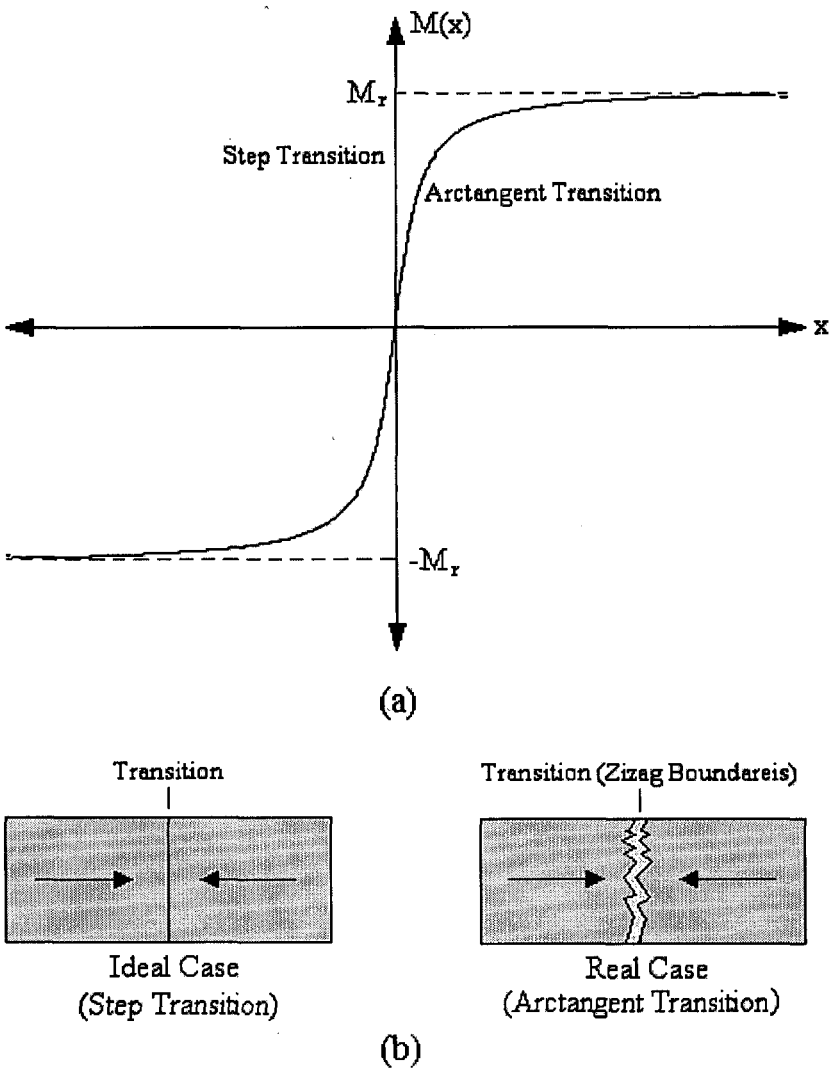

Figure 2.13 (a) Graph of magnetization reversal with a step and arctangent transition. **(b)** An ideal step transition and real case arctangent transition with zigzag boundaries shown in the magnetic media.

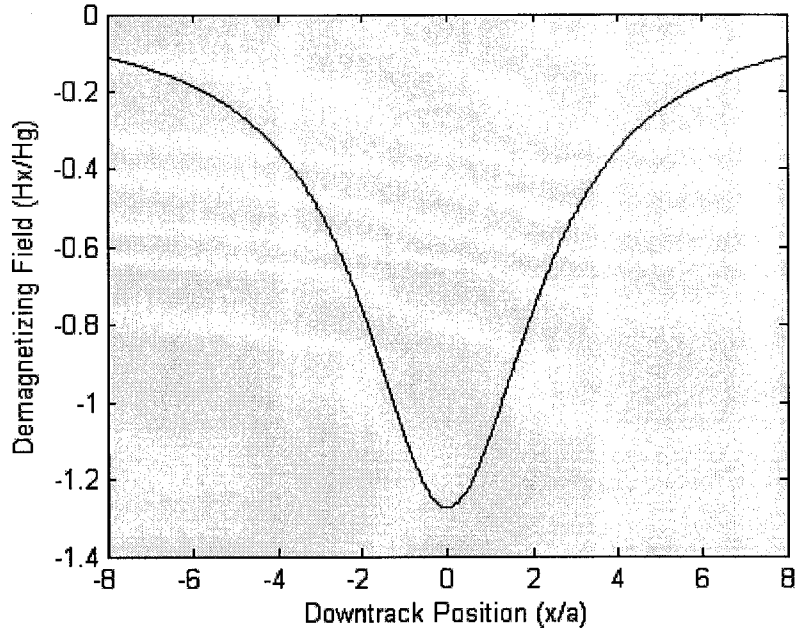

Figure 2.14 The x-component of the demagnetization field produced from the magnetization of the magnetic media.

2.3.3 Macroscopic and Microscopic Properties

The properties of magnetic media can be split into macroscopic and microscopic properties. Macroscopic properties of magnetic media such as coercivity, the remanence thickness product, and coercive squareness determine the pulse shape, amplitude, and resolution of the readback signal. The remanence thickness product is the product of the remanence magnetization and the thickness of the magnetic media. These parameters need to be adjusted accordingly in order to increase areal bit density. The magnetic media needs to possess a high coercivity in order to provide very sharp and narrow transitions. However, the coercive field cannot be allowed to exceed the write capability of the thin-film inductive write head being used. The media needs to exhibit a high remnant magnetization but small magnetic layer thickness. A high remnant magnetization is needed to provide a field large enough for the read sensor to recognize. A small magnetic layer thickness is needed to minimize the spacing thickness loss. Also, the remanence thickness product needs to match that of the spin-valve free layer. Finally, the magnetic media needs to have a squared hysteresis loop to produce sharp transitions and a good overwrite ratio.

Table 2.2 Coercivity of several Co-based alloys and its dependence on the thickness of the magnetic layer [21].

Co-Based Alloy	*Coercivity (kA/m)*	*Layer Thickness, δ (nm)*
CoCrTa	152	30
CoCrTa	168	20
CoCrPtTa	200	15
CoCrPtTaB	200	19
CoCrTa	212	10
CoCrPtTa	225	10

The coercivity of the magnetic layer is largely determined by magnetocyrstalline anisotropy which is an intrinsic property of the material being used. Magnetocrystalline anisotropy is the energy necessary to deflect the magnetic moment in a single crystal from the easy to hard axis. Several approaches aimed towards material alteration can be used to increase the coercivity of the magnetic layer. Various elements are added to form ternary, quaternary, and also higher Co-based alloys in order to enhance coercivity. Coercivity values of Co-based alloys can be seen in table 2.2. Coercivity of the magnetic layer can also be increased by using an ultraclean sputtering process [22]. Furthermore, it has been demonstrated that a multilayer SmCo/Cr/SmCo magnetic film structure exhibits a coercivity of 1120 kA/m after being annealed at 500°C [23]. If Cu or Ni is substituted for Co in the structure, a decrease of saturation magnetization and magnetic switching volume along with an increase in uniaxial anisotropy and coercivity was observed. Altering the materials used in the magnetic layer has been favorable in yielding greater coercivities.

The coercivity of the magnetic layer can also be manipulated by film stress, crystal defects, and grain properties such as size, orientation, and boundaries. The dependence of coercivity on these microscopic properties tends to be quite ambiguous. For example, the influence of grain size or thickness on coercivity is not straightforward. The coercivity of the magnetic layer increases with decreasing grain size or layer thickness until it reaches a peak at a critical thickness of 10 to 30 nm. Therefore, coercivity changes can be split into two regions; one below and one above the critical thickness of the magnetic layer. Above the critical thickness, the coercivity decreases with an increasing magnetic layer thickness due to magnetostatic interactions and an increased disorientation of the c-axis of the Co grains with the disk. Below the critical thickness of the magnetic layer, the coercivity declines rapidly with

decreasing thickness because of the thermal instability of the magnetic grains due to the superparamagnetic effect.

To increase the linear density, the remanence thickness product needs to be reduced. At an areal bit density of 26.5 Gbits/in^2, the remanence thickness product is expected to be 4 mA with a layer thickness of 19 nm [24]. This is the region where the coercivity can decline quickly with the decreasing thickness of the magnetic layer. Therefore, it becomes extremely difficult to attain high coercivities in extremely thin-films. A small magnetic layer thickness is needed to minimize the spacing thickness loss while at the same time a high remanence magnetization is needed to provide a strong enough field for the read sensor to detect during the readback process. At the same time, the overall remanence thickness product needs to be reduced while maintaining a high coercivity to provide increasing linear densities. Usually, a high coercivity and low noise are designed for a specified remanence thickness product.

Microscopic properties such as grain size, grain coupling, and grain crystallographic orientation determine the noise parameters of the magnetic media. The magnetic layer of thin-film media is composed of magnetic grains that have ranged in diameter from 10 to 50 nm in recent years. Typically, at least 100 grains are needed to represent a bit. Any significant decrease in the amount of grains used to represent a bit would cause increases in noise. However, it has to be remembered that the smaller the magnetic grains become the more chance they have of becoming unstable due to the increased effect of thermal energy. This will be discussed in more detail later. Since the magnetic grains are only separated by a couple of nanometers they experience strong magnetostatic and intergranular exchange interactions leading to increased noise levels. Noise is also created by not having the c-axis of the magnetic grains in close alignment with the plane of the disk. Each one of these parameters can be adjusted to provide a low noise magnetic layer by designing the proper Cr underlayer.

The size of grains in the magnetic layer are not uniform, but are spread about an average value. The information stored in smaller grains decays more rapidly because it is affected by thermal energy. On the other hand, larger grains cause higher noise levels. It has been observed that narrowing the grain size distribution can postpone the emergence of thermal effects and also enhance the SNR [25]. There are three main types of distribution models: Gaussian, log-normal, and Rosin-Rammlar distributions. However, since both the Gaussian and Rosin-Rammlar distributions allow for negative values, the log-normal distribution is the only one that can be

used to describe grain size distributions. In other words, a negative distance for a grain size is not possible. The log-normal distribution is defined by

$$y = \frac{1}{\log \sigma_g \sqrt{2\pi}} \exp\left[-\frac{(\log x - \log x_g)^2}{2 \log^2 \sigma_g} \right] \tag{2.16}$$

where x_g is the geometric mean and σ_g is the geometric standard deviation. The log-normal distribution is the Gaussian distribution with the x values substituted by *log(x)* resulting in a geometric mean and standard deviation. Using the logarithm guarantees that there will be no resulting negative values which is what is required when modeling the grain size distribution.

The grain size and grain size distribution of the magnetic layer is primarily controlled by the Cr alloy underlayer structure. This is because the Co-based alloy magnetic grains are epitaxially grown on the Cr-based alloy underlayer [11]. Therefore, a study of how the Cr underlayer is deposited becomes relevant. Atoms of the Cr alloy material nucleate randomly and grow on the ultra smooth NiP sublayer surface. The initial grain size is formed by nucleation and growth models. The average grain diameter can be controlled by the following equation

$$D = 1.448 \times \left(\frac{G}{I} \right)^{2/3} \tag{2.17}$$

where D is the average grain size, G is the grain growth rate, and I is the nucleation rate. The nucleation rate is the rate at which the particles bond to the surface, and the growth rate is the rate at which individual sites grow where a particle has bonded to the surface. If the grain growth rate is relatively high, and the nucleation rate is low, there will be more of a chance of having one large site of a single crystal. This is how a single crystalline structure is created. With these parameters, a continuous film will take longer to develop resulting in larger grains. If the grain growth rate is low and the nucleation rate is high, many individual sites will join together to produce an amorphous material. With this situation smaller grain sizes are produced.

The growth of grains is also affected by the deposition conditions such as substrate temperature and argon (Ar) pressure as seen in Thornton's zone model in figure 2.15. As can be seen, the morphology of the final film varies with the Ar pressure and the substrate temperature,

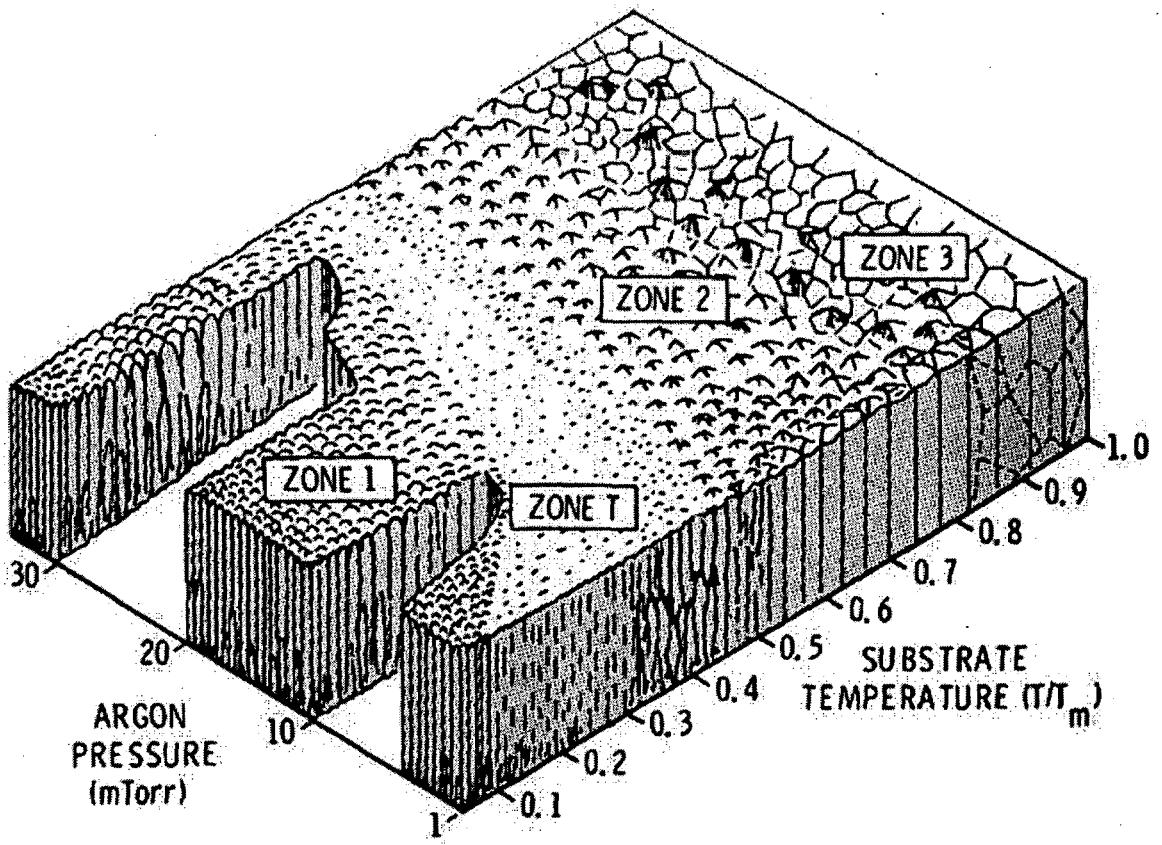

Figure 2.15 Thornton's zone model for sputter deposited metallic films [26].

T, along with the melting temperature, T_m, of the deposited material. As T/T_m increases, the grain size increases. If T/T_m is small value and the Ar pressure is high, the morphology of the underlayer is categorized by zone one in the model. This type of deposition is used to grow thick underlayers and is the most favorable type because it helps to decouple the grains in the magnetic layer resulting in lower media noise. In zone two of the model, columnar shaped grains are separated by dense grain boundaries creating a highly faceted surface. Producing a tight grain size distribution by properly calculated deposition methods of the underlayer will reduce thermal effects and increase SNR.

Narrowing the grain size distribution is not the only method of reducing the noise in magnetic media. Reducing grain coupling in the magnetic layer plays a large role in reducing noise [27]. Exchange coupling is responsible for ferromagnetism and originates from the Pauli exclusion principle of electrons. It states that no two electrons in an atom can be in the same state at the same time. The exchange interaction coupling energy is given by

$$E_{ex} = -2J_{ij}\vec{s}_i \cdot \vec{s}_j \tag{2.1}$$

where i an j are two arbitrary electrons and J_{ij} is the exchange integral which is most significant for nearest neighbor electrons. If $J_{ij}>0$, the spin of the two electrons align parallel minimizing the exchange interaction coupling energy. This condition results in ferromagnetism. If $Jij<0$, the spin of the two electrons is not oriented parallel which leads to antiferromagnetism. Finally, if there is no exchange interaction coupling energy, thermal energy is predominate and aligns magnetic dipoles randomly. This results in paramagnetic materials that do not have a spontaneous magnetization.

Since the exchange integral is most significant for nearest neighbor electrons, exchange coupling becomes non-existent as the separation distance between electrons increases. However, grains in the magnetic layer of thin-film media have become so close to each other that intergranular exchange coupling has become a major issue. In the later part of the 1980's, micromagnetic modeling demonstrated that transition noise is caused by intergranular exchange coupling. If it is considered, it makes sense that intergranular exchange coupling causes transition noise. Intergranular exchange coupling creates clusters of grains; therefore, transitions become larger and zigzag like in order to form around the clusters. Larger zigzag like transitions create higher noise levels.

There are two methods that are used to decrease the noise that is caused by coupling. If the Cr underlayer is sputter deposited at a low temperature and high Ar pressure, a morphology corresponding to zone one of Thornton's model will be created. As mentioned earlier, it produces fine columnar grain with voided boundaries. Therefore, when the magnetic layer is deposited on the underlayer it will have a similar morphology. The voided boundaries are key to reducing noise because the magnetic particles are slightly separated which negates the exchange coupling [11]. A secondary method used to reduce coupling is to induce compositional segregation in the magnetic layer. It has been observed that at high substrate temperatures during the deposition of the magnetic layer, Cr atoms in the Co-based alloy segregate towards the boundaries of the grains. Therefore, Cr atoms tend to form a wall around the magnetic grains reducing intergranular exchange coupling. Furthermore, it has been shown that the addition of Ta into the Co-base alloy increases the Cr segregation further reducing coupling and hence noise to a greater degree.

One final way that is going to be discussed for reducing noise in the magnetic layer is by designing for the proper grain crystallographic orientation. There are particular epitaxial relations that exist between hexagonal close-packed (hcp) and body-centered cubic (bcc) crystal structures. Co-based alloys exhibit the hcp structure and the Cr grains exhibit the bcc structure [28]. Therefore, a Cr underlayer is very suitable because of its good epitaxial relation with Co-based alloys. Also Cr and Co have a similar atomic size. Once again, the Cr underlayer is used to control an aspect of the magnetic layer. With this situation, it is desirable to deposit the underlayer so that an epitaxial relation exists to align the c-axis of the magnetic grains as close as possible to the plane of the disk. Doing this not only reduces noise, but also increases anisotropy and coercivity.

There are several possible orientation relationships between the bcc Cr grains and the hcp Co-based alloy grains. One common scheme to exploit is known as the Pitsch-Schrader relationship. With this scheme, the Cr(001) plane is matched with the Co$(11\bar{2}0)$ plane in order to orient the c-axis of the Co-based magnetic grains close to the plane of the disk. The Cr(001) and Co$(11\bar{2}0)$ planes can be seen in figure 2.16. It can be seen that the Co-based alloy plane is 4.35 Å by 4.08 Å and the Cr plane is 4.07 Å on each side. The planes have a very similar size which yields a favorable lattice match. The mismatch is 0.2% and 6.4% along the c-axis and $[10\bar{1}0]$ directions respectively [10]. Furthermore, the atomic radius of Cr is 1.4 Å and that of Co is 1.35 Å enabling for a favorable lattice match.

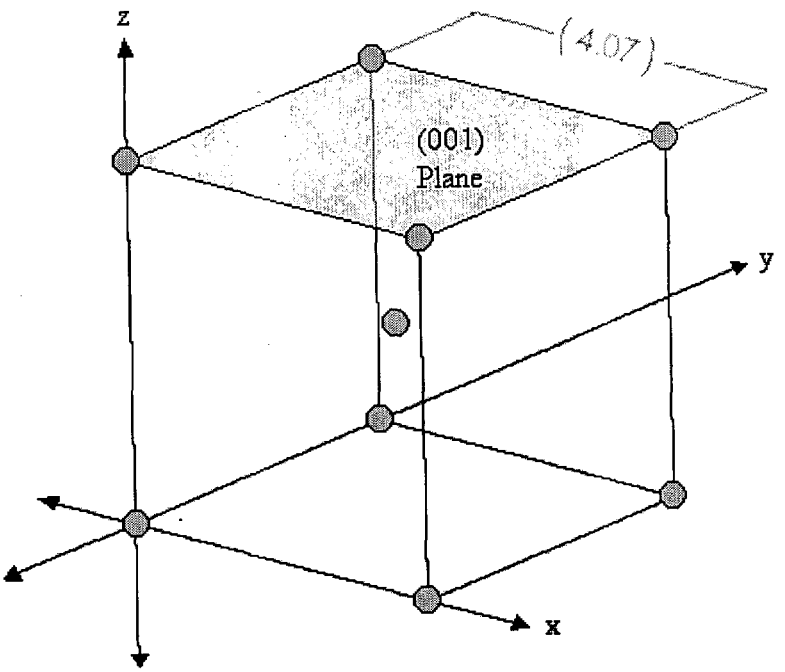

(a)

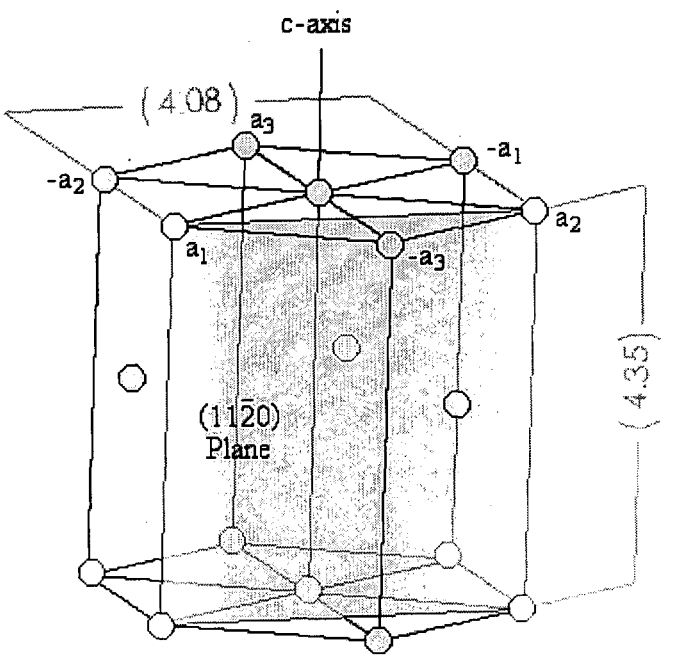

(b)

Figure 2.16 (a) The (001) plane of a body-centered cubic crystallographic orientation which in this case is chromium. **(b)** The $(11\bar{2}0)$ plane of a hexagonal close-packed crystallographic orientation which in this case is a Co-based alloy.

2.4 Limitations of Present-Day Magnetic Recording Technology

Areal bit density has been increased mainly through the principle of scaling in which all relevant head and media dimensions are reduced. There have been several occasions where experts have predicted that magnetic recording used in hard drives would not be able to surpass a certain capacity barrier. None of these barriers dealt with overcoming actual physical limits. Instead, they were practical engineering considerations where it was believed that new technologies could not be discovered to increase capacity at a feasible cost. However, new forms of longitudinal magnetic recording technology such as thin-films and GMR read sensors emerged to extend the ability of scaling. Today, the physical limits of longitudinal magnetic recording on a continuous magnetic media are being approached.

As the stored bit size on a hard drive continues to be reduced, there are staggering limits of physics that arise. A smaller bit size requires smaller magnetic grains because the statistical average of the grains needs to be kept above a minimum value in order to reduce transition noise [29]. The problem with doing this is as the magnetic grains become too small their magnetization is affected by thermal energy. Therefore, thermal variations cause the grains to become superparamagnetic and spontaneous magnetization reversal occurs. When spontaneous magnetization reversal occurs, the information stored in the magnetic media will degrade drastically reducing the lifetime of a hard drive. The superparamagnetic effect also causes dynamic coercivity in the magnetic media. This affects the maximum switching speed because in order to increase the data rate, the switching speed needs to be increased; however, if the coercivity is time dependent, increasing the switching speed will increase the coercivity. These conditions create a tradeoff between the stability of recorded information and achievable SNR with longitudinal magnetic recording on a continuous magnetic media.

The stability of a magnetic grain is compromised as it becomes too small. Its stability is determined by the ratio of its energy barrier to the energy of thermal variations. Therefore, spontaneous magnetization reversal is caused by thermal variations. The Arrhenius-Neel model of magnetization decay shows that the average time for the spontaneous magnetization reversal of a magnetic grain is given by

$$\tau = \tau_o \exp\left(\frac{\Delta E}{kT}\right) \tag{2.19}$$

where $k = 1.3807 \times 10^{-23}$ J/K is Boltzmann's constant, T is the absolute temperature in Kelvin, and $\tau_o = 1/f_o$. The prefactor, f_o, is the thermal attempt frequency to cross the barrier, and it is related to intrinsic material properties such as anisotropy and damping [25]. The commonly used value for Co-based alloy magnetic media is $f_o = 10^9$ Hz [30]. The energy barrier, ΔE, is determined by the anisotropy of magnetic grains undergoing reversal. In the absence of an applied field, the energy barrier is given by

$$\Delta E = K_u V \tag{2.20}$$

where K_u is the uniaxial anisotropy energy density, and V is the magnetic grain volume. For a typical thin-film media the uniaxial anisotropy is $K_u = 0.2$ J/cm^3 [10]. When an applied field is present, the magnetization rotates in the direction of the applied field. Furthermore, the energy in the presence of an external field varies as a function of the field angle and the magnetization angle to the easy axis of the magnetic grain.

If the size of a magnetic particle is continually decreased, it will eventually become superparamagnetic. Its energy barrier becomes comparable to its thermal energy, and the mean time of spontaneous reversal becomes much smaller than the observation time. Figure 2.17 is a plot of how long a magnetic grain is stable depending on its size at room temperature of $T = 300$ K. It can be seen that only a half of a nanometer difference in diameter can decrease the life of a magnetic grain by 30 years. The magnetization reverses easily with smaller grain sizes due to thermal variations. It is comparable to the magnetic dipoles in a paramagnetic material. Since the magnetic moment of the magnetic grain is much larger, the grains are referred to as superparamagnetic.

The lifetime of a hard drive is expected to be at least 10 years. With this consideration in mind, according to figure 2.17 the average grain diameter should be at least 10 nm to achieve several years of stability. This is what is commonly referred to as the superparamagnetic limit. Micromagnetic modeling has also confirmed this analytical observation. It has shown that magnetic grains will become thermally unstable at room temperature if they are smaller than 10 to 12 nm. Since it has been determined that a bit must contain at least 100 thermally stable grains for a readable SNR, the maximum achievable areal bit density of conventional longitudinal magnetic recording before the superparamagnetic effect is encountered is 40 to 70

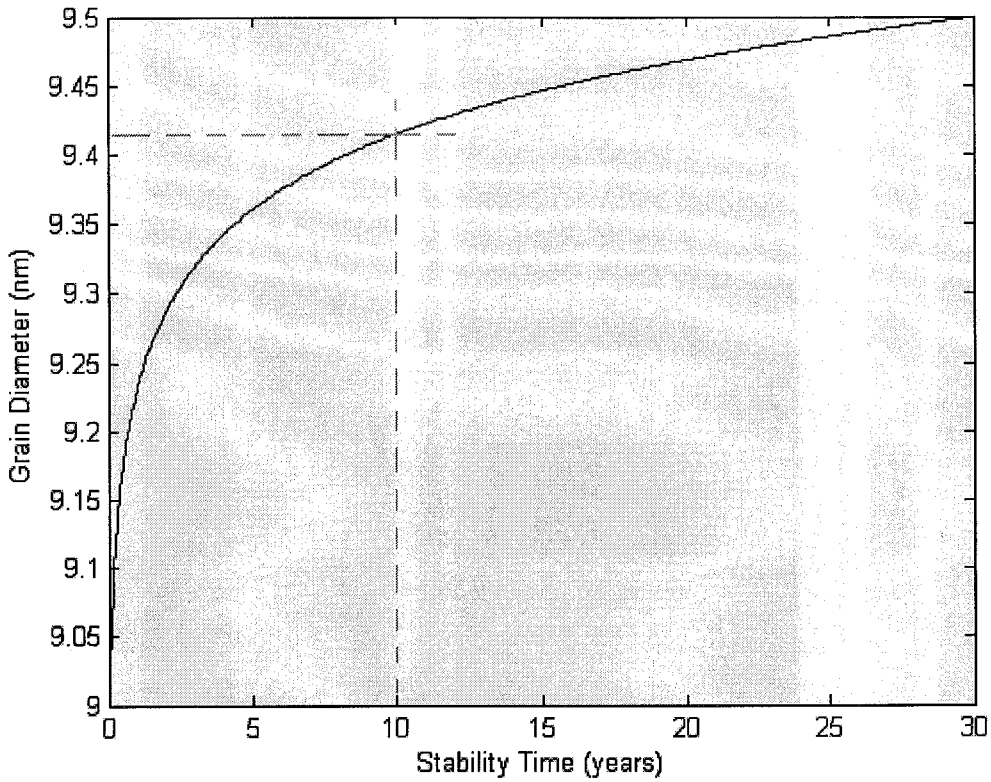

Figure 2.17 A plot of how long the magnetic grains of a hard drive will be thermally stable depending on the average grain size. The Arrhenius-Neel model was used to plot the graph.

Gbits/in^2. Therefore, other types of magnetic recording technologies are needed. It can be seen from equations 2.20 and 2.21 that raising the uniaxial anisotropy constant of the magnetic layer is capable of allowing smaller grain sizes; however, this method has been almost exhausted due to the limitation of greater write head fields.

When the average time of spontaneous magnetization reversal becomes comparable to observation time, magnetic viscosity is experienced. At this point, the measured magnetization is time dependent. The magnetization decays rapidly with time resulting in information loss. In a system of identical, non-interacting magnetic grains, the dynamics of magnetization are given by

$$\frac{dM}{dt} = f_o M \exp\left(\frac{\Delta E}{kT}\right) \tag{2.21}$$

where the solution to equation 2.21 is given by

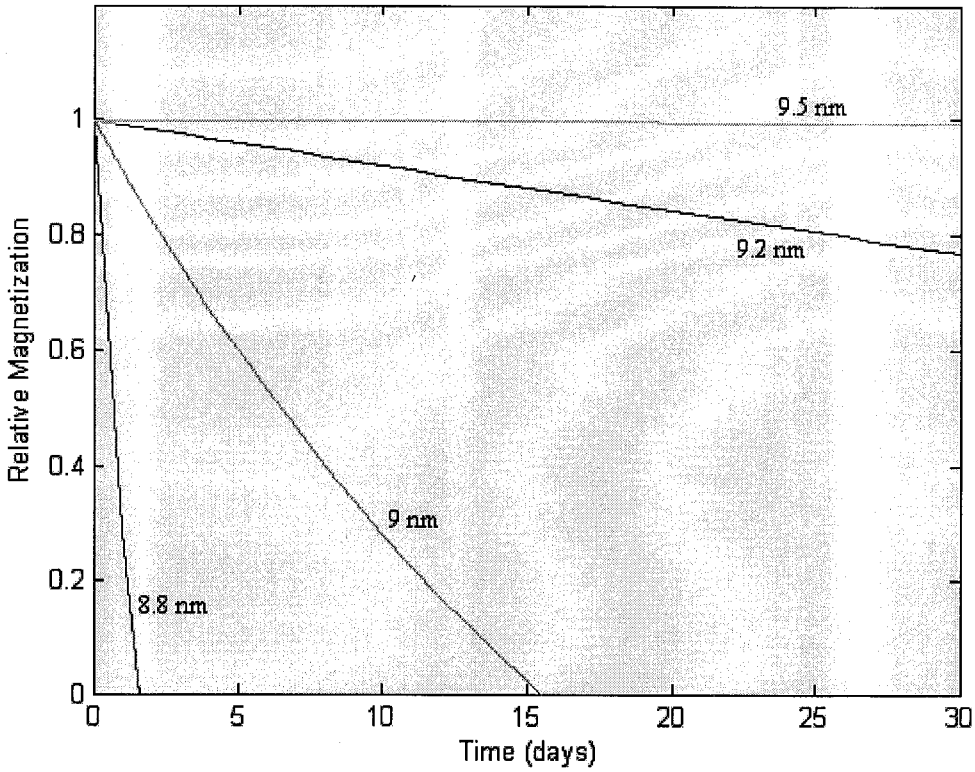

Figure 2.18 A plot of magnetization decay measured in days for various magnetic grain diameters based on equation 2.23.

$$M(t) = M_o\left[2\exp\left(-\frac{t}{\tau_o}\exp\left(-\frac{\Delta E}{kT}\right)\right)-1\right]. \tag{2.22}$$

The exponential within the exponential of equation 2.22 shows that the magnetization decay is extremely sensitive to the thermal effect. This can be seen in figure 2.18 where a plot of equation 2.22 is produced for several magnetic grain diameters. It can be seen that an extremely small reduction in grain diameter results in a large decay of magnetization.

Equation 2.22 is not normally observed because it does not account for grain size and anisotropy distribution in the magnetic layer. These factors need to be accounted for because smaller magnetic grains or anisotropy constants will decay faster than large ones. Therefore another solution to equation 2.21 describing the dynamics of magnetization can be derived in order to account for grain size and anisotropy distributions [21]. The solution provides the time dependence of the average magnetization in the presence of a constant magnetic field. It is given by

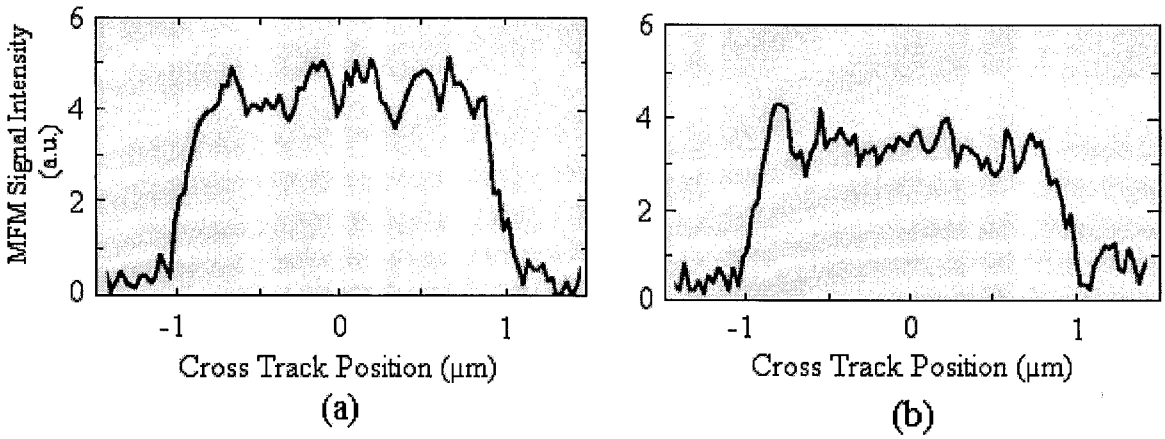

Figure 2.19 MFM signal intensity measured across the track of hard drive at **(a)** 1.5 hours and **(b)** 95 hours after recording [27].

$$M(t) = C - S\ln(t) \tag{2.23}$$

where S is the coefficient of magnetic viscosity, and C is a constant produced from integration. The linear dependence of the magnetization on the logarithm of time is experimentally observed [10]. Magnetization decay can also be observed with magnetic force microscope (MFM) measurements [27]. A reduction in the MFM signal intensity seen in figure 2.19(b) can be attributed to magnetization decay. A transition was recorded in the magnetic media and then measured at 1.5 hours and then 95 hours after recording. The signal intensity is stronger after 1.5 hours seen in figure 2.19(a) than it is at 95 hours seen in figure 2.19(b) because the magnetization has decayed over time.

As seen, the magnetization decay is extremely sensitive to the energy barrier. The energy barrier can be lowered by the presence of a magnetic field. Therefore, when the system is not a single isolated transition, the demagnetizing fields from neighboring transitions will increase the decay. When the magnetization pattern is recorded, the energy barrier is transformed by the demagnetizing field of the recorded transition according to

$$\Delta E = KV\left(1 - \frac{H_d}{H_o}\right)^m \tag{2.24}$$

where H_o is the intrinsic coercivity dependent upon material properties, H_d is the demagnetization field, and m is a value ranging from 1.5 to 2 depending on the grain size distribution and intergranular exchange coupling [31]. The demagnetization field as seen decreases the energy barrier which allows for an accelerated magnetization decay. Since transitions at ultra-high linear densities are subjected to demagnetization fields, they decay faster than isolated transitions.

By now, it has become clear that the superparamagnetic effect causes the magnetic grains and therefore the bits storing information to become unstable. This results in a loss of information and decreases the life of the hard drive. One obvious solution to this might be to increase the coercivity of the magnetic layer until a desired stability is achieved. However, when the magnetic grains are too small, the coercivity increases at smaller time scales comparable to those of the writing time. This severely impacts the writing capability. This problem is observed because the thermal effect causes coercivity to become dependent upon time [10]. The time dependence of coercivity can be described through the combination of equations 2.22 and 2.24 to form the effective coercivity

$$H_c(t) = H_o\left[1-\left(\frac{kT}{K_u V}\ln\left(\frac{f_o t}{0.693}\right)\right)^{1/m}\right]. \tag{2.25}$$

The equation is plotted in figure 2.20 for various grain diameters at an intrinsic coercivity of 240 kA/m and an m value of 1.5. It can clearly be seen that as the time scale becomes larger with smaller grain dimensions, the coercivity drastically decreases.

Dynamic coercivity imposes several problems for magnetic recording. One fundamental problem is measuring the coercivity of the magnetic layer. Typically, this is done using magnetometry at a time scale of several seconds [32]. This is neither the time scale on which the writing process or long-term storage occurs. Therefore, when the thermal effect is substantial enough to cause dynamic coercivity, this measured value will be smaller than the coercivity experienced during writing, and larger than the coercivity experienced during long-term information storage. Magnetometry would not be able to show that the coercivity has become dynamic resulting in design flaws. A smaller write field than needed to overcome the coercivity of the media to change the magnetization direction would be designed.

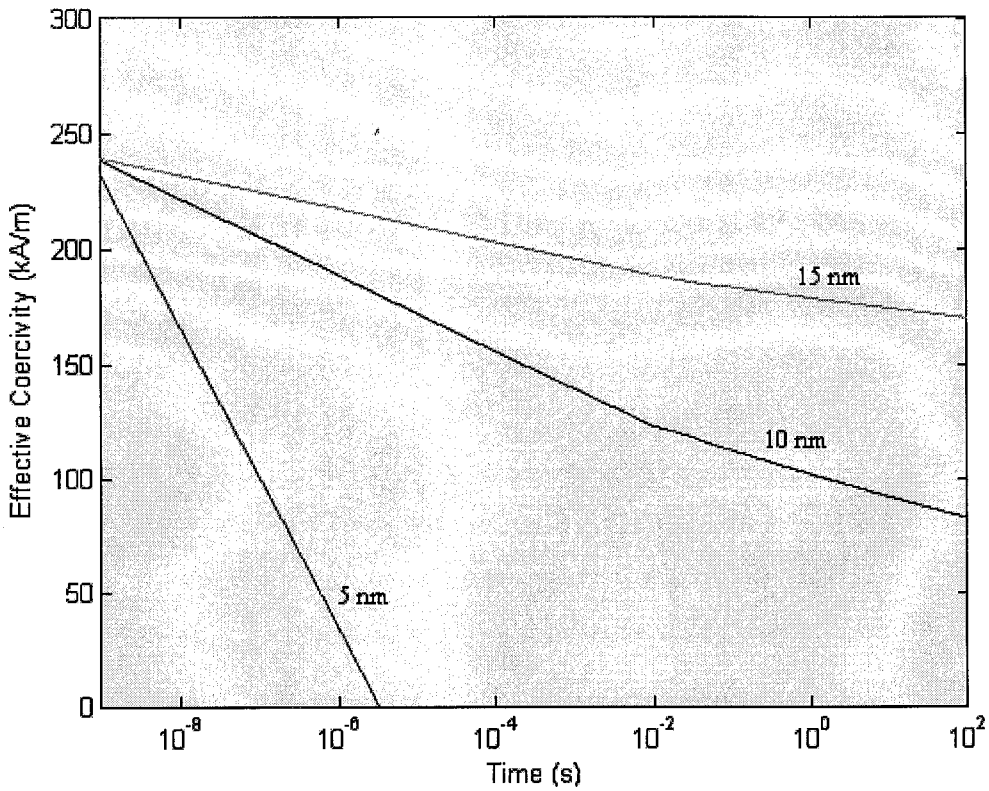

Figure 2.20 A plot of the effective coercivity for various grain size dimensions. As the time scale increases, the coercivity decreases. At shorter time scales, the coercivity of the media will be too great to overwrite. At longer time scales, the coercivity will be too small to maintain the stability of a bit. The intrinsic coercivity was set at 240 kA/m and m was given a value of 1.5. The

Furthermore, the coercivity for long-term storage would be seen as large enough when in fact it would not be. Other methods have been developed to measure dynamic coercivity. A non-destructive and indirect technique has been used to measure coercivity as a function of an applied pulse [33]. It can be seen that dynamic coercivity is another major problem in addition to spontaneous magnetization reversal caused by the thermal effect.

Besides causing spontaneous magnetization reversal and dynamic coercivity, the superparamagnetic effect also indirectly affects the switching time of the magnetization. It is through dynamic coercivity that the superparamagnetic effect is able to increase the magnetization switching time. As mentioned previously, dynamic coercivity results in increased coercivity values at shorter time scales. This increases the time it takes for the reversal of magnetization during the write process. Dynamic coercivity does not solely influence the magnetic media switching time. It is also affected by the gryomagnetic switching speed. As with anything, magnetization reversal in magnetic grains is not instantaneous. Once a magnetic

field is applied to an isolated grain, a damped gryomagnetic precession process occurs [10]. It is described by the Landau-Lifshitz-Gilbert equation

$$\frac{d\vec{M}}{dt} = -\gamma\left(\vec{M} \times \vec{H}\right) + \frac{\alpha}{M_s}\left(\vec{M} \times \frac{d\vec{M}}{dt}\right) \tag{2.26}$$

where γ is the gryomagnetic ratio, $\vec{M}$ is the magnetization of the grain, $\vec{H}$ is the applied magnetic field, α is the damping constant, and M_s is the saturation magnetization. This equation describes a process that is very similar to the wobble of a spinning top except it is done on an atomic level.

The most important aspect of equation 2.26 is the damping constant. The switching speed depends primarily on the damping constant. It describes the loss of energy of a magnetic grain and is similar to a frictional force. If the constant is zero, the precession cycles will last forever, and there would be no reversal of magnetization. This will never occur in this universe because there is always going to be some damping force present. Since the damping constant will always be non-zero, the magnetization will eventually align to the applied field after a number of precession cycles. The maximum switching speed occurs at a damping constant of one. Ferromagnetic resonance experiments have yielded damping constants close to 0.02 for materials used in thin-film magnetic media [34].

The Landau-Lifshitz-Gilbert equation is not used in practice too often because it only accounts for a magnetization reversal for a single isolated magnetic grain. There are no considerations for interactions between grains such as the demagnetizing field and intergranular exchange coupling. This is not the case in actual magnetic media. Therefore, micromagnetic models are used to simulate the magnetization reversal in longitudinal thin-film magnetic media. They show that for damping constants ranging between 0.01 and 0.05, the switching time is 0.5 ns [35]. Some research has shown that switching times on the order of 0.5 ns could be the maximum achievable switching time. If this were true, it would limit the data rate to the order of a few hundreds of megabytes per second.

2.5 Next-Generation Magnetic Recording Technologies

It has been discussed that as scaling continues to increase the areal bit density, the superparamagnetic effect will eventually create major problems with conventional magnetic recording technology. Therefore, new technologies will be needed to take over where longitudinal magnetic recording on continuous thin-film media leaves off. It has been observed that conventional longitudinal magnetic recording becomes susceptible to the effects of thermal energy when grain diameters are reduced in size to 9 to 12 nm [36]. They are scaled down in order to fit 100 magnetic grains in a bit for an acceptable SNR. This translates into an areal bit density of approximately 40 to 70 Gbits/in^2. It was believed that the areal bit density of longitudinal magnetic recording would not be able to surpass this mark; however, a departure from typical scaling proved otherwise.

A deviation from scaling is already being implemented which is postponing the superparamagnetic effect in longitudinal magnetic recording. The deviation is known as antiferromagnetically coupled media. So far, it has achieved areal bit densities of 60 to 75 Gbits/in^2. It is believed that AFC media will be able to increase the areal bit density of hard drives using longitudinal magnetic recording past the 100 Gbits/in^2 mark. After this though, new forms of magnetic or possibly non-magnetic recording will be needed to increase areal bit density. Two different types of technology under research that will extend areal bit density beyond 100 Gbits/in^2 are perpendicular recording and patterned magnetic media.

2.5.1 AFC Media

A cross sectional view of a transition in AFC media is seen in figure 2.21(a). A basic AFC media design contains two ferromagnetic layers separated by a thin non-magnetic layer. The non-magnetic layer induces antiferromagnetic coupling between the ferromagnetic layers. The antiferromagnetic coupling is caused by both Ruderman-Kittel-Kasuya-Yosida (RKKY) interactions across the non-magnetic layer as well as dipolar coupling of the grains in the upper and lower layers [37]. The lower layer is often referred to as the stabilizing layer. The ferromagnetic layers are typically Co-based alloys and the non-magnetic layer is ruthenium (Ru). Figure 2.21(b) shows a sketched hysteresis loop for an AFC media structure. A large applied

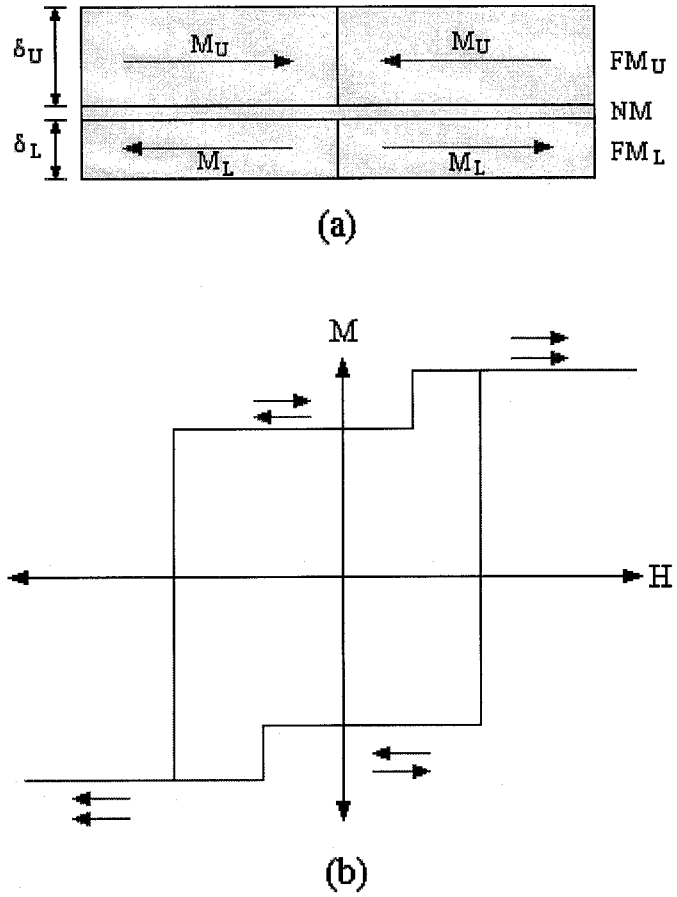

Figure 2.21 (a) Cross sectional area of a transition in an AFC media structure. **(b)** The corresponding hysteresis loop of an AFC media structure.

field will force the magnetizations of the two layers to align parallel to each other pointed in the same direction. In this state, the applied field energy is stronger than the energy associated with the antiferromagnetic coupling. A small applied field will force the magnetizations to switch to opposing directions. In this state, thermal energy has to reverse both layers for the systems to be unstable. This gives AFC media greater thermal stability.

AFC media is now exploited in several hard drive models and has proven an effective design for improving thermal stability without degrading the recording performance. It has the ability of reducing the effective remanence thickness product of a magnetic layer without having to proportionally lower the grain volume. The effective remanence thickness product for an AFC structure is given by

$$M_r\delta_{eff} = M_r\delta_U - M_r\delta_L \tag{2.27}$$

where the first and second terms on the right hand side of the equation are the upper and lower layers respectively. From the equation, it is seen that AFC media can be designed to appear magnetically thin while actually being geometrically thick. Appearing magnetically thin does not degrade recording performance while being geometrically thick enhances thermal stability. Furthermore, if the effective remanence thickness product can be lowered, the transition parameter will be reduced hence yielding larger linear densities. Then, if this can be done without reducing the grain volume, thermal energy will not become substantial.

The design of the stabilizing layer plays a major role in determining the properties of the AFC structure. When the magnetic layers are separated by an ultra-thin Ru layer, there are three competing energies. These are Zeeman energy, anisotropy energy, and interface coupling energy [38]. At applied fields close to zero, the Zeeman energy is no longer a factor. Then anisotropy and interface coupling energy compete with each other. The goal in the design process is to allow the coupling energy to be larger than the anisotropy energy of the stabilizing layer. This is achieved by properly reducing the anisotropy constant, K_{uL}, and thickness, δ_L, of the stabilizing layer because they are proportional to the anisotropy energy. Furthermore, reducing the thickness of the stabilizing layer has proved to increase the readback voltage amplitude and pulse width [39]. By having the coupling energy larger than the anisotropy energy of the stabilizing layer, the magnetization of the stabilizing layer will be pointed in the opposing direction of the upper layer. This will result in a reduction of the remanence thickness product.

A comparison of AFC media to conventional media proves that AFC media can provide enhanced thermal stability. In AFC media, the upper layer provides a good signal resolution while the lower layer provides good media noise performance. The ratio of the thickness of the lower layer to the upper layer is where the SNR can be enhanced [40]. To achieve greater areal bit densities, the coercivity is increased and the remanence thickness product is decreased. To accomplish this with conventional media, the process conditions have to be changed considerably resulting in a decreased SNR performance. However, AFC media can achieve a lower remanence thickness product without a change in process conditions. Figure 2.22 shows the superiority in performance at lower remanence thickness products of AFC media to conventional media. AFC media continues to maintain its original bit error rate (BER) value at a remanence thickness product less than 3.1 mA (0.31memu/cm^2) [41]. The BER for conventional

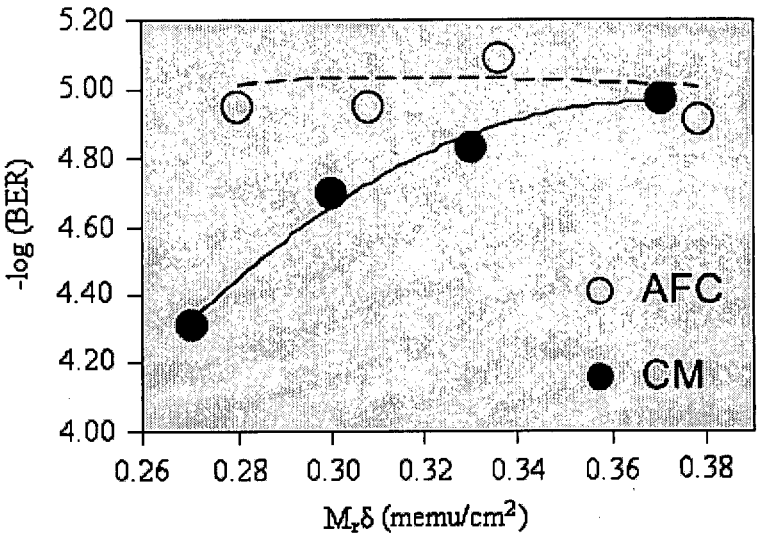

Figure 2.22 BER comparison on AFC and conventional media as the remanence thickness product is decreased. It was done with a coercivity value of 328 kA/m [41].

media deteriorates rapidly below a remanence thickness product of 3.1 mA due to variations in the process conditions to increase coercivity. When the remanence thickness product decreases below 3.1 mA, AFC media offers significant enhancement in thermal stability over conventional media while maintaining its SNR.

2.5.2 Perpendicular Recording

With perpendicular recording, the magnetization of the media lies normal to the disk plane. Figure 2.23 displays a basic perpendicular recording system. There are two main layers in the media used for perpendicular recording. These are the magnetic layer and the underlayer. The underlayer is magnetically soft meaning that its magnetization direction can be easily rotated with a weakly applied field. Magnetically soft materials typically have a coercivity less than 800 A/m [10]. By having a soft underlayer (SUL), a return path for the flux is created during the writing. The main advantage with having this type of recording process is that the magnetic media is subjected to the deep gap field of the head as opposed to the fringe field or write bubble in conventional longitudinal magnetic recording. The effective write field is twice as great with perpendicular recording as it is with longitudinal [11].

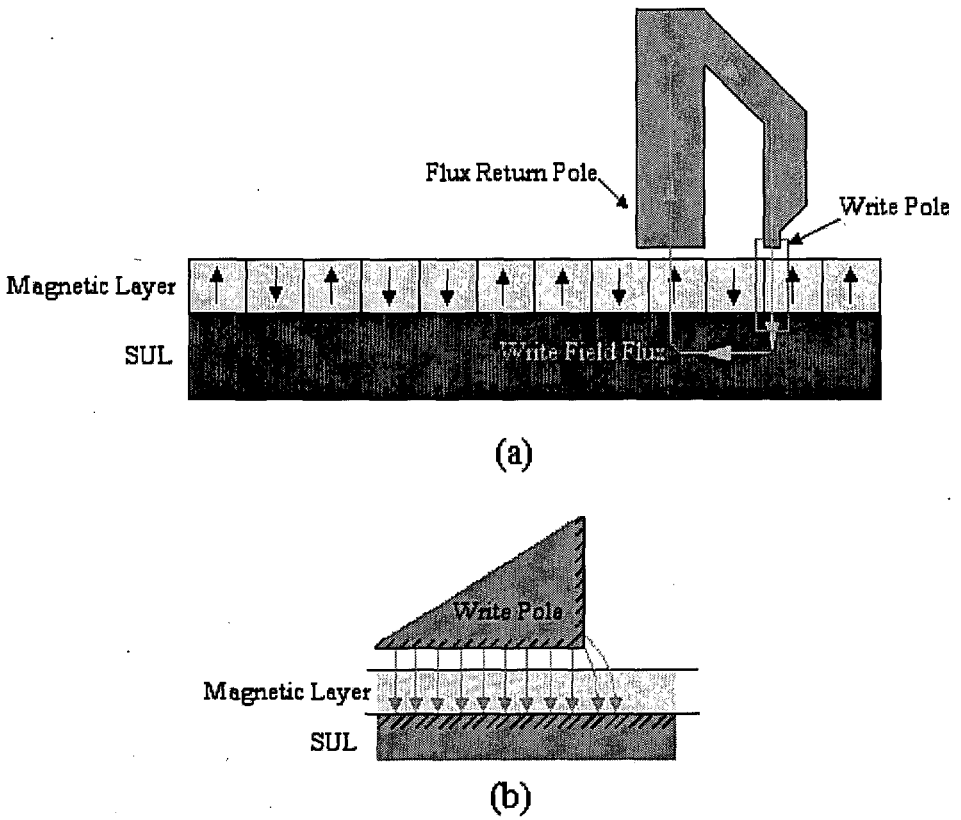

Figure 2.23 (a) Write head and magnetic media used for perpendicular recording. **(b)** Enlarged region of the write pole used to show that with perpendicular recording and a soft underlayer, the magnetic layer is essentially in the write gap.

The write head used for perpendicular recording is structurally similar to one that is used for longitudinal recording. With perpendicular recording, writing is performed with pole head and a SUL. The writing takes place at the trailing edge of the main pole. There is a secondary pole that is wider than the main pole in order to provide a return path for the flux. The SUL is physically part of the media, but is magnetically linked to the write head. It is essentially the same as turning a longitudinal write head on its side and passing the magnetic media through the write gap. Just as with the write head, longitudinal recording read sensors could easily be used for perpendicular recording with only minor modifications, although the readback signal of perpendicular recording would be a different shape than for longitudinal [11]. Also the read gap would need to be decreased for perpendicular recording. This would cause the read sensor to eventually saturate, but a viable solution would be to implement a design using the current perpendicular to the plane.

There are several important requirements of thin-film media for perpendicular recording that are primarily focused on the microscopic properties of magnetic materials. In order to fully exploit perpendicular recording, the media needs to have small grains, minimal intergranular exchange coupling, and small spacing between the soft underlayer and magnetic layer to minimize the effective spacing loss. It is also favorable to have a coercivity in the range of 1.2 to 1.6 MA/m and a near perfect magnetization remanence. There are three types of thin-film constructions used for perpendicular recording. They include multilayer, continuous thin-film, and granular thin-films. As of now granular thin-film media is the most favorable because it can be produced with very small grains and has excellent grain isolation to minimize intergranular exchange coupling. The media can be composed of either hcp Co-based alloys or FePt alloys which have varying effects on recording properties [42].

There are certain fundamental concepts that longitudinal recording is dependent upon whereas perpendicular recording is not. From experiments, it was discovered that the fundamental nature of longitudinal and perpendicular magnetization are complimentary [43]. Longitudinal recording is limited by the macroscopic properties of coercivity, magnetization remanence, and thickness of the magnetic layer. These macroscopic properties are then in turn influenced by the microscopic properties of magnetic materials such as crystalline anisotropy, grain size, and grain coupling. The resolution of perpendicular recording is not limited by any macroscopic properties, but only the microscopic properties of magnetic materials. Therefore, perpendicular recording is essentially only limited by the grain size.

Not being dependent upon macroscopic properties gives perpendicular recording an advantage in achieving greater areal bit densities. There are three main reasons why perpendicular recording is superior to longitudinal recording. The first reason as mentioned earlier is that the implementation of the magnetically soft underlayer essentially places the media in the write gap. In longitudinal recording, the fringe field of the gap is used to write transitions; therefore, the coercivity of the media is limited by the effective write capability of the head. Second, perpendicular recording media can be made much thicker than that of longitudinal media whose demagnetization field increases with thickness. Therefore, perpendicular grains have a smaller area on the disk surface, for a given grain volume yielding greater densities. Finally, the magnetic grains used in perpendicular media are able to achieve a very high degree of orientation [11]. This allows for very small transition lengths resulting in a better SNR for

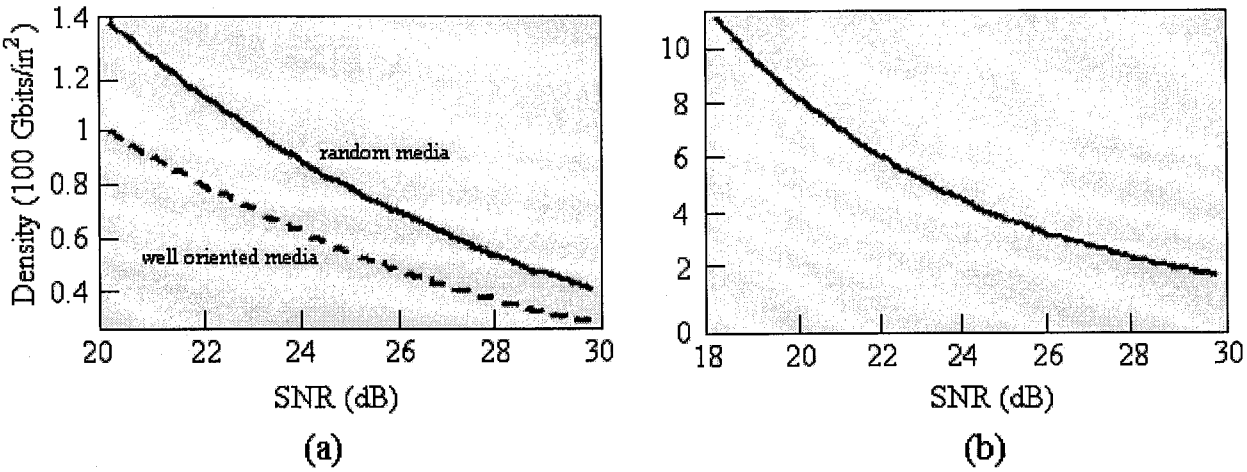

Figure 2.24 (a) Maximum areal bit density versus SNR for random (solid line) and well oriented (dashed line) longitudinal media with M_r = 245 KA/m and δ = 15 nm. **(b)** Maximum density versus SNR for perpendicular recording media for M_r = 350 KA/m and δ = 25 nm [44].

perpendicular recording as seen in figure 2.24. Fewer grains per bit will then be required. Simulations suggest as few as 10 grains per bit would be enough for perpendicular recording.

Perpendicular recording has the potential to continue the increasing trend of areal bit density in hard drives once longitudinal recording fully succumbs to the superparamagnetic effect. Hard drives with perpendicular recording are already making their way into the market. Later this year, Toshiba plans on releasing two hard drive models that will employ perpendicular recording [45]. They will be releasing two models with 1.8-inch drives to be used in Apple's iPod music player. The two models will be capable of storing 40 or 80 GB. The areal bit density of both models is said to be 133 Gbits/in^2 which is 37% greater than current drives. Perpendicular recording will not stop at this mark. An areal bit density of 170 Gbits/in^2 was achieved successfully in the lab with perpendicular recording using a granular CoCrPt-SiO_2 media [46]. Also, areal bit densities of 300 to 500 Gbits/in^2 using perpendicular recording are being investigated with micromagnetic simulations.

2.5.3 Patterned Magnetic Media

In all present day hard drives, magnetic recording, whether it is longitudinal or perpendicular, is accomplished on a continuous magnetic media. The term bit area was used to define divisions on a hard drive disk, but these are not physical divisions. A bit area is

magnetically defined during the write process. In continuous magnetic media, a bit must contain a certain number of thermally stable magnetic grains to decrease transition noise. Currently, high areal bit density and low noise are achieved by decreasing the magnetic grain size as the bit size decreases. However, with grain size approaching the superparamagnetic limit, increasing areal bit density while using longitudinal recording on continuous magnetic media becomes difficult. Therefore, new forms of technology are being implemented such as AFC media and perpendicular recording. AFC media is believed to have the capability to advance longitudinal recording past the 100 Gbits/in^2 mark. With perpendicular recording, an areal bit density of 1 Tbit/in^2 is believed to be possible. However, both of these technologies are still used in conjunction with continuous magnetic media.

Using a continuous magnetic media surface will eventually limit the achievable areal bit density because a certain number of magnetic grains will always be needed to prevent transition noise. Patterned magnetic media will be the solution to this and also other problems. The technology will address SNR problems, switching speed, and thermal decay; however it will not be without several challenges. Patterned magnetic media is a technology that utilizes discrete magnetic islands separated by non-magnetic material. Each island represents a single bit that can contain any number of magnetic grains or theoretically just one. A graphical representation of patterned media is seen in figure 2.25. The bits are predefined lithographically instead of being defined during the write process. The magnetic islands can be fabricated in thin-films having either longitudinal or perpendicular anisotropy allowing the option of implementing longitudinal or perpendicular magnetic recording.

One major advantage of patterned magnetic media is that it will provide a better SNR than conventional continuous magnetic media. Transition noise is a large problem in continuous media. It is created when the transition between two bits is comparable to the bit size. This is caused by exchange coupled magnetic grains or the grain size being too large. With patterned media this is eliminated because each bit cell is isolated by non-magnetic material. A grain from one bit is unable to be exchange coupled to a grain from another bit because the distance is too great. However, if bit packing does become dense resulting in too small of a non-magnetic spacing between bits, magnetostatic interactions between bits will occur [11].

The use of patterned media will allow the superparamagnetic limit to be pushed back even further than simply perpendicular magnetic recording. In conventional longitudinal

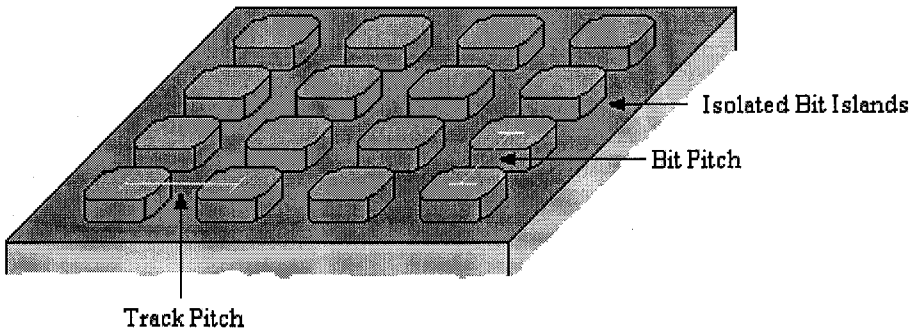

Figure 2.25 A graphical illustration of patterned magnetic media where the raised ovals are the magnetic islands representing bits.

recording the superparamagnetic limit is encountered at densities between 40 to 70 Gbits/in^2. At these densities, the grain size has reached its ultimate limit before thermal energy creates instability. As mentioned, it takes approximately 100 grains to compose a bit. Patterned media has the potential to need only one grain per bit. If only the superparamagnetic limit is considered, patterned media could achieve densities 100 times greater than 40 to 70 Gbits/in^2. It has been calculated that a 10 by 26 nm bit area with a bit pitch distance of 16 nm and a track pitch distance of 40 nm could yield an areal bit density of 1 Tbit/in^2 [11]. If it was assumed that a bit was pushed to the superparamagnetic limit of a magnetic grain and the pitch between bits was decreased, areal bit densities greater than 1 Tbit/in^2 could be achieved. The limit of patterned media will be constrained by patterning defects, SNR, head design, and servo requirements.

Creating patterned magnetic media for magnetic recording is not without its challenges. One of the main challenges for patterned media is synchronization. In an array of nanostructured magnetic islands, the write pulse has to be synchronized to the media pattern in frequency and in position [47]. If it is not, specified bits will never be written to or read from. There are a number of other technology and also system issues that need to be addressed before patterned media will become practical. One in particular is tribological requirements. How will a read/write head be able to fly over a non-planar surface?

The primary challenge in creating patterned magnetic media is finding a low-cost, high throughput pattern generation technology. That will be the main focal point of the rest of this thesis. One thermally stable and isolated grain per bit which patterned magnetic media offers is better than 10 partially stable grains which continuous media with perpendicular recording

offers. However, because patterned media is lithographically defined, it involves greater complexity and cost to create it than continuous magnetic media. Therefore, an efficient method for creating patterned media needs to be developed. The proposed concepts include laser interference lithography, self-assembly patterning, and nanoimprint lithography. These pattern generation methods will be discussed and compared in the next chapter.

2.6 Conclusion

In order to increase areal bit density, the bit size has to be decreased. As it was shown throughout this chapter, decreasing the bit size affects the read sensor, write head, and magnetic media. These components of the hard drive are scaled down as the bit size is reduced; however, at certain points simple scaling is not enough to increase areal bit density, and new technologies need to be developed. This was the case with read sensors. The magnetic field generated from bits in the media became too small for older technologies to detect. Higher sensitivity detection was first found with MR read sensors and then GMR spin valve read sensors. Write heads have less stringent requirements than read sensors do when attempting to achieve greater densities. The size of a bit is defined during the write process. Therefore, the dimensions of the write head are scaled down to decrease the bit size. The strength of the head field diminished in doing this so materials with greater magnetic moments are used for compensation. Finally, the magnetic grains of the media are decreased with the bit size so that a statistical minimum of grains is seen in each bit to promote a readable SNR.

Through all the scaling and development of new technologies for certain components, the primary form of recording technology has remained the same. All present-day hard drives employ longitudinal magnetic recording on a continuous magnetic media. Eventually, this type of technology will no longer be feasible because it will become vulnerable to the superparamagnetic effect. Longitudinal recording on a continuous magnetic media requires approximately 100 magnetic grains per bit. As the magnetic grain size decreases with the bit size and approaches 10 nm in diameter, the grains are no longer thermally stable. The grains become superparamagnetic resulting in spontaneous magnetization reversal and dynamic coercivity. These effects severely reduce the lifetime of the hard drive. It was originally estimated that the superparamagnetic effect would limit areal bit density to somewhere around

40 to 70 Gbits/in^2 in longitudinal magnetic recording. Engineers were able to avoid this with the implementation of AFC media. It creates a more thermally stable magnetic media and is believed to allow longitudinal recording to reach an areal bit density of 100 Gbits/in^2.

A new technology will soon be needed. The limit of longitudinal magnetic recording on a continuous magnetic media will soon be reached. Perpendicular recording has been proposed and is entering the market within the year; however, it is still done on a continuous magnetic media. Therefore, it still needs a certain number of thermally stable magnetic grains to achieve a readable SNR. Patterned magnetic media is a proposed technology that only needs a single magnetic grain to function. It has the ability to achieve grater areal bit densities than all other types of technology. If only the superparamagnetic limit is considered, patterned magnetic media could achieve areal bit densities beyond 1 Tbit/in^2. The technology is not without its challenges. Certainly creating lithographically defined bits is more complicated and costly than current continuous thin-film magnetic media production. However, there are several methods to generate patterned magnetic media.

3 SURVEY OF TECHNOLOGIES CAPABLE OF FABRICATING PATTERNED MAGNETIC MEDIA

The major challenge facing the development of patterned magnetic media today is finding a low-cost, high-throughput pattern generation technology. Patterned magnetic media can be created in the laboratory on a small scale; however, the goal is to eventually move it towards large scale production. To accomplish this, the pattern generation technology needs to be a high throughput method. Most high throughput methods are usually parallel in nature. A parallel process can cover a greater amount of area in a shorter amount of time. The more that can be done in shorter increments of time, the more cost effective it will be. It is a necessity for the generation of patterned magnetic media to be economical if it is going to be the next generation technology in hard drives. If patterned magnetic media is not able to be economically fabricated, its potential to greatly extend areal bit densities will not matter at all. This is common to all emerging technologies. Something may work in the lab, but if mass fabrication is not possible or too costly it will not have much of a future.

The pattern generation technology has to also provide high resolution, densely packed features over a relatively large area. The large area that requires patterning is another reason why a parallel process is needed. The standard desktop hard drive has a disk diameter of 3.5 inches. In terms of lithographic and nanogeneration technologies this is an extremely large area to cover. Any type of serial process would take too much time and hence money to cover this area. Finally, the resolution and density capability need to be very high so that greater areal bit densities can be achieved. If 50 nm diameter features representing bits are created with a pitch, the distance from the center of one feature to that of another, of 100 nm, an areal bit density of only 64.5 Gbits/in^2 would be observed. Patterned magnetic media has the potential to increase areal bit densities into the terabit per square inch regime if sub 20 nm resolution and density can be achieved.

None of the proposed requirements for pattern generation technology to fabricate patterned magnetic media are trivial. The resolution and density that is needed over such a large area is extremely challenging and difficult to make cost-effective. Since the semiconductor industry is mass producing products for commercial use with dimensions comparable to that needed by patterned magnetic media, it can be used as a reference point. Photolithography is

used to manufacture the transistors and various other elements on a microprocessor. Photolithography is a projection method in which a beam of light is passed through a shadow mask exposing a pattern on a photosensitive resist. Presently, the critical dimension that Intel's photolithography process is capable of yielding is 50 nm [9]. Intel plans on decreasing this critical dimension by an upgrade known as extreme ultraviolet (EUV) lithography. However, photolithography's capability of producing larger area patterns is going to remain relatively unchanged. As of now this area is approximately 250 mm^2. The P4 Prescott and extreme edition processors have die sizes of 112 and 237 mm^2 respectively. Even the die area of the larger process is 22 times less than what will be needed for a hard drive platter. While photolithography is capable of producing nanoscale features, it appears that it is not feasible over a large area. A step and repeat technique could be used, but then a problem with registration would arise.

Since photolithography is not capable of producing patterned magnetic media over a large area, attention needs to be directed towards other known lithographic and nanogeneration technologies. Two other known technologies are electron-beam and X-ray lithography. Electron-beam lithography uses irradiation from a focused beam of electrons to expose an electron sensitive resist. It has the capability of producing sub-20 nm closely, spaced features; however, because it is a serial method, it becomes too time consuming. It would not be a cost-effective method to fabricate patterned magnetic media because of the time it would take to pattern the required large areas. There is a derivative of electron-beam lithography developed by Bell Labs that is referred to as scattering with angular limitation in projection electron-beam lithography (SCALPEL) [48]. It is aimed towards providing not only high resolution, but also the throughput of a projection system. However, the areal capability of this system is only comparable to that of a photolithography system and not what is needed for patterned magnetic media. X-ray lithography is the exposure of a resist to X-ray radiation in a parallel process. It has some potential for fabricating patterned magnetic media. Magnetic dots have been fabricated with a diameter of 88 nm and separation of 100 nm over a 5 mm x 5 mm area using the technique [49]. However, the equipment that is required for it is extremely expensive and hard to fabricate. Therefore, a discussion of it in this chapter will be left out. An explanation of the technology can be found in *The Handbook of Microlithography, Micromachining, and Microfabrication* [50].

This chapter will contain a survey of the pattern generation technologies that are being most actively pursued as a means of fabricating patterned magnetic media. These methods include interference lithography (IL), self-assembly pattering, and nanoimprint lithography (NIL). Each of these methods is a parallel process capable of producing large area, high resolution, and densely packed features. Some of them have greater capabilities than others in certain areas. Interference lithography, nanoimprint lithography, and selected self-assembly systems replicate nanoscale patterns in a resist. The patterns in the resist can then be transferred to the substrate by way of an etching or a liftoff process. Selected self-assembly systems are able to directly create a nanoscale pattern of magnetic media on certain substrates. Overall, the three methods do not require relatively elaborate and expensive equipment. Furthermore, despite several obstacles that each faces, they all show a potential for fulfilling the requirements needed to mass manufacture patterned magnetic media

3.1 Interference Lithography

Interference lithography is based on the process of selectively exposing a layer of photoresist to create certain patterns. In this sense, it is similar to photolithography and X-ray lithography. However, it does not use any type of mask to generate the pattern. Instead, the interference of two coherent laser beams is used to expose the photoresist in a variety of patterns. The technology has been around since the invention of the laser beam in the late 1960's. It is now attracting more attention for a wide variety of applications; one of which includes creating patterned magnetic media. Its ability to pattern large areas makes it a favorable tool for creating patterned magnetic media for hard drives.

Interference lithography utilizes the interference of two coherent laser beams to expose a layer of photoresist. In order to observe sustained interference in light waves, the sources must be coherent and monochromatic. Coherent sources maintain a constant phase with respect to each other. Monochromatic sources possess the same wavelength. Interference cannot be observed by placing two ordinary light bulbs next to each other because the light waves emitted from both bulbs are not coherent and not monochromatic. The light waves from each bulb undergo phase changes about once every 10^{-8}s; therefore, the interference only lasts for times on the order of 10^{-8}s. In order to produce two coherent light sources, a single laser can be split into

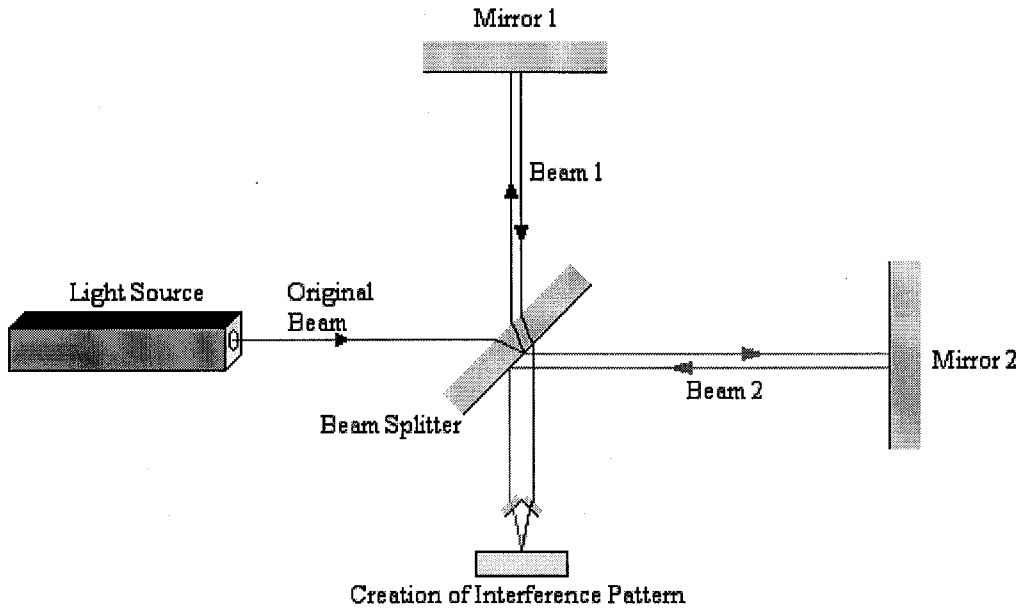

Figure 3.1 An schematic of the original interferometer invented by Michelson.

two beams. The resulting two beams are coherent because they are formed from a single laser beam.

3.1.1 Principle of Interference Lithography

The initial idea of splitting a monochromatic light source into two beams and then recombining them to form an interference pattern was developed by A. A. Michelson. He invented the interferometer in an attempt to prove the theory of relativity. An interferometer basically splits a single beam of monochromatic light into two parts and then recombines the parts to form an interference pattern. It was originally used to measure wavelengths or distances with nanometer resolution [51]. The concept can also be used in the case of interference lithography to expose and pattern a layer of photoresist.

A schematic of an interferometer is shown in figure 3.1. A beam of light from a monochromatic laser source is split into two beams by the half-silvered mirror. Half of the light is transmitted to the mirror on the right, and the other half is reflected to the top mirror. After reflecting off of their respective mirrors, the two beams of light recombine to produce an interference pattern. If the two beams differ by a whole number of wavelengths, constructive

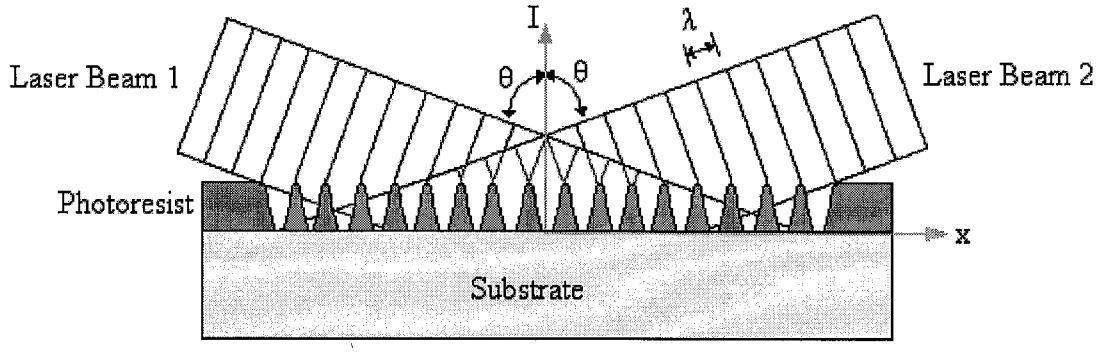

Figure 3.2 A cross sectional illustration of two intersecting laser beams creating a standing wave. The wave exposes the photoresist creating the observed patterned region.

interference is observed. If the beams differ by a whole number and half a wavelength, (i.e. 1.5, 2.5, etc.) destructive interference is observed.

The principle that the interferometer employs is what basic interference lithography operates on. A single monochromatic laser source is split into two coherent beams. The beams are then redirected and illuminate the layer of photoresist on the substrate from opposite directions forming an oblique angle, 2θ. The interference of two laser beams at an oblique incident angle on a layer of photoresist is seen in figure 3.2. The procedure creates a standing wave with a periodic interference pattern of sinusoidal intensity. This pattern is then recorded in the photoresist in a certain manner depending on whether the resist is positive or negative. The pitch of the pattern can be adjusted by either the wavelength of the light or the angle with which the two beams intersect. The equation describing this relation is

$$p = \frac{\lambda}{2} * \sin(\theta) \tag{3.1}$$

where p is the period of the standing wave produced, λ is the wavelength of the light, and θ is half of the angle with which the two beams intersect. The period of the standing wave is approximately equal to the pitch of the pattern formed in the photoresist. When the standing wave is discussed, the term period will be used, and the term pitch will be used when the pattern is discussed. This procedure produces a pattern of parallel lines [49]. More complex patterns can be achieved with successive exposures. Essentially, any pattern that can be formed by intersecting lines can be fabricated. For example, a second exposure after rotating the sample by

90° produces a square array of dots. After the pattern is generated in the photoresist, it can then be transferred to the substrate or used as a template to deposit magnetic materials in order to create patterned magnetic media. A number of post processing techniques such as etching or deposition could be used for this. A detailed explanation of post processing is provided in section 3.3.5.

Interference lithography has certain limitations. The area of the generated pattern is only as large as the diameter of the laser being used. Furthermore, the pitch of the diffraction pattern created in the photoresist is limited to half of the wavelength of the light source that is being used. For example, an Ar laser with a wavelength of 351.1 nm is not capable of generating patterns in the photoresist with pitches smaller than 175 nm. To obtain smaller pitches, lasers with shorter wavelengths are needed. However, there is a problem with using lasers that have extremely short wavelengths. Lasers with very short wavelengths experience poor temporal and spatial coherence [52]. They are not suitable for interference lithography. This usually limits pitches and features sizes above 100 nm using lasers with ultraviolet (UV) wavelengths.

3.1.2 Anti-Reflective Coating

Besides the limitations that were just mentioned, interference lithography has another problem. It not only produces a standing wave that exposes a desired pattern in the photoresist, but also produces a secondary standing wave that is perpendicular to the substrate. This secondary standing wave is produced from the vertical components of the incident light and the light reflected from the photoresist. The period of this vertical standing wave is dependent on the index of refraction in addition to all of the same factors that determine the period of the primary wave. The period of the vertical standing wave is given by

$$p = \frac{\lambda}{2n\cos(\theta)} \tag{3.2}$$

where n is the index of refraction. The index of refraction is the speed of light in a vacuum divided by the speed of light in a specified medium.

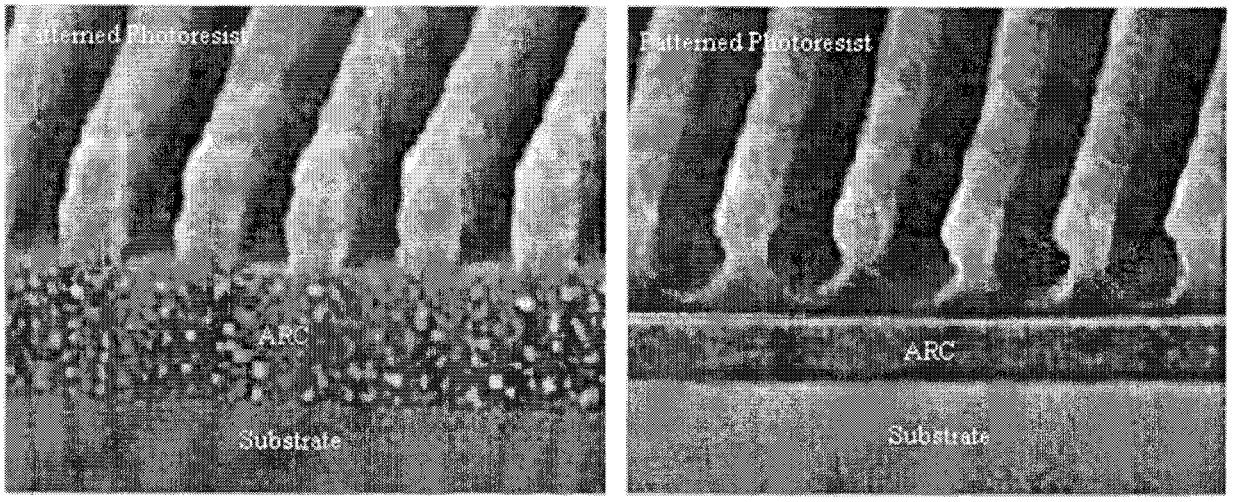

Figure 3.3 A cross sectional view of patterned photoresist created from interference lithography **(a)** with vertical sidewalls due to the elimination of the vertical standing wave and **(b)** non-vertical sidewalls due to the presence of the vertical standing wave [53].

The vertical standing wave that is produced has unwanted effects. It degrades the pattern that is transferred into the photoresist. It does this by attacking the base of the sidewalls in a periodic manner. These effects can be seen by comparing the images in figure 3.3. In figure 3.3 (a), the vertical standing wave has been suppressed resulting in vertical sidewalls. The vertical standing wave in figure 3.3(b) has not been suppressed resulting in non-vertical sidewalls. This effect can weaken the structure enough to collapse during the development process or even worse cut through the bottom section causing the top layer to collapse during exposure.

The effects of the vertical standing wave can be eliminated by using what is known as an anti-reflective coating (ARC). An ARC reduces the effects of the vertical standing wave through a combination of absorption of the wave and cancellation through interference. A coating with the thickness of a quarter of the wavelength can eliminate the reflection of one particular wavelength. If the coating is a quarter of the incident wavelength thick, the two reflections will be 180° out of phase and cancel each other out. The coating is applied between the photoresist and the substrate. Sometimes the index of refraction and absorption properties become the main determining factors of selecting the proper ARC. Other factors become overlooked resulting in undesired effects. Therefore, it is believed that the best method for selecting an ARC is based on the processing that will be done after the lithography is completed [53]. Depending on the post processing, a thin ARC might be more favorable than a think ARC or vice versa. Thin ARCs

reduce the effects of the vertical standing wave more through the interference of the waves. On the other hand, thick ARCs operate by absorbing the light waves. The result of selecting the proper ARC can be seen in figure 3.3. In figure 3.3(a), the ARC was the right thickness resulting in vertical sidewalls. In figure 3.3(b), the thickness of the ARC was not enough to absorb the vertical standing wave resulting in deteriorated sidewalls.

3.1.3 Interference Lithography Systems

The Nanostructures laboratory at MIT has been leading the way in interference lithography research and implementation for the past 30 years. It currently operates four interference lithography systems that are designed for a wide range of applications. The one system that it operates in conjunction with the Space Nanotechnology laboratory is a basic interference lithography scheme shown in figure 3.4. The laser source is located at the top of the schematic where the beam is sent into a primary beamsplitter and divided. The emphasis of the design is the beamsplitter at the bottom of the schematic that directs the two interfering beams to photodiodes. The signals produced from the photodiode are differentially amplified and then used to adjust the Pockels cell which phase shifts one of the beams creating a feedback loop [54]. Hence, the system can be controlled to stabilize the pattern phase eliminating unwanted interferences. The system is specially designed to provide stability and repeatability. It has the capability to produce patterns up to 10 cm in diameter with pitches as small as 200 nm.

Several other interference lithography systems besides the one seen in figure 3.4 have been created to yield fewer errors. One type of system similar to the one in figure 3.4 utilizes a 325 nm wavelength helium-cadmium (HeCd) laser. It also employs a method known as holographic phase shifting interferometry (HPSI). This method is able to measure and map with an extremely high accuracy the linearity and spatial phase of patterns that are produced. The purpose of doing this is to reduce the distortions that create pitch variations.

A more effective method for producing high quality patterns is being researched. It is known as scanning beam interference lithography (SBIL). The two interference lithography systems just described require large diameter laser beams to produce large patterns. Defects in the manufacturing of the optical components can produce errors in the pattern. SBIL uses Gaussian beams that are much smaller than conventional interference lithography systems [55].

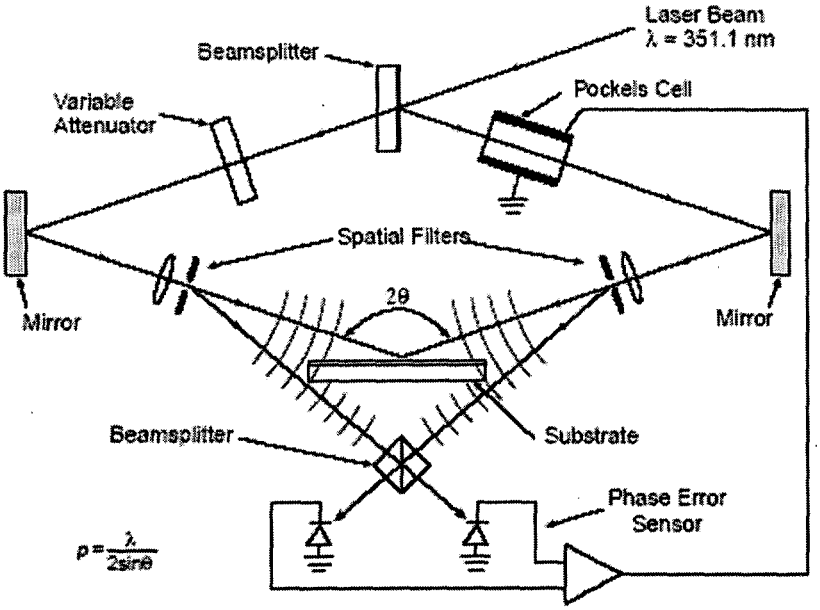

Figure 3.4 A schematic of the conventional interference lithography system that is operated in the Nanostructures Laboratory at MIT [54].

Therefore, a high degree of phase with fewer errors can be achieved since the beam is only passing through a small portion of the lens. The interference pattern created is much smaller than the substrate so to compensate the substrate is scanned under the pattern using a high performance stage with an interferometer as seen in figure 3.5. With this setup two interferometers are used. There is the stage interferometer which uses a 632.8 nm wavelength helium-neon (HeNe) laser beam to determine and control the stage position. The other interferometer uses a 351.1 nm wavelength argon-ion laser to create the interference pattern.

None of the interference lithography systems that were mentioned so far are used for creating patterned magnetic media. The first two methods are unable to vary the period without complex setup changes that take several weeks. Without being able to vary the period, different feature sizes are unable to be created. The SBIL method is not feasible because it is still in the developmental stages. The two methods of interference lithography that are used to create patterned magnetic media are the Lloyds-mirror interferometer setup and achromatic interferometric lithography (AIL).

With the Lloyds-mirror interferometer, a single light source is used with a mirror placed perpendicular to the substrate. This configuration can be seen in figure 3.6(a). The Lloyds-mirror creates an image of a second light source that is spatially separated from the original light

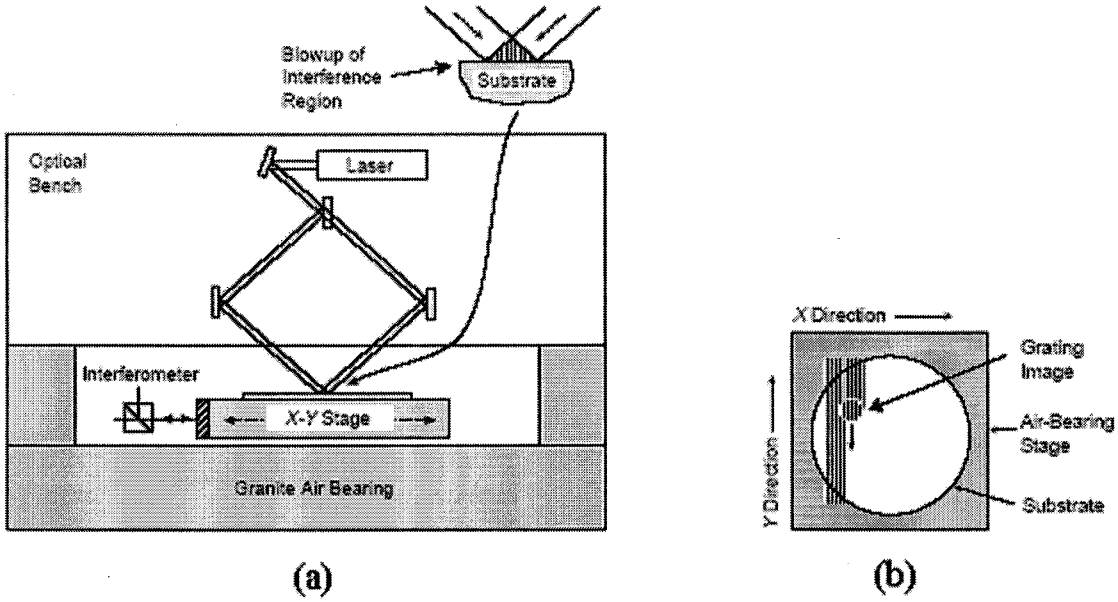

Figure 3.5 Schematic of **(a)** scanning beam interference lithography system and **(b)** top down view of the scanning process to produce a large interference pattern [55].

source. The boundaries of the mirror will receive light directly from the original source and the created source. This produces two beams of light that will intersect to form an interference pattern. The primary advantage of the Lloyds-mirror is that the pitch of the patterns can be varied from several microns down to 170 nm if a 325 nm wavelength laser is used. To change the pitch of the pattern, the substrate is simply rotated about its center point. This can be done with high accuracy and without readjusting the optical pathway. Therefore, a single pattern can have varying degrees of periodicities. This is favorable for patterned magnetic media because to create longitudinal or perpendicular anisotropy, the bit islands have to be certain shapes.

The Lloyds-mirror interferometer is not capable of producing pitches much smaller than 170 nm. This is because the wavelength of the laser used is 325 nm. If all other factors are ignored, this method would not be able to produce an areal bit density greater than approximately 25 Gbits/in^2. While the Lloyds-mirror interferometer has the capability to produce patterns over large regions, it is not able to produce pitches on the order of 100 nm or less. It might seem obvious to use lasers with shorter wavelengths than 325 nm, but as previously mentioned lasers with wavelengths needed for a pitch of 100 nm experience poor temporal and spatial coherence.

There is a solution to this coherence problem. A system known as achromatic interference lithography can be used. To obtain pitches on the order of 100 nm, a 193 nm

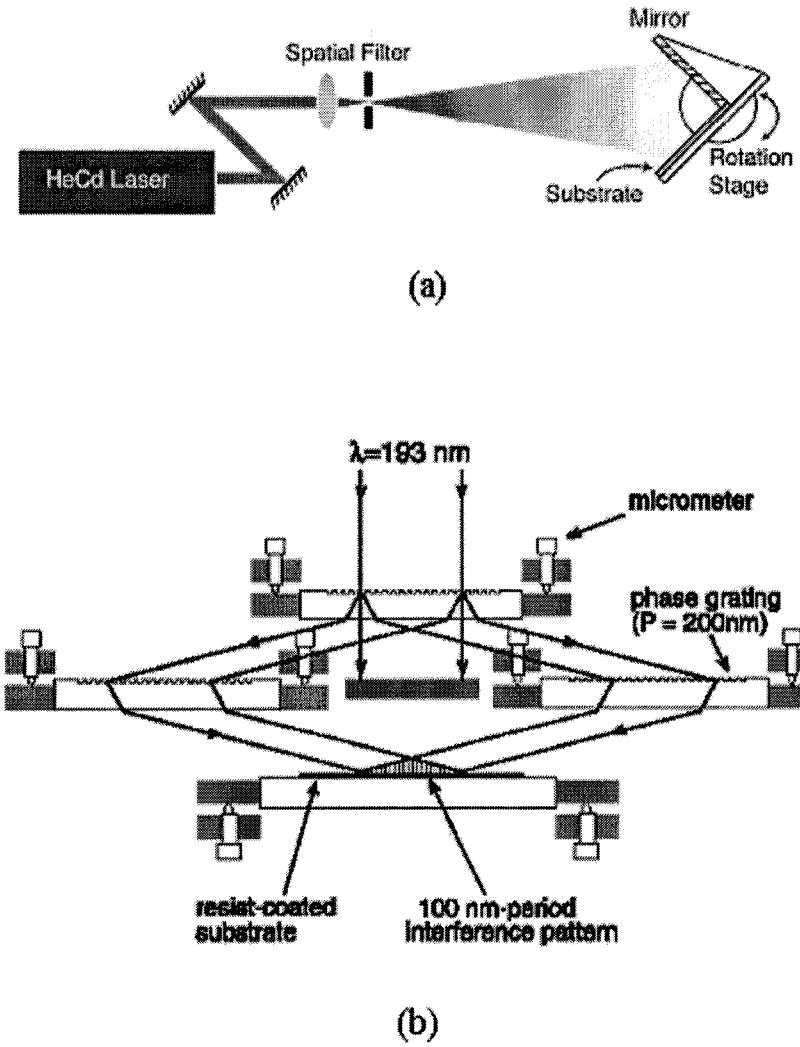

Figure 3.6 Schematics of different interference lithography methods used to create patterned magnetic media. **(a)** Lloyds-mirror interferometer. **(b)** Achromatic interference lithography [54].

wavelength argon-fluorine (ArF) excimer laser is used. To negate the limited temporal and spatial coherence of this source, the AIL setup seen in figure 3.6(b) is implemented. With this method, the pitch of the pattern is only dependent on the phase gratings seen in the center of the setup. The wavelength and coherence of the source is no longer a factor then. Therefore, repeatable results can be obtained. A 100 nm pitch pattern with features smaller than 30 nm has been produced with AIL and successive processing steps [54]. Producing smaller pitched patterns is more complicated because of the limited availability of sources with wavelengths smaller than 100 nm. Also most materials exhibit poor optical properties when exposed to wavelengths below 100 nm.

3.1.4 An Assessment of Interference Lithography

Interference lithography has several favorable qualities which make it a viable method for creating patterned magnetic media. Its ability to create patterned regions over large areas in a short amount of time make it one of the leading technologies for creating patterned magnetic media. It has been reported that a 250 mm x 250 mm region of patterned magnetic media has been created using interference lithography [49]. It is a parallel type process; therefore, it is relatively fast. Fast processing translates into a low-cost fabrication technique. Besides just creating large regions, interference lithography has shown the capability to produce features approximately 30 nm in size. All of these qualities are favorable because to create patterned magnetic media for hard drives, at least a 3.5-inch diameter disk needs to be patterned with nano-sized features at a low-cost. Interference lithography is an efficient and fast method to pattern a large area with nanoscale features.

Despite the advantages that interference lithography has for creating patterned magnetic media, there are also obstacles that hinder it. It can efficiently produce nanoscale features over a large area; however, producing densely packed features is difficult. The pitch of the pattern created by interference lithography is limited to half of the wavelength of the laser being used. To compensate, lasers with shorter wavelengths can be used; however, there are two problems that are presented in doing this. Lasers with wavelengths below 200 nm experience poor temporal and spatial coherence. This problem has been partially solved by passing the laser beam through a grating that negates its dependence on the wavelength and coherence. The second problem is that the optical properties of materials are extremely poor below 100 nm. Therefore, even if the laser beam is coherent, it will not properly pass through optical lenses if the wavelength is too short.

Interference lithography is also hindered by two other factors. The first is more of a nuisance than an obstacle. As mentioned earlier, an anti-reflective coating is often required between the photoresist and substrate to reduce sidewall destruction from the vertical standing wave. This makes post processing more complicated and in some cases even too complicated to use the anti-reflective coating [56]. The last downside to interference lithography is most likely its biggest hindrance. Interference lithography is a periodic pattern generation technology. The structures that it creates are limited to only interference patterns which are highly symmetric. It

is very difficult to incorporate non-regular, non-periodic patterns using interference lithography. These types of patterns are required for tracking and sectoring information for hard drives. While interference lithography appears to have the potential for efficiently creating patterned magnetic media over large areas, it does have several obstacles to overcome.

3.2 Self-Assembly Patterning

Sometimes maybe the best approach to construct something is to not. Simply let nature do the work instead. This is the case with self-assembly. It is an atomically precise parallel fabrication process where an ordered structure is created through the spontaneous organization of certain elements. Components of self-assembled structures find their appropriate locations based on their physical or chemical properties. A self-assembly process can also be guided with external forces and geometrical constraints. The structure formed is the most thermodynamically stable state of the original components. One needs to look no further than him or herself to see the awesome power of self-assembly. Living organisms which are orders of magnitude more complex than any man made structure are continuously and effortlessly being self-assembled.

Self-assembly has become a critical tool in the field of nanotechnology. Scientists and engineers are trying to harness the power of self-assembly for a wide variety of applications. Currently, one the most promising paths of self-assembly is that based on self-assembled monolayers (SAM). The development of self-assembled monolayers and their ability to modify the physical and chemical properties of a surface has been a major area of self-assembly. Self-assembled monolayers are seen in applications such as molecular and bimolecular recognition, sensing and electrode modification, and corrosion prevention. Other self-assembled systems include nanocrystals, heterogeneous nucleation and block copolymers. All of these systems have also recently been drawing attention as a means of creating nanoscale patterns used in microelectronic devices. Patterns created are smaller, denser, more precise, and more uniform than can be achieved with conventional lithography. The ability of self-assembly to create nanoscale features over a large area also makes it a viable candidate for creating patterned magnetic media.

3.2.1 Physical and Molecular Self-Assembly

The self-assembly process can be categorized as either physical or chemical. Physical self-assembly is a process that is driven to produce structures through entropy considerations and reaching a thermodynamically stable state. With microelectronics, physical self-assembly is usually carried out during deposition processes such as molecular beam epitaxy (MBE) or chemical vapor deposition (CVD) [57]. Chemical self-assembly is the complementary binding and molecular recognition of organic molecules and supramolecules [58]. It is often referred to as molecular self-assembly, and is thought of as an extremely advanced chemical reaction. Both self-assembly categories are powerful nanotechnology tools because of their parallel nature and atomic precision. Furthermore, their ability for creating structures on any number of scales make them powerful bottom up techniques.

Protein folding and the pairing of base pairs in DNA are just two common examples of molecular self-assembly that occur naturally. There are hundreds of other examples of molecular self-assembly that take place in nature. These examples that exist throughout nature provide the basic principles of not only molecular, but also physical self-assembly. These principles are then used as a guide to help produce the desired nanostructures in the laboratory. There are five basic principles of molecular self-assembly as outlined by Gregory Timp in his Nanotechnology text [59]. First, molecular self-assembly takes advantage of non-covalent interactions to assemble individual molecular pieces into stable structures. These interactions are ionic bonding, hydrogen bonding, and van der Waals forces.

The following three non-covalent interactions are weaker than covalent bonds, but still have strong enough effects to influence molecular self-assembly. The first type of interaction which is the strongest out of the three is ionic bonding. This is the force of attraction between oppositely charged ions such as Na^+ and Cl^- in water. The next two interactions are considered intermolecular forces whereas ionic bonding is considered a type of bonding. Hydrogen bonds are a strong type of dipole-dipole intermolecular force. They are seen among polar molecules in which hydrogen is bound to highly electronegative atoms such as nitrogen, oxygen, and fluorine. The strength of hydrogen bonds usually influences the boiling point of a material. For example, H_2O has a stronger hydrogen bond than HF resulting in a boiling point 80°C higher. Van der Waals forces are associated with non-polar structures. These forces are derived from certain

atoms having a tendency to develop momentary non-symmetrical electron distributions. This produces an instantaneous, temporary dipolar arrangement of charge that can induce a similar dipole in a neighboring atom. The attraction is usually not strong and does not last too long, but can be significant in larger atoms.

The final principles of molecular self-assembly deal with the final structure and base components that are being used to assemble it. The final structure produced by molecular self-assembly is the most thermodynamically stable. This means that the structure will have a minimal amount of defects. The final structure is predetermined by the properties of the base components. The information for self-assembly is embedded in the base components. Therefore, to modify the final structure, the base components properties need to be altered. The number of different base components used in self-assembly is usually small in order to simplify the information needed to determine the final structure. Finally, to add more simplicity, the base components are small and can be easily synthesized. The principles that govern molecular self-assembly also loosely apply to physical self-assembly. Physical self-assembly relies on non-covalent interactions to produce a thermodynamically stable final structure.

3.2.2 Self-Assembled Monolayers

There are several different types of physical and molecular self-assembling systems which are capable of creating patterned magnetic media. The most well-researched molecular self-assembling system is a self-assembled monolayer (SAM). This is a system which does not occur naturally, but can only be reproduced in a laboratory. SAMs are organic molecules that spontaneously form ordered structures on a compatible substrate surface. To create them, a substrate is immersed in a solution of a certain molecule and organic solvent. Commonly, they have a polar head that is adsorbed to the surface of the substrate and a nonpolar tail that forms the surface of the SAM [58]. It is possible to form a variety of different SAMs. Table 3.1 provides a list of different adsorbate molecules and the type of substrate surface that they self-assemble on. Alkanethiolates (R-SH) are the most prevalent adsorbate molecule. They form SAMs on metals such as gold, silver, copper, iron, platinum, and palladium as well as on certain semiconductors and oxides [61]. The molecular structure of an alkanethiolate molecule is seen

Table 3.1 Adsorbate molecules and the compatible surface substrates they form self-assembled monolayers on [60].

Surface	*Substrate*	*Adsorbate Molecule*
Metal	Au	R-SH, R-SS-R, R-S-R, $R-NH_2$, R-NC, R-Se, R-Te
Metal	Ag	R-COOH, R-SH
Metal	Pt	R-NC, R-SH
Metal	Pd	R-SH
Metal	Cu	R-SH
Metal	Hg	R-SH
Semiconductor	GaAs	R-SH
Semiconductor	InP	R-SH
Semiconductor	CdSe	R-SH
Semiconductor	ZnSe	R-SH
Oxide	Al_2O_3	R-COOH
Oxide	TiO_2	R-COOH, $R-PO_3H$
Oxide	ITO	R-COOH, R-SH, $R-Si(x)_3$
Oxide	SiO2	$R-Si(x)_3$

in figure 3.7(a). The head is composed of a sulfur atom, the body is made up a *n* CH_2 molecules, and the tail can be made of a number of functional groups such as CH_3.

The self-assembly of alkanethiolates on a gold substrate is the SAM that receives the most attention because of its favorable properties. This type of SAM has provided the foundation for more complex and functional nanoscale structures. SAMs with a high degree of structure can also be formed from sulfur based molecules. However, experiments have proven that alkanethiolate molecules are more efficient at self-assembly [60]. Alkanethiolates are more soluble than disulfides (R-SS-R) and sulfides (R-S-R). Once the molecules are adsorbed onto the surface of the substrate, they are stable, but can still be processed. This allows alkanethiolates to be more compatible with a wider variety of organic functional groups [59]. Alkanethiolate molecules form SAMs on gold 1000 times faster than disulfides. The gold substrate is used because of its chemical inertness. It does not form a surface oxide or strongly retain adsorbed components to it. Therefore, SAMs can be created under mild conditions.

The SAM structure formed by the adsorption of alkanethiolate molecules on gold substrates is crystalline in nature. The sulfur atoms of the alkanethiolate molecule tend to form a 30° angled structure on Au(111) as seen in figure 3.7(b). The sulfur atoms adsorb to the gold substrate in the middle of a cluster of three gold atoms. They do this in a hexagonal pattern as seen from a top down view and at a 30° angle as seen from a cross sectional view. The top

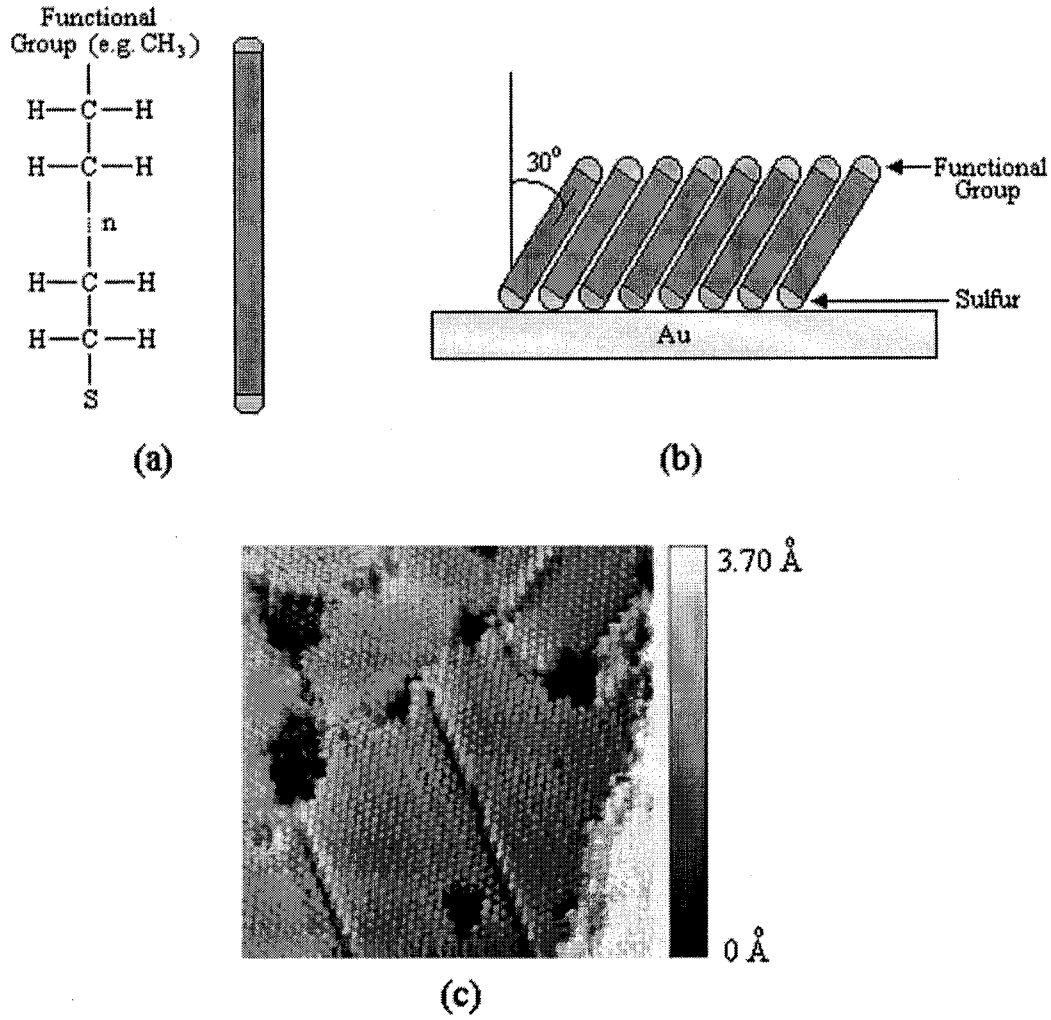

Figure 3.7 (a) Chemical structure of an alkanethiolate molecule. **(b)** A cross-sectional schematic of an alkanethiolate SAM adsorbing to a gold substrate. **(c)** An STM image of a 25 nm x 25 nm area of a decanethiolate SAM on gold [60].

down view of the hexagonal pattern of adsorbed decanethiolate molecules on a gold surface can be seen in the scanning tunneling microscope (STM) image in figure 3.7(c). The SAM of alkanethiolate on gold is formed primarily from the sulfur-gold bond that has a strength of approximately 44 kcal/mol and from the van der Waals forces between the alkyl chains that have a strength of approximately 2 kcal/mol [59]. The distance between the adjacent sulfur atoms is approximately 0.5 nm, and the alkyl chains extend out approximately 2 nm. The properties of the alkyl chains, otherwise known as the tail group of the SAM, can be easily altered to provide different surface properties [61]. For example, SAMs can be used to make surfaces hydrophobic or hydrophilic.

Even though alkanethiolate SAMs on gold are the most researched types, they are not suitable for patterning. Organosilane molecules assembled on silicon dioxide substrates are more favorable to patterning [60]. These SAMs adsorb differently to the substrate than alkanethiolates do to gold. The interaction between the head group and the substrate is stronger. Therefore, organosilane on silicon dioxide is more thermally stable which offers greater stability and robustness needed for patterning. For this reason, organosilane SAMs on silicon dioxide are used as photoresists. Patterning can then be done using energetic beams because of the stability of the SAM.

SAMs can be used as a special type of lithography resist to create patterns. They provide several advantages over normal resists [61]. First, they can provide an atomically precise thickness over a large area. They can also self-assemble on uneven substrate surfaces with areas in the range of several millimeters. They are compatible with a wide range of functional groups which allows for the control of surface properties. SAMs have been patterned using microcontact printing, dip-pen nanolithography, energetic beams such as electron-beams, electrochemical desorption, and STM assisted desorption [60]. The patterning method that conforms well to creating patterned magnetic media is microcontact printing. It is a fast, parallel process that can provide approximately 30 nm features over an area in the centimeter regime. Microcontact printing is a simple method for patterning a monolayer surface. A poly (dimethylsiloxane) PDMS stamp coated with molecules is brought into close contact with the substrate. The molecules from the stamp are transferred to the substrate recreating the pattern. There are some post-processing techniques such as wet-etching that can be utilized to create patterned magnetic media. Most SAMs do not have the durability to be used as masks for reactive ion etching (RIE). However, they can be used to deposit a metal or oxide on top of. A liftoff can then be performed.

3.2.3 Self-Assembly of Nanocrystals

Self-assembly of nanocrystals has not been heavily considered as a means of fabricating patterned magnetic media. However, this self-assembly process has shown the potential to fabricate high coercivity magnetic media that could significantly increase areal bit density.

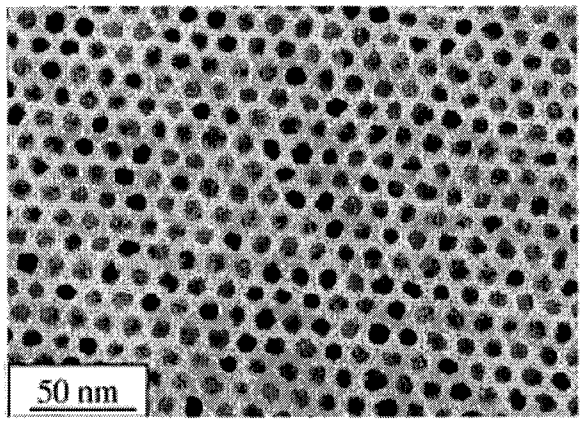

Figure 3.8 A self-assembled hexagonal array of circular FePt nanocrystals [62].

Therefore, it seems relevant to mention it in this section. By controlling the surface chemistry of nanocrystals, they will self-assemble to form ordered two or three-dimensional structures. Different sizes and shapes can be achieved such as circles, rods, teardrops and tetradrops [61]. Van der Waals forces is the interaction that is primarily responsible for controlling the self-assembly of the nanocrystals.

The self-assembly of FePt nanocrystals has been under investigation as a path towards higher areal bit density data storage in hard drives. FePt nanocrystals can be fabricated by reducing $Pt(acac)_2$ and the thermal decomposition of $Fe(CO)_5$ in the presence of oleic acid and oleyl amine [62]. The nanocrystals are then mixed in a solvent which is placed on the substrate. The self-assembly of the FePt nanocrystals occurs during the evaporation of the solvent. A hexagonal array of self-assembled FePt nanocrystals can be seen in figure 3.8. The crystals are shaped like dots and are approximately 6 nm in diameter. It can be seen that there is an extremely narrow size distribution. It was pointed out in the last chapter that a narrow size distribution is favorable for magnetic media grains because it reduces the emergence of thermal effects and enhances SNR. The diameter of the crystals can be varied from 3 to 10 nm depending upon the process conditions. After the crystals assemble, they are annealed to the ferromagnetic $L1_0$ phase. The coercivity increases with the amount of annealing time.

After the magnetic FePt nanocrystals are thermally annealed, they exhibit a phase transformation. They form the ordered $L1_0$ phase which is face-centered tetragonal. The $L1_0$ phase of FePt nanoparticles exhibits a high magnetic anisotropy and coercivity. These are two favorable qualities needed for high areal bit density data storage in hard drives. Ultimately, it

could be possible to store a single bit on each of the nanocrystals seen in figure 3.8. If that were the case then the self-assembly of nanocrystals could be a viable source for fabricating patterned magnetic media. As of now though, it is difficult to achieve a long-range ordered assembly of nanocrystals. This is needed to achieve the goal of one bit per nanocrystal. Therefore, it could be some time before the self-assembly of nanocrystals could be used to create patterned magnetic media.

3.2.4 Self-Assembly through Heterogeneous Nucleation

Heterogeneous nucleation of magnetic islands is a self-assembly system that is similar to the self-assembly of nanocrystals in that the patterned magnetic media can be formed directly on the substrate. This is opposed to SAMs and block copolymers that create a pattern in a resist material that can be transferred to the substrate. The difference between heterogeneous nucleation and the self-assembly of nanocrystals is that the latter is a chemical synthesis process. Also it is a more well researched method for creating patterned magnetic than the self-assembly of nanocrystals. The self-assembly of nanocrystals and SAMs are possible methods for creating patterned magnetic media, but don't seem to have the research emphasis moving in that direction as of now. This section and the following section discuss two self-assembly systems that have been well-researched as methods for creating patterned magnetic media.

Heterogeneous nucleation of magnetic islands involves the deposition of different materials through molecular beam epitaxy or chemical vapor deposition on a substrate. The magnetic islands that are created on the substrate have a close epitaxial relation with the substrate material. The islands are created because when the atoms or molecule from the deposition are brought into close contact with the substrate they can follow one of three paths [63]. One path is that they can adsorb to and diffuse on the surface of the substrate until they nucleate with another atom to form an island. They can attach themselves to an existing island. The final option is to desorb and leave the surface of the substrate. This process needs to be monitored carefully and the nucleation rate needs to be known. At a certain point the creation of new islands will cease, and existing islands will grow in size until a continuous film is formed. Therefore, in order to form magnetic islands, the process needs to be stopped short of this.

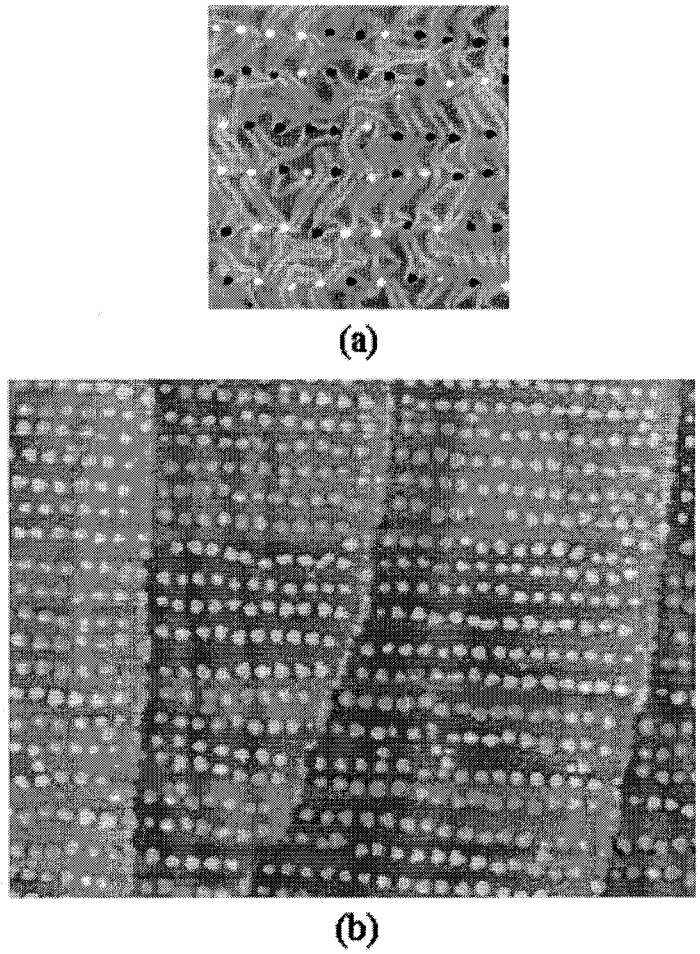

Figure 3.9 (a) The self-assembled array of Co islands on Au(111) can be seen to nucleate on the reconstruction lines of Au(111) **(b)** A 200 nm x 150 nm STM image of an array of self-assembled Co islands on Au(111) [64].

There are several ferromagnetic materials that have favorable epitaxial relations to metallic materials. These epitaxial relations drive the self-assembly system of heterogeneous nucleation of magnetic islands. One example is the epitaxial matches that Co and Ni exhibit for Au(111). Co atoms nucleate to specific regions of the reconstructed Au(111) to form arrays of cylindrical islands [49]. Figure 3.9(a) shows an array of self-assembled Co atoms that nucleated on the reconstruction lines of Au(111). Figure 3.9(b) is just a larger area image of self-assembled Co atoms on Au(111). The same process occurs with Ni atoms. Two other examples of magnetic materials with good epitaxial matches to a metallic surface are Fe and Co on Cu(111). Fe will grow on the raised edges of Cu(111) to form arrays of lines or cylinders. Co lines can also be obtained with this process. These are just a few cases of epitaxial matches between magnetic materials and metallic surfaces that can produce patterned magnetic media

through this self-assembly system. As it can be seen by figure 3.9, this self-assembly system is a viable method for producing patterned magnetic media.

3.2.5 Self-Assembly of Block Copolymers

The self-assembly of block copolymers is another effective system to fabricate patterned magnetic media. It has the potential to create nanoscale features over a macroscopic surface area. Block copolymers are two or more chemically different types of polymeric chains or blocks. If the blocks are immiscible such as oil and water are, they will self-assemble into a variety of nanoscale patterns under the proper conditions. The size, shape, and array from the nanoscale patterns that are developed depend on the preparation method, chain length, polymer type, and several other factors [61]. Patterns with feature sizes in the range of 10 to 100 nm can be developed in the form of such shapes as cylinders or spheres. A variety of nanoscale patterns produced through self-assembled block copolymers can be seen in figure 3.10. These nanoscale patterns can be produced on the surface or in the heart of the material. Block copolymers are useful for fabricating patterned magnetic media because after the self-assembly has occurred, one of the polymer chains can be chemically removed revealing an array of holes. The pattern can then be transferred to the substrate by an etching or liftoff process.

The self-assembly of block copolymers is driven by the phase separation of various parts of the polymer. When the system is heated, the polymers are forced to separate into a variety of nanoscale patterns. Figure 3.11 illustrates the separation of a diblock copolymer. There are two distinct polymeric chains, A and B, and when the system is heated the two chains separate to form a nanoscale pattern. With two polymers, the self-assembly is governed by three parameters [65]. The parameters are the degree of polymerization, the composition of the copolymer and the A-B Flory-Huggins interaction parameter. These parameters are used to calculate the free energy of a diblock copolymer in order to predict the self-assembled pattern. The relation between the parameters and the free energy is given by the Flory-Huggins equation

$$\frac{\Delta G_{mix}}{k_b T} = \frac{1}{N_a}\ln(f_A) + \frac{1}{N_B}\ln(f_B) + f_A f_B \chi \tag{3.3}$$

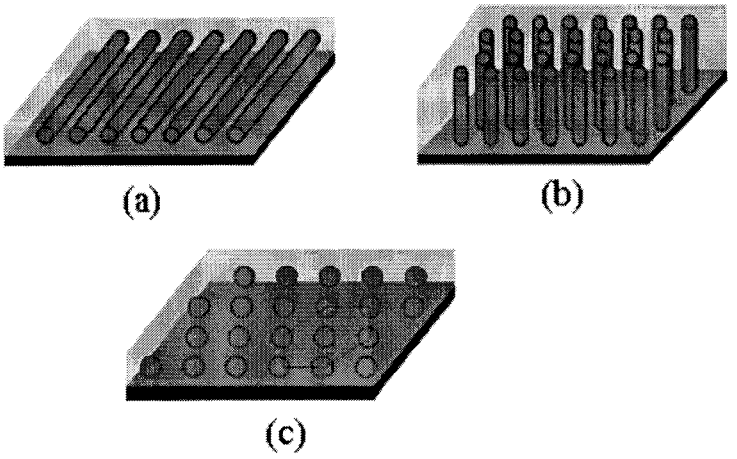

Figure 3.10 An illustration of the various different shaped patterns that can be created with the self-assembly of block copolymers. The shapes include **(a)** cylinders parallel to the substrate **(b)** cylinders perpendicular to the substrate **(c)** spheres [65].

where ΔG is the free energy, k_b is boltzmann's constant, T is the temperature in Kelvin, N_a and N_b are the degrees of polymerization of the two polymers, f_A and f_B are the compositions of the two polymers, and finally χ is the A-B Flory-Huggins interaction parameter. The first two terms on the right side of the equation are related to the entropy of the system [65]. They can be controlled by changing the lengths of the polymer chains and ratio of the length of the polymer A to polymer B. The last term can be controlled by the chemistry of the molecules and the temperature of the system. The composition of the two polymers controls the shapes of the patterns, and the degree of polymerization and interaction parameter are responsible for the size and periodicity.

Experiments have been completed showing that patterned magnetic media can be fabricated using the self-assembly of polystyrene and polymethylmethacrylate (PMMA). Furthermore, it was shown that in conjunction with another method, it could be completed over a large area. If the diblock copolymer of polystyrene and (PMMA) is spun onto a rotating substrate and annealed, the PMMA will form cylinders that are perpendicular to the substrate surface as seen in figure 3.10(b) and completely surrounded by polystyrene. The PMMA can then be removed with an organic etching solvent to form an array of nanoscale holes. Reports have been made of this process yielding holes 20 nm in diameter [66]. These holes are then used as a template to create patterned magnetic media. Magnetic media can be deposited in these holes through sputter coating to create magnetic islands once the polystyrene is lifted off, or the

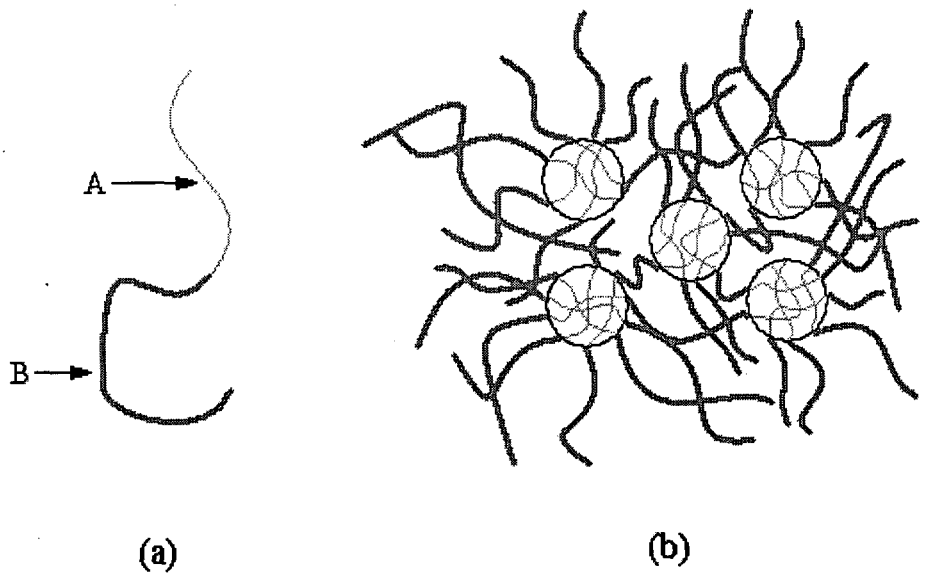

Figure 3.11 (a) Two different polymeric chains of a diblock copolymer. **(b)** After an annealing step, the diblock copolymers self-assemble into separate domains creating a nanoscale pattern.

holes can be created on top of a magnetic layer. In the second case some form of etching would be done to replicate the pattern formed by the diblock copolymers into the magnetic layer.

To achieve a greater long range order with the self-assembly of diblock copolymers, nanoimprint lithography can be utilized. It has been demonstrated that with an artificially assisted self-assembling method, a 2.5-inch disk can be patterned with 40 nm diameter magnetic dots [67]. A nickel master with raised strips ranging from 60 to 250 nm in width separated by 400 nm wide grooves was pressed into a resist layer on top of a sputter coated magnetic film. The raised strips created grooves in the resist. A copolymer of PMMA and polystyrene was poured into these grooves. It was then annealed in order to promote self-assembly into PMMA cylinders surrounded by polystyrene. The PMMA cylinders were removed by an oxygen plasma step. Finally, the pattern was transferred to the underlying magnetic layer by ion milling. Figure 3.12(a) shows the sections of holes separated by solid lines of polymer resist. The holes are the removed sections of PMMA cylinders after self-assembly occurred. Figure 3.12(b) is an SEM image of 40 nm diameter magnetic dots that were created using the holes generated from the self-assembled diblock copolymer.

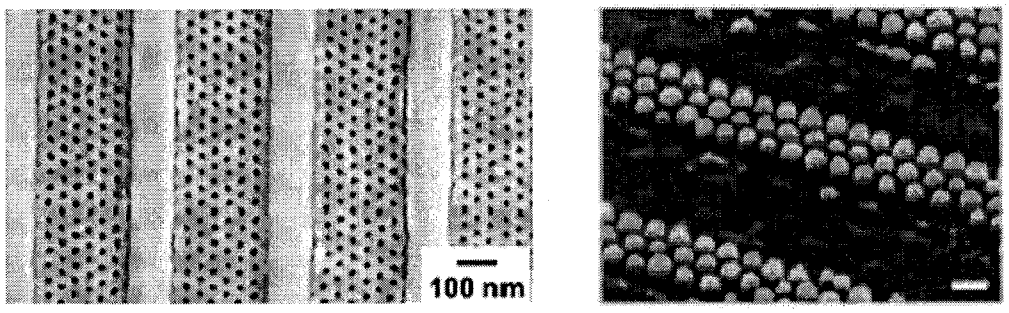

Figure 3.12 (a) Holes created after PMMA cylinders formed from the self-assembly of a diblock copolymer were chemically removed [68]. **(b)** Cylindrical magnetic islands that are 40 nm in diameter created from using the holes as a template similar to those in the left image [67].

3.2.6 An Assessment of Self-Assembly Patterning

There are several advantages to using self-assembly pattern generation technology for fabricating patterned magnetic media. Similar to interference lithography, it is a parallel process which means that it is fast and cost effective. It can also be used to pattern macroscopic areas as evidenced by the patterning of the 2.5-inch diameter disk. These are essential features that are needed by a pattern generation technology for creating patterned magnetic media. Self-assembly patterning also offers several other advantages that interference lithography is unable to. If needed, it is able to generate structures with atomic precision. It can also generate densely packed 20 to 40 nm sized features. Self-assembly is able to produce patterns with pitches of 50 nm or less. This is something difficult to do with interference lithography because of the difficulties in finding lasers with wavelengths shorter than 100 nm and the poor optical properties of materials when exposed to wavelengths that short. The most unique feature of self-assembly is that it is a hands-off technique. Parameters are designated beforehand to generate the desired pattern, and the system automatically creates a pattern. While all of the self-assembly systems mentioned are capable of producing patterned magnetic media, heterogeneous nucleation and block copolymers are at present the most efficient. They seem to be the most well-researched systems of self-assembly for the purpose of creating patterned magnetic media.

There are several negative qualities of self-assembly patterning. Like interference lithography, self-assembly systems can only generate periodic patterns. Therefore, non-periodic patterns that are required for tracking and sectoring information for hard drives can not be

created. Also, self-assembly patterning is a young technology; therefore, there is not enough information known about it yet. At present, the most well-researched path of self-assembly is that based on organic compounds. Finally, the technology is not able to produce long range ordered patterns. It can create patterns on a macroscopic level, but with a lot of defects. A small area might have very few defects, but over a large area, the defects add up to be too many. That was the reason for using an artificially assisted self-assembly system to create the magnetic dots over a 2.5-inch diameter disk. The large amount of defects that are generated when creating a self-assembled pattern over a large area goes back to this being a technology in its infancy. As the technology grows and more is understood, problems like this will be corrected.

3.3 Nanoimprint Lithography

Nanoimprint lithography is the final pattern generation technology that will be discussed as a means of fabricating patterned magnetic media. It will be the focus of the remainder of this thesis. It is similar in style to interference lithography and self-assembly in that it is a parallel process. It also utilizes a similar polymer resist to transfer the pattern to the substrate just as with interference lithography and some of the self-assembly systems that were mentioned. The difference between nanoimprint lithography and the two previous technologies is that it patterns the resist through mechanical deformation instead of through a chemical variation of the resist. Nanoimprint lithography is a method of using a patterned imprinter (i.e. mold or stamp) with sub-100 nm features to mechanically deform a polymer resist in order to transfer the pattern to a substrate. Initial work on the technology was pioneered by Stephen Chou *et al* in the mid 1990's [69]. The advantage of the technology is that a single imprinter can be used repeatedly to create many patterns.

The fundamental principle behind nanoimprint lithography is quite simple compared to other technologies. It is a purely mechanical process similar to a person pressing the top of a Lego into a piece of clay. After they remove it, a pattern of the Lego will have been transferred to the clay. However, since imprint lithography is performed on the nanoscale level, it becomes more involved than compressing clay. There are several problems that can arise if the proper procedure is not completed. Nanoimprint lithography can be divided into four main steps. These include imprinter fabrication, application of an anti-adhesive agent to the imprinter,

pattern replication into the resist (i.e. imprinting), and post processing steps to transfer the pattern to the substrate. The post-processing steps are common to the two previously mentioned pattern generation technologies in order to transfer the pattern from the resist to the substrate. This section will be used to present the theory behind the individual steps of nanoimprint lithography to produce patterned magnetic media. The theory will not only be used to analyze the technology, but will also provide an insight to the research work that is presented in the next chapter.

3.3.1 Imprinter Fabrication

The imprinter is the instrument that transfers a pattern into a resist. In most cases it is more or less a postage stamp sized substrate with part of it containing a patterned array of nanoscale features. It is essentially the Lego of the clay analogy that was just used. There are several different techniques to manufacture an imprinter. Among these include electron-beam, interference, and X-ray lithography. Electron-beam lithography will be the main concentration of this section since interference lithography was already discussed and the difficulties in manufacturing mask and radiation sources for X-ray lithography are too great. Electron-beam lithography creates a pattern by scanning a beam of electrons across an electron sensitive resist thereby chemically altering certain portions of the resist to form a desired pattern. This is done by using an electron gun that is often part of a scanning electron microscope (SEM). Desired patterns are programmed into a PC that controls the electron gun during the process.

Electron-beam lithography as mentioned previously has positive and negative attributes. Electron wavelengths are on the order of 1 Å; however, electron scattering in the resist limits the resolution to greater than approximately 10 nm [58]. Nonetheless, this is an extremely high resolution. Also, any infinite number of different patterns can be generated using electron-beam lithography. Patterns can vary from dots, lines, or crosshatches to drawings of the United States. The downside is that the initial cost for the tools required to perform electron-beam lithography is very high along with maintenance. A SEM system can cost close to a half a million dollars. Also, the process is serial in nature; therefore, for large or complicated patterns it is extremely slow. However, it only needs to create a single patterned imprinter because that imprinter can then be used repeatedly to fabricate many patterns.

There are several different ways to fabricate a patterned imprinter using electron-beam lithography. However, each process is essentially the same with the same goal in mind; to obtain a relief pattern of nanoscale features. The differences lie in the steps, the types of resists used, and the material that the nanoscale features of the imprinter are made out of. There are various electron sensitive resists that can be used for electron-beam lithography. The basic theory behind how to fabricate an imprinter using two different electron-beam lithography methods will be outlined. Both are methods that were used in the research that is presented in the next chapter.

3.3.1.1 SiO_2 Imprinter Fabrication

The first type of electron-beam lithography with six main steps is illustrated in figure 3.13. This method uses several processing steps to produce a silicon dioxide (SiO_2) imprinter. It is important to note that the pattern is written into an electron sensitive resist known as polymethylmethacrylate (PMMA). The first step of the process includes the growth of the SiO_2 layer and spin coating a silicon (Si) substrate with PMMA. Then the specified pattern is written into the resist by electron-beam lithography. After the pattern is written into the PMMA resist, it is then developed. When the developing step is finished, a metal such as Cr or Al is evaporated onto the surface. Then a liftoff step is done to remove the PMMA covered with metal. Finally, the metal pattern is used as a hard mask during a gas-phase etching technique to create a relief structure in the SiO_2 producing an imprinter with raised nanoscale features.

Ideally, the nanoscale features on an imprinter could be made out of either Si or SiO_2. However, it seems that SiO_2 is a better candidate for two reasons [70]. The first is that more control is realized during the etching step if SiO_2 is the material of choice. The second is that SiO_2 is not as brittle as Si. Silicon has an inherently crystalline structure. By the definition of a crystalline material, it possesses a highly regular atomic arrangement along a particular plane. That plane can become weak and break if it is subjected to pressure as would be the case with an imprinter. On the other hand, SiO_2 does not have any crystal plane that can experience weakness in the presence of pressure. This is because it is an amorphous material when it is thermally grown. Therefore, from a standpoint of strength and longevity, a SiO_2-based imprinter is better suited for nanoimprint lithography.

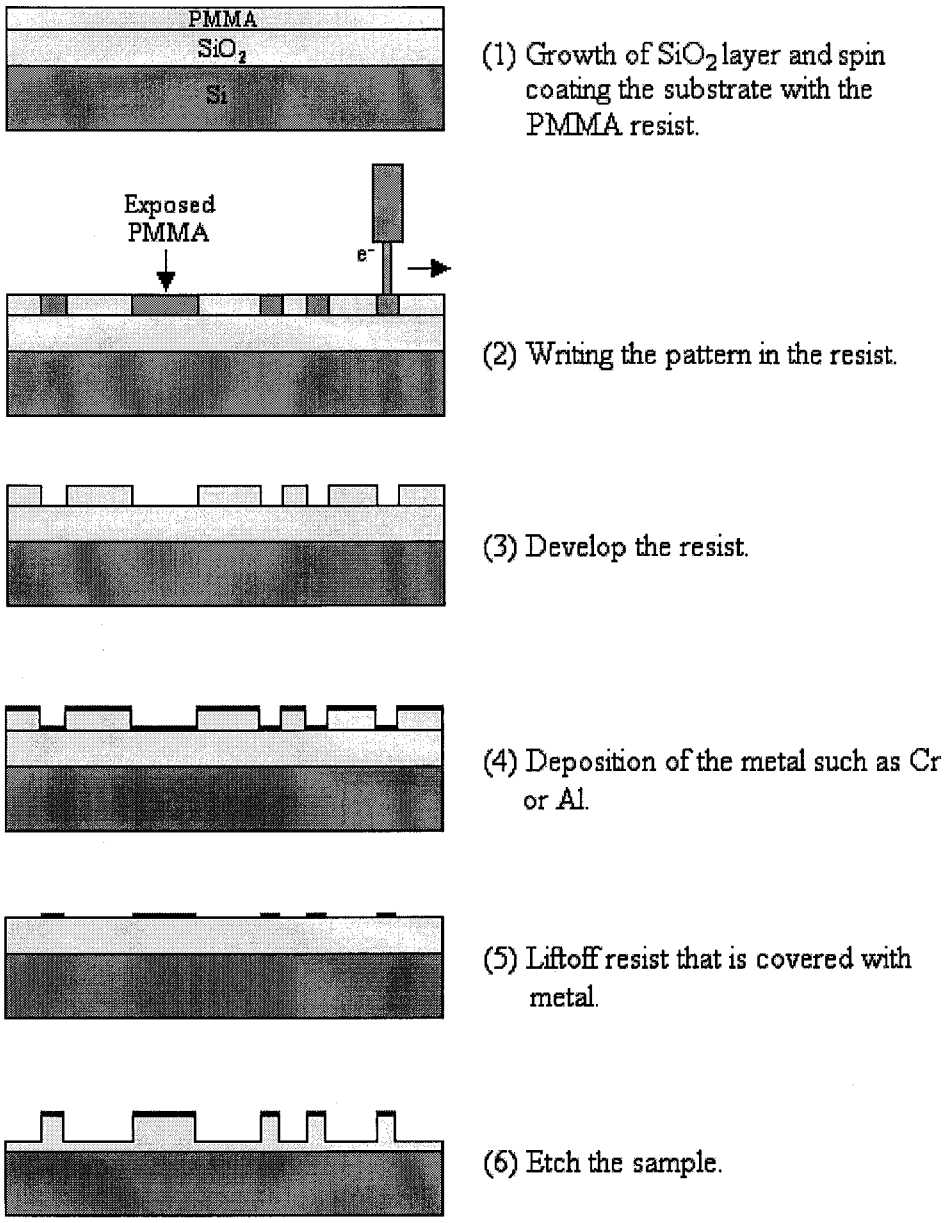

Figure 3.13 An illustration of the steps that are involved with the fabrication of a SiO_2 imprinter through electron-beam lithography.

To complete the first step illustrated in figure 3.13, a layer of SiO_2 is usually grown on top of the Si substrate and the resist layer is applied. To simplify the process, silicon disks can be purchased with an already grown or deposited layer of SiO_2 on them with a specified thickness. Usually resists are polymers dissolved in a liquid solvent. The resist is spin coated onto the substrate. The thickness depends on the concentration of the polymer in the solvent and

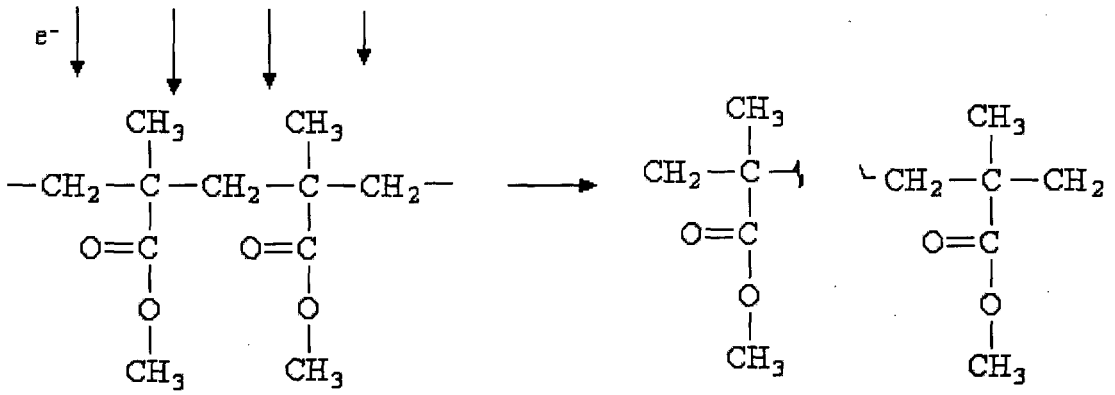

Figure 3.14 A positive PMMA polymer resist chain subjected to electron irradiation on the left. Resulting fragmented PMMA chain on the right.

the speed at which it is spin coated onto the substrate. Then it is baked to drive out the solvent. The precise process will be discussed in the next chapter.

Among the different properties of a resist, its polarity is one of the most important. Polarity refers to whether a resist is positive or negative. A positive resist such as PMMA is one that when exposed to electron irradiation, the polymer chains become fragmented as seen in figure 3.14. These fragments on the right side of the figure are a lower molecular weight than the rest of the resist. Therefore, they dissolve more quickly in a developer leaving a positive tone pattern in the resist layer. A positive resist was needed for this process because raised nanoscale structures were desired. It may not seem to matter by the appearance of figure 3.13. However, the illustration only shows a section of the patterned area of the imprinter substrate. In this case, the patterned area is much smaller than the rest of the imprinter substrate. If a negative resist were used, the patterned area would be an array of holes not pedestals as seen in step six of figure 3.13 with respect to the rest of the imprinter substrate.

PMMA was one of the first resists ever used for electron-beam lithography. It is still one of the most widely used electron sensitive and also photosensitive resists today. What makes it so popular is that it exhibits both a high resolution and sensitivity as compared to other positive resists [50]. This can be seen in a comparison shown in table 3.2. Its superiority over other resists used for electron-beam lithography is why it was used in the research presented in the next chapter. Resolution is defined as the smallest feature size that can be produced in a resist. Obviously, the smaller the features size, the better. Sensitivity is the amount of time needed to begin the chemical reaction that would expose the resist. Therefore, it is apparent that obtaining

Table 3.2 The resolution and sensitivity of positive electron sensitive resists [50].

Resist Type	*Resolution (nm)*	*Sensitivity ($\mu C/cm^2$)*
PMMA	10	100
EBR-9	200	10
PBS	250	1
ZEP	10	30
AZ5206	250	6

both high sensitivity and resolution in a resist is an extremely difficult task. It becomes more or less a tradeoff between resolution and sensitivity.

An endless number of different patterns can be written into a resist by electron-beam lithography. Sometimes some of the simplest such as dots, lines or crosshatches are the most useful as in the case with fabricating patterned magnetic media. Before a pattern is written into a resist, a number of different parameters need to be adjusted. They all affect the quality of the produced pattern. These parameters include the accelerating voltage, magnification, type of dose (i.e. point, line, or area), amount of dose, line spacing, and center-to-center distance. The developer used for patterns written into PMMA is a mixture of methyl isobutyl ketone (MIBK) and isopropanol (IPA). With an accelerating voltage of 30 kV and a 1:3 mixture of MIBK:IPA, the critical dose for PMMA is approximately $300\mu C/cm^2$. Therefore, in order to expose an array of dots down to the substrate with a line and center-to-center spacing of 50 nm, a 7.5 fC point dose is needed. This number might actually need to be adjusted accordingly due to the proximity effect [50].

After the PMMA resist is developed, the next step in the imprinter fabrication is the evaporation of a metal such as Al or Cr onto the surface. This is done through a physical vapor deposition process. The metal is evaporated onto the sample to provide a mask for etching into the SiO_2 as seen in step four of figure 3.13. This is an idealized illustration. In reality, the evaporated metal might coat the sidewalls. To prevent this a bilayer of resist can be used. This will be discussed sections 3.3.3 and 3.3.5. Al and Cr are the most common types of masks used for this. After the metal is deposited, a liftoff is completed to remove the PMMA and any metal that has not come into contact with the substrate. A 1:1 mixture of acetone and methylene chloride can be used for this. Finally, an etch is done to create the nanoscale features in the SiO_2 as seen in step six of figure 3.13. During the etching step, the metal pattern masks certain areas of the underlying SiO_2 from the ions that bombard it. Wherever there is no metal present, the

SiO_2 is etched down to a certain depth to create nanometer-sized columns. The etching step is by far the most complicated because of all the parameters that need to be tuned to obtain vertical sidewalls. A comprehensive study illustrating several parameter setups for etching is given in *Bi-layer Nanoimprint Lithography for Sub-100 nm Features* [70].

3.3.1.2 Hydrogen Silsesquioxane (HSQ) Imprinter Fabrication

The development of SiO_2 imprinters is a complicated process. It involves a minimum of six processing steps that can take at least a day to complete, not to mention that the etching step is a critical one that occurs at the end of the process sequence. Any number of problems can arise causing setbacks or even worse fabricating a defective imprinter. Therefore, if the process could be simplified, the probability of defects arising would be reduced. Recently, a new method of creating imprinters by electron-beam lithography has been proposed. It employs a negative, spin-coatable, organic silicon oxide resist known as hydrogen silsesquioxane (HSQ) [71]. Because HSQ is a negative resist and a derivative of SiO_2, the final pattern of nanoscale features can be directly written into it. This reduces the necessary steps of the PMMA process by half as seen in figure 3.15. The most complicated steps, deposition of a metal, liftoff, and etching, are eliminated in this new process. Essentially, the final pattern is written in the HSQ resist, developed, and post treated with heat.

HSQ displays some very unique properties that enable it to be both a resist, and a robust enough material that can be used for the nanoscale features on an imprinter. It can be purchased as a flowable oxide (FOX-12) from Dow Corning Inc. It is usually dissolved in MIBK. The flowable nature allows it to be spin-coated onto a Si substrate. HSQ has a general molecular formula of

$$(HSiO_3)_{2n},\ n = 2,3,\ \ldots \tag{3.4}$$

Its initial molecular structure as spun onto the substrate is shown in figure 3.16(a). The figure reveals the similarities between SiO_2 and HSQ. One of the four oxygen atoms bonded to every silicon atom in SiO_2 is replaced by a hydrogen atom in HSQ.

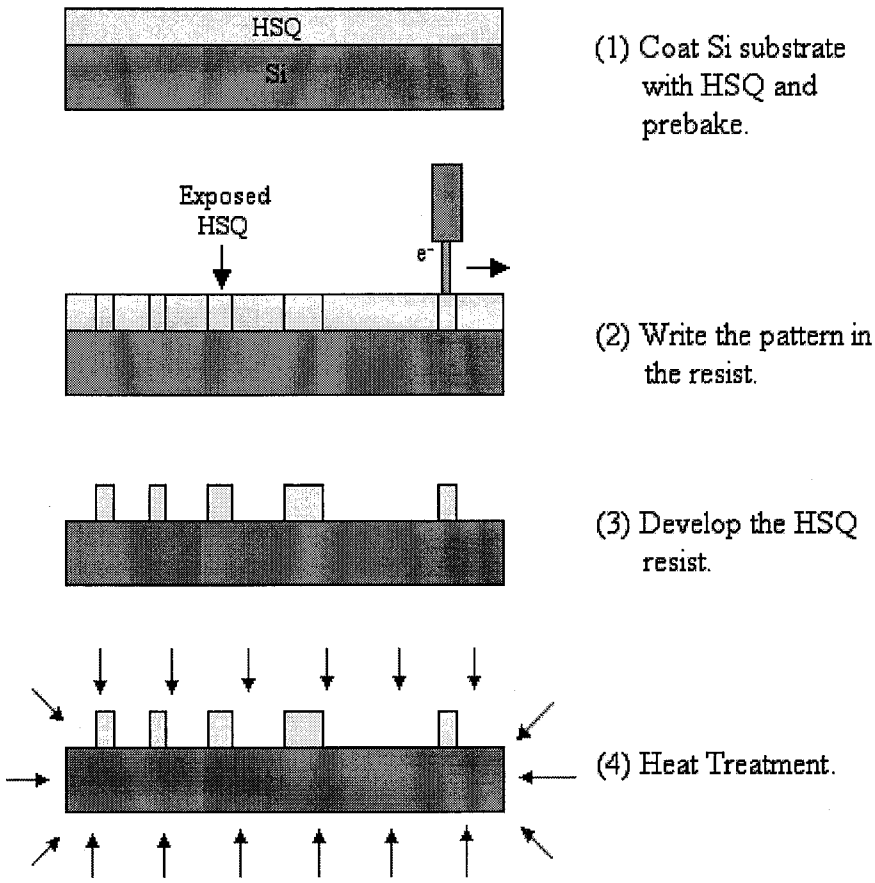

Figure 3.15 An illustration of the necessary steps to create an HSQ-based imprinter through electron-beam lithography.

The initial structure and evolution of the structure of HSQ is described by a class of materials known as caged oligomers [72]. When the HSQ is spun onto the substrate it is in the caged form as seen in figure 3.16(a). When it is exposed to a thermal treatment or electron irradiation, it develops into a three-dimensional network structure as seen in figure 3.16(b). It can be seen that the Si-H bonds disassemble to form the networked structure. This structure is more chemically and mechanically stronger than the initial caged structure. Therefore, when the exposed areas are subjected to electron irradiation, they become less soluble in the developer. That is the definition of a negative polarity resist. Before a pattern is written into HSQ, it is usually baked in order to promote a slight change to a networked structure. By baking the HSQ before electron-beam exposure, the sensitivity is enhanced, but the contrast is reduced. Varying the temperature at which the HSQ is baked will change its network/cage ratio thereby affecting

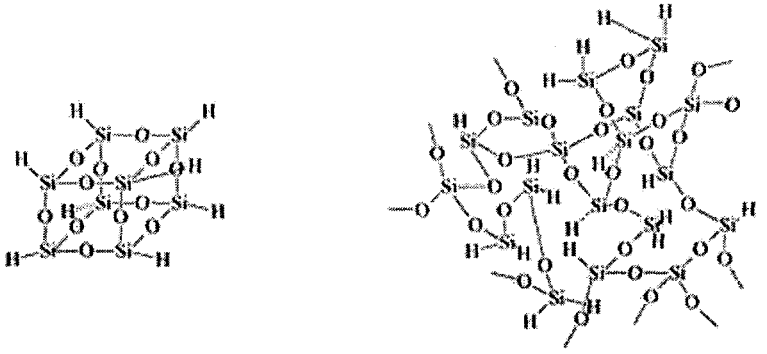

(a) (b)

Figure 3.16 (a) HSQ structure in its caged form. This is the structure that it is in when it is spin coated onto a substrate. **(b)** HSQ network structure produced after it has been thermally annealed or exposed to electron irradiation [72].

the amount of dose needed and the development process [73]. It appears that a lower baking temperature results in a more even surface [73].

Even though HSQ is primarily used as a low-*k* dielectric, several studies have shown it to be a high-quality, negative-tone, electron sensitive resist. It possesses a high resolution with a moderate sensitivity. It has demonstrated the ability to produce sub-10-nm features [73]. Experiments were also conducted that showed that the critical dose to produce semidense lines in HSQ is approximately 1400 $\mu C/cm^2$ [71]. A dose of 1900 $\mu C/cm^2$ is needed for isolated lines. The contrast of HSQ was found to be 1.63 by measuring the remaining film thickness of 100 μm square pads over a dose ranging from 100 to 1000 $\mu C/cm^2$ [71]. While HSQ is not as sensitive as PMMA (300 $\mu C/cm^2$ at 30 kV), it still has an exceptionally high resolution. HSQ also has a good etch resistivity and is stable under SEM inspection. One major downside to HSQ resist is that it experiences a shrinkage of approximately 20 to 25% between 375 to 800°C during the thermal treatment [74]. This means that it will also experience shrinkage when it is exposed to electron irradiation during pattern writing. Another downside is the short shelf life.

After the pattern is written in HSQ, it can be developed. HSQ can be developed using Shipley LDD26W developer, TMAH developer, or simply sodium hydroxide (NaOH). The concentration of the developer has a slight influence on the roughness of the HSQ surface [73]. The more concentrated it is, the rougher the surface will be. Following the development, the HSQ imprinter is subjected to another heat treatment in order to further strengthen the bonds and promote a well-defined network structure. The resulting HSQ structure is chemically similar to

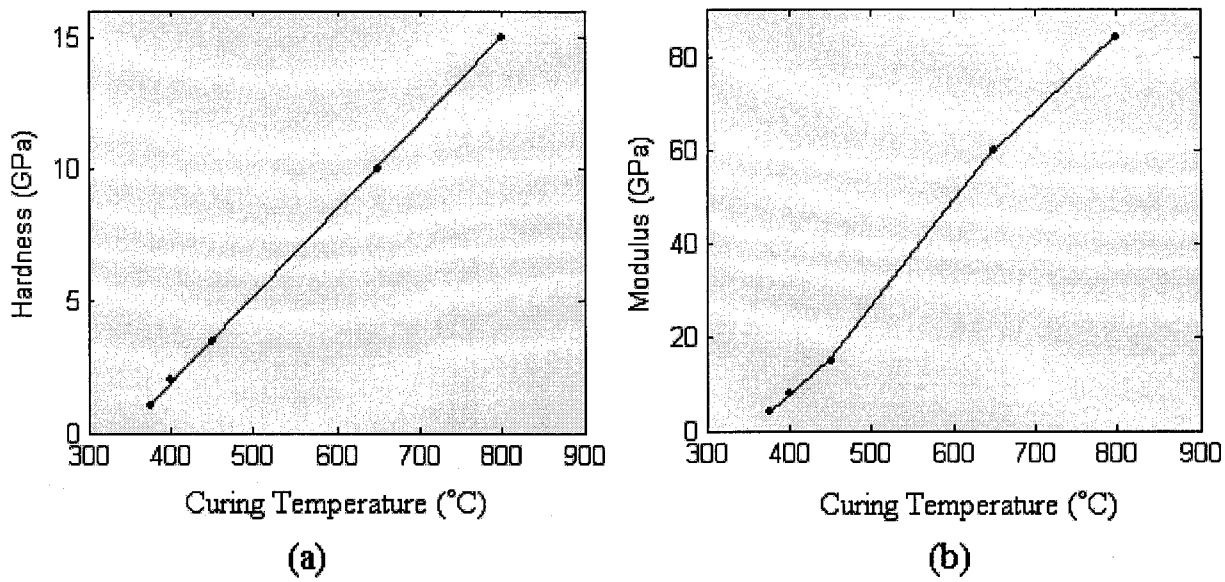

Figure 3.17 (a) The values for the hardness of HSQ resist as the curing temperature is increased. **(b)** The values for the modulus of elasticity of HSQ resist as the curing temperature is increased.

the SiO_2 structure used in the last method. Because of this, an HSQ imprinter has the necessary robustness needed for imprinting. Furthermore, using HSQ resist is an extremely attractive method due to the reduced number of processing steps. Further confirmation of the robust nature of HSQ can be found in *The Effect of Curing Temperature on the Mechanical Properties of Hydrogen Silsesquioxane Thin Films* [74]. HSQ structures exhibit a greater modulus of elasticity and hardness with increased curing temperatures. These values are given in figure 3.17.

3.3.2 Anti-Adhesive Agent

One of the most important aspects of nanoimprint lithography is to prevent the polymer resist of the imprinted sample from adhering to the imprinter. The entire success of the imprinting operation largely depends on this one aspect. If nanoscale features, sub-100 nm, are being imprinted into a polymer resist, it is paramount to employ an imprinter with good anti-adhesive properties. As the features become smaller, there is an increased interaction area between the imprinter and the resist layer. If the surface energy of the imprinter is not sufficiently lower than that of the polymer resist layer, three damaging effects will occur. The polymer resist layer of the imprinted sample will tear and buckle. The nanoscale features of the imprinter could be destroyed. They will either collapse onto the surface of the imprinter or will

be torn off of the imprinter and stuck in the imprinted sample resist layer. Finally, the resist polymer will adhere to the nanoscale features of the imprinter. These effects will be shown in the next chapter.

These unwanted effects can be prevented by applying an anti-adhesive agent to the imprinter. This would chemically alter the surface of the imprinter so that the surface energy would be much less than that of the polymer resist layer on the imprinted sample. The effects of an anti-adhesive layer on the surface can be seen visually by observing the contact angle of a droplet of water placed on it. The greater the contact angle of the water droplet is, the lower the surface energy. Chances are that most people have come face to face with the effects of this process. In order to minimize the sticking of foods, the surfaces of most frying pans are coated with polytetrafluoro ethylene (PTFE) otherwise known as Teflon.

There has been research on two different methods for depositing PTFE or Teflon for the purposes of microelectronics. Thin fluoropolymer films were generated on microscale featured nickel stamps from a CH_4/H_2 plasma [75]. However, this coating would not be suitable for nanoscale features. The extremely large polymer structure of this coating would render a monolayer deposition impossible. A monolayer deposition is needed with nanoscale features so that the features are maintained and not covered up by the anti-adhesive coating. Two other chemical coatings exist that are better suited for nanoscale features. They are a hyper-branched perfluorinated polymer (HBFP) and tridecafluoro-(1,1,2,2)-tetrahydrooctyl-trichlorosilane (F_{13}-TCS) [70,76].

HBFP is a promising anti-adhesive coating because of its low surface energy. The reason for its low surface energy can be seen in its chemical structure shown in figure 3.18. The structure reveals that the anti-adhesive agent is a polymer. Despite being a polymer though, it is still small enough that a coating of only a few nanometers thick can be applied. For most applications this is good enough. The structure also reveals that there are several fluorine atoms hanging off of it. Fluorine is the most electronegative element in the periodic table. It has five valence electrons and strongly desires a sixth. Once the fluorine atoms obtain a sixth electron from bonding with carbon in the structure, they become as stable and non-reactive as a noble gas. The stability and non-reactive nature of all of the fluorine atoms give the HBFP its low surface energy. This makes it a good anti-adhesive agent. The HBFP can also be utilized at temperatures up to 410°C without any degradation which is needed for imprinting [70].

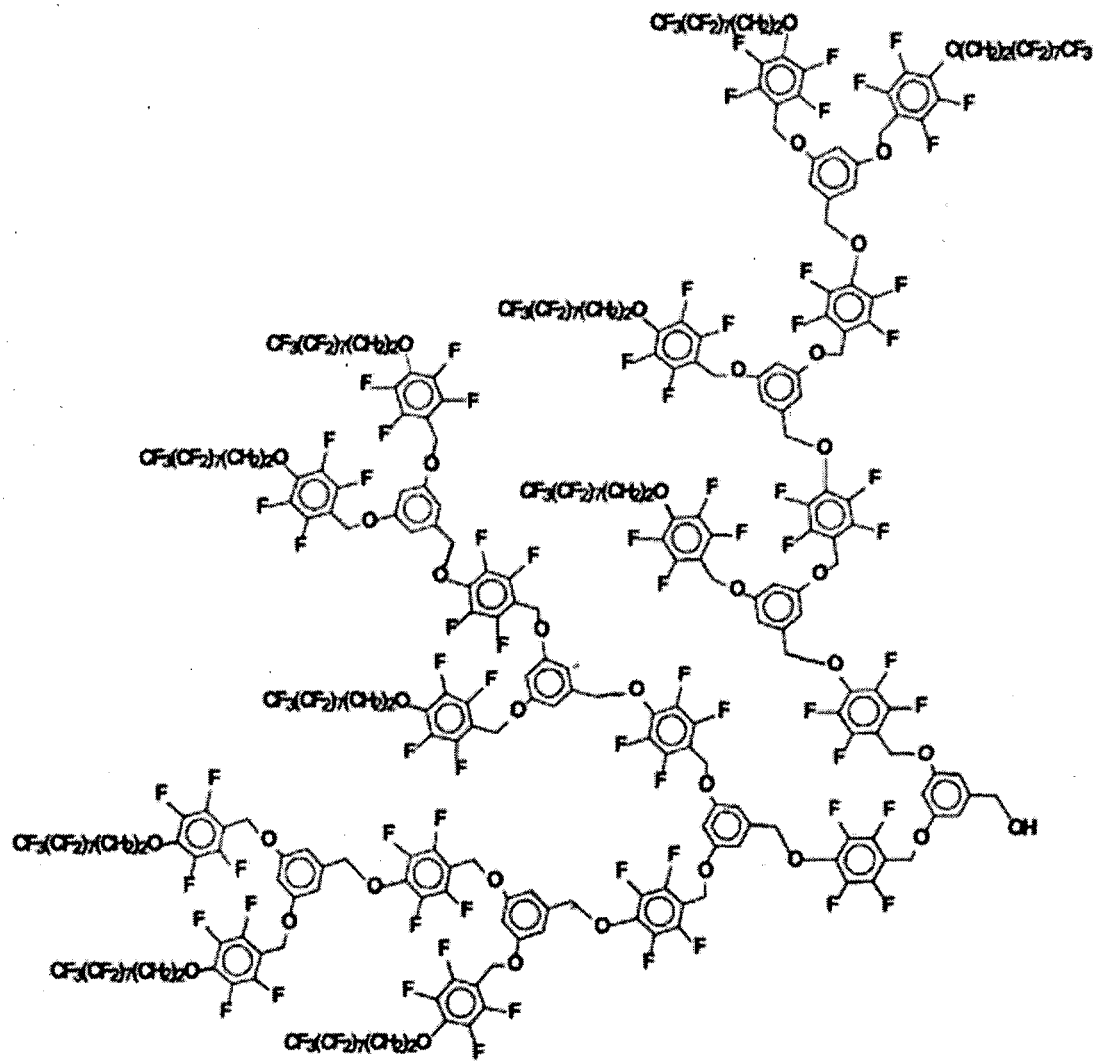

Figure 3.18 Chemical structure of HBFP anti-adhesive agent for imprinters [70].

The HBFP is applied to the surface of the imprinter after fabrication. Just as with a regular resist, it can be spin-coated onto the imprinter. Measurements were taken and show that a 5 to 10 nm coating of the HBFP is produced on the imprinter after application [70]. The solvent of the HBFP coating cannot be driven off thermally because its glass transition temperature (T_g) is too low. The glass transition temperature is a gradual transition in which a polymer's material characteristics change from that of a glass to that of a rubber. Because of this, the imprinter is placed in a vacuum chamber to drive off the solvent from the coating.

The one major problem with using the HBFP as an anti-adhesive agent is that it is not covalently bonded to the surface of the imprinter. Therefore, it needs to be reapplied to the imprinter after every successive imprint. Also, since it is a polymer, it is unable to provide a

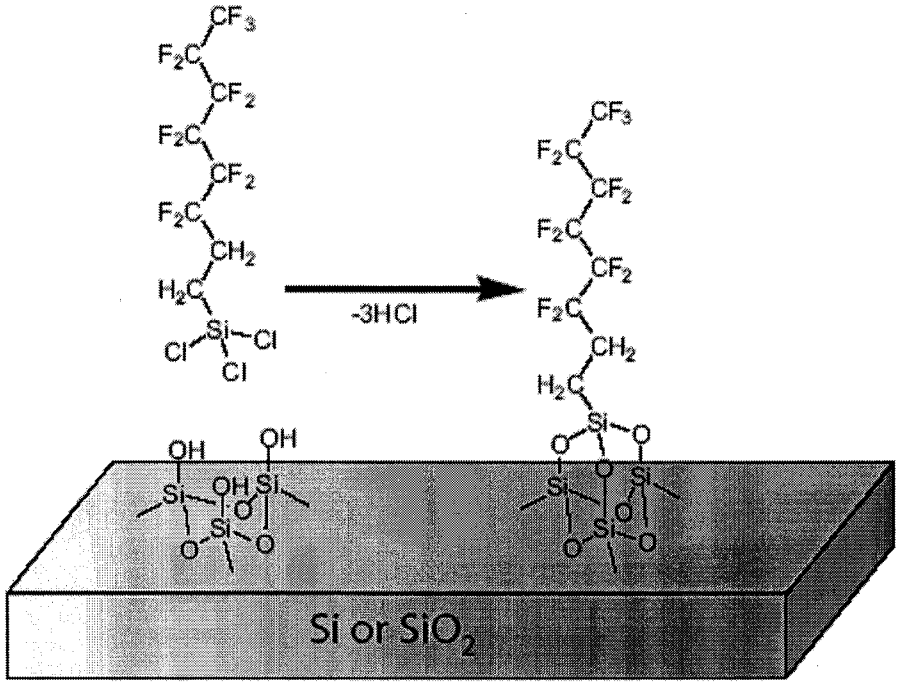

Figure 3.19 The covalent bonding of F_{13}-TCS anti-adhesive agent to a Si or SiO_2 substrate through the elimination of HCl [76].

monolayer coating for applications that require it. The application of the F_{13}-TCS to the surface of the imprinter is a more effecting coating [76]. First it can be covalently bonded through a chemical reaction to either a Si or SiO_2 surface. Therefore, the coating will not deteriorate after every imprint requiring reapplication. The second important aspect is that it is a monolayer coating. If all conditions are set right, it should theoretically provide a 1 nm thick coating. F_{13}-TCS can be purchased from Gelest Inc [76]. It is a chlorosilane that reacts spontaneously with Si or SiO_2 surfaces. The chlorosilane attaches to the Si or SiO_2 substrate through covalent bonding under the elimination of hydrochloric acid (HCl) as seen in figure 3.19. It has also been experimentally shown that the chlorosilane will covalently bond to cured HSQ because of its structural similarity to SiO_2 [71].

There are specific guidelines to applying the F_{13}-TCS anti-adhesive coating. The process is not trivial because certain errors could prevent a monolayer coating from being achieved. First, the reaction has to be done in a glove box that can provide a water-free environment. Typically, a water content of less than 1 ppm is desired. This is needed because chlorosilanes react strongly with water resulting in their polymerization. If the coating polymerizes, it could be several nanometers thick ruining the nanoscale features and not providing adequate anti-

adhesion. Also, to prevent the application of a thick coating, F_{13}-TCS must be applied in the gas phase. Before the imprinter is placed in a glove box, it has to first be hydroxylated with nitric acid. Hydroxylation of the imprinter using nitric acid provides the hydroxide groups that the F_{13}-TCS needs to react with the surface. After hydroxylation the imprinter is placed in a petri dish on top of a hot plate in the glove box. When it has been heated up, several microliters of F_{13}-TCS are placed in the petri dish where it evaporates. As soon as it comes into contact with the surface of the imprinter, the reaction will commence. Finally, after the reaction is complete, the imprinter is soaked in anhydrous hexane to wash away excess F_{13}-TCS. This is done so that the excess F_{13}-TCS does not polymerize when it comes into contact with the atmosphere. The process is not complicated; however, if certain conditions are not precisely met, the anti-adhesive coating will not work properly.

3.3.3 Imprinting

Imprinting or pattern replication is the heart of this entire process. All of the other steps simply lead up to this. There are two different nanoimprint lithography techniques: hot embossing and step-and-flash-imprint lithography (SFIL). They are fundamentally the same methods. They pattern a resist through physical deformation. However, they differ in the type of polymer resist used and the manner in which it is processed to preserve the replicated pattern. Subsequent heating and cooling steps are used with hot embossing to cure a thermoplastic resist polymer. SFIL uses a light source to cure a photocurable polymer resist. Both are efficient techniques because of their parallel nature; however, there are several variables that need to be adjusted in order to produce defect-free and repeatable imprints.

The main thermoplastic resist polymer that is used for hot embossing imprint lithography is PMMA. It not only has excellent properties for electron-beam lithography but also for nanoimprint lithography. It exhibits a small thermal expansion coefficient of 5×10^{-5}/°C and a small pressure shrinkage coefficient of 3.8×10^{-7}/psi. This is favorable for hot embossing because it requires high temperatures and pressures. With values for the thermal expansion and pressure shrinkage coefficients in these ranges, PMMA should easily conform to the nanoscale features on the imprinter. A copolymer known as polymethylmethacrylate methylacrylic acid P(MMA-MAA) can also be used. PMMA can be used by itself if only a single layer of resist is desired.

P(MMA-MAA) is used in conjunction with PMMA if a bilayer resist is needed. A bilayer resist is used in order to provide an undercut. The undercut is performed during post processing in an effort to improve the liftoff procedure after metal deposition [77]. It is possible to obtain a more uniform array of magnetic dots with this method.

For a single layer of resist, the PMMA is spin-coated onto a Si substrate in the same manner as was done with the imprinter fabrication. The thickness of the PMMA layer is controlled by the spin speed and the concentration of PMMA in the solvent. PMMA is usually purchased in an anisole or chlorobenzene solvent [78]. Available concentrations range from 2 to 11% and the most common molecular weights are 495k and 950k. After it is spun onto the Si substrate, it is heated to drive off the solvent. If a bilayer resist is desired, P(MMA-MAA) is usually spun on top of the PMMA after it has been heated. The thickness can be controlled in the same manner. P(MMA-MAA) is usually dissolved in ethyl lactate or anisole [78]. It can be obtained in concentrations similar to PMMA and the available concentrations of methylacrylic acid range from approximately 6 to 17%. After the application of P(MMA-MAA), the substrate is then heated again to drive out the solvent of the second layer. At either of these points (i.e. after baking the single or bilayer) the Si substrate is ready for imprinting.

A general illustration of the hot embossing nanoimprint lithography technique is shown in figure 3.20. The first step is to position the imprinter on top of the sample coated with resist. In the illustration, the sample is coated with a single layer of PMMA. Both the imprinter and the sample are heated above the glass transition temperature of the resist. The glass transition temperature of PMMA is 105°C. This transforms the resist from a hard glass-like material to a soft gel-like material making it easy to deform. Once both the imprinter and sample are at the desired temperature, pressure is applied. A temperature between 140 to 180°C and a pressure ranging between 600 and 1900 psi was used by Chou's group [69]. Temperature and pressure holding times are typically a few minutes [79]. After the temperature and pressure application, the imprinter and sample are cooled to harden the resist. The imprinter and sample are then separated. The reverse pattern of the nanoscale features from the imprinter should be replicated in the resist. A good imprint or pattern replication depends on several factors ranging from the quality of the anti-adhesive agent to the pressure/temperature/times used. Specific guidelines, variable adjustments, and process changes will be given in the next chapter.

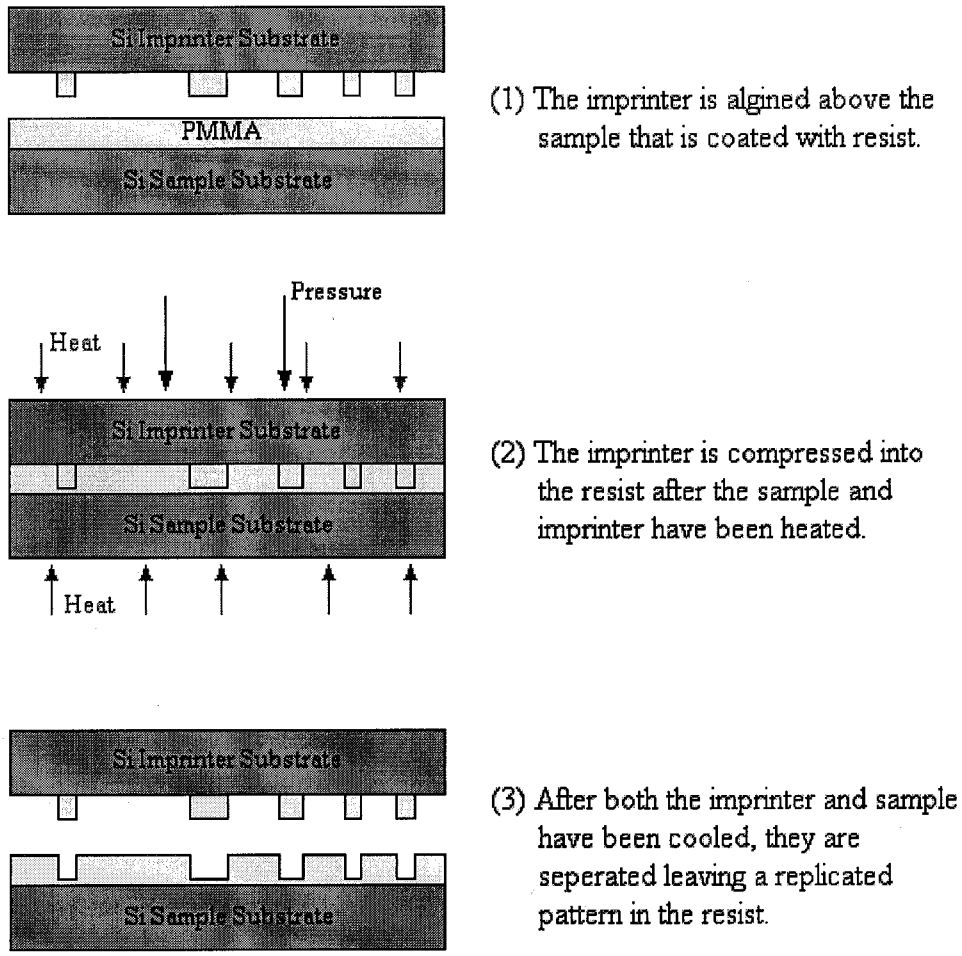

Figure 3.20 A general illustration of the steps involved with hot embossing nanoimprint lithography.

The resist used for SFIL is a photocurable organosilicon polymer. Like the thermoplastic resist used for hot embossing its shrinkage and etch selectivity needs to be considered. Another consideration with the SFIL resist is its polymerization kinetics. The resist is not spin-coated onto the substrate, but instead placed onto it. Therefore, the resist needs to be able to fully wet the substrate. In order to accommodate all of these requirements, the resist can be fabricated from a free radical generator dissolved in a solution of organic monomer, silylate monomer, or a dimethyl siloxane (DMS) oligomer [80]. These monomers and DMS derivatives satisfy each of the requirements that need to be addressed of the SFIL resist. However, as with any type of engineering, certain tradeoffs exist.

A general illustration of the SFIL technique is shown in figure 3.21. A transparent quartz imprinter is positioned on top of a sample coated with photocurable resist. The nanoscale features on the imprinter can be fabricated from HSQ [71]. At the beginning of the process the

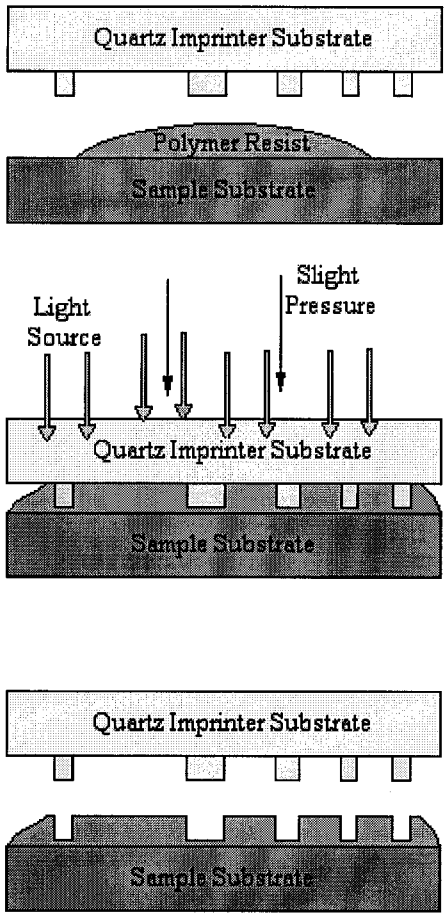

(1) The imprinter is positioned above the sample with photocurable polymer resist on it.

(2) The imprinter is compressed into the resist. A light source shines through the imprinter to harden the resist.

(3) The imprinter is removed from the sample leaving a replicated pattern in the resist.

Figure 3.21 A general illustration of the steps involved with step and flash imprint lithography.

photocurable resist is in the liquid state unlike the thermoplastic resist. Therefore, when the imprinter is pressed into the resist with a small amount of pressure and no heating, it conforms to the features of the imprinter. At this point, a light source shines through the imprinter curing the resist. It has also been shown that a 308 nm XeCl excimer laser can be used to cure the resist in less than 250 ns [58]. This process is known as laser assisted direct imprint (LADI). After the polymer is cured, the imprinter and sample can be separated. Once again the reverse pattern of the imprinter is replicated into the resist. SEM images of a SFIL imprinter and pattern replicated from it in a photocurable resist are shown in figure 3.22. Like hot embossing, the success and repeatability of the SFIL technique depends upon several variables [81].

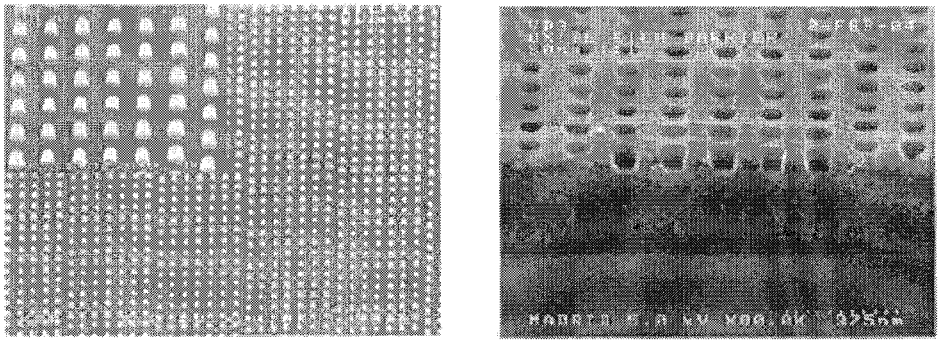

(a) (b)

Figure 3.22 SEM images of a **(a)** transparent imprinter used for SFIL and **(b)** the pattern that it replicated in a photocurable resist [81].

3.3.4 Post Processing

Post processing transfers the pattern of nanoscale features that has been replicated in the resist to the substrate. More importantly it is what will create the final structure of patterned magnetic media. It is not just common with nanoimprint lithography, but also with the other patterned generation technologies outlined in this chapter. Since the full process of nanoimprint lithography was being discussed here as a precursor to the research work offered in the next chapter, it seemed suitable to also discuss post processing here. Post processing is carried out following interference lithography and also the self-assembly systems of SAMs and block copolymers. Other nanofabrication methods also utilize post processing steps such as electron-beam lithography, x-ray lithography, and photolithography. Two types of post processing methods will be discussed that rely on etching, physical vapor deposition, and liftoff.

Etching transfers the pattern in the resist to the substrate by attacking and destroying the exposed material under the resist. It can be broken up into wet and dry categories. A majority of the dry etching methods that are used are plasma based. The three basic ones are high pressure plasma etching, reactive ion etching (RIE), and ion milling. More information on these techniques can be found in *The Springer Handbook of Nanotechnology* [58]. They allow smaller features to be patterned and are better at producing high-aspect-ratio vertical structures than wet etching. However, dry etching provides less selectivity than wet etching. Selectivity is a property of etching that measures the ability with which the etchant can differentiate the masking layer (i.e resist) and the material that needs to be etched. Another important aspect of etching is

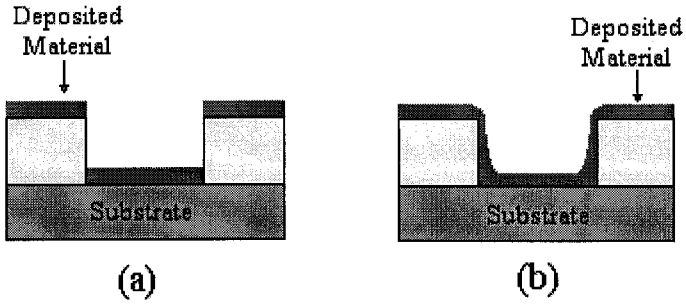

Figure 3.23 The form of deposited material by using **(a)** evaporation **(b)** sputtering physical vapor deposition.

the directionality. An etch can be isotropic or anisotropic. With an isotropic etch, the etchant attacks the material in all directions at the same rate. With an anisotropic etch, the etchant does not attack the material in all directions. An anisotropic etch can create vertical sidewalls.

Physical vapor deposition uses either evaporation or sputtering to deposit a layer of material on a sample. With evaporation, the material to be used is placed in a crucible on the bottom of a vacuum chamber. The samples are placed at the top of the vacuum chamber, and the material is heated up until evaporation occurs. The material can either be heated up by the induction of high currents around the crucible or hitting the material with an electron gun. Evaporation is usually used only for metals. The advantage of this method is that it does not coat the sidewalls of nanoscale features as seen in figure 3.23(a). With sputtering, a target of the material is bombarded with argon (Ar) ions. Individual atoms from the material are physically removed and land on the sample. The bombarding ions are produced in a DC or RF plasma. In a standard parallel plate system the top electrode is the target, and the samples are placed on the bottom electrode. This method can be used with almost any type of material. The downside is that it will coat the sidewalls of the nanoscale features as seen in figure 3.23(b). This will make it hard to liftoff the resist without ripping the material from the substrate.

The bilayer of resist that was discussed in section 3.3.3 is used to help prevent the coating of sidewalls as seen in figure 3.24. Each layer of resist can be independently etched with different solvents without affecting the other layer. An isotropic wet etch of P(MMA-MAA) can be done using methanol or toluene. An isotropic wet etch of PMMA can be done using chlorobenzene or toluene to provide the undercut. Another way of doing the first step would be to do an anisotropic oxygen reactive ion etch to remove the P(MMA-MAA) from the hole. The undercut is then performed in the same manner using an isotropic wet etch. The bilayer in theory

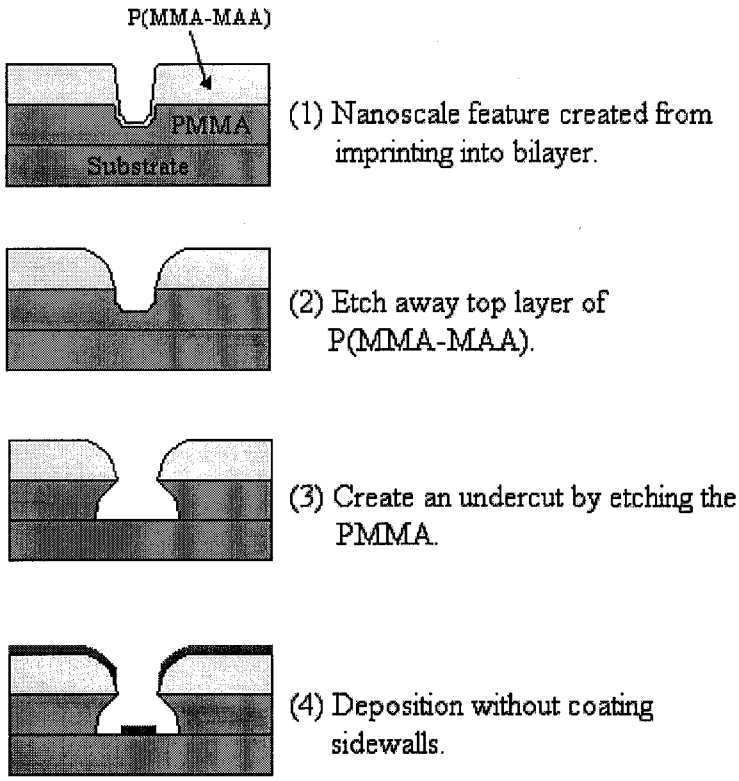

Figure 3.24 An illustration showing the functionality of a bilayer resist.

is supposed to prevent the ripping of a deposited material from the substrate during liftoff [77]. As seen in the fourth step of figure 3.24, the bilayer prevents a continuous coating of metal from the top of the resist to the bottom of the hole. Therefore, it is less likely that the metal deposited on the substrate will be ripped off as easily as that in figure 3.23(b).

One common post processing method is etching. An anisotropic dry etch is commonly done as shown in figure 3.25. With this technique, a layer of magnetic material is deposited on top of the substrate. Then a resist is applied and patterned. An etching method is used to remove the resist at the bottom of the holes. The etching can then be continued in order to transfer the pattern to the substrate. It will destroy all the magnetic material that is not covered by the resist. The resist is then stripped away, and the final outcome is an array of patterned magnetic media. Patterned magnetic media with areal bit densities as high as 29 Gbits/in^2 have been developed using etching [49].

A second post processing method known as liftoff combines etching, physical vapor deposition, and a liftoff as seen in figure 3.26. The illustration is an idealized case because it shows a single layer of resist and no tearing of the magnetic material during liftoff. After

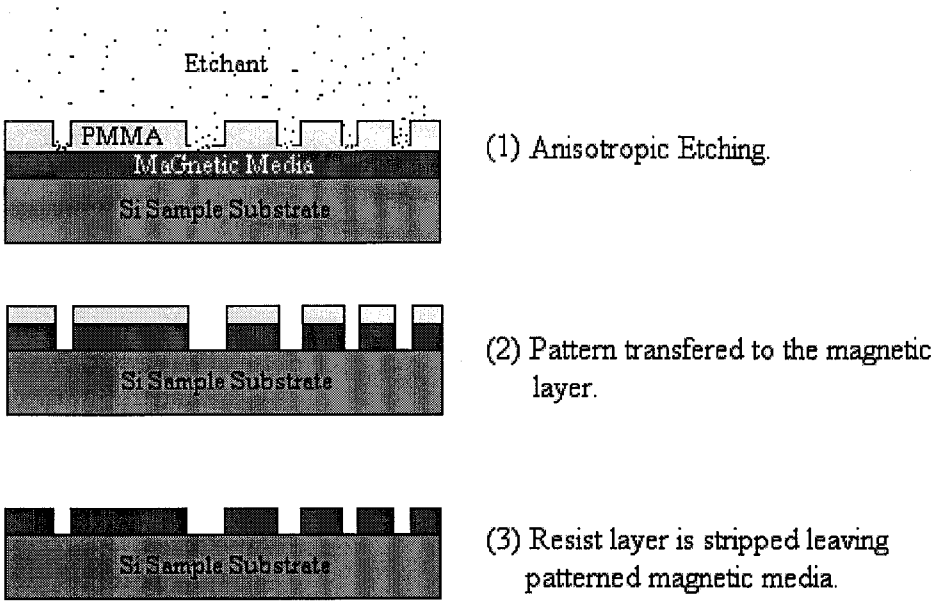

Figure 3.25 The use of anisotropic etching to transfer the pattern in the resist to the substrate in an effort to create patterned magnetic media.

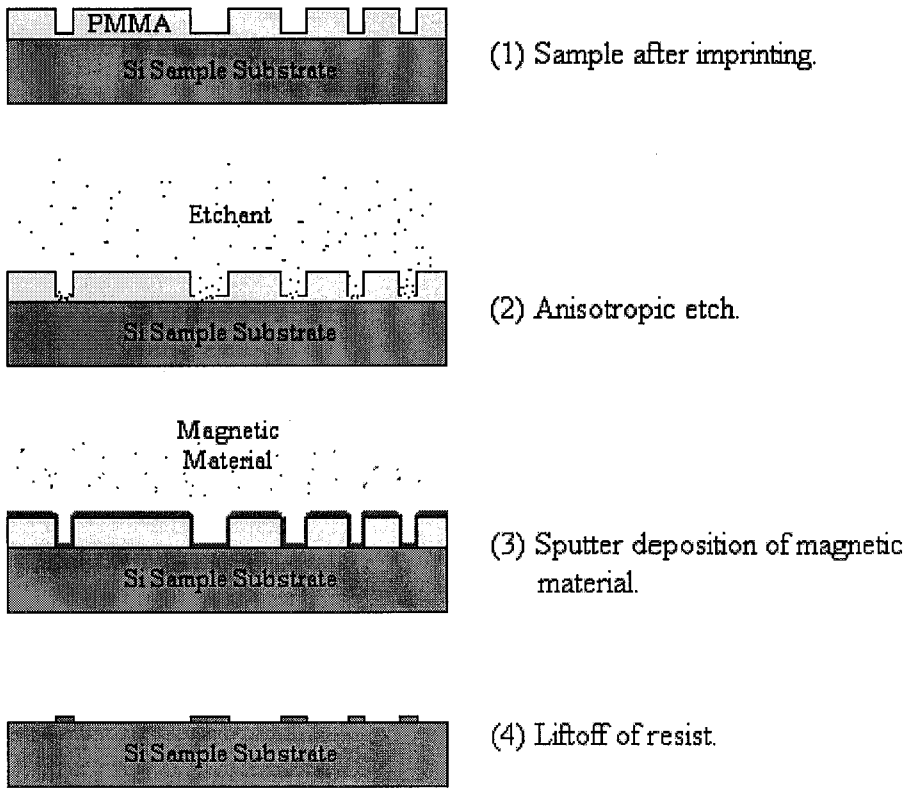

Figure 3.26 The use of anisotropic etching just to remove left over PMMA, sputter coating, and liftoff to transfer the pattern in the resist to the substrate in order to create patterned magnetic media.

imprinting is done, an isotropic or anisotropic, wet or dry etch can be completed to remove the resist from the bottom of the holes. As soon as it reaches the substrate it is stopped. The illustration was done to make it look like an anisotropic etch. This exposes the substrate in certain places. At this point, a coating of magnetic material is applied by a sputter deposition. After the sputter deposition is done, a liftoff is carried out to remove the resist and magnetic material that is not adhered to the sample. The final product is an of array magnetic dots. A very similar method to this produced areal bit densities as high as 18 Gbits/in^2 over a 4 x 4 cm area [82].

3.3.5 An Assessment of Nanoimprint Lithography

Nanoimprint lithography is a promising technology to fabricate patterned magnetic media. It is a parallel process just like interference lithography and self-assembly patterning. Therefore, it is a high-throughput, low-cost pattern generation technology. Due to its parallel nature patterns have been generated over reasonably large areas. Uniform patterns with 25 nm features and minimal defects have been generated over a 30 mm x 30 mm area [49]. With the development of the technology, larger patterns will soon be possible. The technology is capable of easily producing 20 nm features, but also has the capability to produce sub-10 nm features [69]. Furthermore, features in this range are able to be densely packed. Patterns can be produced with a pitch of less than 50 nm. These features are capable because imprinters are primarily fabricated with electron-beam lithography. Despite the slow, serial nature of electron-beam lithography, a single imprinter can be used numerous times for imprinting or pattern replication. Using electron-beam lithography to create the imprinter has one major advantage. Since it can generate almost any thinkable pattern, nanoimprint lithography is capable of producing non-regular, non-periodic patterns. It has been mentioned several times that non-periodic patterns are important for the purpose of including tracking and sectoring information for a hard drive. Finally, if imprinter fabrication is done out-of-house, the laboratory setup required for nanoimprint lithography is extremely cost-effective.

The most visible downside to nanoimprint lithography is the fact that the imprinter comes into physical contact with the polymer resist during imprinting. Very few other pattern generation technologies operate in this manner. Most other technologies use masks held above

the surface or some type of energetic beam. When the imprinter comes into contact with the polymer resist two things can occur. The polymer resist on the sample substrate can be ripped from it or buckle. Also the nanoscale features on the imprinter can be destroyed. As the features become smaller this problem escalates due to an increased area of contact. It was discussed that an anti-adhesive agent could be applied to the imprinter to prevent this. However, it sometimes does not work properly. It can also degrade over time and the number of imprints done. Another problem that exists is the difficulty with alignment using hot embossing; however, it is much easier with SFIL.

3.4 Conclusion

It has become evident from this chapter that interference lithography, self-assembly patterning, and nanoimprint lithography all have the potential to be used for the mass fabrication of patterned magnetic media. Each pattern generation technology is not without obstacles it must overcome. They all have certain advantages and disadvantages over each other as was illustrated. Interference lithography is able to pattern larger areas; however, it is unable to produce features as densely packed and as small as self-assembly patterning and nanoimprint lithography. Research on all of these methods will continue by industry, educational institutions, and the government in a consorted effort for improvement.

At Rowan University, experimental research was completed on nanoimprint lithography. It is highly regarded as a competing technology to develop patterned magnetic media because of its ability to produce non-periodic patterns with densely packed sub-20 nm features. Experiments from other groups have shown imprinted features over areas comparable to that needed for patterned magnetic media. The features are not as small and as densely packed as needed. However, it is believed that it will only be a matter of time and effort before the necessary feature sizes will be replicated over a large enough area using nanoimprint lithography.

4 IMPLEMENTATION AND RESULTS

This chapter presents research work that was performed at Rowan University from the summer of 2003 to the winter of 2004 to produce patterned magnetic media via nanoimprint lithography. It was performed under a collaborative NSF grant awarded to Washington University, Rowan University, NIST, and IBM. After reviewing the upcoming hard drive technologies that would continue the trend of increasing areal bit density, it was believed that patterned magnetic media would offer the greatest long-term potential. To fabricate it, nanoimprint lithography was considered to be the most suitable technology. It has extremely attractive properties such as high throughput, high resolution, and cost-effectiveness for manufacturing patterned magnetic media on a large scale.

Nanoimprint lithography is an attractive technology for fabricating patterned magnetic media; however, it has a few obstacles to overcome. For the most part, features less than 30 nm in diameter with a 50 nm pitch were fabricated. At this level, any problems that were encountered became amplified. There were three main problems that arose during the investigation and implementation of this technology. First, imprinters were difficult to fabricate. The nanoscale features had collapsed on several occasions after the imprinter had been developed. Second, during imprinting, the resist layer on the substrate of the imprinted sample frequently ripped and buckled. This occurred as the imprinter was separated from the imprinted sample. Finally, during post processing, the magnetic dots were occasionally ripped from the surface. When a liftoff was performed to remove the resist, the magnetic dots were ripped up with it instead of adhering to the substrate surface. Throughout the research, each one of these problems was addressed. Attempts were made to solve these problems and any other problems that arose along the way. For the most part, these problems were corrected enough to show that patterned magnetic media could be fabricated using nanoimprint lithography.

It was alluded to in the last chapter that nanoimprint lithography for manufacturing patterned magnetic media can be broken down into four major steps. This chapter discusses the equipment that was used for nanoimprint lithography along with the material processing practices used. It then discusses the research accomplished in each of the four major areas of the fabrication process. Once again, they include imprinter fabrication, application of an anti-adhesive agent to the imprinter, imprinting, and post processing. The two different kinds of

imprinters, SiO_2 and HSQ, discussed in the last chapter were fabricated. The F_{13}-TCS anti-adhesive coating was applied to the imprinters before use. Both a single layer consisting of PMMA and bilayer consisting of PMMA and P(MMA-MAA) were imprinted into. This was done using only the hot embossing method and HSQ imprinters. Finally, the liftoff post processing method was used to create patterned magnetic media. Experiments were completed in which certain variables were adjusted and processing steps were altered in order to obtain the best possible results. The results are shown primarily in SEM images.

4.1 Equipment and Materials

In order to carry out the various steps and experiments involved with nanoimprint lithography, a multitude of chemicals were used. The following chemicals were used for nanoimprint lithography:

- 2% 950k PMMA in chlorobenzene
- 2% 495k PMMA in chlorobenzene
- 10% P(MMA-{17.5%}MAA) in ethyl lactate
- 6% P(MMA-{8.5%}MAA) in ethyl lactate
- 1:2 methyl isobutyl ketone in isopropanol (MIBK:IPA)
- (Tridecafluoro-1,1,2,2-Tetrahydroctyl) Trichlorosilane (F_{13}-TCS)
- hydrogen silsesquioxane (HSQ)
- chlorobenzene
- ethyl lactate
- acetone
- methanol
- hexane
- methylene chloride
- nitric acid
- toluene
- IPA
- sodium hydroxide (NaOH)

The polymer resists, thinners, and developer were purchased from Microchem Inc. The F_{13}-TCS anti-adhesive agent was bought from Gelest Inc. and the HSQ resist was purchased from Dow Corning Inc. Finally, all the other chemical solvents were obtained from Fisher Scientific Inc. All of the laboratory equipment such as beakers, pipettes, and bottles was also purchased from

Fisher. Information on each of the chemicals and a MSDS can be found on the companies web sites.

Several pieces of equipment were vital to the nanoimprint lithography process. The following pieces of equipment were used to perform nanoimprint lithography:

- Laurell Technologies WS-400-6NPP spin coating unit
- VWR Scientific Aquasonic Model 50T sonicator
- Barnstead/Thermolyne Super-Nuova hot plate
- Corning hot plate
- Econotherm laboratory oven
- Laminar flow hood
- Terra Universal glove box
- Newport Corporation pneumatic isolation table
- Leitz Wetzlar optical microscope
- Meiji Techno optical microscope
- Custom built imprinting presses
  - Parker Automation P5T series short stroke thruster models 20 & 100
- Custom built control unit
  - Omega PTC-1A timer
  - Watlow Series 93 heating control unit
  - Watlow E1E43 cartridge heater
  - Watlow 20CJUDB thermocouple
  - Simpson mini 145 digital panel meter
  - Invensys Sensor Systems 19C pressure transducer
  - Parker Pneumatic single solenoid $1/8^{th}$ and $3/8^{th}$ spool valves
- Hewlett Packard E3631A power supply
- Agilent E3633A power supply
- Ambios XP-2 profilometer
- Raith beam blanker
- Leo 1530 VP scanning electron microscope
- Nanometer Pattern Generation System (NPGS)
- T-M Vacuum Products SS24-30T/111 sputtering unit
- Denton Vacuum Desktop II sputtering unit

Most of the equipment was located in Rowan Hall; however, some of the equipment such as the SEM and related components, the profilometer, and the sputtering units were located in the Science Hall. A majority of the equipment in Rowan Hall was either positioned in the fume hood or in the laminar flow hood. The fume hood was used for any process involving chemicals. Almost all of the other work was performed in the laminar flow hood in order to prevent dust contamination. The laminar flow hood was located on top of the pneumatic isolation table to prevent vibration while imprinting or using the optical microscope.

4.1.1 Imprinting Press: Construction

One of the most important pieces of equipment that was used for nanoimprint lithography was the imprinting press. In order to apply the needed pressure for imprinting, two pneumatic slides were purchased. Both slides are Parker Pneumatic P5T series short stroke thrusters. One is a model 20 and the other a model 100. They both have single center piston with two parallel guiding shafts. The model 20 offers a smaller range of forces that can be applied, but has greater control. The model 100 is able to produce much larger forces than the model 20, but with less control.

A housing unit and imprinting platens were designed and machined for both presses. One for the model 20 was completed first. The overall model 20 imprinting press (i.e. housing unit, stage, and pneumatic slide) is seen in figure 4.1. A stainless steel back plate was screwed into a base with predrilled holes. Through holes were then drilled through the back plate in order to attach the pneumatic slide to it. A three layer sandwich structure was used for the upper and lower platens. At the base of the imprinting press structure, from the bottom up is a block of stainless steel, a ceramic tile, and then an aluminum platen. The same structure is attached to the pneumatic slide. When the pneumatic slide is turned on, the upper aluminum platen will press into the lower one.

This three layer structure was used for a particular reason. The aluminum block is the imprinting platen. It contains three holes closer to the ceramic tile for the three cartridge heaters. Two holes closer to the air surface were drilled for the thermocouple. Depending upon the setup, it was sometimes easier to place the thermocouple in one hole over the other. The top of each aluminum block was mechanically polished in a figure eight pattern on top of a mirror with wet sand paper. This was done to ensure a smooth surface for the imprinter and sample to rest on during imprinting. The operating temperature range of the pneumatic slide is -18 to 74°C. If it is heated over 74°C, the Nitrile seals in it will fail. Therefore, the ceramic tile was used to prevent the rest of the system from heating up. It had to be attached to the structure using glue. The purpose of the stainless steel block was to prevent the ceramic block from being permanently glued to the base. This way the stainless steel block was screwed to the base. Therefore, the aluminum platen and ceramic tile could be removed from the structure if need be. The same thing was done for the upper three layer structure attached to the pneumatic slide.

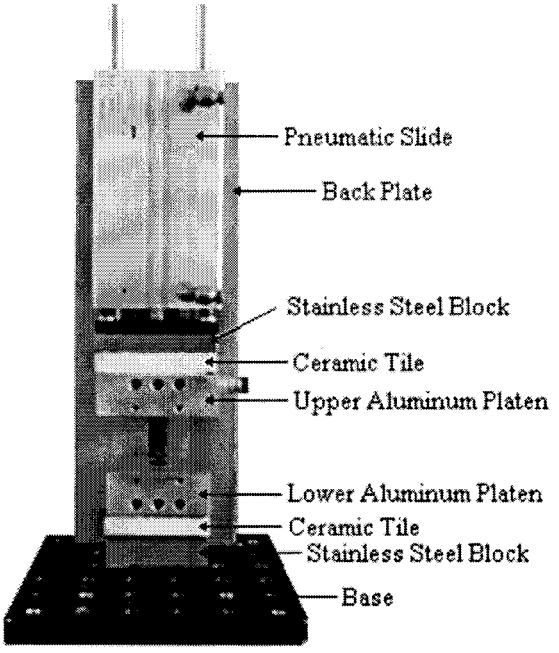

Figure 4.1 Model 20 imprinting press.

Screws could not be used to fasten the ceramic tile to the aluminum block or the rest of imprinting press structure for two reasons. Metal screws would have defeated the purpose of the ceramic insulating block. They would have provided a path for the heat to escape. Second, it was extremely difficult to machine the ceramic tile because of its brittle nature. Therefore, silicone RTV was used as a glue. Silicone RTV was used because of its ability to retain its elastomeric properties at temperatures up to 260°C, its excellent adhesion, and its ability to cure at room temperature. To assemble the three layer structure, the bottom stainless steel block was screwed into the base. A layer of RTV was placed on each side of the ceramic tile. It was then placed on the stainless steel block. Then the aluminum platen was attached to the top of the ceramic tile. The same was done for the upper three layer structure. The pneumatic slide was then turned on and pressed all of the blocks together acting like a vice. By doing this, it was ensured that the two aluminum imprinting platens would be parallel to each other. Because the pneumatic slide needed to be present during the gluing process to ensure that the aluminum imprinting platens were parallel, it was important for the glue to be able to cure at room temperature. The two most important factors of this imprinting press were that the aluminum imprinting platens were precisely parallel to each other and extremely smooth. These two factors are vital to the success of imprinting nanoscale structures.

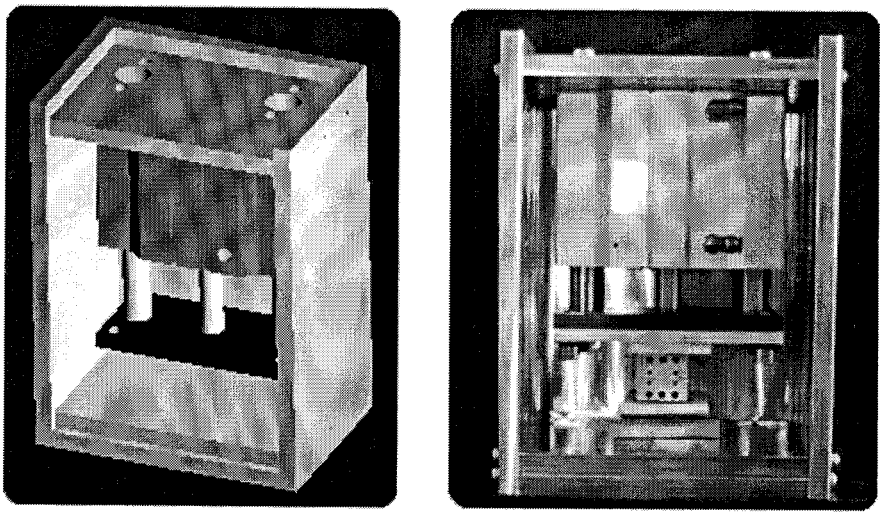

(a) (b)

Figure 4.2 (a) An initial structural design of the model 100 imprinting press in Solid Works. **(b)** The final constructed model 100 imprinting press.

The model 100 imprinting press can be seen in figure 4.2. The exact same imprinting platen design from the model 20 was used for the model 100, but on a slightly larger scale. The housing unit for the model 100 is much more complex because of the weight of the pneumatic slide and the forces that it can produce. The unit was built out of 303 stainless steel. It is enclosed on five sides, and the pneumatic slide is screwed into the top and back plates. The top plate and second plate from the bottom are resting in milled slots to provide more stability than the screws could. Finally, there are two large holes in the top plate for the guiding rails of the pneumatic slide to pass through. This gives extra working room when loading the imprinter and sample.

A control unit was built to operate both imprinting presses. It is seen in figure 4.3. To operate the piston of the imprinting press, the control unit contains a switch, a single solenoid spool valve, and a timing unit. The spool valve controls the position of the piston. A line from a tank of pressurized nitrogen is hooked up to it. It then has a line out to and in from the pneumatic slide. The spool valve is either in the energized or de-energized position. The system was hooked up so that when the spool valve is in the de-energized position, the piston is raised. Once the switch is turned on, 23 Vdc is sent to the spool valve. This places it in the energized position hence lowering the piston and applying pressure to the bottom platen. The switch also activates the timer. Once the timer counts down to zero, the spool valve then raises the piston.

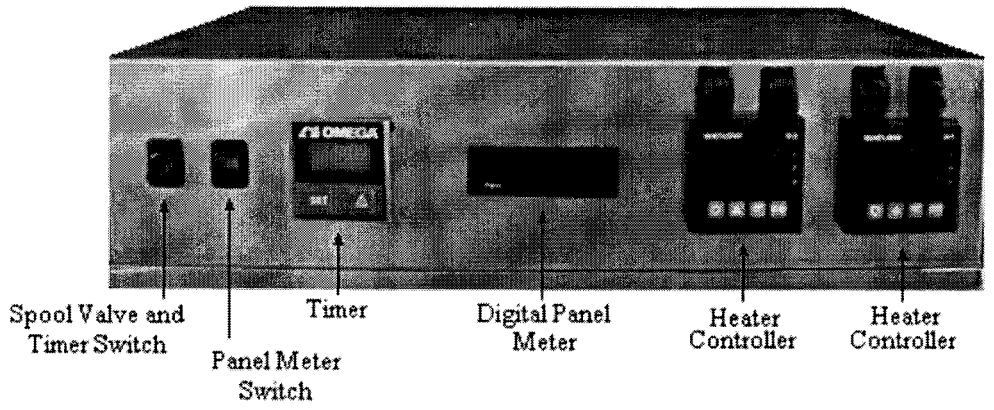

Figure 4.3 The control unit for the imprinting presses.

A pressure transducer that outputs information to a digital panel meter more accurately monitors the pressure than the regulator on the nitrogen supply tank. The transducer is powered with 10 Vdc and the digital panel meter is powered with 5 Vdc. Finally, two heating control units were installed. The one on the left controls three cartridge heaters in the lower aluminum platen. The one on the right controls three cartridge heaters in the upper aluminum platen. A thermocouple is hooked to each heating unit to allow it to monitor the temperature. The control unit can only operate one imprinting press at a time

Each unit is capable of reaching temperatures over 200 °C. The Model 20 can produce a maximum force of 71 lbs and the Model 100 can produce a maximum force of 1765 lbs. A graph displaying the forces of each unit as a function of N_2 pressure is shown in figure 4.4. It can be seen that the smaller unit is capable of far lesser forces, but can be incremented more precisely. The exact opposite is true of the larger model 100 pneumatic slide.

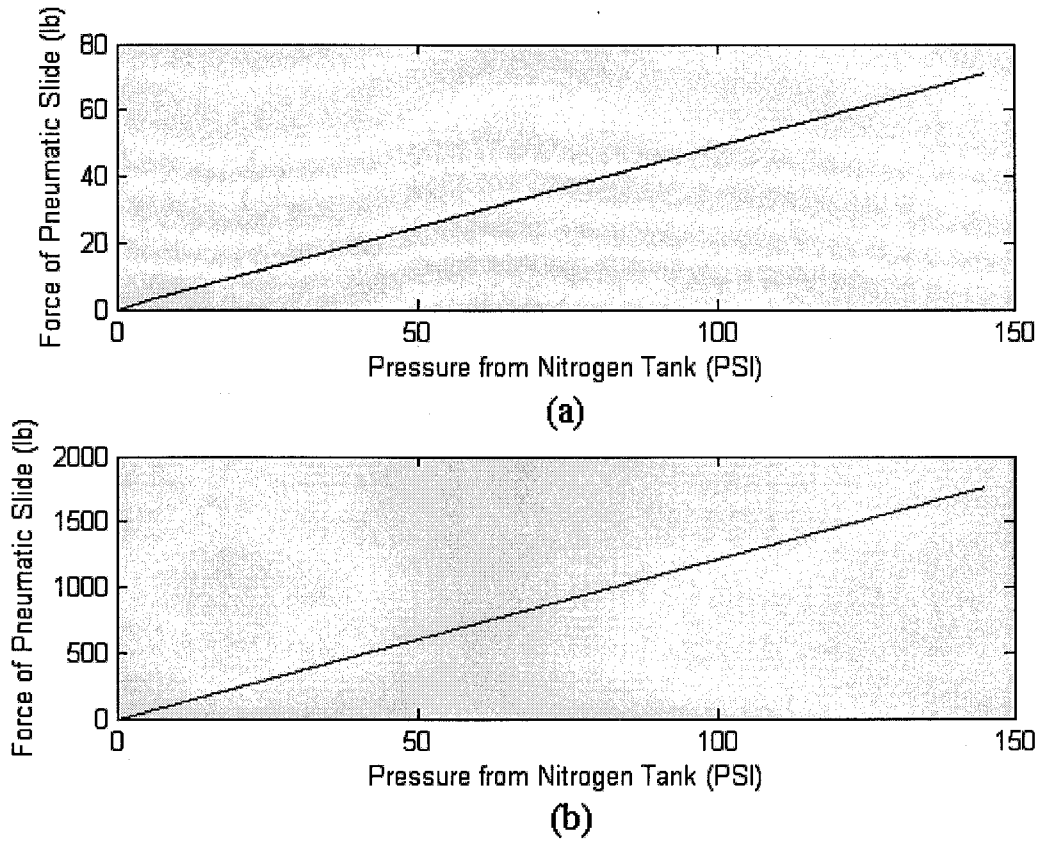

Figure 4.4 A comparison between the forces generated by the **(a)** model 20 **(b)** and model 100 pneumatic slides as a function of N_2 pressure.

4.1.2 SEM: Imaging and Writing a Pattern

The SEM was another essential tool used to carry out the steps of nanoimprint lithography. It was used to image samples for inspection and to perform electron-beam lithography. As stated earlier, electron-beam lithography was used to fabricate imprinters. Imaging a sample was relatively straightforward. The sample was mounted onto a pedestal using carbon tape. The pedestal was then placed in a socket shaped disk that was attached to the SEM stage. The system was then prepared. A vacuum was applied, the accelerating voltage was initiated, the stage was adjusted, the scope detector was initiated, the brightness and contrast were adjusted, and an aperture alignment and stigmation were completed in that order. All of the samples that were inspected were done using the in-lens detector with an accelerating voltage of 6 kV, a working distance of approximately 3 mm, and the 30 μm aperture.

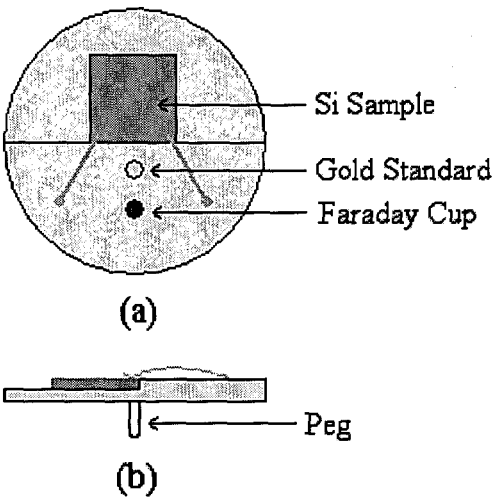

Figure 4.5 An illustration of **(a)** the top down view and **(b)** side view of the specially designed sample holder used during electron-beam lithography.

Using the SEM for electron-beam lithography to write patterns for the fabrication of an imprinter was more involved. To perform electron-beam lithography, the SEM software was used in conjunction with the NPGS software. Before any type of pattern could be exposed in the resist using the SEM and NPGS systems, a pattern needed to be drawn. A pattern was drawn using a CAD program that is linked to the NPGS software. The CAD program enables a user to draw an infinite number of different patterns. However, the pattern has to be made of filled polygons in order to run properly with the NPGS software. After the pattern was drawn, it was checked for errors. It was then saved using a command in the NPGS tab instead of the File tab at the top of the CAD window. Once a CAD file was created, it was converted into a run file. The run file was the file used to control the SEM to write a pattern.

To secure the sample in the SEM before it was written, a specially designed sample holder was used as shown in figure 4.5. The sample holder was designed so that the sample could be wedged against a raised groove and then secured by two clips. The sample holder has a gold standard to accurately perform the stigmation and aperture alignment of the electron-beam. It also has a Faraday cup to measure the current of the electron-beam. The early sample holder was secured to the SEM stage by a peg and hole configuration. A peg on the bottom of the sample holder was inserted into a hole, and it was secured with a screw perpendicular to it. This configuration allowed unwanted movement of the sample holder when the stage was moved.

Therefore, the configuration was later redesigned so that the sample holder was directly screwed into the stage at three different points from the top down.

After the sample was loaded into the SEM, all of the steps mentioned before to prepare the microscope were completed. The multi-purpose secondary electron (MPSE) detector was used for electron-beam lithography. It does not provide as high a resolution as the in-lens, but it had to be used when a sample was electron-beam written. The accelerating voltage normally used for electron-beam lithography was 30 kV, and the in-lens detector is unable to operate at an accelerating voltage greater than 20 kV. The aperture alignment and stigmation were completed using the gold standard on the sample holder with a magnification greater than 100 kX. Then the beam current was measured using the Faraday cup.

Before a pattern was written to a sample at a designated *x,y* location, the surface of the sample at that *x,y* location was brought into focus. This location was not able to be focused using the SEM imaging because that would have exposed the resist before the pattern was written. Therefore, a focused plane was calculated before a pattern was written in a sample. This way, any *x,y* location on the sample had a corresponding *z* or working distance value. This value was used to readjust the working distance bringing the *x,y* location into focus without using the SEM imaging. There were two different methods of focusing and pattern writing that were used. There was a manual method that was used until a more efficient automatic method was ascertained.

For the manual method, four different x,y locations close to the corners of the sample were brought into focus at a magnification greater than 100 kX. Locations too close to the edge were avoided because the resist was built up there from spin coating. Also, the center of the sample was not crossed so that the electron-beam would not expose the resist. To make focusing easier, scratches were made in the resist at the four corners before the sample was loaded into the SEM. The x,y coordinates and the corresponding working distance value at each of these locations were recorded into a Matlab program. The program performed a least squares fit of a plane to the focused points. Now, when any x,y location on the sample was input into the program, a working distance value was calculated. This value that was calculated, was the value at which that *x,y* location would be in focus.

Just before a pattern was written to a sample, the parameters in the run file were adjusted. Normally, if the manual focusing method was used, there was one entity for the pattern in the run

file editor that was being written. The entity of the pattern in the run file editor was where the magnification, pitch, beam current, and dose were adjusted. The three different dose types included area, point, and line. The pitch, amount of dose, and dose type are the parameters that specify what the pattern drawn in the CAD program will be filled with. The pattern could either be solid, a crosshatch array, an of array lines, or an array of pillars. The pitch is the line spacing and center-to-center distance between each point. For simplicity, the values for the line spacing and center-to-center spacing were always kept the same. Therefore, if a pitch of 100 nm is discussed, the line spacing and center-to-center distance are both 100 nm.

After adjusting these parameters, the electron-beam of the SEM was blanked using the SEM software. An external beam blanker was then turned on. The stage was moved to the x,y location of where the first pattern was going to be written using the joystick or by inputting the designated coordinates. The working distance value obtained from the Matlab program to focus that location was input into the SEM software. Then, the run file was activated which took control of the SEM to write the pattern. To write more patterns on the sample, the stage was moved, and this process was repeated until the desired number of written patterns was achieved.

The automatic focusing method eventually became the standard. Gathering focused locations was similar to the manual one. Four different *x,y* locations close to the corners of the sample were brought into focus at a magnification greater than 100 kX. The edges and center of the sample were avoided once again. Also scratches were made on the sample to facilitate focusing. Instead of typing the *x,y* coordinates into a Matlab program, they were entered into the direct stage control which was a tool of the NPGS software. Once a location was focused using the SEM, the spacebar was hit in the direct stage control window to enter the *x,y* coordinates and corresponding working distance. This could only be done if the Remcon32 application was operational. This application allows the NPGS software to interface and thus control the SEM stage. Once four focused locations were acquired in this manner, the enter key was struck to finish acquiring points. The direct stage control, like the Matlab program, performed a least squares fit of a plane to the focused points. A root mean square (RMS) error was then provided. Generally, the goal was to obtain a RMS error value less than 10^{-3}.

The run file editor was set up differently when the automatic focusing and pattern writing method was used. With the manual method, there was usually only one entity for the pattern that was going to be written at a certain location on the sample. To write several patterns

at different locations across the sample, the stage was moved manually using a joystick or by inputting the coordinates of the desired location. The working distance was adjusted, and then the run file was activated to write the pattern at that location. This process was repeated. With the automatic method, the run file editor was set up to include several entities, all of the same pattern created in the CAD program, for the number of patterns that were going to be written on one sample. An *x,y* starting point was designated for where the first pattern was going to be written. It was not mentioned before that besides containing the magnification, pitch, beam current, and dose parameters, each entity also contained an *x,y* move to pattern center location parameter. Once the run file was activated, the first pattern was written at the starting point. Then the stage automatically moved a certain *x,y* distance specified by the *x,y* move to pattern center location parameter in each entity. The next pattern was written at this new location, and this process was continued until all the entities in the run file were written patterns on the sample. Between each pattern, the working distance was adjusted automatically to bring the location of the next pattern to be written into focus. For example, once the run file was activated, 25 different patterns could have been written to a sample without any user interaction.

4.2 Material Processing

Nanoimprint Lithography is a technology based on materials processing. Certain materials are manipulated and transformed to obtain the desired experimental results. It was mentioned in the introduction to this chapter that nanoimprint lithography can be broken into several major steps. A majority of these steps contain the same processes. These processes include cleaving a Si substrate, cleaning it, resist application by spin coating, heat treatments, soaking a sample in a solution, and deposition of Au. These were all simple processes that were used time and time again not only in the several steps involved with nanoimprint lithography, but also in other experiments. They were always performed in the same manner without varying the conditions. This was done so that if the results were not repeatable or a problem arose, these processes were eliminated as a cause. When a problem arises in materials processing, it is always an advantage to quickly eliminate several factors that did not cause it. However, it was impossible to exactly replicate these processes each time they were done because of the human factor involved. For instance, a few drops more of resist might have been placed on some

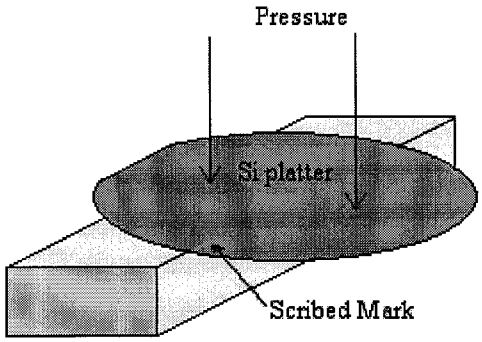

Figure 4.6 An illustration of the cleaving process. A small mark is made parallel to a crystal plane on the Si platter. Pressure is applied to both sides of the mark causing it to be cleaved into two pieces.

samples as compared to others during the spinning process. It was also possible that some samples were coated a second or so longer with Au than others.

All of the resists used for various nanoimprinting steps and experiments were coated onto (100) single crystalline Si substrates. The Si sample had a 200 nm thick layer of SiO_2 that had already been thermally grown on it by the manufacturer. It came in a 6-inch diameter wafer. Therefore, it needed to be cleaved into smaller pieces. A small mark was made on the non-polished side with a diamond scribe. Care was taken to make it parallel or perpendicular to the straight edge of the wafer. This was done to insure that the wafer was cleaved parallel to the crystal plane. Only a small mark was needed because once a crystal plane has been weakened at any point, the rest of the plane can be easily cleaved. The Si wafer to the left of the scribed mark was placed on a raised surface and pressure was applied to hold it down. Then a small amount of pressure was applied on the right half until it was cleaved. This process can be seen in figure 4.6. The process was repeated until the desired sample size was achieved. The size of the pieces depended on the nanoimprinting step or experiment.

Cleanliness was a big issue since all of the work was not performed in a clean room. Before each sample was coated with resist and after it was cleaved to the desired size, it had to be cleaned thoroughly. Cleaning removed the dust particles from the air as well as Si dust produced from cleaving. Dust was a major nuisance throughout all the steps of nanoimprint lithography. If it was present during the spin coating of the resist, it produced streaks in the applied resist. If the streak marks or the actual dust particle were in the location of the yet to be exposed pattern, defects in the pattern were unavoidable. Furthermore, dust was able to easily cover large areas of a pattern on an imprinter as seen in figure 4.7. The piece of dust which is

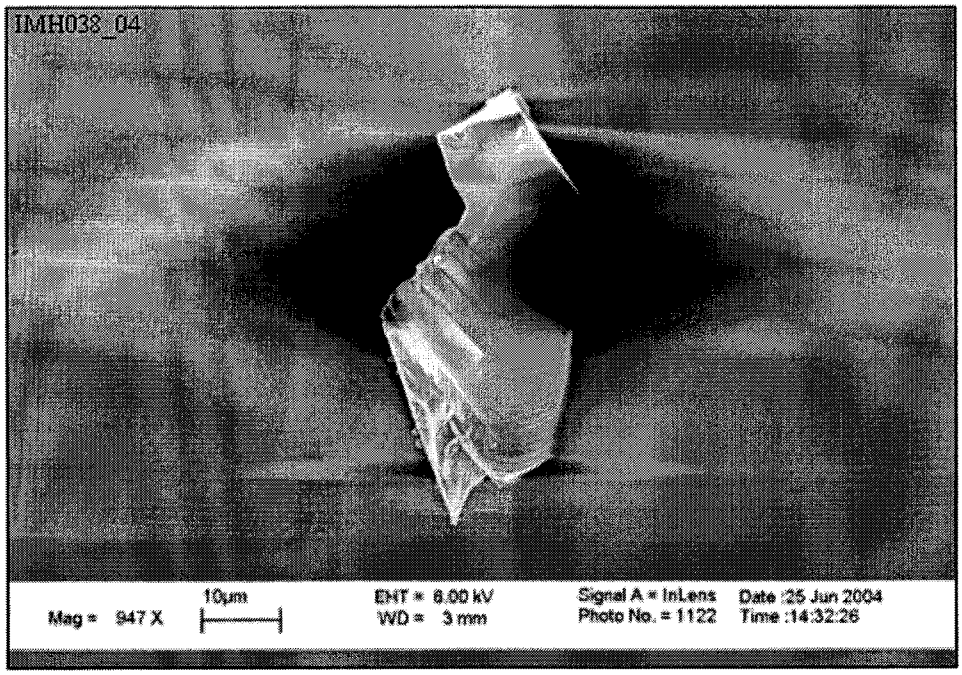

Figure 4.7 A SEM image of a piece of Si dust that has landed on the pattern of an imprinter.

only several micrometers large easily eclipsed a large number of the nanoscale features. This piece of dust could be detrimental to imprinting causing a large number of defects.

Cleaning was done with a process referred to as an acetone or methanol wipe. A sample was secured to the aluminum platter on the spin coating unit by a vacuum. It was then wiped with a lint free wiper soaked in either acetone or methanol. Most of the time acetone was used because it seemed to leave less of a residue after it was washed off. The sample was then blown dry with a stream of pressurized nitrogen (~70 psi). It was eventually decided after a few months of repeating this process that it would also be beneficial to bake the sample on a hot plate to evaporate any leftover acetone or methanol. These steps were repeated until there wasn't any visible dust left on the sample. As a further preventative measure to promote cleanliness, all Si samples were only handled using a pair of gloves and tweezers. This not only prevented dust from coming into contact with the sample, but also prevented fingerprints from marking it. Wearing gloves also prevented people's hands from coming into contact with the hazardous chemicals that were used.

After a sample was cleaned, it was coated with a resist. It was first placed in the center of the aluminum platter on the spin coating unit and secured with a vacuum. It was then repositioned several times by pushing it with a pair of tweezers until it was completely centered.

Great care was taken to center the sample because if it was not, the resist would not spin on evenly. The resist was applied using a disposable plastic pipette. Several drops were placed on the sample until it was completely covered. The resist was either deposited while the sample was stationary or as it started to spin. If there were a lot of streak marks from dust particles, the resist was washed off. Then the sample was cleaned again.

Several steps of nanoimprint lithography require some type of heat treatment and for the sample to be soaked in a solution. Whether it is to drive off a solvent, evaporate a cleaning agent, or strengthen bonds in a material, heating was needed at certain times. Heating was either done in an oven or on a hotplate. When heating was done in the oven, the samples were placed in a petri dish. When the heating was done on a hotplate, the samples were placed directly on it. They were also placed in the center because the outer edges of the hotplate did not heat up to the desired temperature.

Whether it was for development, a liftoff, or wet etching, soaking samples in some type of solution was often performed. The solution was poured into a 100 mL glass beaker and the sample was submerged in it. After a specified time, the sample was removed from the solution with a pair of tweezers. It was placed on the aluminum disk of the spin coating unit and secured with a vacuum. It was either rinsed off or blown dry with a stream nitrogen.

Most of the time, it was extremely difficult to examine a sample in the SEM without a coating of Au on it. This was the case especially if the sample was covered in a resist such as PMMA. The electron-beam exposed the resist resulting in a poor image. To coat a sample with Au, a desktop sputtering system was used. The system was pressurized to 100 mTorr with Ar. Then a layer of Au was sputtered onto the surface of the sample for 15 seconds at 30 mA. It resulted in a thickness of approximately 5 to 10 nm. The only problem with coating a sample with gold was that it was difficult if not impossible for it to be used as an imprinter or in the case of an imprinted sample to be processed further.

4.3 Imprinter Fabrication

The theory behind two imprinter fabrication techniques using electron-beam lithography was presented in the last chapter. One technique used a bilayer resist of positive PMMA to create SiO_2 imprinters. The other technique used a negative HSQ resist that when exposed to

electron or thermal radiation became as durable as SiO_2. The imprinters produced from this method were referred to as HSQ imprinters. Both methods are capable of producing durable imprinters; however, it was pointed out that HSQ imprinters could be fabricated in fewer steps. This translates into an easier fabrication process with fewer possible defects. In this section, the process guidelines, encountered obstacles, and the results of using both methods are presented. There are several terms in this section that were used to describe certain structures. The term "sample" in this section refers to a square piece of Si several millimeters in size before it has been fabricated into an imprinter. The term "imprinter" refers to the same piece of Si that has gone through all of the necessary fabrication steps. Finally, a "pattern" is the term used to describe one of the several regions of nanoscale features on an imprinter.

4.3.1 SiO_2 Imprinter Fabrication

There are six main steps that are involved with the fabrication of a SiO_2 imprinter. These steps contain a number of different variables that can be adjusted and tweaked in order to obtain high-quality results. The primary goal was to figure out what variables needed to be adjusted to produce high-quality SiO_2 imprinters. The method that was used to fabricate each SiO_2 imprinter was derived from the thesis on *Bilayer Nanoimprint Lithography for Sub 100 nm Features* [70]. The first section outlines the conditions required to create a SiO_2 imprinter. This outline was typically followed to fabricate all of the SiO_2 imprinters. The original method was modified at Rowan in order to obtain enhanced results. Any variable changes that were made to the process were done to produce better results. These changes along with the results of fabricating SiO_2 imprinters are discussed in the second section. The most frequently changed variables were the point dose and pitch.

4.3.1.1 Initial Fabrication Process

Before a pattern was written, a substrate was coated with an electron sensitive resist. A bilayer of 2% 100k PMMA and 1% 950k PMMA both dissolved in chlorobenzene was used. Both resists are positive. A bilayer resist was chosen to create an undercut as seen in figure 3.24. For the same exposure time to the electron-beam, a greater volume of the 100k PMMA is exposed than the 950k PMMA because of its lighter molecular weight. This created the required

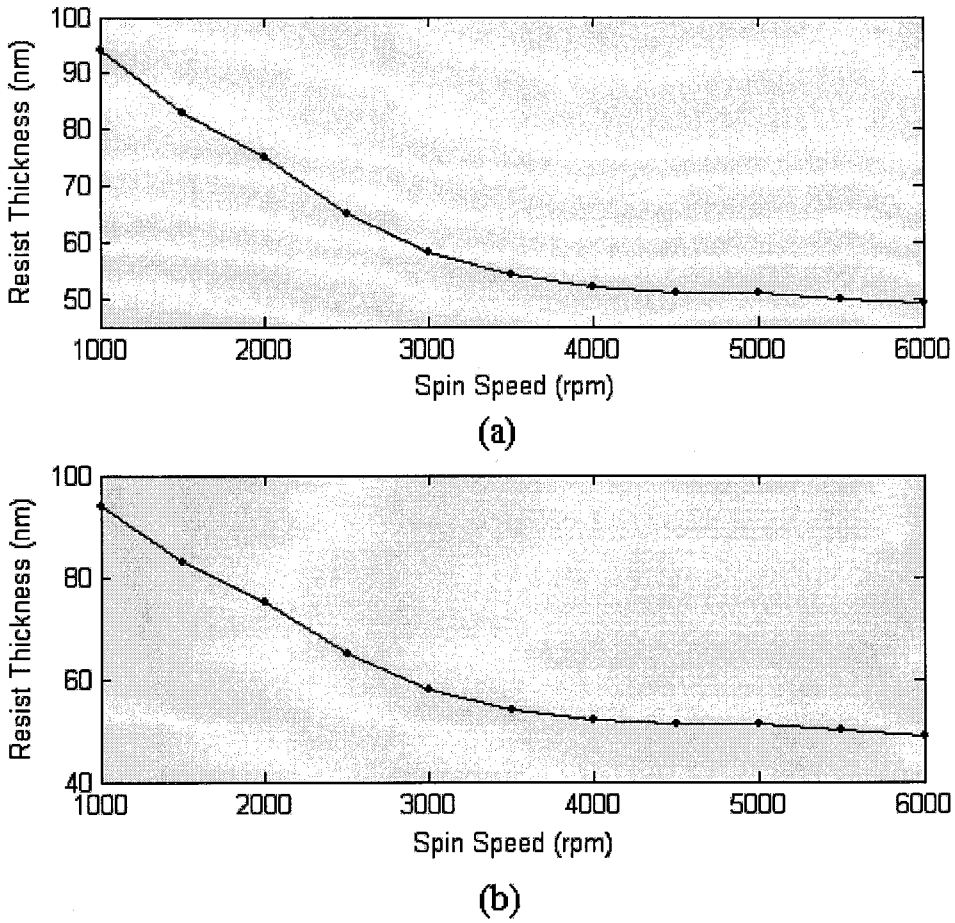

Figure 4.8 Spin Curves for **(a)** 2% 100k PMMA in chlorobenzene and **(b)** 1% 950k PMMA in chlorobenzene on a Si substrate.

undercut. It was used to prevent the metal from tearing off the substrate surface during a liftoff. Therefore, the 100k was chosen to provide a higher sensitivity and the 950k was chosen because it provides the best resolution. The 2% 100k PMMA in chlorobenzene was obtained from Columbia University. It was decided not to dilute this PMMA. It had the right concentration that was needed for the desired thickness. A bottle of 2% 950k PMMA in chlorobenzene had already been purchased from Microchem Inc. In order to obtain the desired concentration for spin coating, 3 mL of 2% 950k PMMA in chlorobenzene was diluted with 3 mL of chlorobenzene to obtain 1% 950k PMMA in chlorobenzene.

A SiO_2 imprinter was fabricated out of a 10 mm x 10 mm sample of Si. A sample was cleaned using the acetone wipe method. Then it was coated with a 2% 100k PMMA. The resist was then spun onto a sample at 4000 rpm for 30 seconds. These settings were used to obtain a 50 nm layer of resist. The spin curve for 2% 100k PMMA in chlorobenzene as seen in figure

4.8(a) was used as a guideline. If there were not a lot of streak marks present from dust contamination, the sample was then transferred to the oven. It was heated for approximately 15 minutes at 170°C to drive off the solvent. If there were too many streak marks, the sample was then run through the cleaning process again.

Once a sample was baked to drive off the solvent of the first layer, it was allowed too cool for several minutes. Before it was coated with the second layer of resist, it had to be blown dry with nitrogen to remove any dust particles. Then, several drops of 1% 950k PMMA were applied to it. To produce a 50 nm thick layer, the resist was spun onto a sample at 3500 rpm for 30 seconds. The spin curve for 1% 950 k PMMA in chlorobenzene is seen in figure 4.8(b). If the spun-on layer of resist had no evident streaks, it was baked to drive off the solvent under the same conditions as the first layer. However, if the second resist layer had too many streak marks to effectively perform electron-beam lithography, the entire process was redone. It was cleaned to wipe off all the resist, and then the resist application was started again from the first layer. Once a sample was coated with a good bilayer of resist, it was secured to the sample holder in the SEM.

Next, a pattern was drawn in the CAD program. A 100 μm x 100 μm pattern with two equilateral triangles pointing to either side of it was drawn as seen in figure 4.9(a). The sides of the triangles were drawn to a length of 50 μm. The idea was to make the triangles solid to provide support and a reference to the square pattern. The square was to contain an array of nanoscale pillars. To make the pillars, an array of holes first had to be exposed in the resist by the electron-beam lithography as seen in figure 3.13. To fabricate a SiO_2 imprinter, ten of these patterns were written onto a sample as shown in figure 4.9(b). The patterns that were written onto a sample to fabricate a SiO_2 imprinter were done using a 25 μm aperture, an accelerating voltage of 30 kV, and a working distance of approximately 6 mm. These parameters were adjusted in the SEM software. Also, the magnification for the square and triangle patterns was always set to 1000 X and 25 X respectively. These magnification values were selected to provide a field of view just large enough to expose each of the patterns. The magnification was adjusted in the run file editor. Finally, the manual focusing and writing method with the external beam blanker was used to write each pattern for a SiO_2 imprinter

The goal of the electron-beam lithography step was to write an array of holes in the square pattern and completely expose the triangles. The pattern was repeated 10 times on a

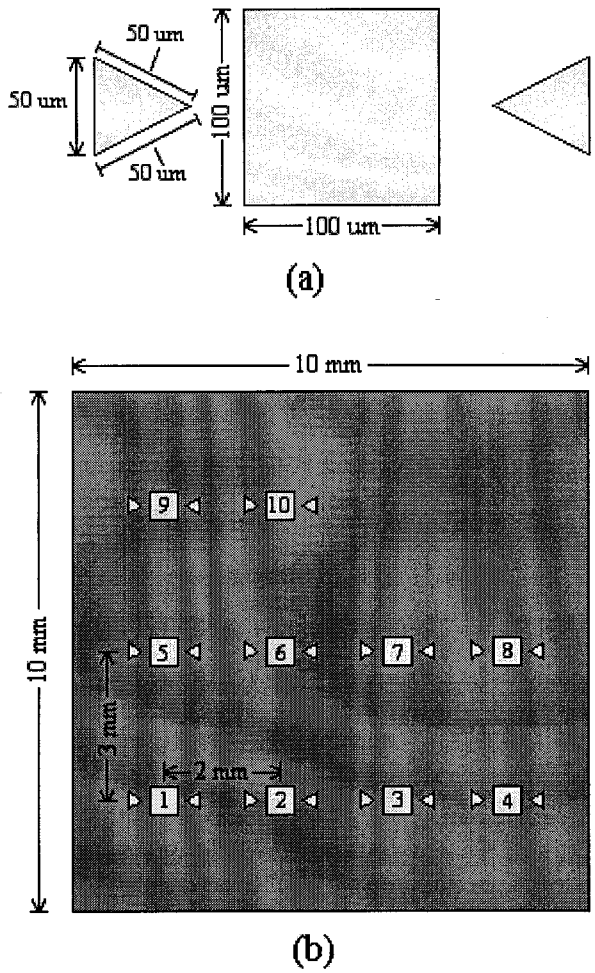

Figure 4.9 (a) An illustration of the pattern used for the SiO_2 imprinters. The triangles are solid reference and supporting structures, and the square is an array of nanoscale pillars. **(b)** An illustration of a SiO_2 imprinter showing the configuration in which the patterns were written onto it.

sample either with the same hole diameter and pitch or with different hole diameters and pitch values for each. Since the PMMA bilayer is a positive resist, any area that was exposed to the electron-beam dissolved in the developer. The critical dose to expose PMMA using an accelerating voltage of 30 kV is 300 $\mu C/cm^2$. Therefore, an area dose of at least 300$\mu C/cm^2$ was used to expose the triangles. This parameter was not varied too much because the triangles were not too important to the research. They merely provided structural support for the pillars and a reference to the square pattern. To produce the required array of holes, a point dose was used. Obviously by selecting a smaller point dose, smaller diameter holes were produced. Table 4.1 provides calculated point dose values needed to produce certain diameter holes. The formula that was used to obtain the calculated point dose values is

Table 4.1 The calculated point doses needed to expose selected diameter nanoscale features in a PMMA resist.

Diameter of Feature (nm)	*Area of Feature (nm^2)*	*Required Dose (fC)*
10	78	0.234
20	314	0.942
30	707	2.12
40	1256	3.77
50	1963	5.89
60	2827	8.48
70	3848	11.5
80	5026	15.1
90	6361	19.1
100	7853	23.6

$$Point\ Dose = (Area_{hole}) \times (300\ \mu C/cm^2). \tag{4.1}$$

For a given point dose, there was a minimum pitch that could be used. If too large of a point dose was used with too small of a pitch, the pattern became overexposed. Instead of having an array of holes, the pattern was more solid. It will be seen that the point dose and pitch were varied systematically to produce a properly exposed array of holes.

The calculated values in table 4.1 were not always trusted to produce the exact hole diameters. This was because of the proximity effect [50]. As the pitch between the holes or features was decreased, adjacent holes received greater doses. This is due to the scattering of electrons. Because of the proximity effect, the calculated values of table 4.1 were not solely used to determine what point dose was needed for certain feature sizes and pitches. Experimental data was also needed. This was accomplished by exposing several patterns and varying either the point dose or the pitch while holding one constant. To gather experimental data, the point dose was held constant and the pitch was varied. It was discovered later that varying the point dose instead was more beneficial. It was done this way originally because the practices involved with electron-beam lithography were still being learned at the time. Also, it was done quickly so that a collection of samples could be sent out to be etched.

After the patterns were written to a sample, it was developed in a 1:3 mixture of MIBK:IPA for 1 minute. It was then blown dry with nitrogen, rinsed with IPA, and then blown dry again. At this point, a sample was either sputter coated with Au or a layer of Cr was

evaporated onto it. A sample was coated with Au in order to inspect it in the SEM. However, once a sample was coated with Au for inspection, it was not developed and used as an imprinter. Evaporation of Cr onto a sample was the next step in the fabrication of a SiO_2 imprinter. However, at the time, an evaporation unit was not available at Rowan University. Therefore, an evaporation unit at Columbia University was used to coat a sample with Cr. A 10 to 15 nm layer of Cr was evaporated onto a sample.

Once a sample was coated with Cr, a liftoff was performed. It was soaked in a 1:1 mixture of methylene chloride and acetone for 30 minutes. The beaker containing this solution and the sample was then placed in a sonicating unit where it was sonicated for 5 minutes. This step removed all of the PMMA from the sample. The only thing left on the SiO_2 surface after this was an array of Cr dots. Finally, a sample was subjected to plasma etching using a machine at Cornell University. Etching physically removed most of the SiO_2 layer, lowering the entire surface except where the Cr dots were positioned. This created ten 100 μm x 100 μm patterns of SiO_2 pillars on a sample. The etching created approximately 100 nm tall SiO_2 pillars. After this, the fabrication of a SiO_2 imprinter was complete.

4.3.1.2 Results and Variable Adjustments

Four Si samples were created with 10 patterns written on each of them as shown in figure 4.9(b). Three of the samples were developed into SiO_2 imprinters. One of the samples was used to gather experimental data. The ten patterns written on it were used to determine what size features a certain point dose created. They were also used to determine what the minimum pitch was for a selected dose. Table 4.2 lists the images of nine of the ten patterns and the conditions in which they were written in the resist of the experimental sample. The measured hole diameter of each pattern is also given. The sample and pattern number is also provided. The *IMS* prefix before the sample number denotes that it is a SiO_2 imprinter. The pattern number corresponds to the numbers in figure 4.6(b),

A dose of 14 fC was used for the patterns shown in images A.1-7. It can be seen from images A.1-2 that the dose was too great for a 75 and 100 nm pitch. Both patterns were entirely exposed in the same way as the triangles instead of creating an array of dots. A few holes were

Table 4.2 A list of several patterns after being developed and coated with gold. They were written on the same sample. Each line with a point dose and pitch is a different pattern on the sample shown in the designated image(s).

Image Number	*Sample #_Pattern #*	*Point Dose (fC)*	*Pitch (nm)*	*Measured Hole Diameter (nm)*
A.1	IMS002_01	14	75	No features
A.2	IMS002_02	14	100	No features
A.3-4	IMS002_03	14	200	84
A.5	IMS002_04	14	400	77
A.6	IMS002_05	14	800	84
A.7	IMS002_06	14	1000	84
A.8	IMS002_08	13	100	No features
A.9	IMS002_09	13	200	107
A.10	IMS002_10	13	400	106

created along the border of the pattern as seen in image A.2. However, the rest of the pattern was fully exposed because a point dose of 14 fC was too great for a pitch of 100 nm. The patterns in images A.3-7 turned out better because the pitch was greater. The diameter of the holes produced in these patterns is in agreement with the calculated values in table 4.1. A majority of the measured diameters produced with a 14 fC point dose are approximately 84 nm. A point dose of 14 fC was calculated to produce a feature diameter of just less than 80 nm. A dose of 13 fC was used for the patterns shown in images A.8-10. The pattern in images A.8 which has a pitch of 100 nm contains a very messy array of holes. Because the dose was decreased, the entire pattern was not exposed like the pattern created with a 14 fC point dose and 100 nm pitch in image A.2. The patterns in image A.9-10 were written with pitches of 200 and 400 nm respectively. The measured diameters of the holes are approximately 107 nm. Since a lesser dose was used for these patterns with the same pitches as the patterns shown in image A.3-5, the hole diameters should be less. These feature sizes are anomalies that were possibly caused by improper focusing techniques or an uneven surface.

The 10 patterns on the experimental sample demonstrated that a point dose of 14 fC produced approximately 80 nm diameter holes when a pitch greater than 200nm was used. Therefore, another sample was written using a 14 fC point dose and various pitches to produce an imprinter. A smaller point dose could have been used in order to decrease the feature size and hence be able to produce patterns with shorter pitches. However, it seemed more beneficial to start with larger features and pitches at first. Moreover, it was believed that the SiO_2 pillars created after etching would be smaller in diameter than the holes created in the PMMA. Also,

Table 4.3 A list of several imprinter patterns after being etched. Each line is a different pattern on an imprinter shown in the designated image(s).

Image Number	*Sample #_Pattern #*	*Point Dose (fC)*	*Pitch (nm)*	*Measured Pillar Diameter (nm)*
A.11-12	IMS004_10	13	150	65
A.13-14	IMS004_03	13	200	52
A.15-16	IMS004_04	13	400	54
A.17	IMS004_07	13	2000	58
A.18	IMS003_03	14	200	40
A.19	IMS003_02	14	400	50
A.20	IMS001_02	15	200	47

two more samples with various pitches were written with 13 and 15 fC doses in order to produce imprinters. At the time, it seemed practical to use 13 and 15 fC doses to see what the results would be.

The patterns on the three SiO_2 imprinters were inspected after plasma etching was completed. Table 4.3 provides a list of images of different patterns on certain imprinters. These patterns were written with the point dose and pitch listed in the table. Furthermore, the measured diameter of the pillars for these patterns is provided. The feature size or diameter of the pillars ranges from 40 to 70 nm. The prediction that the SiO_2 pillars would be smaller in diameter than the holes in the PMMA was correct. This effect is seen because there will be some imperfections that will cause the Cr dots created through evaporation to be smaller than the holes. The pitch used for each pattern varied from 150 to 2000 nm. The pillar height was approximated by inspecting the pattern shown in images A.21-22. The images show the height or depth of the plasma etching. The PMMA in this pattern was completely exposed because the point dose, 14 fC, used was too great for the pitch, 100 nm. Therefore, a solid 100 μm x 100 μm plateau of SiO_2 was created from etching. It appears to be 126 nm tall. Therefore, the pillars created in the other patterns are comparable to this measurement. Finally, the patterns were examined for defects. The ones mentioned thus far are relatively free of defects as evidenced by the images.

There were several other patterns that were not free of defects. A majority of these damaged patterns were a result of overexposure of the resist to the electron-beam. This was something that could have been easily fixed by making an adjustment before the patterns were written. There were also several other defects that were spotted. It was concluded that these defects had to have occurred during etching. Since etching was not done at Rowan University, it would have been very difficult to correct the problems that caused these defects. All of the

imprinters had noticeable discolorations that were first detected in the optical microscope as seen in image A.23. Upon further inspection using the SEM, it seemed that these discolorations were a result of the plasma etching not working on certain areas as seen in images A.24-25. Therefore, the surface in certain areas of the imprinter had been lowered and in other regions it had not been. The cause of this is still unknown. Another defect that was noticed was that certain patterns were significantly scratched and covered in debris as seen in images A26-28.

Only a small amount of time in the beginning of the research was devoted towards the fabrication of SiO_2 imprinters. The one sample mentioned in which it was developed and then coated with Au to gather experimental data was the only one of its kind made. The three SiO_2 imprinters with 10 patterns on each were the only ones made. Further research was not conducted for three reasons. First, the process of fabricating a SiO_2 imprinter involved too many steps. Another method was discovered that could be done in a fewer number of steps. The etching step could not be completed at Rowan University. Therefore, it became very difficult to correct the problems that caused the aforementioned defects. Finally, it took close to three months for the three samples to be etched and returned to Rowan University. This was partially due to the plasma etching unit at Cornell University being non-operational at the time. However, it was felt that something similar to this could occur again. Even if it didn't, the shortest amount of time to fabricate an imprinter with this method was estimated to be around a week. Remember that the Cr evaporation had to be done elsewhere also. This was too long of a time especially with a more efficient method available.

4.3.2 HSQ Imprinter Fabrication

As it turned out, a more efficient method of fabricating imprinters was identified in the winter of 2003. With it, imprinters were fabricated using a spin coatable oxide resist known as HSQ. It was noted that the required number of steps to fabricate an imprinter using HSQ were cut in half. The steps of fabricating a HSQ imprinter include spin coating HSQ resist onto a Si sample, the exposure of a pattern in the resist, development of the pattern, and a post bake treatment. The three trickiest steps of Cr evaporation, liftoff, and etching were eliminated by using this method. With Cr evaporation and etching eliminated, all of the steps were completed at Rowan University in a matter of approximately 4 to 6 hours. This was a tremendous

improvement over the previous method. For this reason, an extensive amount of research was completed towards the fabrication and implementation of HSQ imprinters. The first section outlines the conditions used to create a HSQ imprinter. This outline was typically followed to fabricate all of the HSQ imprinters. Any variable changes that were made to the process were done to produce better results. These changes along with the results of fabricating HSQ imprinters are discussed in the second section. Once again, the most frequently changed variables were the point dose and pitch.

4.3.2.1 Initial Process

HSQ is known as a flowable oxide (FOX-12) and is available exclusively from Dow Corning Inc. It had to be shipped in a thermally insulated container. As soon as it arrived, it was immediately stored in the refrigerator. HSQ needs to be kept cool at all times because at room temperature, it will begin to chemically breakdown. In an effort to prolong the life of the HSQ, a small amount was poured into an auxiliary container. Before a sample was coated with HSQ, the auxiliary container was taken out of the refrigerator. It was then allowed to sit at room temperature for approximately 15 minutes. This allowed it to acclimate to room temperature and guaranteed a relatively consistent coating of a sample.

Initially, a 10 mm x 10 mm sample was used to fabricate a HSQ imprinter. Eventually an 8 mm x 8 mm sample size was used. This was done in order to accommodate the samples that were imprinted into. After a sample was cleaved, it was washed using the acetone wipe method. HSQ was then spun onto it at 2000 rpm for 30 seconds. The HSQ was not diluted so this speed produced a 100 nm thick layer. A 150 or 160 nm layer of HSQ could have been produced by spin coating at 1500 or 1000 rpm respectively. If a sample contained dust streaks, it was cleaned and recoated with HSQ. After a sample was coated with HSQ, it was then heated on a hotplate for 3 minutes at 250°C. Heating a sample before it was written was in a sense a pre-exposure. It enhanced the sensitivity of the HSQ [73]. This reduced the contrast, but not by any substantial amount. After a sample was coated with HSQ and heated, it was secured to the sample holder in the SEM.

A pattern similar to the one used for a SiO_2 imprinter was used for a HSQ imprinter. A 100 μm x 100 μm pattern was drawn as seen in figure 4.9(a) except it was without the triangles

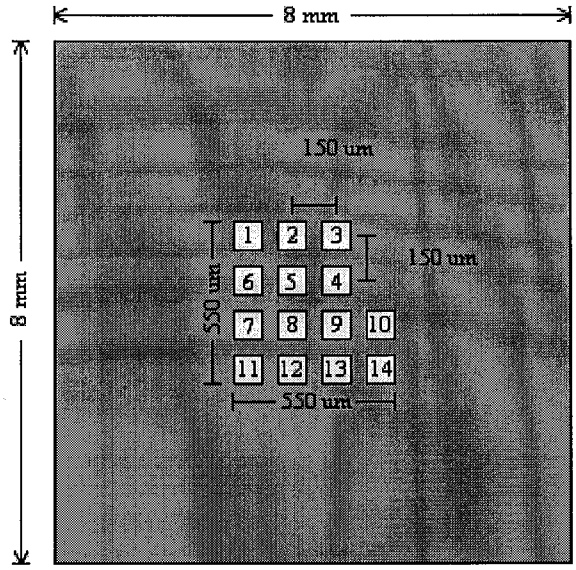

Figure 4.10 An illustration of an HSQ imprinter showing the configuration in which the 100 μm x 100 μm patterns were written onto it.

flanking it on either side. For a HSQ imprinter, 14 patterns were written onto a single sample in the configuration shown in figure 4.10. All 14 patterns were written in the center of the sample. A starting point was calculated for the first pattern to achieve this. It was done by first obtaining the center point of the sample from the *x,y* coordinates of the edges. Then half the length, 225 μm, of the overall structure was added to the *x* coordinate and subtracted from the *y* coordinate of the center point of the sample. All of the patterns that were written in the resist of a sample to produce a HSQ imprinter were done using a 30 μm aperture, an accelerating voltage of 30 kV, and a working distance of approximately 6 mm. Also, the magnification to write the square pattern was set to 1000 X. Finally, the automatic focusing and writing method without the external beam blanker was used to write each pattern for each HSQ imprinter.

The goal was to write an array of pillars in the square pattern that was drawn in the CAD program. The pattern was repeated 14 times on a sample either with the same pillar diameter and pitch or with different pillar diameters and pitch values for each. Since HSQ is a negative resist, any area that was exposed to the electron-beam became strengthened. The unexposed regions dissolved in the developer. Once again, to produce the array of pillars, a point dose was used. One experiment showed that the critical dose of HSQ is approximately 1900 $\mu C/cm^2$ for isolated features and 1400 $\mu C/cm^2$ for features with a spacing of 100 to 200 nm [71]. The densities used in these experiments were much too great for what was needed. Also, the accelerating voltage

for each critical dose was not given. To complicate matters more, the proper dose needed to expose a HSQ resist depends on the amount of time it is left at room temperature before it is exposed. Therefore, it seemed only plausible to determine the required dose for certain pitch values through experimentation. At first, a point dose of 25 fC with a pitch of 50 nm produced high quality features.

After the patterns were written to a sample, it was developed. A sample was developed with 25% NaOH in DI water for 2 minutes. After it was developed, it was secured on the spin coating unit with the vacuum and rinsed with DI water. Then it was blown dry with pressurized nitrogen. After this, a sample was either coated with Au for inspection or exposed to a heat treatment. The heat treatment was done to increase the strength of the HSQ pillars. It was heated at 400°C for 2 hours. After a sample was heated, the fabrication of the HSQ imprinter was complete. Sometimes, a sample was coated with Au after the heat treatment. However, once a sample was coated with Au, it was not used as an imprinter.

4.3.2.2 Results and Variable Adjustments

The first HSQ imprinter, IMH005, that was fabricated was done using all of the conditions stated in the last section. It was subjected to a final heat treatment and was then coated with Au for inspection. The 14 different patterns on the imprinter were exposed using a different point dose and pitch. Three different patterns were exposed with a point dose of 10 fC and pitch values of 75, 100, and 125 nm. Another three were exposed with a point dose of 14 fC and the same pitch values. Four were exposed with a point dose of 18 fC and pitch values of 75, 100, 125, 150 nm. Finally, another four patterns were exposed with a point dose of 25 fC and pitch values of 50, 75, 125, and 150 nm.

All of the patterns that were produced except for one were underexposed. The point doses of 10, 14, and 18 fC were not great enough. A point dose of 25 fC was still not strong enough for pitch values of 75, 125, and 150 nm. The underexposed patterns were covered with collapsed pillars as shown in images A.29-30. The point dose of these patterns was not strong enough to fully promote a change in the chemical structure of the HSQ from the caged structure to the more robust network structure. Therefore, the HSQ pillars that had been exposed to the electron-beam either dissolved or collapsed when the sample was developed. It was obvious that

the dose needed to expose HSQ was not in the range of that needed for PMMA. Also, the greater dose that HSQ required increased the exposure time.

The only pattern with a high-quality array of pillars was the 13th one that was exposed. A 25 fC point dose and a 50 nm pitch were used to expose it. The pillars of the pattern can be seen in images A.31-36. A majority of the pattern was free of defects and uniform. A uniform and defect free 3.5 μm x 5 μm area of pillars can be seen in image A.31. The measured diameter of the pillars is 31 nm and the measured pitch is 51.2 nm as seen in image A.32. The measured height of the pillars varied between 87 and 100 nm. This is relatively consistent with the 100 nm thick layer of HSQ that was spun onto the sample. The height of the pillars was measured by using pillars that had collapsed as seen in images A.33-34. The beam blanker was not used when the HSQ resist was exposed because it had failed. The result of not having a beam blanker can be seen in image A.35. There is a line of HSQ residue left between each pillar. This line was exposed because the beam passed over it. Finally, image A.36 shows an angled view of the upper right corner of the pattern near the SEM dump point. The dump point is a location where the electron-beam is positioned before it begins writing a pattern. It is only produced when a beam blanker is not used in conjunction with writing.

A 25 fC point dose worked for a 50 nm pitch and not for pitches of 75, 125, and 150 because the proximity effect was greater when the spacing of the features was reduced to 50 nm. Even though pattern 13 had a well exposed array of pillars, it still contained a number of collapsed pillars around the edges of it. This can be observed in images A.37-40. Near the edges of the pattern, the proximity effect is not as great because there are not as many adjacent areas that were exposed as in the center of the pattern. There is a slight change in texture from the bottom to the top of the pattern seen in image A.40. At the bottom near the edge, all of the pillars have collapsed. Towards the center of the pattern, more and more pillars are free standing until all of them are.

An appreciable amount of information was obtained from the fabrication and inspection of the first HSQ imprinter. At least a 25 fC point dose was needed to expose an array of pillars in the HSQ for a pitch of 50 nm or less. If a lesser point dose or greater pitch was used, the pillars collapsed when the imprinter was developed. Furthermore, the processing conditions were assumed to be slightly narrow. A point dose of 25 fC was enough to expose the center of the pattern with a pitch of 50 nm. However, it was not enough to expose the edges of the pattern.

The mere absence of the proximity effect around the edges of the pattern caused the pillars to collapse. The proximity effect increases the dose to a certain point or area. A lesser dose around the edges prevented the HSQ from fully strengthening and cause the pillars to collapse. At first, it was thought that maybe a 25 fC point dose was on the very edge of the necessary point dose needed to expose a pattern with a 50 nm pitch. To negate this theory, the same effect around the edges was also seen when a 30.5 fC point dose was used with a 50 nm pitch to expose the pattern seen in image A.41. No matter what the dose was used, the pillars around the edges of all the patterns were collapsed. The pillars around the edges always collapsed. Although, this was attributed to the absence of the proximity effect, it could have been some other factor that could not be identified.

Since a 25 fC point dose was needed, a majority of the other patterns on all the imprinters were exposed with a point dose equal or greater. In the beginning of the research, a point dose less than 25 fC was occasionally used. It was used to expose a pattern with a pitch less than 50 nm. However, with limited attempts, this was unsuccessful. Patterns in six other HSQ imprinters were exposed using pitches other than 50 nm. Then it was decided to expose the rest of the patterns on imprinters with a 50 nm pitch. This was done because successful results on imprinter IMH005 had already been obtained using a 50 nm pitch. By using just one pitch, it was believed that results using this pitch could be finely tuned. Also, a pitch of 50 nm provided an appreciable areal bit density of 258 Gbits/in^2.

Despite the fewer steps needed to fabricate a HSQ imprinter compared to that of a SiO_2 imprinter, there were two problems that impeded the fabrication of HSQ imprinters. Both problems dealt with the quality of the pillars. The first problem was noticed after observing the patterns on several imprinters that had been fabricated. It was discovered that the point dose needed to expose the patterns varied. A point dose that produced a high quality array of pillars in one pattern sometimes under or overexposed another pattern. In the underexposed case, the pillars collapsed after development. In the overexposed case, a mostly solid plateau of HSQ was formed. It was just demonstrated that a 25 fC point dose and 50 nm pitch produced a high quality array of pillars. However, the same dose and pitch produced underexposed patterns on imprinters IMH023-25. This is evidenced by the collapsed pillars seen in images A.42-44 respectively. The pillars shown are in the center of the pattern and not near the edges. Moreover, the same dose and pitch also overexposed a pattern on imprinter IMH022 as seen in

image A.45. A 24.5 fC point dose also overexposed a pattern on IMH022 as seen in image A.46. If anything, a lesser dose should have underexposed the pattern. The problem was also observed using other doses besides 25 fC. A 28.5 fC point dose underexposed, properly exposed, and overexposed different patterns as seen in images A.47-49 respectively.

After time, it was noticed that this problem could be detected optically. After a sample was developed, the color of the patterns on it indicated whether they were underexposed, properly exposed or overexposed. An underexposed pattern appeared light purple like the ones seen on imprinter IMH048 in image A.50. The patterns in the optical image proved to indeed be underexposed after a SEM observation. The pillars in the center of pattern 1 had collapsed as seen in image A.51. A properly exposed pattern appeared dark purple. Image A.52 shows an optical image of properly exposed patterns on imprinter IMH089, and image A.53 shows an SEM image of pattern 1 on it. Finally, an overexposed pattern appeared green as seen in image A.54.

The problem did not always occur. Several imprinters were produced using a certain dose that did not contain any under or overexposed patterns. However, the problem did occur from time to time. It made it difficult to determine the needed dose to expose a pattern with a 50 nm pitch. It also made it difficult to quickly produce a collection of imprinters. A list of several different variables that were thought to cause the problem was recorded. By changing one variable and holding all others constant during the fabrication of imprinters, a number of variables were ruled out. Ones that were eliminated included the preparation of the sample, the development time used, variation of the working distance for writing, aperture alignment of the SEM, stigmation adjustment of the SEM, and noise created by other machinery in the lab.

The problem turned out to be a simple mistake. The four focus points that were collected before each imprinter was written were not always focused well enough. Therefore, the sample was not always in focus at the points where the patterns were written. This resulted in patterns that were under or overexposed using a point dose that properly exposed other patterns. It became even more apparent that this was the cause of the problem when a single pattern was seen to have collapsed pillars on the left half of it and free standing pillars on the right half as seen in images A.55-56. Patterns with a combination of either collapsed pillars, free standing pillars, or a plateau of HSQ appeared two toned optically like those at the top of image A.57.

To solve the misfocusing problem, Au was sputter coated around the edges of a sample. A shadow mask was placed over the center of the sample to prevent it from being coated with Au. Then patterns were written like they normally were. This made focusing the four needed points much easier. However, when the imprinter was developed, the HSQ around the edges that was coated with Au did not come off. This created a new problem that needed to be solved. It was worth solving because using the Au to focus enabled perfectly exposed patterns to be created each time.

Attempts to remove the Au coated HSQ around the edges of an imprinter were made using four different methods. The first method used was developing the imprinter for a longer time, 30 minutes, in a higher concentration NaOH, 100%. It was also sonicated. This removed the Au coated HSQ around the edges; however, it caused the pillars to collapse as seen in image A.58. An attempt was then made to etch the Au and some of the HSQ away. The T-M Vacuum Systems sputtering unit was used to perform etching. A shadow mask was used to cover the center of the imprinter to protect the patterns. It was then etched for 2 minutes at 200 W. This did not improve the removal of the Au coated HSQ around the edges when the imprinter was developed. Therefore an Au etchant solution was purchased from Transene Inc. to remove the Au. The imprinter was soaked in the gold etchant, but this still did not aid in the removal of the HSQ around the edges of the imprinter. At this point, it was apparent that the Au coated HSQ edges had to simply be cut off. Therefore, a 15 mm x 15 mm sample was used to write 14 patterns on. After it was developed, the Au coated HSQ edges were cut off with a diamond blade. The resulting imprinter was approximately 8 mm x 8 mm.

The second problem associated with fabricating HSQ imprinters dealt with the height of the pillars. It was noticed while inspecting imprinter IMH011 that the pillars in the middle of the pattern are shorter than the thickness of HSQ that was spun on. This can be observed in images A.59-61. HSQ was spun onto imprinter IMH011 at 2000 rpm producing a 100 nm thick layer. The measured height of the pillars in the centers of patterns one, five, and eight are 72, 53, and 41 nm respectively. Point doses of 24, 26, and 27.5 fC were used to expose these patterns respectively. Furthermore, the pillars around the edges are taller than the ones in the center as seen in image A.62. The pillars here are between 70 and 100 nm. This problem was also seen in other imprinter patterns. Imprinter IMH012 also contained a 100 nm layer of HSQ that was spun onto it; however, the pillars in the center of its patterns were between 60 and 75 nm tall.

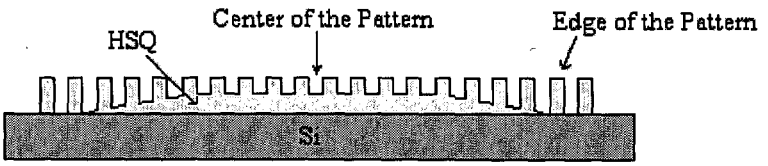

Figure 4.11 An illustration of the cross section of an HSQ imprinter pattern. The center of the pattern contains HSQ between the pillars lowering their effective height. The HSQ is present between the pillars in the center of the pattern and not around the perimeter because the center experiences greater doses due to the proximity effect. Therefore HSQ between the pillars also becomes exposed.

This problem was initially believed to be a result of the fact that HSQ shrinks when it is cured or exposed to electron irradiation [74]. Therefore, it was believed that if a thicker layer of HSQ was spun onto a sample, taller pillars could be obtained. Starting with imprinter IMH016, all imprinters were coated with a 150 nm layer of HSQ. It was spun on at 1500 rpm to produce this. However, this did not help the problem. The measured pillar height in the center of patterns was still much shorter than the thickness of the spun on HSQ. Also, the height of the pillars in the center of the patterns continued to be lower than around the edges. This can be seen in images A.63-70. The point dose used to expose all of the patterns in the images was 32 fC. The measured height of the pillars in the center of the patterns is approximately 40 nm. The measured height around the edges is between 70 and 100 nm.

It seemed that the pillars in the center of the pattern shown in images A.67-70 were lower because the surface between them had been raised. The surface was most likely raised by exposed HSQ. The greater dose that was seen in the center of the pattern exposed the HSQ between the pillars. This raised the surface lowering the effective height of the pillars as illustrated in figure 4.11. If this was happening on this pattern, it was most likely occurring on all of the patterns. It seemed like a realistic solution to lower the dose to reduce this effect. After all, the pillars around the perimeter of each pattern were taller. However, lowering the dose to create taller pillars caused them to collapse. Therefore, there is a slight possibility that HSQ might not be the best material to produce small diameter reasonably tall pillars. It is useful for creating high aspect ratio lines, but lines are much more robust than individual 30 nm diameter pillars.

Despite the fact that the HSQ pillars were not as tall as the spun on material or what was originally desired, their reduced height did not cripple the imprinting process as will soon be seen. Imprinting or pattern replication was done into resists with thickness in the 50 to 70 nm

regime. Therefore, with pillars that ranged mostly from 40 to 50 nm, the worst case scenario was that several nanometers of resist would be left in the imprinted holes. This was not a major issue since post processing steps were done to remove the remaining resist in the holes. Therefore, the HSQ imprinters were sufficient for the required task.

The final process that was developed produced the highest quality HSQ imprinters. The HSQ was coated onto a 15 mm x 15 mm sample at 1500 rpm and then the sample was heated on the hotplate for 3 minutes at 250°C. The edges of the sample were coated with Au. It was exposed using a point dose of 32 fC and a 50 nm pitch. After the imprinter was developed in a 25% NaOH solution for 2 minutes, it was baked for 2 hours at 400°C. The Au coated HSQ edges were then cut off. Spinning the HSQ on at 1500 rpm did not help the height problem. However, coating the edges with Au made focusing much easier. It allowed for the repeatable production of defect free imprinters at least from the standpoint of under or overexposed patterns. A pattern from imprinter IMH101 that was fabricated under these conditions is seen in images A.71-74. The pattern is properly exposed and the arrays of pillars seen are near perfect. The measured pillar diameter was 25 nm and the pitch was 50 nm. The height ranged from 40 to 50 nm in the center of the patterns.

4.4 F_{13}-TCS Anti-Adhesive Application

As pointed out in the last chapter, it is necessary for an imprinter to have an anti-adhesive coating. The anti-adhesive coating decreases the surface energy of the imprinter so that it is lower than the polymer resist layer on the imprinted sample. This, in theory, is supposed to reduce not only the amount of resist that is torn from the sample and but also the amount that sticks to the imprinter. After a HSQ imprinter was fabricated, it was coated with the F_{13}-TCS anti-adhesive agent. F_{13}-TCS forms a covalent bond with Si, SiO_2, or HSQ with the release of hydrochloric acid. The covalent bond that is created is very robust; therefore, the coating is not removed after every imprint that is done. This was the reason that the F_{13}-TCS was chosen as the anti-adhesive agent over HBFP. It did not seem efficient to have to keep reapplying the HBFP coating after every imprint. Furthermore, the F_{13}-TCS anti-adhesive agent is more capable of providing a monolayer coating than the HBFP.

4.4.1 Initial Process

The initial overall process of applying the F_{13}-TCS anti-adhesive coating was not substantially altered. The imprinter was first hydroxylated in nitric acid for 3 minutes. After hydroxylation, it was blown dry with a stream of pressurized nitrogen. If there were any streak marks present on the imprinter, this step was repeated. After several imprinters had been coated with the F_{13}-TCS anti-adhesive agent, it was discovered that the imprinter needed to be rinsed in DI water after hydroxylation to remove any contaminants. Once this information was obtained, this practice was implemented. The imprinter was transferred to the glove box in a small petri dish after it was hydroxylated, rinsed in DI water, and blown dry. Tools such as a pair of tweezers, a pipette, a hot plate, a beaker, and a larger petri dish were placed in the glove box. Also a bottle containing the F_{13}-TCS and a bottle containing hexane were taken out of a vacuum storage and placed in the glove box.

At this point, the rest of the coating process was performed in the glove box. Reasons for this were explained in the previous chapter. Chlorosilanes present in the F_{13}-TCS react violently in the presence of a small amount of water. They quickly polymerize forming large chain aggregates. These structures would have formed on the imprinter making the goal of obtaining a monolayer coating impossible. Therefore, the entire reaction was performed in an anhydrous environment created by the glove box. A vacuum was pulled in the glove box and then it was purged with nitrogen. This was completed three times. Then, a steady flow of nitrogen at approximately 3 psi was allowed to pass through the glove box the rest of the time.

The imprinter was placed in the center of the larger 90 mm diameter petri dish. The petri dish was placed on the hotplate and allowed to heat up to 250°C. After 10 minutes elapsed, 65 to 70 μL of F_{13}-TCS was released into the side of the petri dish. The petri dish was immediately covered with the top to contain all of the F_{13}-TCS. The required amount of F_{13}-TCS that was placed in the petri dish was calculated from the size of the dish and information that was obtained from *Improving Nanoimprinting Lithography Stamps for the 10 nm Features* [76]. After the petri dish was covered, the reaction was allowed to continue for 2 hours. At the end of 2 hours, the imprinter was taken out of the petri dish and soaked in hexane for 1 minute. The imprinter was then taken out of the hexane. Any remaining hexane on it evaporated within

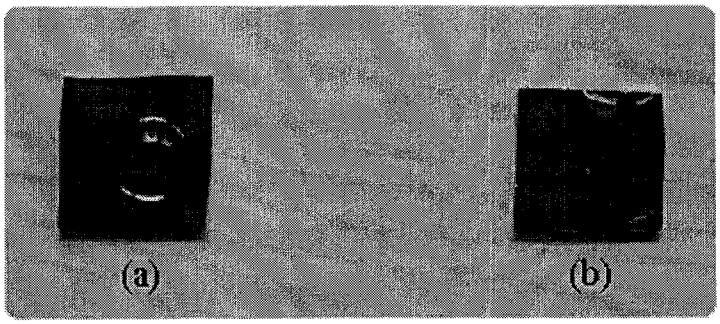

Figure 4.12 An imprinter (a) with a coating of F_{13}-TCS applied to it (b) and one without any type of anti-adhesive coating.

several seconds. This removed any excess F_{13}-TCS so that it would not polymerize when it was taken out of the anhydrous environment.

Once the imprinter was rinsed in hexane, it was taken out of the glove box. It was then ready for the imprinting process. Imprinters were usually tested to see if the coating had been applied properly. The easiest way to test for this was to place a drop of water on the coated imprinter. If it was coated properly, the contact angle that the drop of water formed with the surface was much larger than that of a drop of water on a non-coated piece of silicon. Figure 4.12(a) is an image of an imprinter coated with F_{13}-TCS and figure 4.12(b) is an image of an imprinter that was never coated. The effect of the coating can clearly be seen. The water droplet on the coated imprinter is completely symmetric and does not wet the surface. On the other hand, the water droplet on the non-coated imprinter wets the surface. The contact angle of the water drop on the coated imprinter is much greater than the one on the non-coated imprinter because the surface energy is much less. With a smaller surface energy, it is harder for anything to adhere to the coated imprinter.

4.4.2 Results of Implementing the Anti-Adhesive Coating

A drop of water was placed on each imprinter after it was coated with F_{13}-TCS. On every imprinter that had been coated, the drop of water formed a symmetrical circle and large contact angle with the surface as seen in figure 4.12(a). However, this did not always mean that the coating prevented certain unwanted effects. There were many instances when the resist of the patterned region was ripped from the surface of the imprinted sample. There were many

instances when the resist adhered to the imprinter patterns. There were also many instances when the pillars broke off from the imprinter. Furthermore, when the pressure was released after imprinting, the imprinter was bonded to the imprinted sample on many occasions. The two were forcefully pried apart using tweezers.

At the time, the main reason for these problems could not be targeted. Even today, there is still some uncertainty. Nonetheless, it was initially suspected that the anti-adhesive coating was not working properly. The F_{13}-TCS coating appeared to be applied properly from the standpoint of the water droplet test. An initial test was eventually carried out to determine why the imprinter often became bonded to the imprinted sample. A blank piece of Si without any nanoscale patterns on it was coated with F_{13}-TCS. It was then used in the same manner as an imprinter. Several imprinting runs were conducted with it. There was not one instance when the blank piece of Si coated with the anti-adhesive agent became bonded to the imprinted sample. Therefore, it was clear that the nanoscale features had not been properly coated with the F_{13}-TCS anti-adhesive agent.

The fact that the nanoscale patterns were not coated properly resulted in the ripping and sticking that was observed during imprinting. The question then was why was the coating not working on the nanoscale patterns? The coating was specifically applied in the gas phase so that a near monolayer could be produced over the features. It was thought that maybe the F_{13}-TCS and hexane used were old or had been contaminated with water. If either of these two things were true, the coating applied to the imprinters was much too thick. This would have resulted in a poor coating of the nanoscale patterns. Therefore, new chemicals were purchased and then stored in a vacuum to prevent water contamination. However, the same problems were still seen during imprinting. The water droplet test on the coated imprinters worked well, but the imprinters still often ripped the resist away and often became bonded to the imprinted sample.

Other reasons that potentially caused these problems were formulated. One idea was that using the bilayer resist caused more patterns to rip up and the imprinter to stick to the sample. An in depth discussion of the bilayer is presented in the next section. It was also observed that a major portion of patterns were ripped up from an imprinted sample the first time an imprinter was used. Besides a poor anti-adhesive coating, it was also possible that the HSQ surface was too rough because the sample was baked at 250°C before it was exposed [73]. In this case, it

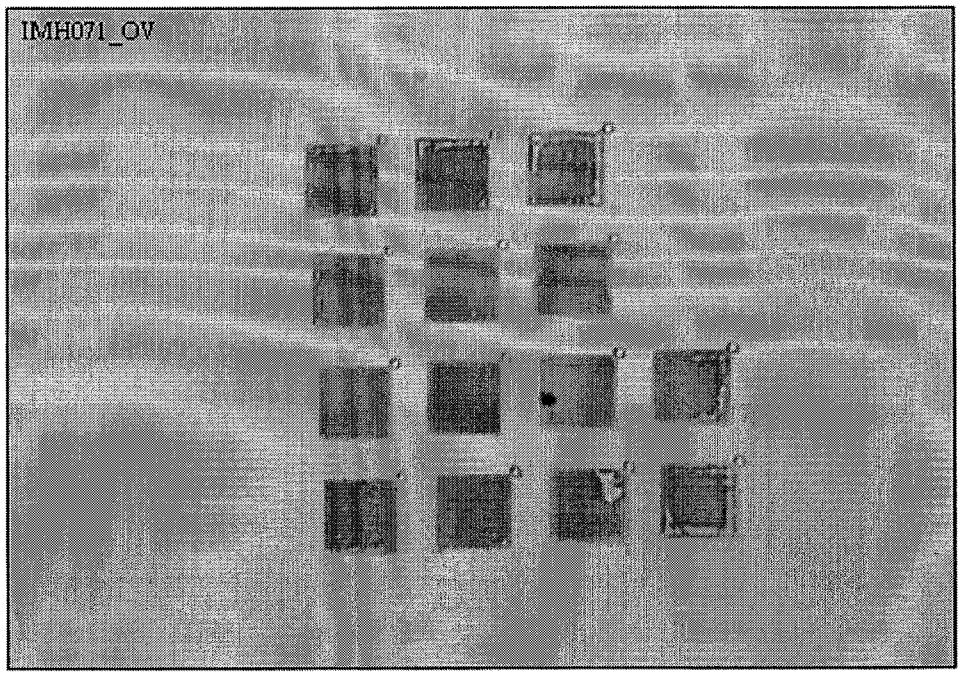

Figure 4.13 An optical image of imprinter IMH071 after a fourth imprint was done to it. The residue around the edges of some patterns is resist that was ripped from the imprinted sample.

would have been easier for the rough features to grab and rip up the resist. After a few imprints, the features would have been smoothed over from the adhered resist resulting in better imprints.

While the ripped-up resist was a hindrance at times, it did not completely impede imprinting. The ripped resist usually adhered to the imprinter as seen in figure 4.13. An optical image of all the patterns on imprinter IMH071 is seen. The greenish outline on some of the patterns is the resist that was ripped from the sample. This was observed after the fourth imprint. An imprinter was usually washed and sonicated in either acetone or another solvent to remove the resist. This also removed other contaminants such as dust and dirt. The cleaning step was not 100% effective. Therefore any leftover resist on the imprinter usually produced defects in the next imprint. The ripped-up resist in the patterned regions and the imprinter sticking to the imprinted sample were two problems that were never fully solved. Most likely they were caused by a deficiency in the F_{13}-TCS anti-adhesive coating. Nonetheless, the overall durability of the imprinters was adequate for the current research to proceed. Well over 30 imprints were done with imprinter IMH071. The 32nd imprint that was done with the imprinter is seen in figure 4.14. The imprint is acceptable with only a fraction of defects. Approximately 25% of the imprinted holes are shallow and have an imprint depth of 5 nm.

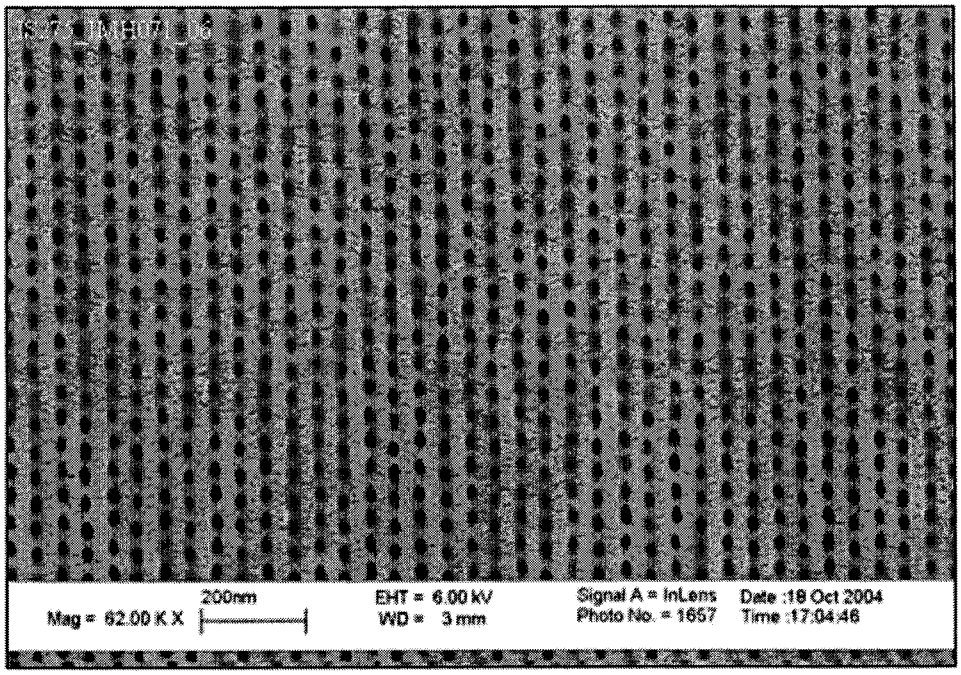

Figure 4.14 An SEM image of a pattern of imprinted holes that was the 32nd imprint completed with imprinter IMH071.

4.5 Imprinting

The fabrication of patterned magnetic media using nanoimprint lithography relied heavily on deriving a robust and repeatable imprinting process. The goal was to use hot embossing nanoimprint lithography to replicate the fourteen 100 μm x 100 μm patterns of the HSQ imprinter in a thermoplastic resist coated substrate. In the end, relatively defect free patterns of holes in the resist were needed. There were a number of different variables ranging from the designated imprinting pressure to the resist type that were adjusted to yield favorable results. The process was continually refined to solve problems as they arose. Several different imprinters were used to produce 155 imprinted samples in order to achieve the desired process. The initial and final processes are outlined in this section along with the results of imprinting.

4.5.1 Initial Imprinting Process

The initial imprinting process that was developed was essentially a set of guidelines. For a time, imprinting was carried out adhering strictly to these guidelines so that when a problem

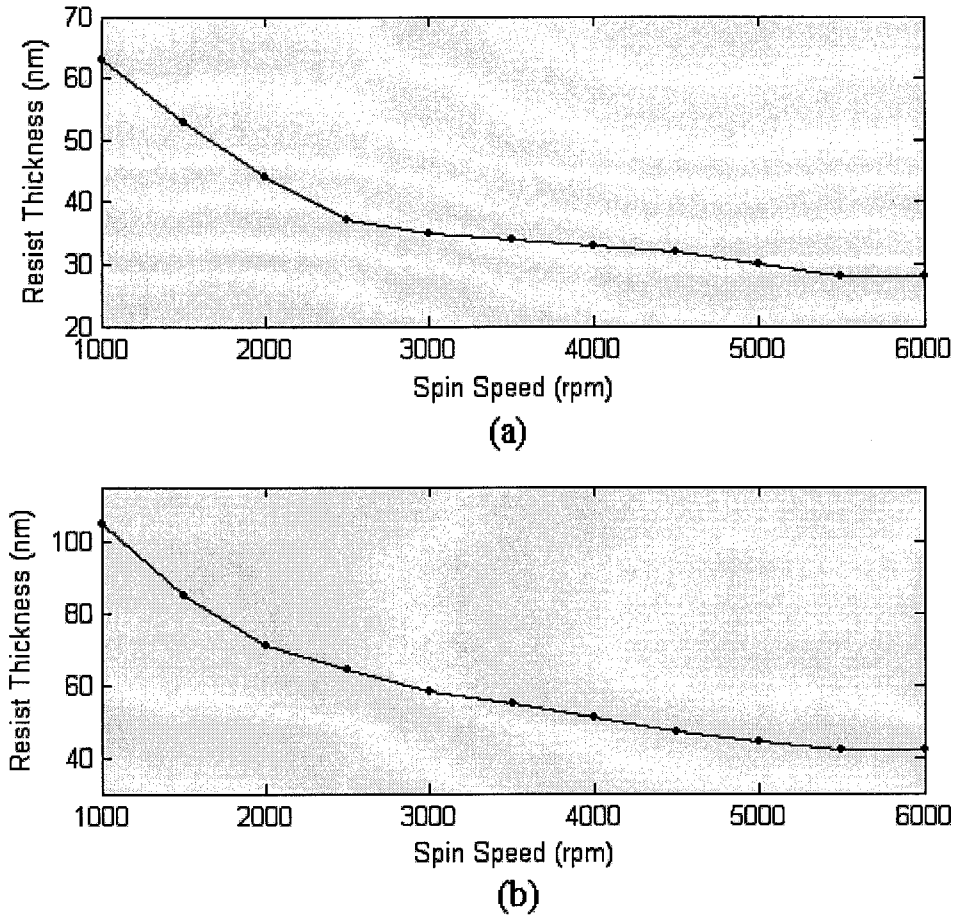

Figure 4.15 Spin curves for **(a)** 1% 495k PMMA in chlorobenzene and **(b)** 2.2% P(MMA-{17.5%}MAA) in ethyl lactate on a Si substrate.

arose there was a better chance of diagnosing it. There was not by any means a shortage of problems that arose. This was understandable because it was the early stages of imprinting at Rowan University. Quite often the resist in the patterned regions ripped away, imprinters became bonded to the imprinted samples, and patterns were not replicated in the resist. The goal was to produce imprinted patterns relatively free of defects; however, at first it was difficult to simply achieve imprinted patterns.

For the initial imprinting process, a 10 mm x 10 mm sample was coated with either a single or bilayer resist for imprinting. The single layer consisted of 1% 495k PMMA. It was spun onto the sample at 1800 rpm to produce a 50 nm thick layer. The bilayer consisted of 1% 495k PMMA on the bottom and 2.2% P(MMA-{17.5%}MAA) on the top. The PMMA was spun onto the sample at 1800 rpm to produce a 50 nm thick layer, and the P(MMA-MAA) was spun on at 4000 rpm to produce a 50 nm thick layer. The spin curves seen in figure 4.15 for 1%

495k PMMA in chlorobenzene and 2.2% P(MMA-{17.5%}MAA) in ethyl lactate were used for guidance. The spin time for PMMA was always 30 seconds, and it was always 45 seconds for P(MMA-MAA). After each of the resist layers were applied, the sample was heated at 170°C for 15 minutes.

After the sample was coated with either a single or bilayer resist, it was ready for imprinting. The larger model 100 imprinting press was initially used. The sample was placed on top of the lower aluminum platen of the model 100 imprinting press. It was placed over the vacuum hole. A vacuum hole was located in the center of the lower and upper platens directly under the piston. The purpose of each hole was to pull the imprinter from the imprinted sample after imprinting. The imprinter was then placed on top of the sample with the patterned side touching the resist. A pressure of 6 psi coming from the regulator on the nitrogen tank was then applied. This pressed the imprinter into the sample. The vacuum was then turned on. Once the vacuum was turned on, the lower platen was heated to 170°C. It took approximately one minute for the platen to reach this temperature. The upper platen was not heated because at the time there were no heaters for it. When the lower platen reached 170°C, the system was left alone for approximately 2 to 4 minutes. On this first imprinting trial, this amount of time proved to be long enough for the pillars to penetrate the resist and replicate the pattern. Therefore, the imprinting time was never changed. The system was then cooled passively which took 30 to 45 minutes. Once it was cooled to approximately 50°C, the pressure was released to retract the piston hence pulling the imprinter off of the imprinted sample. The system was cooled with the imprinter in place because if the imprinter and sample are separated at a temperature close to or greater than the glass transition temperature of the resist, the resist will flow back into the imprinted holes. The imprinted sample was then inspected using an optical microscope.

A pressure of 6 psi was used because it was the minimum pressure at which the piston could extend. A regulator pressure of 6 psi extended the piston with a force of 73 lb. This information can be obtained from the graph seen in figure 4.4(b). A force of 73 lb applied a pressure of 1.2×10^6 psi across all of the nanoscale pillars to push them into the resist. This value was calculated for the HSQ imprinters that were used. Each imprinter had fourteen 100 μm x 100 μm patterns of pillars that were approximately 30 nm in diameter and spaced with a 50 nm pitch. The total number of pillars on each imprinter is 56 million. The pressure turned out to

be too great from previous guidelines found from other research work and from the high amount of broken pillars seen in the sample. Therefore, an adjustment is seen in the final process.

4.5.2 Most Effective Imprinting Process

There were several flaws with the original imprinting process that had to be fixed. The resist in the patterned regions of the sample ripped and the imprinter stuck to the sample far too often for the process to be efficient. Also, there were too many instances when the imprinter pattern was not even replicated in the resist of the sample after imprinting. When this occurred, there was no evidence of replicated patterns in the resist. Some of these problems might have been a result of an ineffective anti-adhesive coating. However, there was no way of knowing this. Therefore, attempts were made to alleviate the problems by altering the imprinting process. The initial imprinting process was not used too long before it was modified, and the process was continually refined until an effective process was achieved. The problems were not completely eliminated, but their occurrence was reduced making the process more effective.

It was ascertained that using samples the same size of the imprinter presented a major problem. Both the samples used for the initial imprinting process and the original HSQ imprinters were 10 mm x 10 mm. When a sample was coated with resist, the resist built up around the edges as seen in figure 4.16 because they were not beveled. The height of the resist reached a few hundred nanometers. The imprinter was then placed on top of the sample and pressure was applied for imprinting. However, there was a high probability that the features of each pattern never reached the resist because the imprinter was resting on the built up resist around the edges as seen in figure 4.16(a). This explained why in some cases a pattern was not replicated in the resist after imprinting. To correct this, samples were cleaved into 15 mm x 15 mm pieces and the HSQ imprinters were reduced in size to 8 mm x 8 mm. A smaller imprinter and larger sample prevented the imprinter from resting on the built up resist around the perimeter during imprinting as seen in figure 4.16(b). After this adjustment, the efficiency of pattern replication was increased.

Most of the parameters of the final imprinting process that was developed were held constant except the resists that were used. A variety of different resists were used to imprint into. The single layer and the bilayer that were discussed in the initial process were used. A

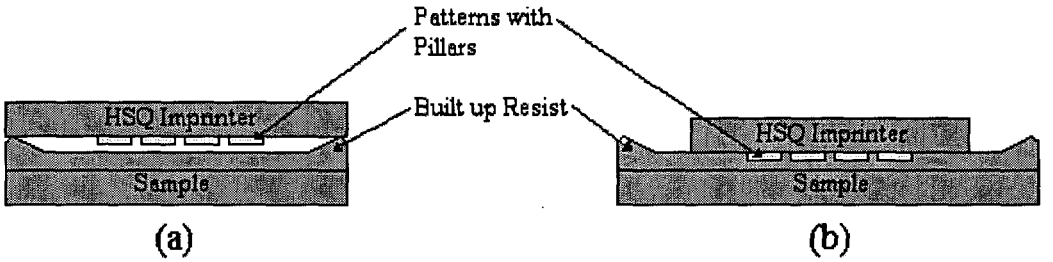

Figure 4.16 An illustration of **(a)** the imprinting process with the same size imprinter and sample, and **(b)** the imprinting process with a smaller imprinter and larger sample. Imprinting was more effective with the smaller imprinter and larger sample because the imprinter was not resting on the built up resist around the edges of the sample.

single layer was easier to work with, but a bilayer had better processing capabilities. The bilayer was challenging to imprint into. It was noticed that the imprinter stuck to the sample and ripped resist away when a bilayer was used at least twice as much more than compared to a single layer. Therefore, three different types of bilayers were used besides the initial one. The parameters of the three new bilayers along with the original bilayer and single layer can be seen in table 4.4. A more in-depth discussion of the types of resist layers used will be provided in the next section. Once again, the spin time for PMMA was always 30 seconds, and it was always 45 seconds for P(MMA-MAA). Also, after each of the resist layers were applied, the sample was heated at 170°C for 15 minutes.

After a sample was coated with resist, imprinting was carried out. The sample was secured to the lower aluminum platen of the smaller model 20 imprinting press with a 12 mm diameter piece of carbon tape. It was centered directly below the piston. Before the imprinter entered the setup, it was sonicated in acetone, chlorobenzene, or ethyl lactate. An imprinter exposed with a 32 fC point dose was used. It was then rinsed with DI water and blown dry. A piece of carbon tape was cut into a square just smaller than the imprinter and pressed onto the back of the imprinter. The imprinter was then centered face down on top of the sample. The piston was lowered manually so that the upper aluminum platen touched the carbon tape on the back of the imprinter. The imprinter was now adhered to the upper platen. The pressure at this point had not yet been applied.

Once the piston was lowered so that the upper platen was touching the back of the imprinter, the setup was complete. Both the upper and lower platens of the imprinting press were heated to 170°C according to their respective heating curves seen in figure 4.17(a). The upper platen was equipped with heaters this time. It took approximately a minute and forty

Table 4.4 The table lists the parameters of each type of resist coating that was used for the final improved imprinting process. The PMMA is 495k PMMA

Type of Coating	*Layer of Resist*	*Spin on Speed (rpm)*	*Thickness (nm)*
Single Layer	1% PMMA	1800	50
Bilayer 1	Top: 2.2% P(MMA-{17.5}MAA)	4000	50
	Bottom: 1% PMMA	1800	50
Bilayer 2	Top: 1% P(MMA-{17.5}MAA)	4000	25
	Bottom: 1% PMMA	1800	50
Bilayer 3	Top: 1% P(MMA-{17.5}MAA)	4000	25
	Bottom: 1% PMMA	4000	30
Bilayer 4	Top: 1% P(MMA-{8.5}MAA)	4000	25
	Bottom: 1% PMMA	4000	30

seconds for the two platens to reach 170°C. Once this temperature had been reached, a regulator pressure of 40 psi was applied to the piston. The system was left under pressure at 170°C for 4 minutes. It was then cooled actively by pointing a pressurized stream of air at the upper platen. Using this active cooling method, the platens cooled according to the curves seen in figure 4.17(b). It took 12 minutes for the system to cool to under 40°C using the active cooling method. Once the upper platen was at 45°C, the pressure was gradually reduced to zero without separating the imprinter and imprinted sample. The piston was retracted pulling the imprinter away from the imprinted sample when the upper platen reached 39°C. The imprinter and imprinted sample were removed from each piece of carbon tape with a razor. The imprinted sample was then inspected in the optical microscope.

This modified imprinting process was drastically different from the initial one. The decision was made to clean the imprinter before imprinting to remove any resist or dust from it. The acetone worked nicely to clean off any dust. Naturally, the chlorobenzene was effective at removing PMMA entrenched between the pillars. Furthermore, the ethyl lactate was effective at removing the copolymer, P(MMA-MAA). The imprinter and sample were secured to the upper and lower platens respectively by carbon tape. This was used because the vacuum supply was not strong enough to hold on to each when they were separated. The introduction of the heating was done differently also. The imprinter and sample were heated before the pressure was applied. This was done because it seemed more logical to soften the resist before the imprinter was pressed into it. It seemed to lessen the number of pillars that broke off.

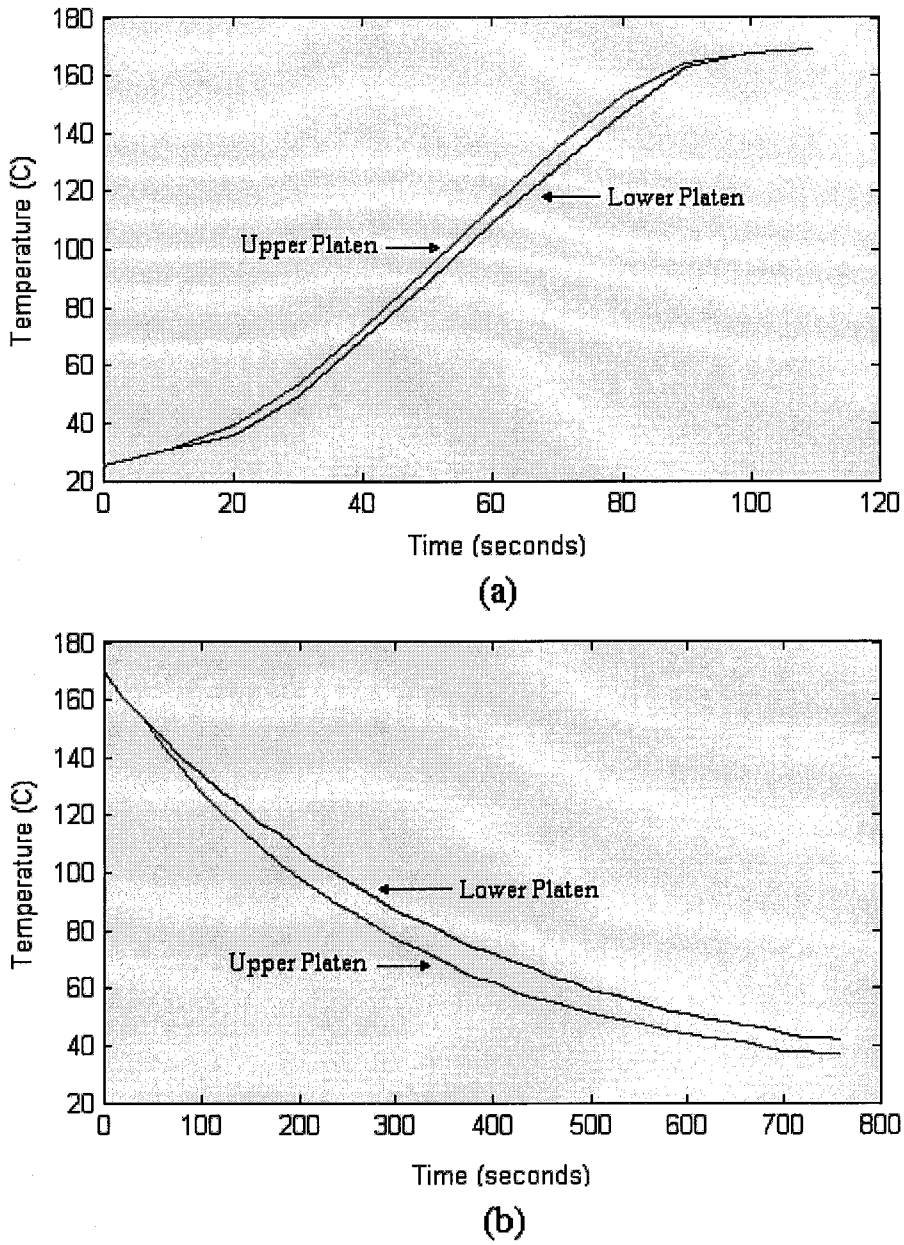

Figure 4.17 (a) The amount of time it took the upper and lower platens to reach 170°C. **(b)** The amount of time it took the upper and lower platens to cool to the desired separation temperature.

The most prominent difference with this process was that the smaller model 20 imprinting press was used with heaters in the upper platen. It was absolutely essential to have heaters in the upper platen. Without the heaters in the upper platen to heat the imprinter, replication of the patterns in the resist of the sample was exceedingly difficult. When the imprinter was not heated and pressed into the sample, it simply cooled the resist below its glass transition temperature of 105°C. Therefore, there was not much of a chance for the replication of

patterns in the resist. The model 20 imprinting press was used because the model 100 was unable to employ the lower pressures that were needed. According to one experiment, only a pressure in the range of 145,000 to 350,000 psi was needed to imprint into a 50 to 100 nm thick resist [70]. The smallest pressure that could be applied with the HSQ imprinters and the model 100 was 1.2×10^6 psi. This was far too great for what was needed. It was most likely another cause for the large quantity of broken pillars that were seen on imprinters. Using a regulator pressure of 40 psi with the model 20 imprinting press and the HSQ imprinters, an applied pressure of 320,000 psi was produced across the surface of all of the pillars. This was more in the range of what was needed.

The final steps of the imprinting process were also altered. An active cooling method was implemented. The main reason for this was to reduce the amount of time it took to imprint a sample. The longest period of the imprinting process was always the cooling phase. With the active cooling method, the amount of time was reduced from 45 minutes to 12 minutes. The pressure of the imprinting press was gradually reduced to zero before the imprinter and imprinted sample were pulled apart. This was done because it was theorized that it would decrease the amount of resist that was ripped from the patterned regions. It was unable to be determined if this actually helped.

4.5.3 Results of Imprinting

Along the way from the initial to final imprinting process that proved to be the most effective there were five primary variables that were adjusted for each imprinted sample that is shown. These include the imprinter used and its dose to expose it, the type of resist coating that was used corresponding to table 4.4, the imprinting press used, the applied regulator pressure, and the average temperature that the upper and lower platens were cooled to before separation. The patterns on the imprinted samples that will be shown were imprinted with both the upper and lower platens of the press heated to 170°C. Furthermore, the duration of the imprint (i.e. amount of time the system was left at 170°C under pressure) was always 4 minutes.

4.5.3.1 Single Layer

Most of the imprinting was initially carried out using a single layer of PMMA. A single layer was easier to work with than a bilayer. Obviously, coating a sample with a single layer took less time. Also, imprinting into a single layer of PMMA yielded better results. Therefore, it was perfect for obtaining initial results and refining the process. Imprinted patterns from sample IS170 are seen in images A.75-80. They were imprinted into a single layer of PMMA using imprinter IMH008 and the larger model 100 imprinting press. A regulator pressure of 6 psi was used. The system was cooled to 50°C before the imprinter and sample were separated.

The imprint created on sample IS170 contains an assortment of defects which can be seen in image A.75. It appears that a deeper, more pronounced imprint was achieved on the left side. Since the imprinter and sample were the same size, the imprinter was resting on one of the raised edges of PMMA. This most likely caused an unequal distribution of pressure resulting in a deeper imprint as seen on the left side. A higher magnification image of pattern 2, which is on the right side of image A.75, is shown in image A.70. It is seen that the imprint achieved in pattern 2 is very shallow because of a lack of pressure. A higher magnification image of pattern 3, which is more towards the left side of image A.75, is shown in image A.77. It is seen that a lot of the pillars broke away from the imprinter and are embedded in the pattern. This was probably caused by the extra pressure that this area received since the imprinter and sample were not completely parallel. The enormous pressure that was applied by the model 100 imprinting press was probably also a factor. Nonetheless, there were several areas of holes with few defects as seen in figures A.78-80. The measured hole diameter and pitch of these areas was 35 nm and 53 nm respectively.

The rest of the imprinted patterns that are shown in this thesis were produced differently. The model 20 imprinting press was used to apply a smaller pressure. Also, the patterns were imprinted utilizing a smaller imprinter and larger sample. Finally, the point dose used to expose the imprinters was increased. This was not mentioned previously, but a lesser point dose might have also been a factor in the destruction of the pillars during imprinting. Using a smaller imprinter and larger sample, allowed for the two to be more parallel to each other. Their degree of parallelism was unable to be measured; however, the effectiveness of pattern replication increased by at least 50%. This provided a more even distribution of pressure which allowed for

equal depth imprints across all of the patterns. All of the changes helped to reduce the number of pillars that were broken off from the imprinter and embedded in the PMMA.

Imprinting into a single layer of PMMA was relatively successful and a compilation of high quality results was obtained. Once the changes that were discussed in the previous paragraph were implemented, the imprinted patterns had less noticeable defects and appeared cleaner. Also, the depth of the imprinted holes was more consistent across all of the patterns. Overviews of the fourteen 100 μm x 100 μm patterns on several different imprinted samples are provided in images A.81-88. As seen, each successive imprinted sample has less noticeable defects and appears cleaner. Higher magnification images of the imprinted holes of several patterns on various imprinted samples can be seen in images A.89-105. The arrays of holes seen in these images do have a certain amount of defects. Approximately 20 to 40% of each image contains defects.

Despite the success of imprinting into a single layer of PMMA, at least 5% of each sample contained defects. This percentage on some samples probably was as high as 50%. Therefore, from time to time, several defects such as the presence of dust, broken pillars, shallow imprinted holes, and ripped PMMA were seen in some areas of certain patterns. A piece of Si dust that contaminated pattern 10 of sample IS207 is seen in images A.106-107. The dust is only several microns in size; however, it completely covered the pattern. Pillars that have broken off of the imprinter and adhered to the imprinted sample are seen in images A.108-109. The shallow imprint seen in image A.110 was probably caused by broken pillars on the imprinter in that location. Finally, the PMMA of several patterns had torn away as seen in images A.111-116. In the case of sample IS320 shown in image A.111, the PMMA of all the patterns was torn away. This level of imperfection was not usually seen with a single layer, but more so with a bilayer of resist.

4.5.3.2 Type 1 Bilayer Coating

Imprinting into a single layer of PMMA was easier than using a bilayer. However, an undercut was not able to be performed on a single layer to facilitate the liftoff process. Only a bilayer was capable of this. Therefore, imprinting into a bilayer resist was carried out. The type 1 bilayer coating listed in table 4.4 was the first one used for imprinting. It consisted of a 50 nm

thick bottom layer of 1% PMMA and a 50 nm thick top layer of 2.2% P(MMA-{17.5%}MAA). Varying results were obtained from using this type of bilayer coating. The resist in the patterned areas was commonly ripped up when the imprinter was separated from the sample. This was the case with almost every imprinted sample. However, there were regions on several of the patterned areas that were comprised of high quality imprinted holes.

The common outcome of imprinting into a type 1 bilayer coating is seen in images A.117-119. The images show that the resist of all 14 patterns of imprinted sample IS220 was ripped off. There was a small amount left at the top of pattern 3. An image of the imprinted holes in this remaining piece of resist is shown in image A.120. The sample was imprinted using imprinter IMH033 and the model 20 imprinting press. A regulator pressure of 70 psi was used, and the imprinter and sample were separated at 40.5°C. The patterns on the imprinter were exposed with a 28.5 fC point dose. After this imprint was done, it was thought that the pressure was too great because of the substantial amount of defects seen in the imprint.

Since the pressure was thought to be too great, it was lowered in other imprints. Sample IS223 was imprinted using imprinter IMH034 and the model 20 imprinting press. The patterns on imprinter IMH034 were exposed with a 28.5 fC point dose. A regulator pressure of 55 psi was used this time. The imprinter and sample were separated at 41.5°C. Resist had ripped off only a few of the patterns, but some of the patterns did not show up as evidenced by image A.121. Higher magnification images revealed that not only were both layers of resist ripped off in places, but also in some places only the top layer of resist ripped off as seen in images A.122-126 respectively. Finally, the imprinted holes of some of the patterns are shown in images A.127-129. The imprinted holes are free of defects and are 28 nm in diameter. The measured pitch was 48 nm.

The pressure used to imprint sample IS223 was lowered from that used on IS220. The result was less resist torn away from the patterns. Therefore, the pressure was reduced even further for the successive imprints thinking there would be less torn away resist. This was not the case. Other samples that were imprinted had either all of the resist torn away as in sample IS220 or some of the resist torn away as in sample IS223. Sample IS227 was imprinted using imprinter IMH040 and the model 20 imprinting press. The patterns on imprinter IMH040 were exposed with a 28.5 fC point dose. A regulator pressure of 40 psi was used this time. The imprinter and sample were separated at 41°C. Even with lower pressure, sample IS227 still had

40% of its resist ripped from the patterned regions as seen in image A.130 similar to sample IS223. A higher magnification image of the ripped resist is seen in image A.131. This imprinted sample, like IS223, contained areas of high quality imprinted holes as seen in images A.132-134. The measured hole diameter and pitch was 30 and 44 nm respectively.

Decreasing the pressure with which a sample was imprinted did not substantially fix the problem of torn resist. While samples IS223 and IS227 had less resist ripped from the patterned regions than IS220, approximately a third of their patterns still had torn resist. Furthermore, there were several more imprinted samples that were not displayed. The resist of all the patterns on these imprinted samples was ripped away, even though the regulator pressure used was between 40 and 55 psi. It became apparent that there was a problem using a bilayer. It was possible that the problem was a result of a poor anti-adhesive coating on the imprinters that were used. However, even though the resist in a single layer ripped away on several occasions, it was never as severe as what was experienced with a bilayer.

4.5.3.3 Type 2-4 Bilayer Coatings

Several attempts were made to alleviate the dilemma of torn up resist in the patterned areas of a bilayer. It was first thought that the bilayer was too thick. If this was the case, there was too much surface contact between the imprinter and resist. The increased surface contact probably caused the resist to adhere to the imprinter and rip up. Therefore, a thinner bilayer was employed. The type 2 bilayer coating listed in table 4.4 was first used. It consisted of a 50 nm thick bottom layer of 1% PMMA and a 25 nm thick top layer of 1% P(MMA-{17.5%}MAA). The results that were obtained using this bilayer were improved. The amount of instances in which the resist was not pulled up with this bilayer compared to the type 1 bilayer was reduced by 20%.

Sample IS275 was coated with a type 2 bilayer and imprinted. Imprinter IMH071 and the model 20 imprinting press were used. The patterns on imprinter IMH071 were exposed with a 32 fC point dose. A regulator pressure of 50 psi was used this time. The imprinter and sample were separated at 35°C. It can be seen in image A.135 that there was no evidence of large areas of ripped up resist on the sample. A few small areas of resist ripped as seen in images A.136-137, but nothing significant. Imprinted holes of the several patterns can be seen in image A.138-

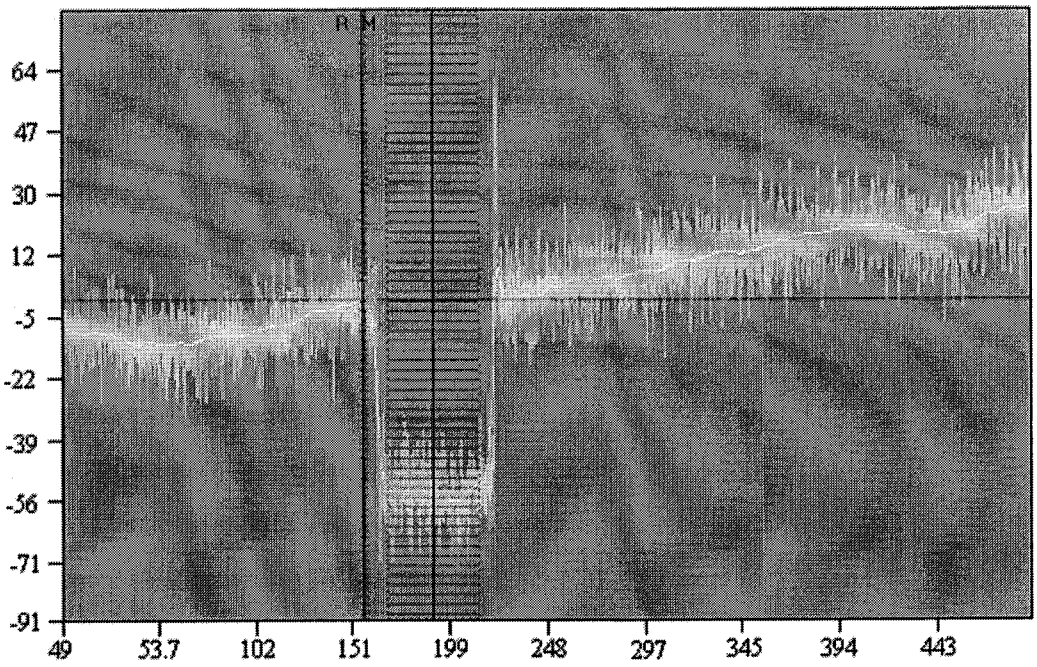

Figure 4.18 A profilometer measurement of the thickness of the type 3 bilayer coating. The thickness is approximately 55 nm.

140. Some of the holes are not as deep as others. The pillars of the imprinter had most likely broken off in these areas due to extensive use. This was the 32nd imprint performed with imprinter IMH071. The measured hole diameter was 28 nm and the measured pitch was 51 nm.

Since reducing the thickness of the bilayer partially alleviated the problem of ripped resist, the idea was taken one step further. It was decided to not only reduce the thickness of the top layer, but also the bottom layer. Therefore an even thinner bilayer was utilized. It is listed in table 4.4 as a type 3 bilayer. It consisted of a 30 nm thick bottom layer of 1% PMMA and a 25 nm thick top layer of 1% P(MMA-{17.5%}MAA). A profilometer measurement of the total thickness of the bilayer is seen in figure 4.18. The type 3 bilayer was not much more effective than the type 2 bilayer. Around the time that the type 3 bilayer started to be used, it was confirmed that the pillars of the imprinters were on average 50 nm tall. Therefore, a bilayer of 55 nm became beneficial.

An imprint into a type 3 bilayer coating is shown in image A.141. The resist of several patterns ripped as seen in the image; however, the imprinted holes that it contained were the best observed to this point. Imprinter IMH081 and the model 20 imprinting press were used. The patterns on imprinter IMH081 were exposed with a 32 fC point dose. A regulator pressure of 50 psi was used, and the imprinter and sample were separated at 45°C. One area of the imprinted

sample contained detached pillars from the imprinter as seen in image A.142. The pillars measured 78 nm in height. It is possible that the pillars broke because they were so long. The imprinted holes on the sample that are seen in images A.143-144 were the best seen to date in terms of uniformity and shape. They measured 22 nm in diameter.

A fourth type of bilayer coating was used for imprinting in one last attempt to completely alleviate the problem of ripped away resist. The 495k PMMA and P(MMA-{17.5%}MAA) had been expired for at least two years. Even though using expired resist probably only had effects in the application of electron-beam lithography, it was considered that maybe it may affect imprinting. Therefore, a new bottle of 495k PMMA in chlorobenzene and a new bottle P(MMA-{8.5%}MAA} in ethyl lactate was purchased. A bottle of P(MMA-{8.5%}MAA}was purchased with an 8.5% methylacrylic acid instead of a 17.5% simply because the lead time was shorter. Therefore, the fourth type of bilayer coating consisted of a 30 nm thick bottom layer of brand new 1% PMMA and a 25 nm thick top layer of 1% P(MMA-{8.5%}MAA). The type 4 bilayer did not alleviate the ripping problem any more than the type 2 or 3.

Even though the type 4 did not alleviate the ripping problem any more than the previous two, it did provide for several beautiful imprints. Sample IS323 was imprinted using the most effective imprinting process that had been developed. Imprinter IMH099 and the model 20 imprinting press were used. The patterns on imprinter IMH099 were exposed with a 32 fC point dose. This imprinter was exposed using the gold around the perimeter process. A regulator pressure of 40 psi was used, and the imprinter and sample were separated at 36.5°C. One of the cleanest looking imprints with the highest amount of defect free imprinted holes was accomplished. The overview of the patterns is shown in image A.145. Ripped up resist was only really seen in patterns 1, 10, and 11. High magnification images of the ripped resist are shown in images A.146-147. The sample was 90% filled with high quality imprinted holes in terms of shape, uniformity, and size. The edges of some of the imprinted patterns are shown in images A.148-150. Defect free imprinted holes can be seen in images A.151-159. The measured depth of the imprint was 32 nm. The measured hole diameter was 20 nm and the measured pitch was 44 nm. These are the best results to date!

4.6 Post Processing

After the patterns of the imprinter were replicated in the resist of the sample via imprinting, the patterns were transferred to the surface of the sample in the form of magnetic media. The imprinted sample was subjected to three post processing steps to achieve this. The steps were etching, physical vapor deposition, and a liftoff performed in this order. Etching removed the resist in the bottom of the imprinted holes in order to expose the surface of the sample. In the case of a bilayer resist, etching also produced an undercut. Physical vapor deposition deposited the magnetic media onto the sample surface that had been exposed by the imprinted holes. Finally, a liftoff removed the resist leaving behind patterns of magnetic media.

Certain parameters of each post processing step were adjusted to obtain the best possible array of patterned magnetic media. Two different etching methods were used. A dry etching method was used exclusively for single layer imprinted samples. An isotropic wet etching method that provided an undercut was used exclusively for bilayer imprinted samples. The magnetic media used was Permalloy. It was sputtered onto the imprinted samples after they were etched using a RF sputtering system. It was always sputtered onto the imprinted samples at 300 W. Various different times were used. Finally, a liftoff was performed after the sputter deposition was completed. The sample was soaked in a 1:1 mixture of methylene chloride and acetone for approximately 30 minutes. This solution was then poured out, and the sample was sonicated in a clean solution for 5 minutes. The sample was taken out of the solution, rinsed with IPA, and blown dry with a stream of nitrogen.

4.6.1 Fabrication of Patterned Magnetic Media Using a Single Layer

A single layer of PMMA was imprinted and in conjunction with dry etching was used to produce patterned magnetic media. Dry etching was done in order to remove the excess resist in the bottom of the holes of a single layer imprinted sample. Wet etching was not used because it was too isotropic. The wet etching was unable to clear all of the resist in the bottom of the holes before it washed away the sides. Sample IS249 was soaked in toluene for 20 seconds after it was imprinted. After it was soaked, it was rinsed with DI water, dried with a stream of nitrogen, and then coated with Au. Toluene was used instead of chlorobenzene because it dissolves PMMA

slower allowing for greater control. The results of the wet etching are shown in images A.160-162. It can be seen that the resist looks washed away in most areas. What happened was analogous to throwing paint thinner onto a painted canvas. Some of the holes were etched, but most of the PMMA simply washed away.

Dry etching was performed using Ar plasma from the RF sputtering system. Even though it was not completely anisotropic it produced better results than wet etching. Ideally, a RIE machine should have been used. However, the laboratory was not equipped with one. Several different runs were completed to obtain the needed power and time to remove the resist in the bottom of the holes. It was finally narrowed down to two sets of parameters. The first was an etching time of 20 seconds at a power of 200 W. Sample IS238 was etched using this set of parameters. The results are shown in images A.163-165. It can be seen that etching did not distort the imprint in any direction except the vertical one. The measured diameter of the holes was still 30 nm and the measured pitch was still 50 nm after etching.

The second set of parameters used was an etching time of 20 seconds at a power of 100 W. The results of etching sample IS247 with this set of parameters are shown in images A.166-172. Once again the etching did not distort the imprint in any direction except the vertical one. The measured diameter of the holes in pattern 1 was 30 nm and the measured pitch was 50 nm as seen in image A.167. The measured diameter of the holes in pattern 5 was 25 nm as seen in image A.170. Furthermore, it can be seen that the resist was cleared out of the holes as seen in images A.171-172. The substance that is seen in the holes in images A.171-172 is the Au that was deposited for focusing. Because the resist layer was thin enough as seen in images A.171-172, etching at 100 W was used instead of 200 W. Etching at 200 W worked nicely, but there was no need to etch away more resist than necessary. Therefore, all single layer imprinted samples were etched using 100 W to remove the resist in the holes.

Several samples were initially coated with Permalloy using various deposition times. Sample IS244 was coated with Permalloy for 5 minutes at 300W. A 5 minute deposition time at 300 W produced an 8 nm layer of Permalloy as seen in figure 4.19. The liftoff did not work very well at first. The sample had to be placed feature side down in the beaker when it was sonicated to get the PMMA to come off. Basically, what was happening here was the beaker was scratching the PMMA away due to the vibrations caused by the sonicating unit. A lot of the Permalloy dots were ripped from the surface of the sample in the areas where the PMMA came

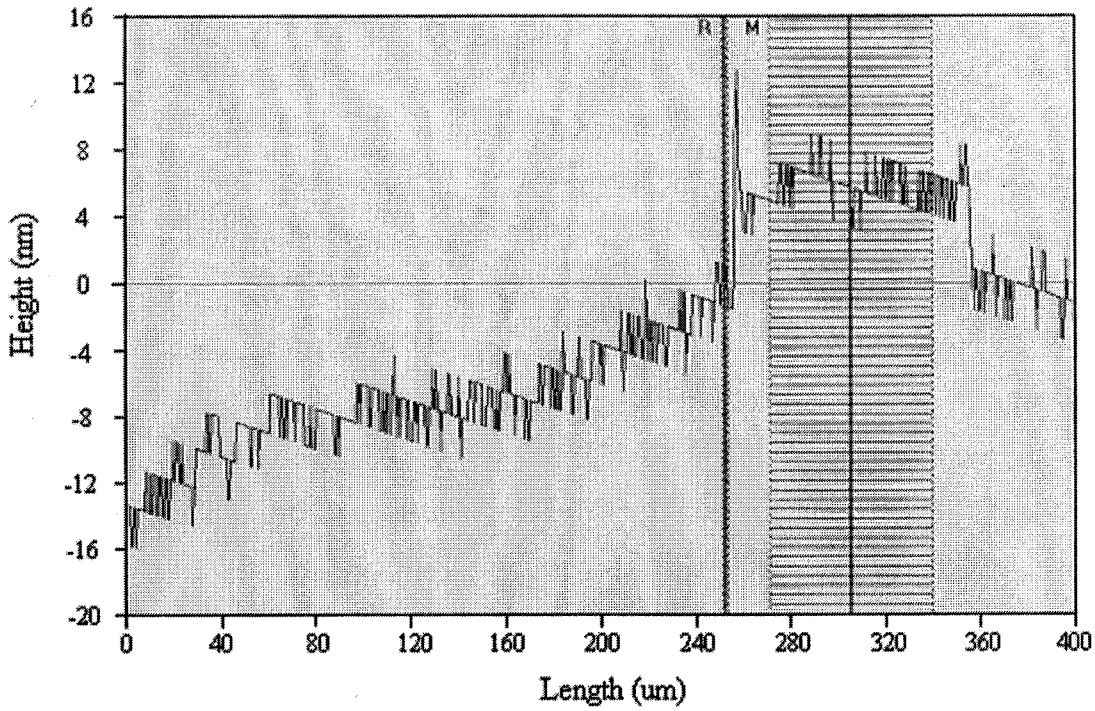

Figure 4.19 A profilometer measurement of the thickness of Permalloy when deposited at 300 W for 5 minutes. The thickness is approximately 8 nm.

off. This can partially be seen in images A.173-174 of sample IS244 after a liftoff was performed. The dark colored dots are not Permalloy, but instead indentations that the dots left after they were ripped up. Initially, this was blamed on sonicating the sample with the feature side facing the glass.

Two more samples were coated with Permalloy, and then a liftoff was performed. Once again, the PMMA did not come off easily, and a lot was still left on the sample. Sample IS246 was coated with Permalloy for 5 minutes at 300 W. An overview of the sample patterned with Permalloy dots after a liftoff can be seen in image A.175. All of the scratches that are seen on it are from sonicating it with the features rubbing against the beaker. Higher magnification images seen in images A.176-178 show the Permalloy dots. The light colored dots are Permalloy and the dark colored ones are where it was ripped off. Sample IS251 was coated with Permalloy for 7 minutes at 300 W. An overview of the sample is shown in image A.179, and the Permalloy dots can be seen in images A.180-183. These areas show less dots ripped off, but more PMMA that has been left on the sample. The measured diameter of the Permalloy dots was 28 nm and the measured pitch was 46 nm.

The problem that was experienced with the liftoff of the PMMA was eventually solved. It was first thought that the liftoff solution was blocked from breaking up the PMMA by too thick of a Permalloy layer covering too thin of a resist layer. This was not accurate. Since the PMMA had been expired for over two years, its chemical properties were altered over time. Therefore, a 1:1 mixture of methylene chloride and acetone had no effect on the PMMA. Once new PMMA was used, the liftoff worked as expected. The new PMMA was used for sample IS251. The sample was coated with Permalloy for 10 minutes at 300 W. It only took 30 minutes to liftoff most of the PMMA. An overview of the patterned sample can be seen in images A184. The sample is not as scratched as the others because its feature side was not touching the glass during the liftoff. Other patterned areas are shown in images A.185-191. There were a higher percentage of Permalloy dots, and they looked better than in the previous samples that were shown. This was most likely a result of a more effective liftoff. Also a deposition time of 10 minutes was believed to be a slight factor. The measured diameter of the Permalloy dots ranged from 19 to 23 nm, and the measured pitch was 50 nm.

Even though there were more Permalloy dots and they looked more uniform, a significant number had still been ripped off of the surface of the sample. The particle size of the Permalloy was only about 2 to 3 nm as seen in image A.192. Therefore, the problem was not a result of the Permalloy particles being too large for the imprinted holes. It was then thought that the Permalloy dots were ripped up because a single layer was used and this cannot achieve an undercut. Without an undercut, the sidewalls of the imprinted holes became coated with a continuous layer of Permalloy as seen in image A.192. Some of the Permalloy that landed on the sample surface was not able to withstand the force with which the PMMA was lifted off. Therefore, some of it was ripped from the surface by the PMMA as seen in image A.193. To try to correct this problem, a bilayer imprint was used to produce patterned magnetic media.

4.6.2 Fabrication of Patterned Magnetic Media Using the Type 4 Bilayer

A bilayer resist was imprinted and in conjunction with only wet etching was used to produce patterned magnetic media. The type 4 bilayer, which consisted of a 30 nm thick bottom layer of brand new 1% PMMA and a 25 nm thick top layer of 1% P(MMA-{8.5%}MAA), was predominantly used. This bilayer was used because it was shown that patterns of imprinted holes

with minimal defects were effectively produced in it. Furthermore, the resists used for the bilayer were brand new so there was more of a chance that the wet etching or liftoff solutions would be effective. The duration of time that was needed to etch the sample was quickly ascertained. A 5 second rinse in methanol successfully washed away a thin layer of the P(MMA-{8.5%}MAA). Then a 5 second rinse in chlorobenzene dissolved enough of the underlying PMMA layer to produce the undercut.

Several samples were fabricated using a type 4 bilayer coating to produce patterned magnetic media. Consider sample IS336. It was imprinted using the final, most effective, imprinting process that had been developed. The model 20 imprinting press and imprinter IMH100 were used. The imprinter was exposed with a 32 fC point dose, and Au was sputtered around the edges of it for optimal focusing. A regulator pressure of 40 psi was used for imprinting, and the separation temperature was 33°C. The sample was subjected to a wet etch using the parameters specified in the last paragraph. The sample was sputter coated with Permalloy for a duration of 10 minutes at 300 W. According to the profilometer measurement shown in figure 4.19, these parameters produced a 16 nm thick layer of Permalloy. The liftoff was performed using a 1:1 mixture of methylene chloride and acetone. Within 30 minutes, most of the resist was removed form the surface of the sample. Some of the resist did not come off the patterns and in the circular region around the patterns.

The best looking expanse of patterned magnetic media was seen on sample IS336. The sample contained a higher percentage of Permalloy dots than was produced with the single layer. The dots also appeared more circular and much sharper. Regions containing Permalloy dots can be seen in images A195-A206. A 4.3 μm x 2.8 μm region is approximately 50% filled with Permalloy dots as seen in image A.197. The measured dot diameter ranged from 17 to 19 nm. The measured pitch ranged from 40 to 45 nm. A pitch of 45 nm equates to a bit density of 320 Gbits/in^2.

Despite the higher level of success achieved with the bilayer, there were still areas where the Permalloy dots had been ripped from the surface. The only possible reason for this was that the bilayer was too thin. It was 55 nm thick before etching was carried out. With such a thin bilayer, the sidewalls were still susceptible to a continuous coating of Permalloy. This was even more of a case with sputter coating. Sputter coating is a form of physical vapor deposition in which the material is fired at the sample from every direction. A thicker bilayer was not

plausible because of the short height of the HSQ pillars. The increased surface interaction that occurred with a thicker bilayer caused the resist to tear and the imprinter to stick to the sample. Remember that the type 1 bilayer coating had to be curtailed due to this. Evaporating the Permalloy onto the sample might have further reduced the tearing that was observed. With evaporation, the targeted material is only deposited on the sample from the vertical direction. However, Permalloy could not have been evaporated onto the sample with our equipment.

4.7 Magnetic Measurements

Sample IS340 was sent to Washington University in St. Louis so that magnetic measurements could be performed on it. Experiments revealed that the Permalloy dots were magnetized in the perpendicular direction. However, most of the other tests were unsuccessful. The stray fields from the sample were too weak to provide adequate phase information. Attempts were made to reverse the magnetization of the Permalloy dots with a permanent magnet and also pin the magnetization of the dots in the horizontal direction. The phase information which was produced showed no evidence that these two tests were successful. It was stated that the stray field of the magnetic force measurement (MFM) probe perturbed the magnetization of the Permalloy dots. This was a result of the magnetically soft property of the dots.

4.8 Conclusion

The research in this chapter established that nanoimprint lithography was able to effectively fabricate patterned magnetic media. Various apparatuses and an assortment of chemicals were utilized along with specific material processing guidelines to carry out the steps of nanoimprint lithography. Two types of imprinters were fabricated. It was elected to use HSQ imprinters for imprinting because, unlike the SiO_2 imprinters, all of the fabrication steps could be done in one day at Rowan University. The HSQ imprinters were coated with the F_{13}-TCS anti-adhesive agent. The imprinting process was refined several times to obtain optimal results. A single layer and an assortment of bilayer resist coatings were used to imprint into. Finally,

fourteen 100 μm x 100 μm patterns containing Permalloy dots were produced after post processing was completed. Dry etching, a sputter deposition of Permalloy, and a liftoff were the post processing steps used to fabricate patterned magnetic media with a single layer of resist. Isotropic wet etching, a sputter deposition of Permalloy, and a liftoff were the post processing steps used to fabricate patterned magnetic media with a bilayer resist.

A handful of problems were experienced throughout the steps of nanoimprint lithography. The first two problems occurred with the fabrication of HSQ imprinters. The pillars collapsed after the sample was developed, and their height in the center of the pattern was not as tall as the thickness of the spun-on HSQ. The collapsed pillars were simply a case of poor focusing. The height problem was more involved. A certain thickness of HSQ was exposed between the pillars either due to the proximity effect or the absence of a beam blanker. Thus, the effective height of the pillars in the center of the pattern was lowered. A spun on thickness of 150 nm of HSQ produced 50 nm tall pillars. This problem was never corrected, but a solution to work around it was used. The height of the resist used for imprinting was lowered.

The height of the resist used for imprinting provides a good transition to the next problem that was encountered. The resist of an imprinted pattern had a tendency to rip or tear after the imprinter was separated from the sample. One of the causes was believed to be that the F_{13}-TCS anti-adhesive coating was not working effectively. This is still assumed to be part of the problem. It was also though that the resist tore away because the pillars were not the desired height. The thickness of the resist was reduced mostly with the bilayer and less ripping and buckling occurred.

Finally, there was one last problem that was detected. The resist ripped up the Permalloy dots when a liftoff was performed. Also, the liftoff was not working properly. It was discovered that because the PMMA was expired, the liftoff solution was ineffective. With the new PMMA, the liftoff worked fine, and more Permalloy dots were seen per pattern. However, a certain percentage of dots were still ripped from the surface of the sample. It was thought that a single layer allowed the Permalloy to form a continuous layer from the top of the holes to the bottom which caused it to rip up. A bilayer resist was then used because it was able to provide an undercut. A higher percentage of Permalloy dots was seen with a bilayer; however, there was still a percentage that was being ripped off. It was finally determined that the resist of both the single layer and bilayer was not thick enough to prevent a continuous coating of Permalloy from

the top of the holes to the bottom. However, the thickness was unable to be increased because the pillars of the imprinter could not be made taller.

Some aspects of the nanoimprint lithography process performed at Rowan University do need to be altered even further to prevent the eventual tearing of the Permalloy dots. Nonetheless, a considerable amount of results were compiled showing that nanoimprint lithography is an effective way of producing patterned magnetic media. The measured pillar diameter and pitch of HSQ imprinters was 25 nm and 50 nm respectively. The effective height of the pillars measured between 30 and 50 nm. Patterns of imprinted holes were produced with hole diameters as small as 20 nm and pitches of 44 nm. Finally, patterns of Permalloy dots were produced. The smallest dot diameter measured was 17 nm and pitch was 40 nm. A pitch of 40 nm equates to a bit density of 403 Gbits/in^2.

5 CONCLUSION

Advances in technology continually change and reshape everyday life and the manner in which things are done. The truth of this can be seen in the way that information is stored. Paper has been the primary form of information storage for thousands of years. However, with advances in technology, more efficient, low cost, and greater capacity information storage systems have been developed. There is now an increasing demand for high performance and low cost information storage. This demand has fueled the growth of the hard disk drive industry. In 2002, a study was conducted which showed that hard drives were the primary form of information storage for that year. Approximately 2 exabytes of original information was stored on hard drives in 2002 alone. Two exabytes of information is ten times the amount of all the printed material in the world.

The wealth of available information to be stored along with the growth of storage-hungry graphics and multimedia applications has created a demand for greater capacity hard drives. The hard drive industry has been trying to keep up with this demand. The capacity of hard drives has increased by at least 61% annually since 1991. In 1957, the first hard drive which was the size of a small room was capable of storing 5 MB. Today, there is a commercially available hard drive capable of storing 500 GB on just a few 3.5 inch platters. As the trend to store more information continues to increase, the capacity of hard drives will also need to increase to stay competitive in the storage field. As of now, hard drives are the most popular type of information storage. They are able to store massive amounts of information at a price of $0.001/MB. Information storage on paper and film is between ten cents and a dollar per megabyte. It has been stated that semiconductor flash memory could eventually compete with hard drives. However, this is pure speculation because the price per megabyte of this type of memory is currently two orders of magnitude greater than that of hard drives.

In order to keep increasing the capacity of hard drives, all major components of the head-disk assembly are scaled down in size. These include the read sensor, write head, and the magnetic media. The capacity of a hard drive is measured in areal bit density. To increase this parameter, the bit size is reduced. Bits on a hard drive platter are not physical barriers, but instead magnetic barriers. The write process defines the size of a bit; therefore, the dimensions of a bit are dependent upon the size of the write head. The write head has been scaled down over

the years to yield smaller bit dimensions. There exist certain tradeoffs in doing this as defined by the transition parameter. One of the tradeoffs is maintaining a large enough remanence thickness product to produce a detectable readback signal. As the dimensions of a bit decrease, so does its emanating stray fields. Scaling of inductive read sensors eventually proved to be ineffective. To compensate, GMR spin valve read sensors were eventually employed. They were able to provide the needed sensitivity to detect the extraordinarily small signals of a bit.

Eventually a limit to increasing the areal bit density through scaling of relevant head and media dimensions will be reached. A bit has to be composed of on average 100 magnetic grains to promote a readable SNR. As the bit dimensions are reduced, the size of the magnetic grains must also be reduced to maintain this average. However, there is a limit to how small the grain size can become. Once a grain reaches approximately 10 to 12 nm in diameter, it becomes superparamagnetic. Its magnetization is affected by thermal energy. The thermal energy is pivotal in causing the magnetization of a grain to spontaneously switch directions. Once this begins to occur, the lifetime of a hard drive greatly diminishes. It has been predicted that the superparamagnetic limit will be encountered between areal bit densities of 40 to 70 Gbits/in^2.

Despite the previous prediction, a hard drive has just been released with an areal bit density of 76 Gbits/in^2 using conventional longitudinal recording on continuous magnetic media. A concept known as "pixie dust" or AFC media initially developed by IBM has made this possible. The technology antiferromagnetically couples two layers of magnetic media to increase the thermal stability of smaller grains. Eventually, this will not be enough to prolong the life of conventional magnetic recording in hard drives. Therefore, a next generation recording technology will be instrumental in continuing the increase of areal bit density. Perpendicular recording has the potential to provide larger areal bit densities than longitudinal because the required average of magnetic grains per bit is about 10. A hard drive using perpendicular recording technology will soon be commercially available in Apple's iPod music player. The areal bit density is said to be 133 Gbits/in^2. There is a possibility of achieving far greater areal bit densities. The perpendicular recording of this new hard drive will still be done on continuous magnetic media. If magnetic media can be physically patterned one grain per bit can be achieved. This would enable areal bit densities to surpass 1 Tbit/in^2.

Fabricating patterned magnetic media is indeed challenging. Finding a low-cost, high-throughput pattern generation technology is difficult. Patterned magnetic media can be created

in the laboratory on a small scale; however, the goal is to eventually move it towards large scale production. There are three pattern generation technologies that are being actively pursued to fabricate patterned magnetic media. These are interference lithography, self-assembly patterning, and nanoimprint lithography. All three have their advantages and disadvantages. Interference lithography has been shown to pattern an area as large as 250 mm x 250 mm. However, there are difficulties in producing sub-50 nm densely packed features due to issues with optics. Furthermore, only highly regular, periodic patterns can be created with the technology. Self-assembly patterning has also shown the capability to produce large area patterns. The patterning of a 2.5-inch diameter disk was demonstrated using self assembly. Densely packed sub-50 nm features can be fabricated using self-assembly. The downside to self-assembly patterning is that, like interference lithography, it is only capable of producing periodic patterns. Also, it is not able to consistently produce long range ordered patterns. Finally, nanoimprint lithography is capable of producing sub- 20 nm densely packed features. It is also able to produce non-periodic patterns. The disadvantage of nanoimprint lithography is that it has not yet been shown to fabricate patterns as large as the previous two.

Research was completed to show that nanoimprint lithography is a competing technology and capable of fabricating patterned magnetic media. Electron-beam lithography was used to fabricate HSQ imprinters. The imprinters were then coated with a F_{13}-TCS anti-adhesive agent to decrease the surface energy. Imprinting was completed using the hot embossing method. A single layer and several bilayer resist coatings were used to imprint into. Dry etching, a sputter deposition of Permalloy, and a liftoff were used to fabricate patterned magnetic media with a single layer resist. The same procedure except with wet etching instead of dry was used to fabricate patterned magnetic media with a bilayer. In the end, fourteen 100 μm x 100 μm patterns per sample containing Permalloy dots were produced.

Several problems were encountered. It was found that the pillars of the imprinter collapsed after they were developed and were not as tall as the spun on layer of HSQ. The resist occasionally ripped and buckled after the imprinter was separated from the sample. Finally, the areas of Permalloy dots were torn away from the surface of the sample by the resist when it was removed. The problems were either fixed or worked around. Despite the problems that were encountered, a large quantity of results were amassed that proved nanoimprint lithography is an effective technology to fabricate patterned magnetic media. HSQ imprinters were produced with

a measured pillar diameter of 25 nm, a pitch of 50 nm, and a height of 30 to 50 nm. Imprinted patterns were produced with a hole diameter of 20 nm and a pitch of 44 nm. Finally, fourteen 100 μm x 100 μm patterns of Permalloy dots were produced. They were usually 50% full of dots. The smallest dot diameter measured was 17 nm and pitch was 40 nm. A pitch of 40 nm is equal to a bit density of 403 Gbits/in^2. These results illustrate the tremendous potential that nanoimprint lithography possesses to fabricate patterned magnetic media.

6 FUTURE RECOMMENDATIONS

If further research is going to be performed down this direction, a few problems need to be addressed more specifically. First, experiments should be conducted to determine why the HSQ between the pillars in the center of patterns is exposed. The solution to this might be as simple as using a beam blanker. Either that or the HSQ is not well suited for fabricating pillars. More research should be done with SiO_2 imprinters. If the necessary equipment is supplied at Rowan University, it might be a good idea to fabricate and use SiO_2 imprinters for imprinting. Even though there are more steps involved, the pillar height of these imprinters will be greater. This will allow the resist to be thicker. A thicker resist will prevent the sidewalls of holes from being coated with Permalloy. In the end, this should prevent the Permalloy dots from tearing off the surface. Also, experiments need to be completed with the anti-adhesive coating to make sure it is effective. The possibility of it not being effective and causing the resist to rip up has to be eliminated. Finally, larger areas of patterned magnetic media need to be created. One way to start experimenting with this is to imprint a sample several times.

APPENDIX A: IMAGES

This appendix contains all of the SEM and optical images of imprinters, imprinted samples, and magnetic dots produced from the research work that was completed. These images are the primary form of results that were gathered. Each image has a sample number on the top left of it. The sample number of an image of an imprinter can be broken into three parts. The first part is the abbreviation where IMS indicates a SiO_2 imprinter and IMH indicates a HSQ imprinter. The number immediately following this is the specific imprinter sample. Finally the number after the dash is the pattern number that corresponds to figure A.1 for a SiO_2 imprinter and figure A.2 for a HSQ imprinter. The sample number of an imprinted sample image can be broken into four parts. The abbreviation IS indicates that it is an imprinted sample and the numbers immediately following indicate which specific one. The abbreviation and numbers after the first dash are what type and specific imprinter was used to create it. Finally, the last numbers are what pattern created from the imprinter the image is of. If the final numbers are replaced by OV, the image is an overview of all of the patterns on an imprinter or imprinted sample. The patterns on the imprinted samples are mirror image of the patterns on the HSQ imprinter seen in figure A.2. Each type of resist used for the imprinted samples is shown in table A.1.

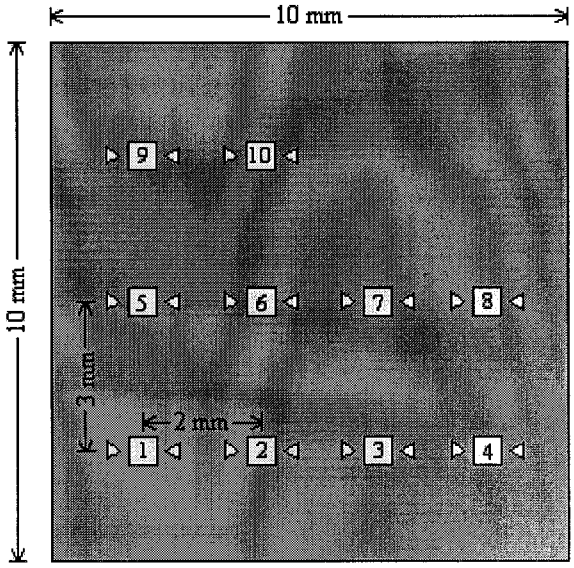

Figure A.1 An illustration of a SiO_2 imprinter showing the configuration in which the patterns were written onto it.

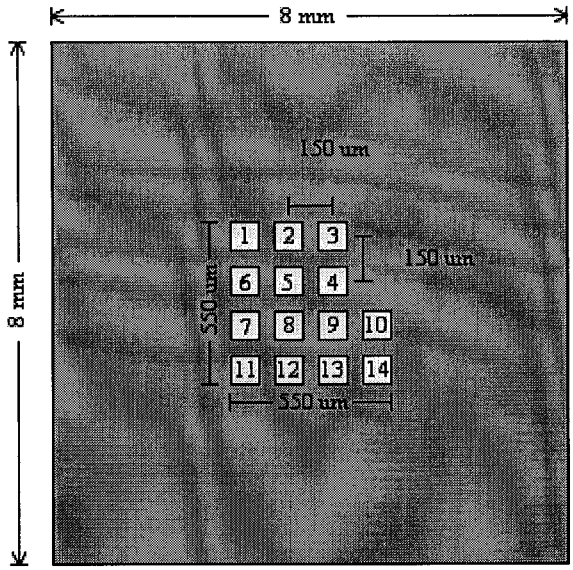

Figure A.2 An illustration of an HSQ imprinter showing the configuration in which the 100 by 100 μm patterns were written onto it.

Table A.1 The table lists the parameters of each type of resist coating that was used for the final improved imprinting process. The PMMA is 495k PMMA

Type of Coating	*Layer of Resist*	*Spin on Speed (rpm)*	*Thickness (nm)*
Single Layer	1% PMMA	1800	50
Bilayer 1	Top: 2.2% P(MMA-{17.5}MAA)	4000	50
	Bottom: 1% PMMA	1800	50
Bilayer 2	Top: 1% P(MMA-{17.5}MAA)	4000	25
	Bottom: 1% PMMA	1800	50
Bilayer 3	Top: 1% P(MMA-{17.5}MAA)	4000	25
	Bottom: 1% PMMA	4000	30
Bilayer 4	Top: 1% P(MMA-{8.5}MAA)	4000	25
	Bottom: 1% PMMA	4000	30

A.1 Imprinters

A.1.1 SiO_2 Imprinters

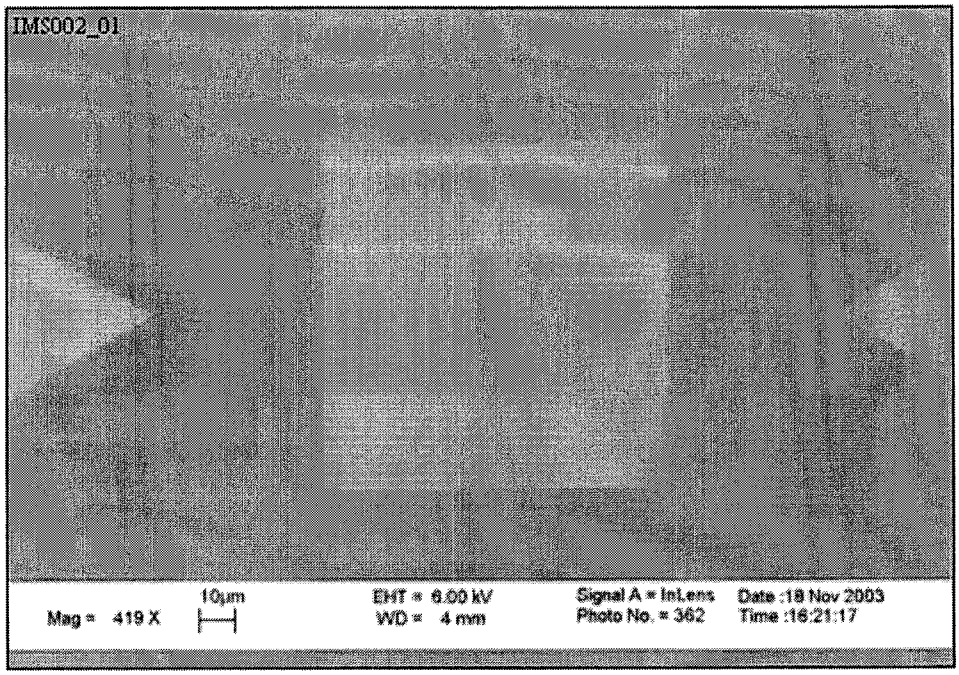

Image A.1 A low resolution, large field of view image of a pattern 1 on sample IMS002 after it was written, developed, and coated with Au. A dose of 14 fC and a pitch of 75 nm were used.

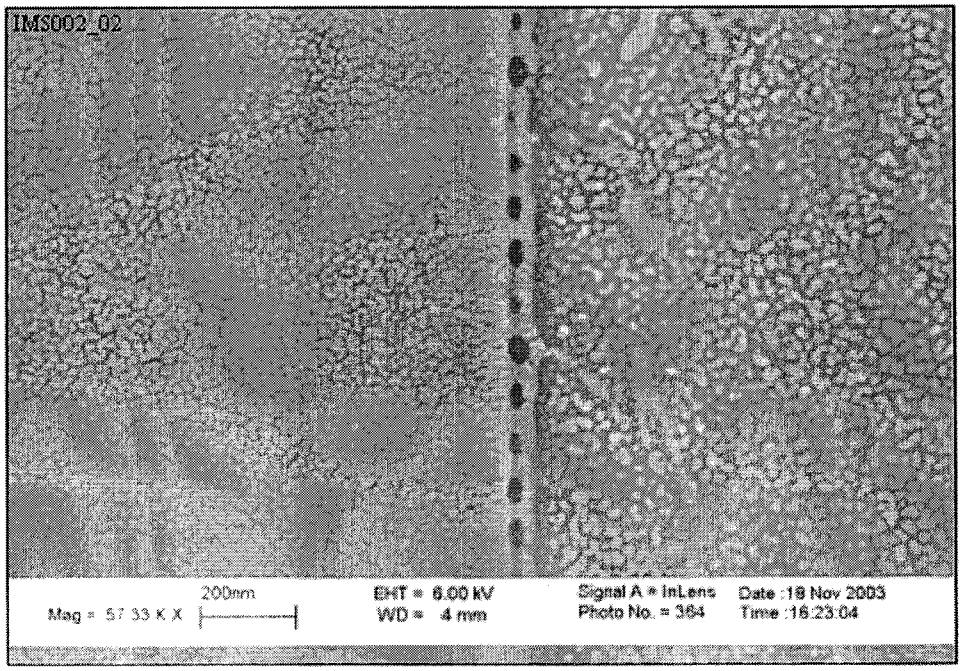

Image A.2 A relatively high resolution image of pattern 2 on sample IMS002 after it was written, developed, and coated with Au. A dose of 14 fC and a pitch of 100 nm were used.

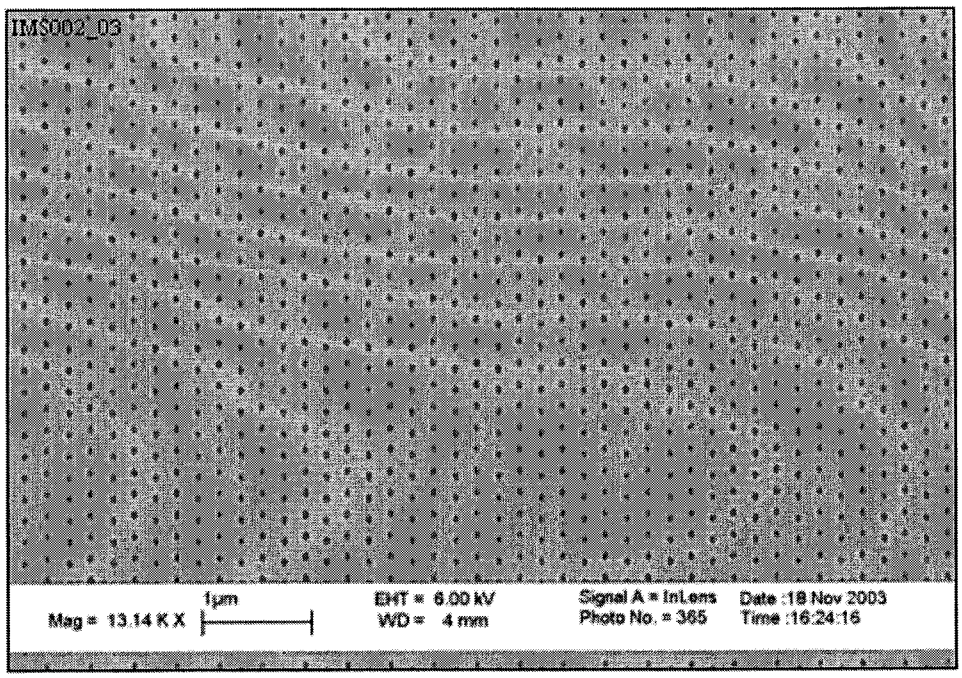

Image A.3 Image of pattern 3 on sample IMS002 after it was written into a bilayer PMMA resist, developed, and coated with Au. A dose of 14 fC and a pitch of 200 nm were used.

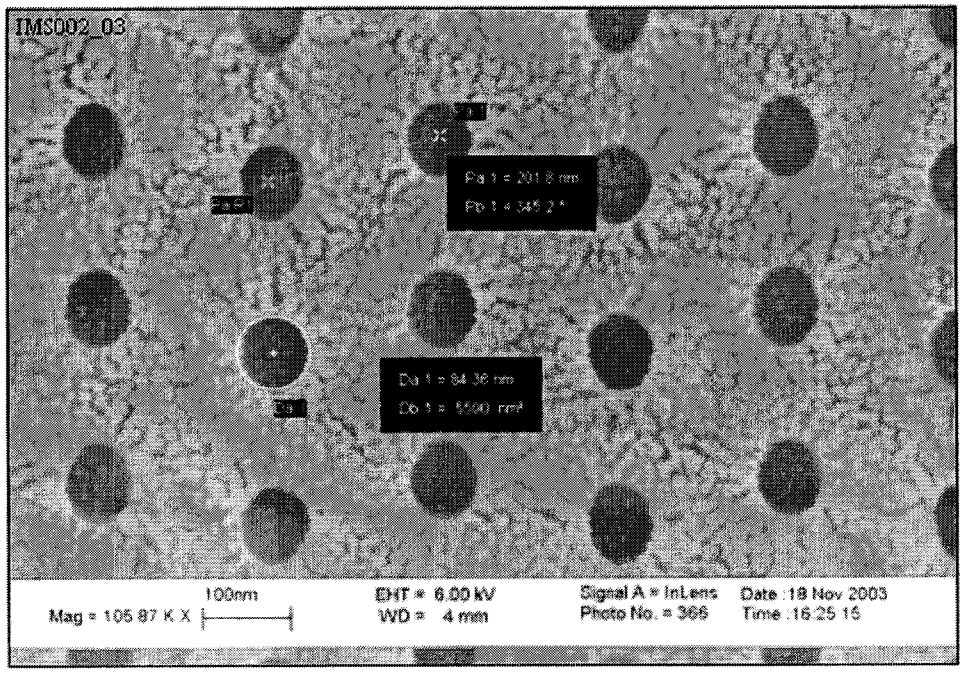

Image A.4 Image of pattern 3 on imprinter IMS002 after it was written into a bilayer PMMA resist, developed, and coated with Au. A dose of 14 fC and a pitch of 200 nm were used.

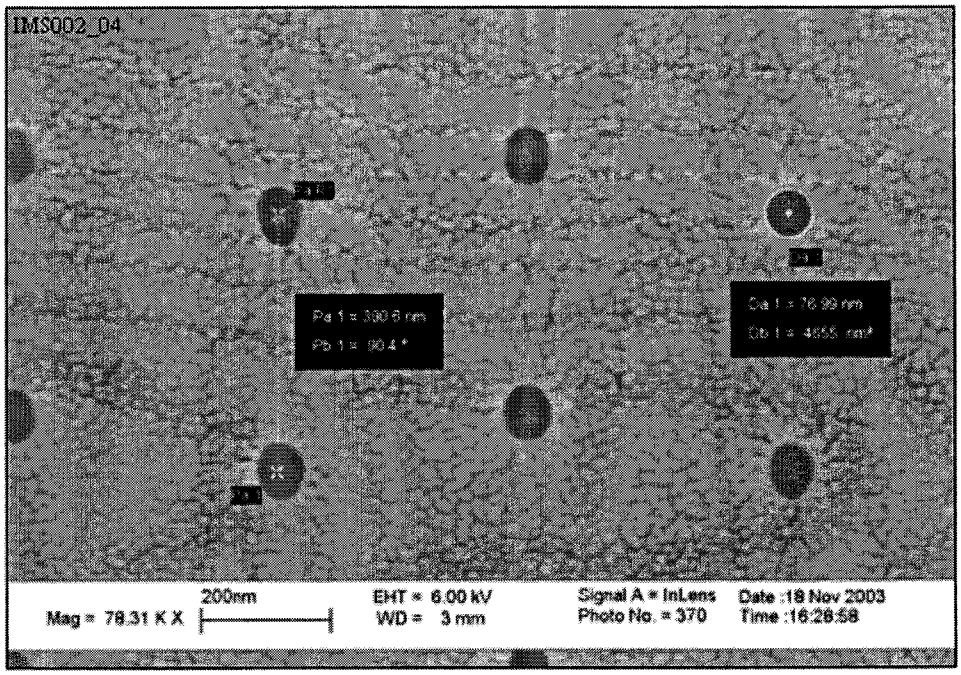

Image A.5 Image of pattern 4 on imprinter IMS002 after it was written into a bilayer PMMA resist, developed, and coated with Au. A dose of 14 fC and a pitch of 400 nm were used.

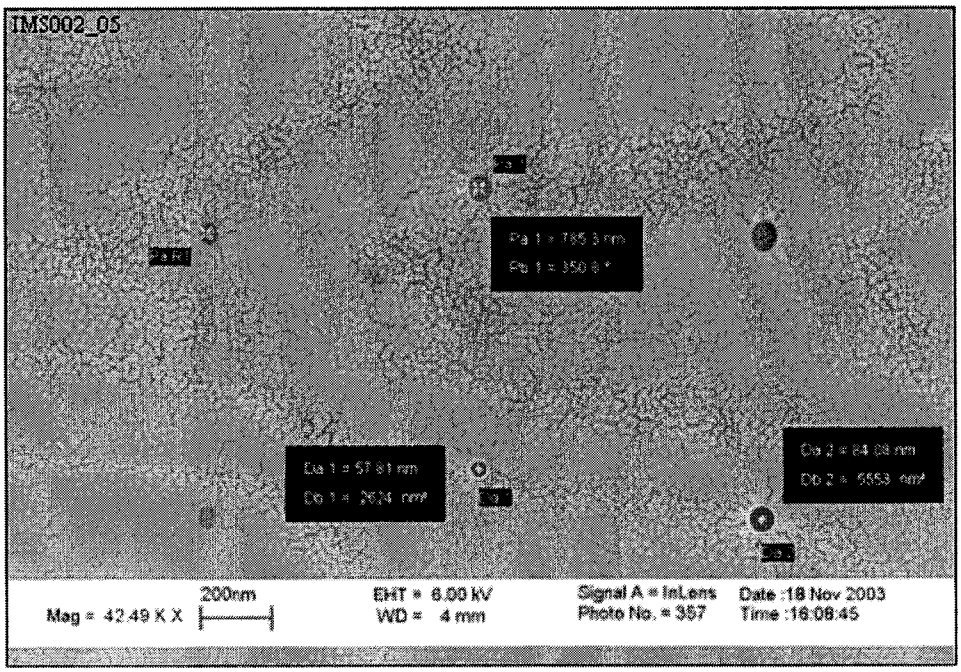

Image A.6 Image of pattern 5 on imprinter IMS002 after it was written into a bilayer PMMA resist, developed, and coated with Au. A dose of 14 fC and a pitch of 800 nm were used.

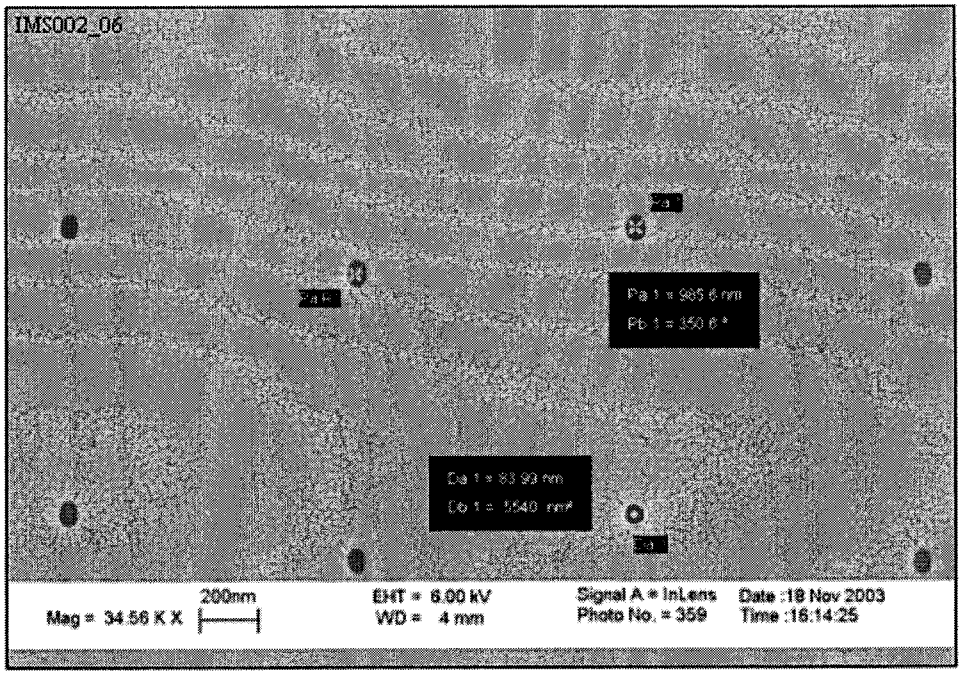

Image A.7 Image of pattern 6 on imprinter IMS002 after it was written into a bilayer PMMA resist, developed, and coated with Au. A dose of 14 fC and a pitch of 1000 nm were used.

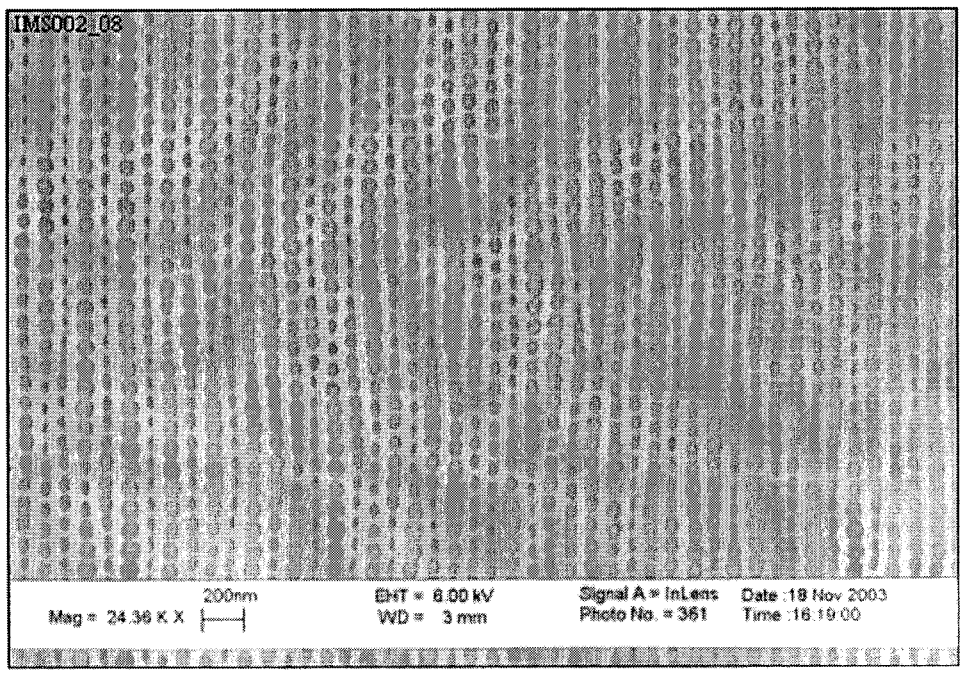

Image A.8 Image of pattern 8 on imprinter IMS002 after it was written into a bilayer PMMA resist, developed, and coated with Au. A dose of 13 fC and a pitch of 100 nm were used.

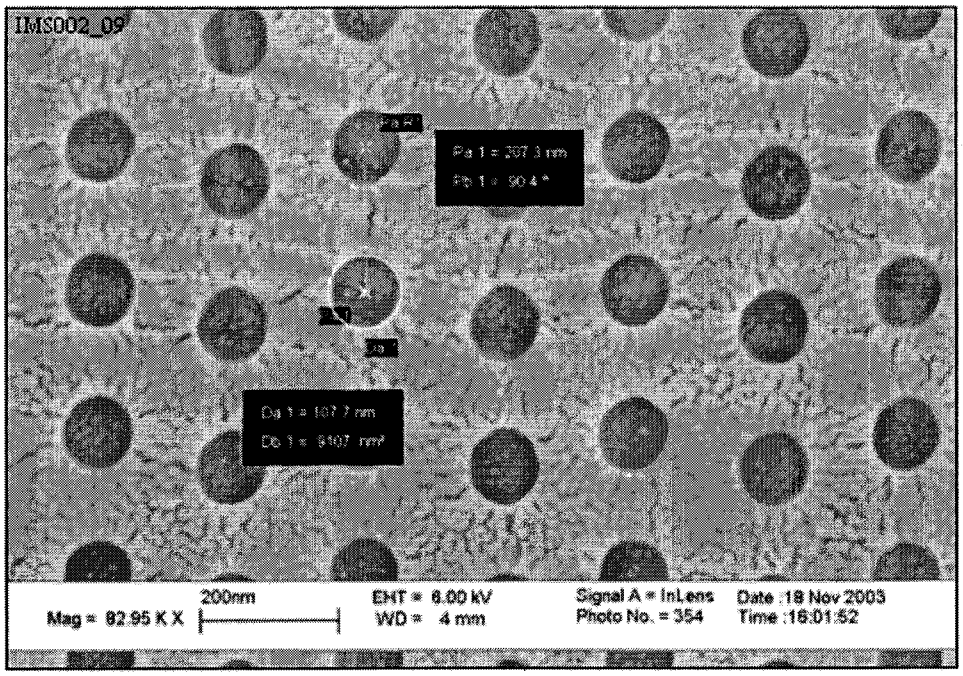

Image A.9 Image of pattern 9 on imprinter IMS002 after it was written into a bilayer PMMA resist, developed, and coated with Au. A dose of 13 fC and a pitch of 200 nm were used.

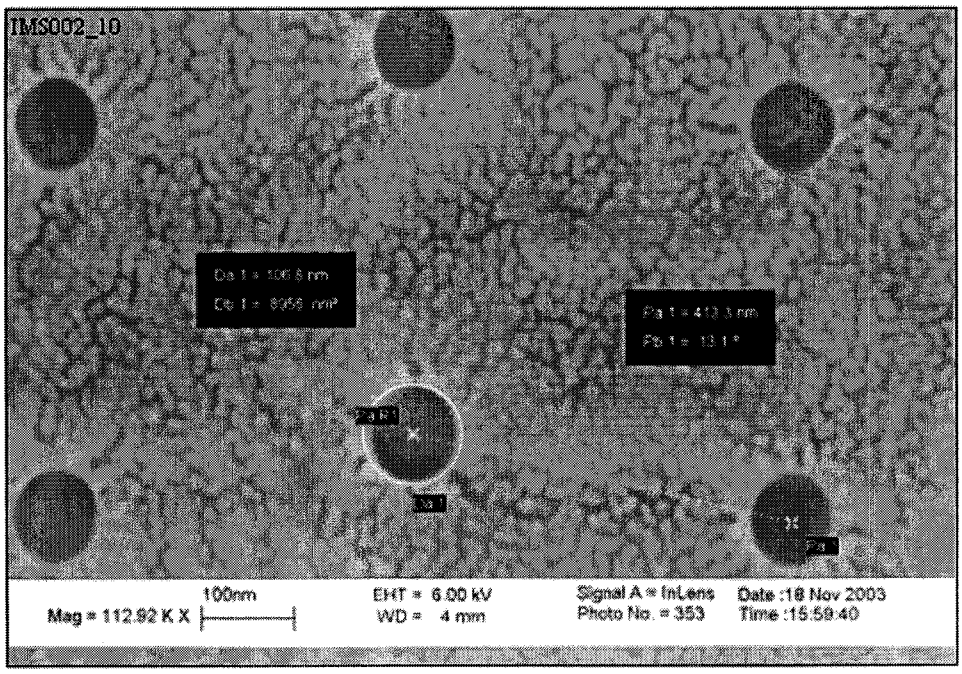

Image A.10 Image of pattern 10 on imprinter IMS002 after it was written into a bilayer PMMA resist, developed, and coated with Au. A dose of 13 fC and a pitch of 400 nm were used.

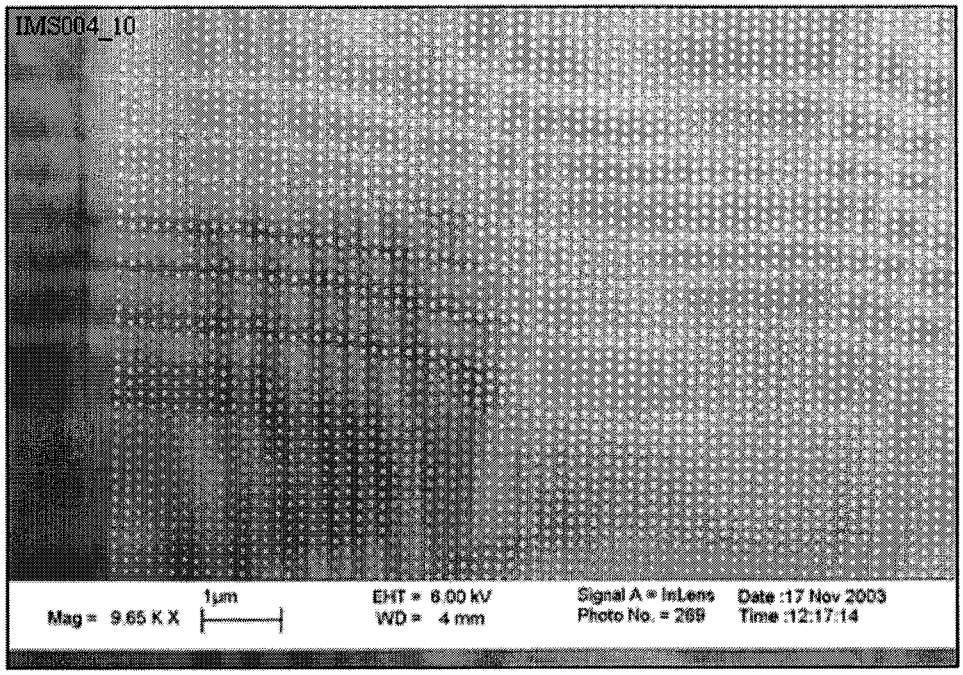

Image A.11 Pattern 10 on imprinter IMS004 after it was etched. It was produced using a 13 fC point dose and a 150 nm pitch revealing a flawless array of SiO_2 pillars.

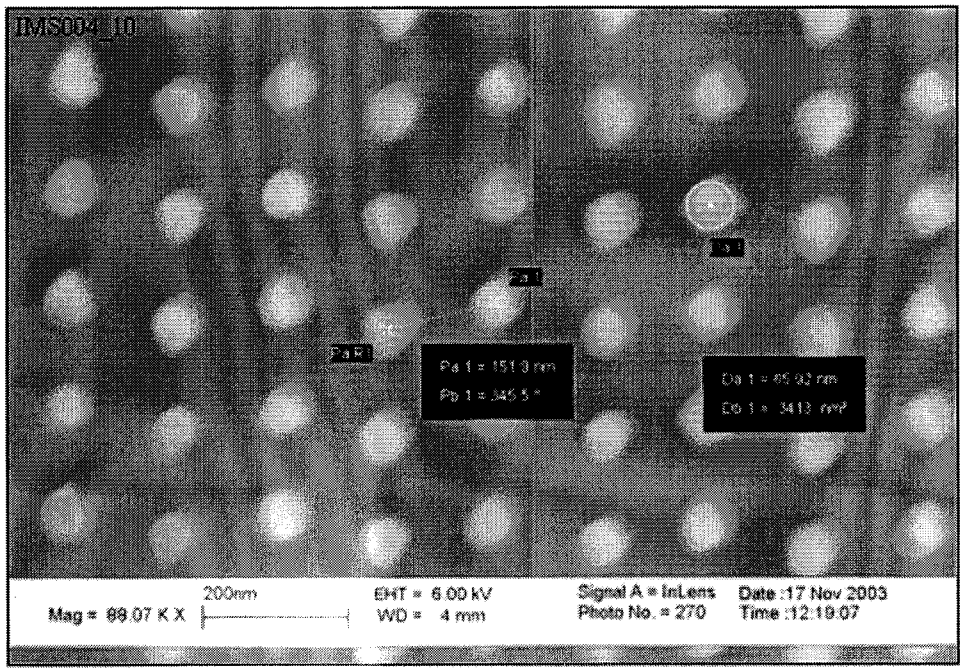

Image A.12 A higher magnification image of pattern 10 on imprinter IMS004. The pillars were measured to be 65 nm in diameter. Also the measured pitch value agrees with the value set before writing.

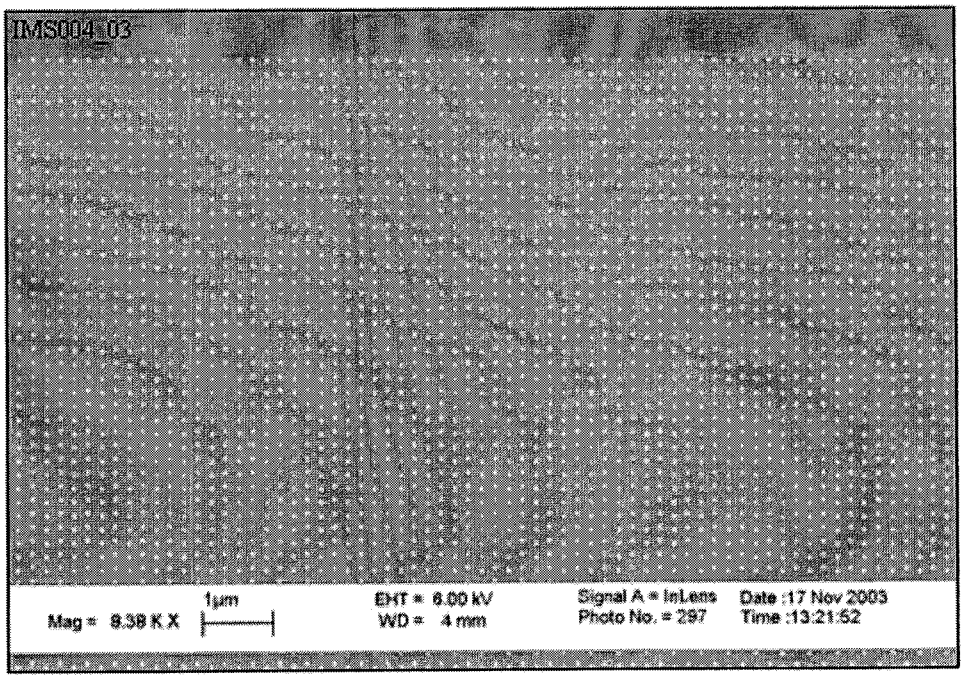

Image A.13 Pattern 3 on imprinter IMS004 produced using a 13 fC point dose and a 200 nm pitch revealing a flawless array of SiO_2 pillars.

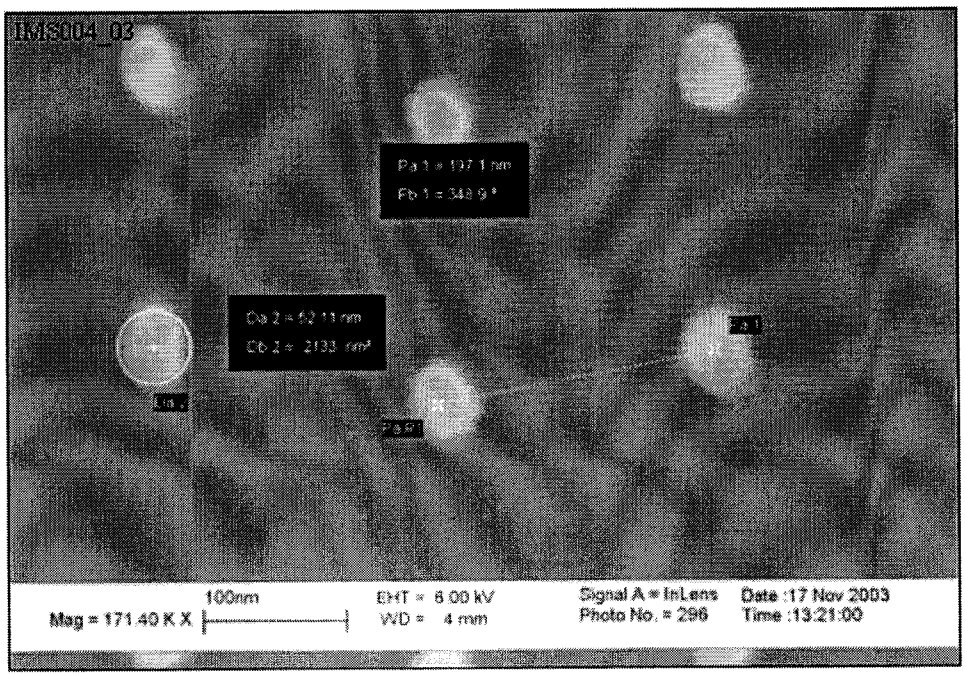

Image A.14 A higher magnification image of pattern 3 on imprinter IMS004. The diameter of the pillars was measured to be 52 nm and the pitch value agreed with the one that had been designated.

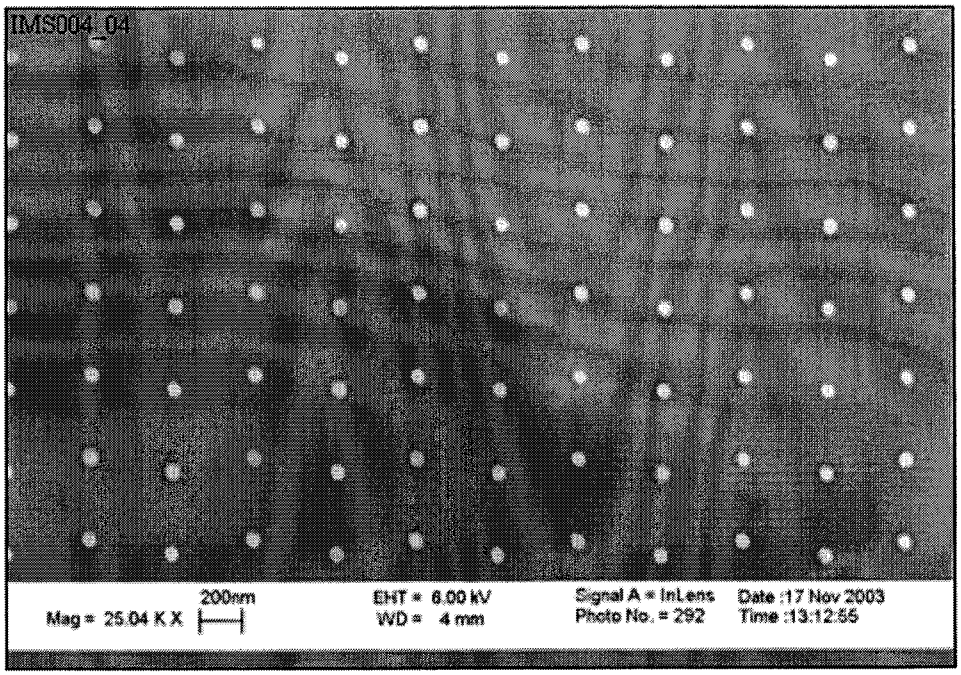

Image A.15 Pattern 4 on imprinter IMS004 produced using a 13 fC point dose and a 400 nm pitch revealing a flawless array of SiO_2 pillars.

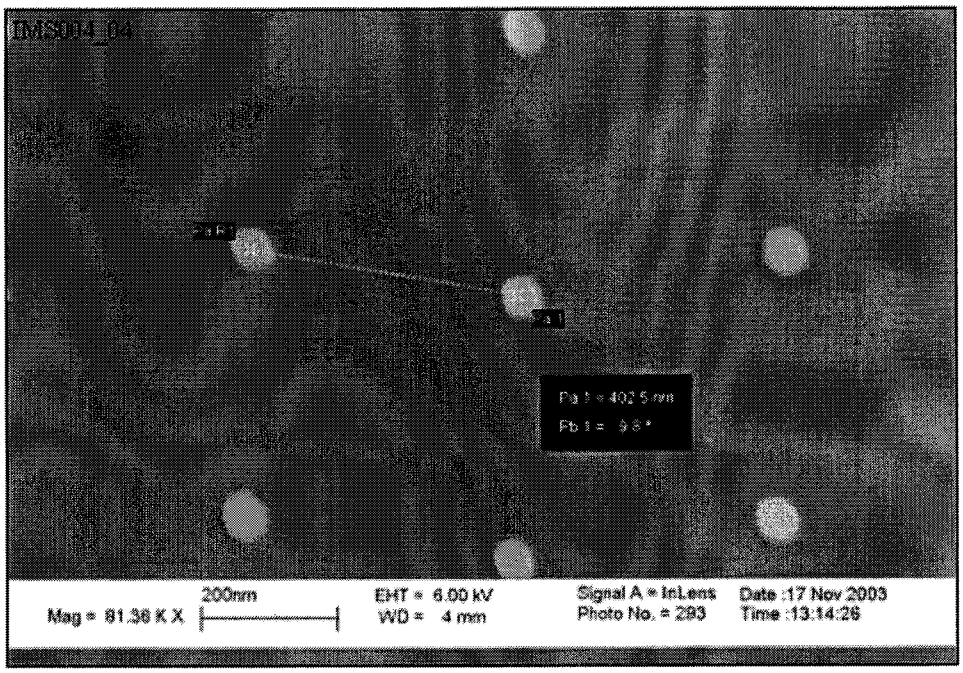

Image A.16 A higher magnification image of pattern 4 on imprinter IMS004. The pillars are about 54 nm in diameter and the value of the pitch agrees with the one that was initially set.

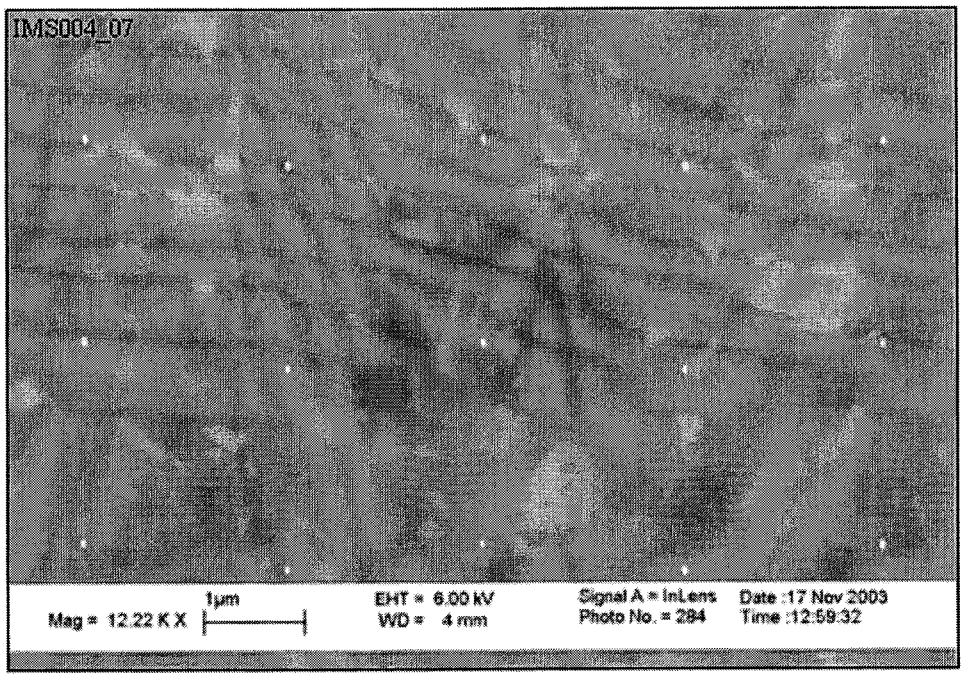

Image A.17 Pattern 7 on imprinter IMS004 written using a 13 fC point dose and a pitch of 2000 nm. The pillars were measured to be 58 nm in diameter.

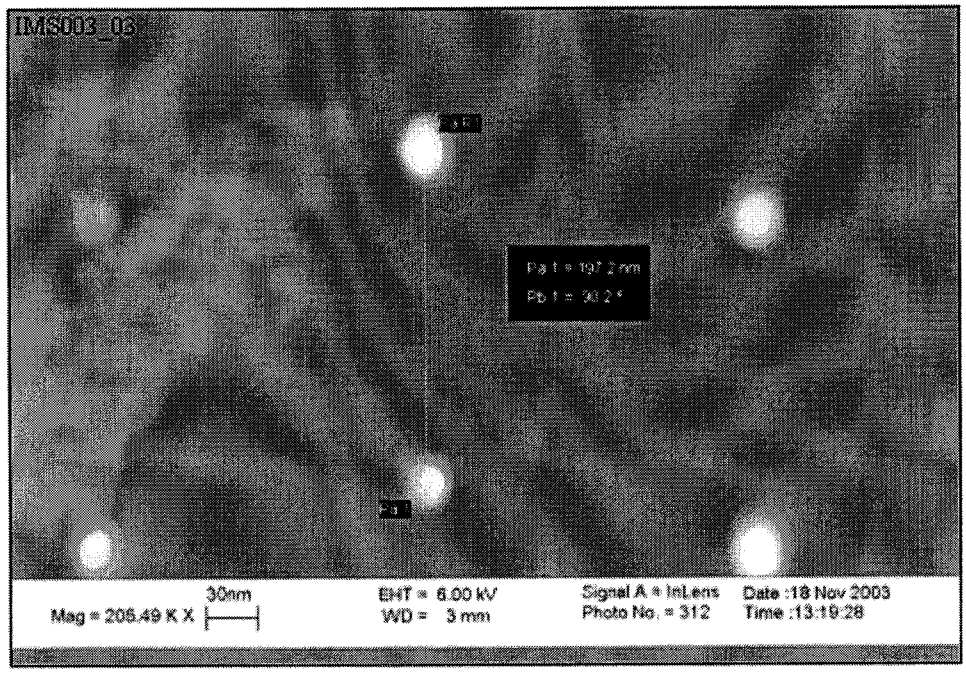

Image A.18 Pattern 3 on imprinter IMS003 produced using a point dose of 14 fC and a pitch of 200 nm. The measured pillar diameter was 40 nm and the measured pitch was 197 nm.

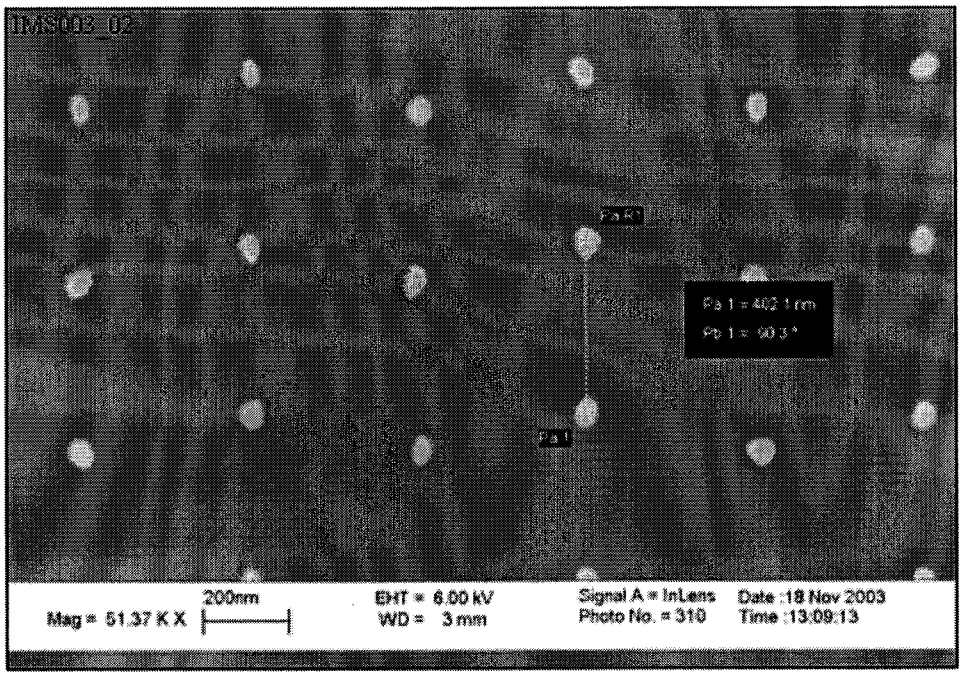

Image A.19 Pattern 2 on imprinter IMS003 written using a point dose of 14 fC and a pitch of 400 nm. The measured pillar diameter was 50 nm and the measured pitch was 402 nm.

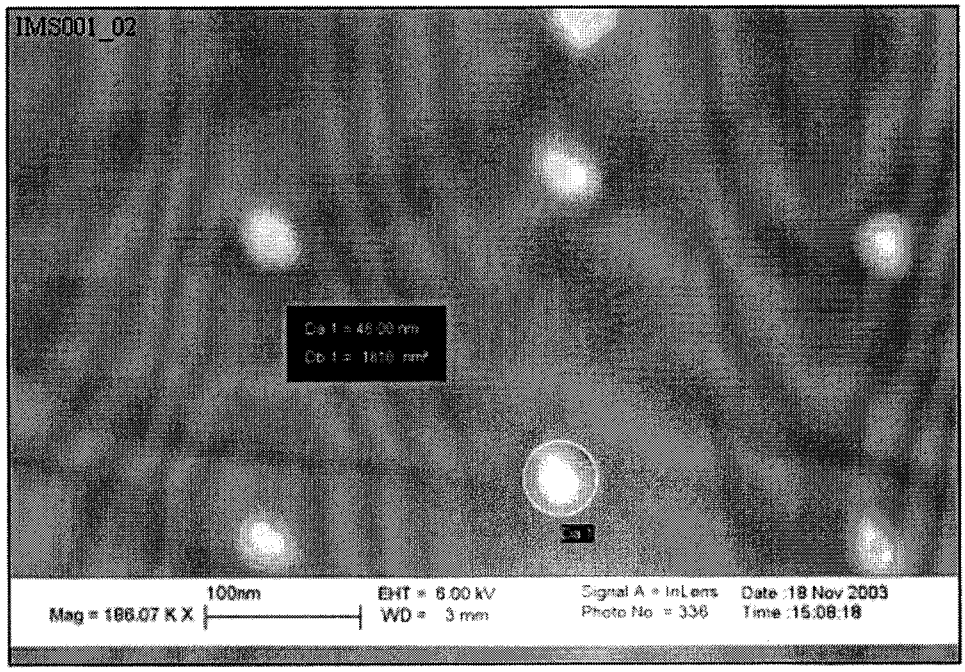

Image A.20 Pattern 2 on imprinter IMS001produced using a 15 fC dose and a 200 nm pitch. The measured diameter of the pillars was 48 nm.

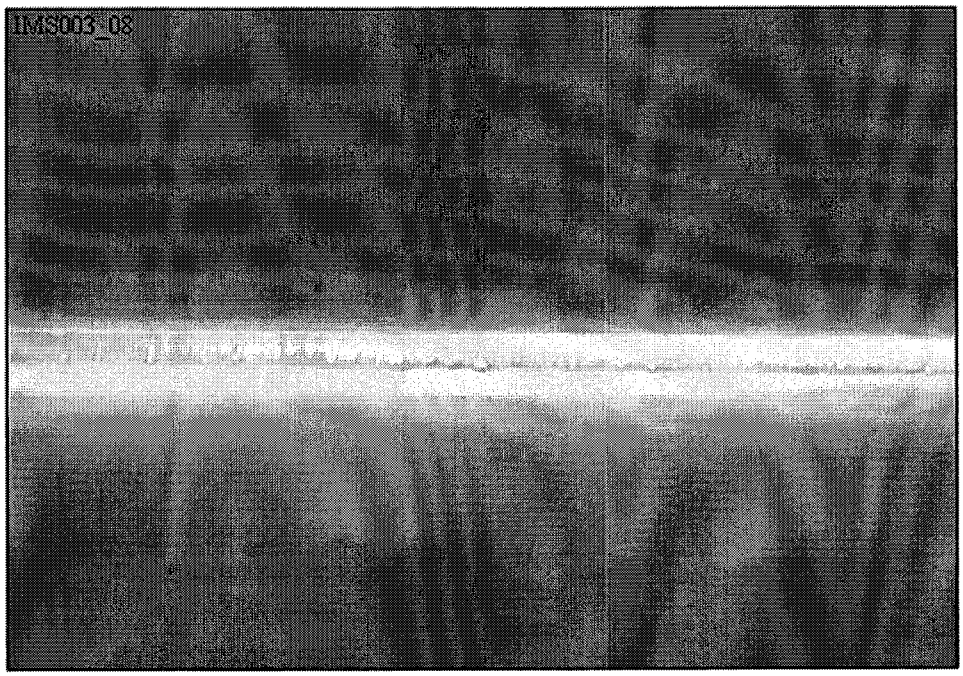

Image A.21 Pattern 8 on imprinter IMS003 was overexposed. A 13 fC point dose was used with a 100 nm pitch during electron beam writing resulting in a continuous plateau of SiO_2 instead of pillars after etching. The SEM image was shot at a 40° angle.

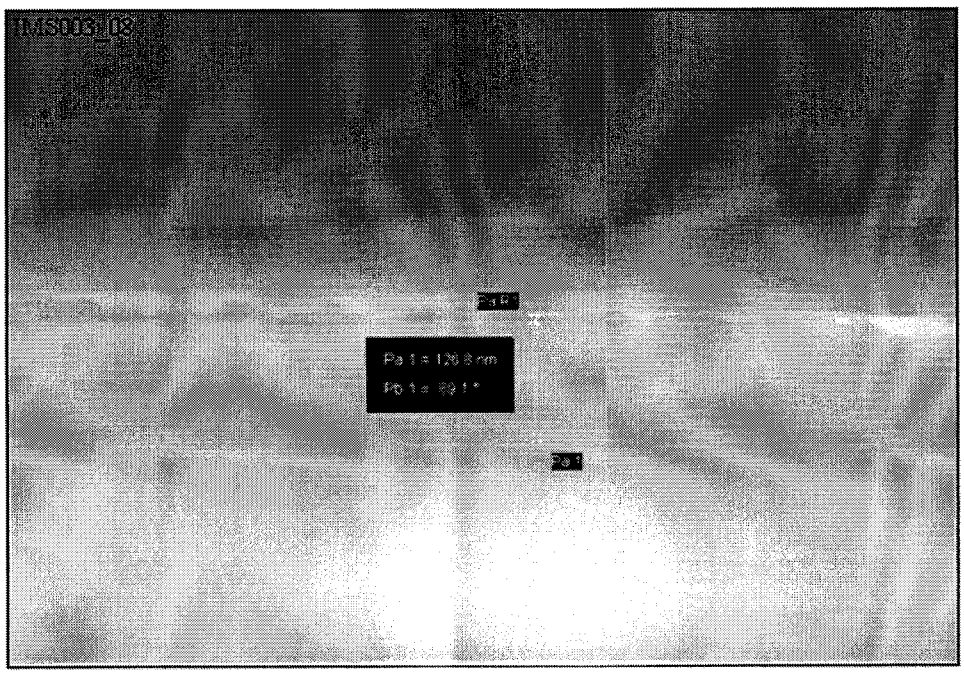

Image A.22 Pattern 8 on imprinter IMS003 was used to measure the height or depth of the SiO_2 plateau from plasma etching. This image was also shot at a 40° angle.

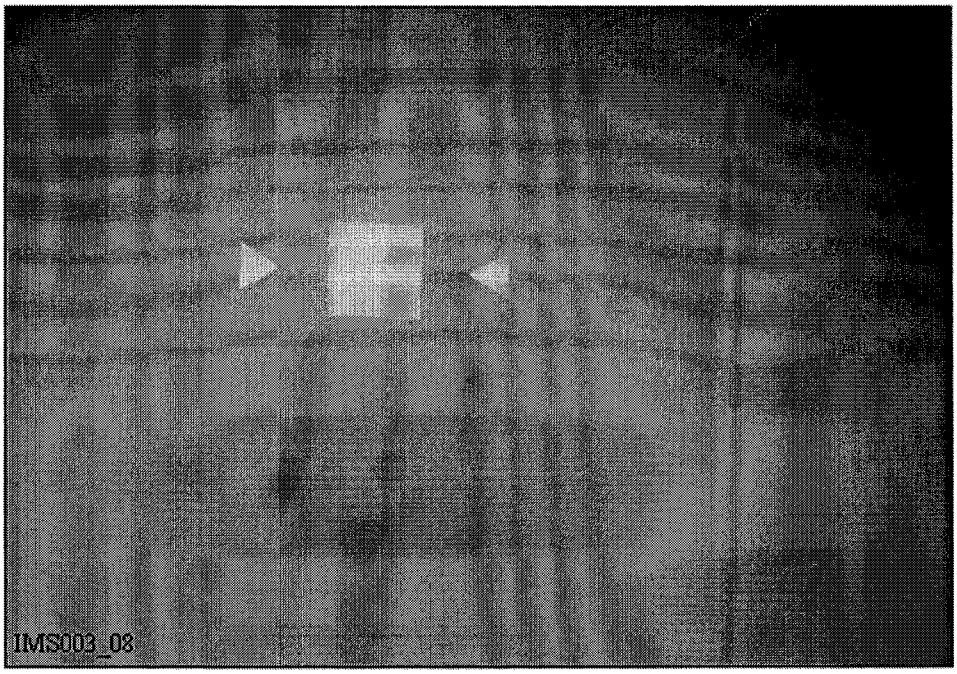

Image A.23 An optical microscope image of pattern 8 on imprinter IMS003 surrounded by a discoloration. The discoloration is SiO_2 that was not etched properly.

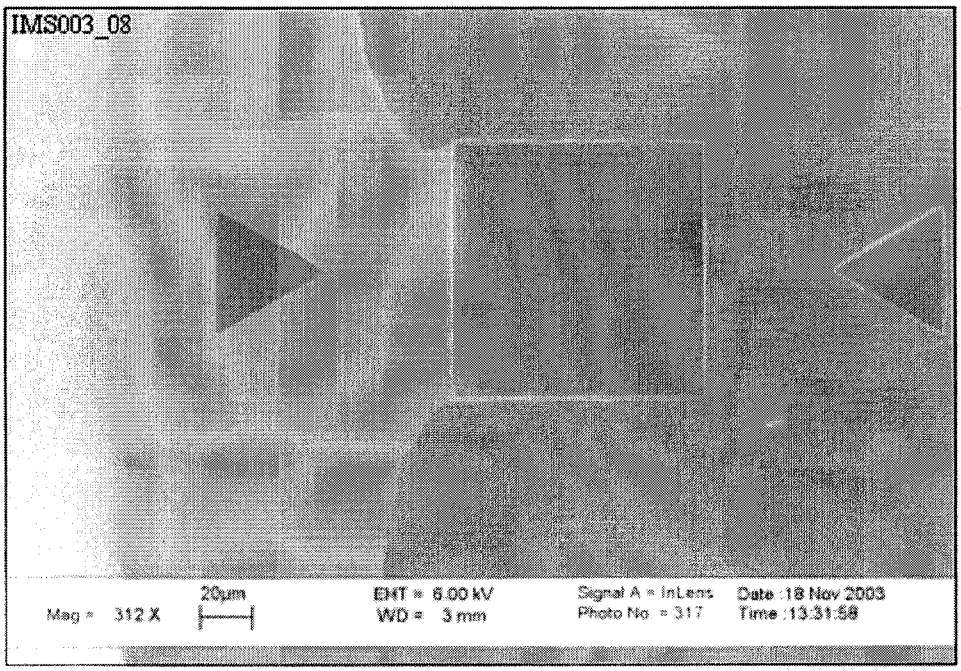

Image A.24 A SEM image of pattern 8 on imprinter IMS003. It is now clearly apparent that the darker surface on the right is higher than that on the left because it was not fully etched.

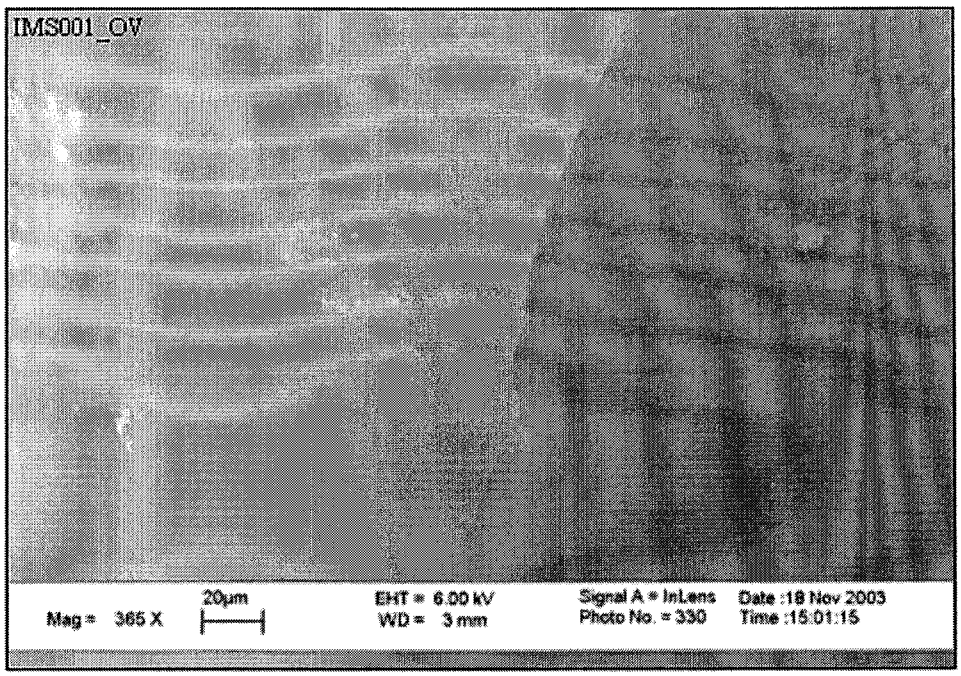

Image A.25 An image of an unetched surface as seen on the right side.

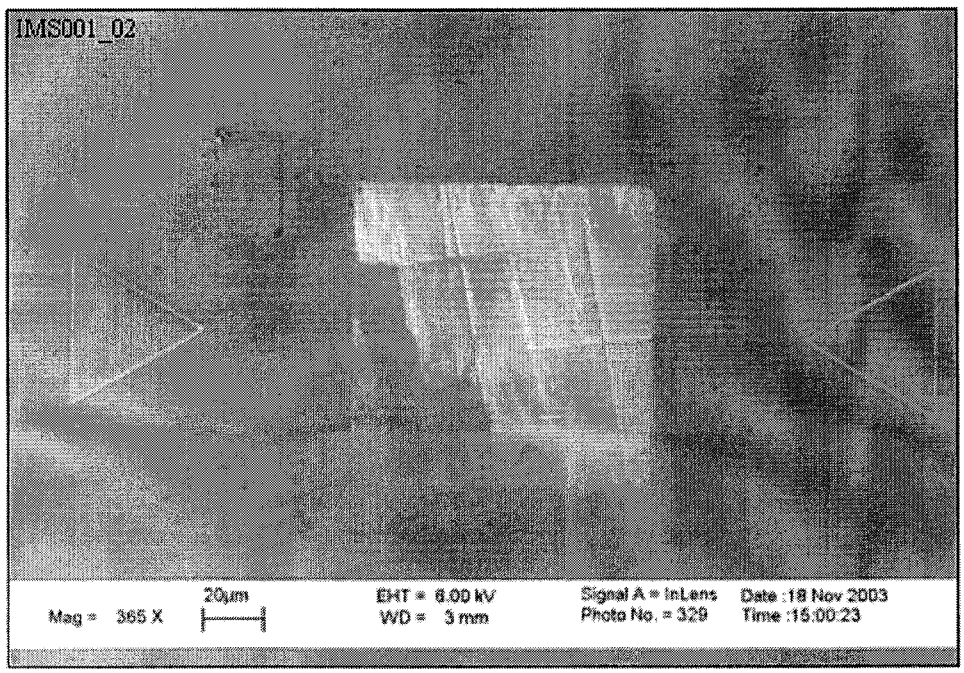

Image A.26 Pattern 2 on imprinter IMS001 with a high percentage of defects.

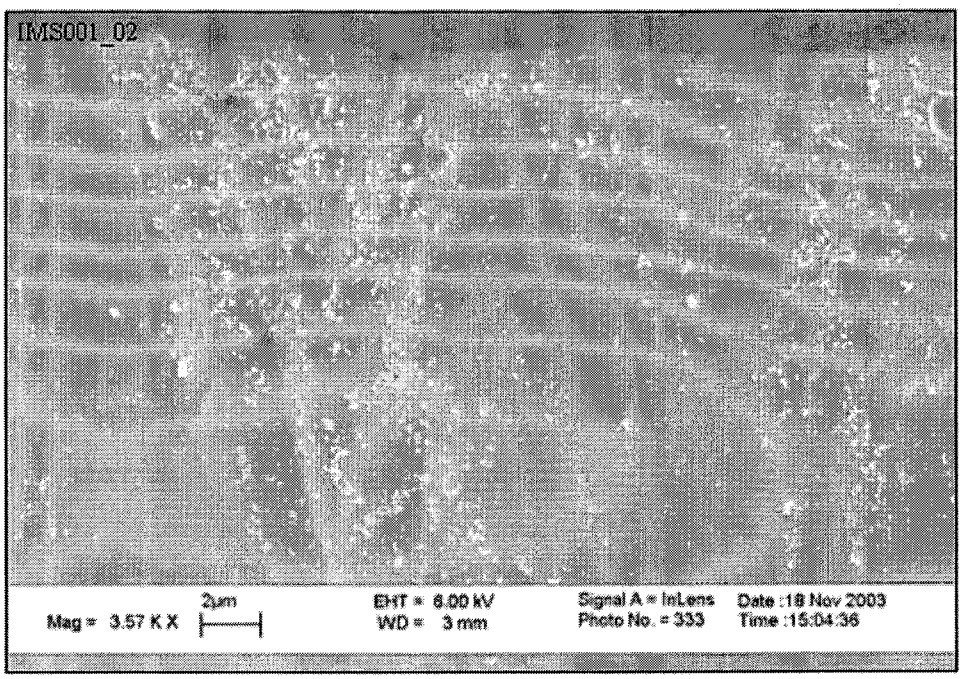

Image A.27 A higher magnification image of the pattern 2 on imprinter IMS001. There is a significant amount of debris, scratches, and collapsed pillars.

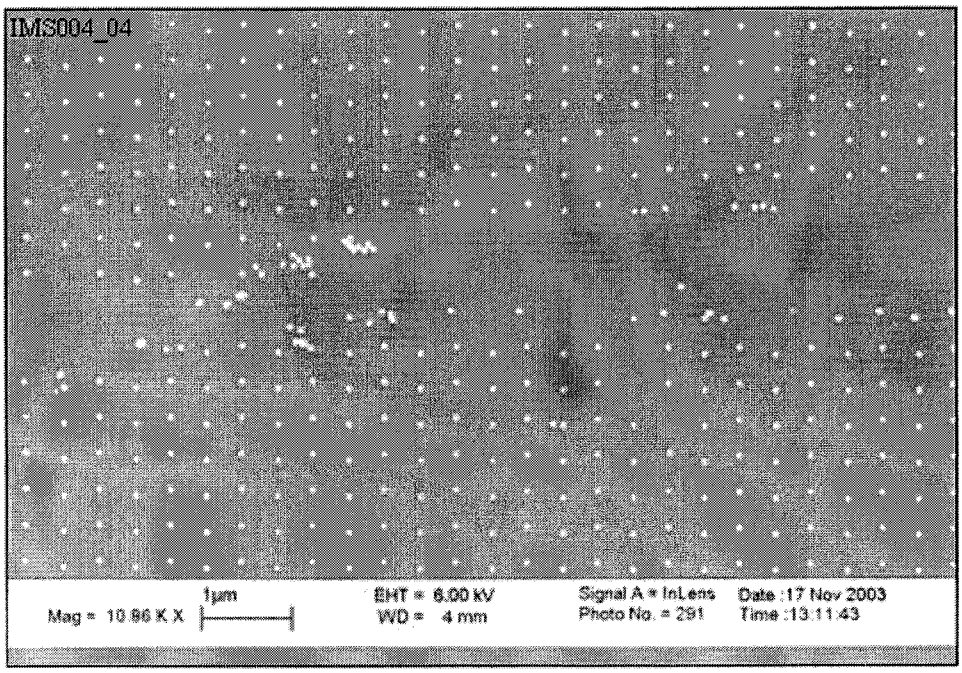

Image A.28 The image displays an area of wiped out pillars on pattern 4 of imprinter IMS004. Some of the pillars collected towards the left side of the image.

A.1.2 HSQ Imprinters

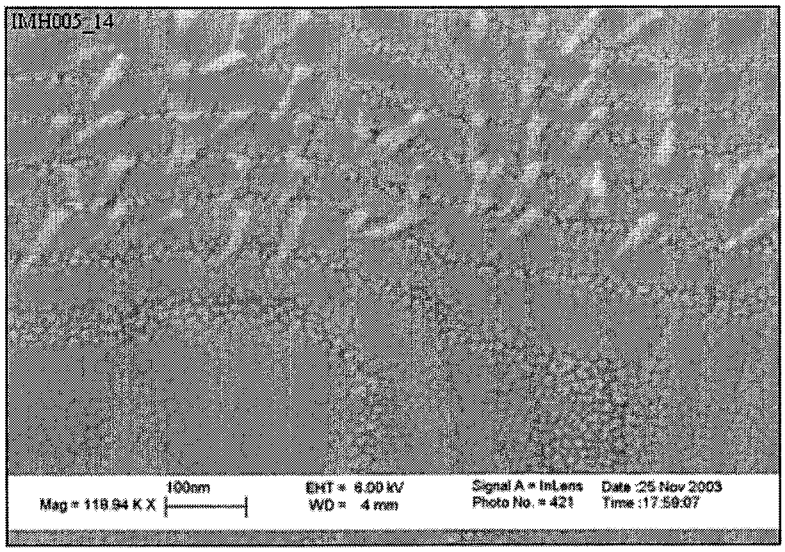

Image A.29 Collapsed pillars of pattern 14 on HSQ imprinter IMH005 caused from an underexposure. The pattern was exposed using a point dose of 25 fC and a pitch of 75 nm.

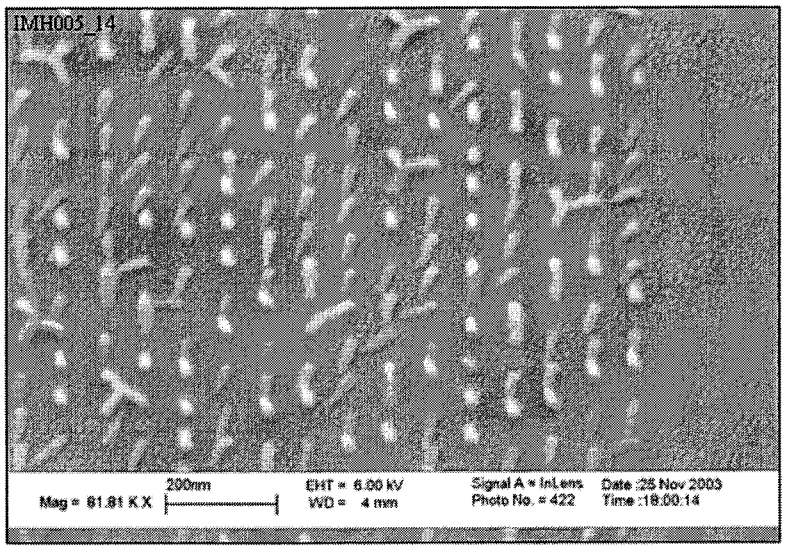

Image A.30 A different area of pattern 14 on imprinter IMH005. The pattern was underexposed by using a point dose of 25 fC and 75 nm pitch. That is why the pillars have collapsed.

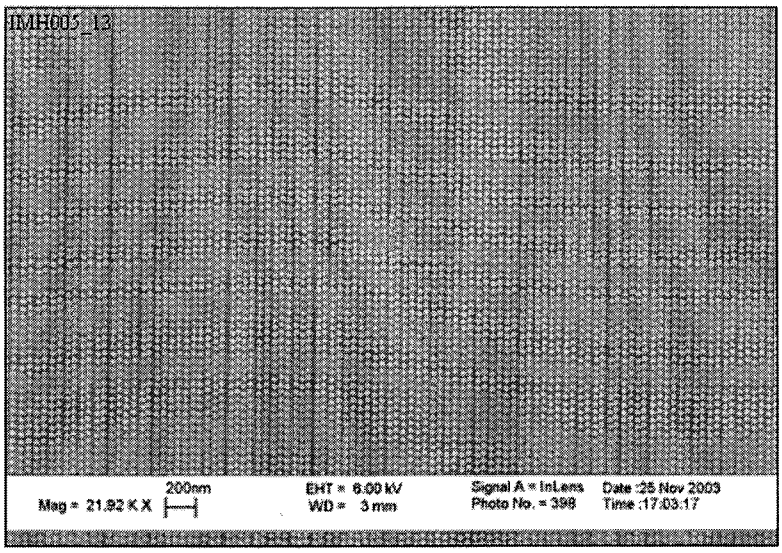

Image A.31 A flawless area of pillars of pattern 13 on imprinter IMH005. The area is approximately 3.5 by 5 μm. The pattern was exposed using a point dose of 25 fC and a pitch of 50 nm.

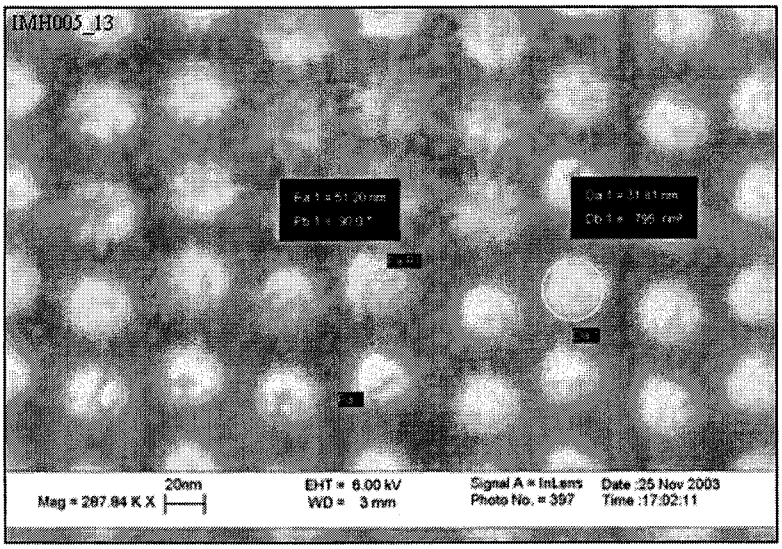

Image A.32 The measured pillar diameter and pitch of pattern 13 on imprinter IMH005. The pillar diameter is 31.81 nm and the pitch is 51.20 nm. The pattern was exposed using a 25 fC point dose and a 50 nm pitch.

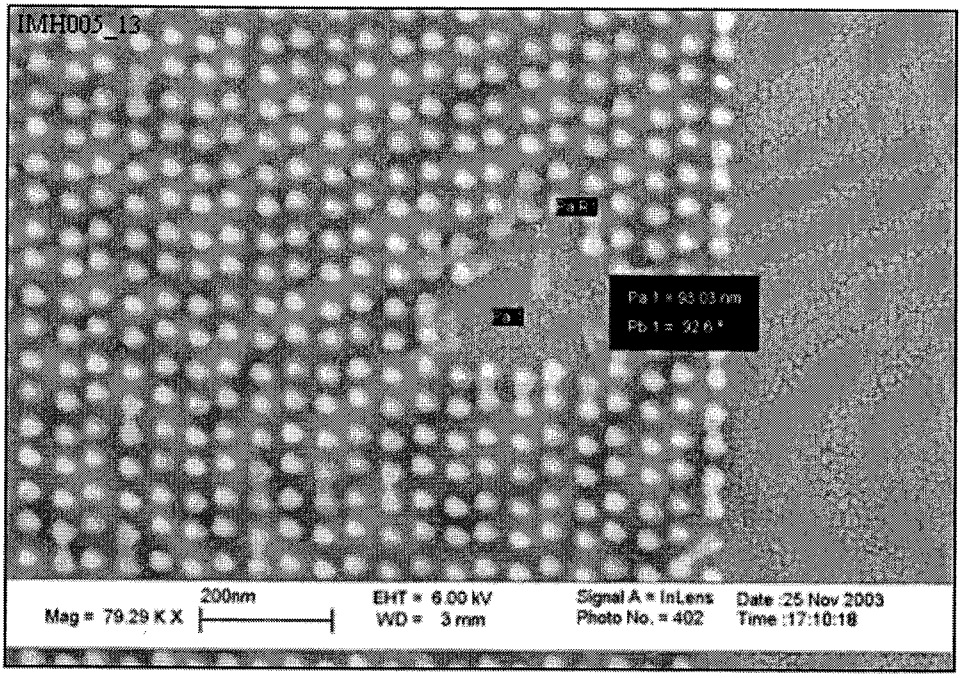

Image A.33 Knocked over pillars of pattern 13 on imprinter IMH005 were used to measure the pillar height. The height seen here is 93 nm. The pattern was exposed with a 25 fC point dose and a 50 nm pitch.

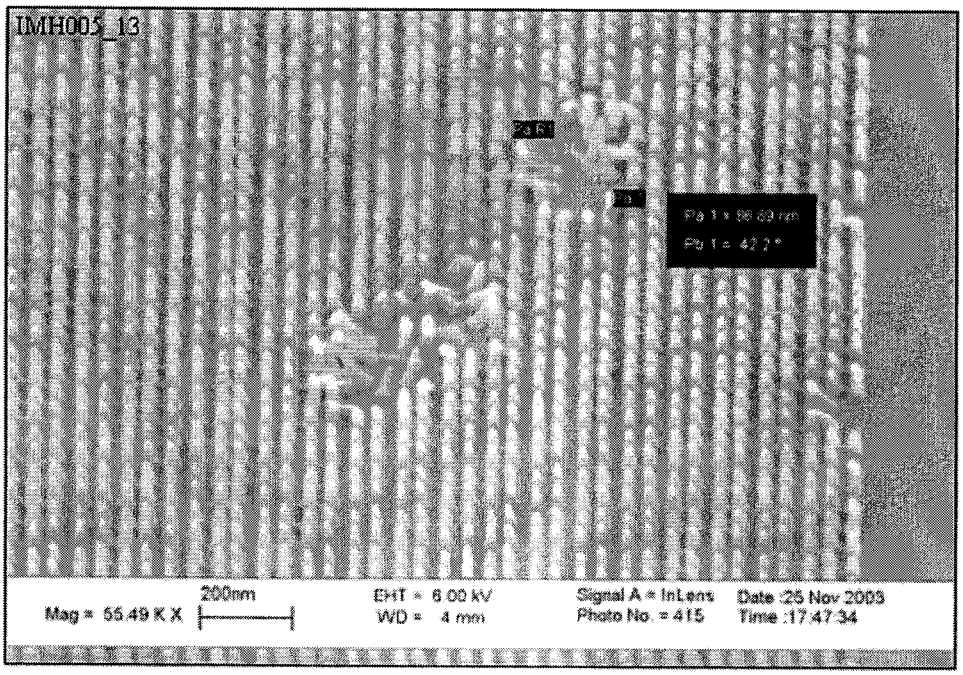

Image A.34 Measured pillar height of patter 13 on imprinter IMH005. Here the pillar height is 86.89 nm. The pattern was exposed with a 25 fC point dose and a 50 nm pitch.

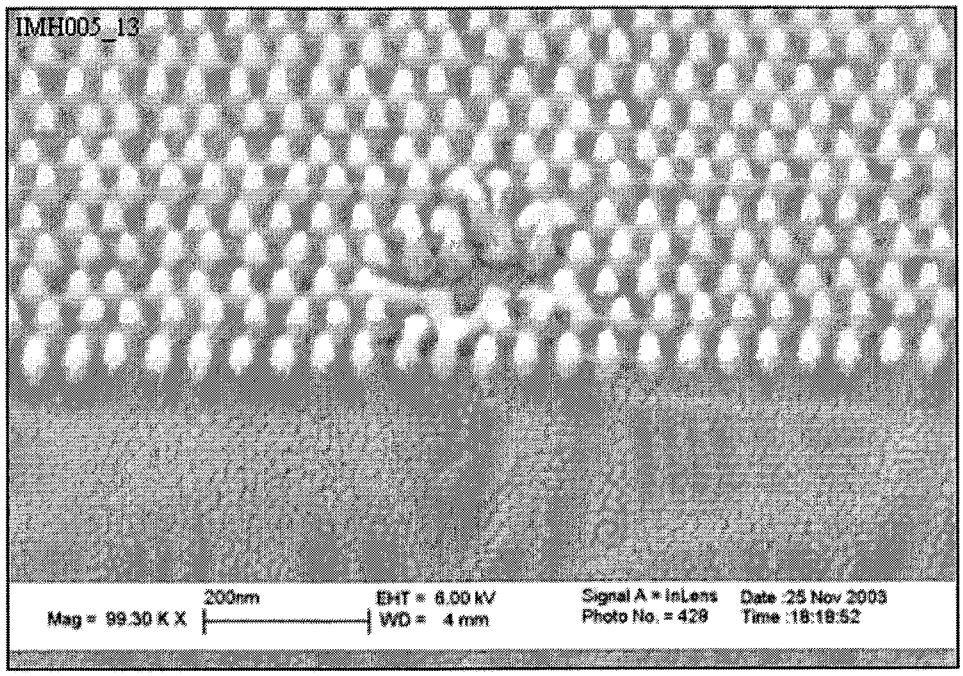

Image A.35 This image of pattern 13 on imprinter IMH005 displays the results of not using a beam blanker. HSQ residue is left between the pillars because it was exposed. The pattern was exposed with a 25 fC point dose and a 50 nm pitch.

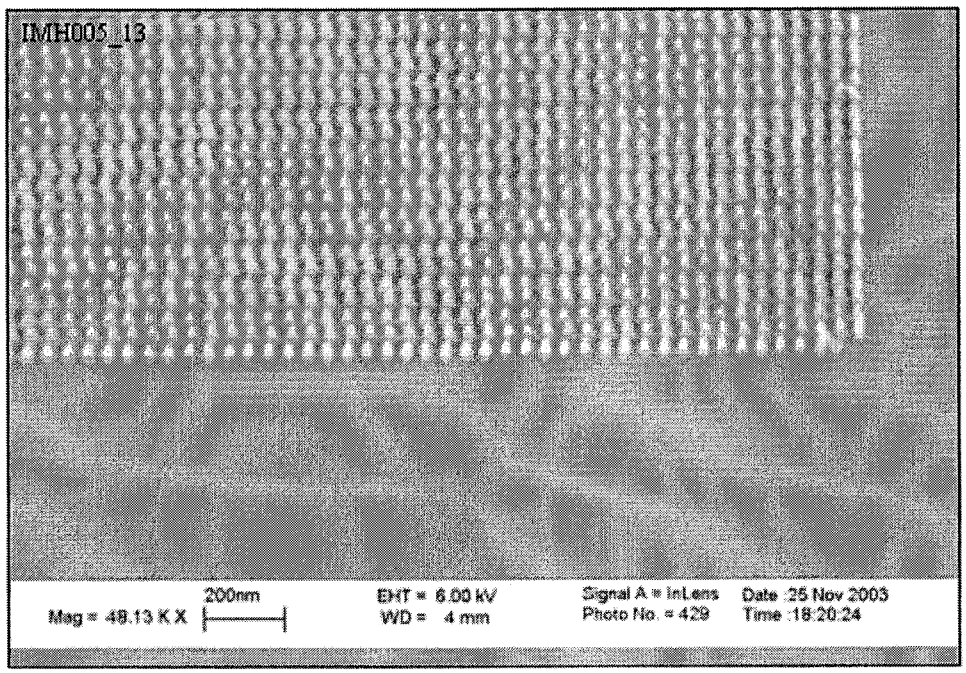

Image A.36 An image of the top corner of pattern 13 on imprinter IMH005. The residue of HSQ left between the resist is also visible here. The pattern was exposed using a 25 fC point dose and a 50 nm pitch.

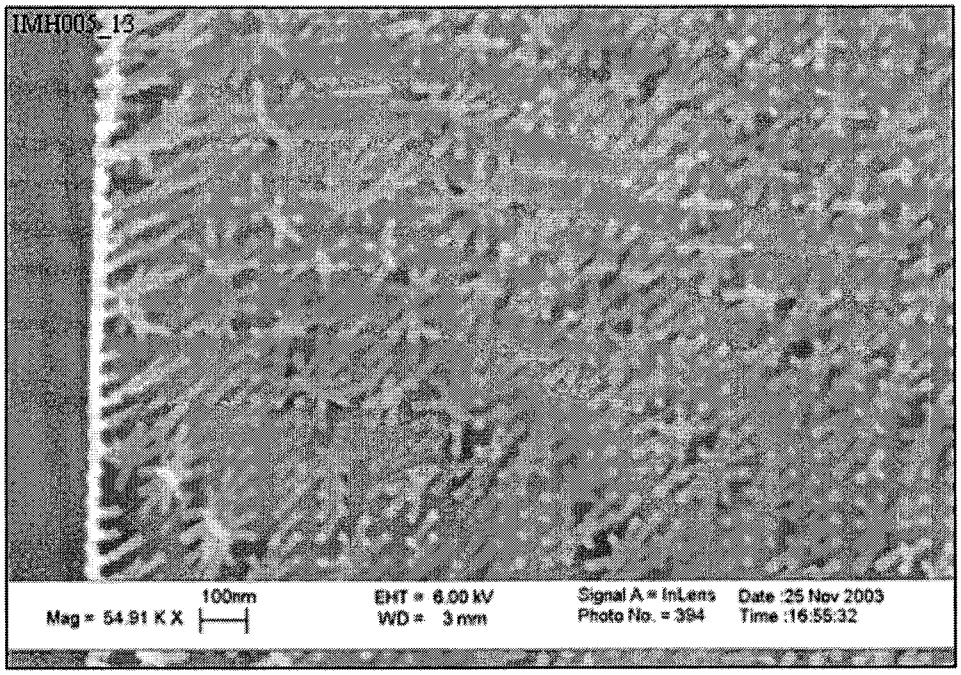

Image A.37 The corner of pattern 13 on HSQ imprinter IMH005. It was exposed using a 25 fC point dose and a 50 nm pitch. The pillars collapsed because the proximity effect is minimal around the edges of the pattern.

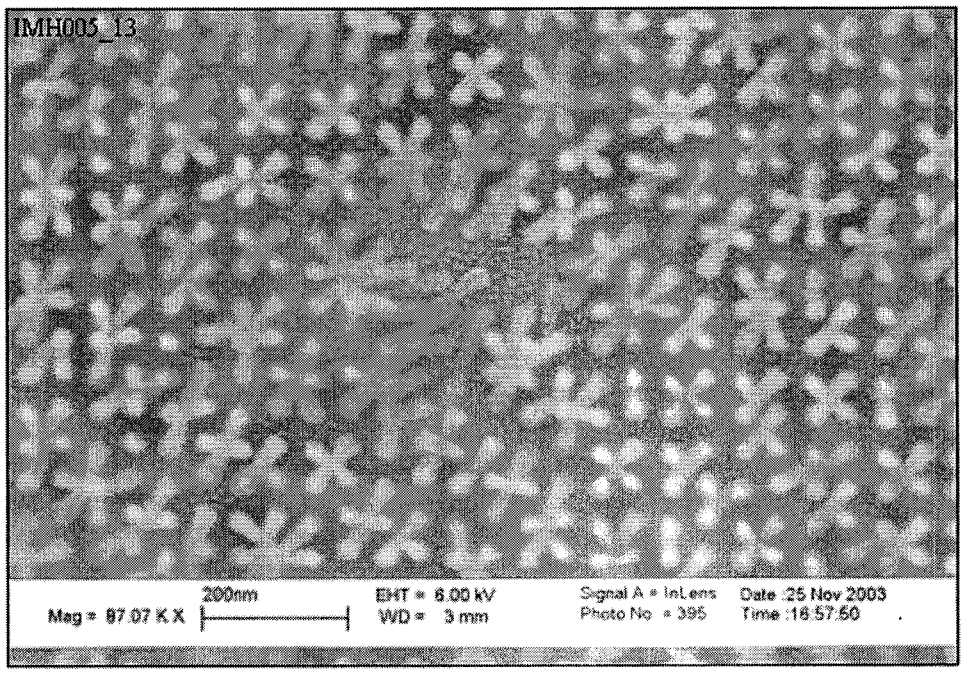

Image A.38 One of the edges of pattern 13 on imprinter IMH005. The pattern was exposed using a 25 fC point dose and a 50 nm pitch. The pillar collapsed because the proximity effect is not present around the edges of the pattern.

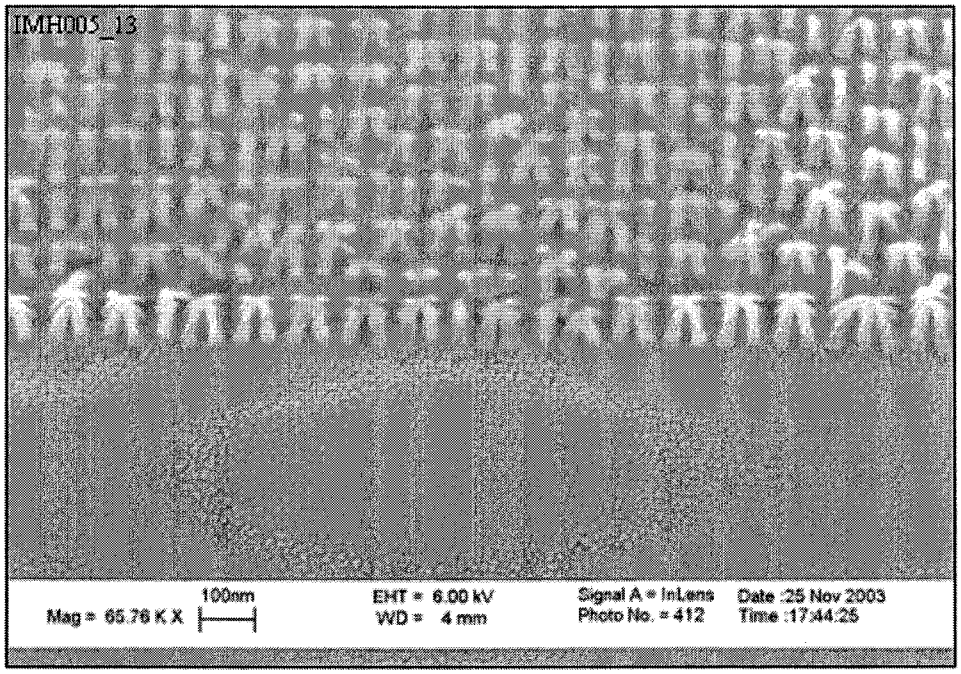

Image A.39 One of the edges of pattern 13 on imprinter IMH005. The pattern was exposed using a 25 fC point dose and a 50 nm pitch. An angled view of the collapsed pillars can be seen.

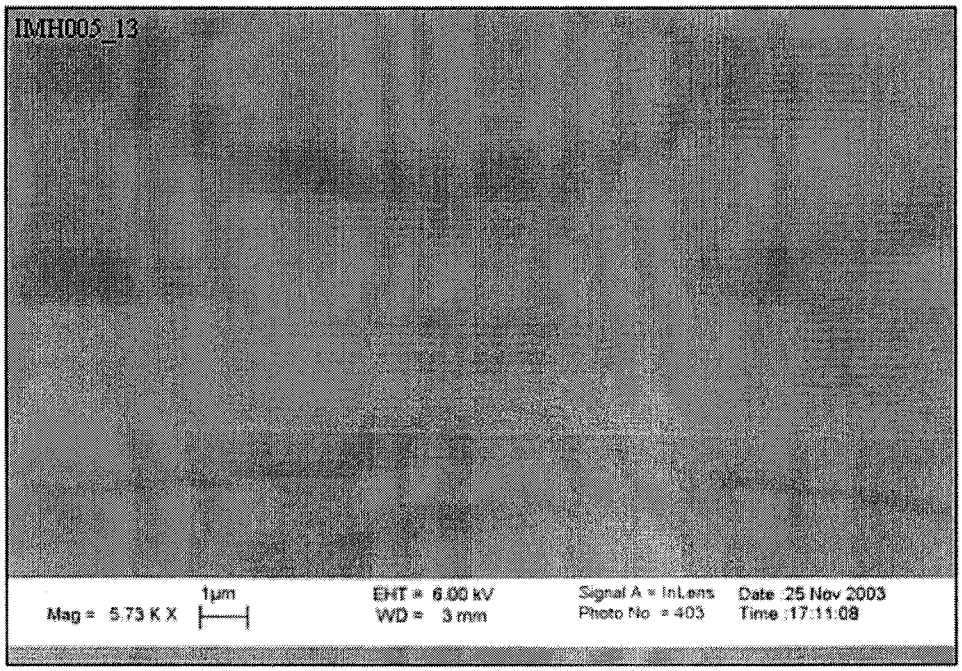

Image A.40 A low magnification overview image of one of the edges of pattern 13 on imprinter IMH005. The pattern was exposed using a 25 fC point dose and a 50 nm pitch. The border between the collapsed pillars and the standing pillars can be seen.

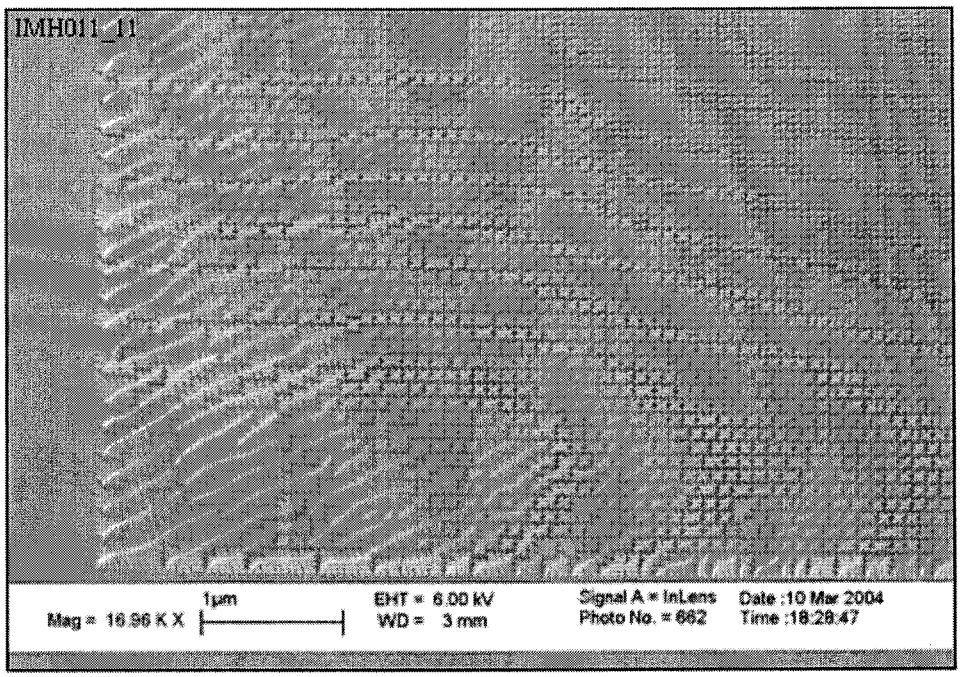

Image A.41 The lower left corner of pattern 11 on imprinter IMH011. Even though a 30.5 fC point dose was used with a 50 nm pitch, the pillars around the edges still collapsed.

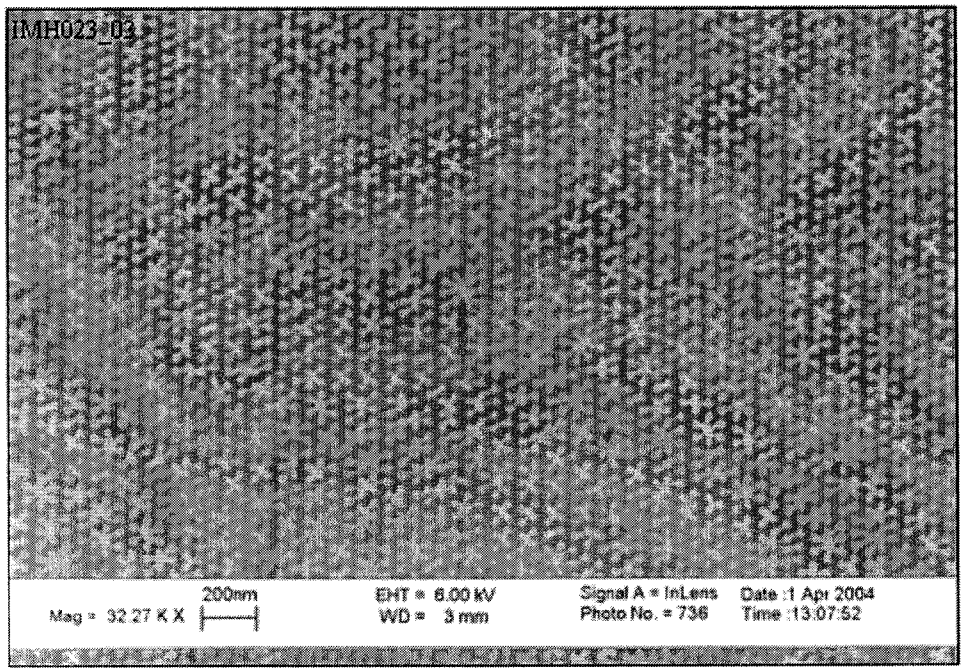

Image A.42 The collapsed pillars of pattern 3 on imprinter IMH023 are a result of underexposure. A 25 fC point dose and 50 nm were used to expose the pattern.

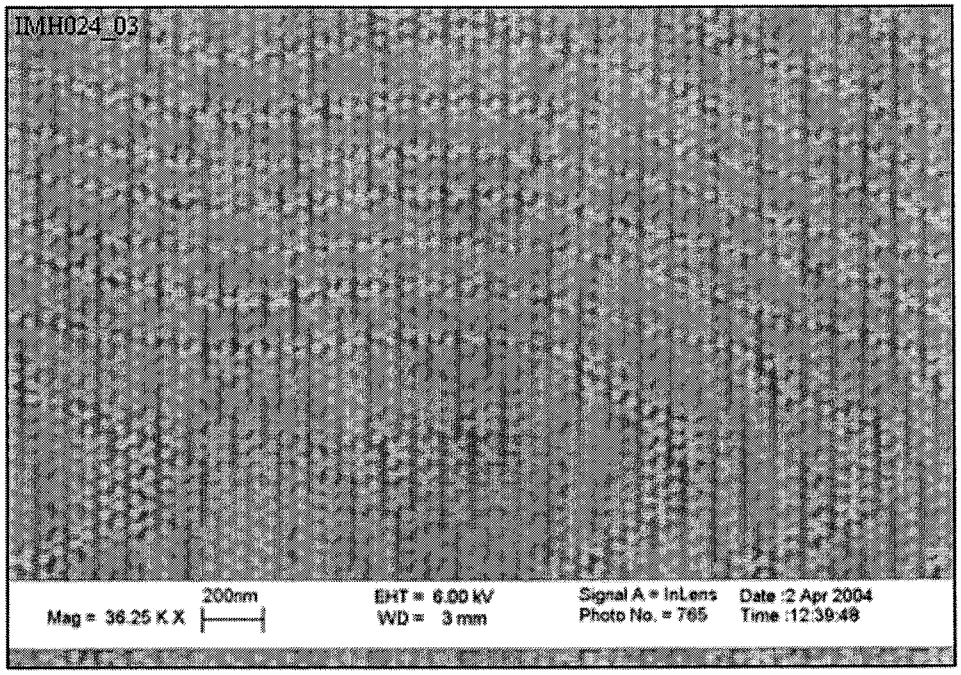

Image A.43 The pillars also collapsed on pattern 3 of imprinter IMH024 due to underexposure. A 25 fC point dose and 50 nm pitch were used to expose the pattern.

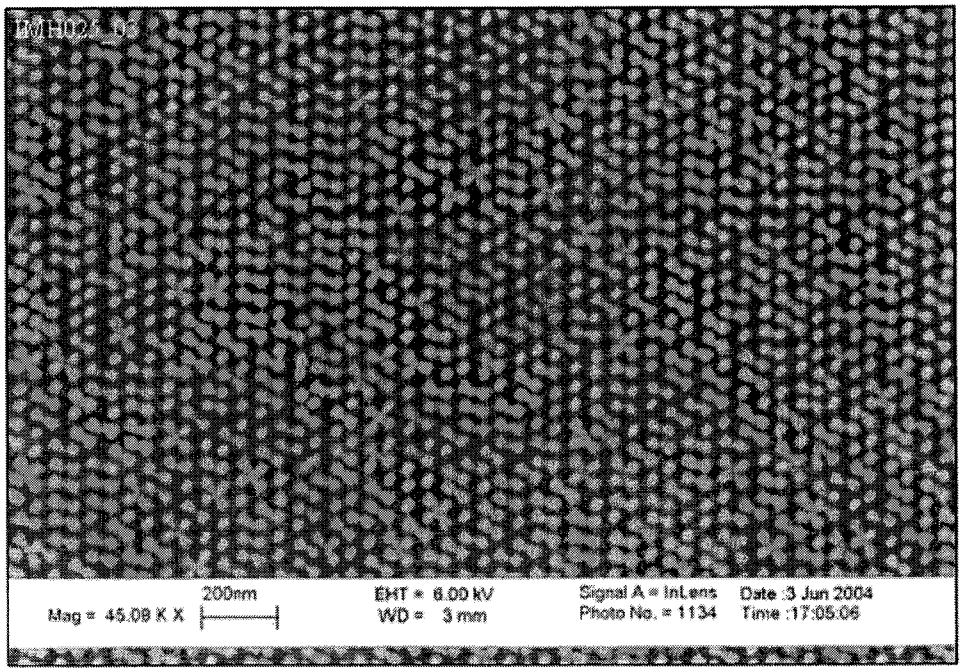

Image A.44 The pillars on pattern 3 of imprinter IMH025 collapsed due to an underexposure. A point dose of 25 fC and pitch of 50 nm were used to expose the pattern.

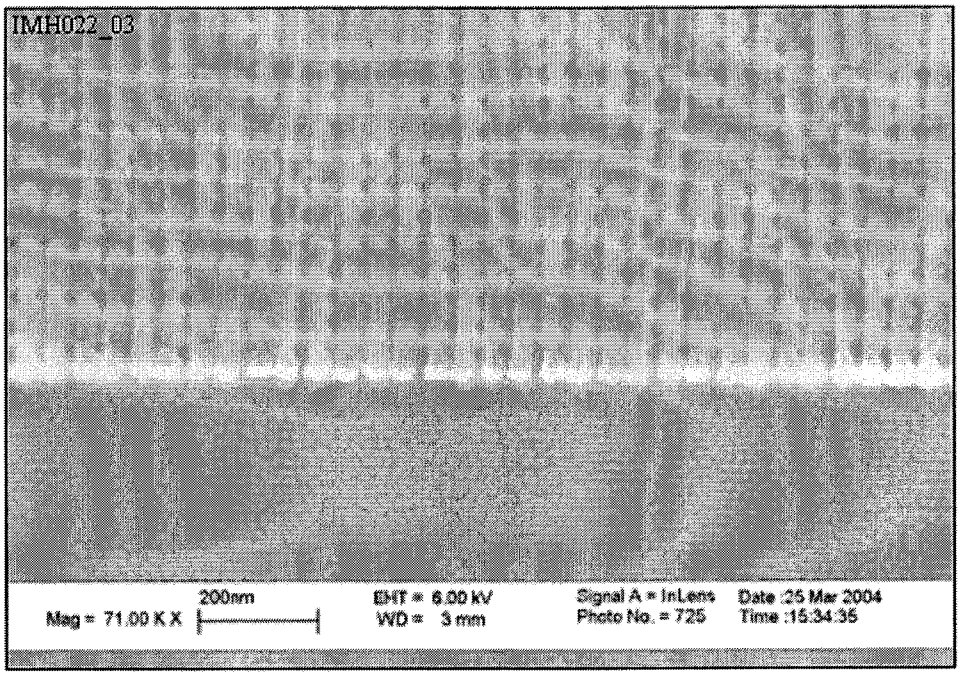

Image A.45 Pattern 3 on imprinter IMH022 was overexposed as seen here. A 25 fC point dose and 50 nm pitch were used to expose the pattern.

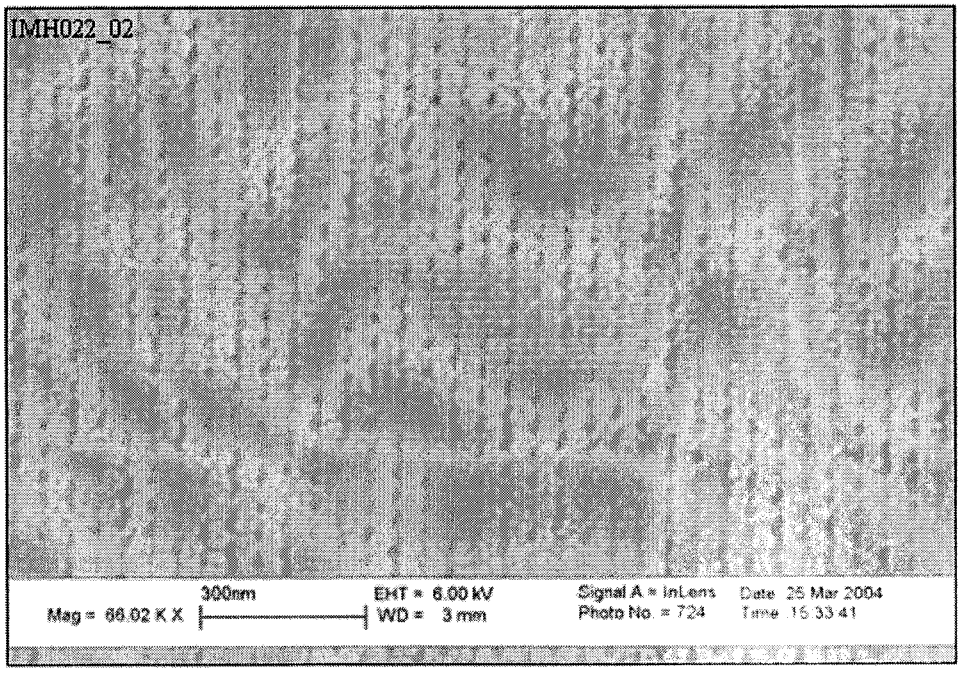

Image A.46 Pattern 2 on imprinter IMH022 was overexposed as seen in this image. A 25 fC point dose and 50 nm pitch were used.

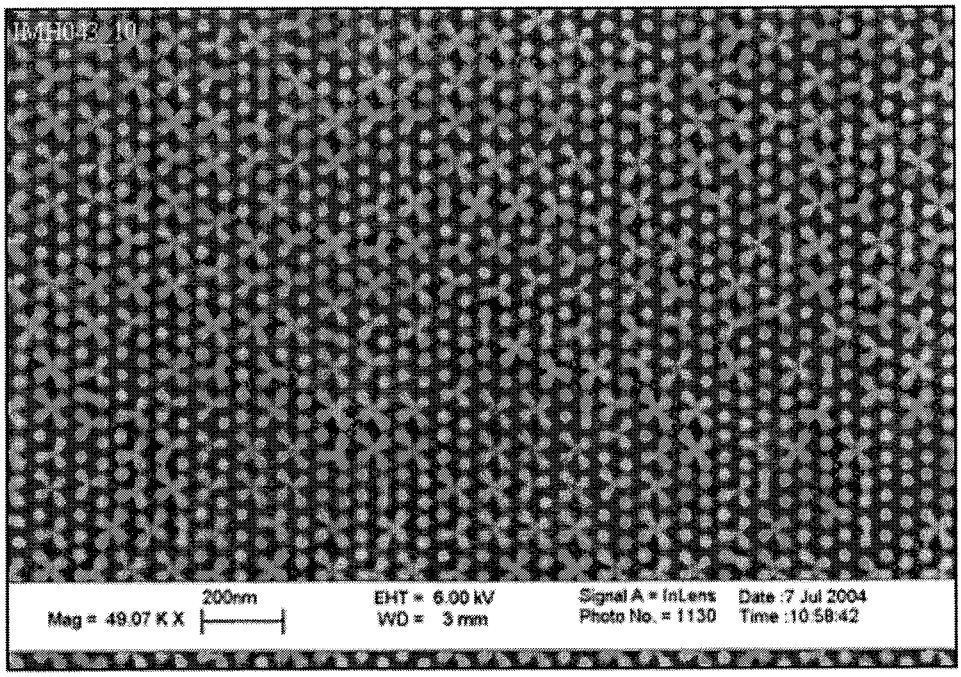

Image A.47 Pattern 10 on imprinter IMH043 was underexposed resulting in collapsed pillars as seen here. A 28.5 fC point dose and 50 nm pitch were used to expose the pattern.

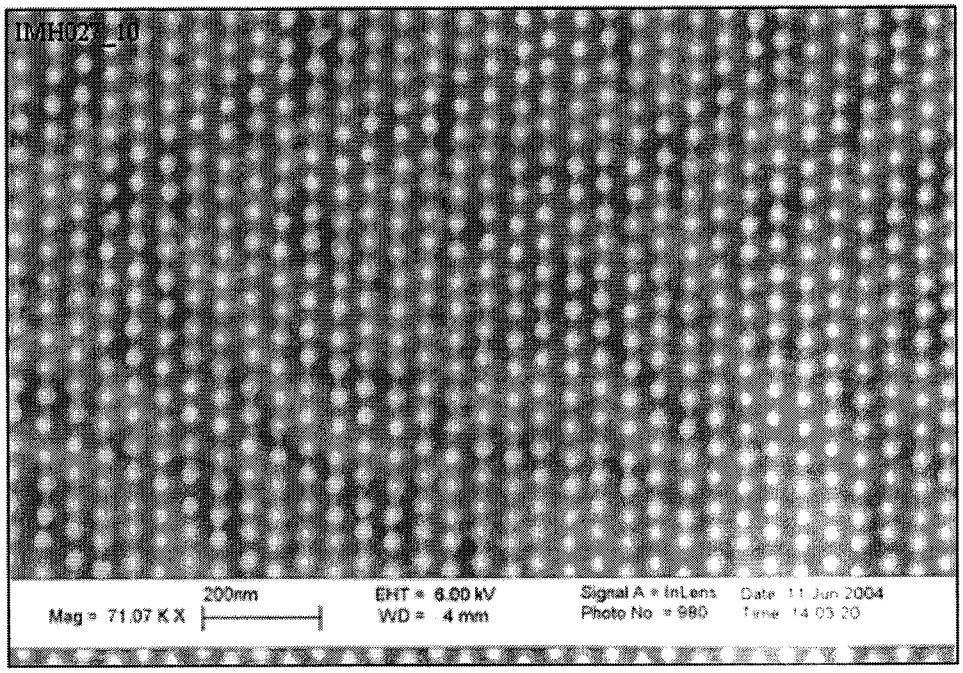

Image A.48 Pattern 10 on imprinter IMH027 contains a high quality array of pillars. A point dose of 28.5 fC and a 50 nm pitch were used to expose the pattern.

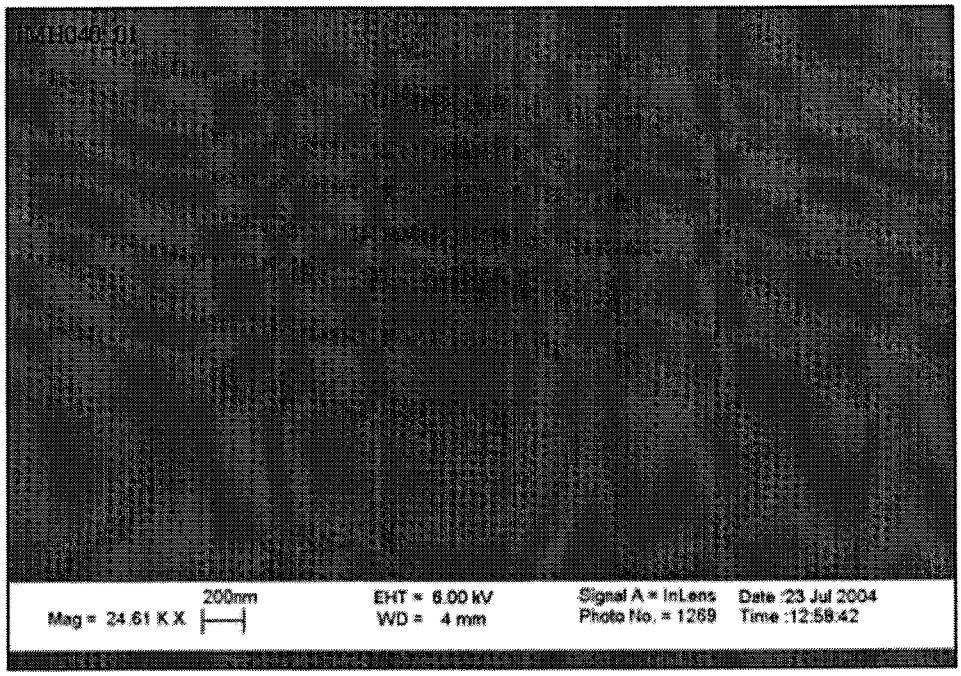

Image A.49 Pattern 1 on imprinter IMH040 was overexposed resulting in a plateau of HSQ. A 28.5 fC point dose and 50 nm pitch were used.

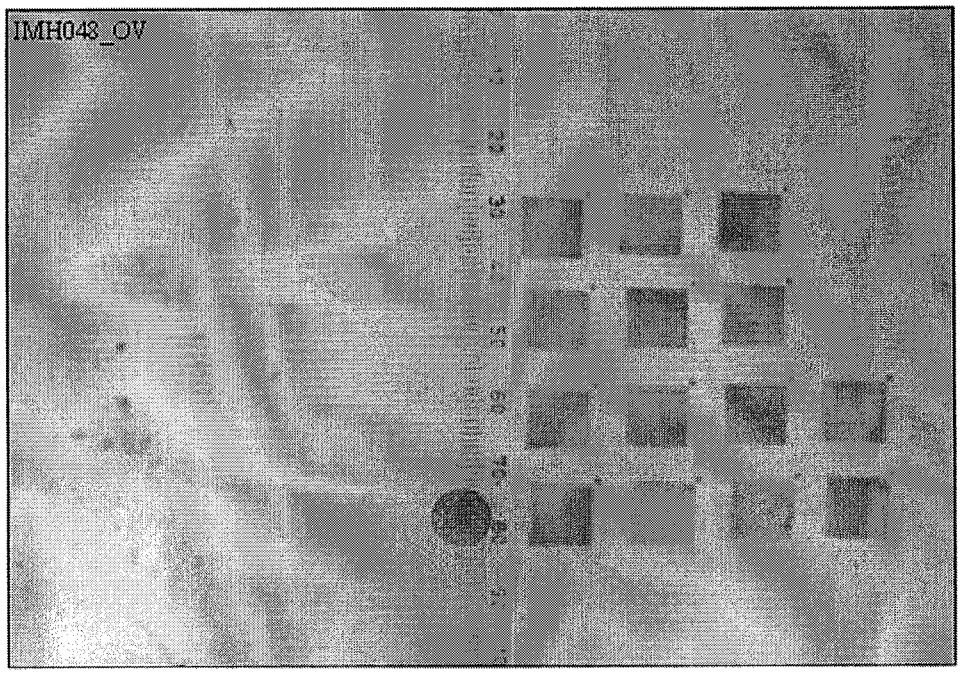

Image A.50 An optical image of imprinter IMH048. The light purple hue of the patterns indicates that they are underexposed. A 28.5 fC point dose and 50 nm pitch were used to expose all of the patterns except the circle in the lower left corner.

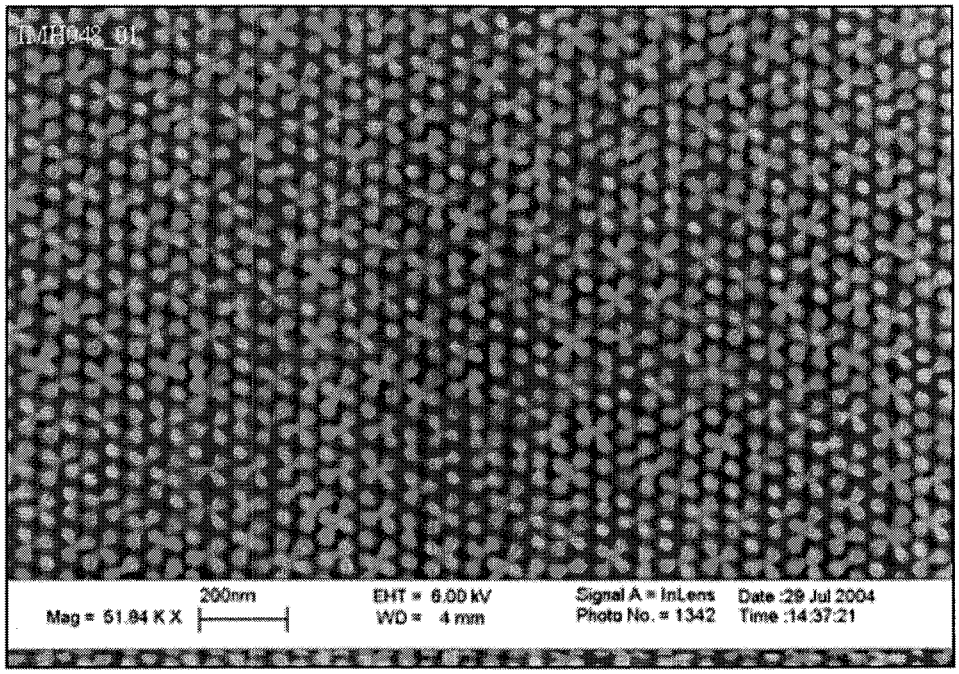

Image A.51 Collapsed pillars of pattern 1 on imprinter IMH048. They collapsed because the pattern was underexposed. A 28.5 fC point dose and 50 nm pitch were used to expose the pattern.

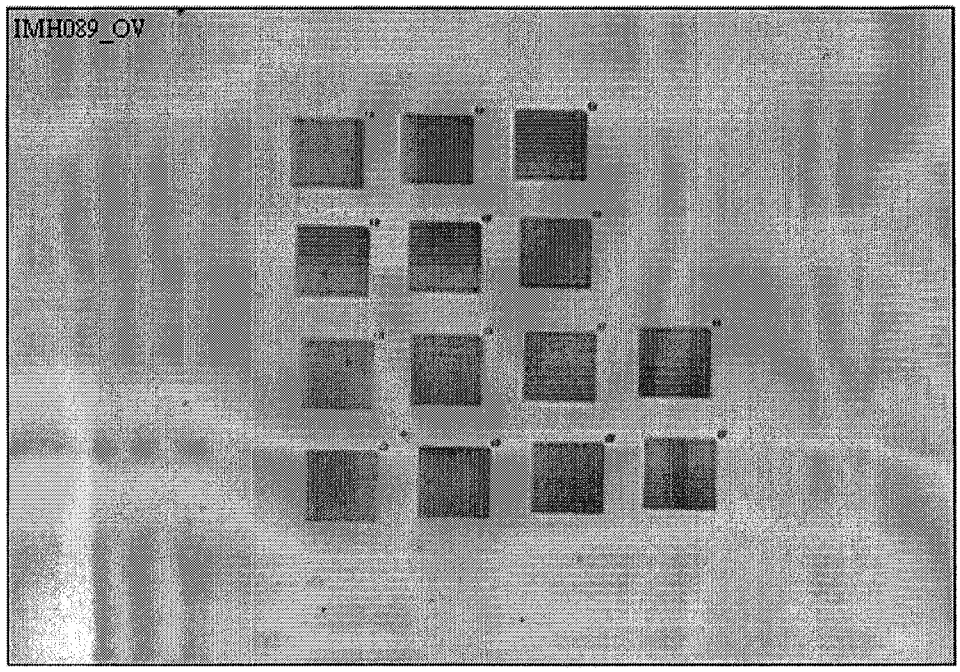

Image A.52 An optical image of imprinter IMH089. The dark purple hue indicates that the patterns were properly exposed. A 32 fC point dose and 50 nm pitch were used to expose all of the patterns.

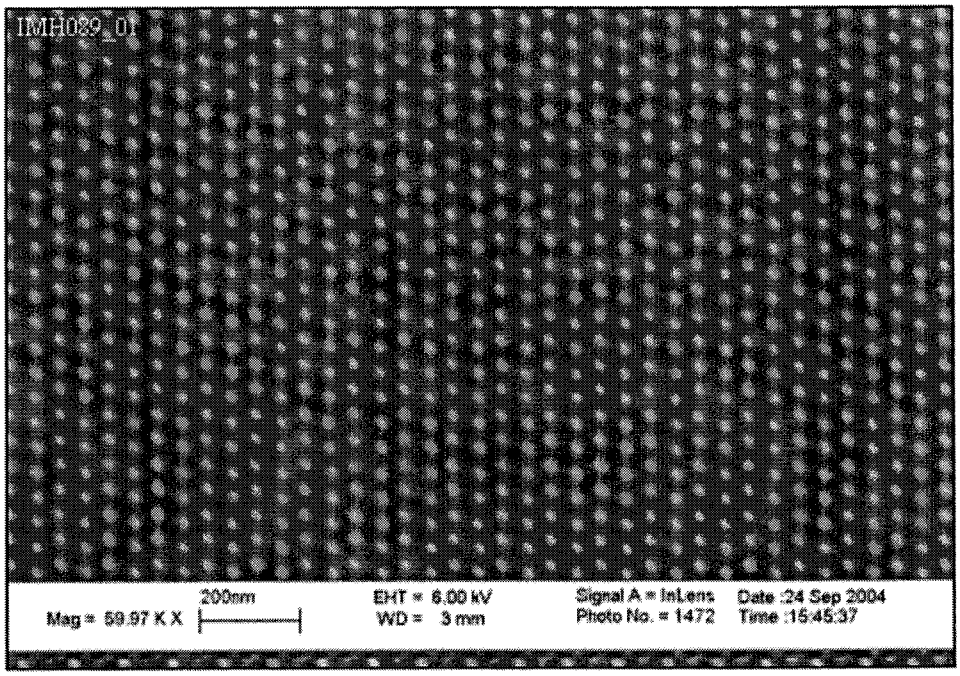

Image A.53 An area of free standing defect free pillars of pattern 1 on imprinter IMH089. A point dose of 32 fC and a pitch of 50 nm were used to expose the pattern.

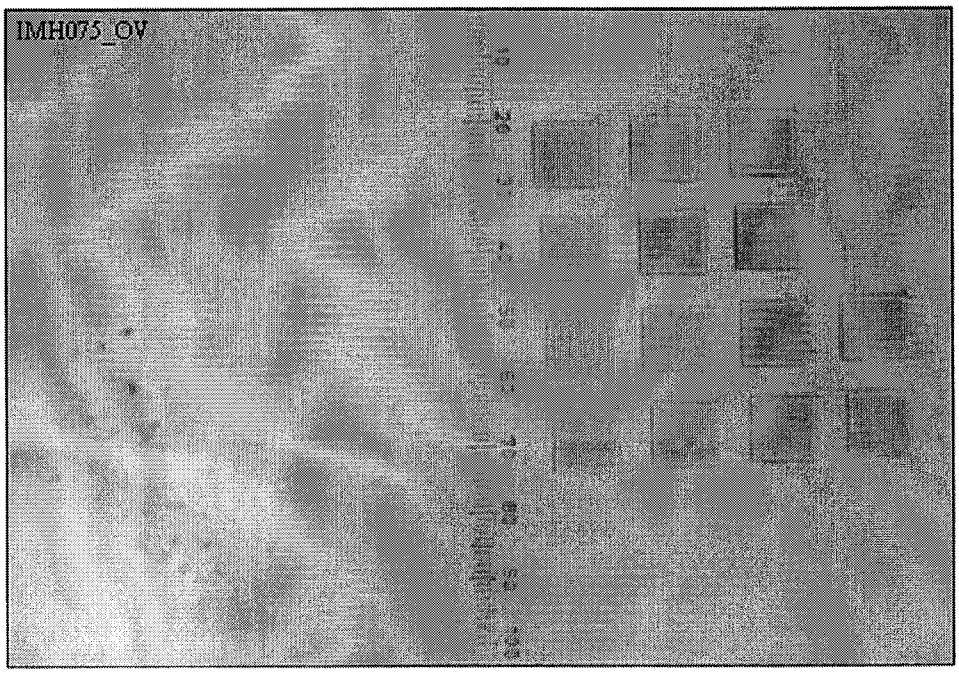

Image A.54 An optical image of imprinter IMH075. The greenish color of the patterns indicates that they were overexposed.

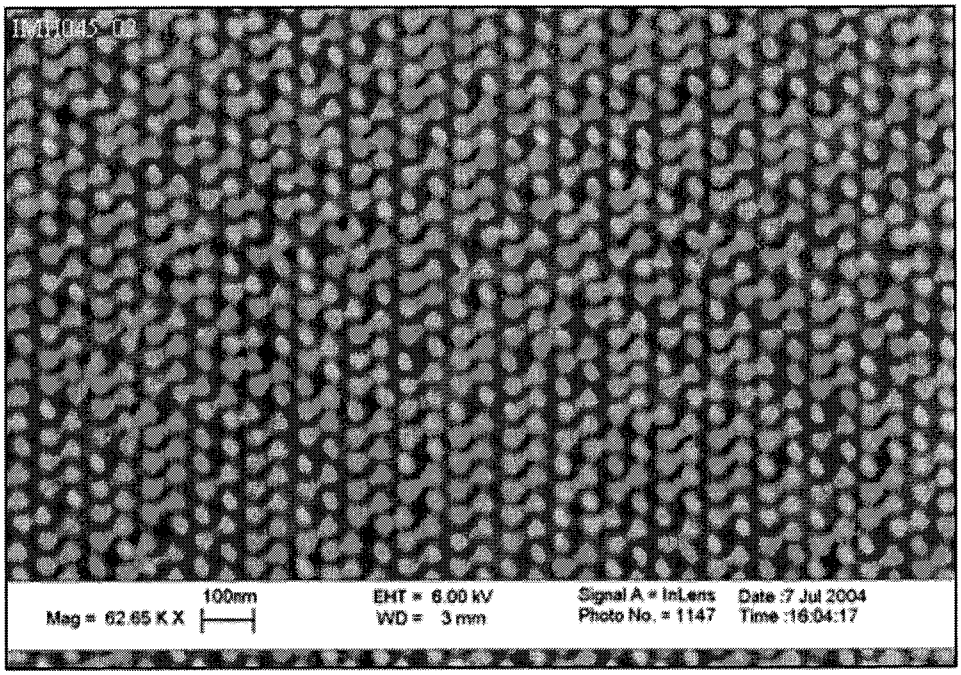

Image A.55 Collapsed pillars on the left half of pattern 2 on imprinter IMH045. This side of the pattern was underexposed because the sample was not in focus. The pattern was exposed with a 28.5 fC point dose and a 50 nm pitch.

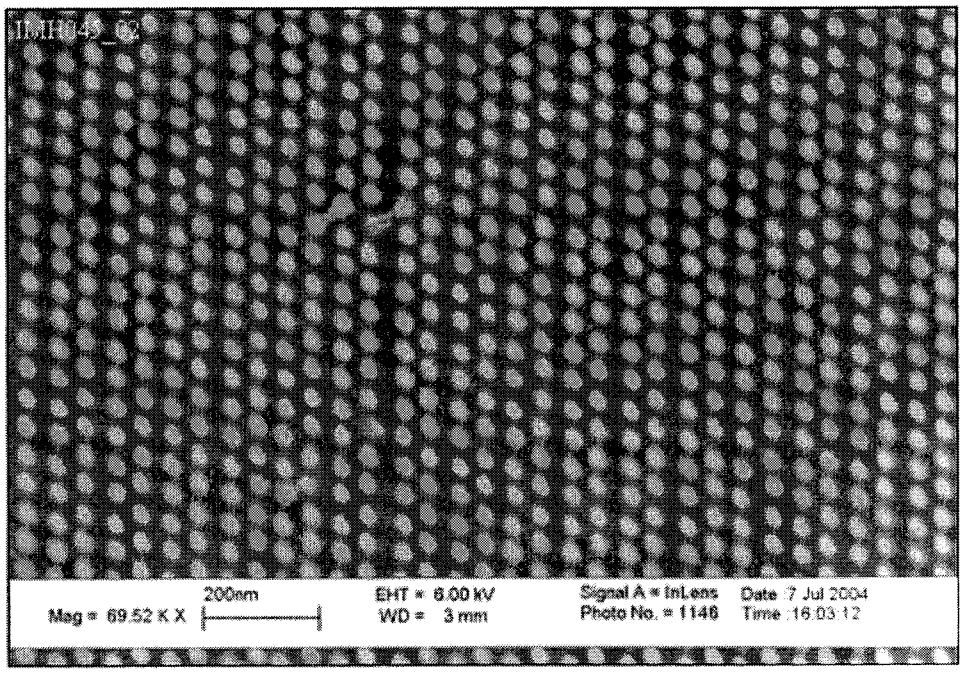

Image A.56 An almost defect free area on the right side of pattern 2 on imprinter IMH045. The pattern was exposed using a point dose of 28.5 fC and a 50 nm pitch.

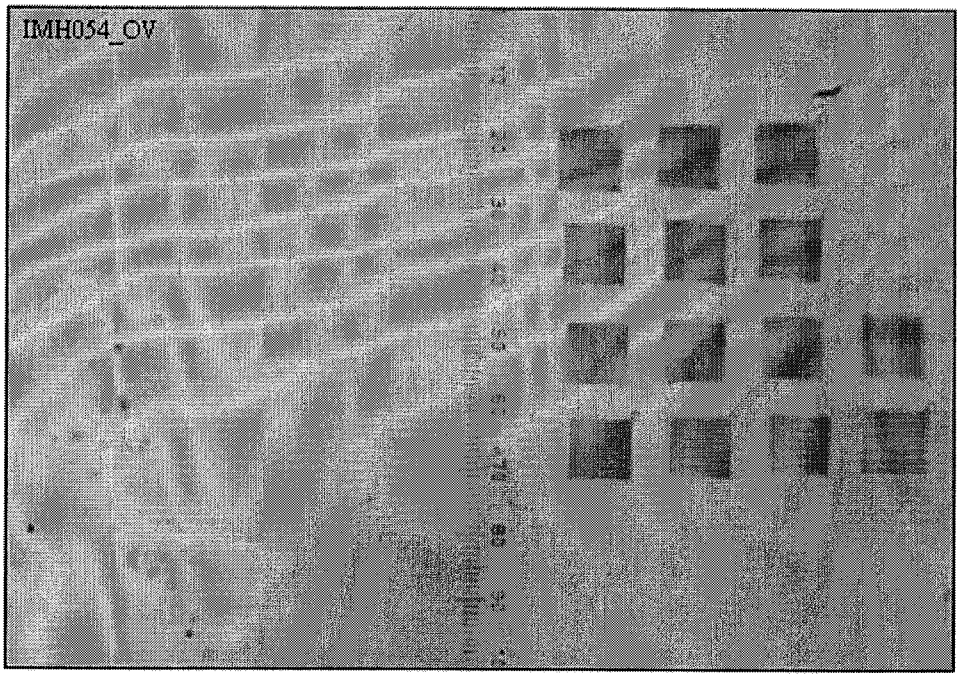

Image A.57 An optical image of imprinter IMH054. The patterns on the top appear to have two colors because part of each of them was exposed properly and the other part was not. This was due to improper focusing. All the patterns were exposed using a point dose of 28.5 fC and a pitch of 50 nm.

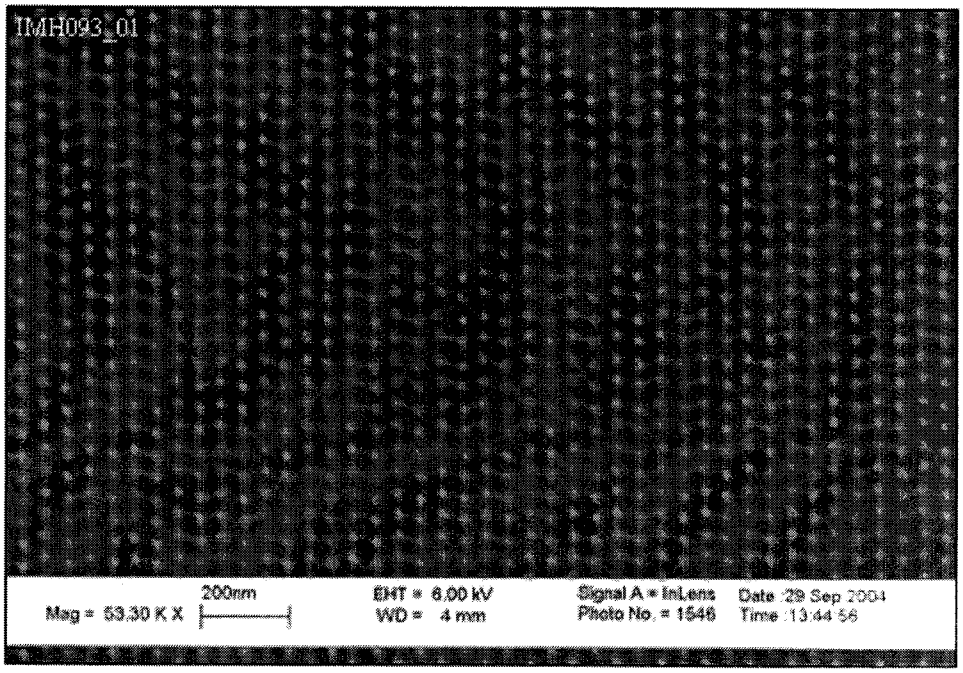

Image A.58 Pattern 1 on imprinter IMH093 after it was developed for 30 minutes in NaOH. The pattern was exposed with a 32 fC point dose and a 50 nm pitch.

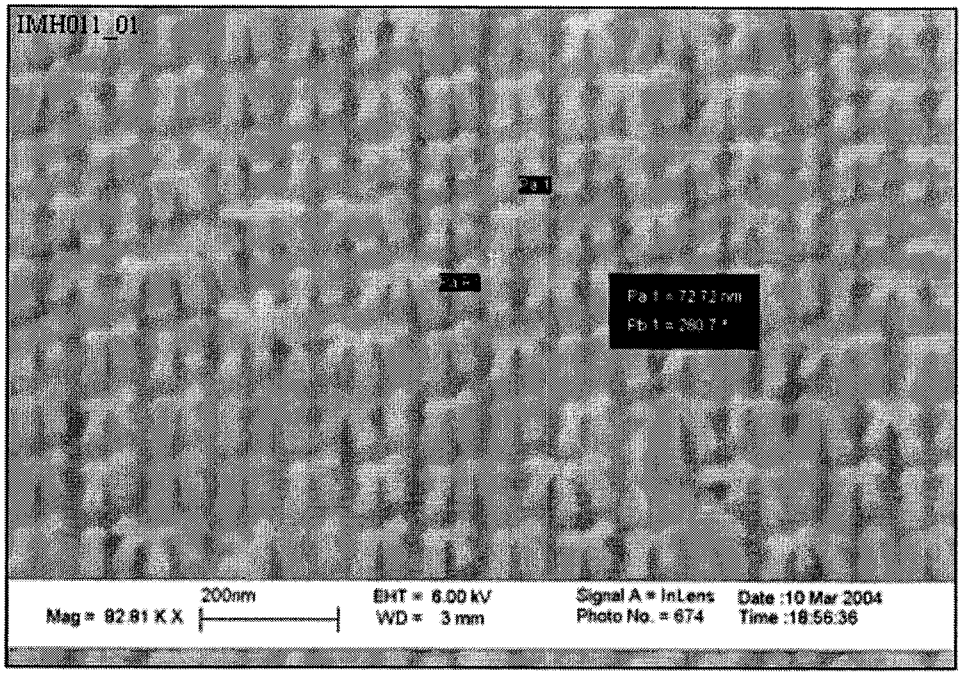

Image A.59 The measured height of the pillars in the center of pattern 1 on imprinter IMH011 is 72 nm. The pattern was exposed with a 24 fC point dose and a 50 nm pitch.

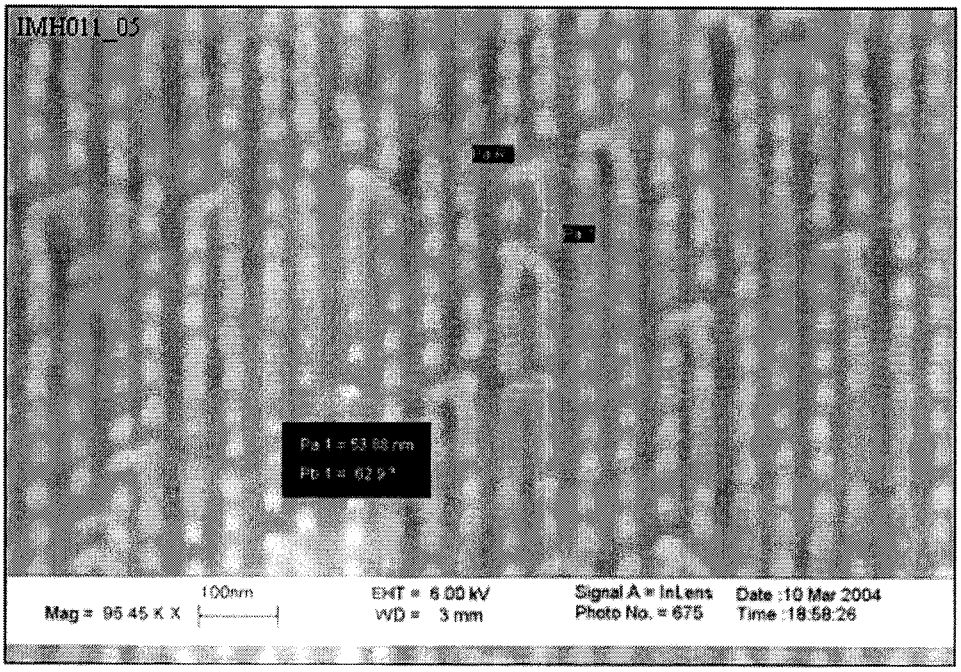

Image A.60 The measured height of the pillars in the center of pattern 5 on imprinter IMH011 is 54 nm. A 26 fC point dose and a 50 nm pitch were used to expose the pattern.

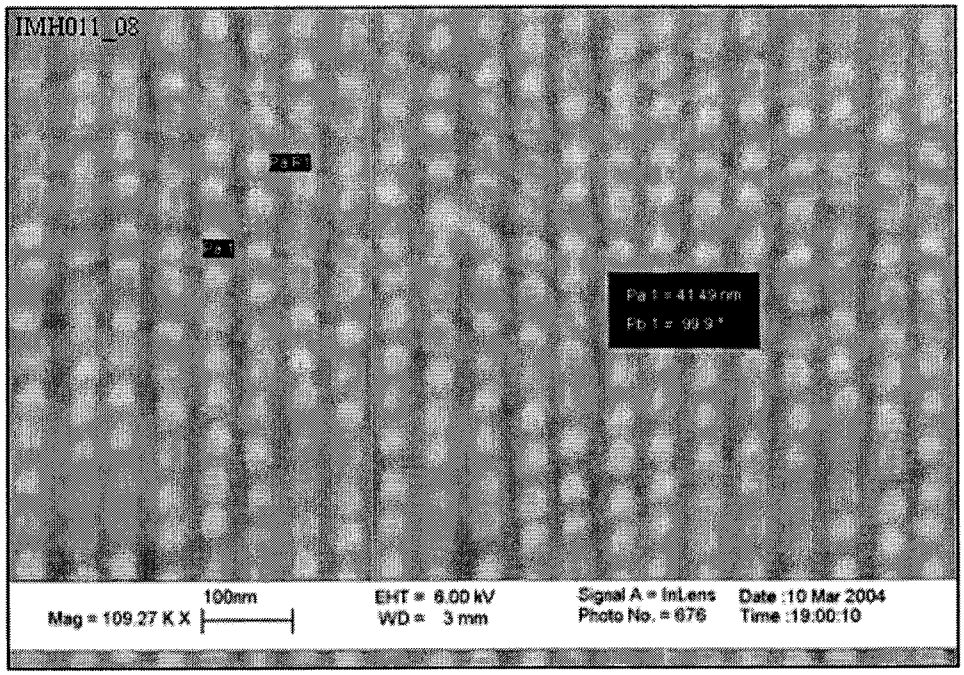

Image A.61 The measured height of the pillars in the center of pattern 8 on imprinter IMH011 is 42 nm. A 27.5 fC point dose and a 50 nm pitch were used to expose the pattern.

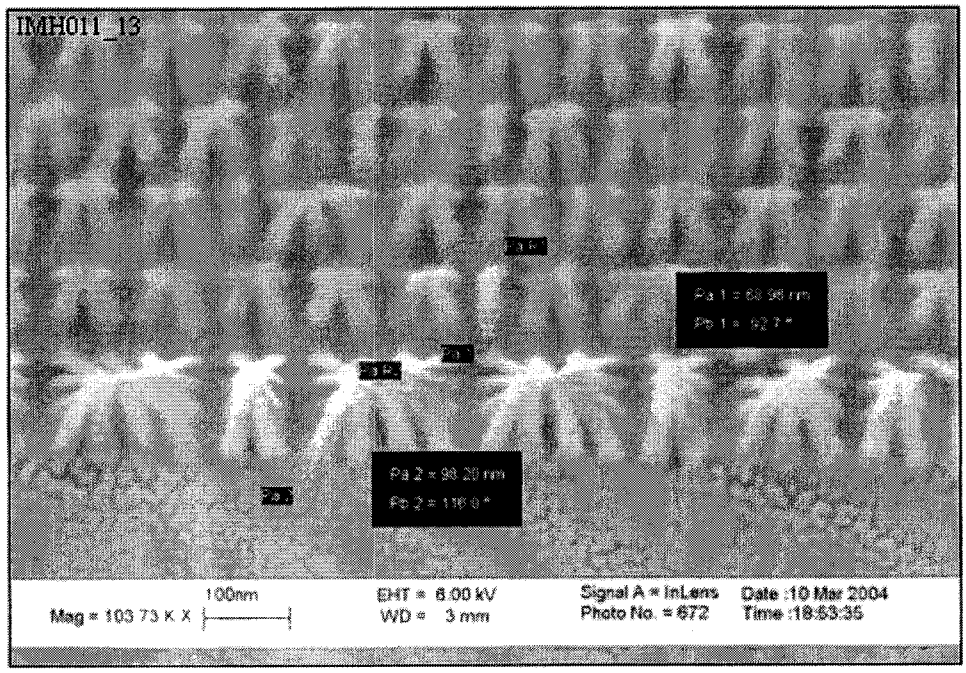

Image A.62 The measured height of the pillars around the edge of pattern 13 on imprinter 11 is between 70 and 100 nm. A 29.5 fC point dose and 50 nm pitch were used to expose the pattern.

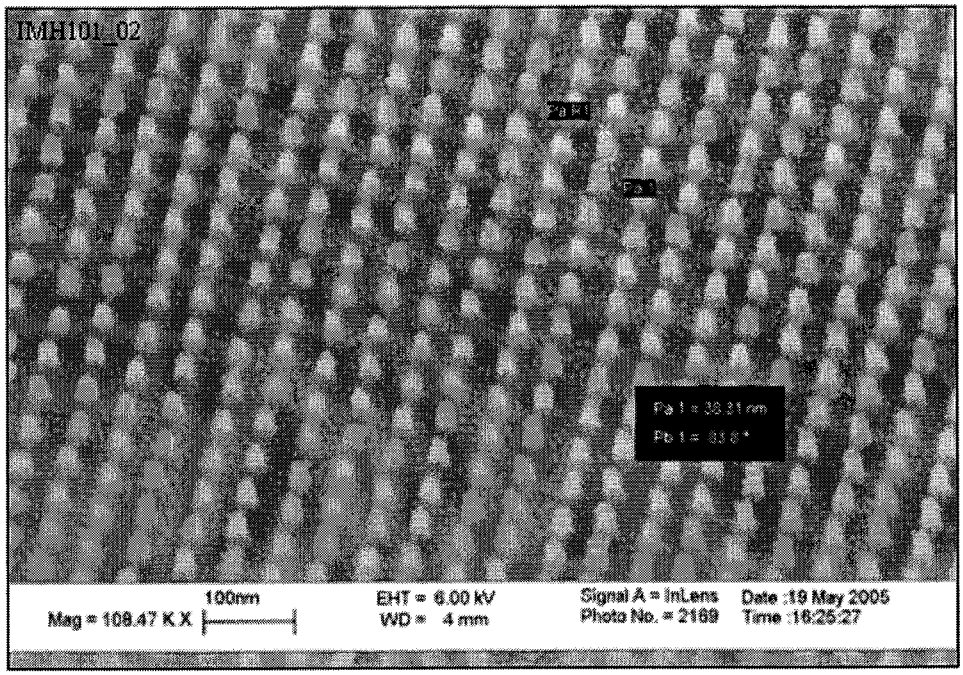

Image A.63 The measured height of the pillars in the center of pattern 2 on imprinter IMH101 is 38 nm. The pattern was exposed using a 32 fC point dose and 50 nm pitch.

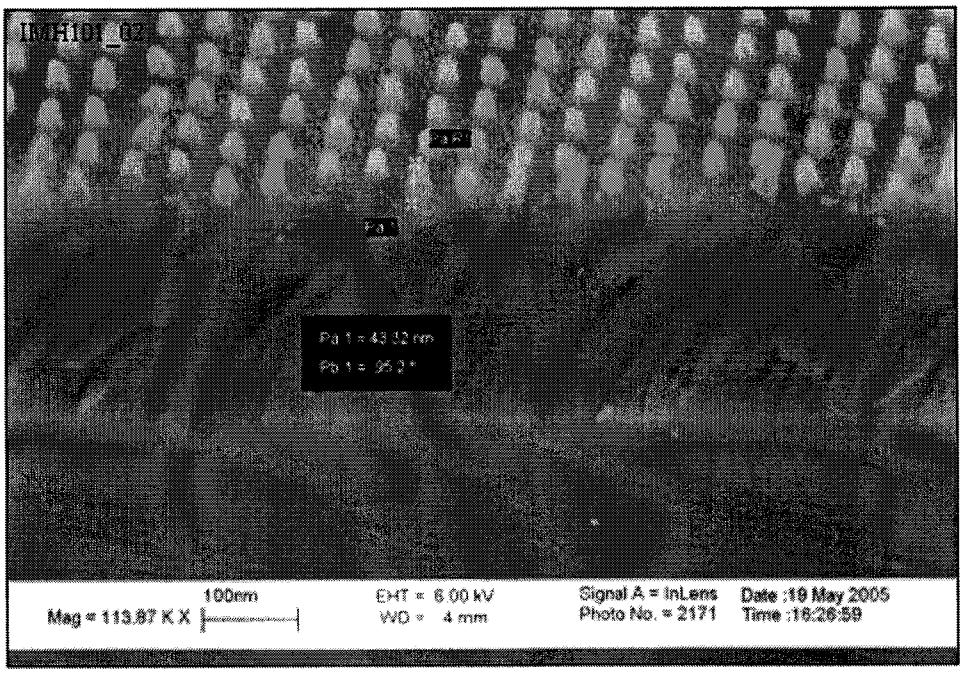

Image A.64 The image shows the measured pillar height near the center of pattern 2 on imprinter IMH101 to be 43 nm. A 32 fC point dose and 50 nm pitch were used to expose the pattern.

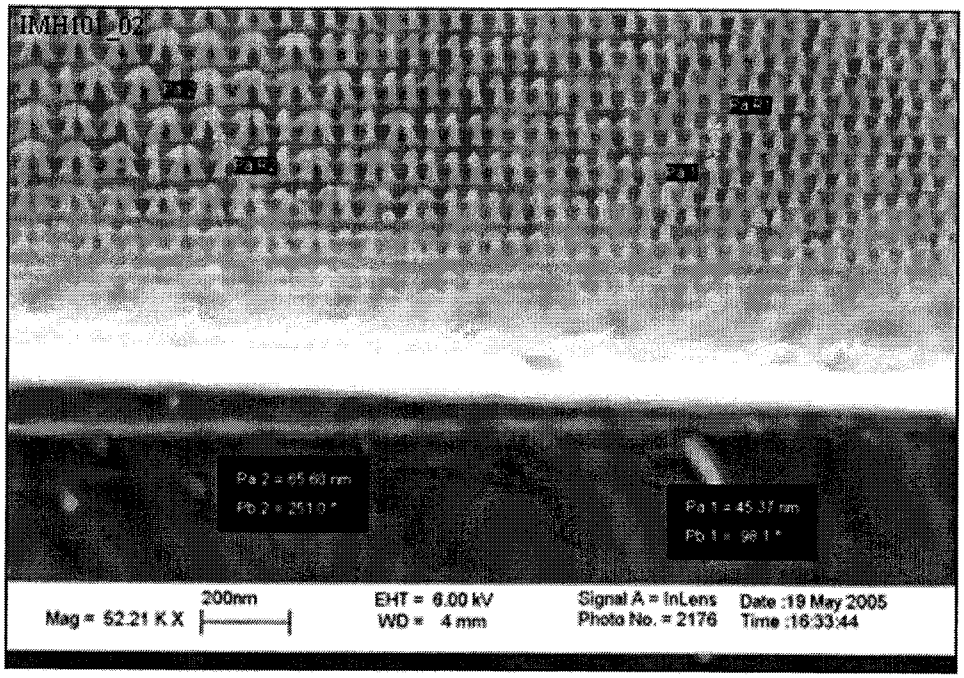

Image A.65 The image shows the border of where the pillars in the center of pattern 2 on imprinter IMH101 meet those by the edge. The pillars in the center are 45 nm tall and those near the edge are 65 nm tall. A 32 fC point dose and 50 nm pitch were used to expose the pattern.

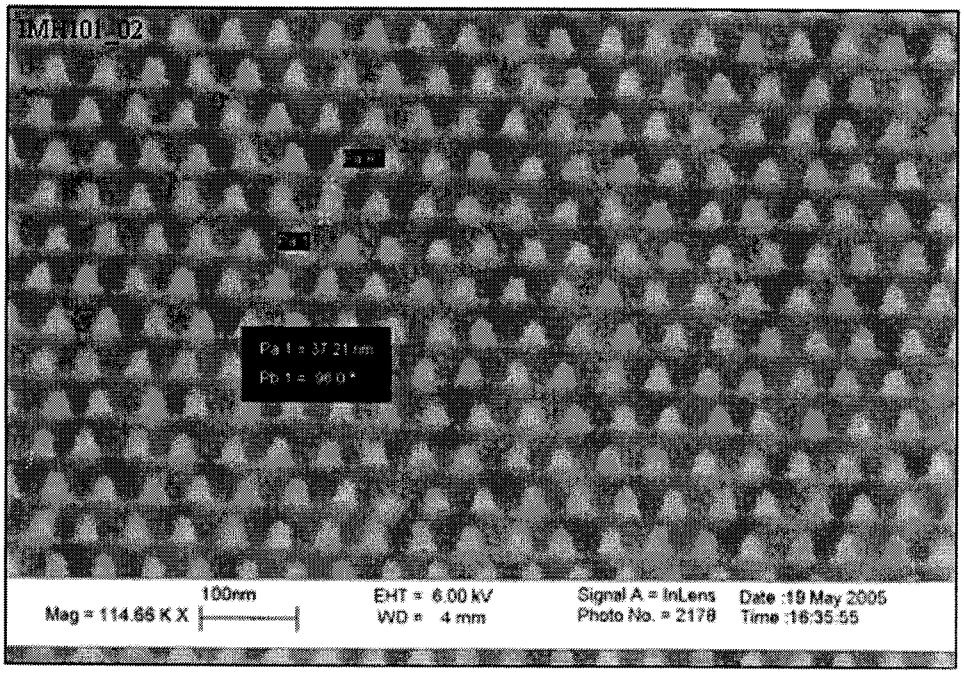

Image A.66 The image shows the measured pillar height near the center of pattern 2 on imprinter IMH101 to be 37 nm. A 32 fC point dose and a 50 nm pitch were used to expose the pattern.

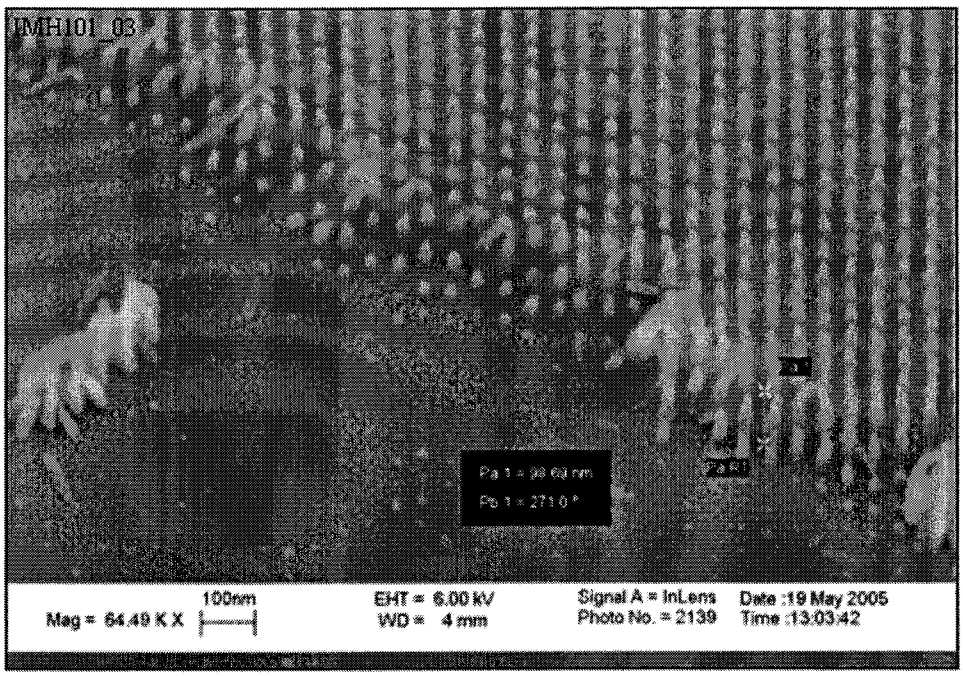

Image A.67 The image shows a cut out area near the center of pattern 3 on imprinter IMH101. It reveals the cross section of the HSQ pillars. The overall height is 99 nm. The pattern was exposed with a 32 fC point dose and a 50 nm pitch.

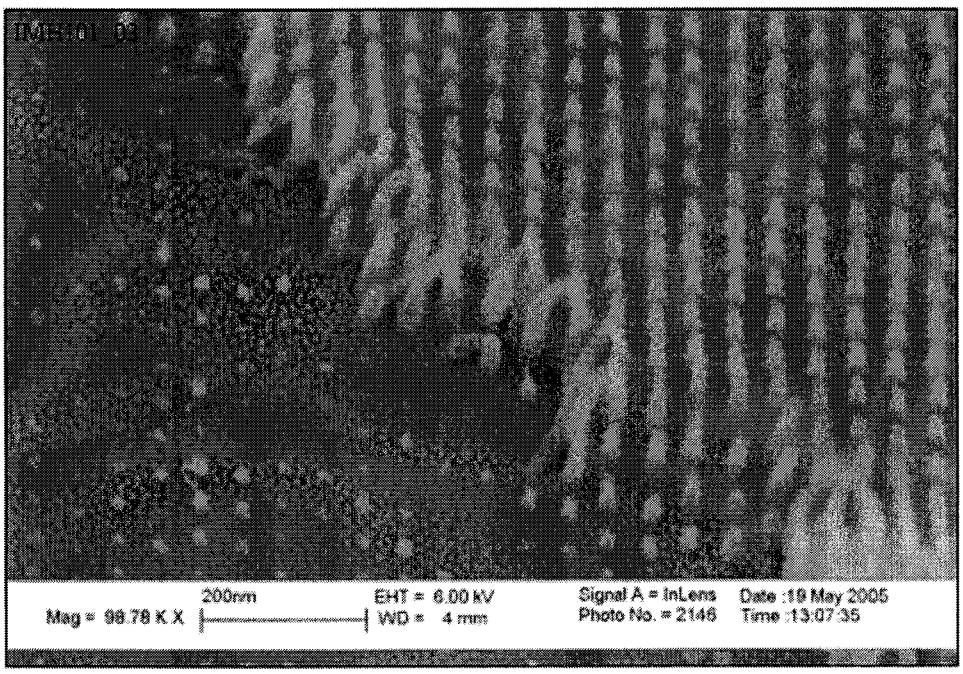

Image A.68 The image reveals the cross sectional structure of HSQ pillars near the center of pattern 3 on imprinter IMH101. A 32 fC point dose and a 50 nm pitch were used to expose the pattern.

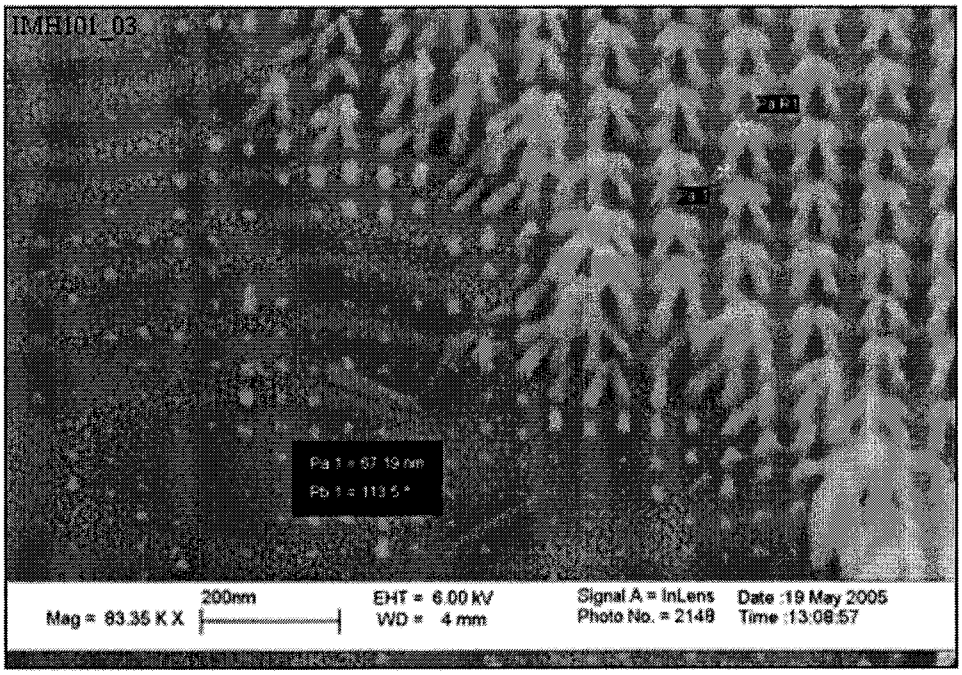

Image A.69 The image shows the pillars near the edge of pattern 3 on imprinter IMH101. The measured height is 67 nm. The pattern was exposed with a 32 fC point dose and a 50 nm pitch.

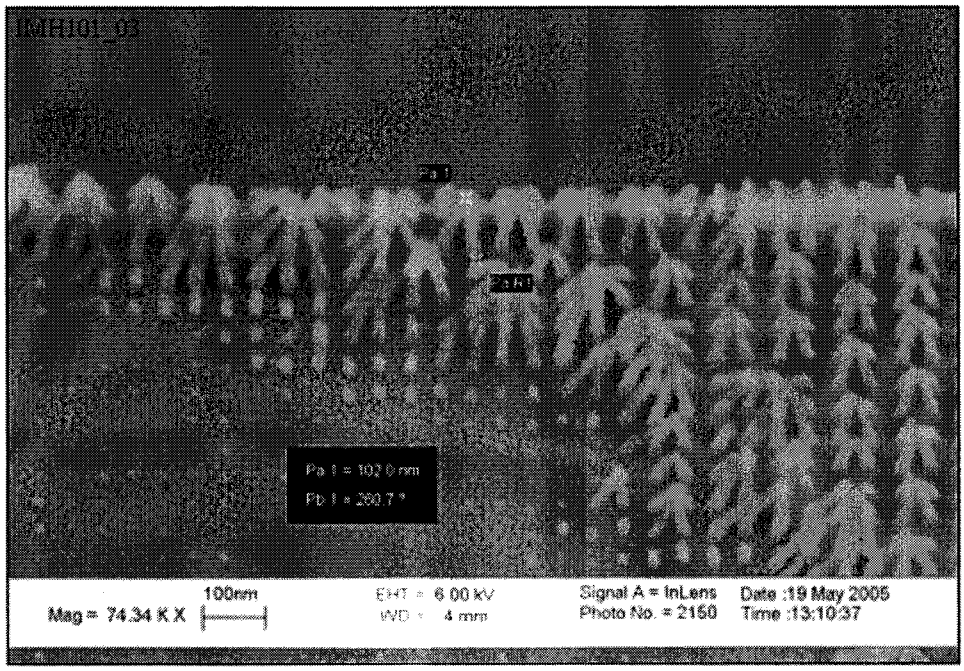

Image A.70 The image shows the pillars on the very edge of pattern 3 on imprinter IMH101. The measured height is 102 nm. The pattern was exposed using a 32 fC point dose and a 50 nm pitch.

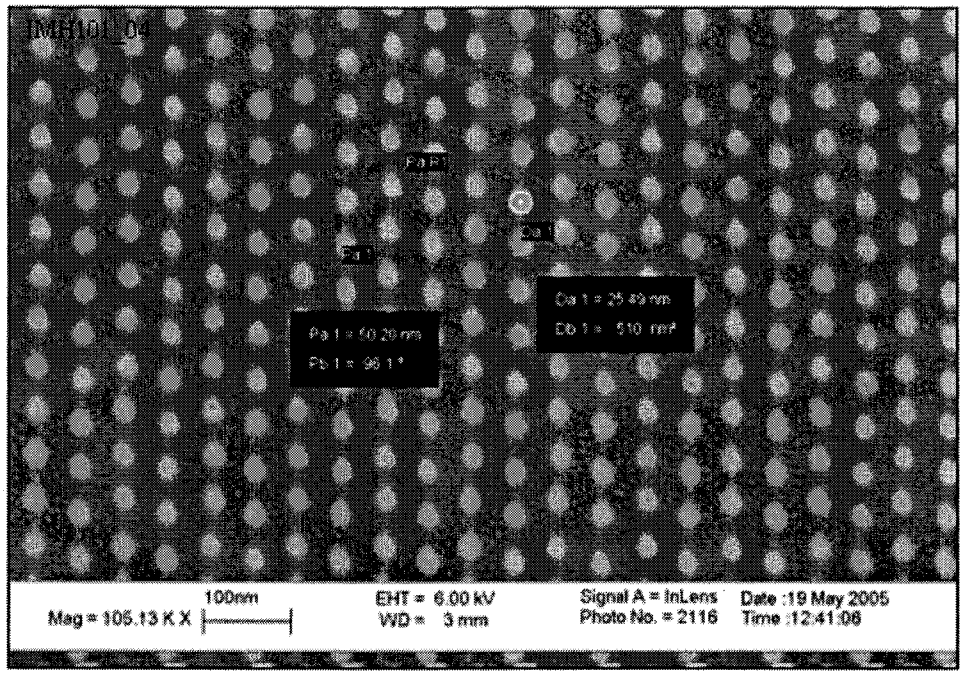

Image A.71 The image displays the measured pillar diameter and pitch of pattern 4 on imprinter IMH101. The pillar diameter is 25 nm and the pitch is 50 nm. The pattern was exposed with a 32 fC point dose and a 50 nm pitch.

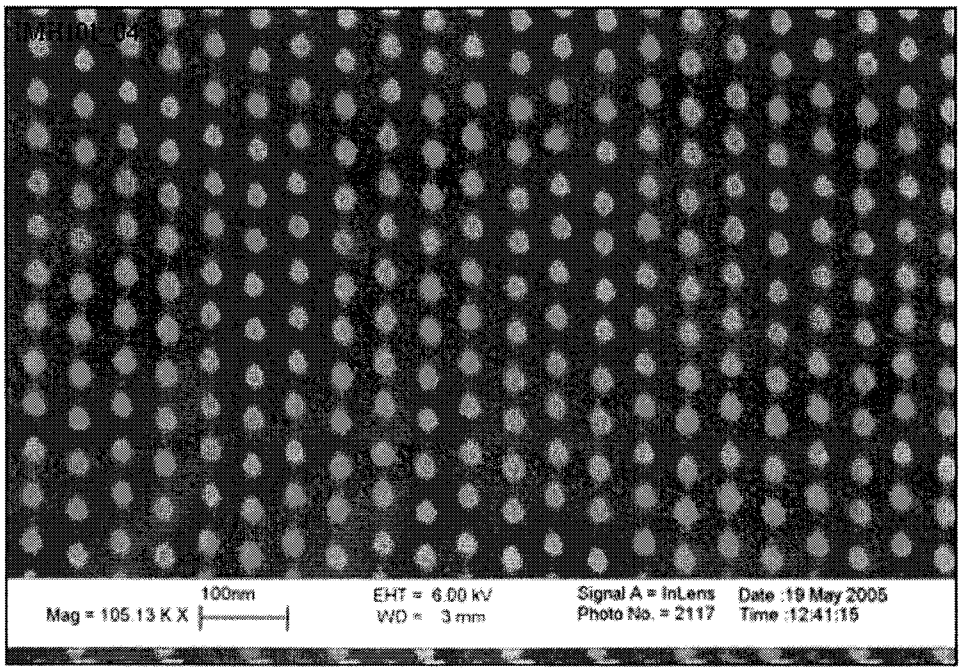

Image A.72 A clean, defect free array of pillars in pattern 4 on imprinter IMH101. The pattern was exposed using a 32 fC point dose and a 50 nm pitch.

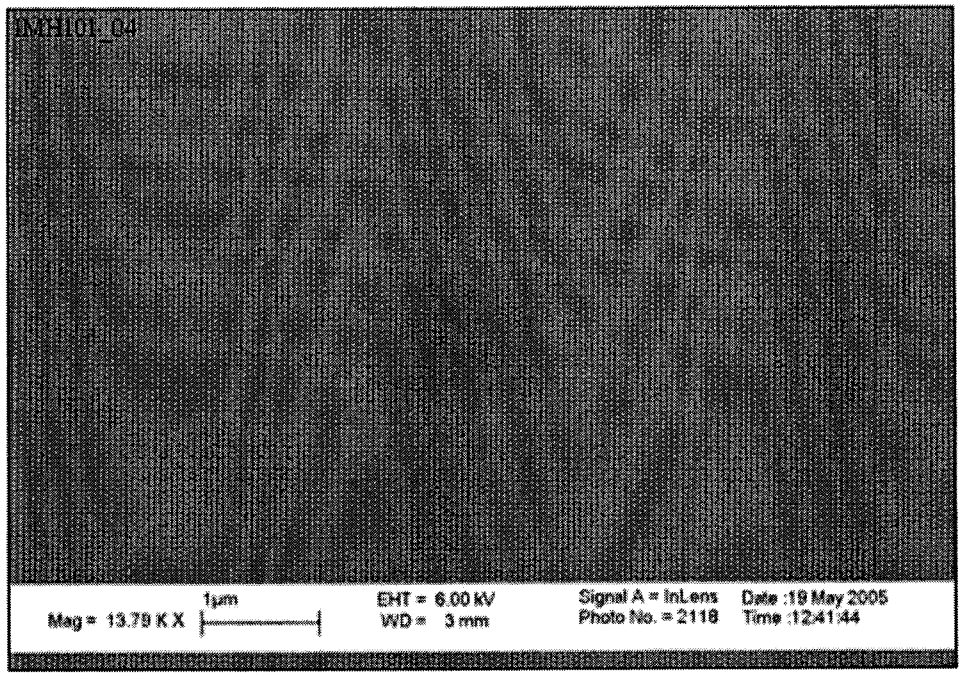

Image A.73 A several micron wide and long completely defect free area of pattern 4 on imprinter IMH101. A 32 fC point dose and 50 nm pitch were used to expose the pattern.

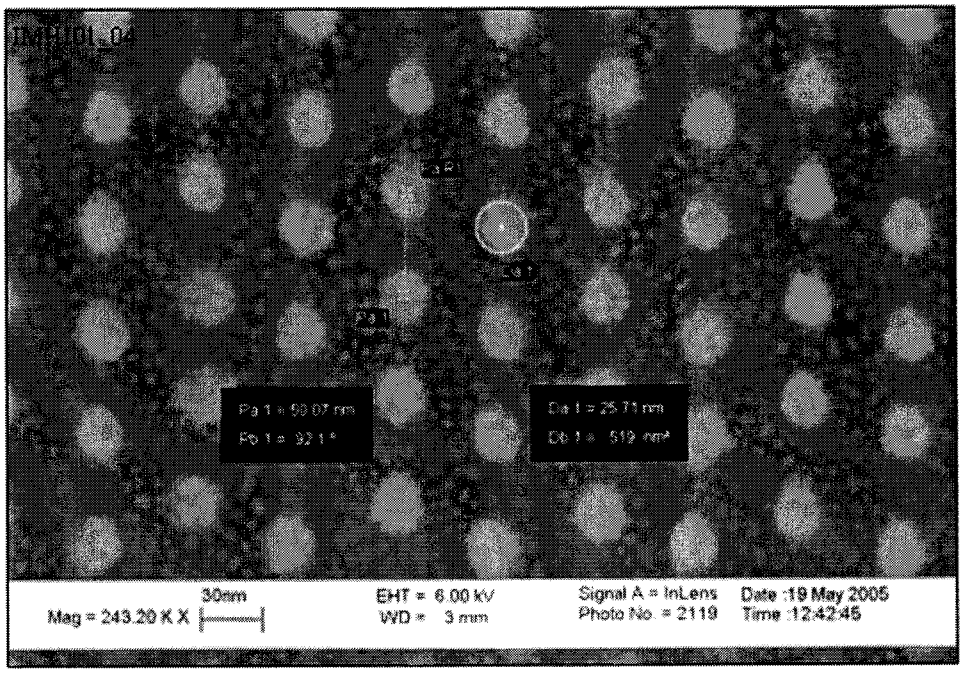

Image A.74 The measured pillar diameter and pitch of pattern 4 on imprinter IMH101. The pattern was exposed using a 32 fC point dose and a 50 nm pitch.

A.2 Imprinted Samples

A.2.1 Single Layer Resist

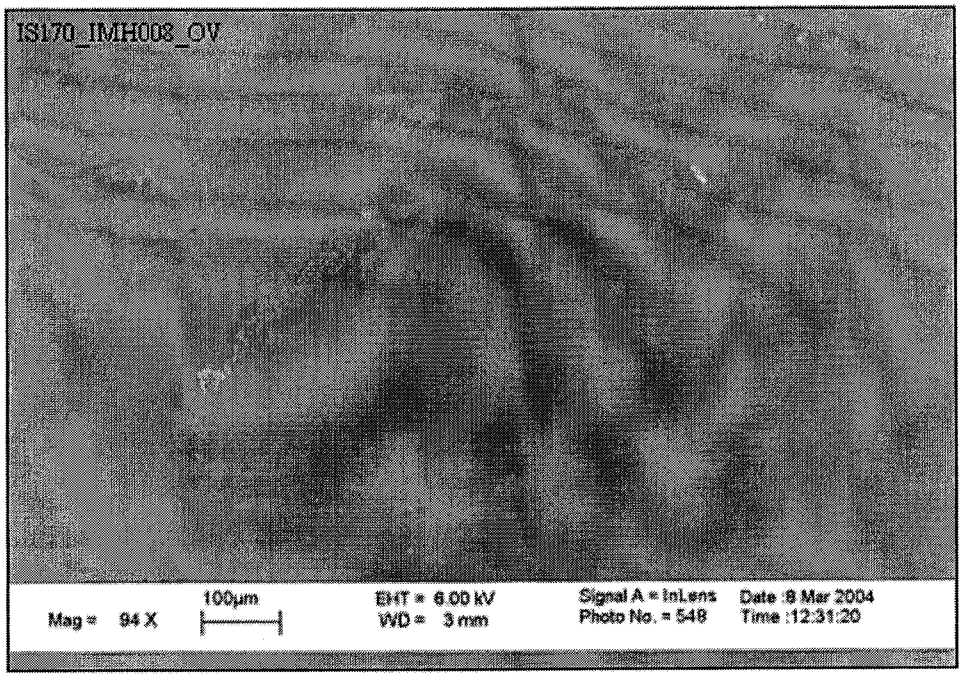

Image A.75 The image displays an overview of all the imprinted patterns on sample IS170. The following parameters were used: single layer of PMMA, model 100 imprinting press, imprinter IMH008 (several doses), regulator pressure of 6 psi, and a separation temperature of 50°C.

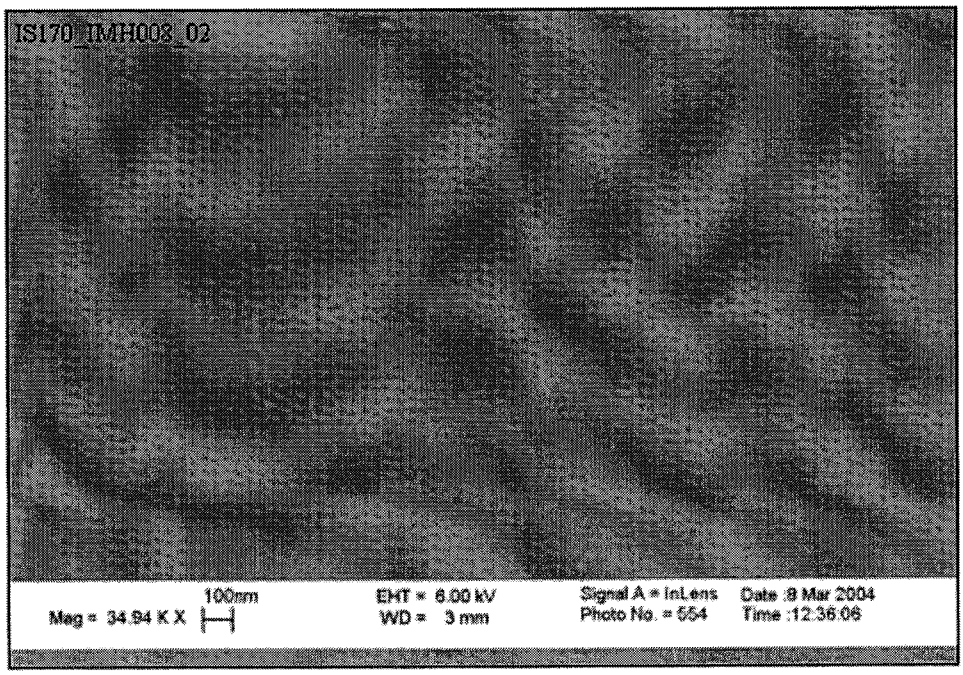

Image A.76 The image displays an area of pattern 2 on sample IS170 with a shallow imprint depth. The following parameters were used: single layer of PMMA, model 100 imprinting press, imprinter IMH008 (24 fC point dose), regulator pressure of 6 psi, and the imprinter and sample were separated at 50°C.

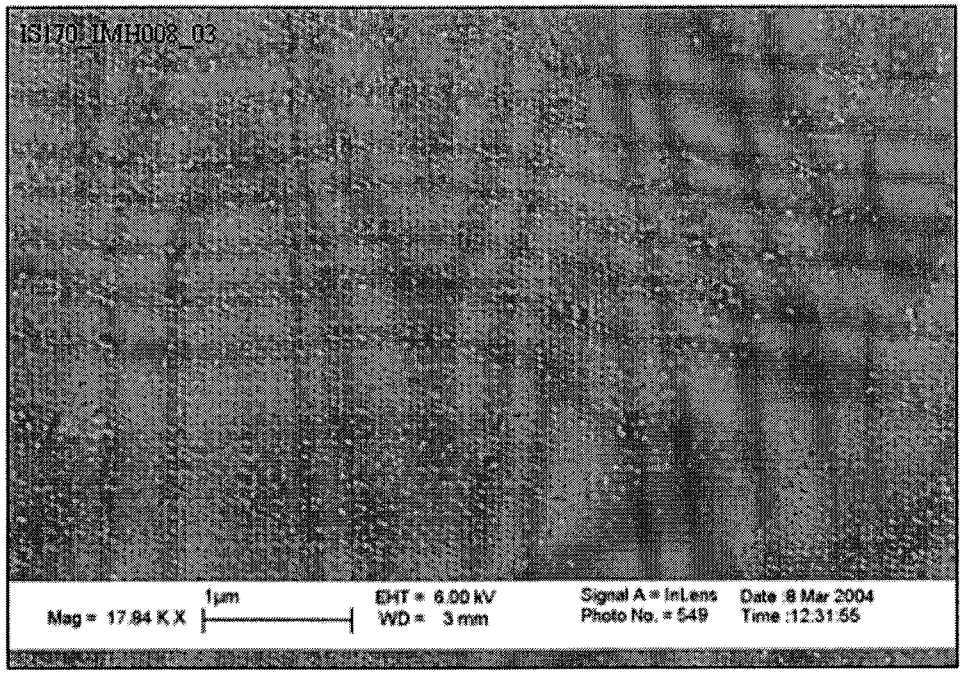

Image A.77 The image displays broken pillars from the imprinter imbedded into the PMMA. The imprinted sample was produced with the following parameters: single layer of PMMA, model 100 imprinting press, imprinter IMH008 (24 fC point dose), regulator pressure of 6 psi, and the imprinter and sample were separated at 50°C.

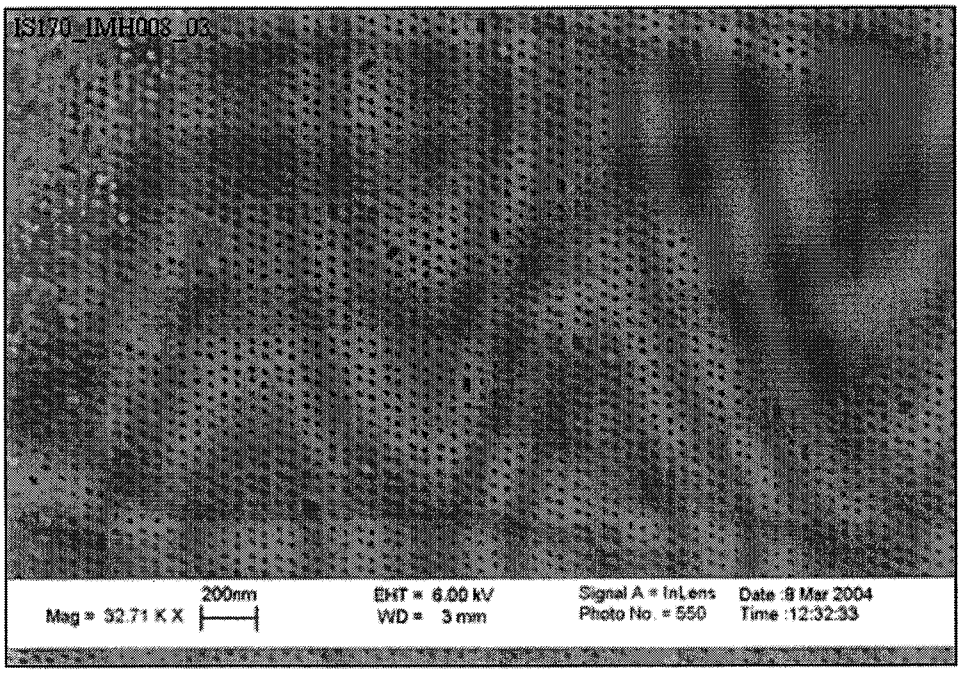

Image A.78 The image displays an area containing imprinted holes and a certain amount of defects. The imprinted sample was produced with the following parameters: single layer of PMMA, model 100 imprinting press, imprinter IMH008 (24 fC point dose), regulator pressure of 6 psi, and the imprinter and sample were separated at 50°C.

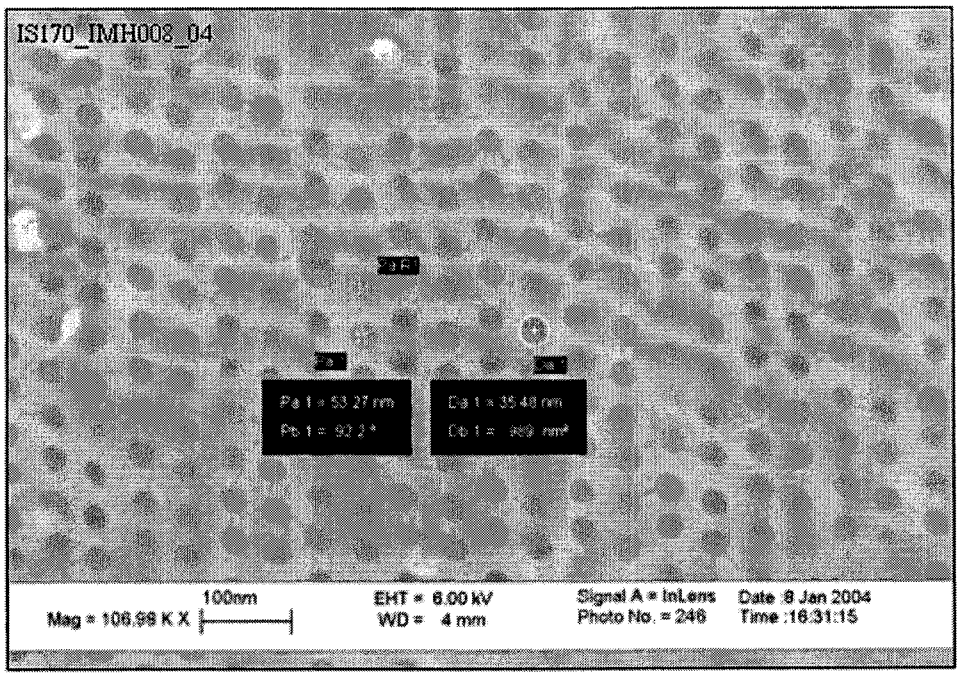

Image A.79 The image displays the measured hole diameter and pitch of pattern 4 on sample IS170. The imprinted sample was produced with the following parameters: single layer of PMMA, model 100 imprinting press, imprinter IMH008 (26 fC point dose), regulator pressure of 6 psi, and the imprinter and sample were separated at 50°C.

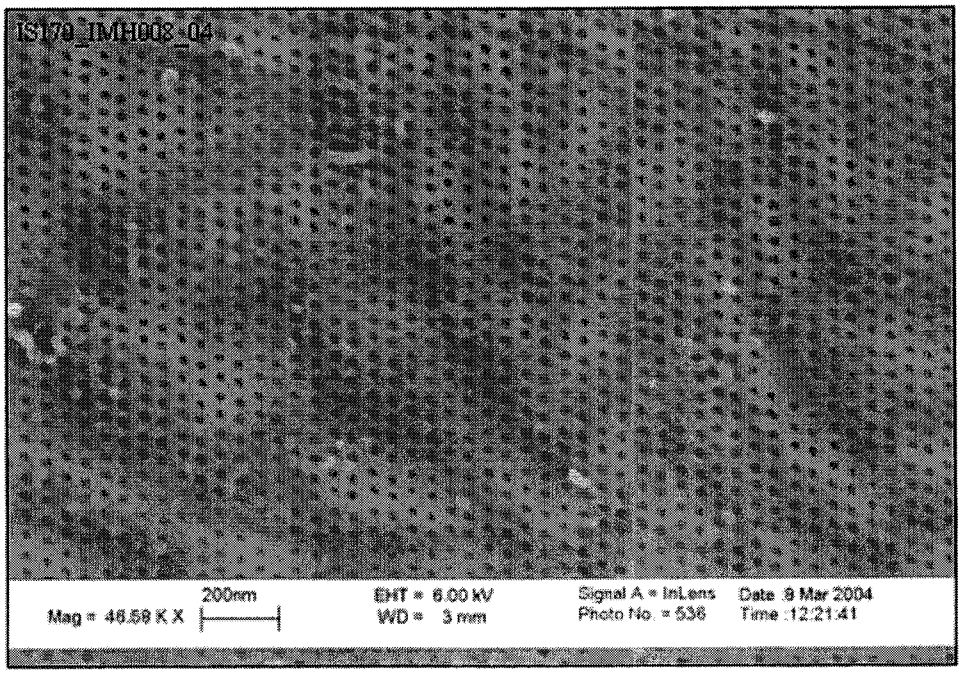

Image A.80 The image displays an area of pattern 4 on sample IS170 containing imprinted holes and several defects. The imprinted sample was produced with the following parameters: single layer of PMMA, model 100 imprinting press, imprinter IMH008 (26 fC point dose), regulator pressure of 6 psi, and the imprinter and sample were separated at 50°C.

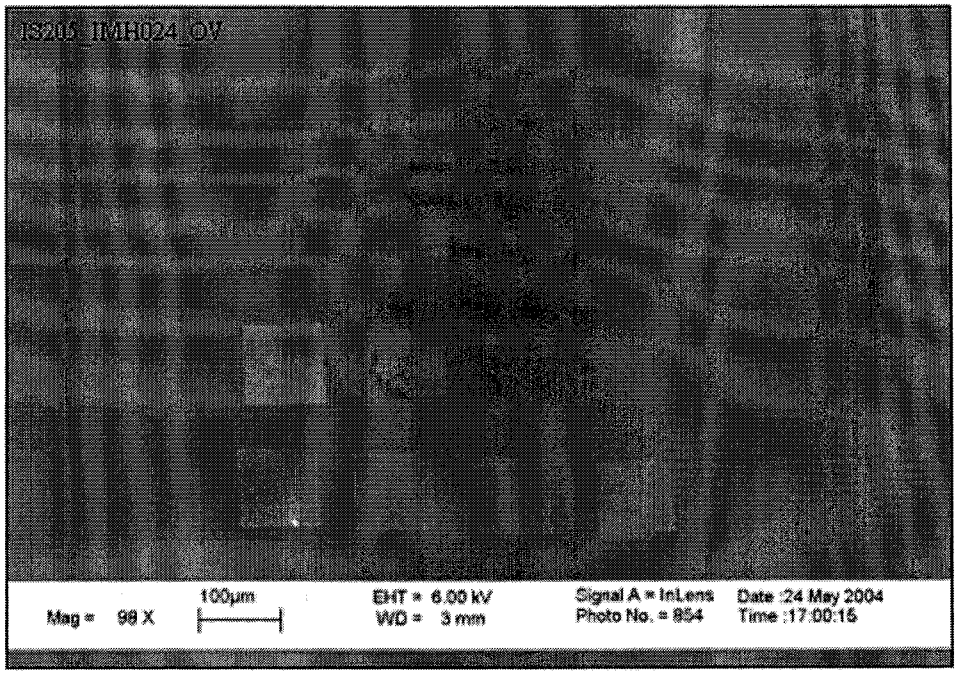

Image A.81 The image displays an overview of the patterns on imprinted sample IS205. The imprinted sample was produced with the following parameters: single layer of PMMA, model 20 imprinting press, imprinter IMH024 (several doses), regulator pressure of 80 psi, and the separation temperature was 39.5°C.

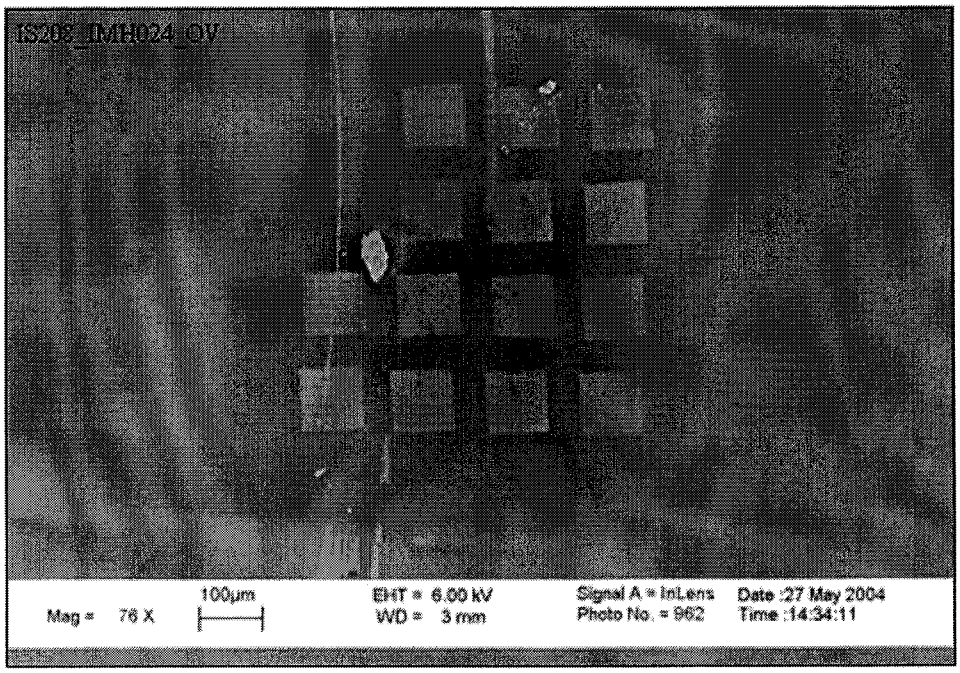

Image A.82 The image is an overview of all the patterns on imprinted sample IS208. The imprinted sample was produced with the following parameters: single layer of PMMA, model 20 imprinting press, imprinter IMH024 (several doses), regulator pressure of 40 psi, and the separation temperature was 36.5°C.

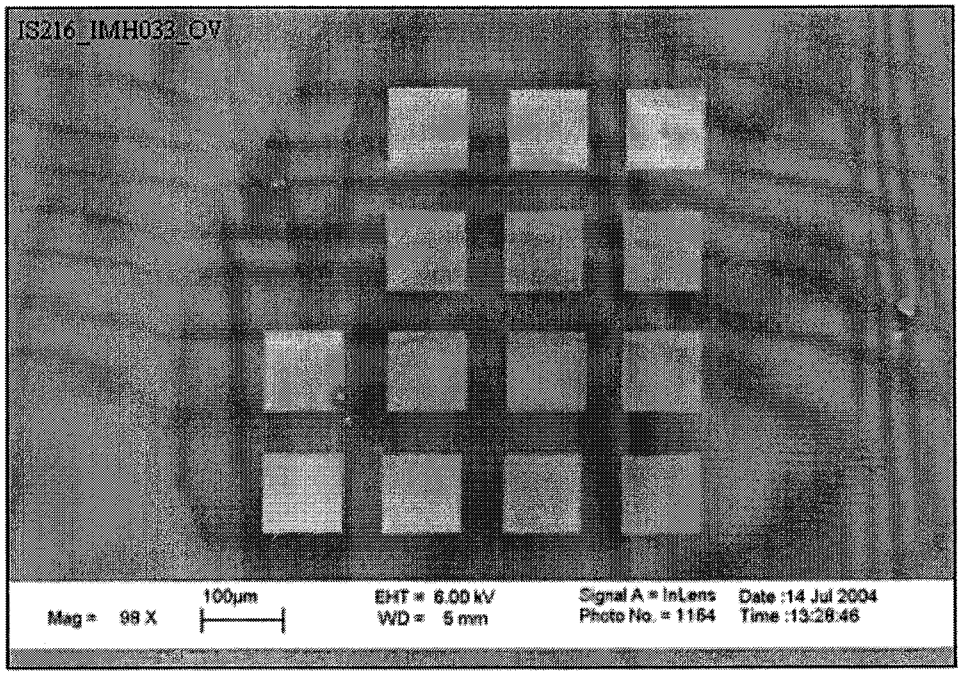

Image A.83 The image displays an overview of all the patterns on imprinted sample IS216. The following parameters were used: single layer of PMMA, model 20 imprinting press, imprinter IMH033 (28.5 fC point dose), regulator pressure of 40 psi, and the separation temperature was 40°C.

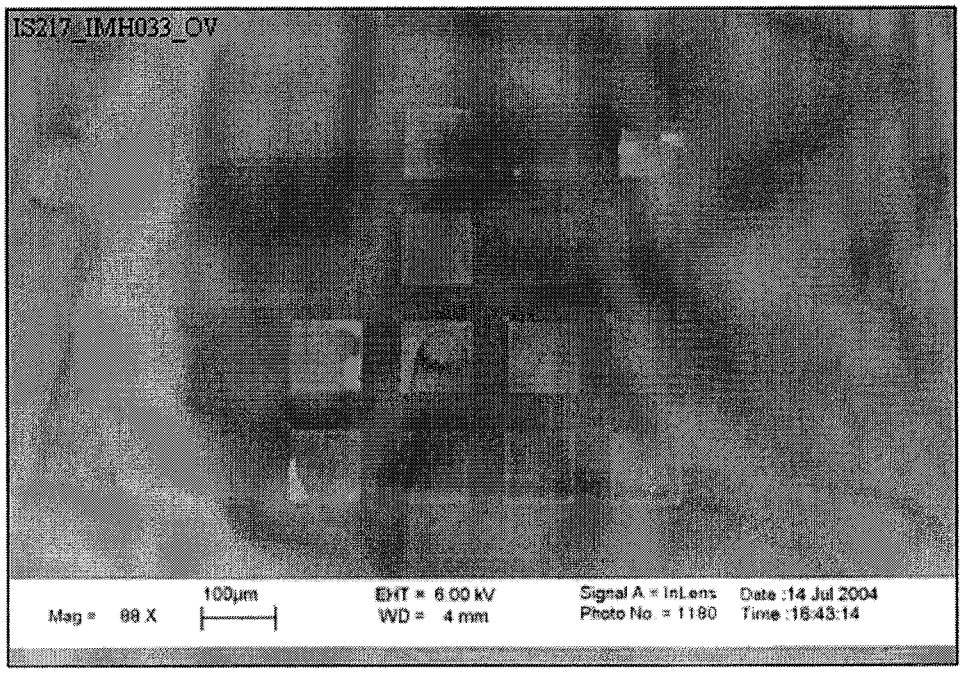

Image A.84 The image displays an overview of the patterns on imprinted sample IS217. The following parameters were used: single layer of PMMA, model 20 imprinting press, imprinter IMH033 (28.5 fC point dose), regulator pressure of 40 psi, and the separation temperature was 39.5°C.

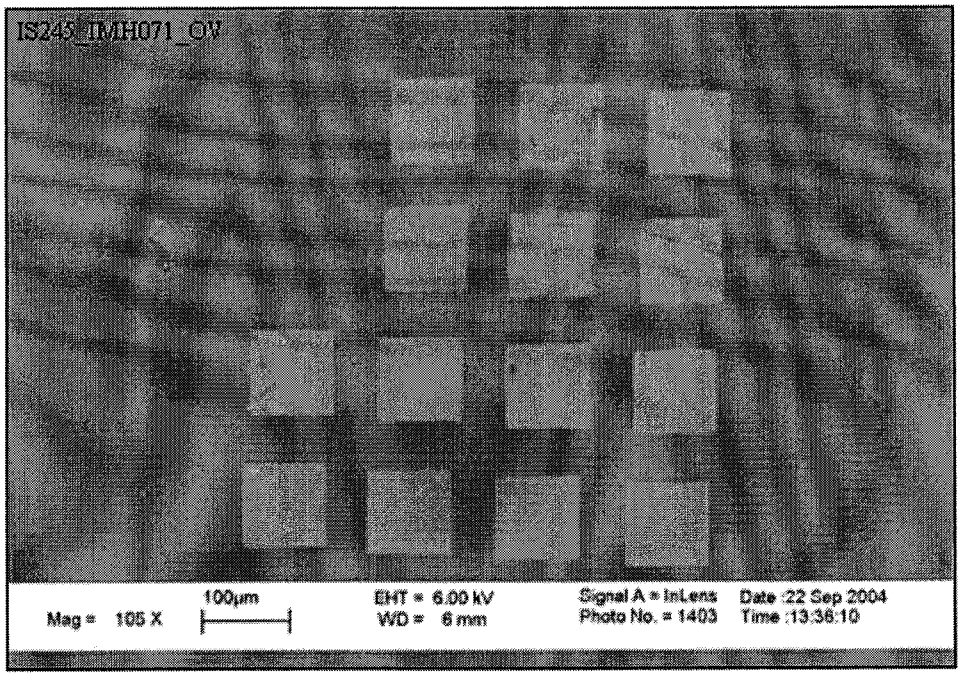

Image A.85 The image displays an overview of the patterns on imprinted sample IS245. The following parameters were used: single layer of PMMA, model 20 imprinting press, imprinter IMH071 (32 fC point dose), regulator pressure of 50 psi, and the separation temperature was 42.5°C.

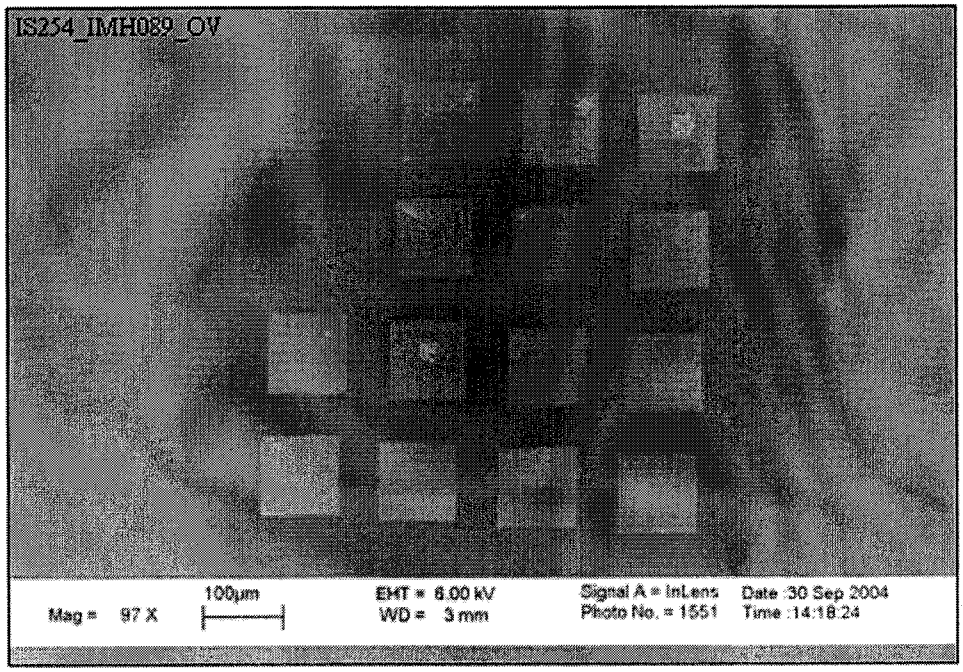

Image A.86 The image displays an overview of the patterns on imprinted sample IS254. The following parameters were used: single layer of PMMA, model 20 imprinting press, imprinter IMH089 (32 fC point dose), regulator pressure of 50 psi, and the separation temperature was 35°C.

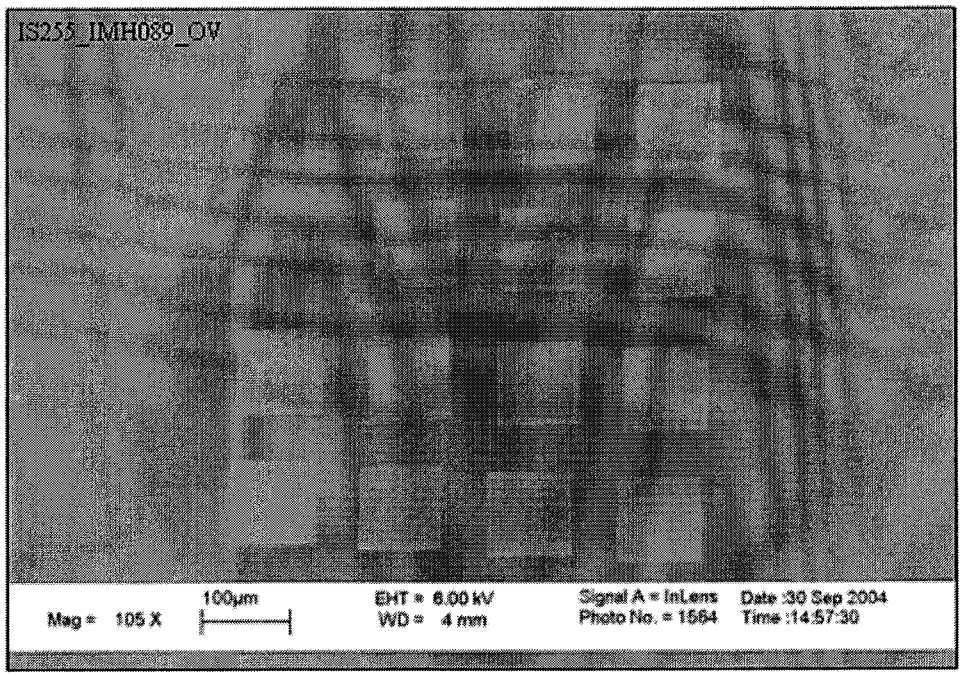

Image A.87 The image displays an overview of the patterns on imprinted sample IS255. The following parameters were used: single layer of PMMA, model 20 imprinting press, imprinter IMH089 (32 fC point dose), regulator pressure of 50 psi, and the separation temperature was 34.5°C.

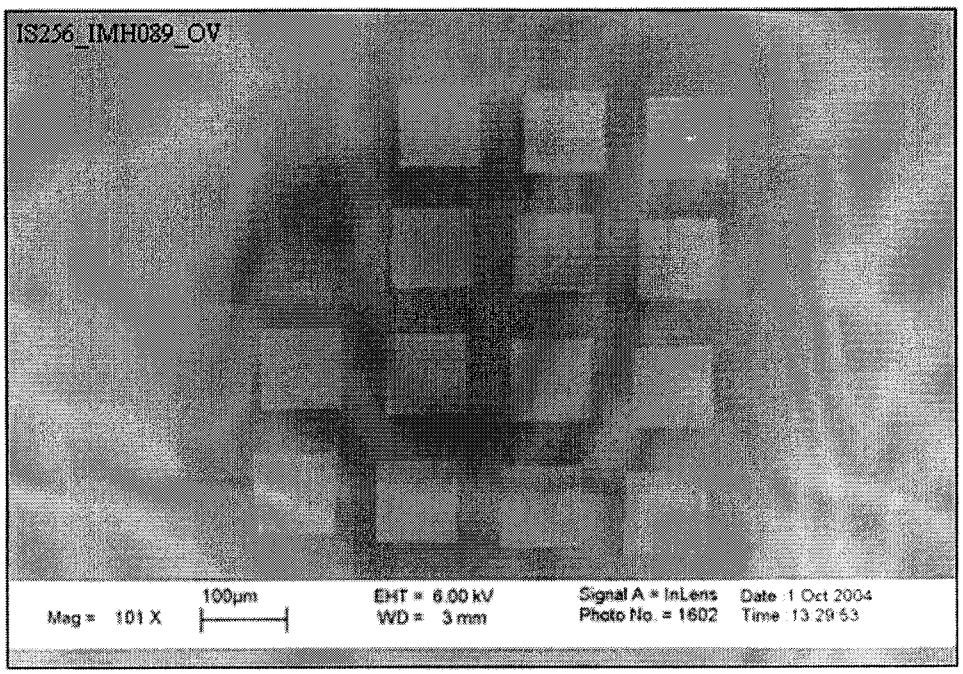

Image A.88 The image displays an overview of the patterns on imprinted sample IS256. The following parameters were used: single layer of PMMA, model 20 imprinting press, imprinter IMH089 (32 fC point dose), regulator pressure of 50 psi, and the separation temperature was 35.5°C.

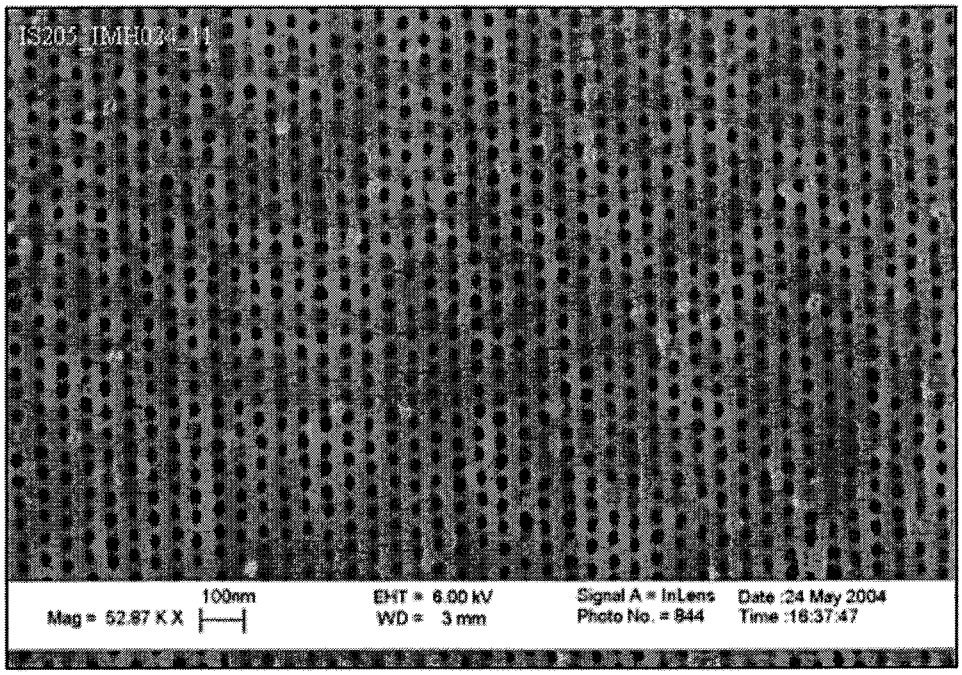

Image A.89 Imprinted holes of pattern 11 on sample IS205. The following parameters were used: single layer of PMMA, model 20 imprinting press, imprinter IMH024 (30.5 fC point dose), regulator pressure of 80 psi, and the separation temperature was 39.5°C.

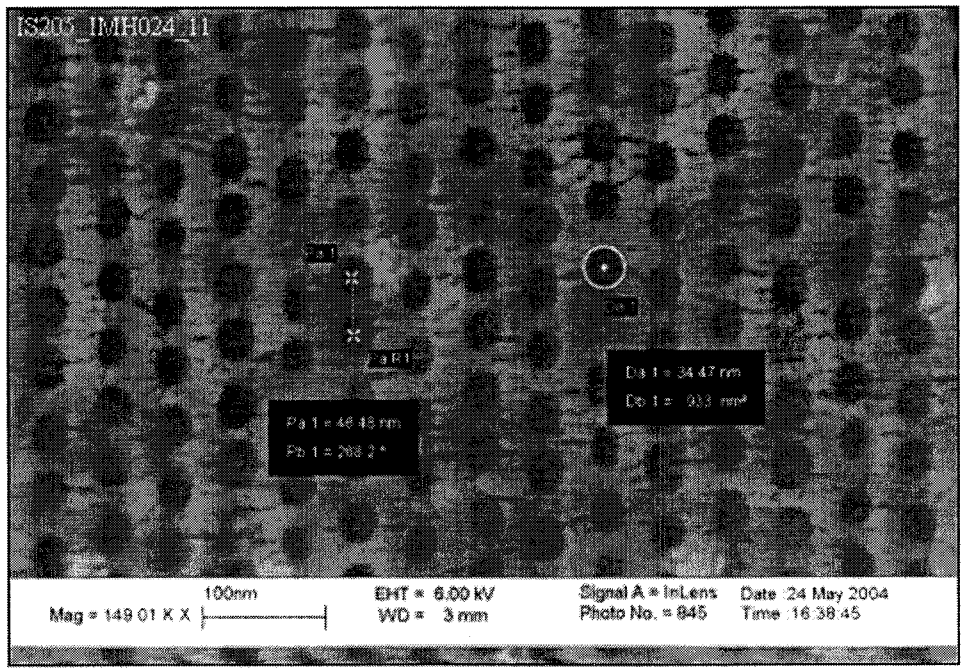

Image A.90 Imprinted holes of pattern 11 on sample IS205. The following parameters were used: single layer of PMMA, model 20 imprinting press, imprinter IMH024 (30.5 fC point dose), regulator pressure of 80 psi, and the separation temperature was 39.5°C.

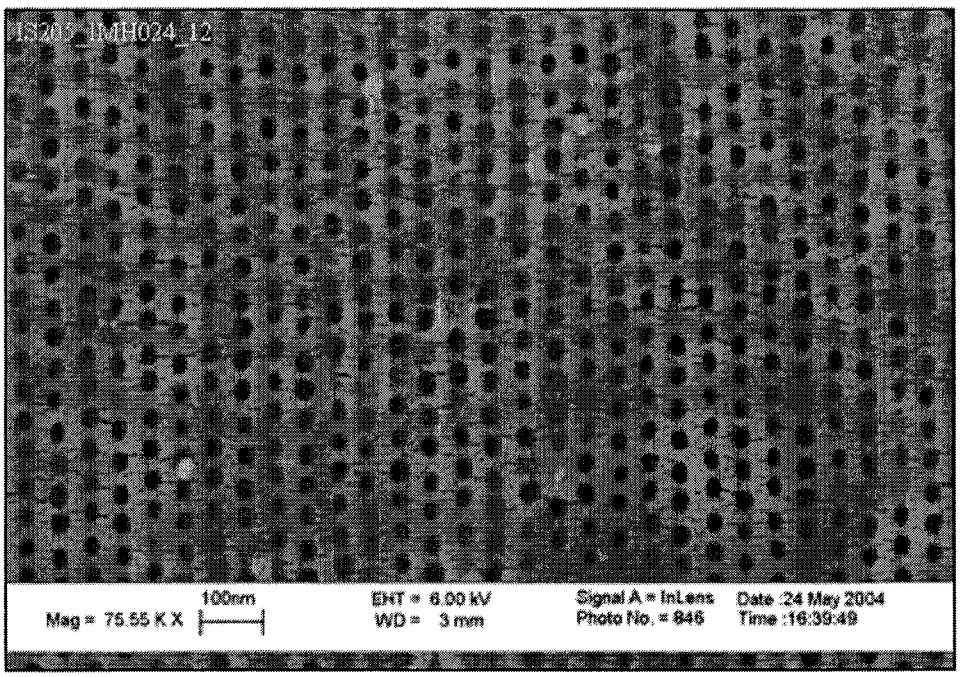

Image A.91 Imprinted holes of pattern 12 on sample IS205. The following parameters were used: single layer of PMMA, model 20 imprinting press, imprinter IMH024 (30 fC point dose), regulator pressure of 80 psi, and the separation temperature was 39.5°C.

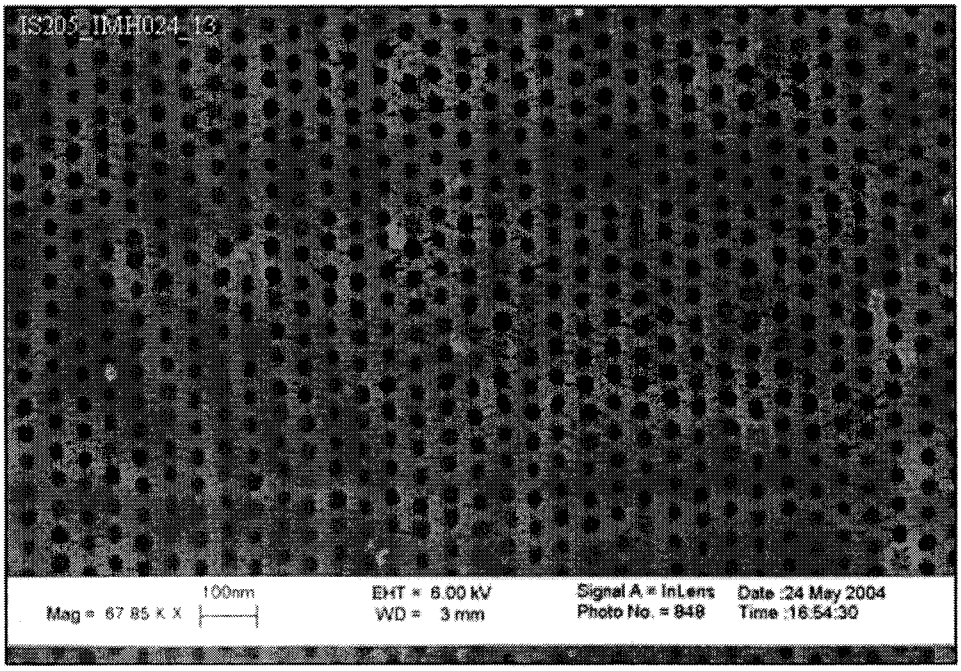

Image A.92 Imprinted holes of pattern 13 on sample IS205. The following parameters were used: single layer of PMMA, model 20 imprinting press, imprinter IMH024 (29.5 fC point dose), regulator pressure of 80 psi, and the separation temperature was 39.5°C.

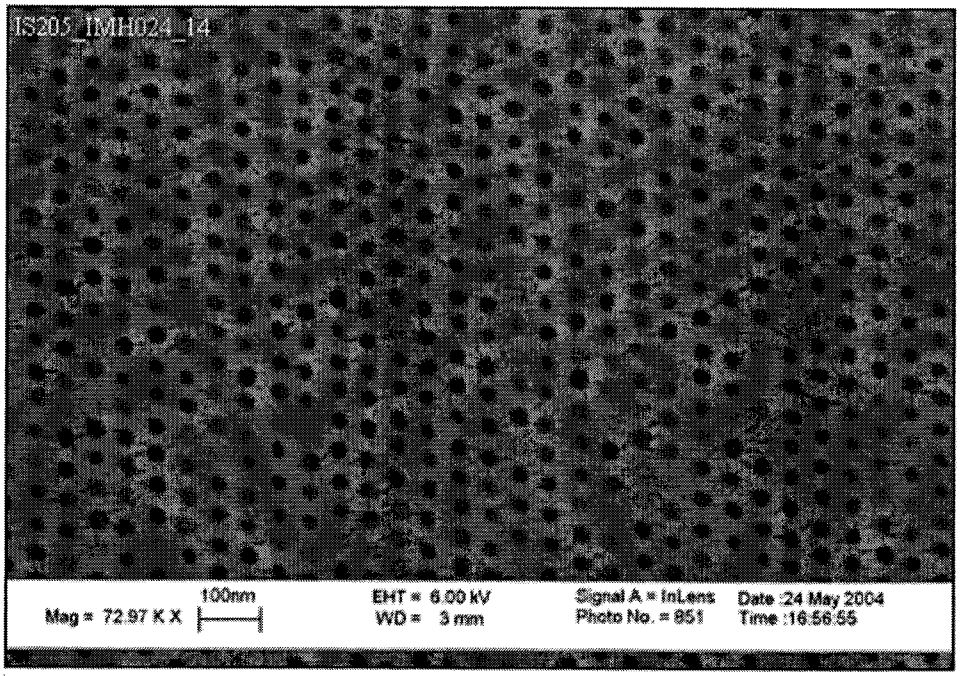

Image A.93 Imprinted holes of pattern 14 on sample IS205. The following parameters were used: single layer of PMMA, model 20 imprinting press, imprinter IMH024 (29 fC point dose), regulator pressure of 80 psi, and the separation temperature was 39.5°C.

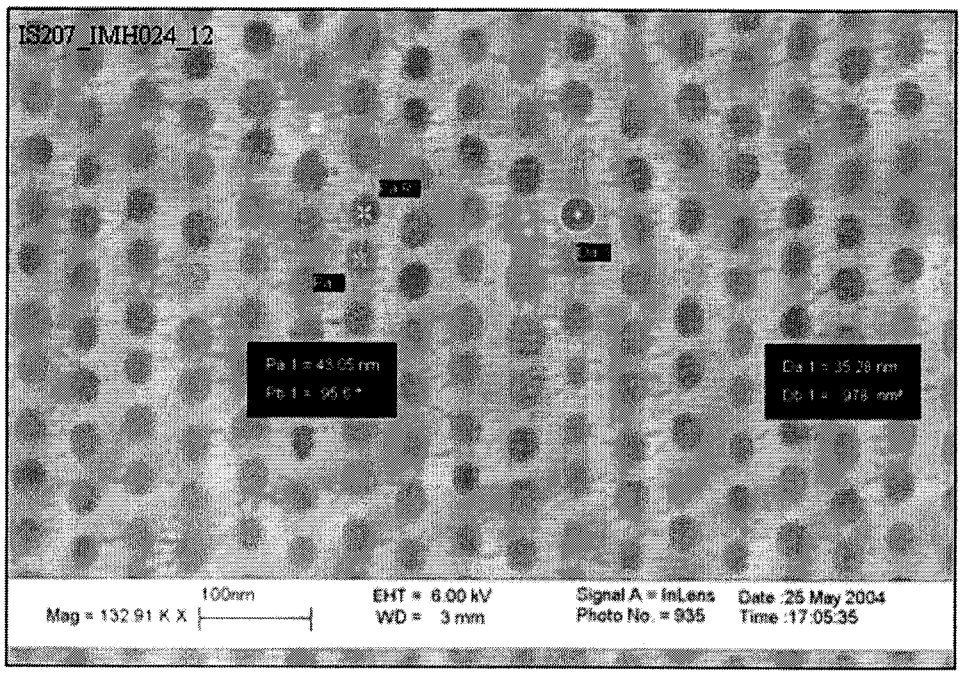

Image A.94 Imprinted holes of pattern 12 on sample IS207. The following parameters were used: single layer of PMMA, model 20 imprinting press, imprinter IMH024 (30 fC point dose), regulator pressure of 80 psi, and the separation temperature was 31.5°C.

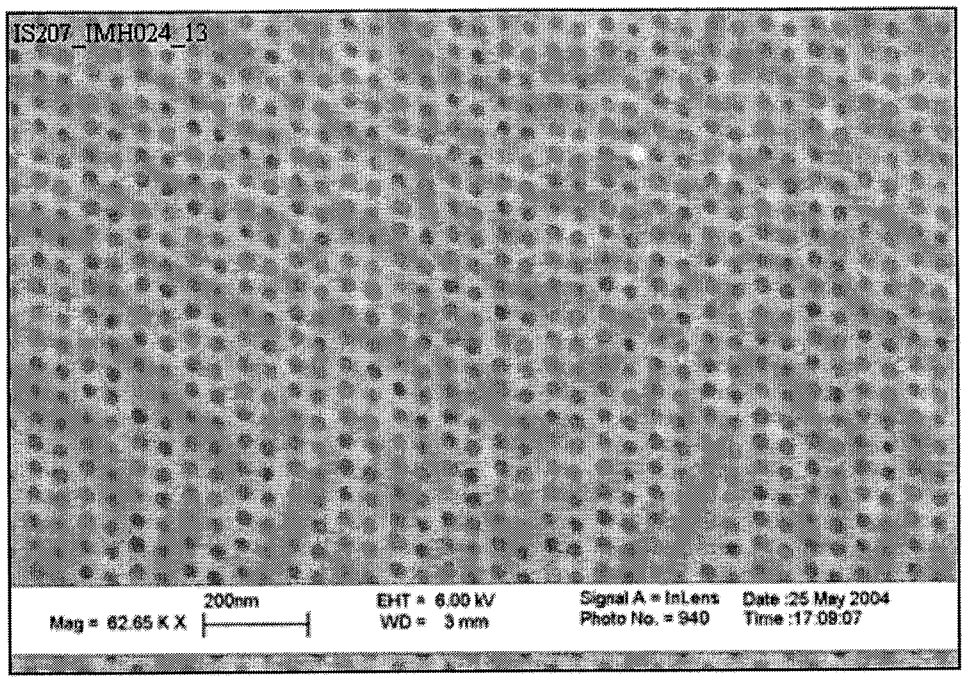

Image A.95 Imprinted holes of pattern 13 on sample IS207. The following parameters were used: single layer of PMMA, model 20 imprinting press, imprinter IMH024 (29.5 fC point dose), regulator pressure of 80 psi, and the separation temperature was 31.5°C.

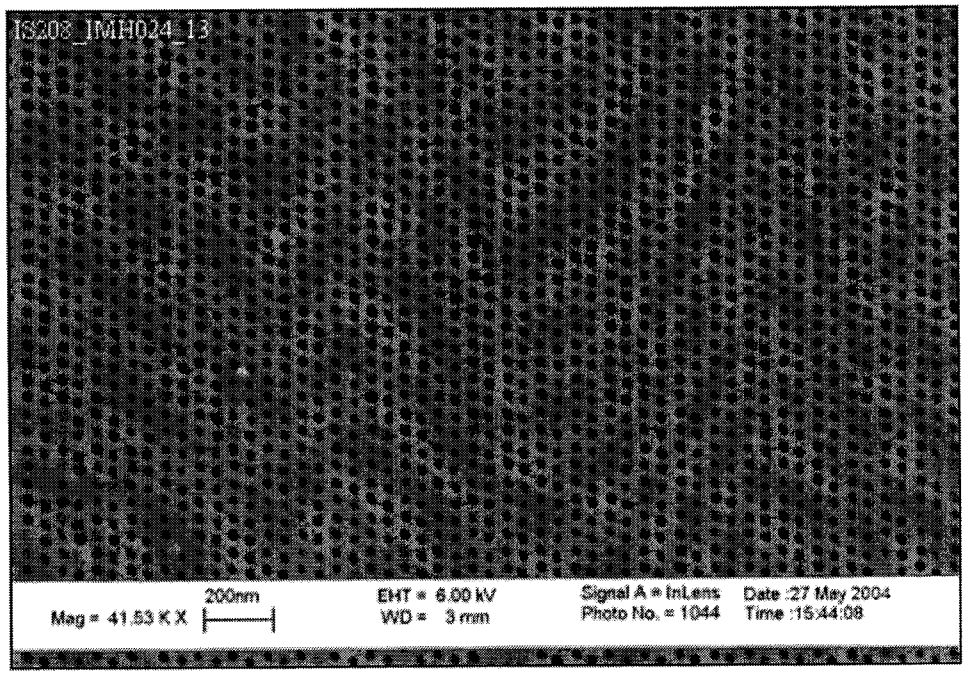

Image A.96 Imprinted holes of pattern 13 on sample IS208. The following parameters were used: single layer of PMMA, model 20 imprinting press, imprinter IMH024 (29.5 fC point dose), regulator pressure of 40 psi, and the separation temperature was 36.5°C.

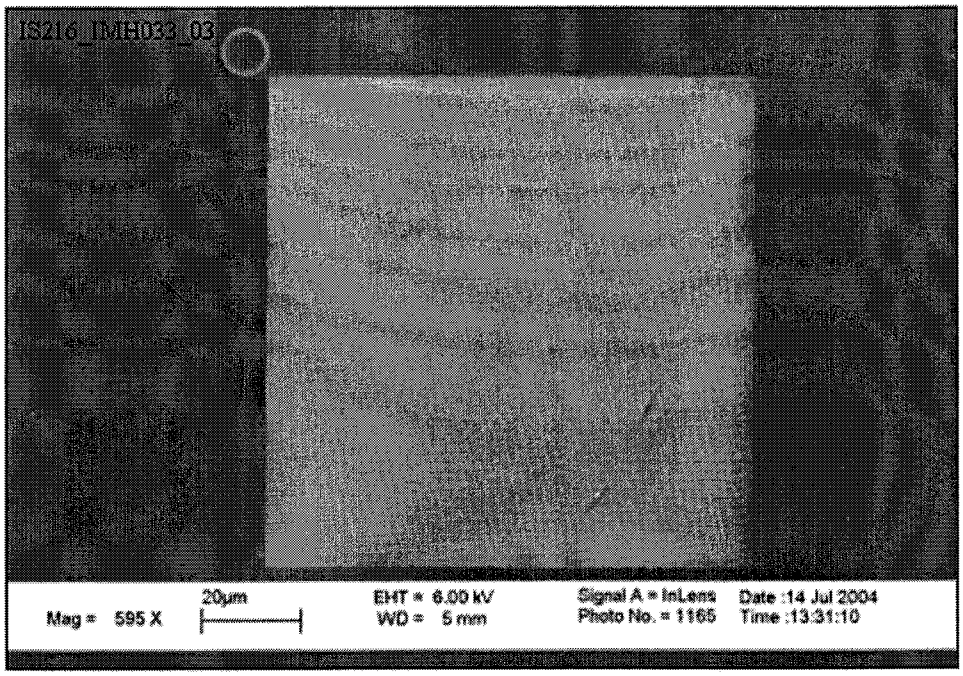

Image A.97 An overview of pattern 3 on sample IS216. The following parameters were used: single layer of PMMA, model 20 imprinting press, imprinter IMH033 (28.5 fC point dose), regulator pressure of 40 psi, and the separation temperature was 40°C.

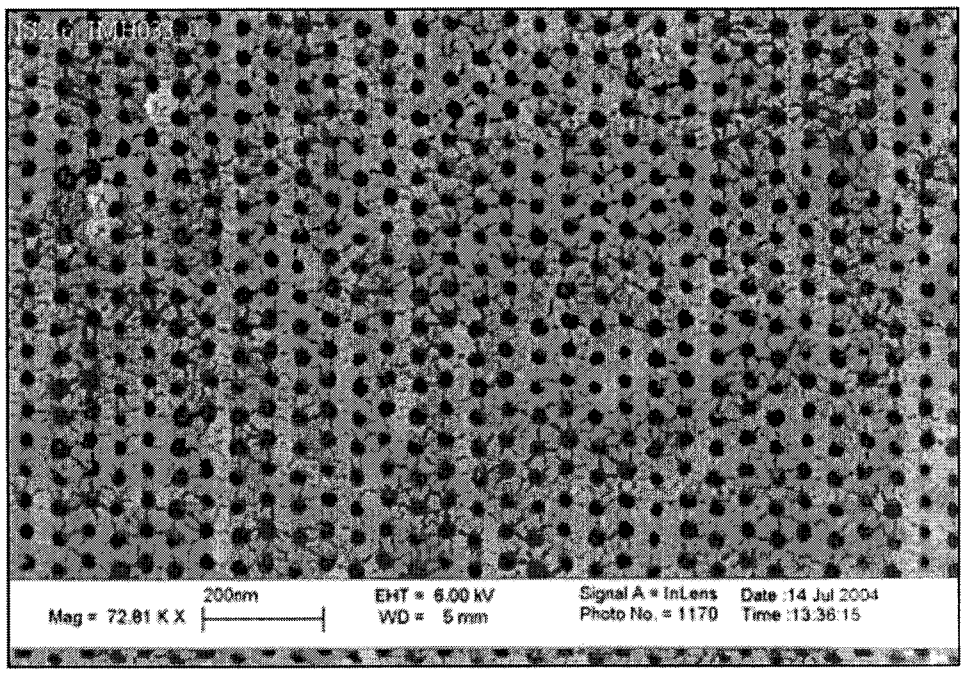

Image A.98 Imprinted holes of pattern 3 on sample IS216. The following parameters were used: single layer of PMMA, model 20 imprinting press, imprinter IMH033 (28.5 fC point dose), regulator pressure of 40 psi, and the separation temperature was 40°C.

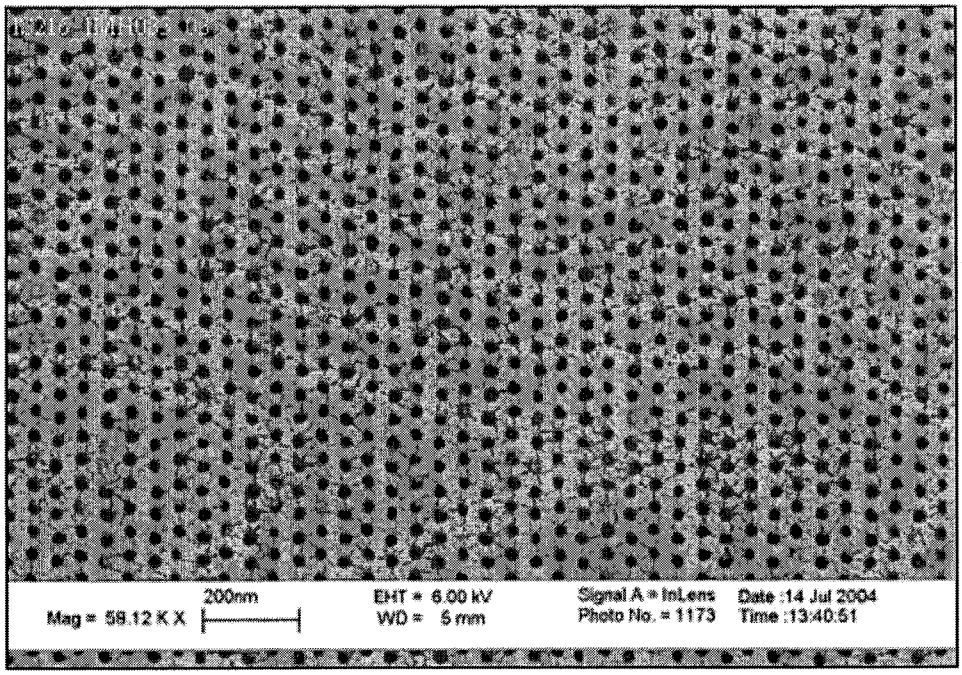

Image A.99 Imprinted holes of pattern 3 on sample IS216. The following parameters were used: single layer of PMMA, model 20 imprinting press, imprinter IMH033 (28.5 fC point dose), regulator pressure of 40 psi, and the separation temperature was 40°C.

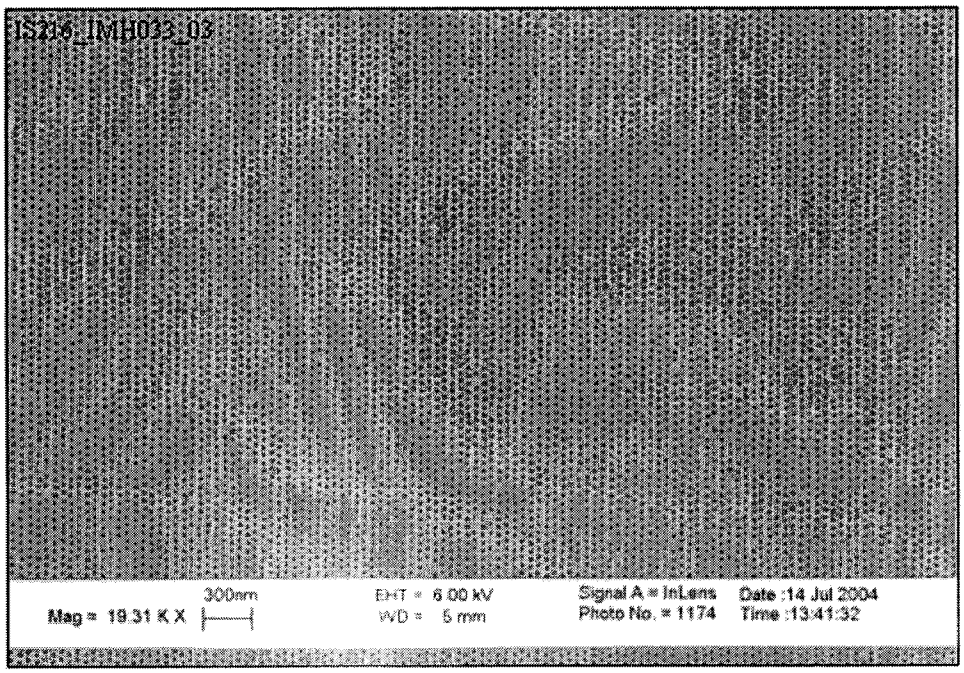

Image A.100 Imprinted holes of pattern 3 on sample IS216. The following parameters were used: single layer of PMMA, model 20 imprinting press, imprinter IMH033 (28.5 fC point dose), regulator pressure of 40 psi, and the separation temperature was 40°C.

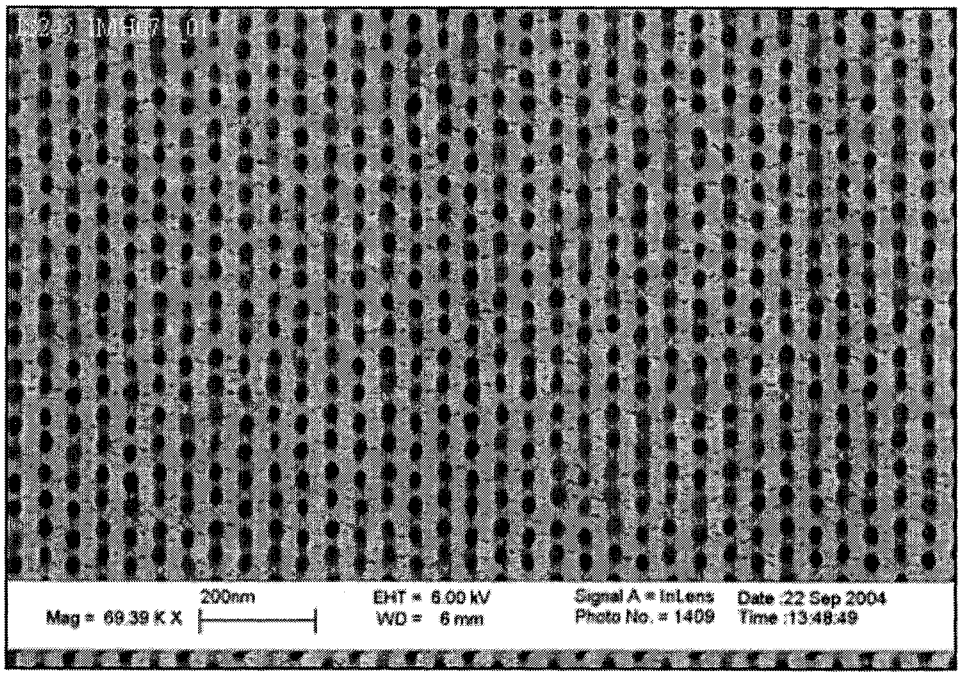

Image A.101 Imprinted holes of pattern 1 on sample IS245. The following parameters were used: single layer of PMMA, model 20 imprinting press, imprinter IMH070 (32 fC point dose), regulator pressure of 50 psi, and the separation temperature was 42.5°C.

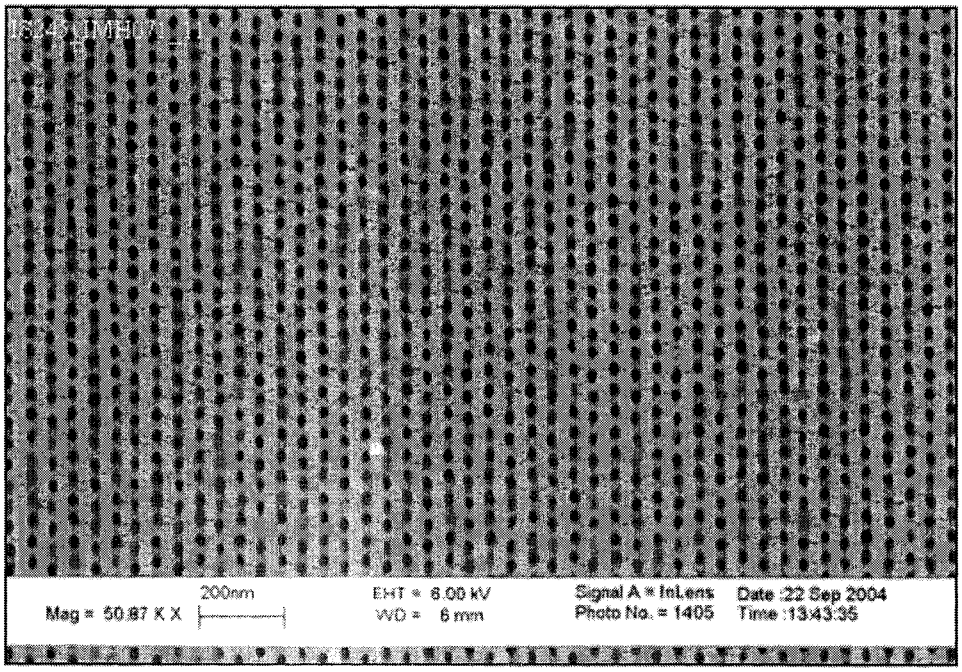

Image A.102 Imprinted holes of pattern 11 on sample IS245. The following parameters were used: single layer of PMMA, model 20 imprinting press, imprinter IMH071 (32 fC point dose), regulator pressure of 50 psi, and the separation temperature was 42.5°C.

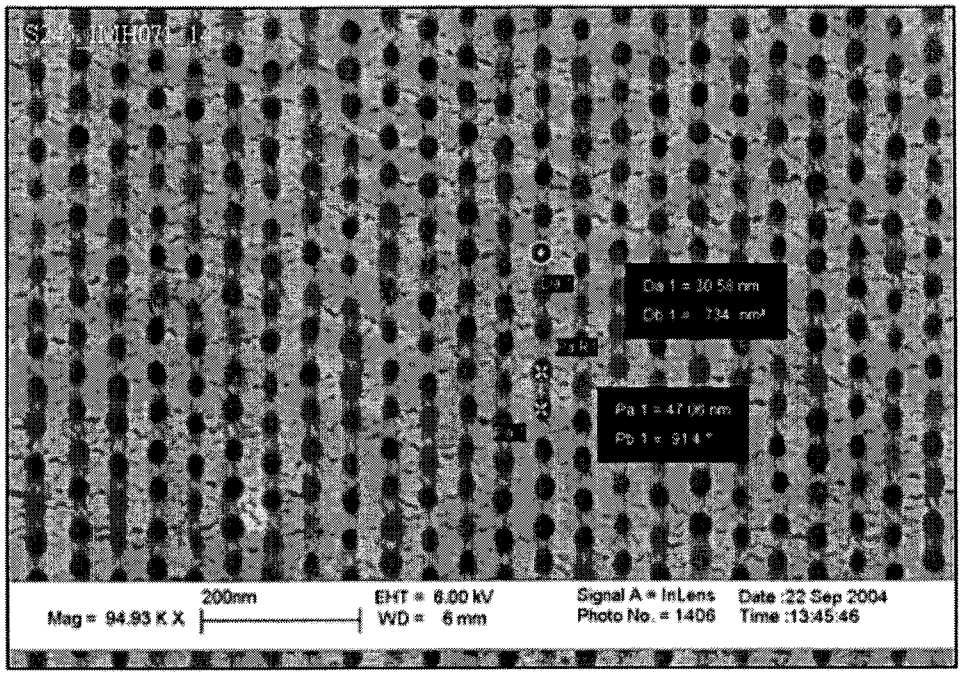

Image A.103 Imprinted holes of pattern 14 on sample IS245. The following parameters were used: single layer of PMMA, model 20 imprinting press, imprinter IMH071 (32 fC point dose), regulator pressure of 50 psi, and the separation temperature was 42.5°C.

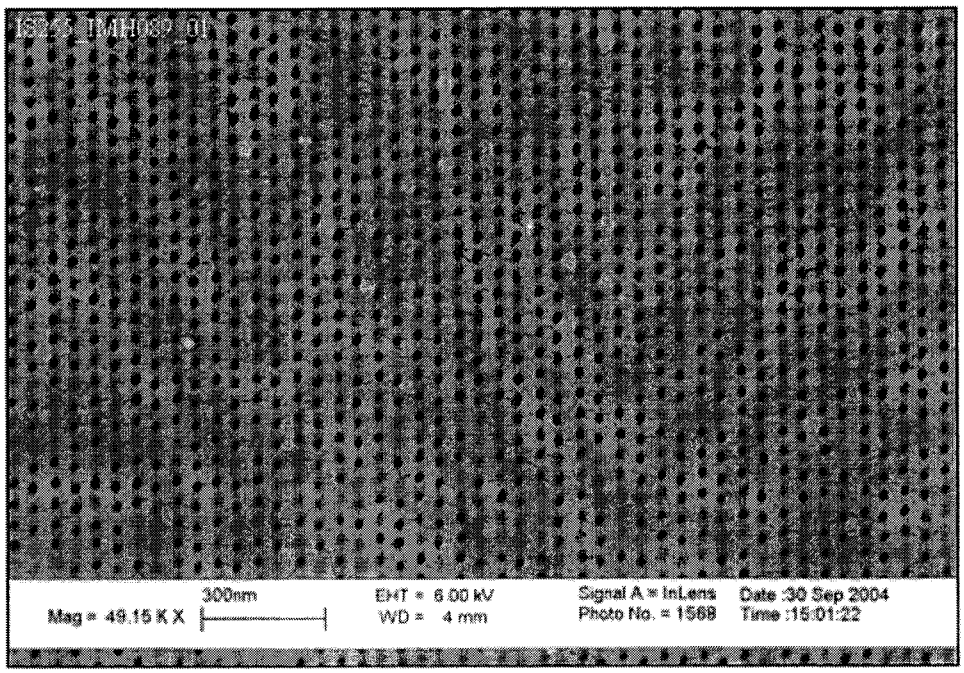

Image A.104 Imprinted holes of pattern 1 on sample IS255. The following parameters were used: single layer of PMMA, model 20 imprinting press, imprinter IMH089 (32 fC point dose), regulator pressure of 50 psi, and the separation temperature was 35°C.

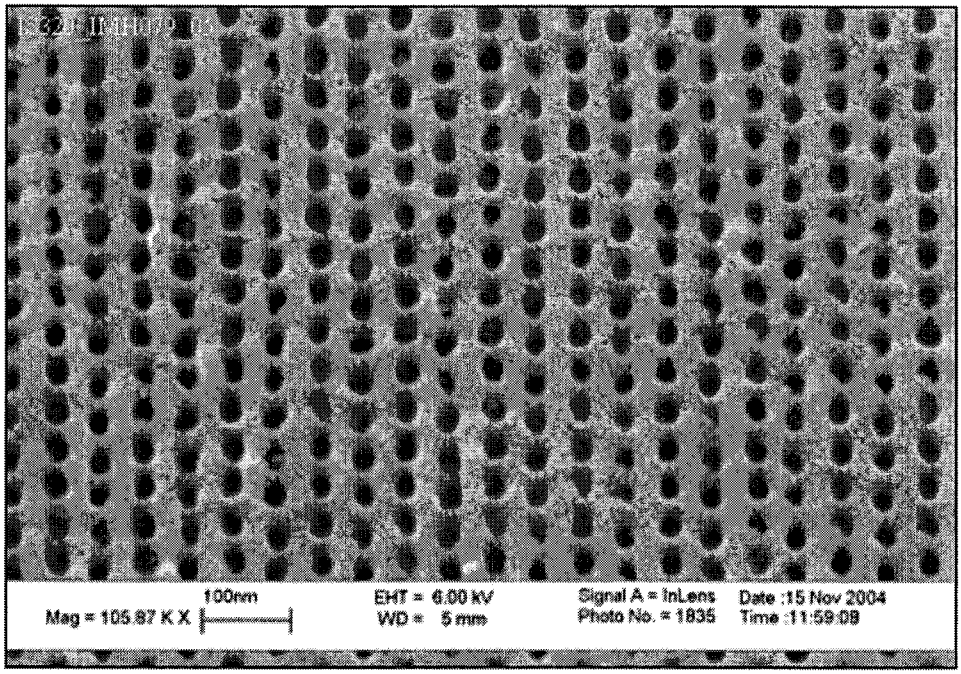

Image A.105 Imprinted holes of pattern 5 on sample IS320. The following parameters were used: single layer of PMMA, model 20 imprinting press, imprinter IMH079 (32 fC point dose), regulator pressure of 50 psi, and the separation temperature was 33.5°C.

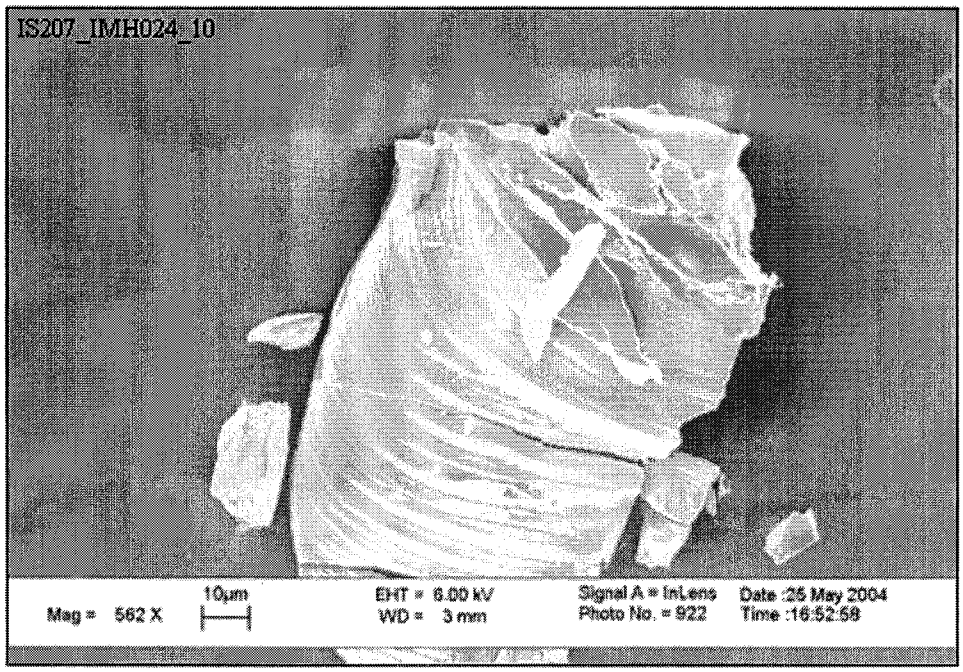

Image A.106 A piece of Si dust covering pattern 10 on sample IS207. The following parameters were used: single layer of PMMA, model 20 imprinting press, imprinter IMH024 (28.5 fC point dose), regulator pressure of 50 psi, and the separation temperature was 31.5°C.

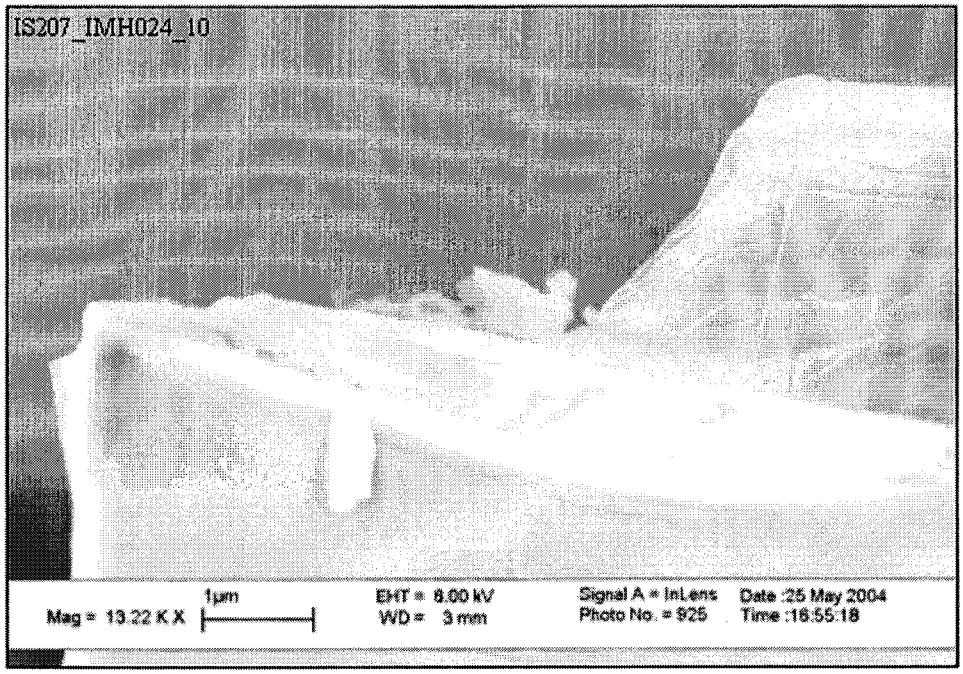

Image A.107 A piece of Si dust covering pattern 10 on sample IS207. The following parameters were used: single layer of PMMA, model 20 imprinting press, imprinter IMH024 (28.5 fC point dose), regulator pressure of 50 psi, and the separation temperature was 31.5°C.

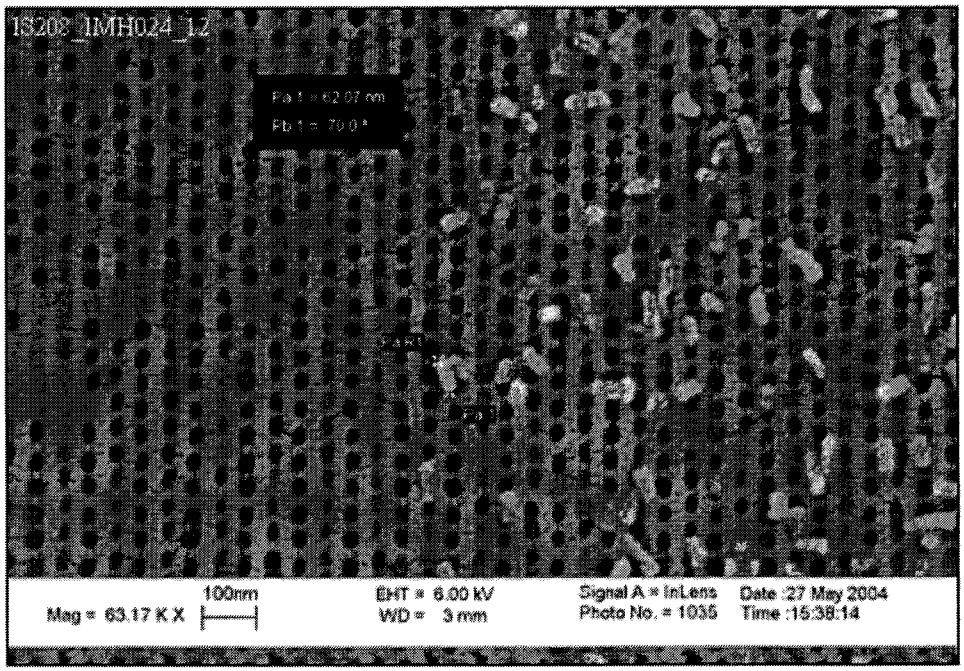

Image A.108 Broken pillars of Imprinter IMH024 seen in pattern 12 on imprinter IS208. The following parameters were used: single layer of PMMA, model 20 imprinting press, imprinter IMH024 (30 fC point dose), regulator pressure of 40 psi, and the separation temperature was 36.5°C.

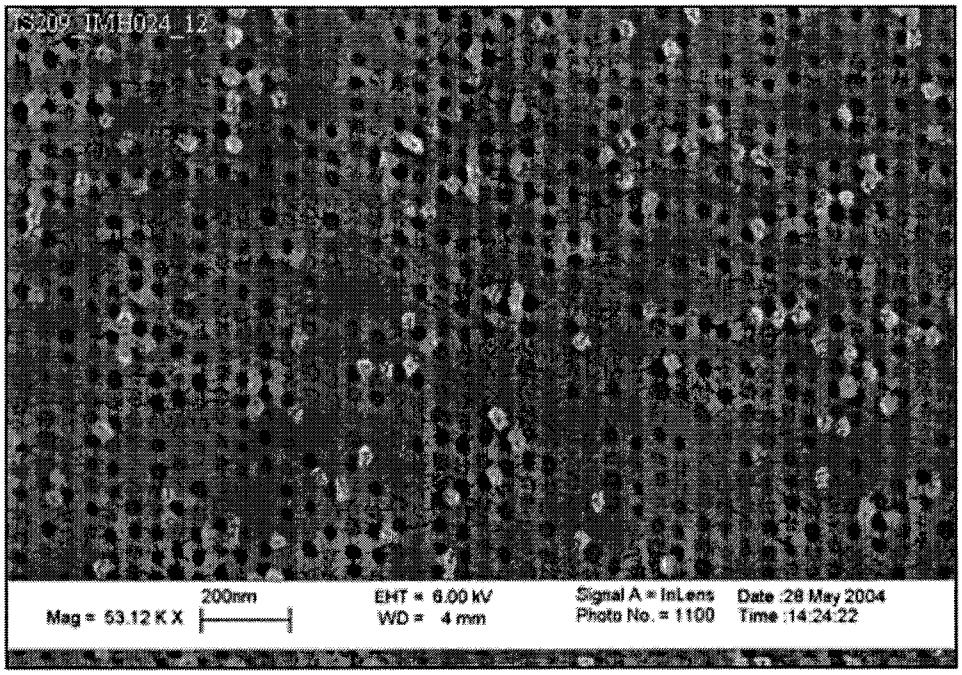

Image A.109 Broken pillars of Imprinter IMH024 seen in pattern 12 on imprinter IS209. The following parameters were used: single layer of PMMA, model 20 imprinting press, imprinter IMH024 (30 fC point dose), regulator pressure of 40 psi, and the separation temperature was 34.5°C.

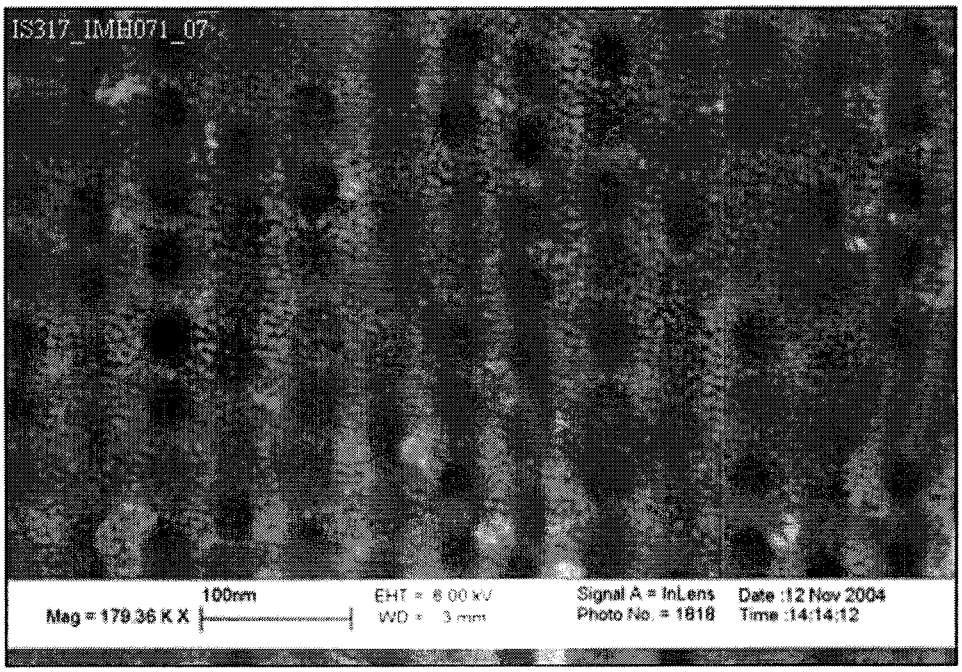

Image A.110 An area of pattern 7 on sample IS317 with a shallow depth imprint. The following parameters were used: single layer of PMMA, model 20 imprinting press, imprinter IMH071 (32 fC point dose), regulator pressure of 50 psi, and the separation temperature was 25.5°C.

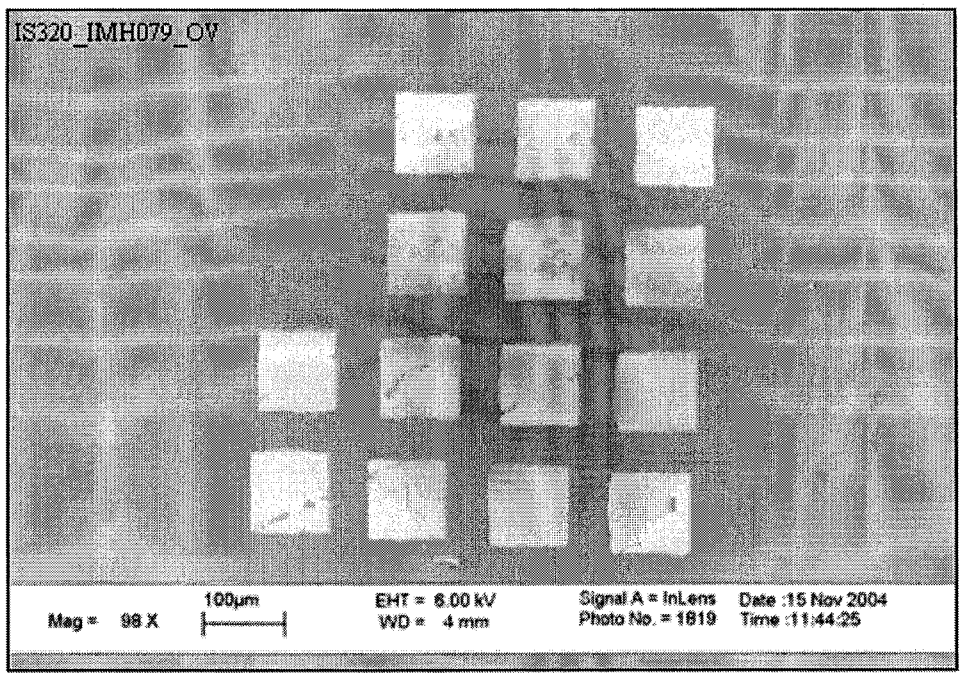

Image A.111 The image displays the torn away PMMA of all of the patterns on sample IS320. The following parameters were used: single layer of PMMA, model 20 imprinting press, imprinter IMH079 (32 fC point dose), regulator pressure of 50 psi, and the separation temperature was 33.5°C.

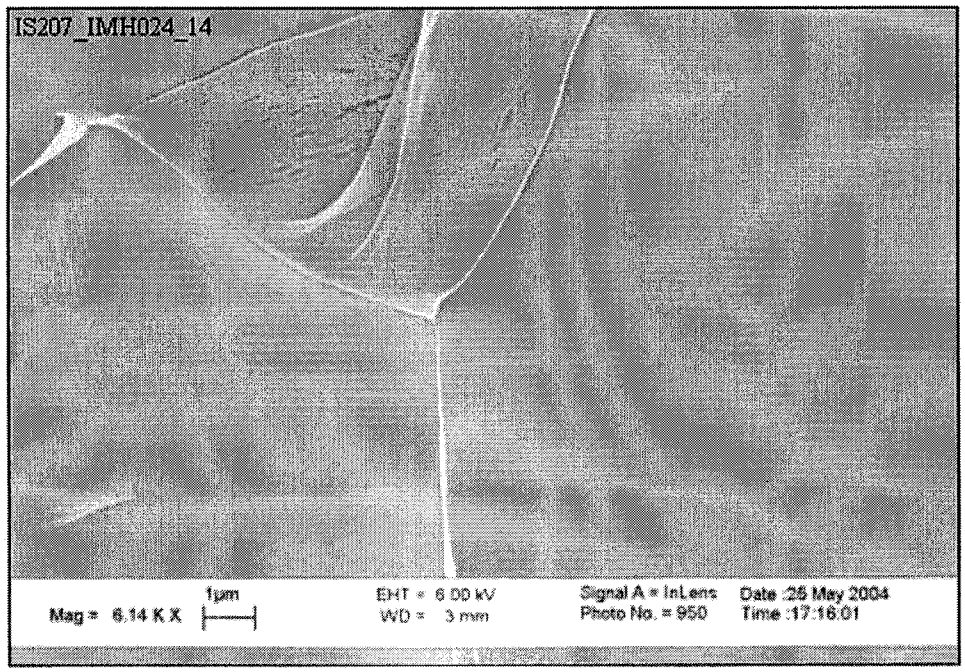

Image A.112 The image displays a portion of PMMA from pattern 14 on sample IS207 torn away. The following parameters were used: single layer of PMMA, model 20 imprinting press, imprinter IMH024 (29 fC point dose), regulator pressure of 80 psi, and the separation temperature was 31.5°C.

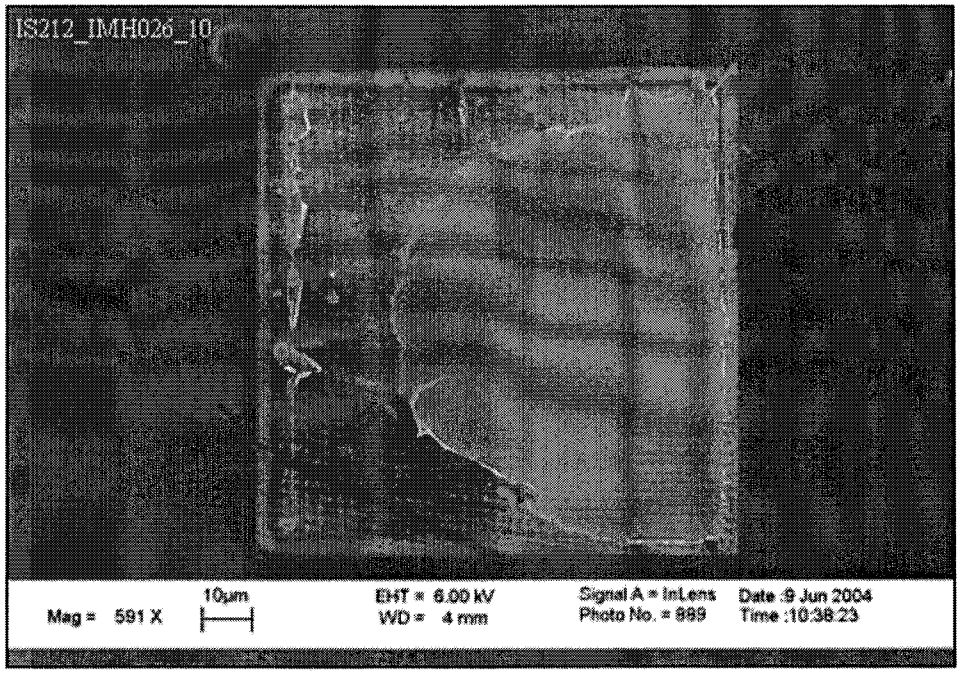

Image A.113 The image displays half of the PMMA from pattern 10 on sample IS212 ripped away. The following parameters were used: single layer of PMMA, model 20 imprinting press, imprinter IMH026 (28.5 fC point dose), regulator pressure of 40 psi, and the separation temperature was 40.5°C.

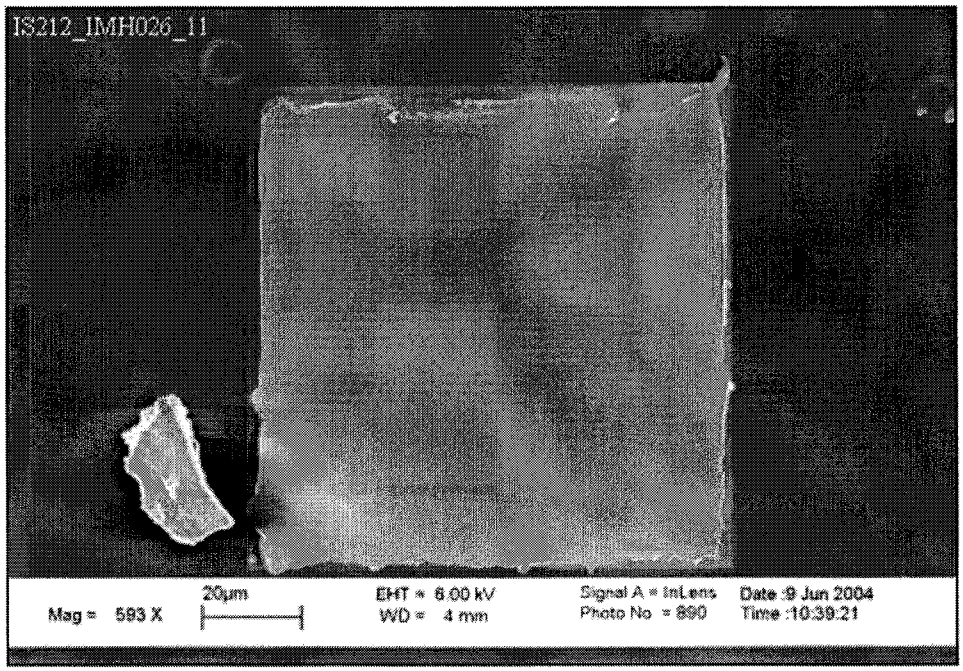

Image A.114 The image displays almost all of the PMMA from pattern 11 on sample IS212 ripped away. The following parameters were used: single layer of PMMA, model 20 imprinting press, imprinter IMH026 (30.5 fC point dose), regulator pressure of 40 psi, and the separation temperature was 40.5°C.

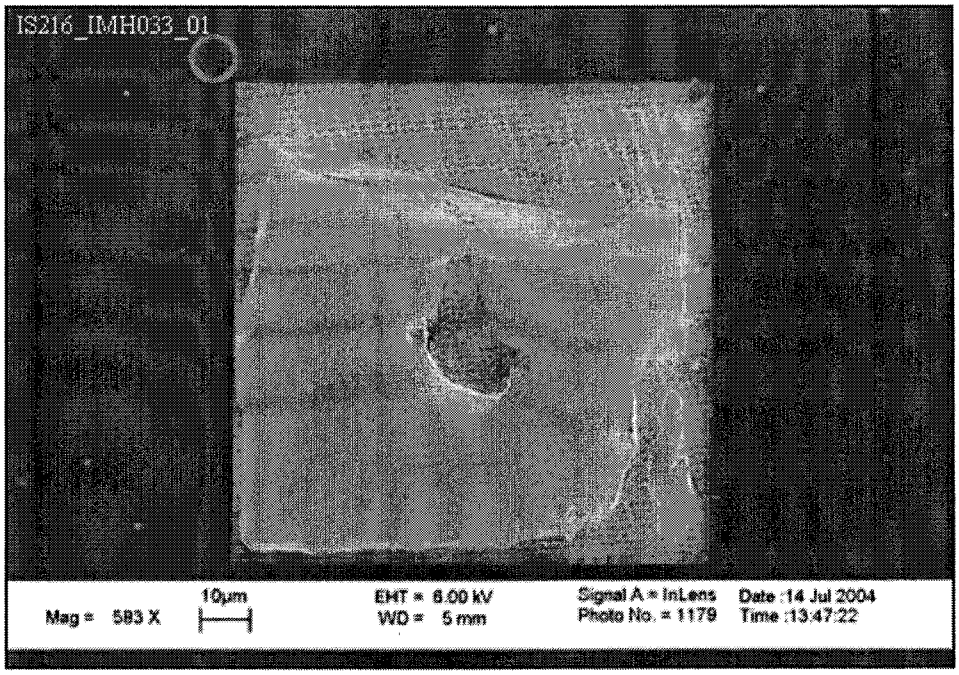

Image A.115 The image displays more than half of the PMMA from pattern 1 on sample IS216 torn away. The following parameters were used: single layer of PMMA, model 20 imprinting press, imprinter IMH033 (28.5 fC point dose), regulator pressure of 40 psi, and the separation temperature was 40°C.

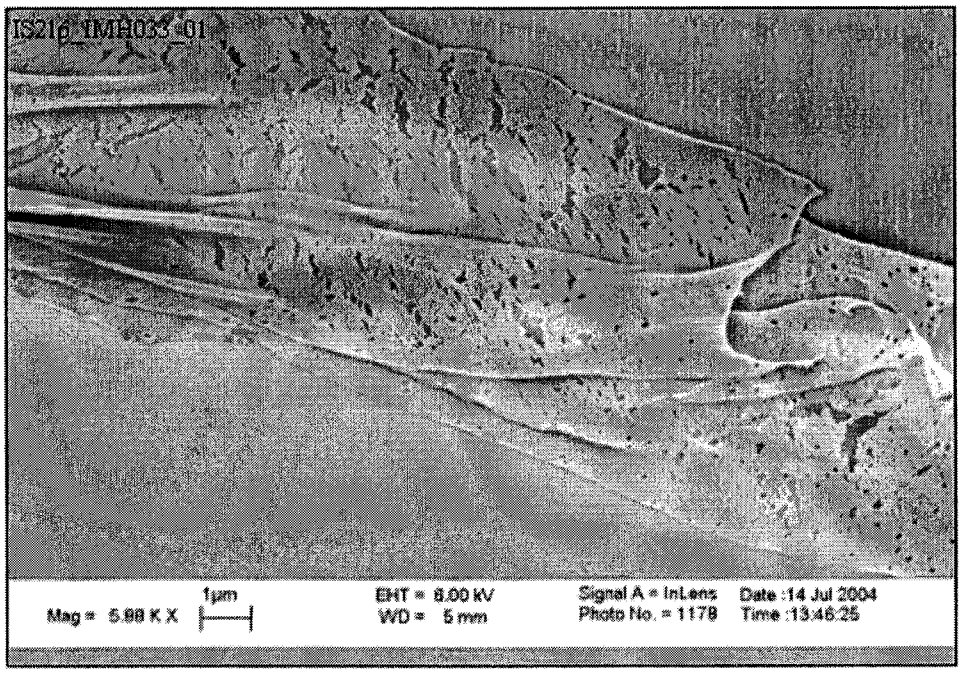

Image A.116 The image displays the PMMA from pattern 1 on sample IS216 ripped away. The holes of the pattern can be seen on and above the torn PMMA. The following parameters were used: single layer of PMMA, model 20 imprinting press, imprinter IMH033 (28.5 fC point dose), regulator pressure of 40 psi, and the separation temperature was 40°C.

A.2.2 Type 1 Bilayer Coating

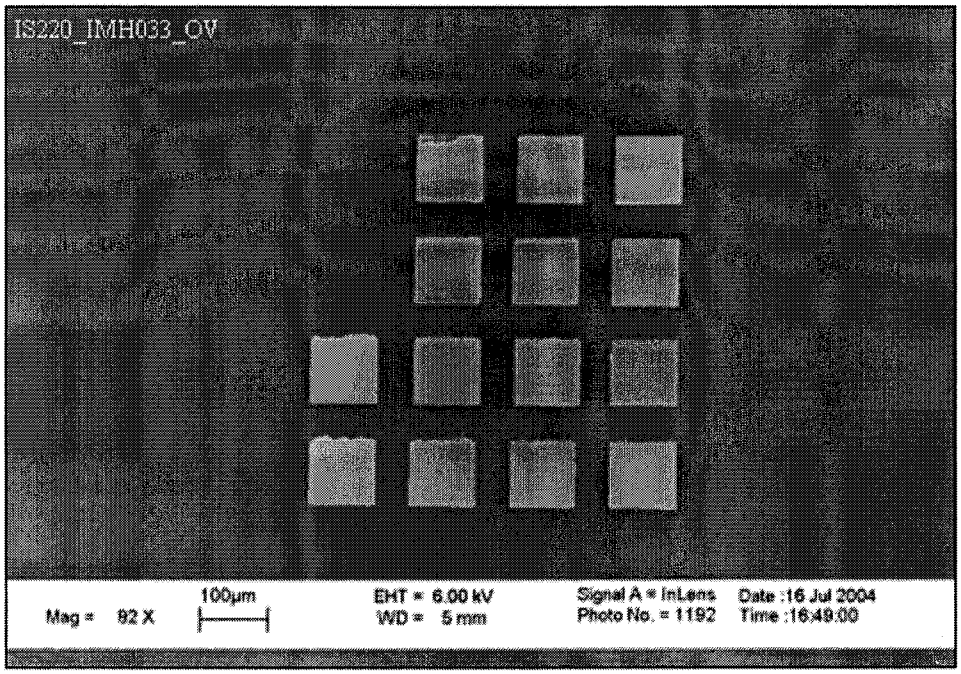

Image A.117 The image displays torn resist from all of the patterns on sample IS220. The following parameters were used: type 1 bilayer coating, model 20 imprinting press, imprinter IMH033 (28.5 fC point dose), regulator pressure of 70 psi, and the separation temperature was 40.5°C.

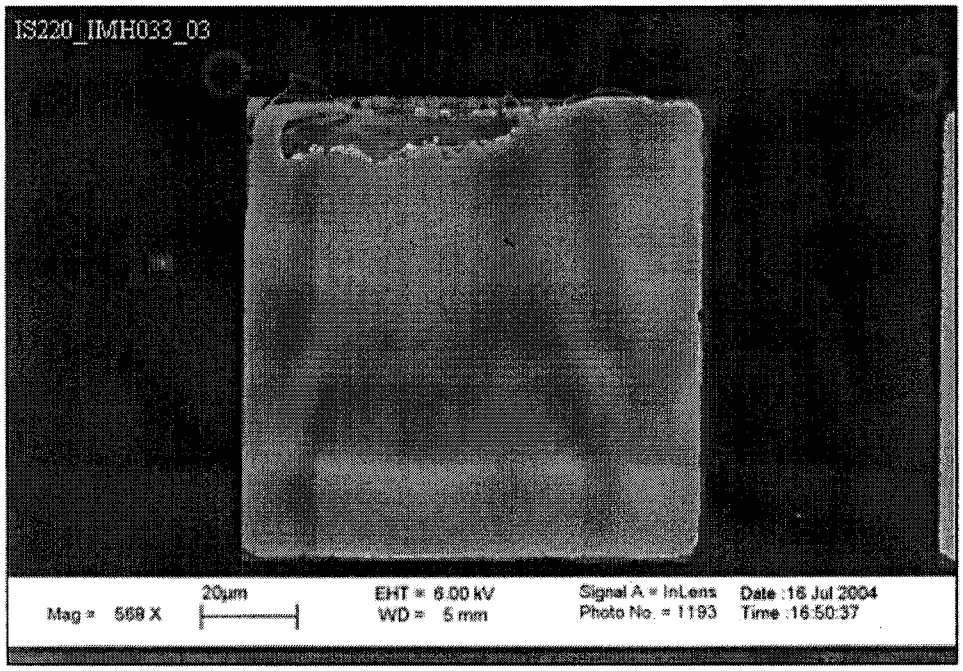

Image A.118 The image displays torn resist from pattern 3 on sample IS220. The following parameters were used: type 1 bilayer coating, model 20 imprinting press, imprinter IMH033 (28.5 fC point dose), regulator pressure of 70 psi, and the separation temperature was 40.5°C.

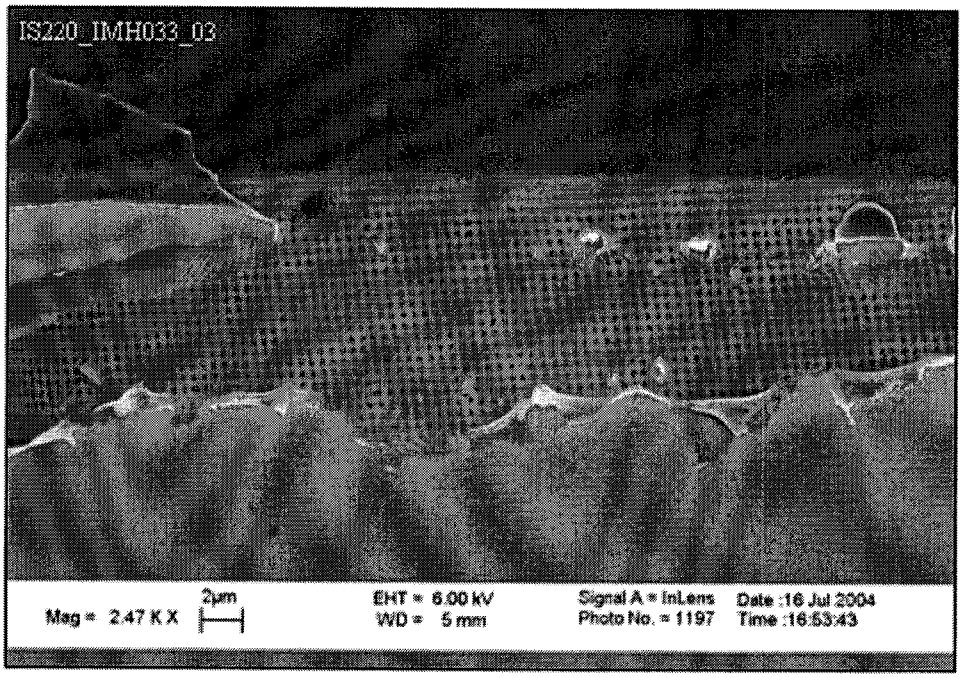

Image A.119 The image displays a small portion of remaining resist at the top of pattern 3 on sample IS220. The following parameters were used: type 1 bilayer coating, model 20 imprinting press, imprinter IMH033 (28.5 fC point dose), regulator pressure of 70 psi, and the separation temperature was 40.5°C.

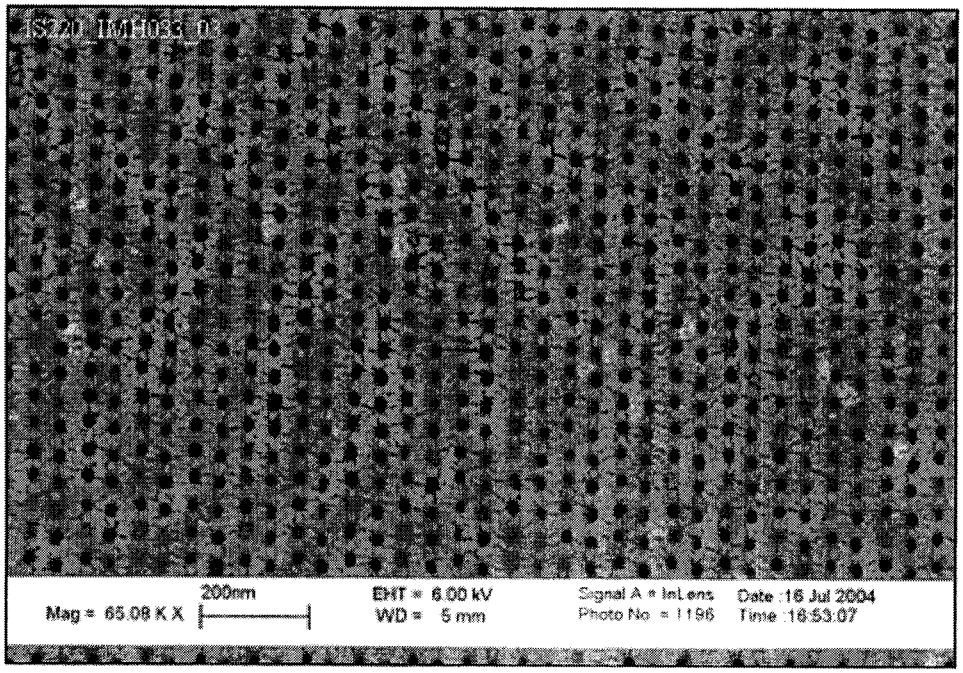

Image A.120 The image displays imprinted holes of pattern 3 on sample IS220. The following parameters were used: type 1 bilayer coating, model 20 imprinting press, imprinter IMH033 (28.5 fC point dose), regulator pressure of 70 psi, and the separation temperature was 40.5°C.

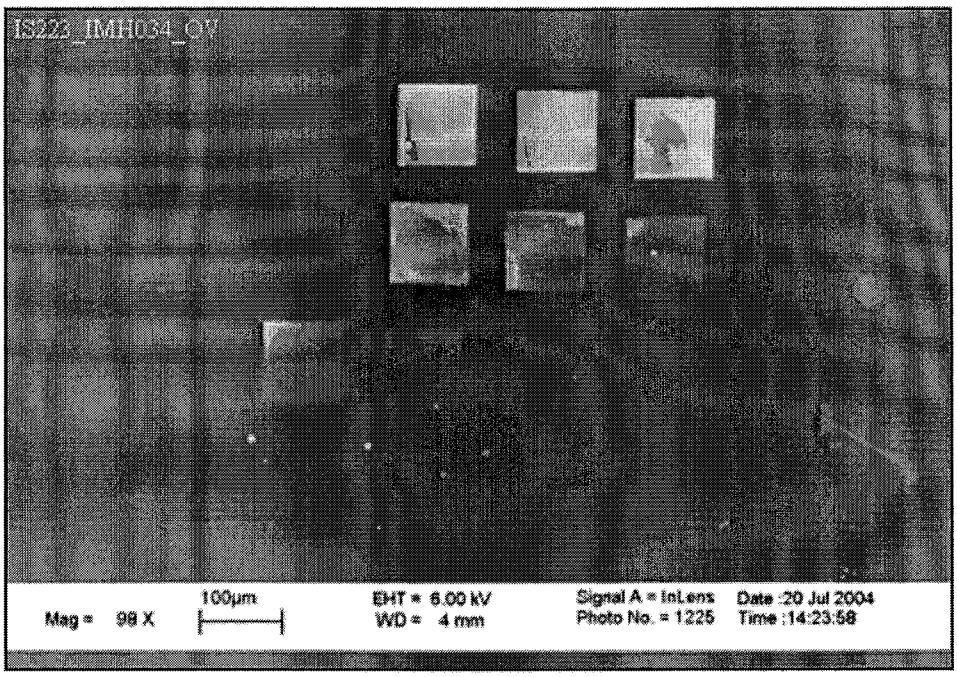

Image A.121 The image displays all of the patterns on sample IS223. The following parameters were used: type 1 bilayer coating, model 20 imprinting press, imprinter IMH034 (28.5 fC point dose), regulator pressure of 55 psi, and the separation temperature was 41.5°C.

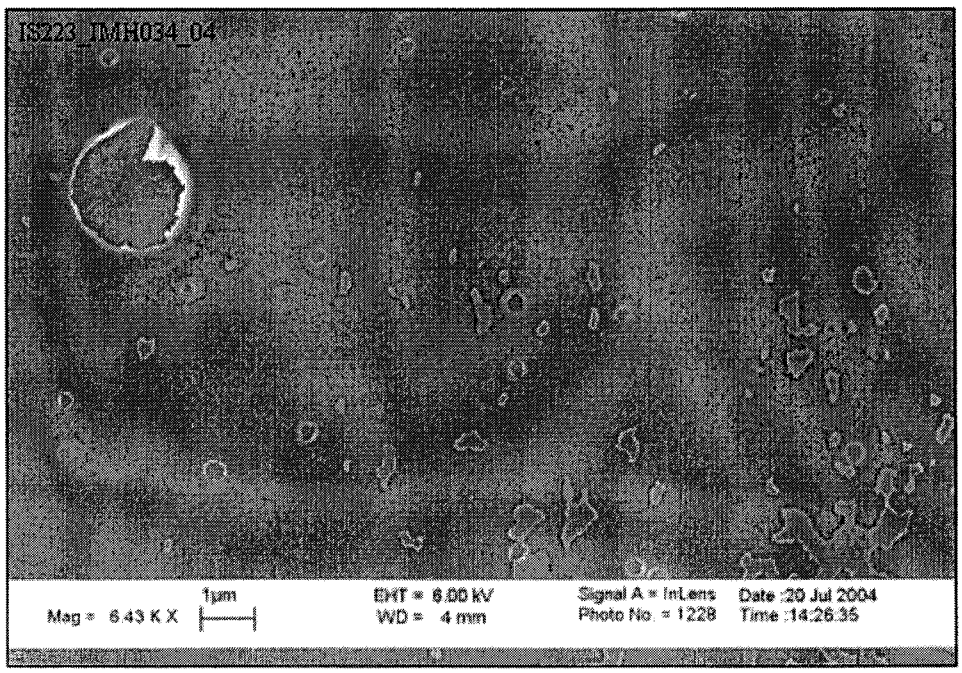

Image A.122 The image displays the top layer of resist torn up in places of pattern 4 on sample IS223. The following parameters were used: type 1 bilayer coating, model 20 imprinting press, imprinter IMH034 (28.5 fC point dose), regulator pressure of 55 psi, and the separation temperature was 41.5°C.

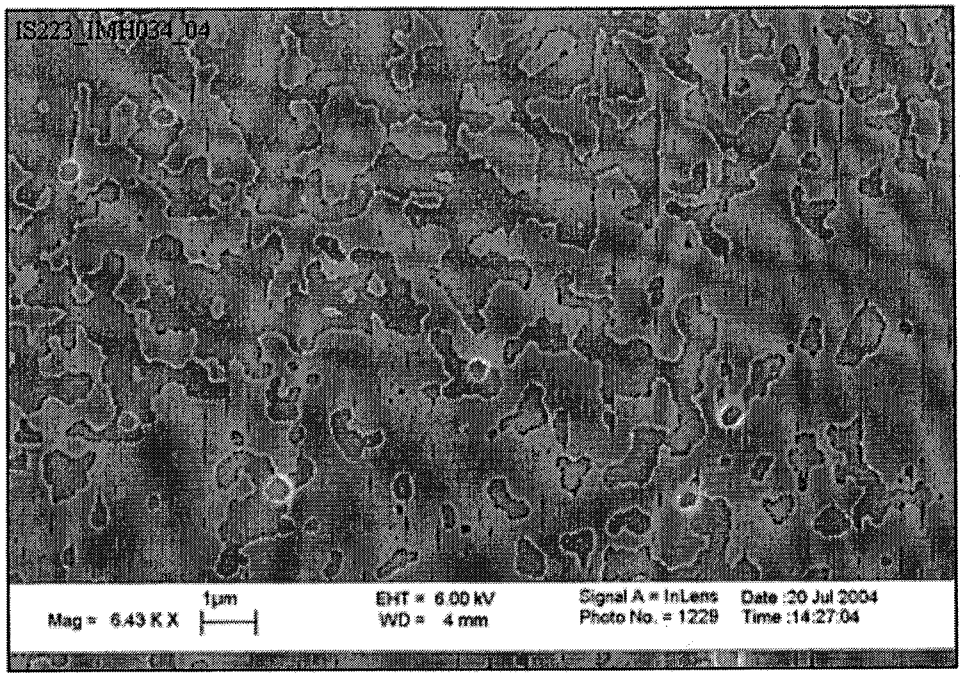

Image A.123 The image displays the top layer of resist torn up in places of pattern 4 on sample IS223. The following parameters were used: type 1 bilayer coating, model 20 imprinting press, imprinter IMH034 (28.5 fC point dose), regulator pressure of 55 psi, and the separation temperature was 41.5°C.

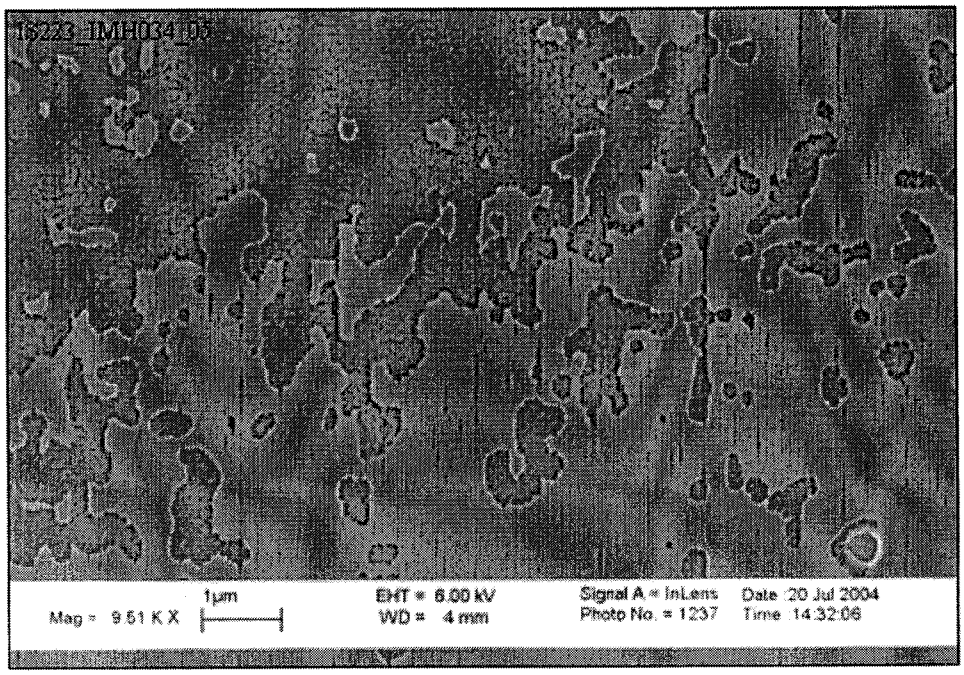

Image A.124 The image displays the top layer of resist torn up in places of pattern 5 on sample IS223. The following parameters were used: type 1 bilayer coating, model 20 imprinting press, imprinter IMH034 (28.5 fC point dose), regulator pressure of 55 psi, and the separation temperature was 41.5°C.

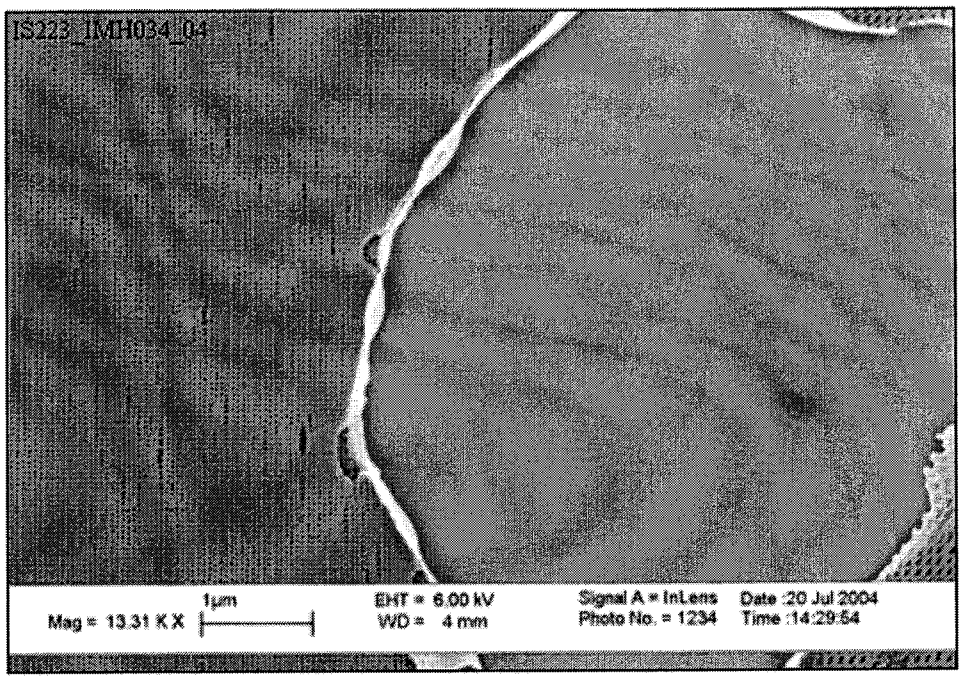

Image A.125 The image displays a circular area of resist torn from pattern 4 on sample IS223. The following parameters were used: type 1 bilayer coating, model 20 imprinting press, imprinter IMH034 (28.5 fC point dose), regulator pressure of 55 psi, and the separation temperature was 41.5°C.

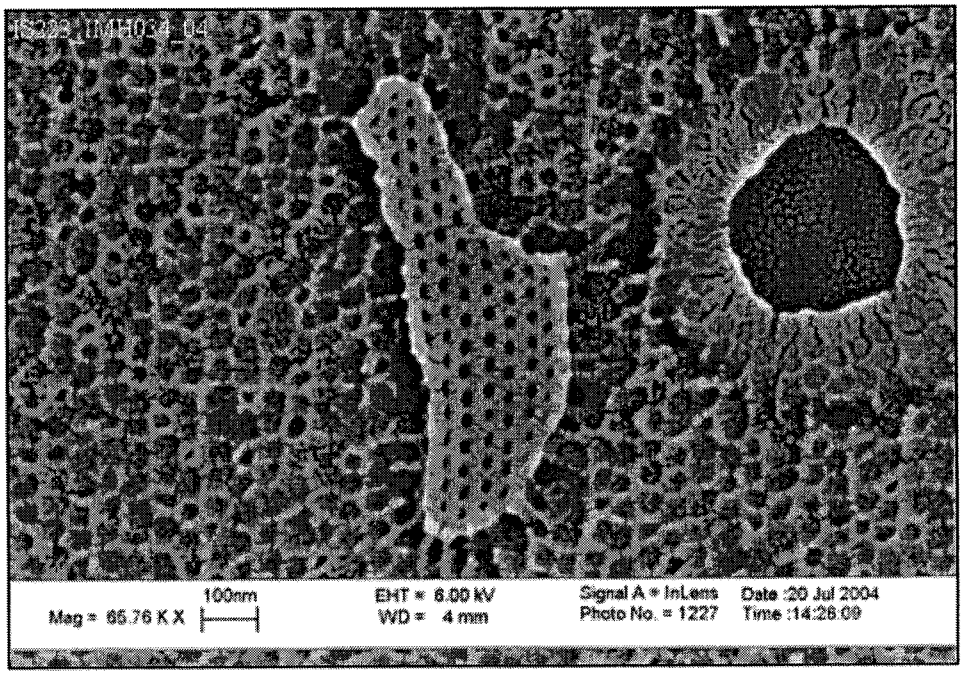

Image A.126 The image displays a remaining piece of the top layer of resist to the left and circular area of both layers torn up to the right in pattern 4 on sample IS223. The following parameters were used: type 1 bilayer coating, model 20 imprinting press, imprinter IMH034 (28.5 fC point dose), regulator pressure of 55 psi, and the separation temperature was 41.5°C.

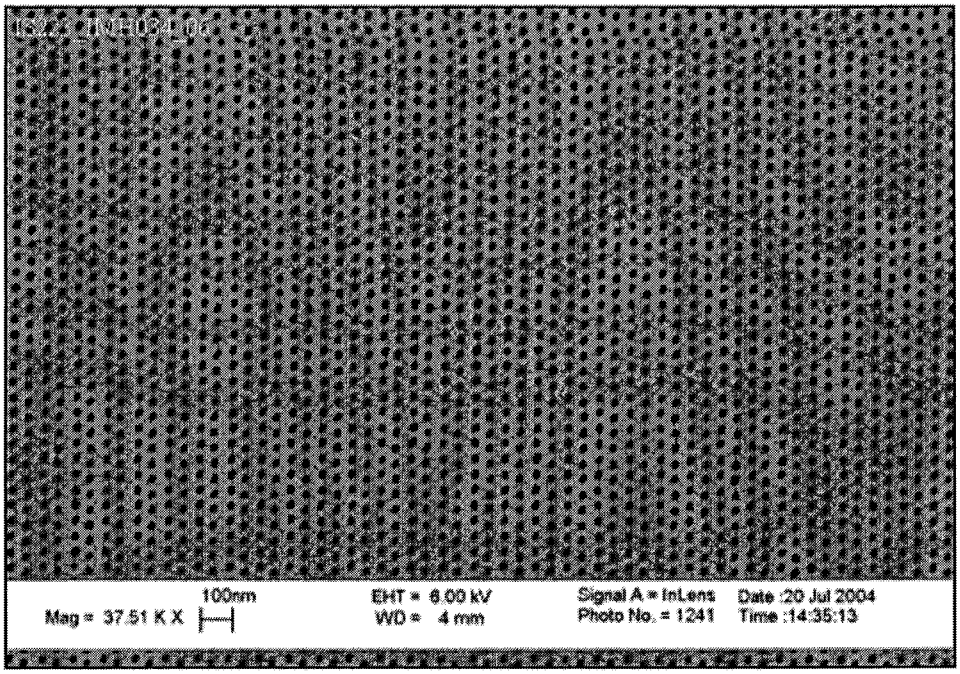

Image A.127 The image displays a defect free area of imprinted holes of pattern 6 on sample IS223. The following parameters were used: type 1 bilayer coating, model 20 imprinting press, imprinter IMH034 (28.5 fC point dose), regulator pressure of 55 psi, and the separation temperature was 41.5°C.

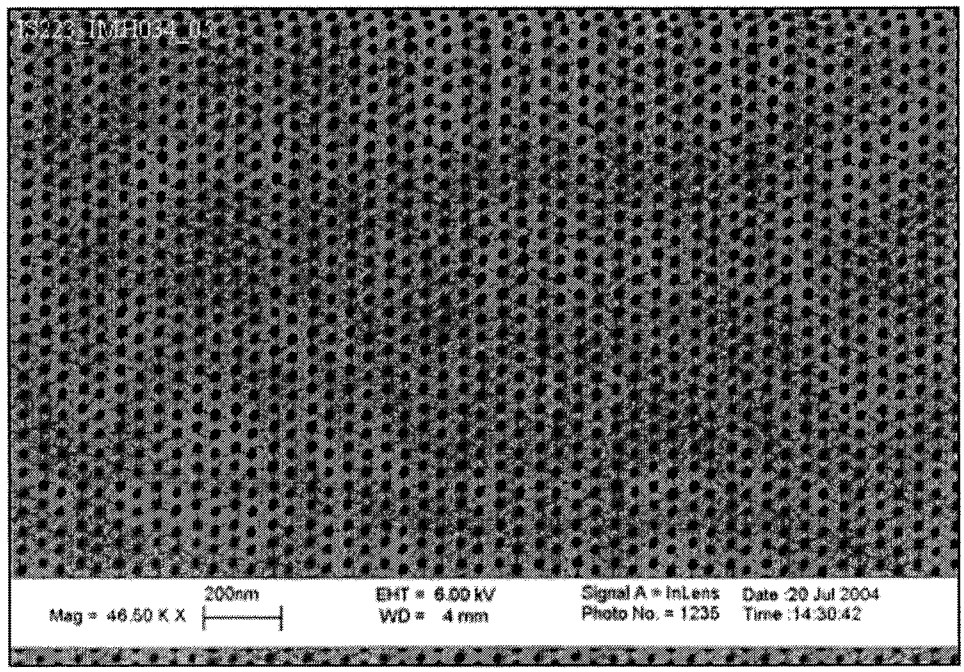

Image A.128 The image displays a defect free area of imprinted holes of pattern 5 on sample IS223. The following parameters were used: type 1 bilayer coating, model 20 imprinting press, imprinter IMH034 (28.5 fC point dose), regulator pressure of 55 psi, and the separation temperature was 41.5°C.

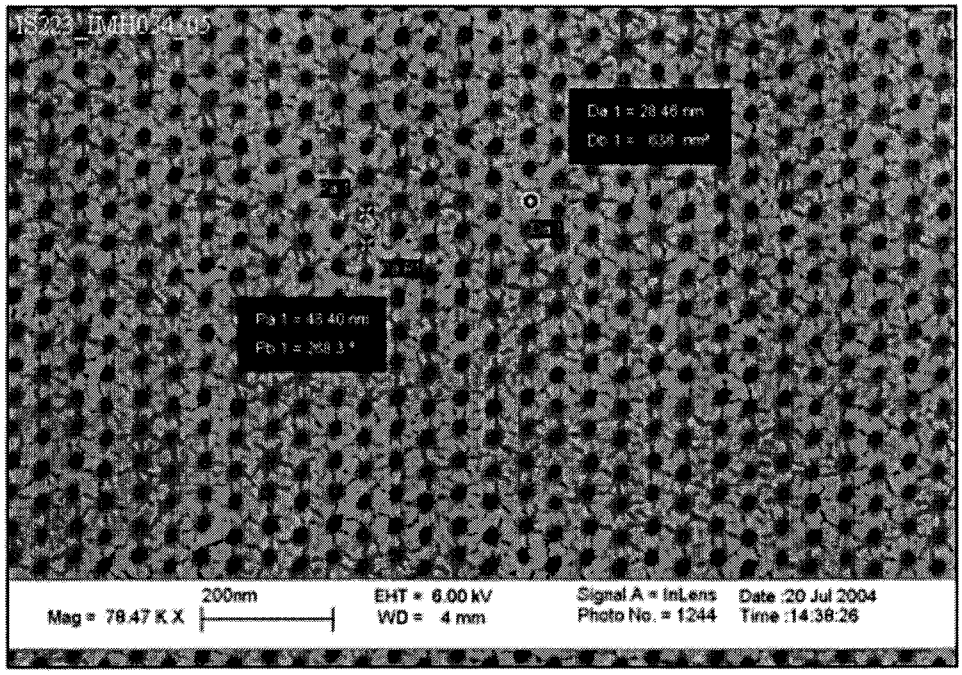

Image A.129 The image displays the measured hole diameter and pitch of pattern 5 on sample IS223. The following parameters were used: type 1 bilayer coating, model 20 imprinting press, imprinter IMH034 (28.5 fC point dose), regulator pressure of 55 psi, and the separation temperature was 41.5°C.

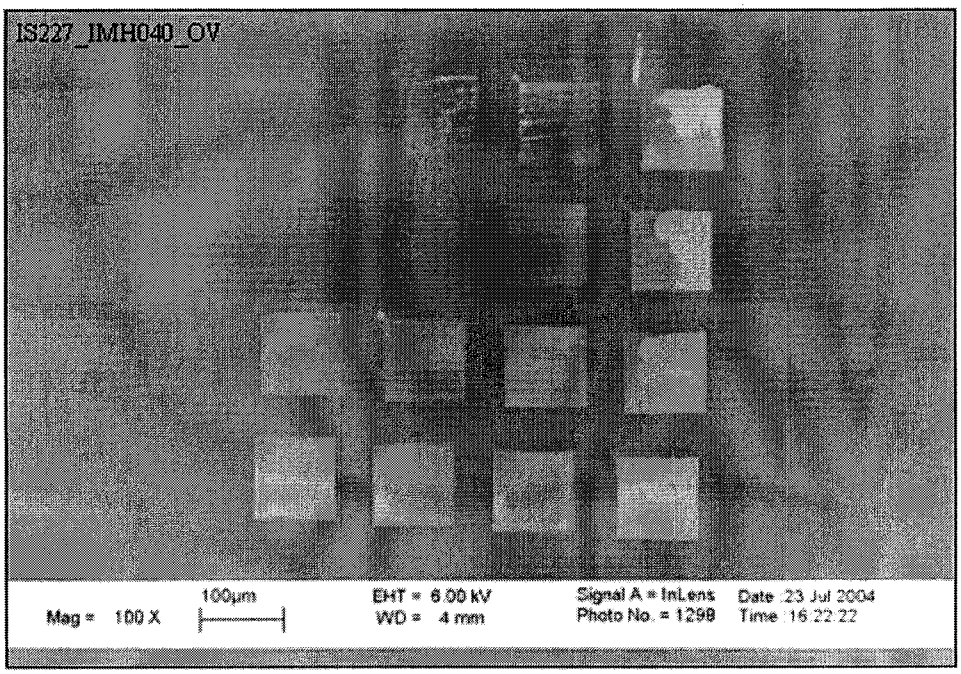

Image A.130 The image displays an overview of all of the patterns on sample IS227. The following parameters were used: type 1 bilayer coating, model 20 imprinting press, imprinter IMH040 (28.5 fC point dose), regulator pressure of 40 psi, and the separation temperature was 41°C.

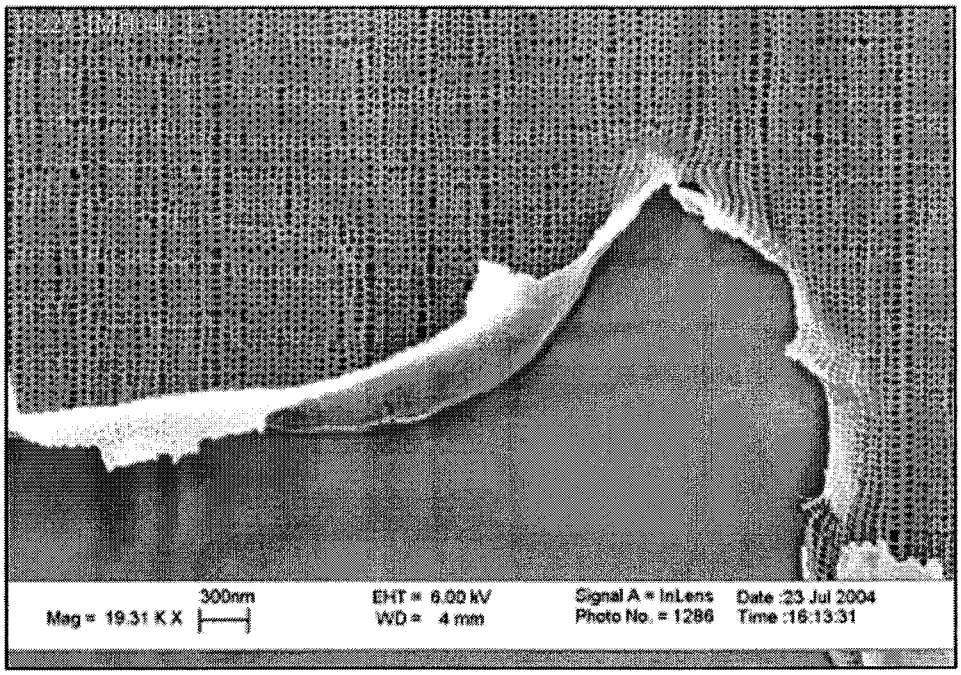

Image A.131 The image displays ripped resist of pattern 13 on sample IS227. The following parameters were used: type 1 bilayer coating, model 20 imprinting press, imprinter IMH040 (28.5 fC point dose), regulator pressure of 40 psi, and the separation temperature was 41°C.

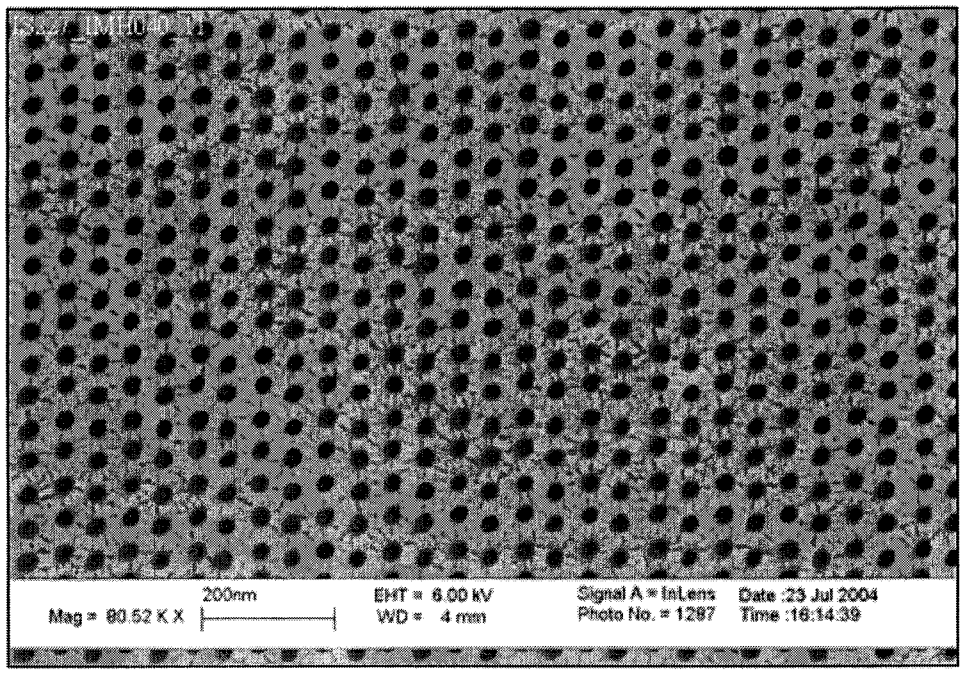

Image A.132 The image displays an area of the pattern 11 on sample IS227 containing defect free imprinted holes. The following parameters were used: type 1 bilayer coating, model 20 imprinting press, imprinter IMH040 (28.5 fC point dose), regulator pressure of 40 psi, and the separation temperature was 41°C.

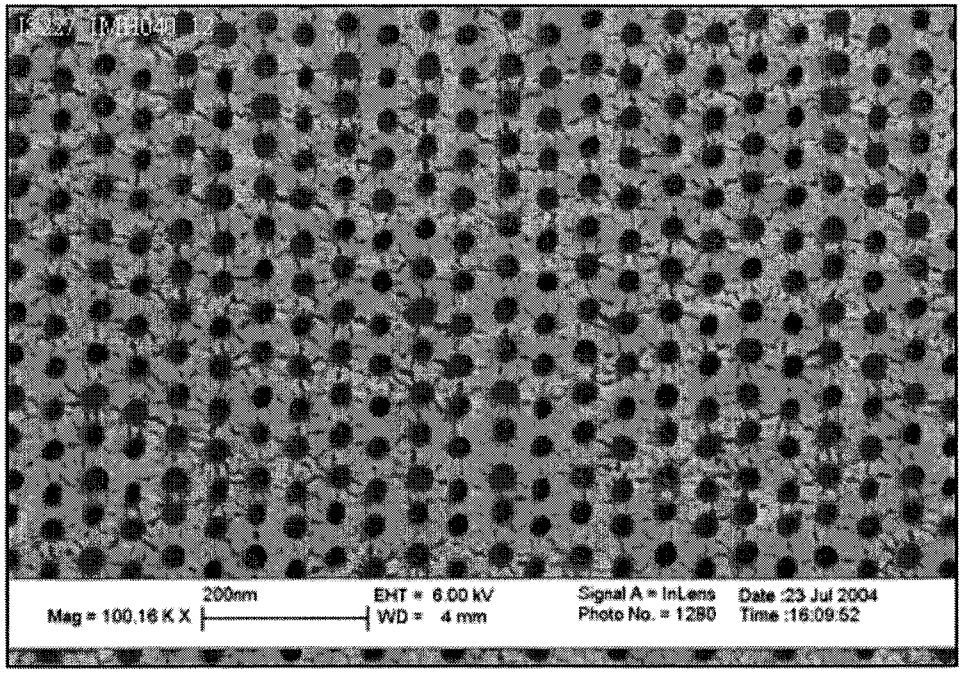

Image A.133 The image displays an area of the pattern 12 on sample IS227 containing defect free imprinted holes. The following parameters were used: type 1 bilayer coating, model 20 imprinting press, imprinter IMH040 (28.5 fC point dose), regulator pressure of 40 psi, and the separation temperature was 41°C.

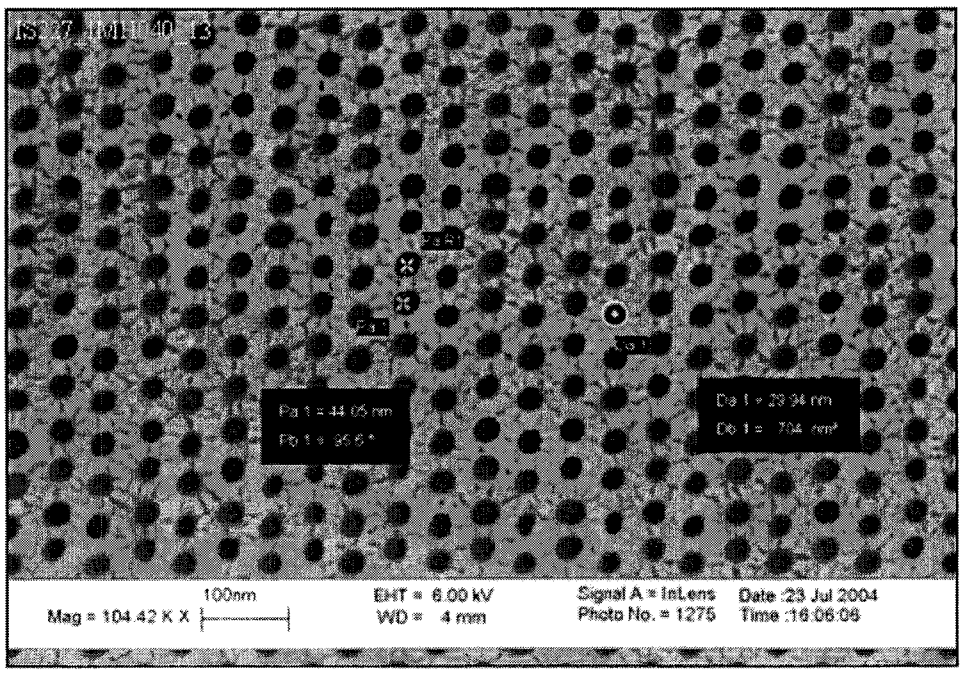

Image A.134 The image displays the measured hole diameter and pitch of pattern 13 on sample IS227. The following parameters were used: type 1 bilayer coating, model 20 imprinting press, imprinter IMH040 (28.5 fC point dose), regulator pressure of 40 psi, and the separation temperature was 41°C.

A.2.3 Type 2 Bilayer Coating

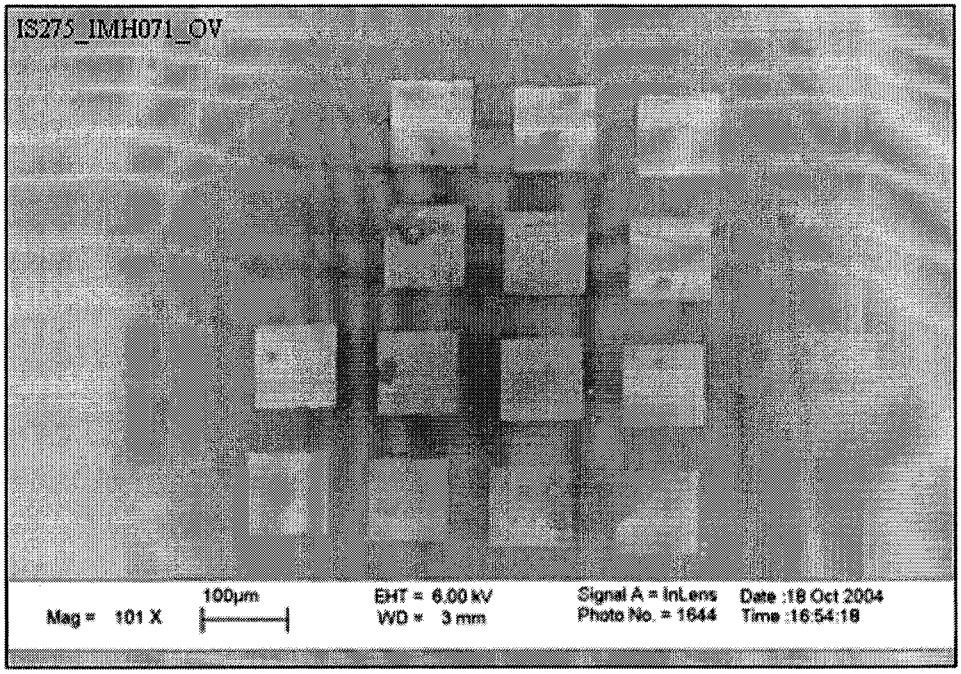

Image A.135 The image displays an overview of the patterns on sample IS275. The following parameters were used: type 2 bilayer coating, model 20 imprinting press, imprinter IMH071 (32 fC point dose), regulator pressure of 50 psi, and the separation temperature was 35°C.

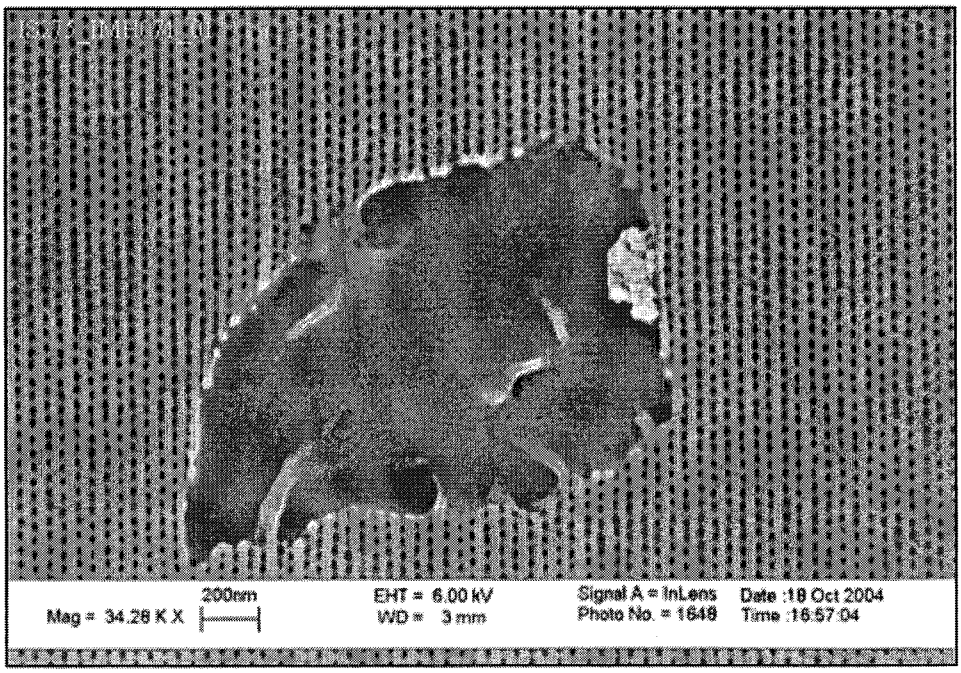

Image A.136 The image displays an area of pattern 1 on sample IS275 where the resist has ripped. The following parameters were used: type 2 bilayer coating, model 20 imprinting press, imprinter IMH071 (32 fC point dose), regulator pressure of 50 psi, and the separation temperature was 35°C.

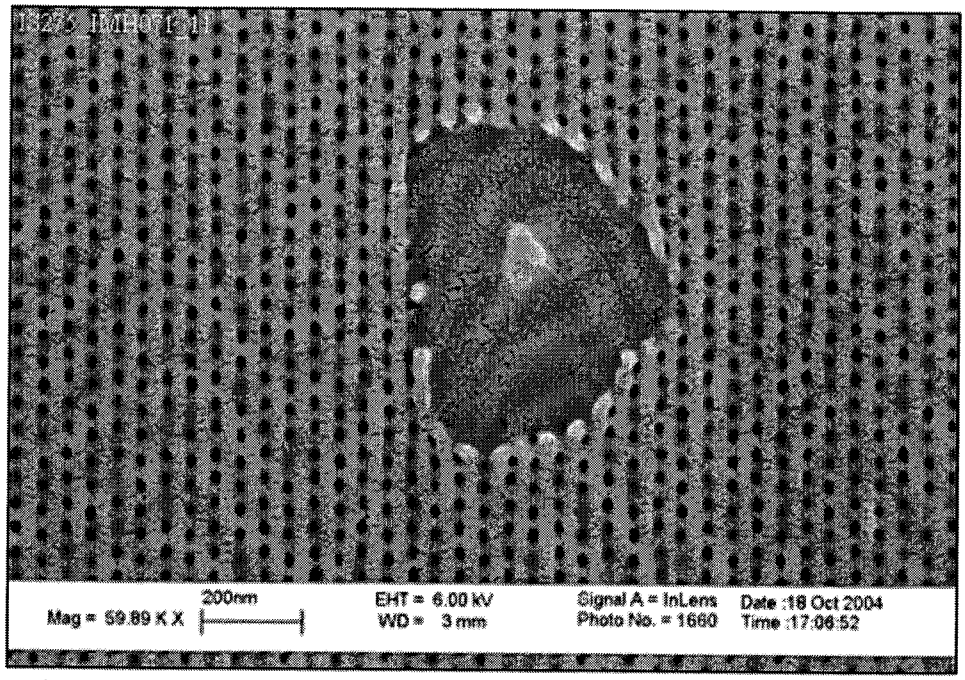

Image A.137 The image displays an area of pattern 11 on sample IS275 where the resist has ripped. The following parameters were used: type 2 bilayer coating, model 20 imprinting press, imprinter IMH071 (32 fC point dose), regulator pressure of 50 psi, and the separation temperature was 35°C.

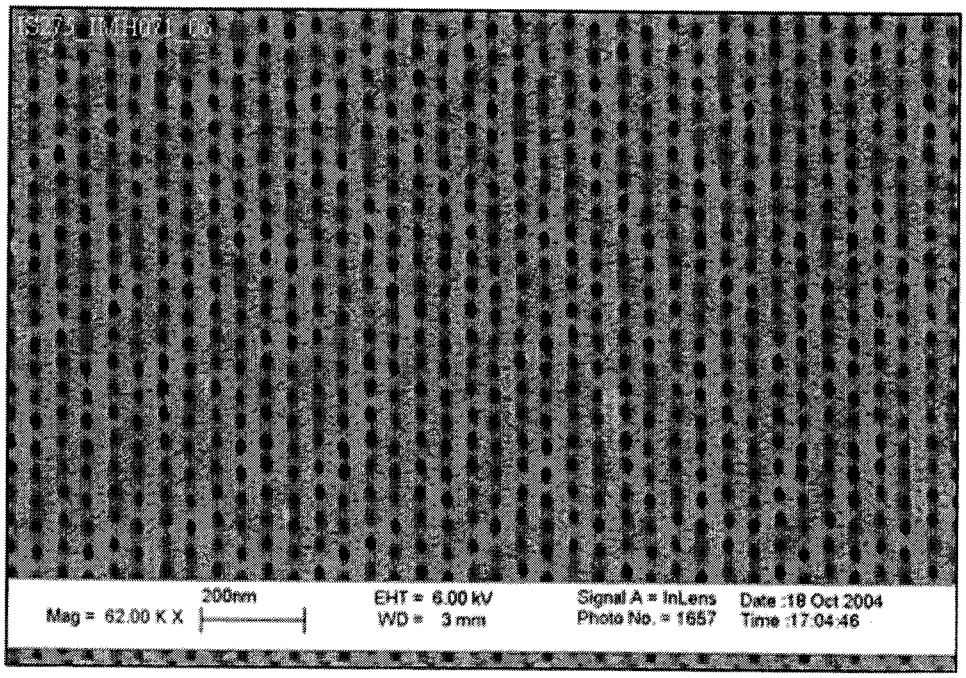

Image A.138 The image displays an area of pattern 6 on sample IS275 containing imprinted holes with minimal defects. The following parameters were used: type 2 bilayer coating, model 20 imprinting press, imprinter IMH071 (32 fC point dose), regulator pressure of 50 psi, and the separation temperature was 35°C.

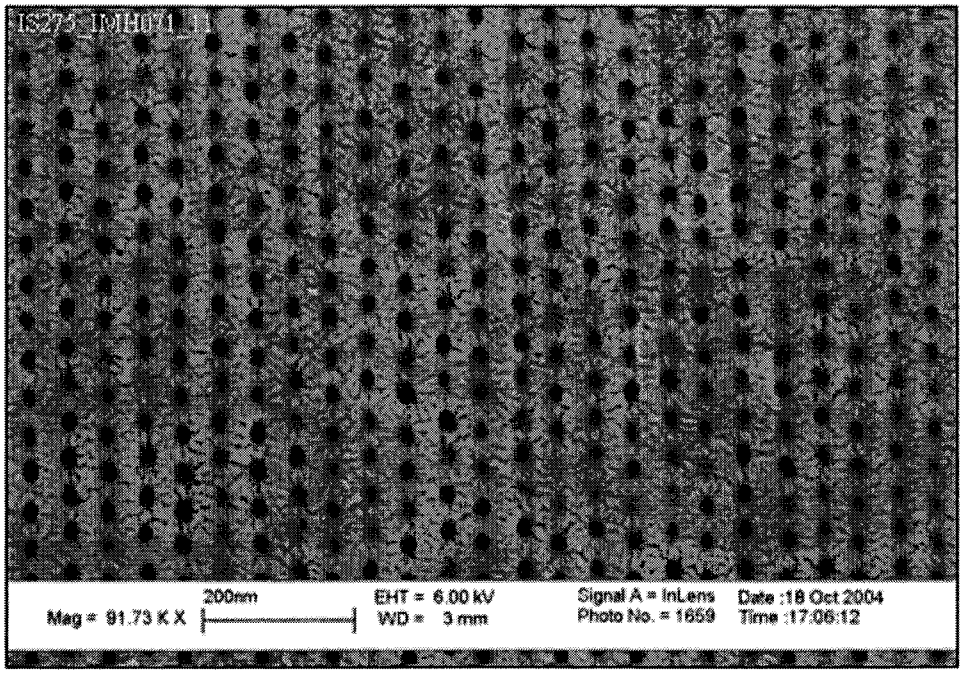

Image A.139 The image displays an area of pattern 11 on sample IS275 containing imprinted holes with minimal defects. The following parameters were used: type 2 bilayer coating, model 20 imprinting press, imprinter IMH071 (32 fC point dose), regulator pressure of 50 psi, and the separation temperature was 35°C.

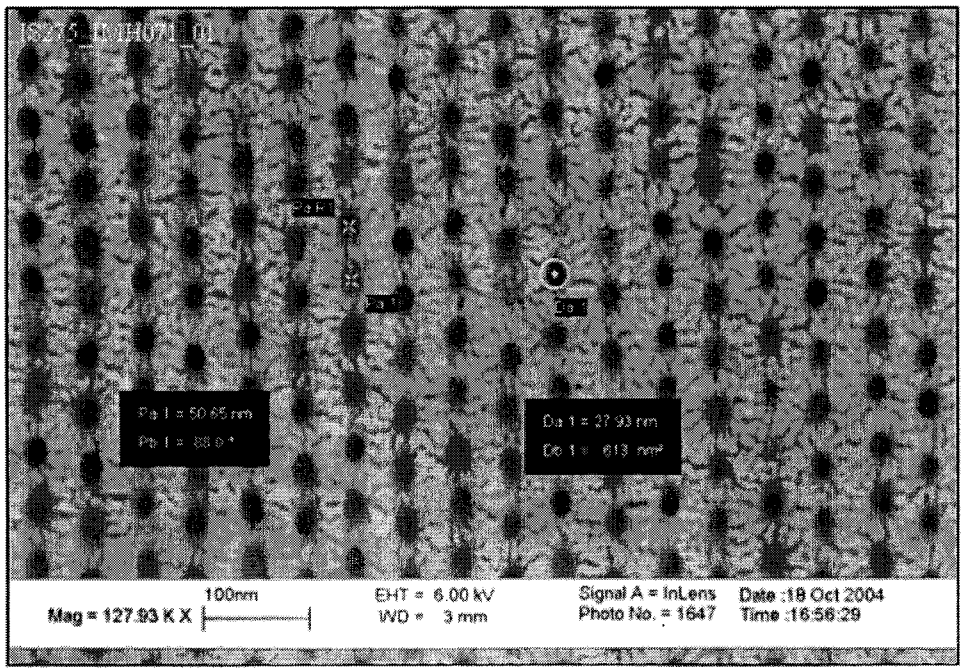

Image A.140 The image displays the measured hole diameter and pitch of pattern 1 on sample IS275. The following parameters were used: type 2 bilayer coating, model 20 imprinting press, imprinter IMH071 (32 fC point dose), regulator pressure of 50 psi, and the separation temperature was 35°C.

A.2.4 Type 3 Bilayer Coating

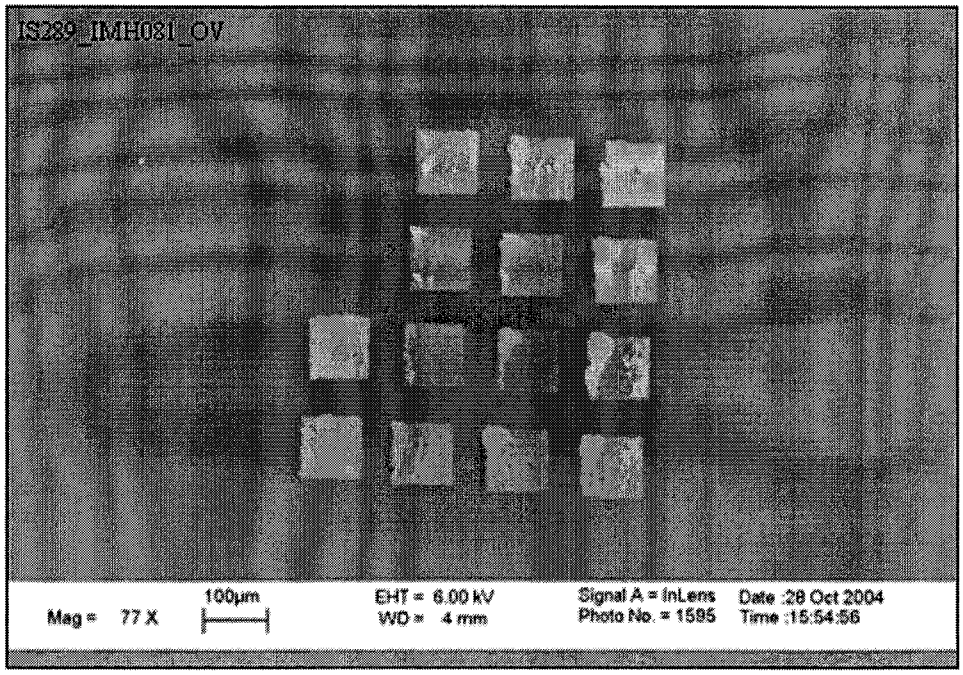

Image A.141 The image displays an overview of the patterns on sample IS289. The following parameters were used: type 3 bilayer coating, model 20 imprinting press, imprinter IMH081 (32 fC point dose), regulator pressure of 50 psi, and the separation temperature was 45°C.

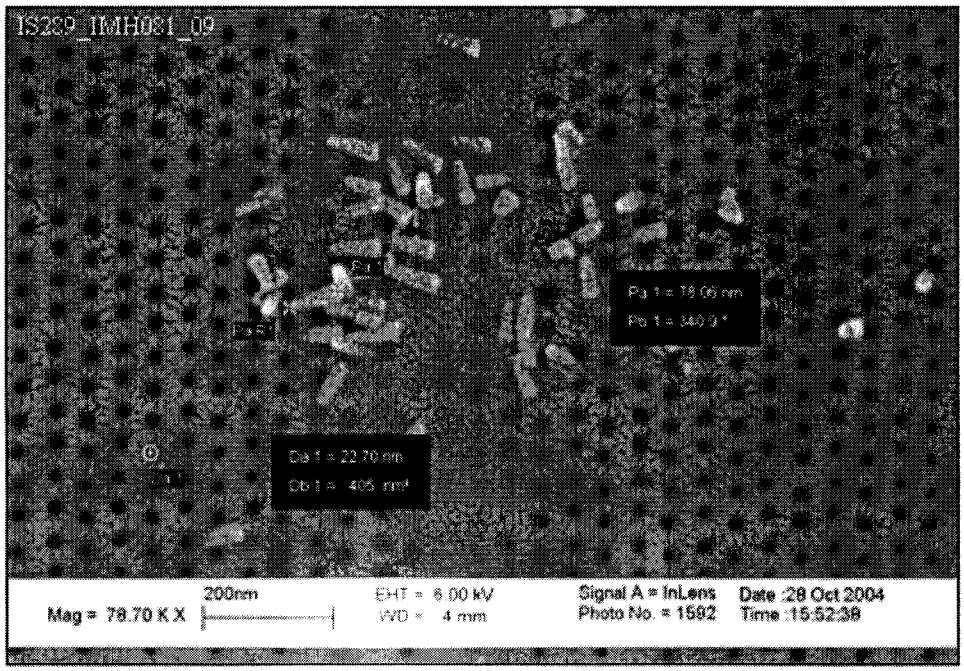

Image A.142 The image displays an area of pattern 9 on sample IS289 where broken off pillars from the imprinter were collected. The following parameters were used: type 3 bilayer coating, model 20 imprinting press, imprinter IMH081 (32 fC point dose), regulator pressure of 50 psi, and the separation temperature was 45°C.

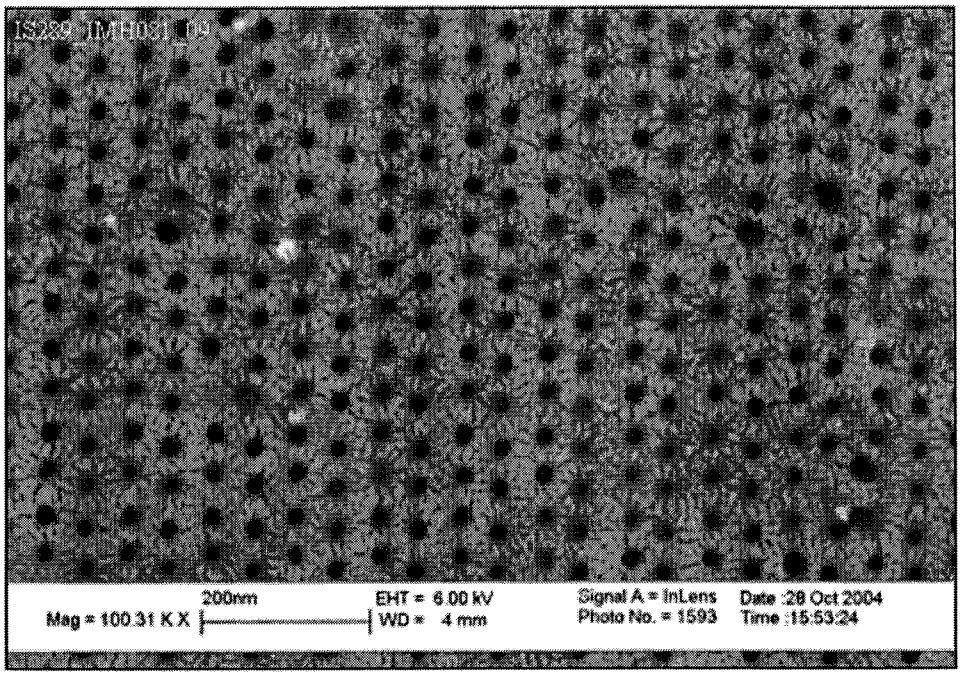

Image A.143 The image displays an area of pattern 9 on sample IS289 containing imprinted holes with minimal defects. The following parameters were used: type 3 bilayer coating, model 20 imprinting press, imprinter IMH081 (32 fC point dose), regulator pressure of 50 psi, and the separation temperature was 45°C.

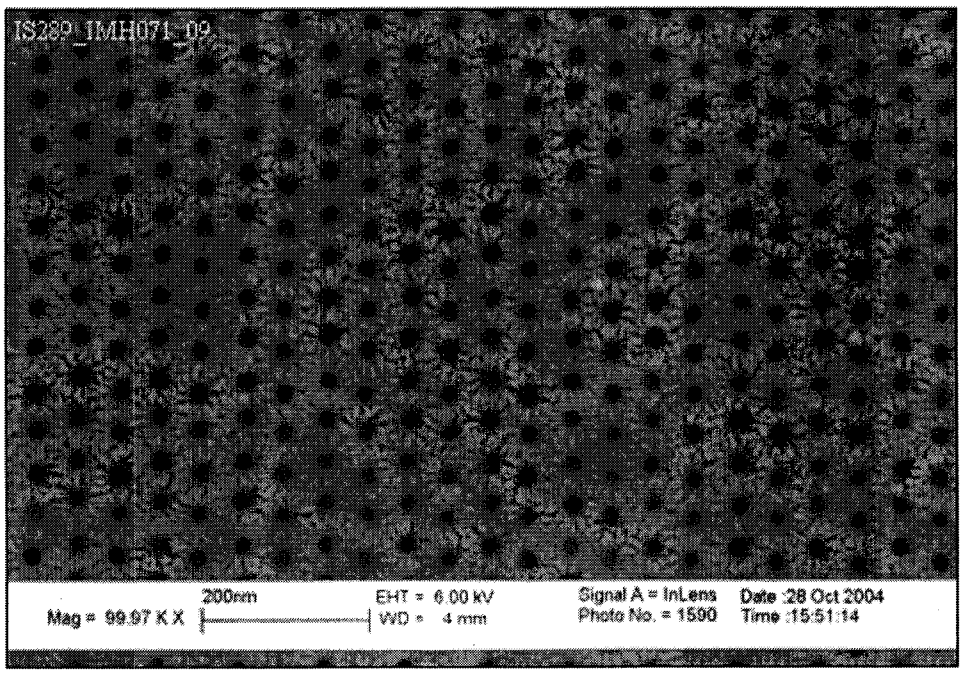

Image A.144 The image displays an area of pattern 9 on sample IS289 containing 100% defect free imprinted holes. The following parameters were used: type 3 bilayer coating, model 20 imprinting press, imprinter IMH081 (32 fC point dose), regulator pressure of 50 psi, and the separation temperature was 45°C.

A.2.4 Type 4 Bilayer Coating

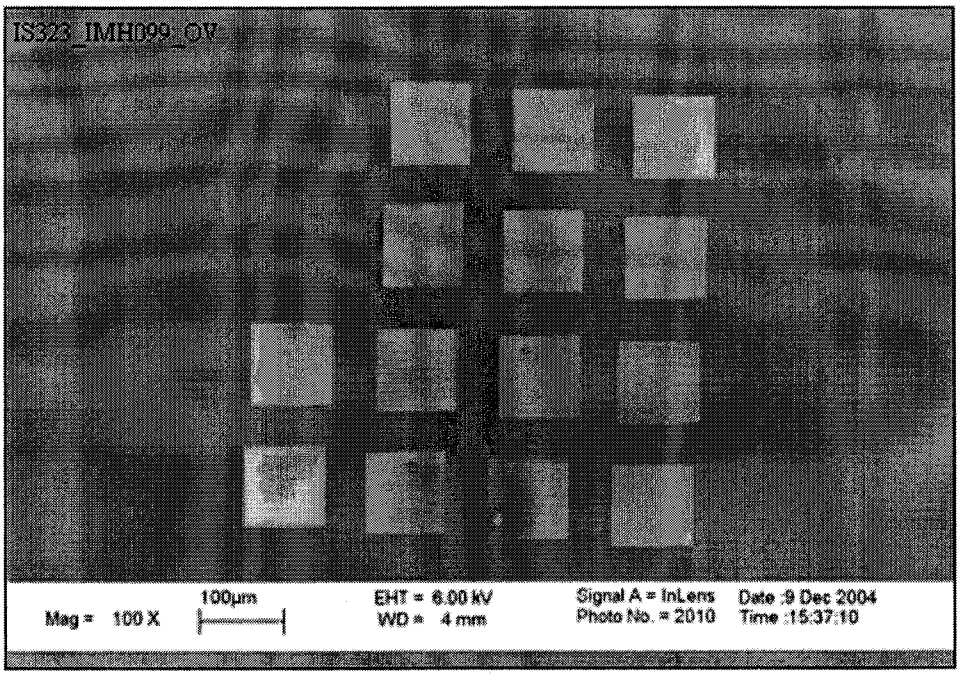

Image A.145 The image displays an overview of the patterns on sample IS323. The following parameters were used: type 4 bilayer coating, model 20 imprinting press, imprinter IMH099 (32 fC point dose), regulator pressure of 40 psi, and the separation temperature was 36.5°C.

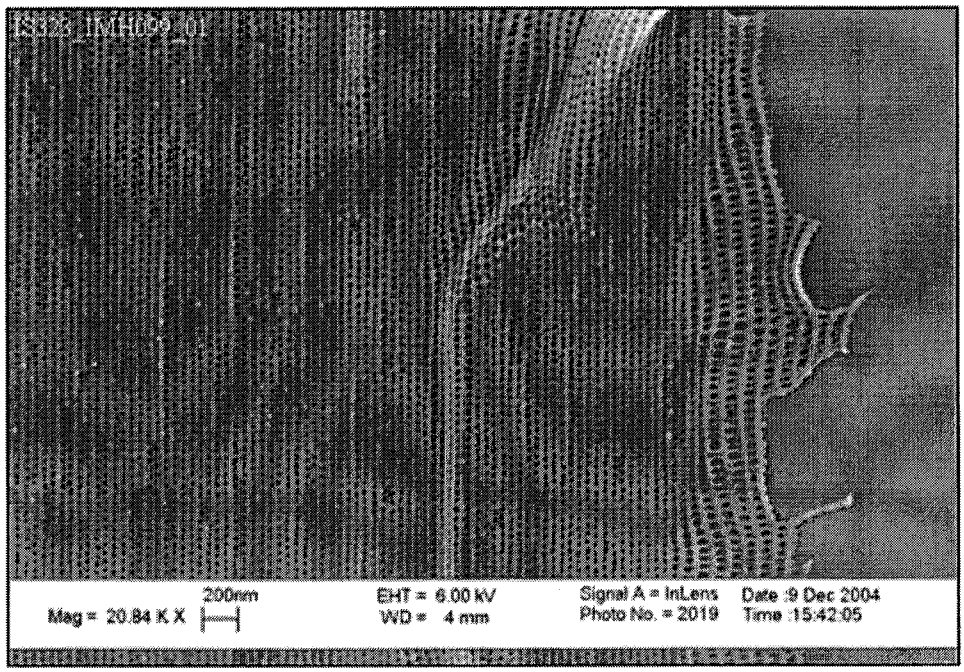

Image A.146 The image displays an area of pattern 1 on sample IS323 where the resist has ripped. The following parameters were used: type 4 bilayer coating, model 20 imprinting press, imprinter IMH099 (32 fC point dose), regulator pressure of 40 psi, and the separation temperature was 36.5°C.

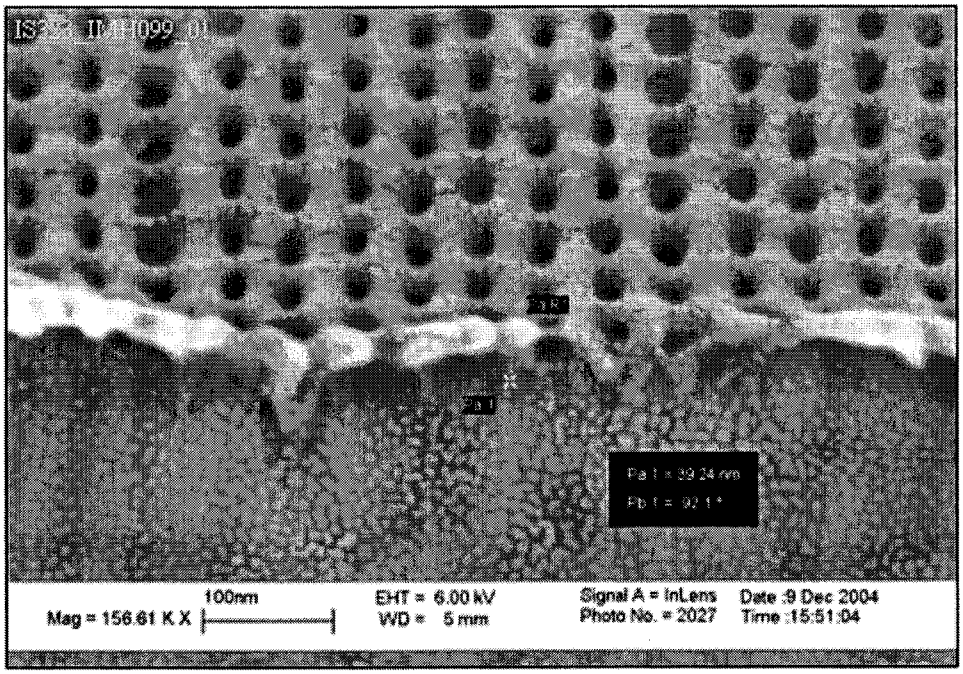

Image A.147 The image displays an area of pattern 1 on sample IS323 where the resist has ripped. The following parameters were used: type 4 bilayer coating, model 20 imprinting press, imprinter IMH099 (32 fC point dose), regulator pressure of 40 psi, and the separation temperature was 36.5°C.

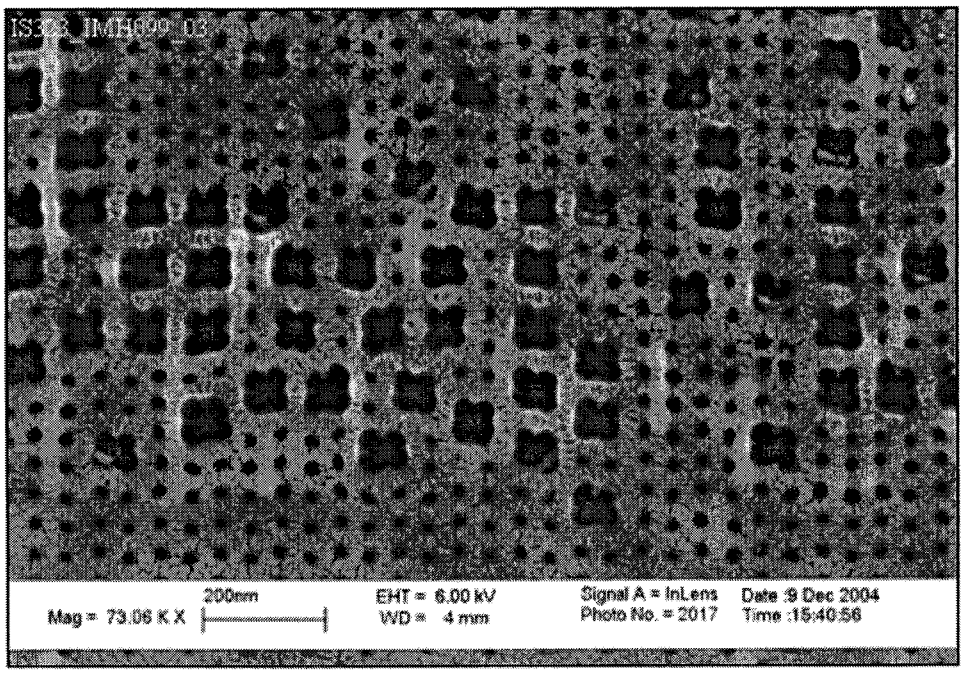

Image A.148 The image displays the top edge of pattern 3 on sample IS323. The following parameters were used: type 4 bilayer coating, model 20 imprinting press, imprinter IMH099 (32 fC point dose), regulator pressure of 40 psi, and the separation temperature was 36.5°C.

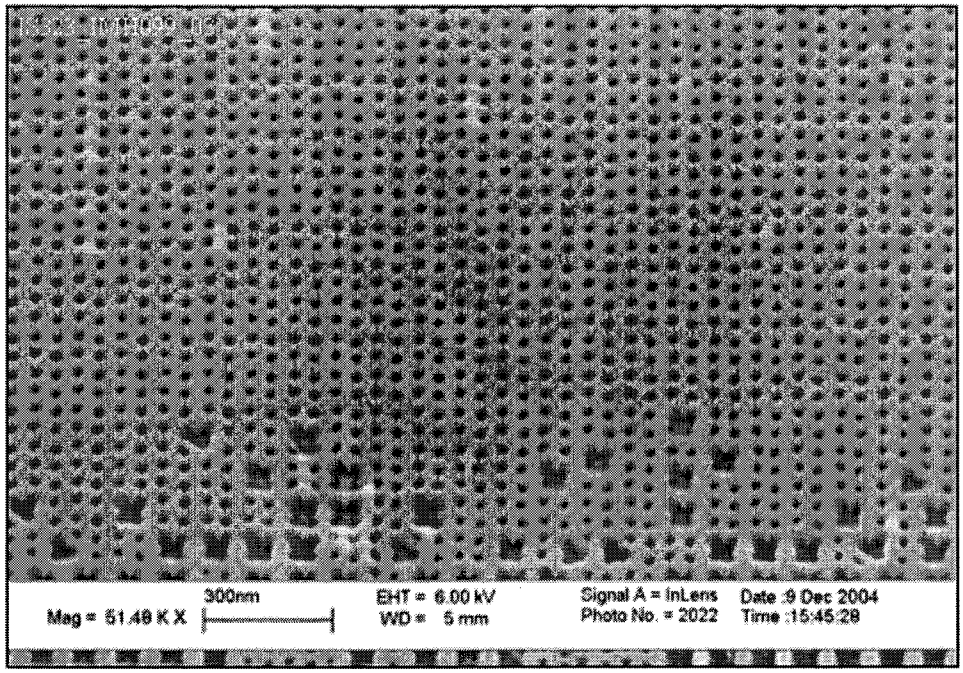

Image A.149 The image displays the bottom edge of pattern 3 on sample IS323. The following parameters were used: type 4 bilayer coating, model 20 imprinting press, imprinter IMH099 (32 fC point dose), regulator pressure of 40 psi, and the separation temperature was 36.5°C.

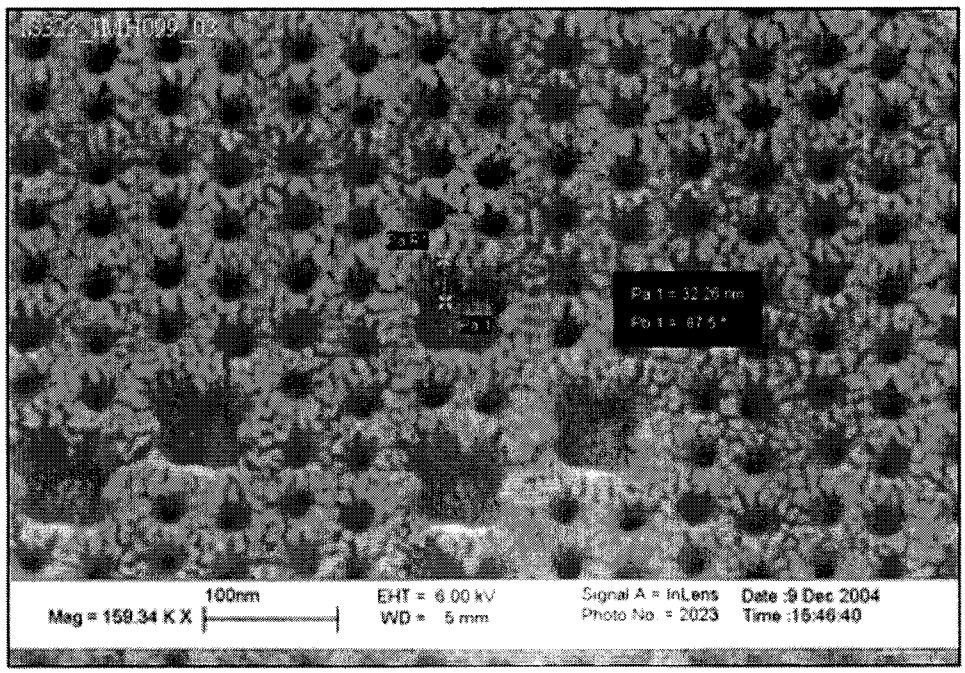

Image A.150 The image displays the top edge of pattern 3 on sample IS323. The following parameters were used: type 4 bilayer coating, model 20 imprinting press, imprinter IMH099 (32 fC point dose), regulator pressure of 40 psi, and the separation temperature was 36.5°C.

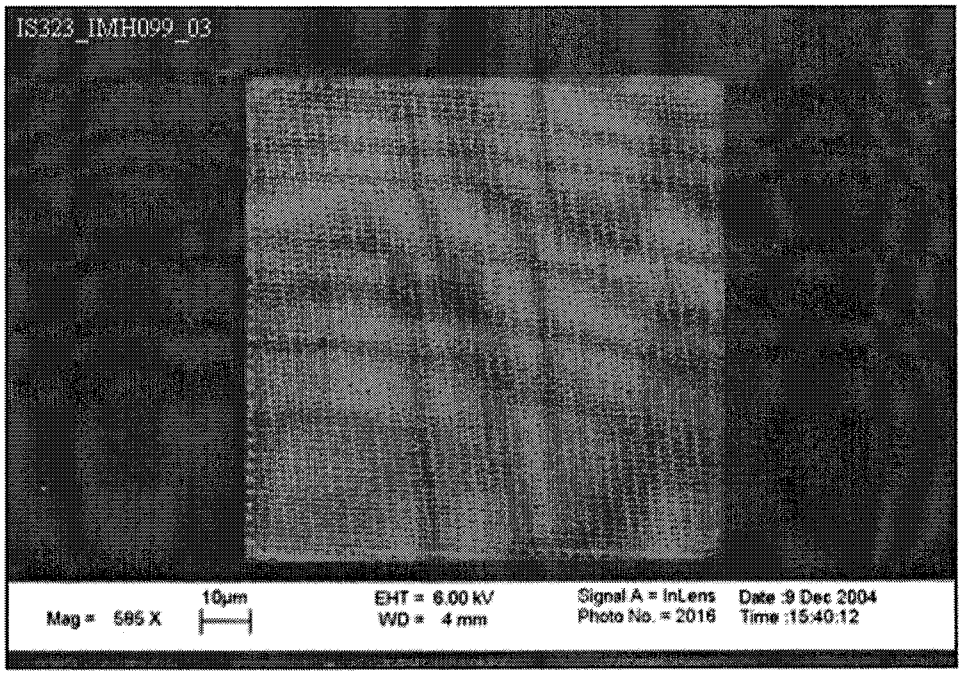

Image A.151 The image displays an overview of the defect free pattern 3 on sample IS323. The following parameters were used: type 4 bilayer coating, model 20 imprinting press, imprinter IMH099 (32 fC point dose), regulator pressure of 40 psi, and the separation temperature was 36.5°C.

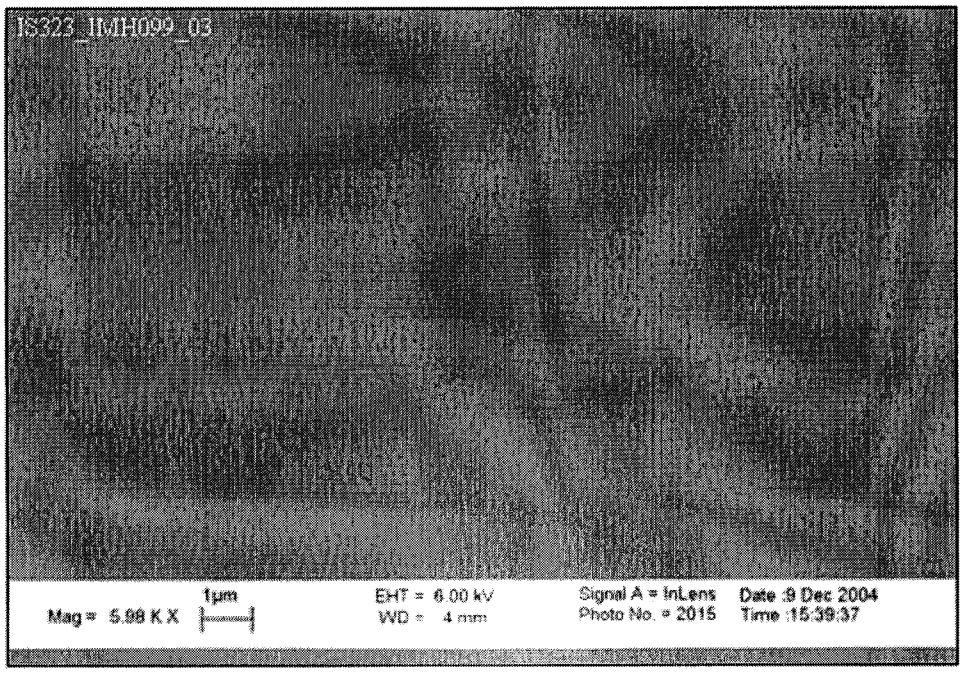

Image A.152 The image displays an area of pattern 3 on sample IS323 containing defect free imprinted holes. The following parameters were used: type 4 bilayer coating, model 20 imprinting press, imprinter IMH099 (32 fC point dose), regulator pressure of 40 psi, and the separation temperature was 36.5°C.

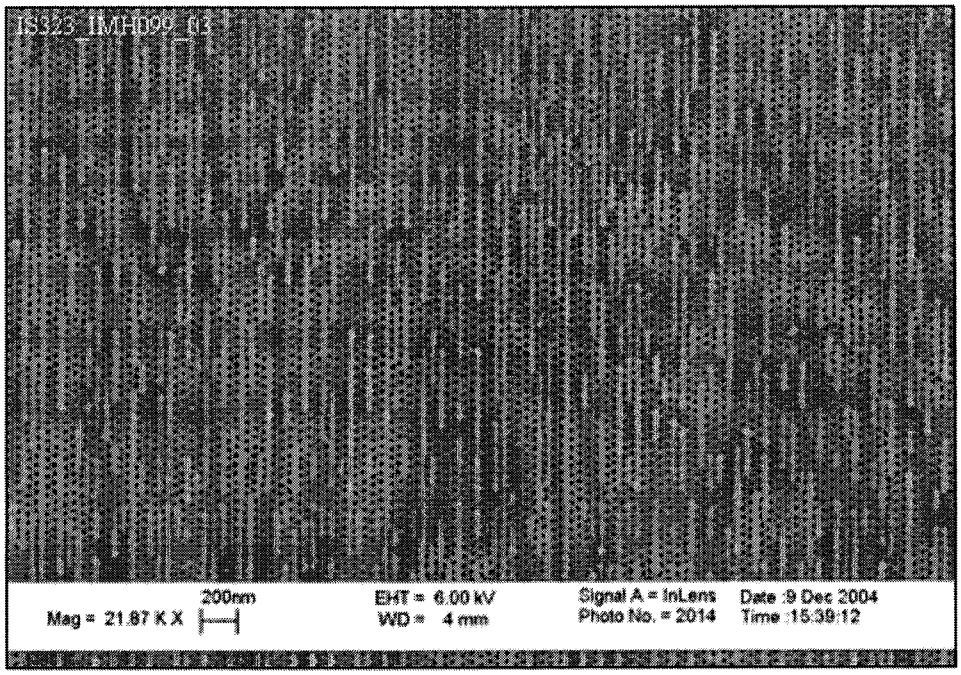

Image A.153 The image displays an area of pattern 3 on sample IS323 containing defect free imprinted holes. The following parameters were used: type 4 bilayer coating, model 20 imprinting press, imprinter IMH099 (32 fC point dose), regulator pressure of 40 psi, and the separation temperature was 36.5°C.

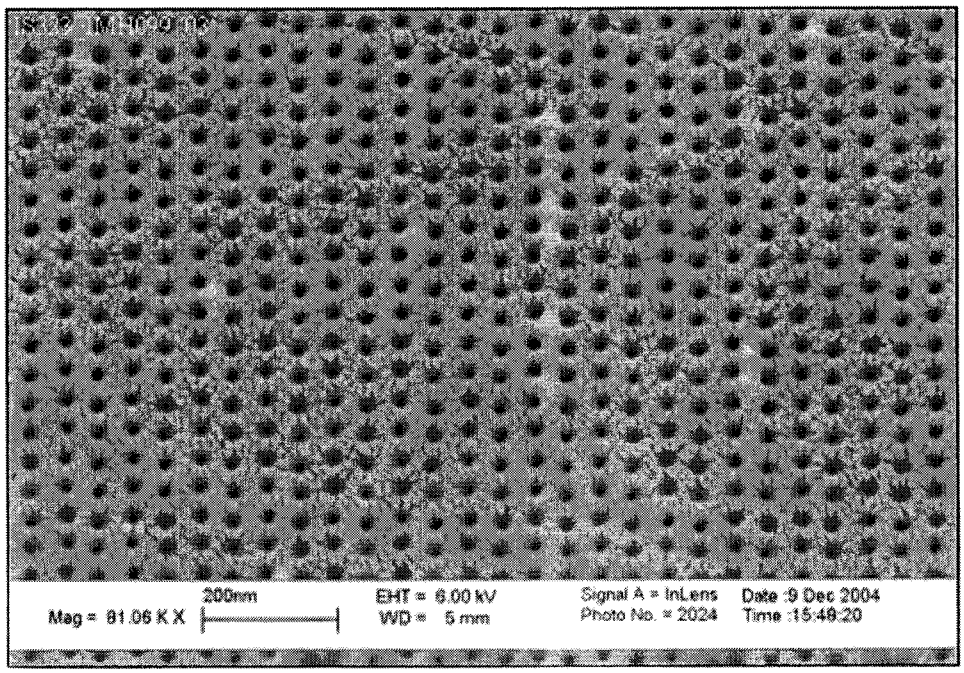

Image A.154 The image displays an area of pattern 3 on sample IS323 containing defect free imprinted holes. The following parameters were used: type 4 bilayer coating, model 20 imprinting press, imprinter IMH099 (32 fC point dose), regulator pressure of 40 psi, and the separation temperature was 36.5°C.

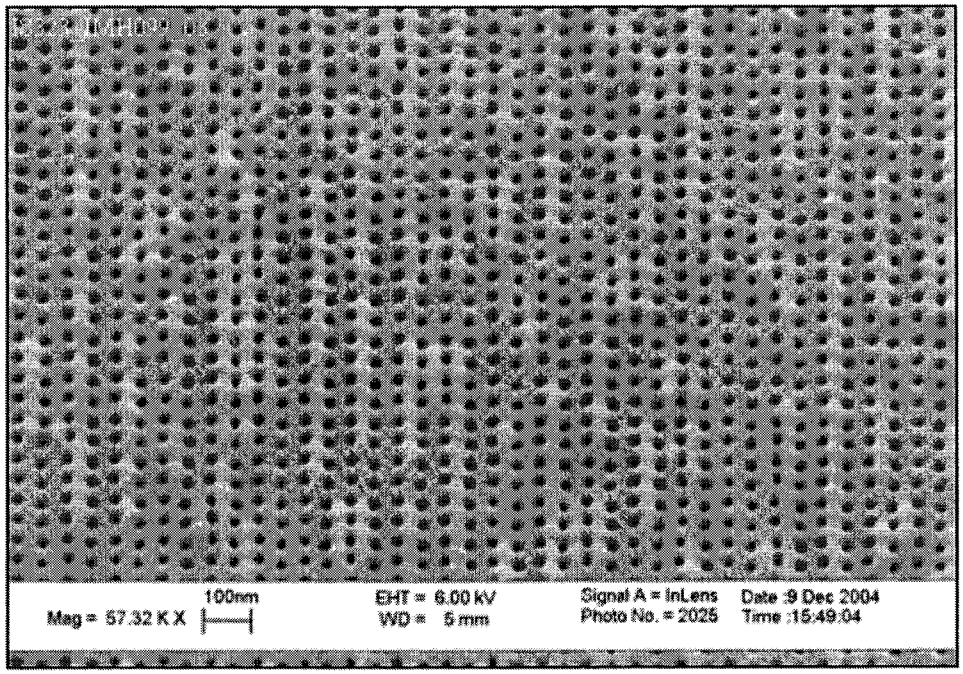

Image A.155 The image displays an area of pattern 3 on sample IS323 containing defect free imprinted holes. The following parameters were used: type 4 bilayer coating, model 20 imprinting press, imprinter IMH099 (32 fC point dose), regulator pressure of 40 psi, and the separation temperature was 36.5°C.

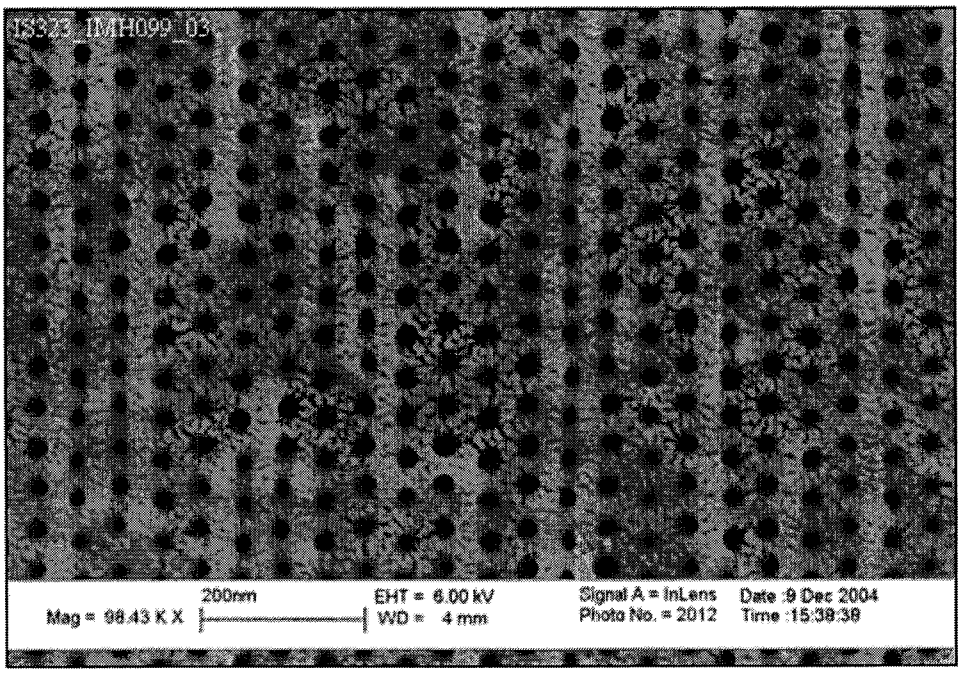

Image A.156 The image displays an area of pattern 3 on sample IS323 containing defect free imprinted holes. The following parameters were used: type 4 bilayer coating, model 20 imprinting press, imprinter IMH099 (32 fC point dose), regulator pressure of 40 psi, and the separation temperature was 36.5°C.

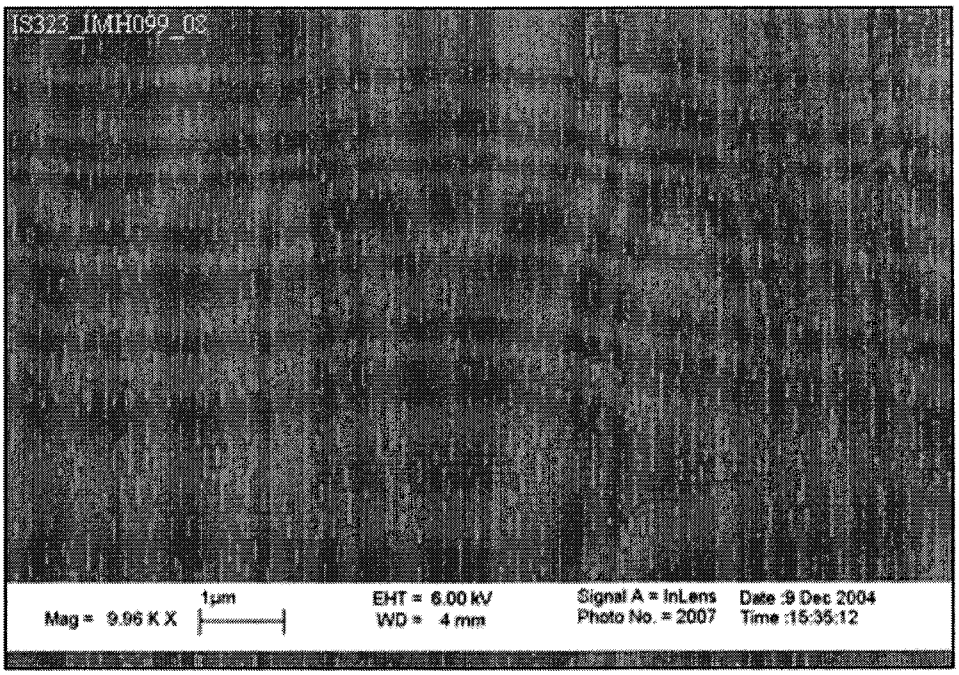

Image A.157 The image displays an area of pattern 8 on sample IS323 containing defect free imprinted holes. The following parameters were used: type 4 bilayer coating, model 20 imprinting press, imprinter IMH099 (32 fC point dose), regulator pressure of 40 psi, and the separation temperature was 36.5°C.

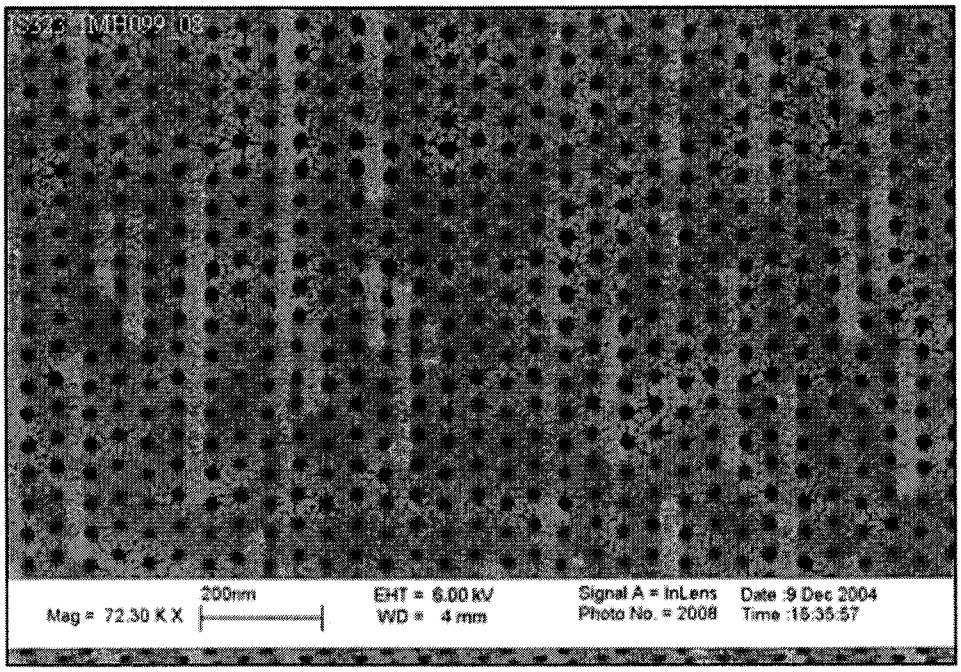

Image A.158 The image displays an area of pattern 8 on sample IS323 containing defect free imprinted holes. The following parameters were used: type 4 bilayer coating, model 20 imprinting press, imprinter IMH099 (32 fC point dose), regulator pressure of 40 psi, and the separation temperature was 36.5°C.

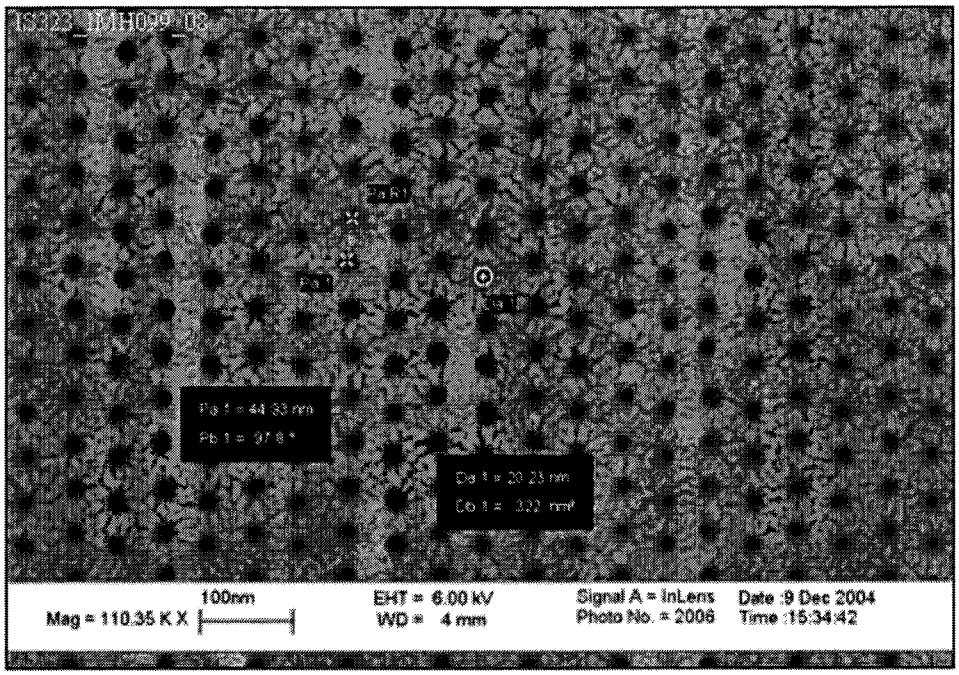

Image A.159 The image displays the measured hole diameter and pitch of a defect free area of pattern 8 on sample IS323. The following parameters were used: type 4 bilayer coating, model 20 imprinting press, imprinter IMH099 (32 fC point dose), regulator pressure of 40 psi, and the separation temperature was 36.5°C.

A.3 Samples: Etched and Patterned Permalloy Dots

A.3.1 Single Layer

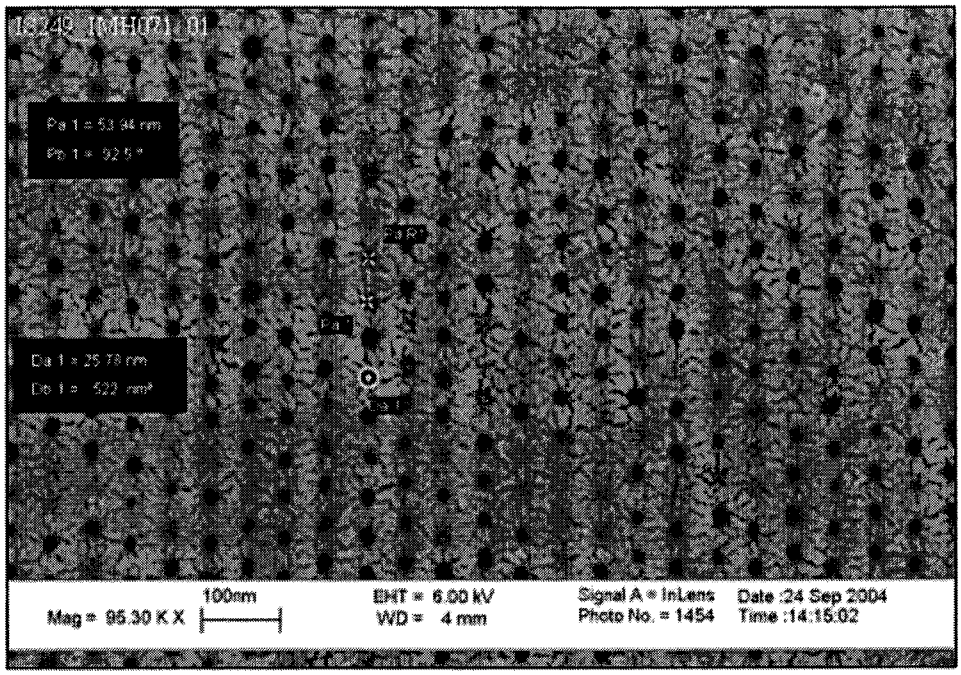

Image A.160 The image displays pattern 1 on sample IS249 after it was subjected to a wet etch in toluene for 20 seconds. The parameters were: single layer, model 20 imprinting press, imprinter IMH071 (32 fC point dose), regulator pressure of 50 psi, and the separation temperature was 36°C.

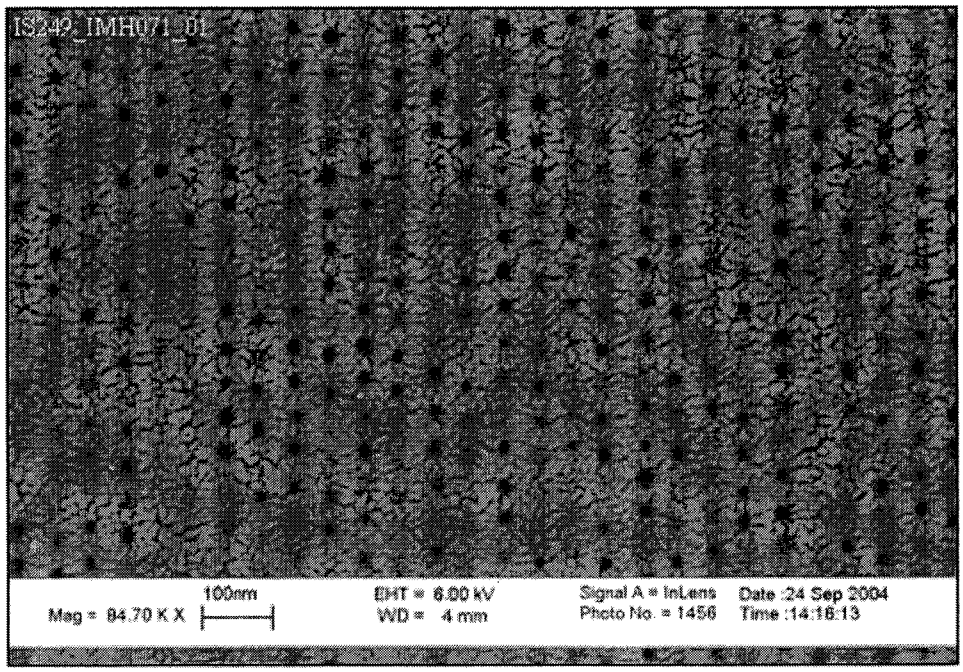

Image A.161 The image displays pattern 1 on sample IS249 after it was subjected to a wet etch in toluene for 20 seconds. The parameters were: single layer, model 20 imprinting press, imprinter IMH071 (32 fC point dose), regulator pressure of 50 psi, and the separation temperature was 36°C.

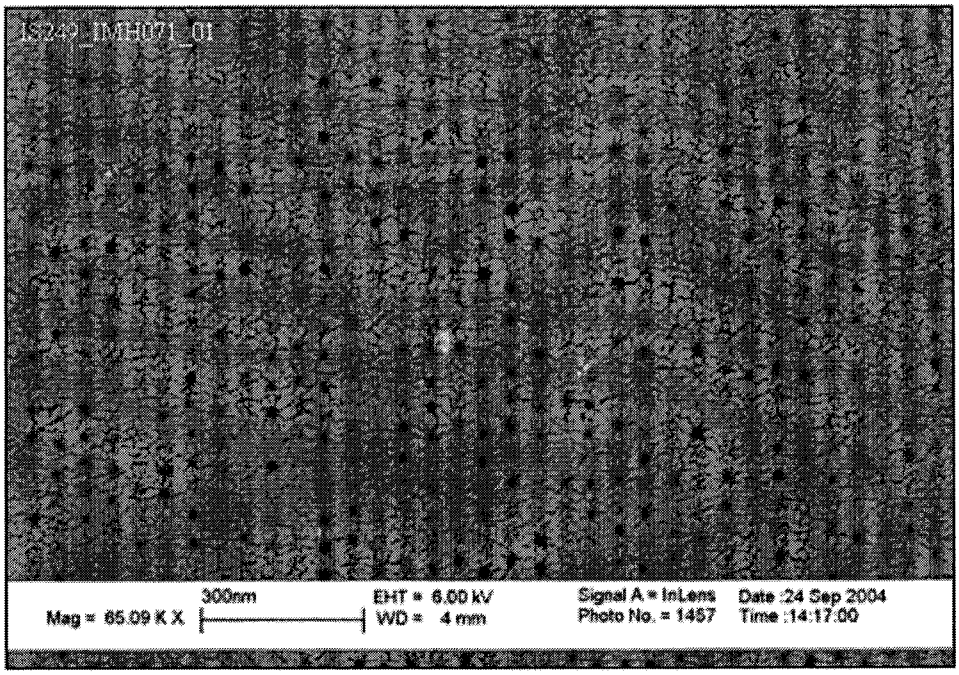

Image A.162 The image displays pattern 1 on sample IS249 after it was subjected to a wet etch. The following parameters were used: single layer of PMMA, model 20 imprinting press, imprinter IMH071 (32 fC point dose), regulator pressure of 50 psi, the separation temperature was 36°C, and the etching was done for 20 seconds in toluene.

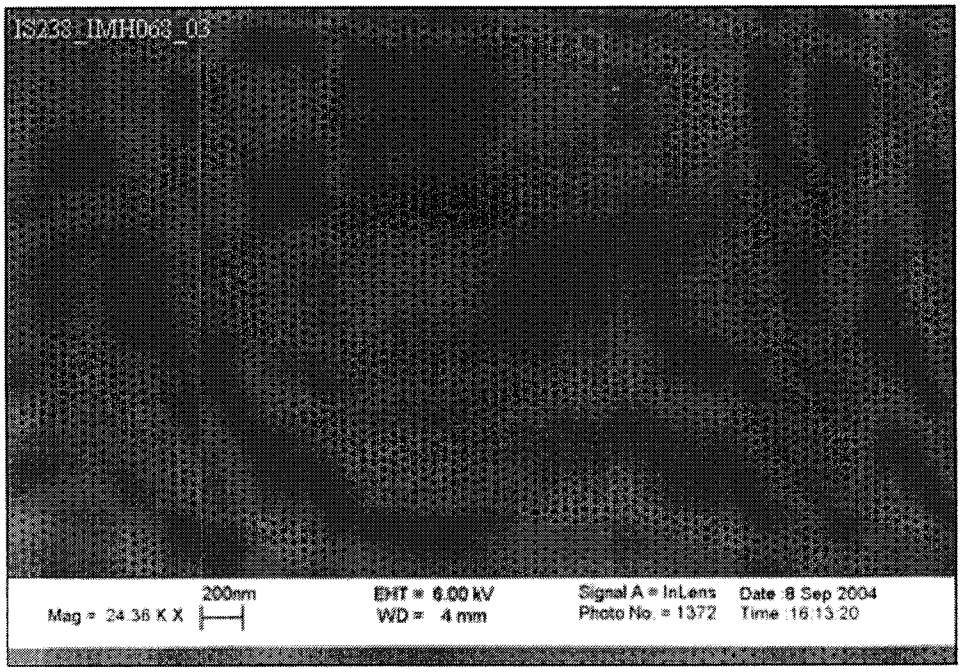

Image A.163 The image displays pattern 3 on sample IS238 after it was subjected to a dry etch. The following parameters were used: single layer of PMMA, model 20 imprinting press, imprinter IMH068 (32 fC point dose), regulator pressure of 50 psi, the separation temperature was 41°C, and the etching was done for 20 seconds at 200W.

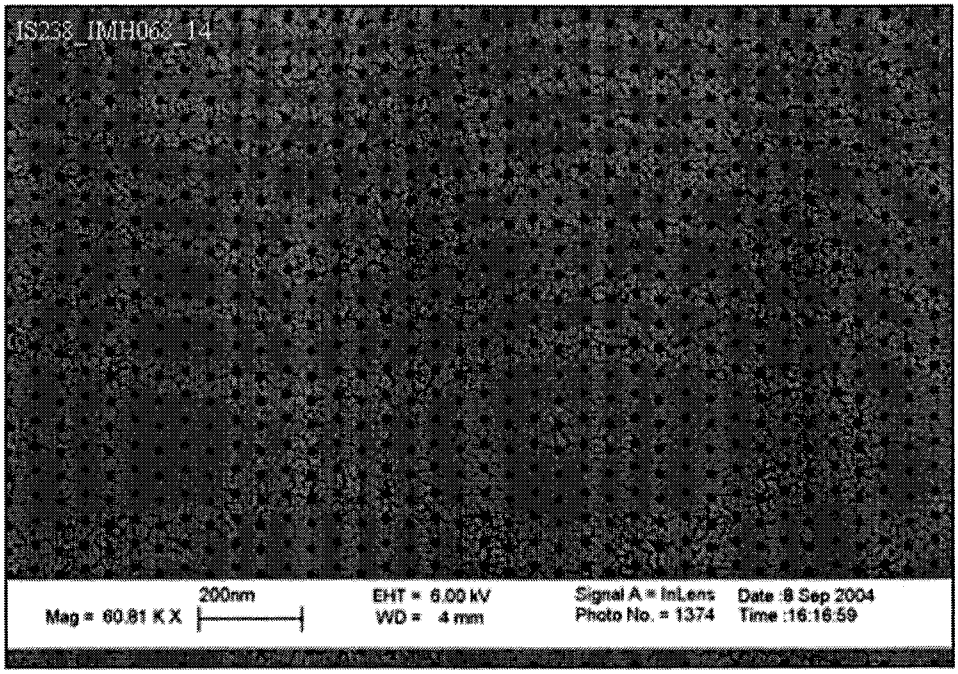

Image A.164 The image displays pattern 14 on sample IS238 after it was subjected to a dry etch. The following parameters were used: single layer of PMMA, model 20 imprinting press, imprinter IMH068 (32 fC point dose), regulator pressure of 50 psi, the separation temperature was 41°C, and the etching was done for 20 seconds at 200W.

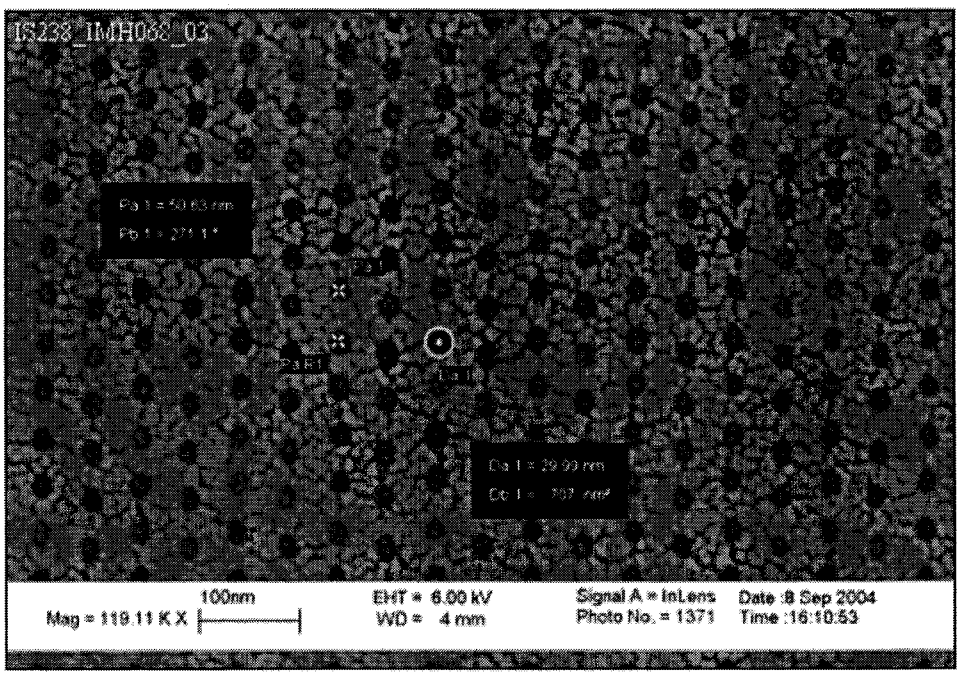

Image A.165 The image displays pattern 3 on sample IS238 after it was subjected to a dry etch. The following parameters were used: single layer of PMMA, model 20 imprinting press, imprinter IMH068 (32 fC point dose), regulator pressure of 50 psi, the separation temperature was 41°C, and the etching was done for 20 seconds at 200W.

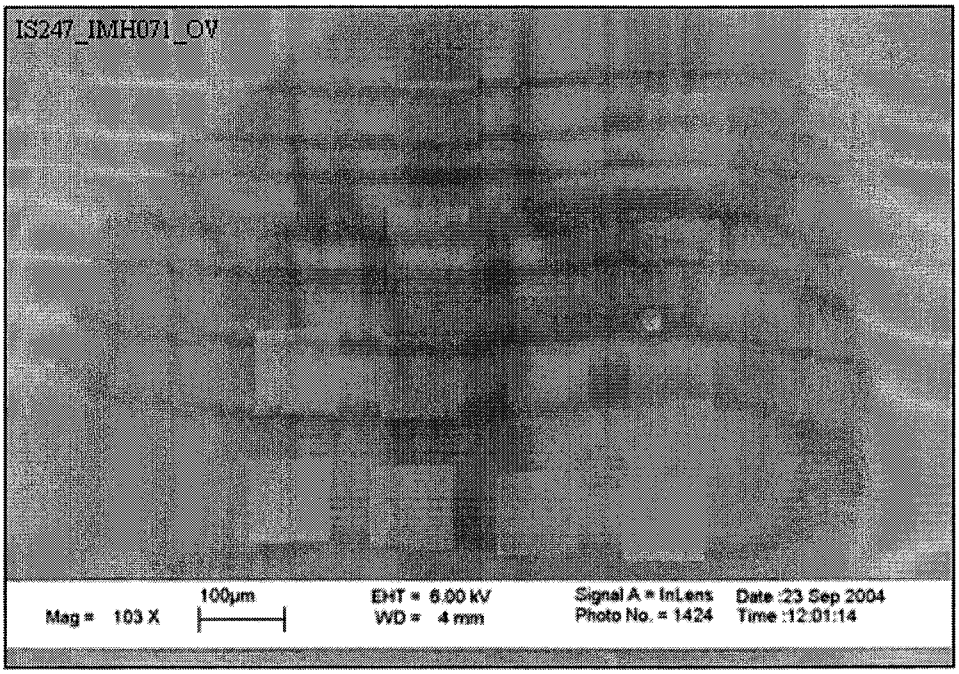

Image A.166 The image displays all of the patterns on sample IS247 after it was subjected to a dry etch. The following parameters were used: single layer of PMMA, model 20 imprinting press, imprinter IMH071 (32 fC point dose), regulator pressure of 50 psi, the separation temperature was 35.5°C, and the etching was done for 20 seconds at 100W.

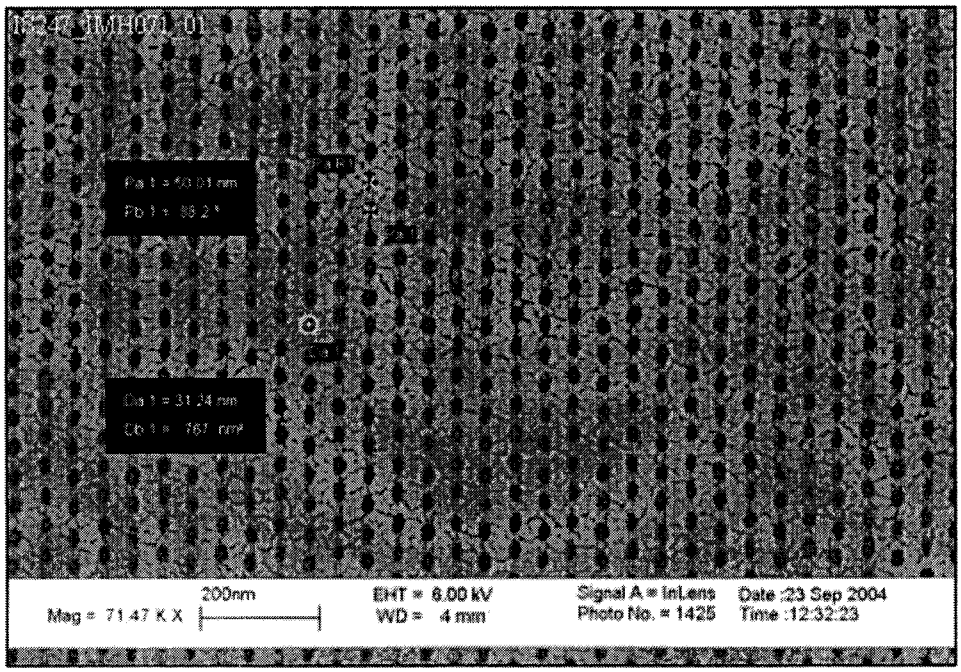

Image A.167 The image displays pattern 1 on sample IS247 after it was subjected to a dry etch. The following parameters were used: single layer of PMMA, model 20 imprinting press, imprinter IMH071 (32 fC point dose), regulator pressure of 50 psi, the separation temperature was 35.5°C, and the etching was done for 20 seconds at 100W.

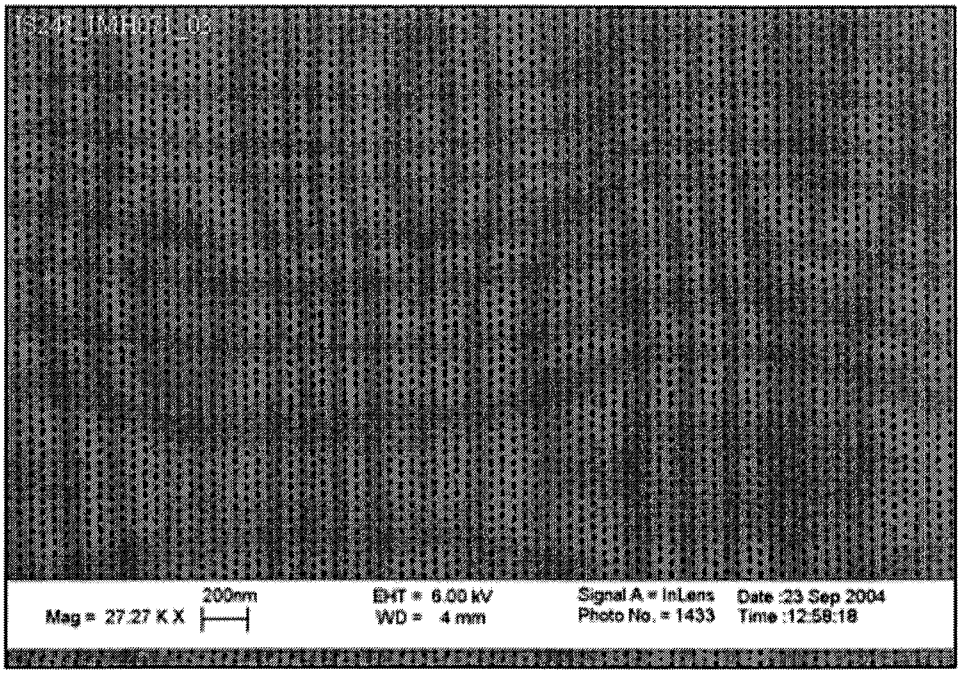

Image A.168 The image displays pattern 3 on sample IS247 after it was subjected to a dry etch. The following parameters were used: single layer of PMMA, model 20 imprinting press, imprinter IMH071 (32 fC point dose), regulator pressure of 50 psi, the separation temperature was 35.5°C, and the etching was done for 20 seconds at 100W.

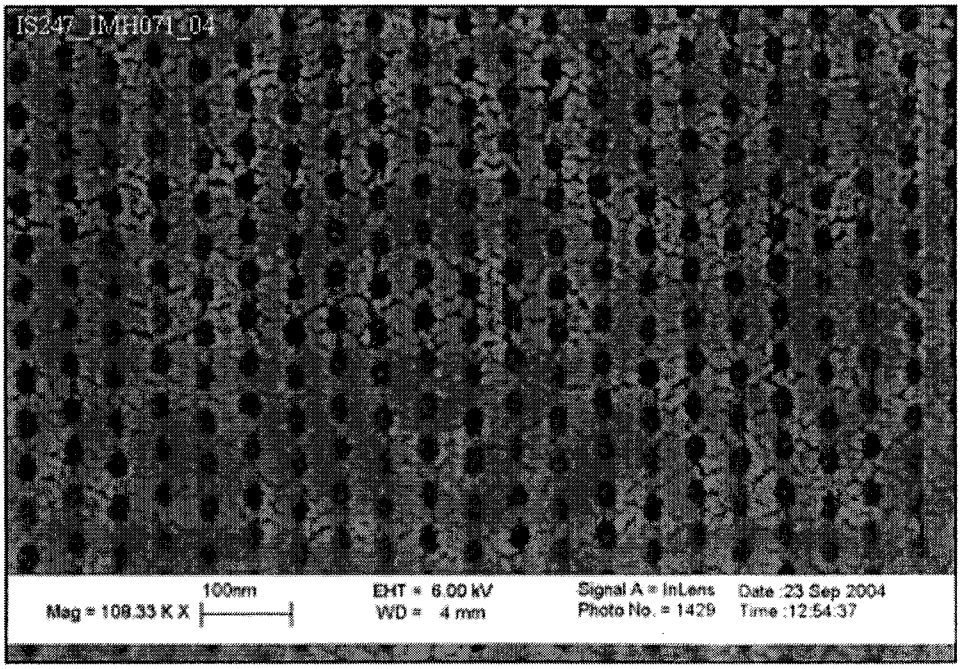

Image A.169 The image displays pattern 4 on sample IS247 after it was subjected to a dry etch. The following parameters were used: single layer of PMMA, model 20 imprinting press, imprinter IMH071 (32 fC point dose), regulator pressure of 50 psi, the separation temperature was 35.5°C, and the etching was done for 20 seconds at 100W.

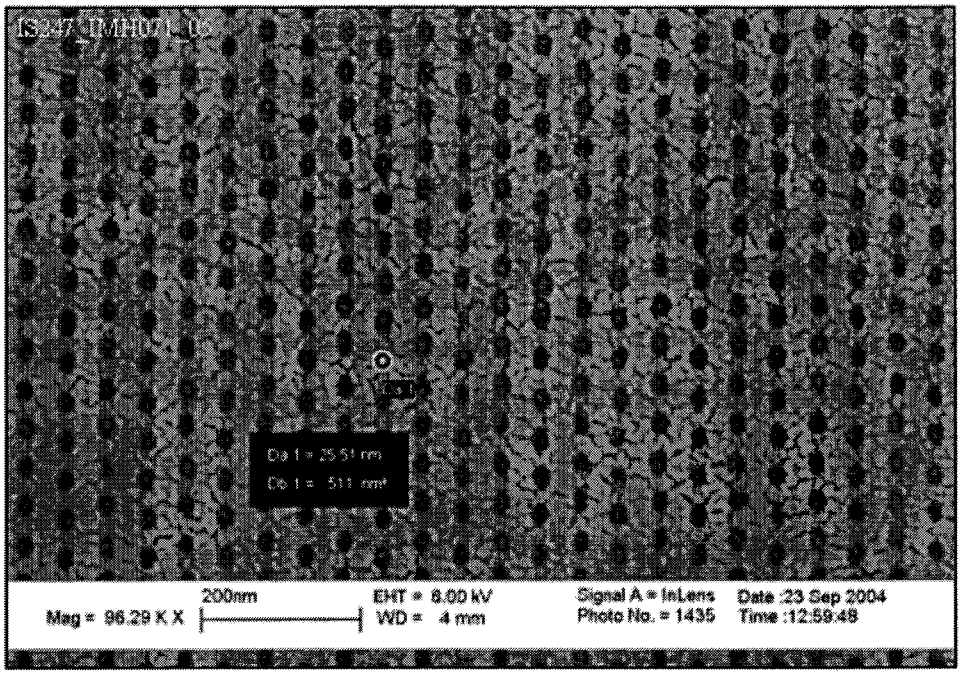

Image A.170 The image displays pattern 5 on sample IS247 after it was subjected to a dry etch. The following parameters were used: single layer of PMMA, model 20 imprinting press, imprinter IMH071 (32 fC point dose), regulator pressure of 50 psi, the separation temperature was 35.5°C, and the etching was done for 20 seconds at 100W.

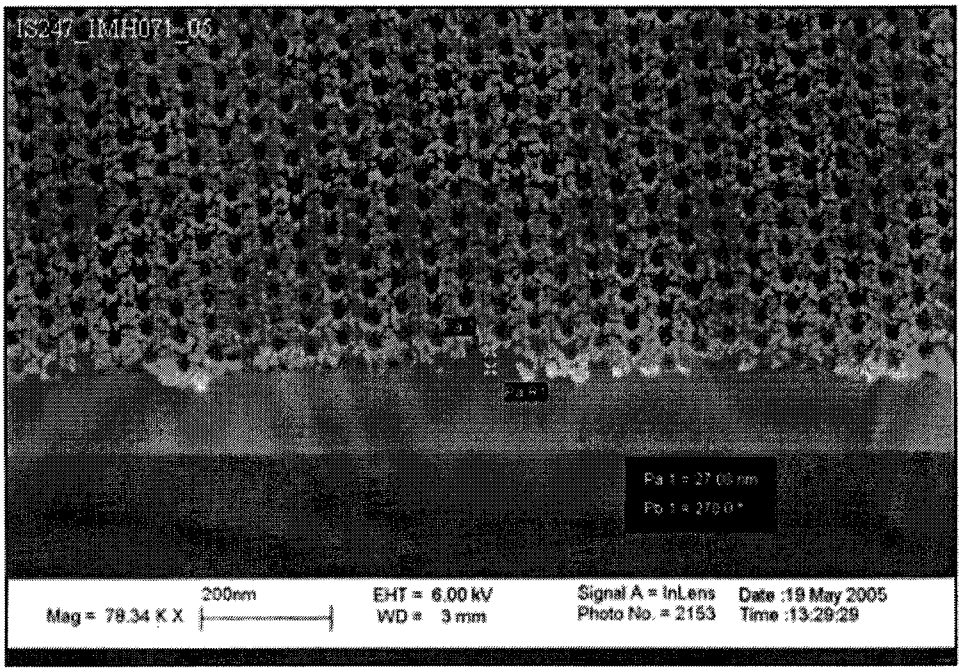

Image A.171 The image displays pattern 5 on sample IS247 after it was subjected to a dry etch. The following parameters were used: single layer of PMMA, model 20 imprinting press, imprinter IMH071 (32 fC point dose), regulator pressure of 50 psi, the separation temperature was 35.5°C, and the etching was done for 20 seconds at 100W.

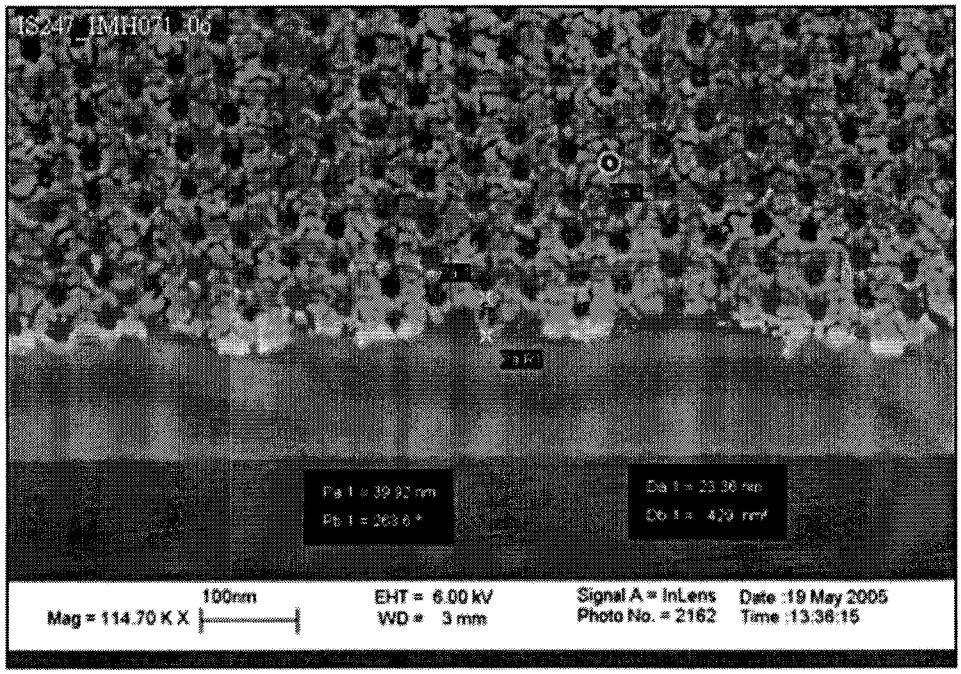

Image A.172 The image displays pattern 6 on sample IS247 after it was subjected to a dry etch. The following parameters were used: single layer of PMMA, model 20 imprinting press, imprinter IMH071 (32 fC point dose), regulator pressure of 50 psi, the separation temperature was 35.5°C, and the etching was done for 20 seconds at 100W.

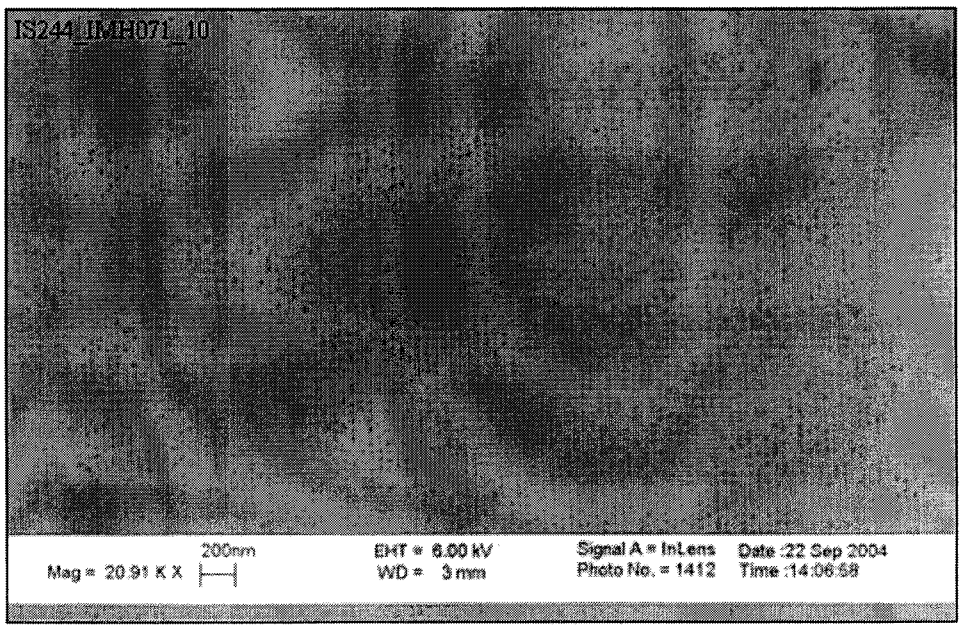

Image A.173 The image displays an area of pattern 10 on sample IS244 containing mostly ripped up Permalloy dots. The following parameters were used: single layer of PMMA, model 20 imprinting press, imprinter IMH071 (32 fC point dose), regulator pressure of 50 psi, a separation temperature of 42.5°C, etching for 20 seconds at 100W, and a Permalloy deposition of 5 minutes at 300W.

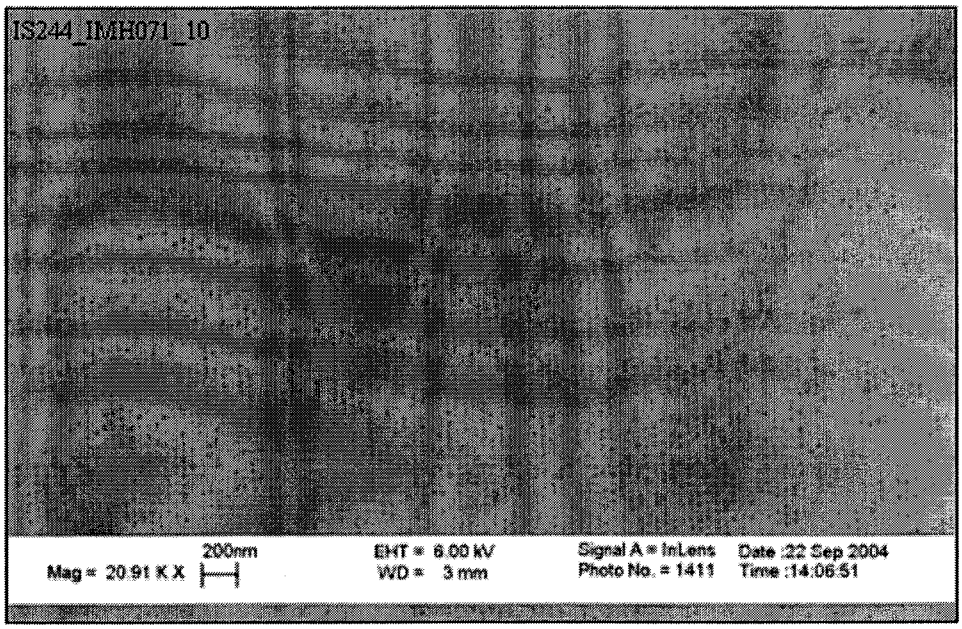

Image A.174 The image displays an area of pattern 10 on sample IS244 containing mostly ripped up Permalloy dots. The following parameters were used: single layer of PMMA, model 20 imprinting press, imprinter IMH071 (32 fC point dose), regulator pressure of 50 psi, a separation temperature of 42.5°C, etching for 20 seconds at 100W, and a Permalloy deposition of 5 minutes at 300W.

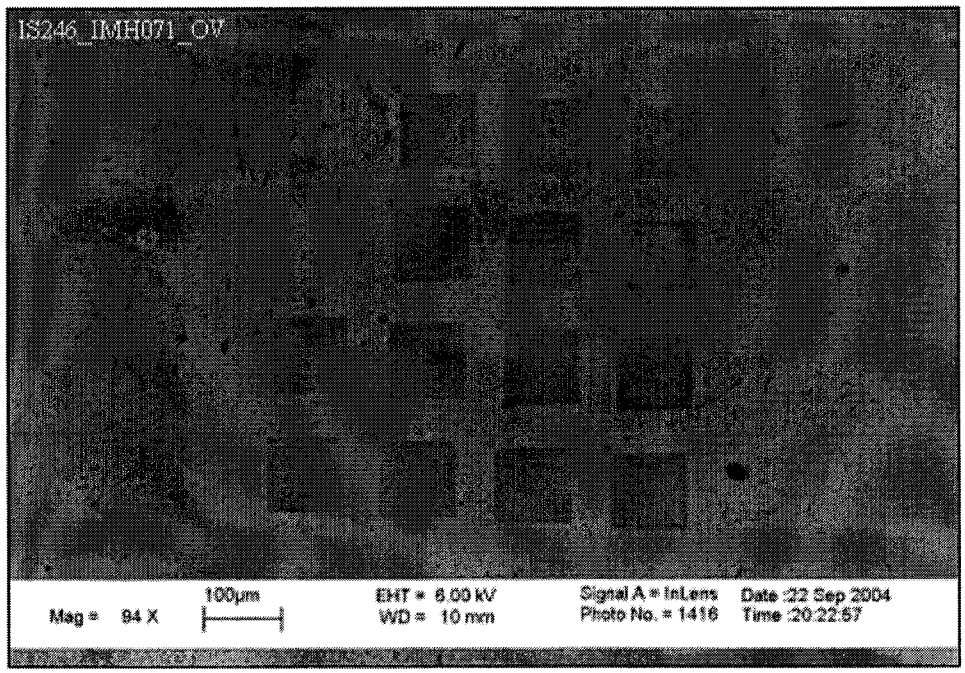

Image A.175 The image displays an overview of the patterns on sample IS246 after a liftoff. The following parameters were used: single layer of PMMA, model 20 imprinting press, imprinter IMH071 (32 fC point dose), regulator pressure of 50 psi, a separation temperature of 38°C, etching for 20 seconds at 100W, and a Permalloy deposition of 5 minutes at 300W.

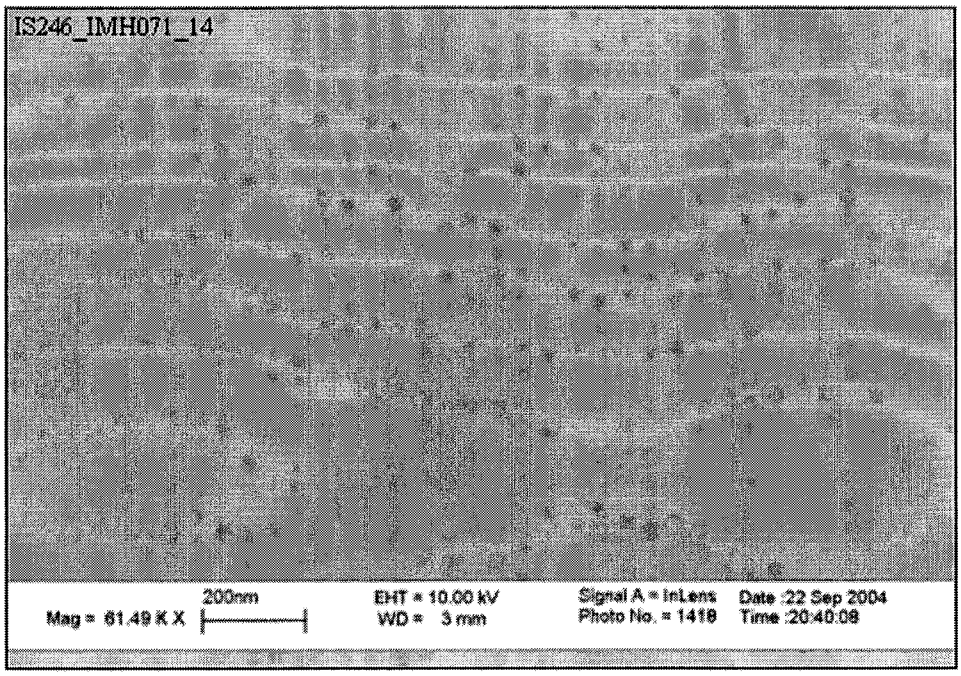

Image A.176 The image displays an area of pattern 14 on sample IS246 containing Permalloy dots. The following parameters were used: single layer of PMMA, model 20 imprinting press, imprinter IMH071 (32 fC point dose), regulator pressure of 50 psi, a separation temperature of 38°C, etching for 20 seconds at 100W, and a Permalloy deposition of 5 minutes at 300W.

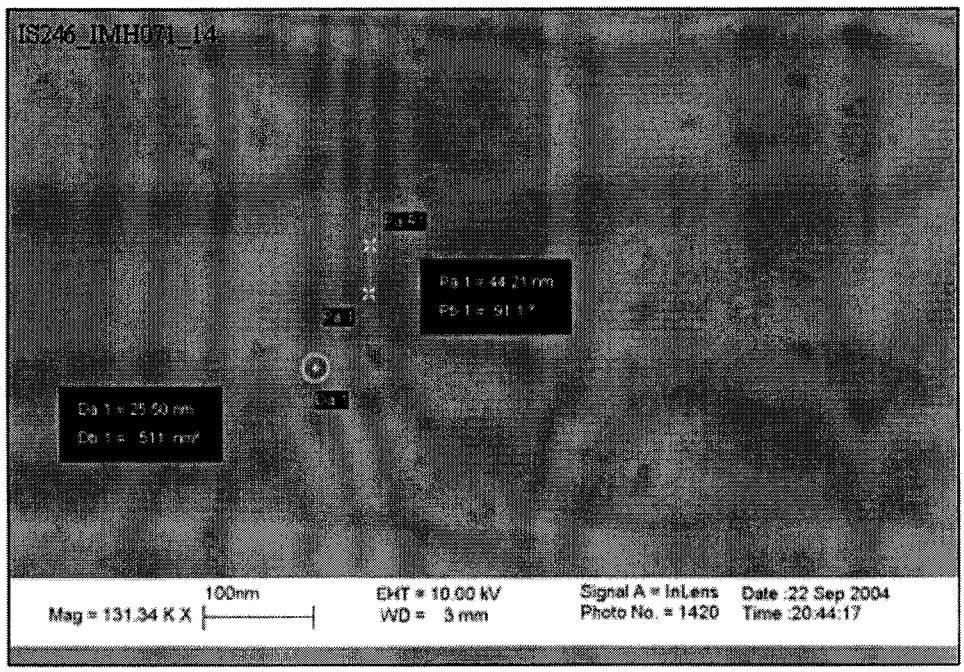

Image A.177 The image displays an area of pattern 14 on sample IS246 containing Permalloy dots. The following parameters were used: single layer of PMMA, model 20 imprinting press, imprinter IMH071 (32 fC point dose), regulator pressure of 50 psi, a separation temperature of 38°C, etching for 20 seconds at 100W, and a Permalloy deposition of 5 minutes at 300W

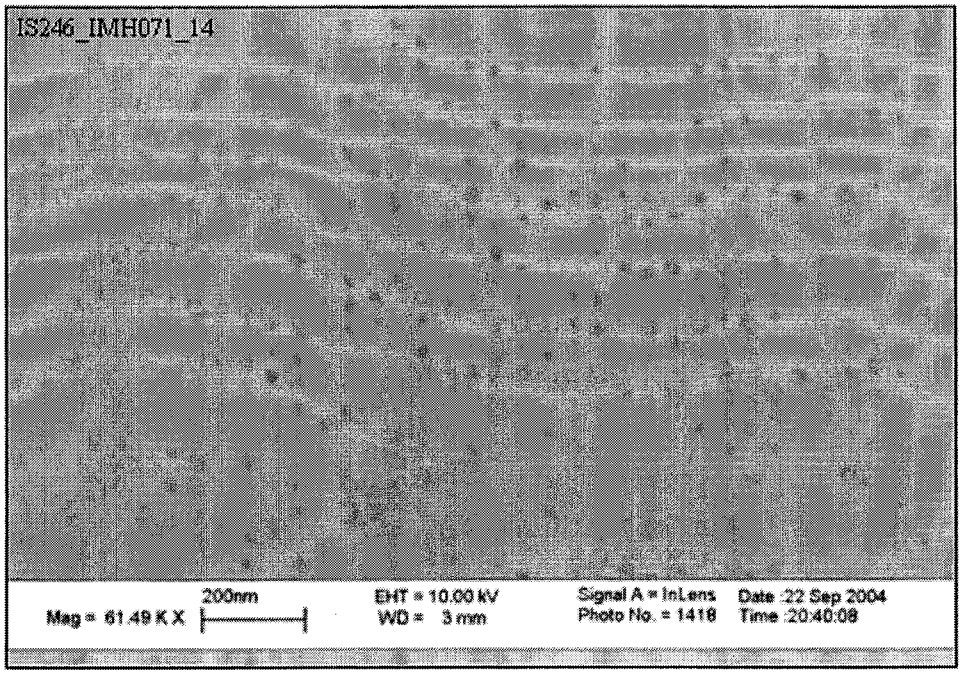

Image A.178 The image displays an area of pattern 14 on sample IS246 containing Permalloy dots. The following parameters were used: single layer of PMMA, model 20 imprinting press, imprinter IMH071 (32 fC point dose), regulator pressure of 50 psi, a separation temperature of 38°C, etching for 20 seconds at 100W, and a Permalloy deposition of 5 minutes at 300W

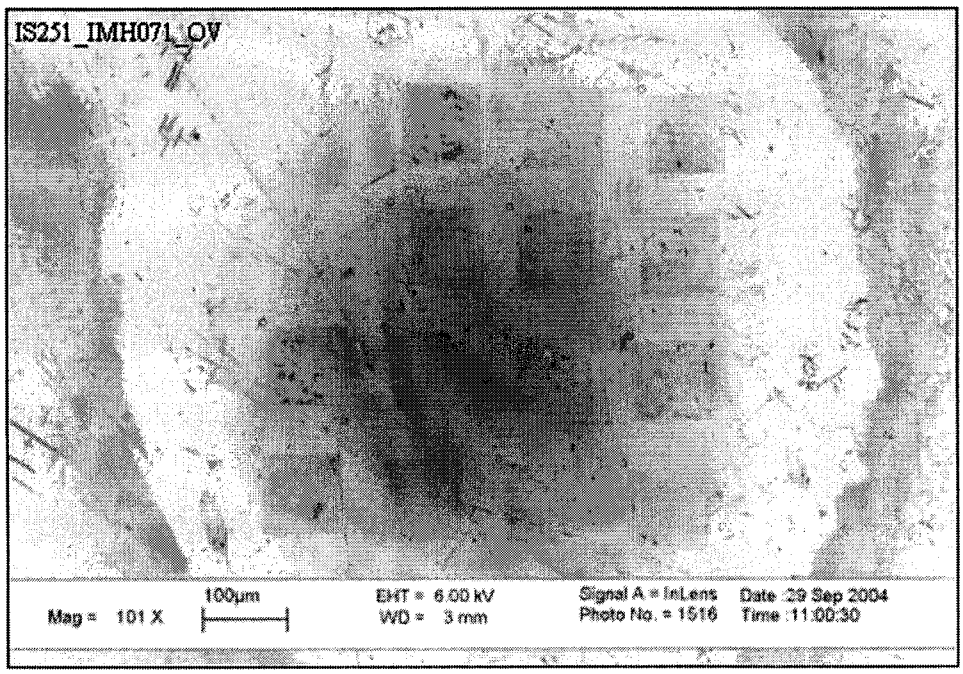

Image A.179 The image displays an overview of the patterns on sample IS251 after a liftoff. The following parameters were used: single layer of PMMA, model 20 imprinting press, imprinter IMH071 (32 fC point dose), regulator pressure of 50 psi, a separation temperature of 34.5°C, etching for 40 seconds at 100W, and a Permalloy deposition of 7 minutes at 300W.

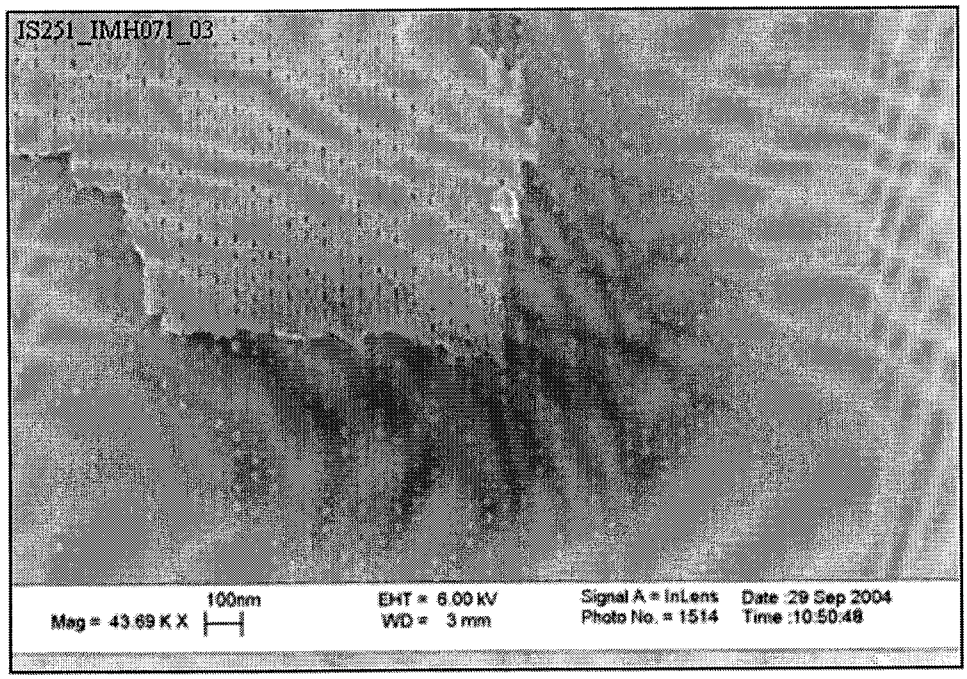

Image A.180 The image displays an area of pattern 3 on sample IS251 containing Permalloy dots. The following parameters were used: single layer of PMMA, model 20 imprinting press, imprinter IMH071 (32 fC point dose), regulator pressure of 50 psi, a separation temperature of 34.5°C, etching for 40 seconds at 100W, and a Permalloy deposition of 7 minutes at 300W.

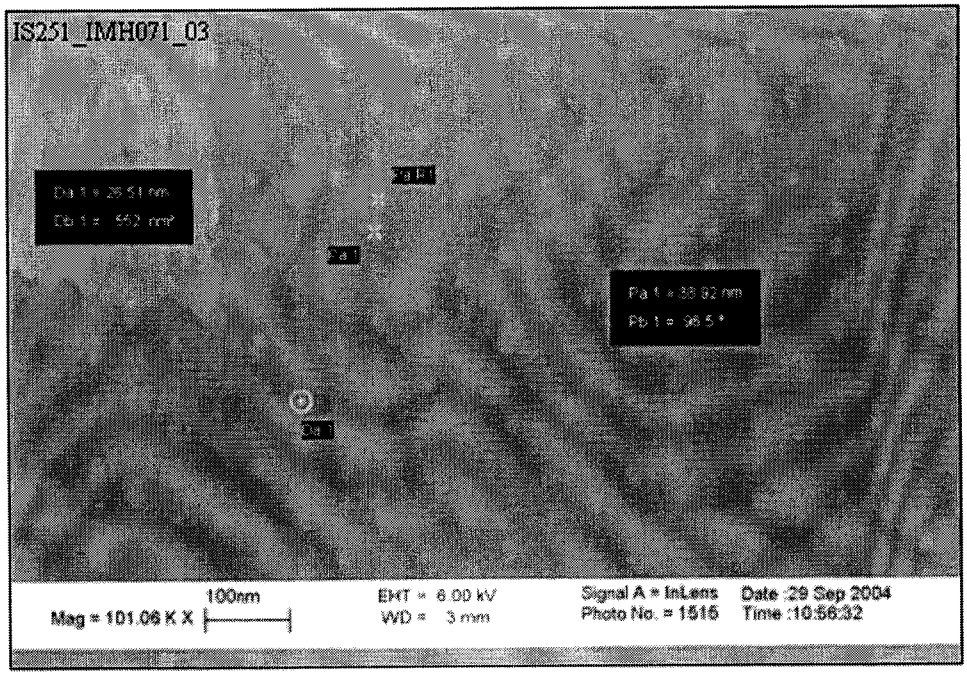

Image A.181 The image displays the measured diameter and pitch of Permalloy dots seen in pattern 3 on sample IS251. The following parameters were used: single layer of PMMA, model 20 imprinting press, imprinter IMH071 (32 fC point dose), regulator pressure of 50 psi, a separation temperature of 34.5°C, etching for 40 seconds at 100W, and a Permalloy deposition of 7 minutes at 300W.

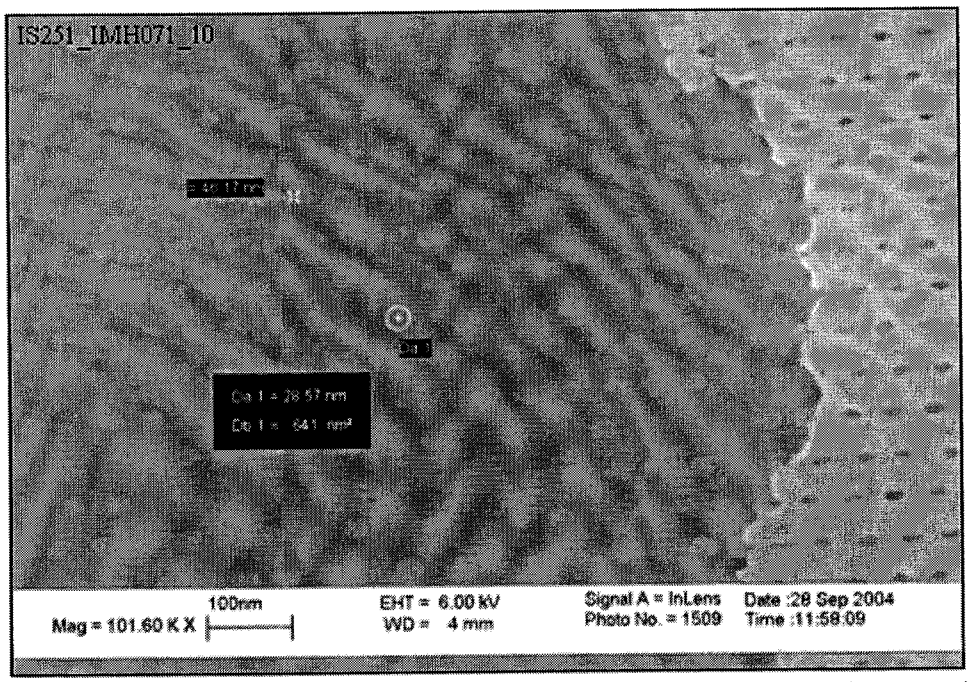

Image A.182 The image displays the measured diameter and pitch of Permalloy dots seen in pattern 10 on sample IS251. The following parameters were used: single layer of PMMA, model 20 imprinting press, imprinter IMH071 (32 fC point dose), regulator pressure of 50 psi, a separation temperature of 34.5°C, etching for 40 seconds at 100W, and a Permalloy deposition of 7 minutes at 300W.

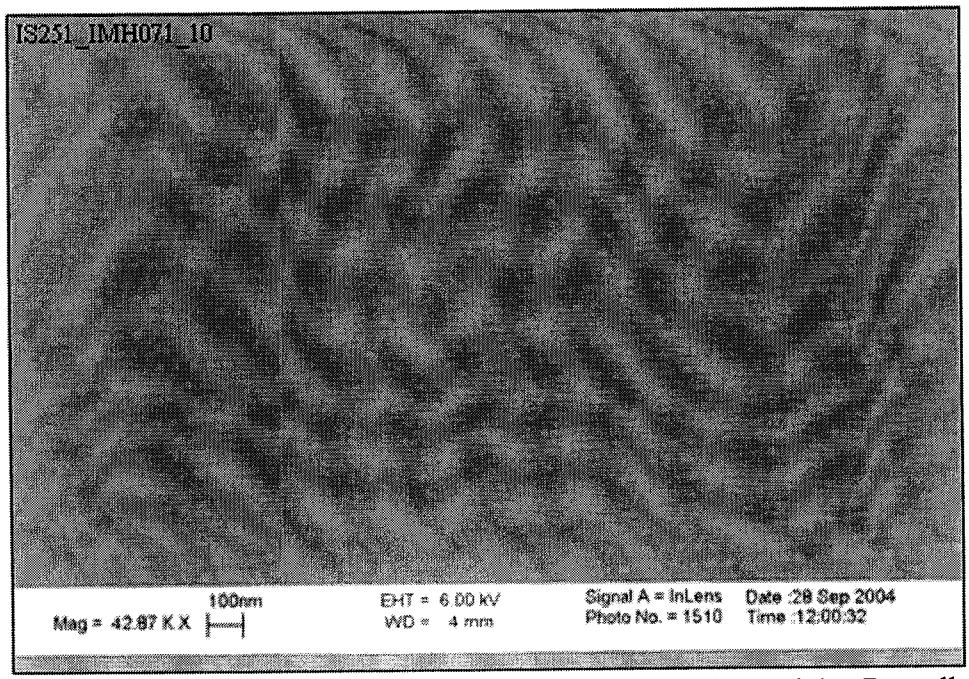

Image A.183 The image displays an area of pattern 10 on sample IS251 containing Permalloy dots. The following parameters were used: single layer of PMMA, model 20 imprinting press, imprinter IMH071 (32 fC point dose), regulator pressure of 50 psi, a separation temperature of 34.5°C, etching for 40 seconds at 100W, and a Permalloy deposition of 7 minutes at 300W.

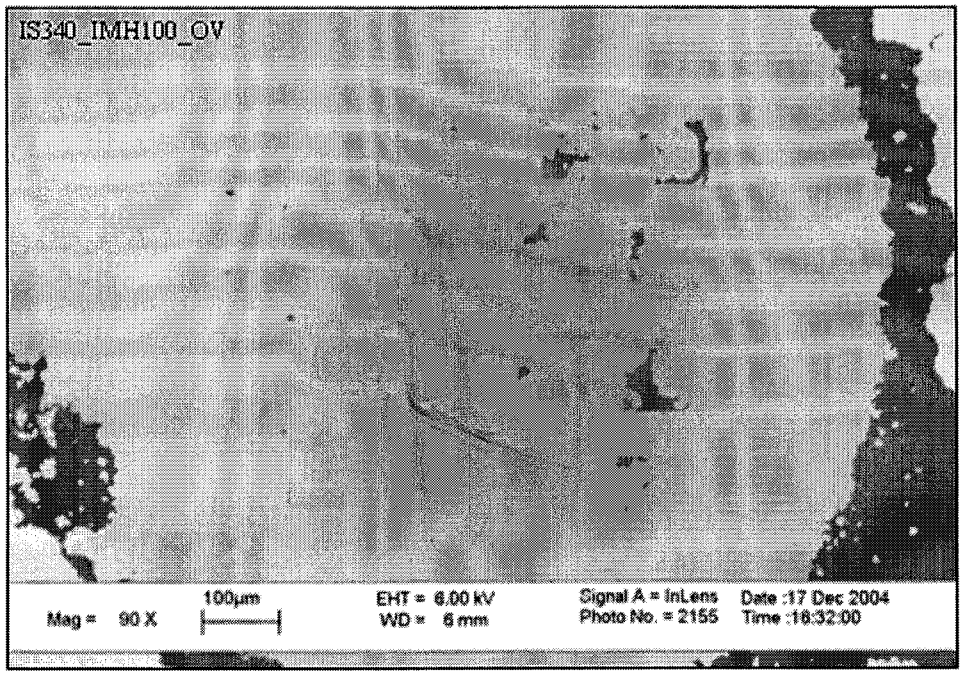

Image A.184 The image displays an overview of the patterns on sample IS340 after a liftoff. The following parameters were used: single layer of PMMA, model 20 imprinting press, imprinter IMH100 (32 fC point dose), regulator pressure of 40 psi, a separation temperature of 40.5°C, etching for 1 minute and 20 seconds at 100W, and a Permalloy deposition of 10 minutes at 300W.

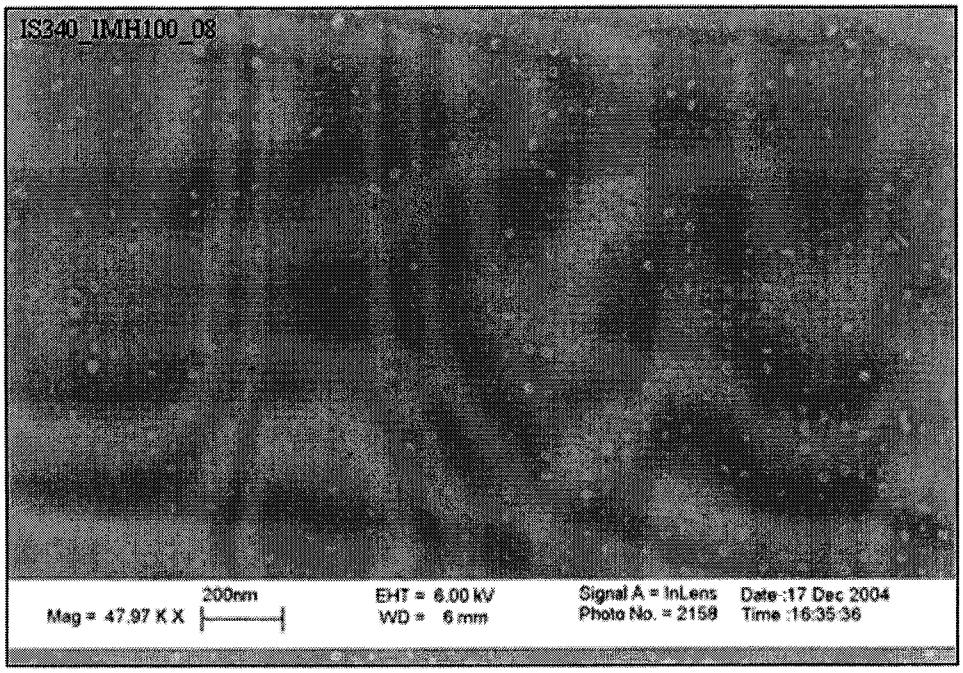

Image A.185 The image displays an area of pattern 8 on sample IS340 containing Permalloy dots. The following parameters were used: single layer of PMMA, model 20 imprinting press, imprinter IMH100 (32 fC point dose), regulator pressure of 40 psi, a separation temperature of 40.5°C, etching for 1 minute and 20 seconds at 100W, and a Permalloy deposition of 10 minutes at 300W.

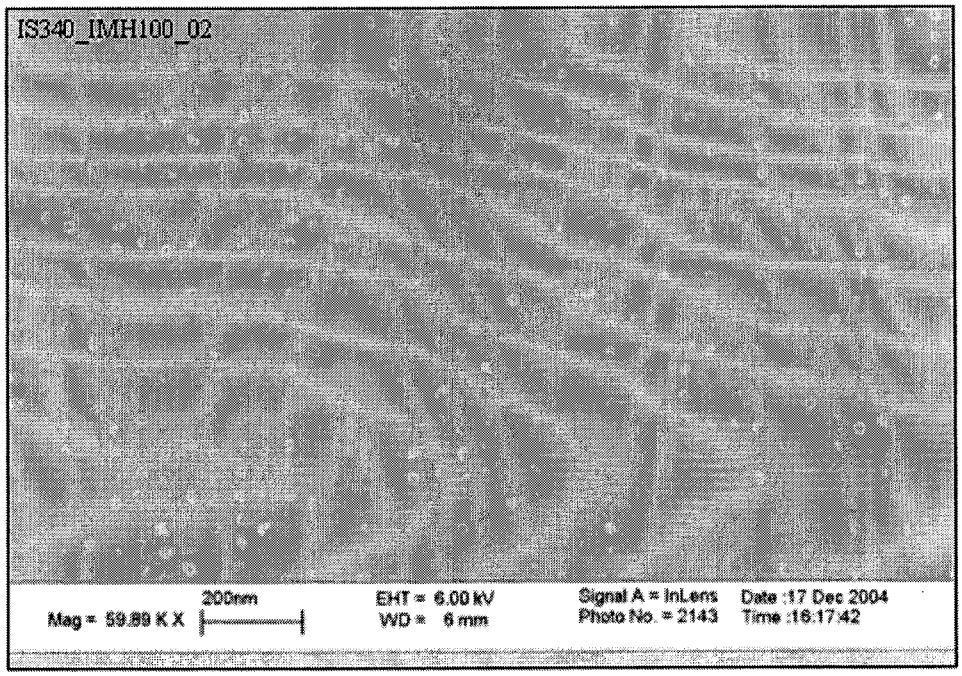

Image A.186 The image displays an area of pattern 2 on sample IS340 containing Permalloy dots. The following parameters were used: single layer of PMMA, model 20 imprinting press, imprinter IMH100 (32 fC point dose), regulator pressure of 40 psi, a separation temperature of 40.5°C, etching for 1 minute and 20 seconds at 100W, and a Permalloy deposition of 10 minutes at 300W.

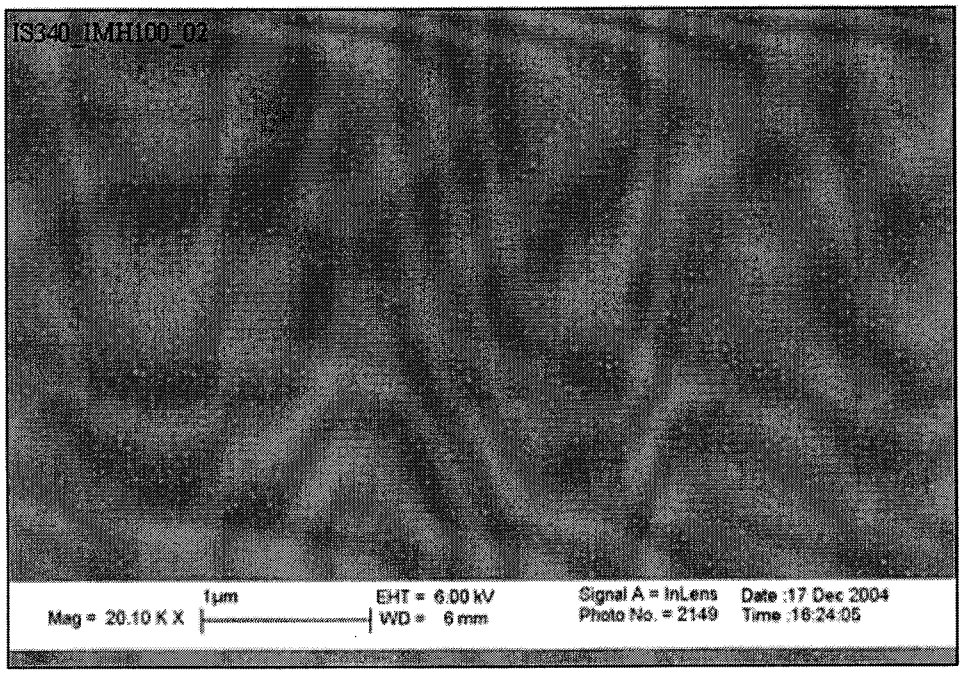

Image A.187 The image displays an area of pattern 2 on sample IS340 containing Permalloy dots. The following parameters were used: single layer of PMMA, model 20 imprinting press, imprinter IMH100 (32 fC point dose), regulator pressure of 40 psi, a separation temperature of 40.5°C, etching for 1 minute and 20 seconds at 100W, and a Permalloy deposition of 10 minutes at 300W.

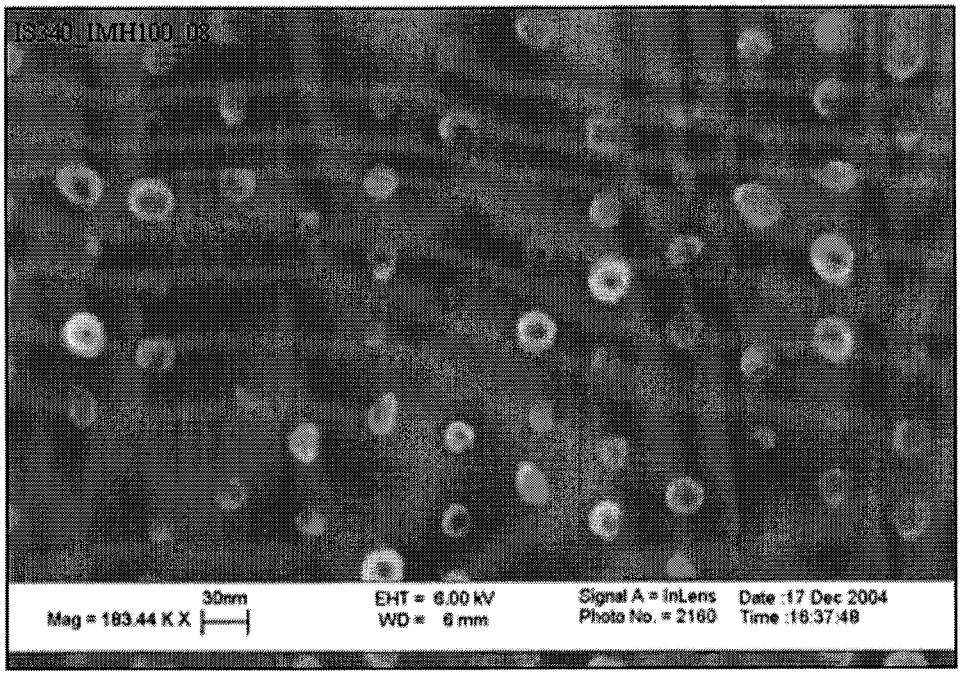

Image A.188 The image displays an area of pattern 8 on sample IS340 containing Permalloy dots. The following parameters were used: single layer of PMMA, model 20 imprinting press, imprinter IMH100 (32 fC point dose), regulator pressure of 40 psi, a separation temperature of 40.5°C, etching for 1 minute and 20 seconds at 100W, and a Permalloy deposition of 10 minutes at 300W.

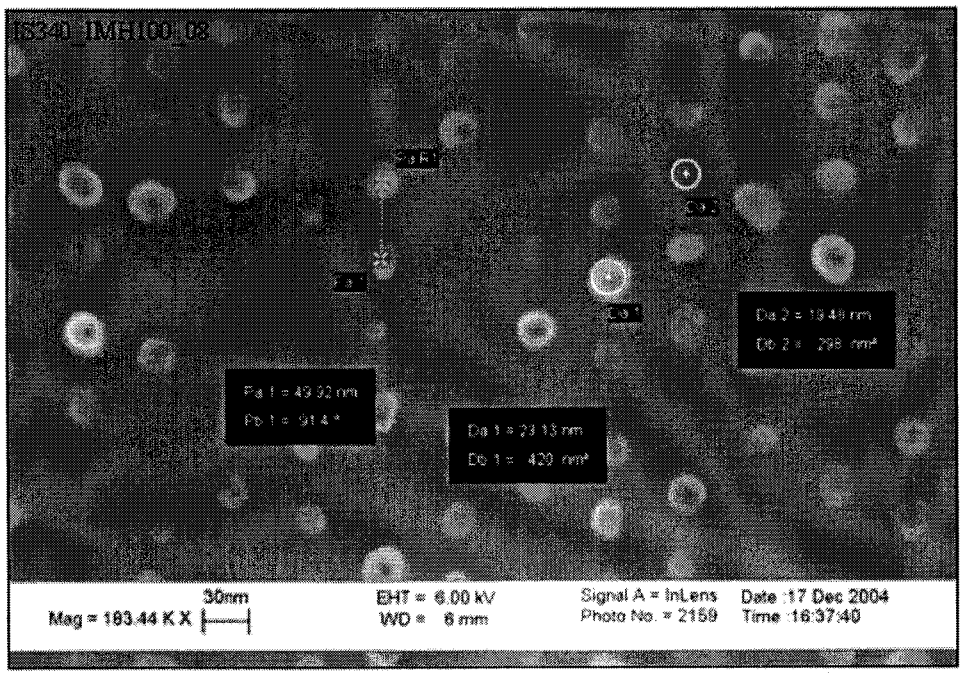

Image A.189 The image displays the measured diameter and pitch of Permalloy dots seen in pattern 8 on sample IS340. The following parameters were used: single layer of PMMA, model 20 imprinting press, imprinter IMH100 (32 fC point dose), regulator pressure of 40 psi, a separation temperature of 40.5°C, etching for 1 minute and 20 seconds at 100W, and a Permalloy deposition of 10 minutes at 300W.

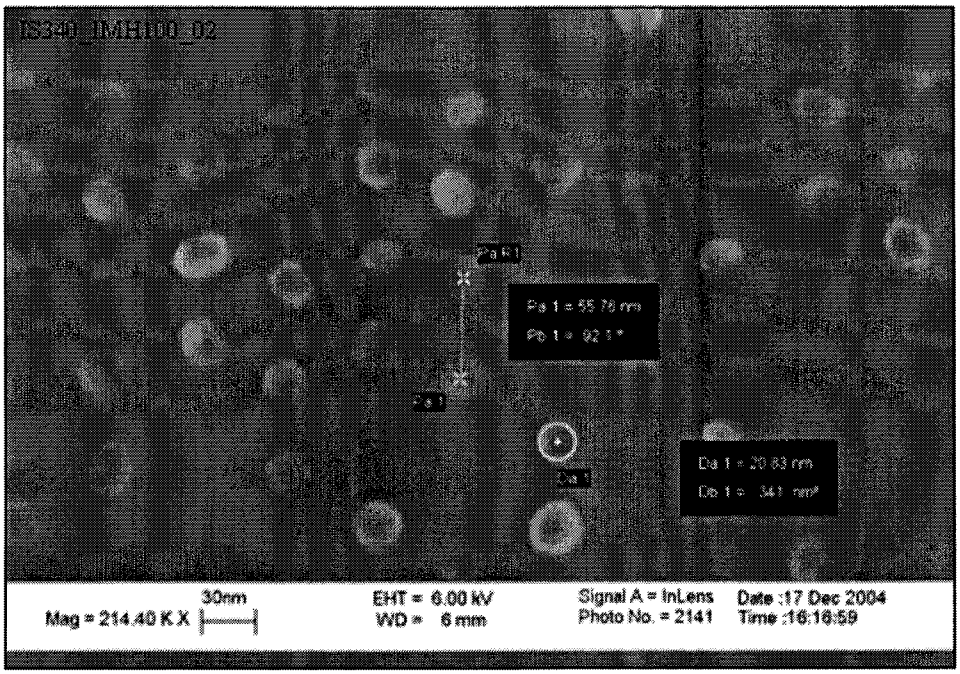

Image A.190 The image displays the measured diameter and pitch of Permalloy dots seen in pattern 2 on sample IS340. The following parameters were used: single layer of PMMA, model 20 imprinting press, imprinter IMH100 (32 fC point dose), regulator pressure of 40 psi, a separation temperature of 40.5°C, etching for 1 minute and 20 seconds at 100W, and a Permalloy deposition of 10 minutes at 300W.

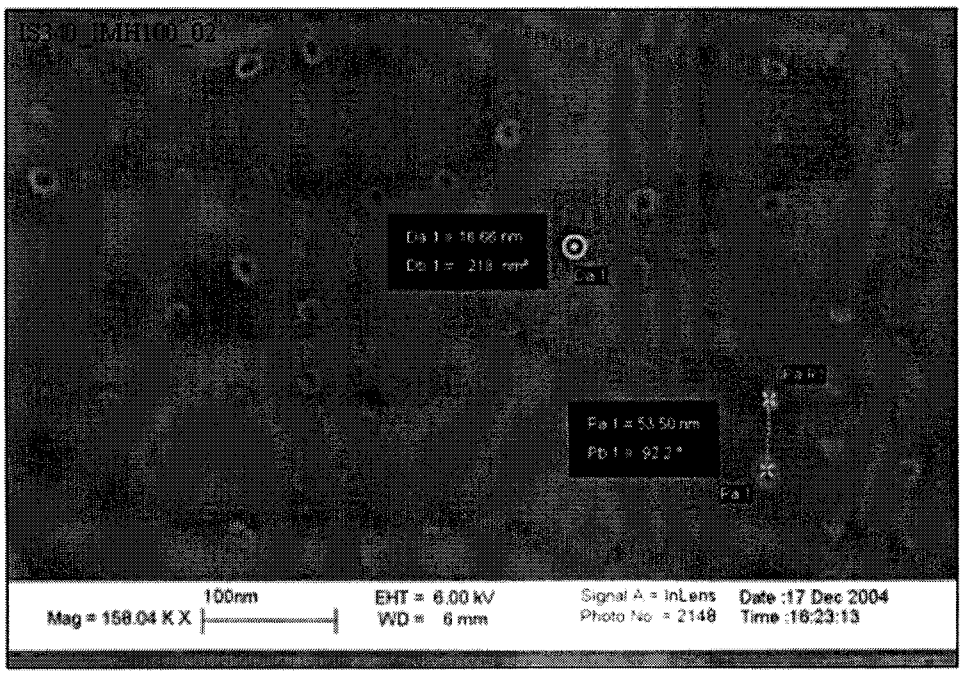

Image A.191 The image displays the measured diameter and pitch of Permalloy dots seen in pattern 2 on sample IS340. The following parameters were used: single layer of PMMA, model 20 imprinting press, imprinter IMH100 (32 fC point dose), regulator pressure of 40 psi, a separation temperature of 40.5°C, etching for 1 minute and 20 seconds at 100W, and a Permalloy deposition of 10 minutes at 300W.

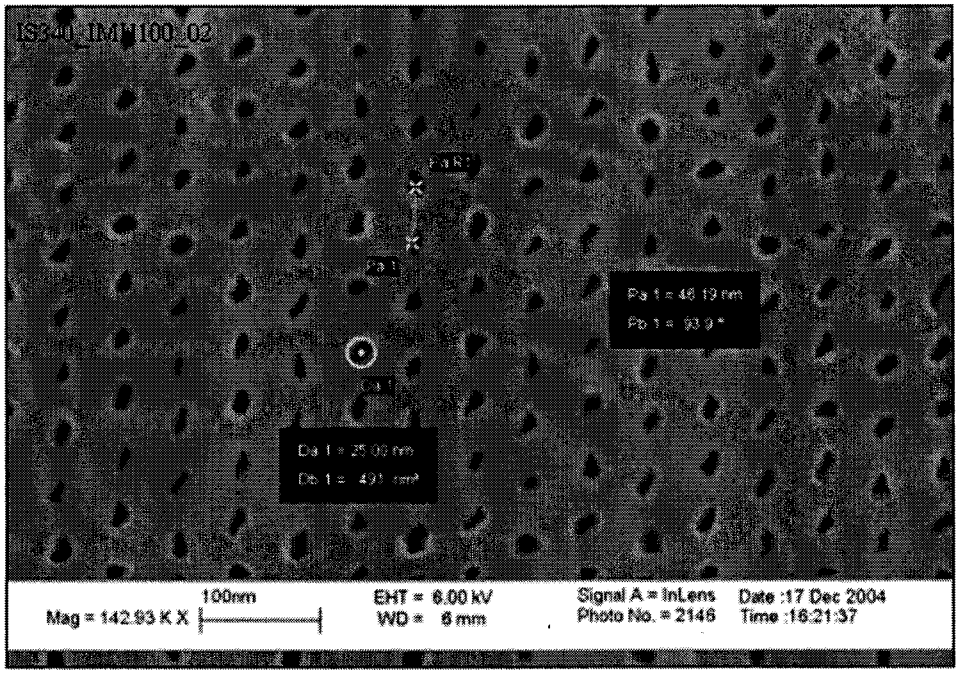

Image A.192 The image displays an area of pattern 2 on sample IS340 where the PMMA is covered with Permalloy. The following parameters were used: single layer of PMMA, model 20 imprinting press, imprinter IMH100 (32 fC point dose), regulator pressure of 40 psi, a separation temperature of 40.5°C, etching for 1 minute and 20 seconds at 100W, and a Permalloy deposition of 10 minutes at 300W.

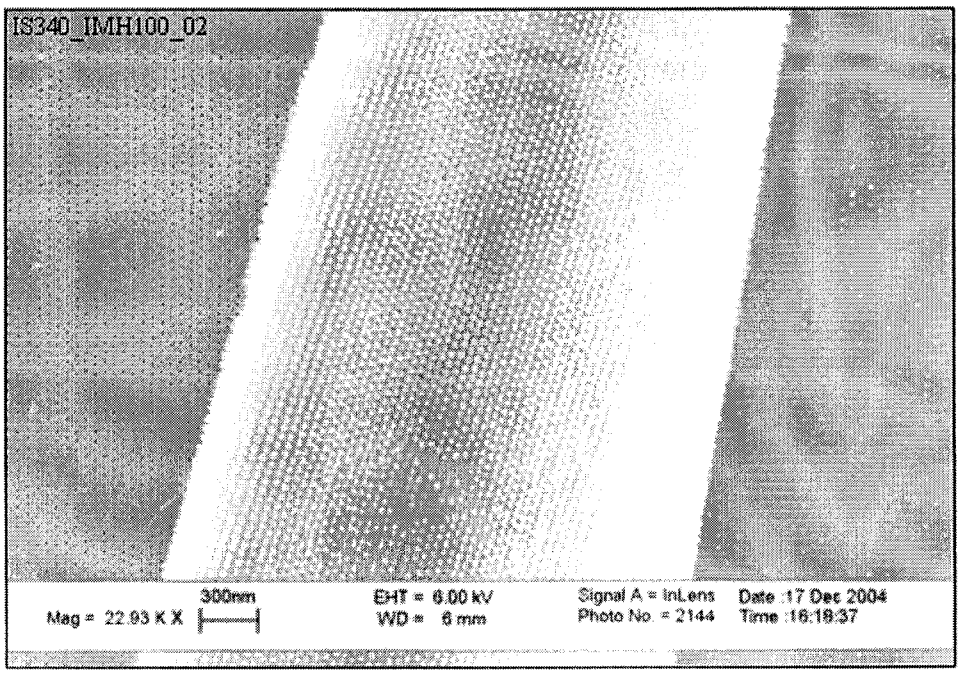

Image A.193 The image displays an area of pattern 2 on sample IS340 where the PMMA is shown ripping up the Permalloy dots. The following parameters were used: single layer of PMMA, model 20 imprinting press, imprinter IMH100 (32 fC point dose), regulator pressure of 40 psi, a separation temperature of 40.5°C, etching for 1 minute and 20 seconds at 100W, and a Permalloy deposition of 10 minutes at 300W.

A.3.2 Type 4 Bilayer

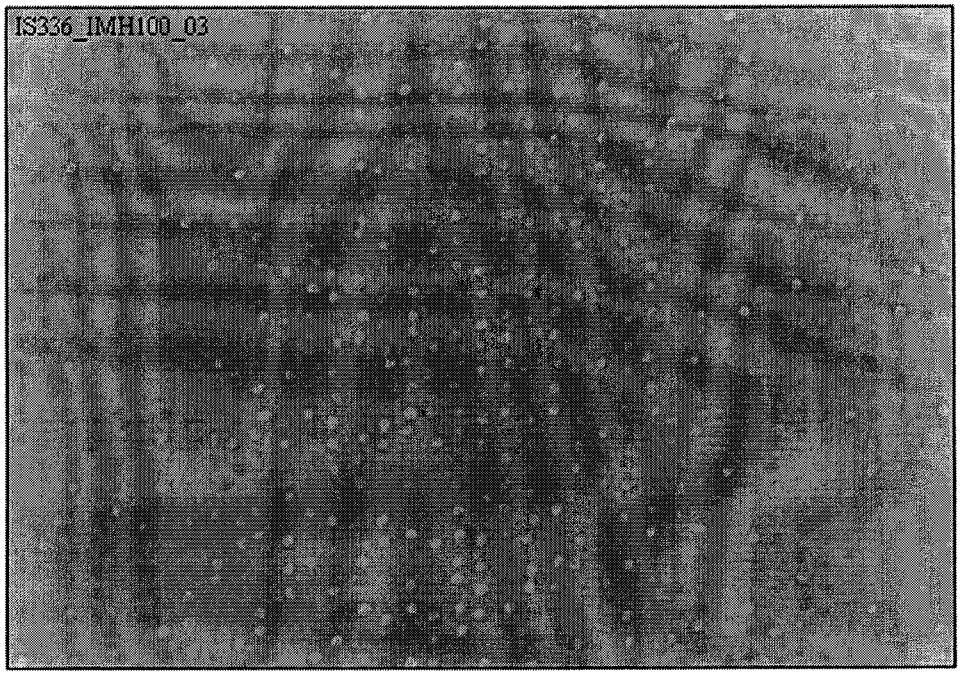

Image A.194 The image displays an area of pattern 3 on sample IS336 containing Permalloy dots. The following parameters were used: type 4 bilayer coating, model 20 imprinting press, imprinter IMH100 (32 fC point dose), regulator pressure of 40 psi, a separation temperature of 38°C, 5 second etch in methanol and a 5 second etch in chlorobenzene, and a Permalloy deposition of 10 minutes at 300W.

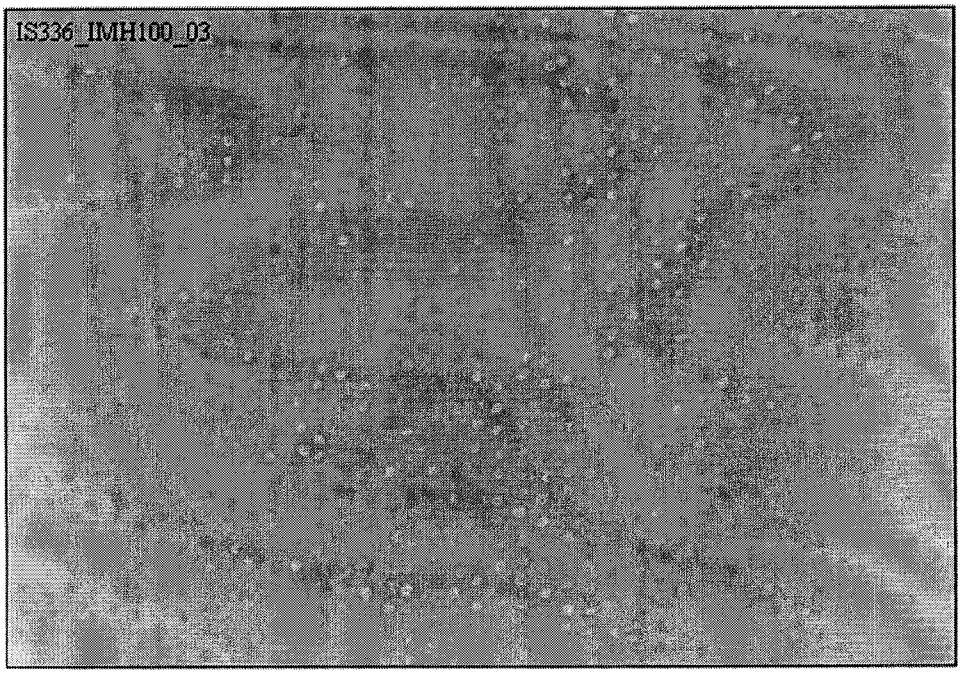

Image A.195 The image displays an area of pattern 3 on sample IS336 containing Permalloy dots. The following parameters were used: type 4 bilayer coating, model 20 imprinting press, imprinter IMH100 (32 fC point dose), regulator pressure of 40 psi, a separation temperature of 38°C, 5 second etch in methanol and a 5 second etch in chlorobenzene, and a Permalloy deposition of 10 minutes at 300W.

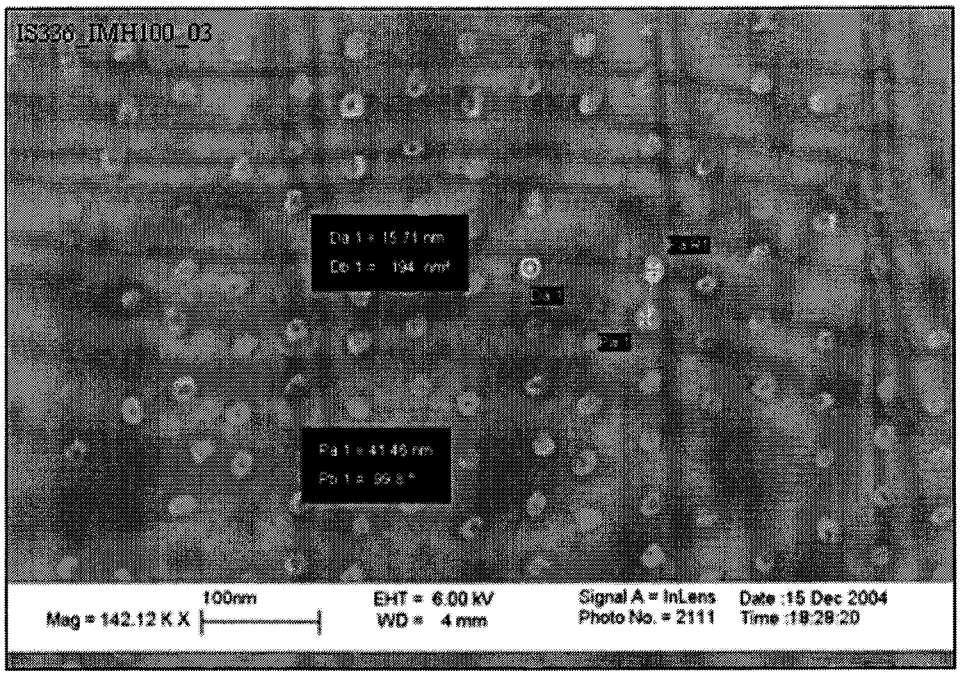

Image A.196 The image displays the measured diameter and pitch of Permalloy dots seen in pattern 3 on sample IS336. The following parameters were used: type 4 bilayer coating, model 20 imprinting press, imprinter IMH100 (32 fC point dose), regulator pressure of 40 psi, a separation temperature of 38°C, 5 second etch in methanol and a 5 second etch in chlorobenzene, and a Permalloy deposition of 10 minutes at 300W.

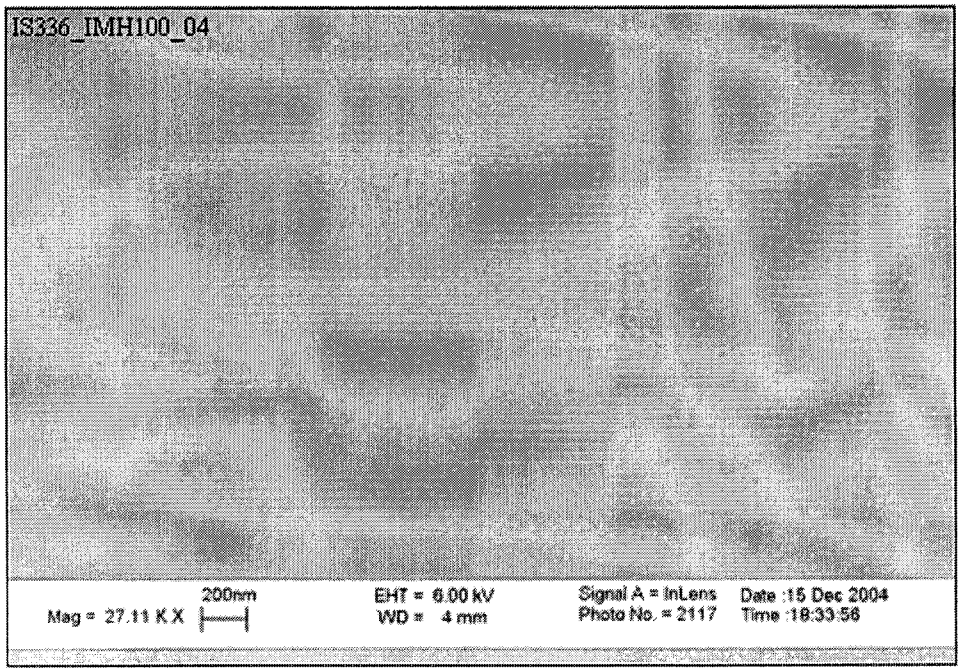

Image A.197 The image displays an area of pattern 4 on sample IS336 containing Permalloy dots. The following parameters were used: type 4 bilayer coating, model 20 imprinting press, imprinter IMH100 (32 fC point dose), regulator pressure of 40 psi, a separation temperature of 38°C, 5 second etch in methanol and a 5 second etch in chlorobenzene, and a Permalloy deposition of 10 minutes at 300W.

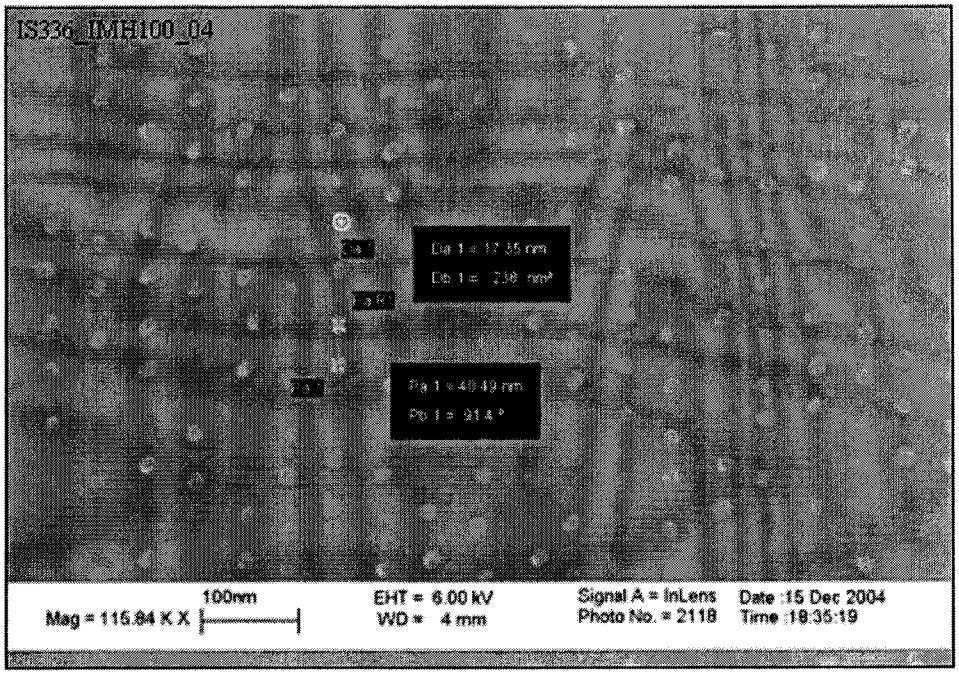

Image A.198 The image displays the measured diameter and pitch of Permalloy dots seen in pattern 4 on sample IS336. The following parameters were used: type 4 bilayer coating, model 20 imprinting press, imprinter IMH100 (32 fC point dose), regulator pressure of 40 psi, a separation temperature of 38°C, 5 second etch in methanol and a 5 second etch in chlorobenzene, and a Permalloy deposition of 10 minutes at 300W.

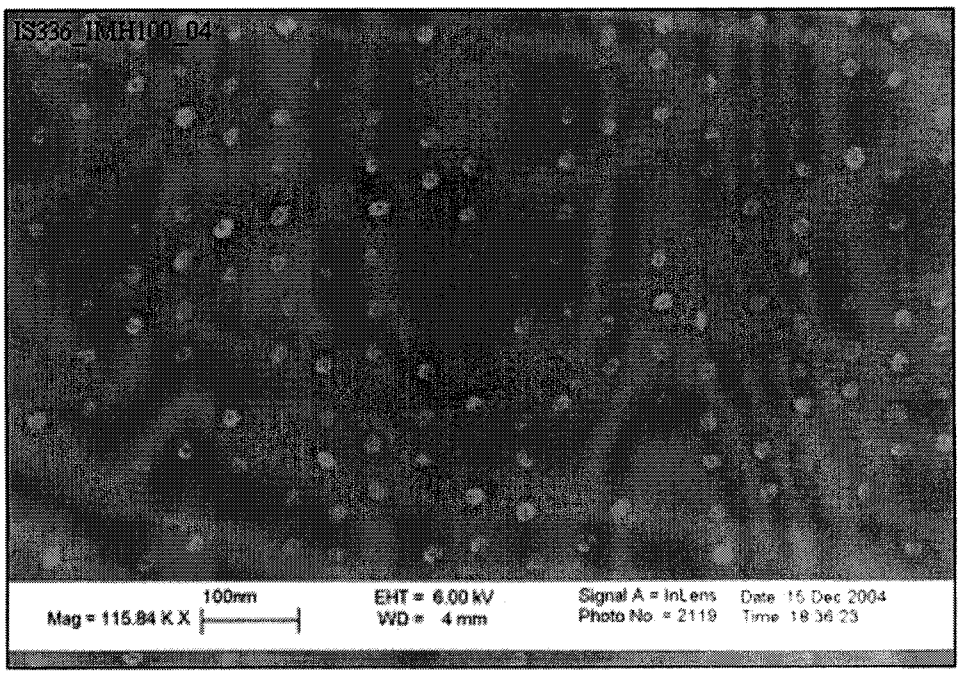

Image A.199 The image displays an area of pattern 4 on sample IS336 containing Permalloy dots. The following parameters were used: type 4 bilayer coating, model 20 imprinting press, imprinter IMH100 (32 fC point dose), regulator pressure of 40 psi, a separation temperature of 38°C, 5 second etch in methanol and a 5 second etch in chlorobenzene, and a Permalloy deposition of 10 minutes at 300W.

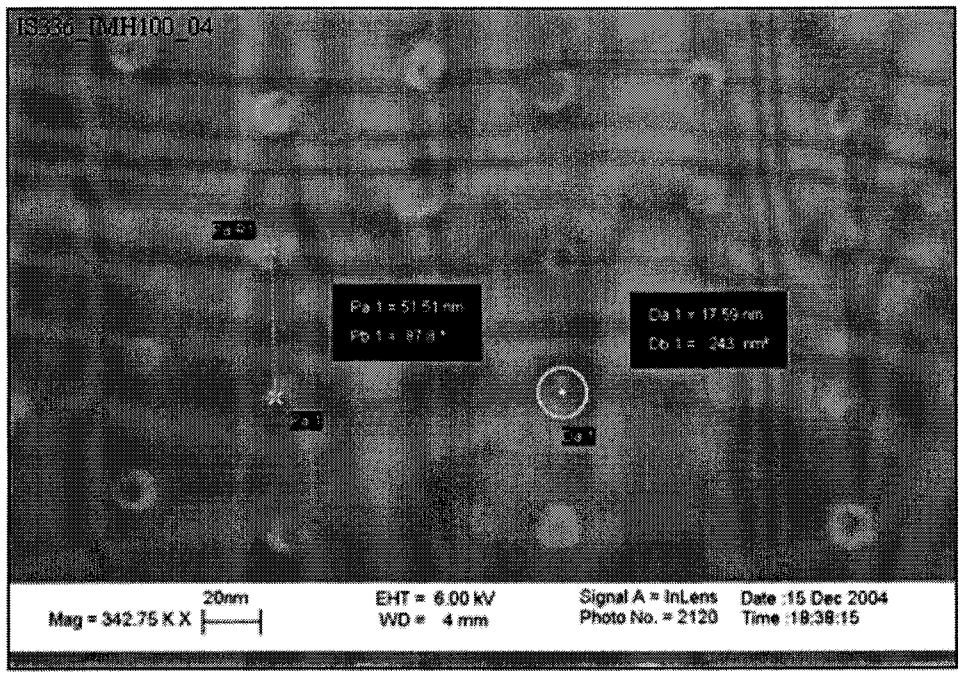

Image A.200 The image displays the measured diameter and pitch of Permalloy dots seen in pattern 4 on sample IS336. The following parameters were used: type 4 bilayer coating, model 20 imprinting press, imprinter IMH100 (32 fC point dose), regulator pressure of 40 psi, a separation temperature of 38°C, 5 second etch in methanol and a 5 second etch in chlorobenzene, and a Permalloy deposition of 10 minutes at 300W.

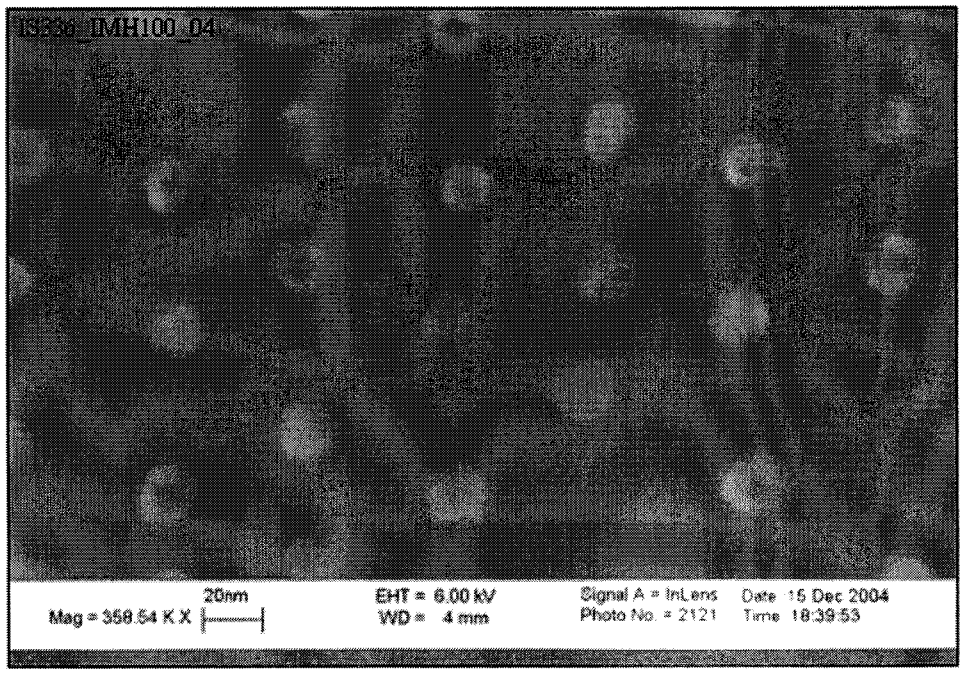

Image A.201 The image displays an area of pattern 4 on sample IS336 containing Permalloy dots. The following parameters were used: type 4 bilayer coating, model 20 imprinting press, imprinter IMH100 (32 fC point dose), regulator pressure of 40 psi, a separation temperature of 38°C, 5 second etch in methanol and a 5 second etch in chlorobenzene, and a Permalloy deposition of 10 minutes at 300W.

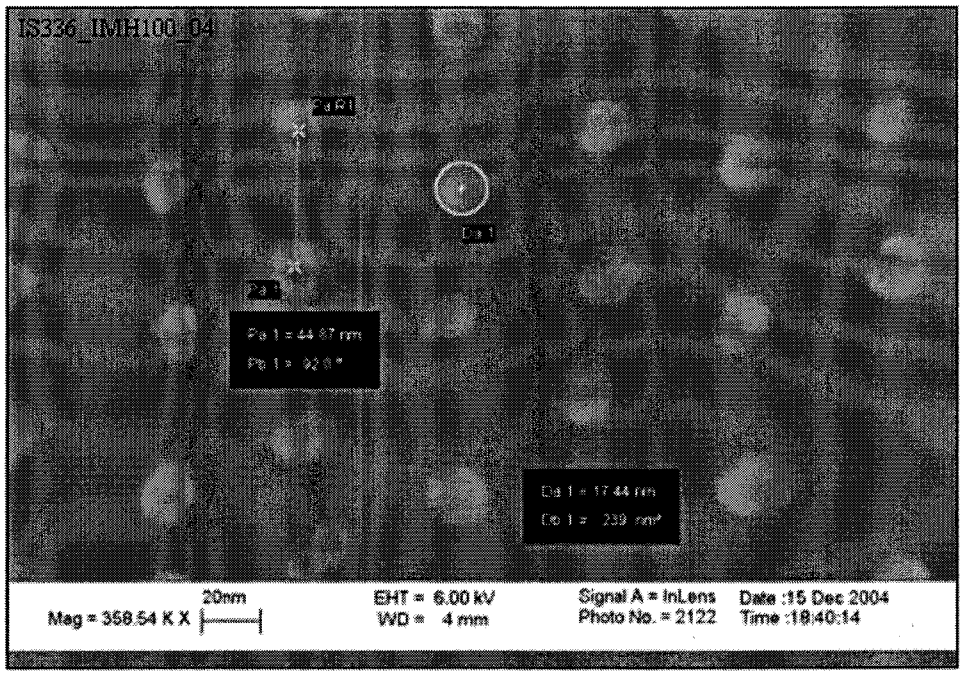

Image A.202 The image displays the measured diameter and pitch of Permalloy dots seen in pattern 4 on sample IS336. The following parameters were used: type 4 bilayer coating, model 20 imprinting press, imprinter IMH100 (32 fC point dose), regulator pressure of 40 psi, a separation temperature of 38°C, 5 second etch in methanol and a 5 second etch in chlorobenzene, and a Permalloy deposition of 10 minutes at 300W.

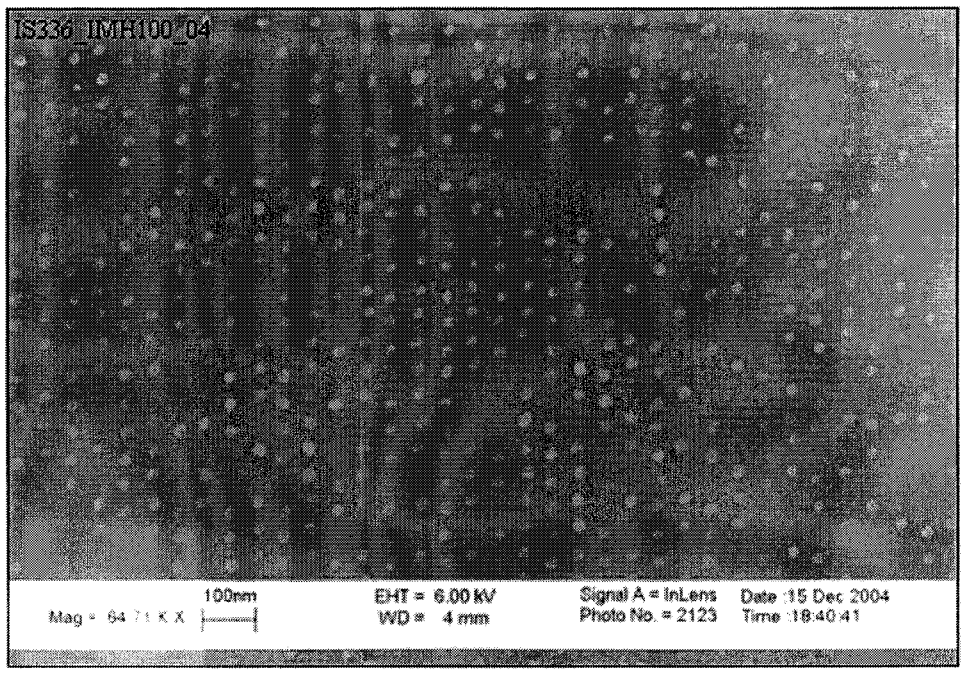

Image A.203 The image displays an area of pattern 4 on sample IS336 containing Permalloy dots. The following parameters were used: type 4 bilayer coating, model 20 imprinting press, imprinter IMH100 (32 fC point dose), regulator pressure of 40 psi, a separation temperature of 38°C, 5 second etch in methanol and a 5 second etch in chlorobenzene, and a Permalloy deposition of 10 minutes at 300W.

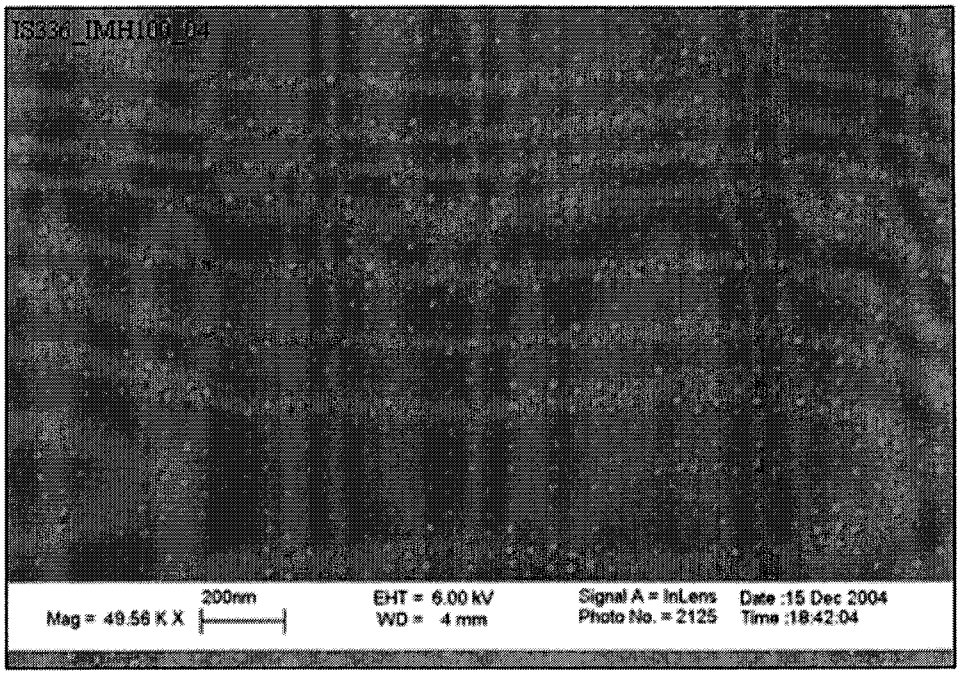

Image A.204 The image displays an area of pattern 4 on sample IS336 containing Permalloy dots. The following parameters were used: type 4 bilayer coating, model 20 imprinting press, imprinter IMH100 (32 fC point dose), regulator pressure of 40 psi, a separation temperature of 38°C, 5 second etch in methanol and a 5 second etch in chlorobenzene, and a Permalloy deposition of 10 minutes at 300W.

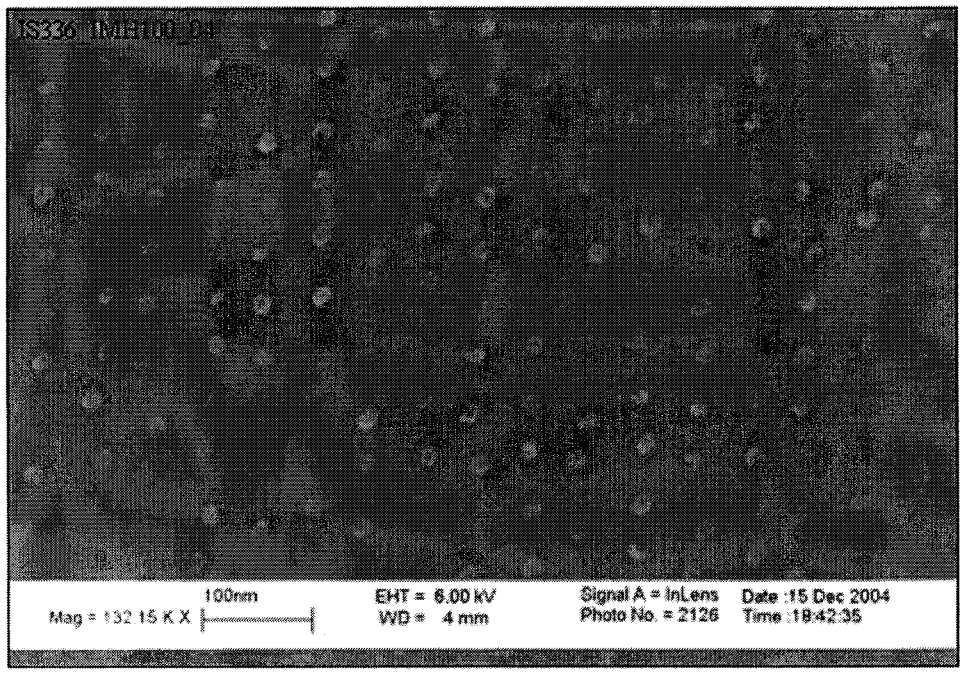

Image A.205 The image displays an area of pattern 4 on sample IS336 containing Permalloy dots. The following parameters were used: type 4 bilayer coating, model 20 imprinting press, imprinter IMH100 (32 fC point dose), regulator pressure of 40 psi, a separation temperature of 38°C, 5 second etch in methanol and a 5 second etch in chlorobenzene, and a Permalloy deposition of 10 minutes at 300W.

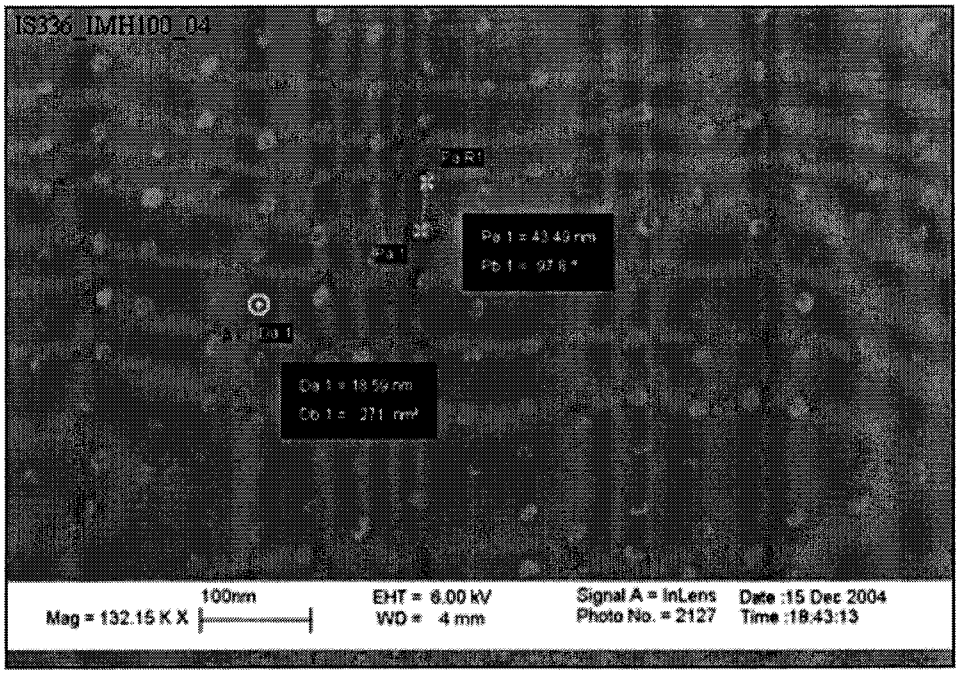

Image A.206 The image displays the measured diameter and pitch of Permalloy dots seen in pattern 4 on sample IS336. The following parameters were used: type 4 bilayer coating, model 20 imprinting press, imprinter IMH100 (32 fC point dose), regulator pressure of 40 psi, a separation temperature of 38°C, 5 second etch in methanol and a 5 second etch in chlorobenzene, and a Permalloy deposition of 10 minutes at 300W.

REFERENCES

[1] How Much Information? 2003. 27 October 2003. <http://www.sims.berkeley.edu/research/projects/how-much-info-003/execsum.htm#report>.

[2] E. Grochowski and Halem, R.D. "Technological Impact of Magnetic Hard Disk Drives on Storage systems." IBM Systems Journal. 42 (2003): 338-346.

[3] J.R. Wilson. "Solid-State Memory Takes Over in Niche Military and Aerospace Applications." Military and Aerospace Electronics Magazine. December 2001.

[4] Hitachi Global Storage Technologies. 2005. <http://www.hitachigst.com/hdd/research/>.

[5] Kanu G. Ashar. Magnetic Disk Drive Technology – Heads, Media, Channel, Interfaces, and Integration. New York: The Institute of Electrical and Electronics Engineers, Inc., 1997.

[6] C. Denis Mee and Eric D. Daniel. Magnetic Storage Handbook. New York: McGraw-Hill, 1990.

[7] IBM's 'Pixie Dust' Breakthrough to Quadruple Disk Drive Density. 21 May 2001. <http://domino.research.ibm.com/comm/pr.nsf/pages/news.20010518_pixie_dust.html>.

[8] Seagate Sets Aerial Density Storage Record. <http://www.seagate.com/newsinfo/technology/d4g.html>.

[9] 90 nm: The World's Most Advanced Chip-Making Process. <http://www.intel.com/research/silicon/nanometer.htm>.

[10] Shan X. Wang and Alexander M. Taratorin. Magnetic Information Storage Technology. New York: Academic Press, 1999.

[11] M.L. Plummer, J. Van Ek, D. Weller., eds. The Physics of Ultra-High Density Magnetic Recording. New York: Springer, 2001.

[12] The Giant Magnetoresistive Head: A Giant Leap for IBM Research. <http://www.research.ibm.com/research/gmr.html>.

[13] Richard Liboff. Introductory to Quantum Mechanics. New York: Benjamin Cummings, 2002.

[14] M. Takagishi, K. Koi, M. Yoshikawa, T. Funayama, H. Iwasaki, and M. Sahashi. "The Applicability of CPP-GMR Heads for Magnetic Recording." IEEE Transactions on Magnetics. 38(2002): 2277-2282.

[15] D.E. Heim. "Design and Operation of Spin Valve Sensors." IEEE Transactions on Magnetics. 30(1994): 316-321.

[16] Y. Chen and C. Tong. "Inductive Write Heads for Greater Than 60Gb/in^2 Demonstration." IEEE Transactions on Magnetics. 37 (2001): 1719-1722.

[17] S.X. Wang and P.R. Webb. "Modeling of Submicron Trackwidth Inductive Write Head Designs." IEEE Transactions on Magnetics. 31 (1995): 2687-2689.

[18] H. Neal Bertram. Theory of Magnetic Recording. New York: Cambridge University Press, 1994.

[19] H.C. Tong. "The Micromagnetics of Thin-Film Disk Recording Tracks." IEEE Transactions on Magnetics. 20 (1984): 1831-1833.

[20] Yingjian Chen. "Inductive Write Heads Using High-Moment Pole Materials for Ultrahigh-Density Demonstrations." IEEE Transactions on Magnetics. 39 (2003): 2368-2370.

[21] G. Bottoni, D. Candolfo, and A. Cecchetti. "Thermal Stability of Magnetic Properties in Ternary and Quaternary Co-Based Alloy Thin-Film Media." Journal of Magnetism and Magnetic Materials. (2004): 1-4.

[22] M. Takahashi, A. Kikuchi, and J. Nakai. "The Ultra-Clean Sputtering Process and High Density Magnetic Recording Media." IEEE Transactions on Magnetics. 33 (1997): 2938.

[23] X. Wang, Z.Y. Li, P. Tan, D.C. Zhang, and X. Zhang. "High Coercivity Sm(Co, Cu, Ti)/Cr Sputtered Thin Films for Longitudinal Recording." Advanced Nanomaterials and Nanodevices. 10-14 (2002): 695-699.

[24] Marilee A. Schultz, Sudhir S. Malhotra, Brij B. Lal, Jay M. Kimmal, Michael A. Russak, Francis Liu, Kroum Stoev, Stone Shi, Hua-Ching Tong, and Subrata Dey. "26.5 Gb/in^2 Aerial-Density Longitudinal Thin Film Media." IEEE Transactions on Magnetics. 36 (2000): 2143-2147.

[25] Dieter Weller and Andreas Moser. "Thermal Effect Limits in Ultrahigh-Density Magnetic Recording." IEEE Transactions on Magnetics. 35(1999): 4423-4439.

[26] J.A Thornton. "Influence of Apparatus and Geometry Deposition Conditions on the Structure and Topography of Thick Sputtered Coatings." Journal of Vacuum Science and Technology. 11(1974): 667-670.

[27] Yuzuru Hosoe, Tetsuya Kanbe, Kiwamu Tanabashi, Ichiro Tamai, Satoshi Matsunuma, and Yoshio Takahashi. "Thermal Aftereffects in Thin Film Magnetic Recording Media." IEEE Transactions on Magnetics. 34 (1998): 1528-1533.

[28] David W. Oxtoby, H.P. Gillis, and Norman H. Nachtrieb. Principles of Modern Chemistry. Philadelphia: Saunders College Publishing, 1999.

[29] H.J. Richter. "Longitudinal Recording at 10 to 20 Gbit/inch^2 and Beyond." IEEE Transactions on Magnetics. 35(1999): 2790-2795.

[30] D.C. Crew, P.G. McCormick, and R. Street. "The Interpretation of Magnetic Viscosity." The Journal of Applied Physics. 29(1996): 2313.

[31] M.P. Sharrock. "Time Dependent Magnetic Phenomena and Particle Size Effects in Recording Media." IEEE Transactions on Magnetics. 26(1990): 193-201.

[32] P. Bruno, G. Bayreuther, P. Beauvillain, C. Chappert, G. Lugert, D. Renard, J.P. Renard, and J. Seiden. "Magnetic Properties of Ultrathin Ferromagnetic Films." Journal of Applied Physics. 68(1990): 5759.

[33] H.J Richter, S.Z. Wu, and R. Malmhall. "Dynamic Coercivity Effects in Thin Film Media." IEEE Transactions on Magnetics. 34(1998): 1540-1542.

[34] N. Inaba, Y. Uesaka, A. Nakamura, M. Futamoto, and Y. Sugita. "Damping Constants of CoCrTa and CoCrPt thin films." IEEE Transactions on Magnetics. 33(1997): 2989-2991.

[35] Q. Peng and H.N. Bertram. "Micromagnetic Studies of Recording Dynamics and Switching Speed in Longitudinal Thin Film Media." IEEE Transactions on Magnetics. 33(1997): 2677-2679.

[36] Alexander Taratorin, David Cheng, and Ernesto Marinero. "Media Noise, Nonlinear Distortions, and Thermal Stability in High Density Recording." IEEE Transactions on Magnetics. 36(2000): 80-85.

[37] Eric E. Fullerton, David T. Margulies, Natacha Supper, Hoa Do, Manfred Schabes, Andreas Berger, and Andreas Moser. "Anitferromagnetically Coupled Magnetic Recording Media." IEEE Transactions on Magnetics. 39 (2003): 639-644.

[38] S.N. Piramanayagam, J.P. Wang, X. Shi, S.I. Pang, C.K. Pock, Z.S. Shan, and T.C. Chong. "Magnetic Properties and Switching Field Control of Antiferromagnetically Coupled Recording Media." IEEE Transactions on Magnetics. 37 (2001): 1438-1440.

[39] Manfred E. Schabes, Eric E. Fullerton, and David T. Margulies. "Theory of Antiferromagnetically Coupled Magnetic Recording Media." IEEE Transactions on Magnetics. 37(2001): 1432-1434.

[40] Bo Bian, Mike Avenell, Jackie Tsoi, Larry Mei, Sudhir Malhotra, and Gerardo Bertero. "Thermal Stability Improvement for Longitudinal Magnetic Recording Media." IEEE Transactions on Magnetics. 41(2005): 648-653.

[41] J.N. Zhou, B.R. Acharya, E.N. Abarra, G. Choe, J. Gao, and K.E. Johnson. "Performance Comparison Between Conventional and AFC Media at Different Orientation Ratios." IEEE Transactions on Magnetics. 40(2004): 2428-2430.

[42] David E. Laughlin, S. Kumar, Yingguo Peng, and Anup G. Roy. "Engineering the Microstructure of Thin Films for Perpendicular Recording." IEEE Transactions on Magnetics. 41(2005): 719-723.

[43] Shun-ichi Iwasaki. "Guiding Principle for Research on Perpendicular Magnetic Recording." IEEE Transactions on Magnetics. 41(2005): 683-686.

[44] H.N. Bertram and M. Williams. "SNR and Density Limit Estimates: A Comparison of Longitudinal and Perpendicular Recording." IEEE Transactions on Magnetics. 36(2000): 4-9.

[45] Martyn Williams. "Toshiba To Use Perpendicular Recording in New HDDs." PCWorld. December 2004.

[46] Masukazu Igarashi, Miki Hara, Atsushi Nakamura, Yuzuru Hosoe, and Yutaka Sugita. "High-Density Perpendicular Recording Media With Large Grain Separation." IEEE Transactions on Magnetics. 41(2005): 549-554.

[47] Manfred Albrecht, Srikanth Ganesan, Charles T. Rettner, Andreas Moser, Margaret E. Best, Robert L. White, and Bruce D. Terris. "Patterned Perpendicular and Longitudinal Media: A Magnetic Recording Study." IEEE Transactions on Magnetics. 39(2003): 2323-2325.

[48] <http://www.bell-labs.com/project/SCALPEL/>.

[49] J.I. Martin, J. Nogues, Kai Liu, J.L. Vicent, and Ivan K. Schuller. "Ordered Magnetic Nanostructures: Fabrication and Properties." Journal of Magnetism and Magnetic Materials. 256(2003): 449-501.

[50] P. Rai-Choudhury, ed. Handbook of Microlithography, Micromachining, and Microfabrication. Washington: The International Society for Optical Engineering and The Institution for Electrical Engineers, 1997.

[51] Raymond A. Serway and Robert J. Beichner. Physics for Scientists and Engineers. United States: Thomson Learning, Inc., 2000.

[52] J.C. Lodder. "Methods for Preparing Patterned Media for High-Density Recording." Journal of Magnetism and Magnetic Materials. 272-276(2004): 1692-1697.

[53] Michael E. Walsh. "Nanostructuring Magnetic Thin-Films Using Interference Lithography." Dissertation Massachusetts Institute of Technology, 2000.

[54] J.M. Carter, R.C. Fleming, T.A. Savas, M.E. Walsh, and T.B. O'Reilly. "Interference Lithography." MTL Annual Report 2003. (2003): 186-188.

[55] M.L. Schattenbrug, C.G. Chen, R.K. Heilmann, P.T. Konkola, and G.S. Patti. "Progress Towards a General Gratting Patterning Technology Using Phase-Locked Scanning Beams." Proceedings of the SPIE. 4485(2001): 1-7.

[56] R. Murillo, H.A. Van Wolferen, L. Abelmann, J.C. Lodder. "Fabrication of Patterned Magnetic Nanodots by Laser Interference Lithography." Microelectronic Engineering. 78-79(2005): 260-265.

[57] Victor V. Zhirnov and Daniel J.C. Herr. "New Frontiers: Self-Assembly and Nanoelectronics." Computer. (2001): 34-43.

[58] Bharat Bhushan, ed. Springer Handbook of Nanotechnology. Germany: Springer-Verlag Berlin Heidelberg, 2004.

[59] Gregory Timp, ed. Nanotechnology. New York: Springer-Verlag Inc., 1999.

[60] Rachel K. Smith, Penelope A. Lewis, Paul S. Weiss. "Patterning Self-Assembled Monolayers." Progress in Surface Science. 75(2004): 1-68.

[61] Babak Amir Parviz, Declan Ryan, and George M. Whitesides. "Using Self-Assembly for the Fabrication of Nano-Scale Electronic and Photonic Devices." IEEE Transactions on Advanced Packaging. 26(2003): 233-241.

[62] S. Ander, S. Sun, C.B. Murray, C.T. Rettner, M.E. Best, T. Thomson, M. Albrecht, J.-U. Thiele, E.E. Fullerton, and B.D. Terris. "Lithography and Self-Assembly for Nanometer Scale Magnetism." Microelectronic Engineering. 61-62(2002): 569-575.

[63] Charles P. Poole Jr. and Frank J. Owens. Introduction to Nanotechnology. Hoboken: John Wiley & Sons Inc., 2003.

[64] Laboratory of Louis Neel. 12 January 2005. <http://lab-neel.grenoble.cnrs.fr/themes/couches/ext/gallery/index-en.html>.

[65] Rachel A. Segalman. "Patterning with Block Copolymer Thin-Films." Materials Science and Engineering. 48(2005): 191-226.

[66] Gary Stix. "Nano Patterning: IBM Brings Closer to Reality Chips that Put Themselves Together." Scientific American. March 2004.

[67] Katsuyuki Naito, Hiroyuki Hieda, Masatoshi Sakurai, Yoshiyuki Kamata, and Koji Asakawa. "2.5-Inch Disk Patterned Media Prepared by an Artificially Assisted Self-Assembling Method." IEEE Transactions on Magnetics. 38(2002): 1949-1951.

[68] Charles T. Black and Odile Bezencenet. "Nanometer-Scale Pattern Registration and Alignment by Directed Diblock Copolymer Self-Assembly." IEEE Transactions on Nanotechnology. 3(2004): 412-415.

[69] Stephen Y. Chou, Peter R. Krauss, and Preston J. Renstrom. "Nanoimprint Lithography." Journal of Vacuum Science and Technology. 14(1996): 4129-4133.

[70] Brian O. Faircloth. "Bi-layer Nanoimprint Lithography for Sub 100 nm Features." Dissertation Washington University, 1998.

[71] D.P. Mancini, K.A. Gehoski, E. Ainley, K.J. Nordquist, D.J. Resnick, T.C. Bailey, S.V. Sreenivasan, J.G. Ekerdt, and C.G. Willson. "Hydrogen Silsesquioxane for Direct Electron-Beam Patterning of Step and Flash Imprint Lithography Templates." Journal of Vacuum Science and Technology. 20(2002): 2896-2901.

[72] Chang-Chung Yang and Wen-Chang Chen. "The Structures and Properties of Hydrogen Silsesquioxane (HSQ) Films Produced by Thermal Curing." Journal of Material Chemistry. 12(2002): 1138-1141.

[73] Y.M. Georgiev, W. Henschel, A Fuchs, and H. Kurz. "Surface Roughness of Hydrogen Silsesquioxane as a Negative Tone Electron Beam Resist." Vacuum. (77): 117-123.

[74] Huey-Chiang Liou and John Pretzer. "Effect of Curing Temperature on the Mechanical Properties of Hydrogen Silsesquioxane Thin Films." Thin Solid Films. 335(1998): 186-191.

[75] R.W. Jaszewski, H. Schift, P. Groning, and G. Margaritondo. "Properties of Thin Anti-Adhesive Films Used for the Replication of Microstructures in Polymers." Microelectronic Engineering. 35(1997): 381-384.

[76] M. Beck, M. Graczyk, I. Maximov, E.-L. Sarwe, T.G.I Ling, and L. Montelius. "Improving Nanoimprint Lithography Stamps for the 10 nm Features." Division of Solid State Physics & Nanometer Structure Consortium.

[77] Brian Faircloth, Henry Rohrs, Richard Tiberio, Rodney Ruoff, Robert R. Krchnavek. "Bilayer Nanoimprint Lithography." Journal of Vacuum Science and Technology. 18(2000): 1-8.

[78] Nano PMMA and Copolymer Processing Guidelines. Microchem.

[79] S. Zankovych, T. Hoffmann, J. Seekamp, J.U. Bruch, and C.M. Sotomayor Torres. "Nanoimprint Lithography: Challenges and Prospects." Nanotechnology. 12(2001): 91-95.

[80] T. Bailey, B.J. Choi, M. Colburn, A. Grot, M. Meissl, M. Stewart, J.G. Ekerdt, S.V. Sreenivasan, and C.G. Willson. "Step and Flash Imprint Lithography: A Technology Review." The University of Texas at Austin. 11(2000): 54-67.

[81] Douglas J. Resnick, S.V. Sreenivasan, and C. Grant Wilson. "Step and Flash Imprint Lithography." Materials Today. Feb. 2005: 34-42.

[82] Wei Wu, Bo Cui, Xiao-yun Sun, Wei Zhang, Lei Zhuang, Linshu Kong, and Stephen Y. Chou. "Large Area High Density Quantized Magnetic Disks Fabricated Using Nanoimprint Lithography." Journal of Vacuum Science and Technology. 16(1998): 3825-3829.